

**Synthesis and Photophysical Characterization of
New Azaphthalocyanines and
Azanaphthalocyanines
for Semiconductor Interface Design**

Dissertation

zur

Erlangung des Doktorgrades der Naturwissenschaften

(Dr. rer. nat.)

dem Fachbereich Chemie
der Philipps-Universität Marburg

vorgelegt von

Martin Bernhard Liebold

aus

Heidelberg

Marburg (Lahn) 2016

Die vorliegende Arbeit wurde in der Zeit von November 2012 bis Juli 2016 am Fachbereich Chemie der Philipps-Universität Marburg in der Arbeitsgruppe und unter Leitung von Herrn Prof. Dr. Jörg Sundermeyer angefertigt.

Vom Fachbereich Chemie der Philipps-Universität Marburg (Hochschulkennziffer: 1180) als Dissertation angenommen am 14.07.2016.

Erstgutachter: Prof. Dr. Jörg Sundermeyer

Zweitgutachter: Prof. Dr. Eric Meggers

Tag der mündlichen Prüfung: 20.07.2016

To my friends in Syria!

Who always believed in me to become a “German doctor”.

"One of the things Ford Prefect had always found hardest to understand about humans was their habit of continually stating and repeating the very very obvious. "

Douglas Adams, *The Hitchhiker's Guide to the Galaxy*

Erklärung

Ich erkläre, dass eine Promotion noch an keiner anderen Hochschule als der Philipps-Universität Marburg, Fachbereich Chemie, versucht wurde.

Ich versichere, dass ich meine vorgelegte Dissertation mit dem Titel

**Synthesis and Photophysical Characterization of
New Azaphthalocyanines and
Azanaphthalocyanines
for Semiconductor Interface Design**

selbst und ohne fremde Hilfe verfasst, nicht andere als die in ihr angegebenen Quellen oder Hilfsmittel benutzt, alle vollständig oder sinngemäß übernommenen Zitate als solche gekennzeichnet habe sowie die Dissertation in der vorliegenden oder einer ähnlichen Form noch bei keiner anderen in- oder ausländischen Hochschule anlässlich eines Promotionsgesuches oder zu anderen Prüfungszwecken eingereicht habe.

Marburg, den ____ . ____ . ____ .

Unterschrift: _____.

Published parts of this work

Presentations

M. Liebold and J. Sundermeyer, *Tailoring Phthalocyanines for Internal Interface Alignment*, SFB Workshop, 18. Dez. 2014.

M. Liebold, *Phthalocyanines – with Equatorial and Axial Anchors for Organic Interfaces with Tailored Properties*, SFB Kick-Off Meeting, 28. Nov. 2013.

M. Liebold, *Hybrid Subphthalocyanines, Porphyrazines, and Phthalocyanines*, Koordinationschemietreffen Bayreuth, 25. Feb. 2013.

Poster (Auswahl)

M. Liebold, J. Sundermeyer, *Experimental and Computational Study of Soluble Azaphthalocyanines and Azasubphthalocyanines of Varying Number of Aza Units*, ICII-2016, Marburg, 31.05.-03.06.2016.

M. Liebold, M. Kothe, G. Witte, J. Sundermeyer, *Aza(sub)phthalocyanines with Equatorial and Axial Anchors for Heterojunction Interfaces*, Marburg, 9. Juli 2015.

M. Liebold, *Phthalocyanines - with Equatorial Anchors for Organic Interfaces with Tailored Properties*, Hirschegg – Kleinwalsertal, 8. Feb. – 12. Feb. 2015.

M. Liebold and J. Sundermeyer, *Interfacial Bonding of Phthalocyanines and Pyrazinoporphyrazines with Axial and Equatorial Anchors*, San Sebastian, Spain, 27. – 31. Juli 2014.

M. Liebold and J. Sundermeyer, *Interfacial Bonding of Phthalocyanines and Pyrazinoporphyrazines with Axial and Equatorial Anchors*, 8th ICPP Istanbul, Turkey, 22. – 28. Juni 2014.

I. Meyenburg, M. Kothe, A. Karthäuser, M. Liebold, T. Breuer, G. Witte, W. Heimbrod, *Optical Spectroscopy on Organic-Inorganic Hybrid Structures*, Materialforschungstag Gießen, Juni 2014.

M. Liebold, M. Bartlett, A. Ibrahim, J. Sundermeyer, *Interfacial Bonding of Phthalocyanines and Pyrazinoporphyrazines with Axial and Equatorial Anchors*, Materialforschungstag Gießen, Juni 2014.

List of Abbreviations

Ac	acetyl
Acac	acetylacetonate
MeCN	acetonitrile
AFM	atomic force microscope
APCI	atmospheric pressure chemical ionisation
Bu	butyl
calc	calculated
cat	catalytic
CB	chlorobenzene
CC	column chromatography
CNP	1-chloronaphthalene
Conc	concentrated
COSY	correlation spectroscopy
CV	cyclic voltammetry
DAMN	diaminomaleonitrile
Dpbf	1,3-diphenylisobenzofuran
DBU	1,8-diazabicyclo[5.4.0]undec-7-en
DBN	1,5-diazabicyclo[4.3.0]non-5-ene
DC	Dünnschichtchromatographie
DCB	dichlorobenzene
DCM	dichloromethane
DDQ	2,3-dichloro-5,6-dicyano-1,4-benzoquinone
DFT	density functional theory
DISN	diiminosuccinonitrile
dme	dimethoxyethane

DMF	dimethylformamide
DMSO	dimethyl sulfoxide
DSSC	dye sensitized solar cell
EE	ethyl acetate
EI	electron ionisation
EPR	electron paramagnetic resonance
ESI	electron spray ionisation
eq	equivalents
Et	ethyl
EXAFS	extended X-ray absorption fine structure
FD	field desorption
FS	fluorescence
FTO	fluorine doped tin oxide
<i>hf</i>	<i>hyperfine</i>
HOMO	highest occupied molecular orbital
IR	infra red spectroscopy
ITO	indium tin oxide
LUMO	lowest unoccupied molecular orbital
M	metal, molecule (in MS) or molar mass, depending on context
MALDI-ToF	matrix-assisted laser desorption/Ionisation – time-of-flight mass spectrometer
Me	methyl
MEK	methyl ethyl ketone
MPLC	medium pressure liquid chromatography
M _{RE}	rare earth metal
MS	mass spectrometry
NBS	<i>N</i> -bromosuccinimide

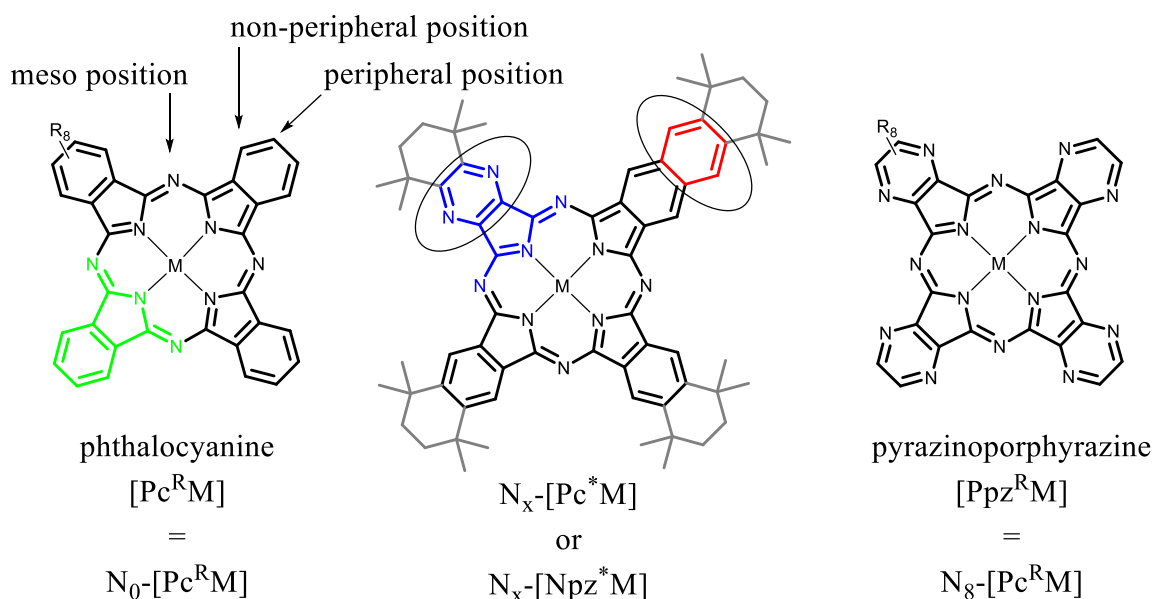
NDN	naphthalonitrile
Nc	naphthalocyanine
NEXAFS	X-ray absorption near-edge structure spectroscopy
NMP	<i>N</i> -methyl-2-pyrrolidine
NMR	nuclear magnetic resonance
Ox	oxidation
Pc	phthalocyanines
PDT	photodynamic therapy
PE	pentane or petrolether (chosen by boiling point)
PDN	phthalonitrile
Ppz	pyrazinoporphyrazine
PS	photosensitizer
Py	pyridine
PyzDN	pyrazinenitrile
Pz	azaphthalocyanine
Red	reduction
RFA	X-ray fluorescence spectroscopy
<i>shf</i>	<i>superhyperfine</i>
TBA	tetra <i>n</i> -butyl ammonium
TBTAP	tetrabenzotriazaporphyrin
TBDAP	tetrabenzodiazaporphyrin
TBMAP	tetrabenzomonoazaporphyrin
TD-DFT	time dependent density functional theory
TDS	thermal desorption spectroscopy
TFA	trifluoroacetic acid
THF	tetrahydrofuran
TLC	thin layer chromatography

TOCSY	total correlated spectroscopy
Tol	toluene
UV-Vis	UV and visible light
XAS	X-ray absorption spectroscopy
XPS	X-ray photoelectron spectroscopy

Table of Discussed Compounds

All compounds, which already have been discussed in literature, are marked with the corresponding reference. All other compounds in this thesis have been synthesised for the first time. The precursors/dinitriles are marked with a number and some, e. g. target compounds, with an abbreviation. Commercially available compounds are marked with a € sign. Intermediates are marked with Roman numerals. The completed ligands and complexes are named with an abbreviation.

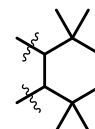
The following abbreviations are used for the compounds listed below: Pc (**P**hthalocyanine), Ppz (**P**yrazinoporphyrzine), Pz (**P**orphyrzine), Spc (**S**ubphthalocyanine), Sppz (**S**ubpyrazinoporphyrzine), PDN (**P**hthalo(**d**i)nitrile), Pyz (**P**yrzine), PyzDN (**P**yrzine(**d**i)nitrile), NDN (**N**aphthalo(**d**i)nitrile), NpzDN (**N**aphthalopyrazine(**d**i)nitrile), NqnDN (**N**aphthaloquinoxalin(**d**i)nitrile), NppzDN (**N**aphthalopyrazinopyrazine(**d**i)nitrile).



On the left, a phthalocyanine $[PcM]$ is shown, on the right, a pyrazinoporphyrazine $[PpzM]$. Hybrid compounds, so called **azaphthalocyanines** $N_x-[PcM]$, are shown in the middle. If $[-CH=]$ (black) units of an **isoindoline** (green) unit are exchanged by $[-N=]$ (blue) these azaphthalocyanines are abbreviated with $N_x-[PcM]$. The x, in N_x , gives the number of exchanged $[-CH=]$ by $[-N=]$ units. When the π -system is annulated with an additional benzene unit, these **naphthalocyanine-pyrazine** hybrid systems are named as $N_x-[NpzM]$ (red). C_{4v} symmetrical, A_4 azanaphthalocyanines, are abbreviated with $N_{x,y}-[NcM]$; x and y give the number and position

of exchanged [-CH=] by [-N=] units. Smaller ring-contracted subphthalocyanines are abbreviated with [Spc], azasubphthalocyanines with N_x -[Spc] and subpyrazinoporphyrazines with [Sppz]. If the Pc is annulated with an additional 2,2,5,5-tetramethylcyclohexane ring, the compounds are marked with a " * ", such as "[Pc**M*]", following the common terminology of prominent organometallic ligands Cp (C₅H₅) and Cp* (C₅Me₅).

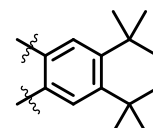
* annulated 2,2,5,5-tetramethylcyclohexane ring



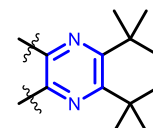
° annulated cyclohexane ring



Pc* annulated tetramethyltetraline system

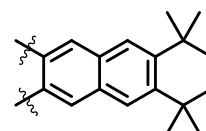


Ppz* annulated tetramethyltetrahydroquinoxaline system

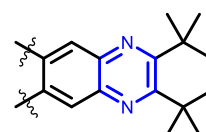


For corresponding Naphthalocyanines:

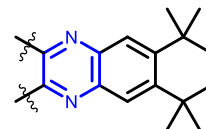
Nc* annulated tetramethyltetraline system



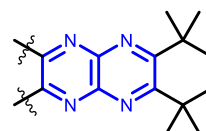
Npz* tetramethyltetrahydrophenazine system



Nqn* annulated tetramethyltetrahydroquinoxaline system



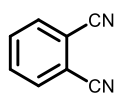
Nppz* annulated tetramethyltetrahydropyrazino-[2,3-b]-pyrazine



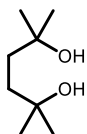
When non-/peripheral functional groups are added to an A₃B system, the functional group is written in superscript after the complex, while the A₃ system is written within square brackets such as [Pc^{alkyl-ligands}M]^(functional group). The corresponding derivatives are named by the number of units: A₂B₂-[Pc^{alkyl-ligands}M]^(functional group)/ AB₃-[Pc^{alkyl-ligands}M]^(functional group). Axial ligands, coordinated at the central metal atom are written within the square brackets, such as [PcTiO].

Organic precursors

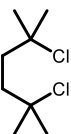
Phthalonitriles



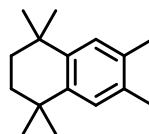
PN I ^ε



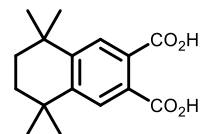
II ^ε



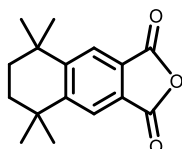
III [a]



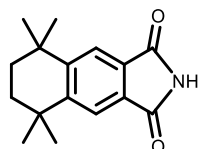
IV [a]



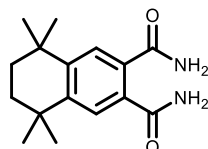
V [a]



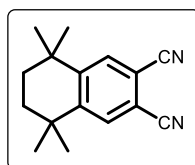
VI [a]



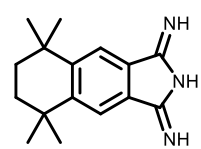
VII [a]



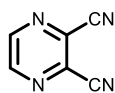
VIII [a]



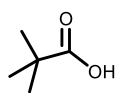
PDN* 1 [a]



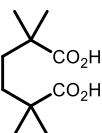
Isoindoline of 1 [b]



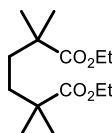
PызDN IX [c]



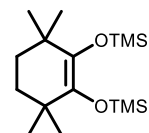
X ^ε



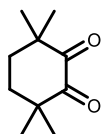
XI [d]



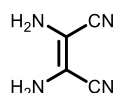
XII [e]



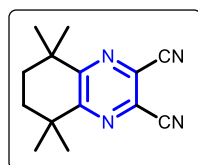
XIII [e]



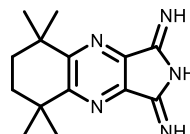
XIV [e]



DAMN ^ε



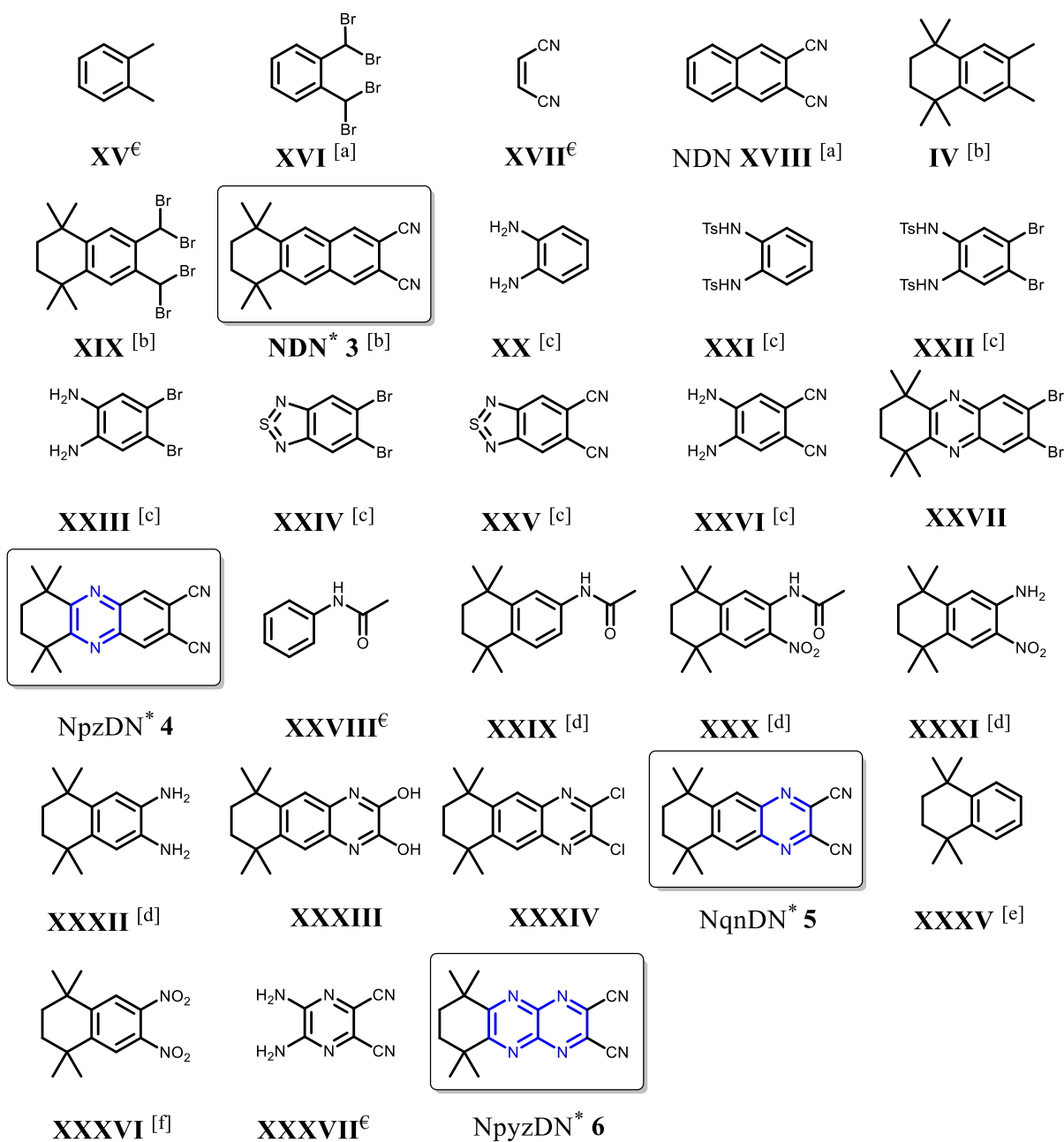
PызDN* 2 [b]



Isoindoline of 2 [b]

[a] S. A. Mikhalenko, L. I. Solov'eva, E. A. Luk'yanets, *J. Gen. Chem. USSR* **1988**, *58*, 2618-2619. [b] E. Seikel, *Dissertation*, Philipps-Universität Marburg, **2012**. [c] T. Tsude, K. Fujisjima, H. Ueda, *Agricultural and Biological Chemistry* **1981**, *45*, 2129-2130. [d] D. D. Coffman, E. L. Jenner, R. D. Lipscomb, *J. Am. Chem. Soc.* **1958**, *80*, 2864-2872. [e] P. Jones, G. B. Villeneuve, C. Fei, J. DeMarte, A. J. Haggarty, K. T. Nwe, D. A. Martin, A.-M. Lebus, J. M. Finkelstein, B. J. Gour-Salin, T. H. Chan, B. R. Leyland-Jones, *J. Med. Chem.* **1998**, *41*, 3062-3077.

Naphthalonitriles

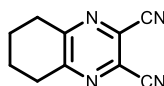


[a] E. V. Kovshev, V. A. Puchnova, E. A. Luk'yanetz, *J. Org. Chem. USSR (Engl. Trans.)* **1971**, *71*, 364. [b] S. A. Mikhalenko, L. I. Solov'eva, E. A. Luk'yanets, *J. Gen. Chem. USSR* **1988**, *58*, 2618-2619. [c] C. Burmester, R. Faust, *Synthesis* **2008**, 1179-1181. [d] L. Eyrolles, H. Kagechika, E. Kawachi, H. Fukasawa, T. Iijima, Y. Matsushima, Y. Hashimoto, K. Shudo, *J. Med. Chem.* **1994**, *37*, 1508-1517. [e] H. A. Bruson, J. W. Kroeger, *J. Am. Chem. Soc.* **1940**, *62*, 36-44. [f] H. Kagechika, E. Kawachi, Y. Hashimoto, K. Shudo, T. Himi, *J. Med. Chem.* **1988**, *31*, 2182-2192.

Other Precursors

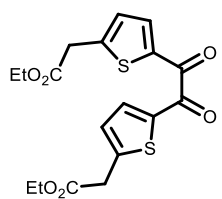


XXXVIII^e

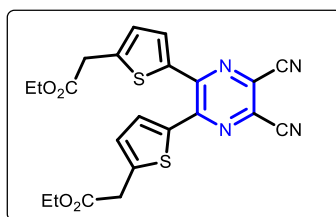


PzDN° 7 [a]

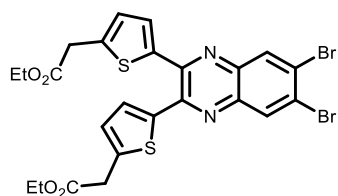
Thiophenenitriles



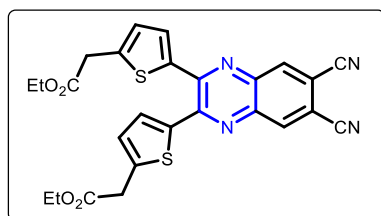
IXL [b]



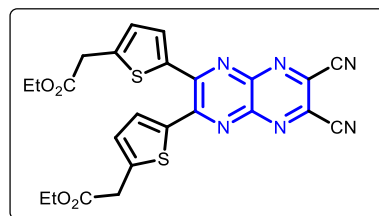
8 [b]



XL

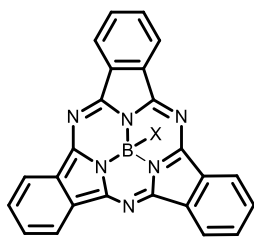


QnDN^{Tp} 9



PzDN^{Tp} 10

Aza-/Subphthalocyanines



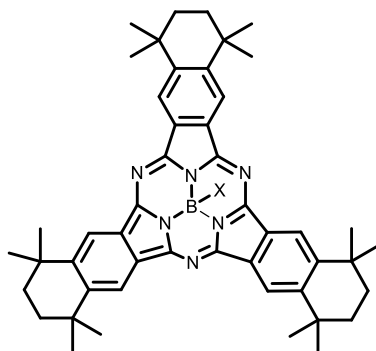
[SpcB-X^{Hal}]

with X^{Hal} = F [c]

X^{Hal} = Cl [c]

X^{Hal} = OH [c]

X^{Hal} = carbazol



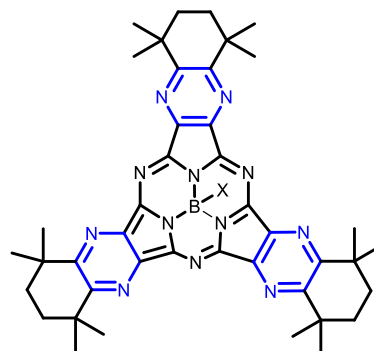
[SpC* B-X^{Hal}]

with X^{Hal} = F

X^{Hal} = Cl [b]

X^{Hal} = Br

X^{Hal} = OH [d]



[Sppz* B-X^{Hal}]

with X^{Hal} = F

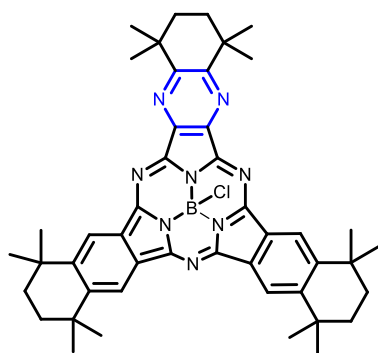
X^{Hal} = Cl [b]

X^{Hal} = Br

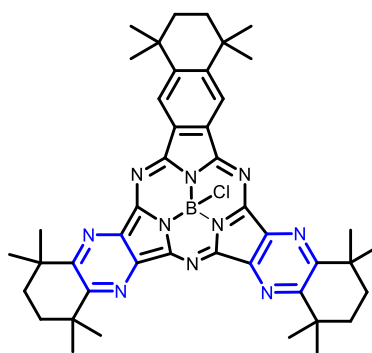
X^{Hal} = OH [d]

[a] H. Onay, B. Esat, R. Öztürk, *Polyhedron* **2010**, 29, 1314-1316. [b] E. Seikel, *Dissertation*, Philipps-Universität Marburg, **2012**. [c] J. Guilleme, D. González-Rodríguez, T. Torres, *Angew. Chem. Int. Ed.* **2011**, 50, 3506–3509. [d] E. Sharikow, *Bachelorarbeit*, Philipps-Universität Marburg, **2013**.

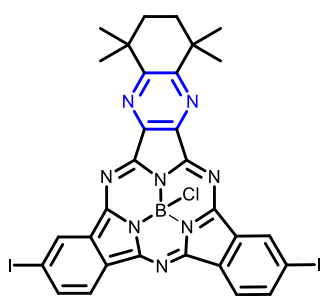
Asymmetrical Aza/-Subphthalocyanines



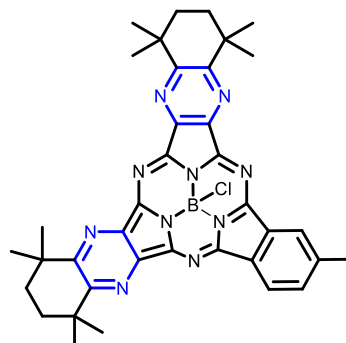
N_2 -[Spc*BCl]



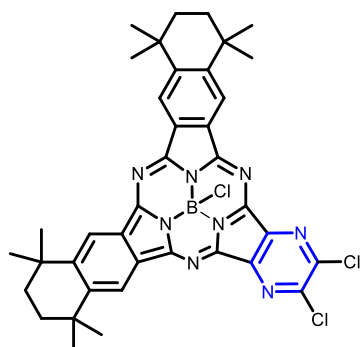
N_4 -[Spc*BCl]



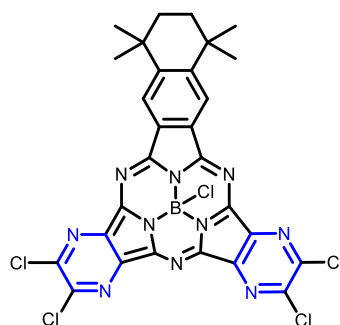
N_2 -[Spc*BCl]^I



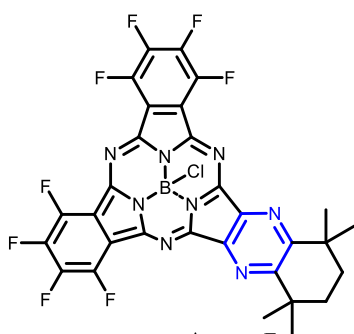
N_4 -[Spc*BCl]^I



N_2 -[Spc*BCl]^{Cl} [a]

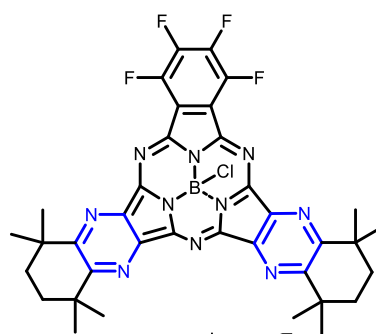


N_4 -[Spc*BCl]^{Cl} [a]



N_2 -[Spc*BCl]^F

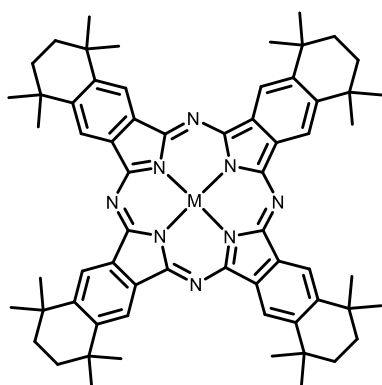
Bisazasubporphyrazine



N_4 -[Spc*BCl]^F

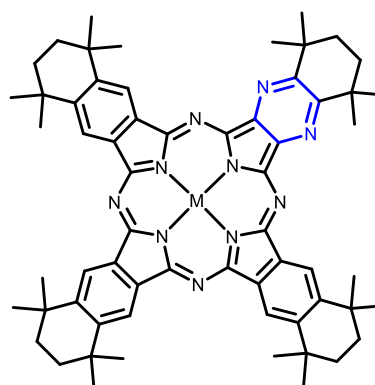
Tetraazasubporphyrazine

Phthalocyanines and Azaphthalocyanines – N_x -[Pc* M]



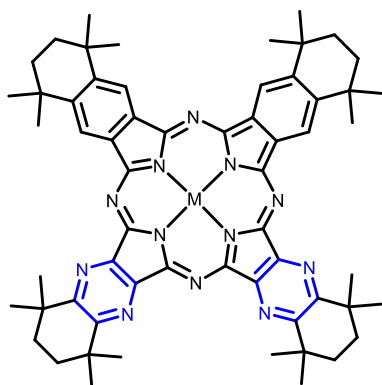
A_4 ; [Pc* M] ^[a]

Phthalocyanine with $M = 2 \text{ H, Zn}$



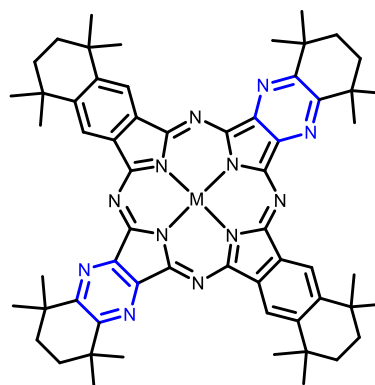
A_3B ; N_2 -[Pc* M] ^[b]

Diazaphthalocyanine with $M = 2 \text{ H, Zn}$



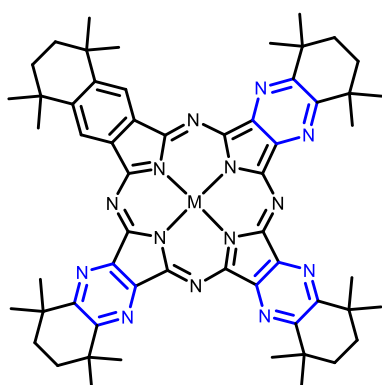
A_2B_2 ; N_4 -[Pc* M] ^[b]

Tetraazaphthalocyanine with $M = 2 \text{ H, Zn}$



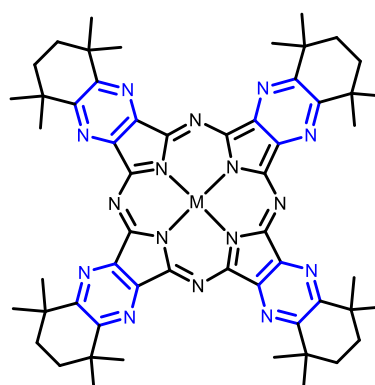
ABAB; N_4 -[MPc* M]

Tetraazaphthalocyanine with $M = 2 \text{ H, Zn}$



AB_3 ; N_6 -[Pc* M] ^[b]

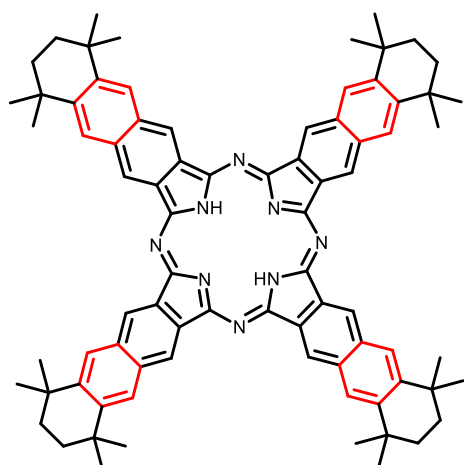
Hexaazaphthalocyanine with $M = 2 \text{ H, Zn}$



B_4 ; N_8 -[Pc* M] ^[b]

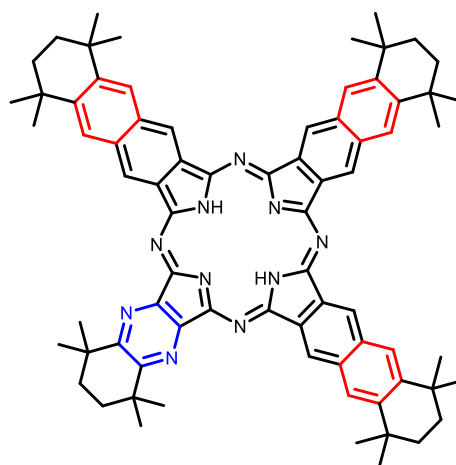
Octaazaphthalocyanine with $M = 2 \text{ H, Zn}$
or Pyrazinoporphyrazine [Ppz* M]

Naphthalopyrazines – $N_x\text{-Npz}^*\text{H}_2$



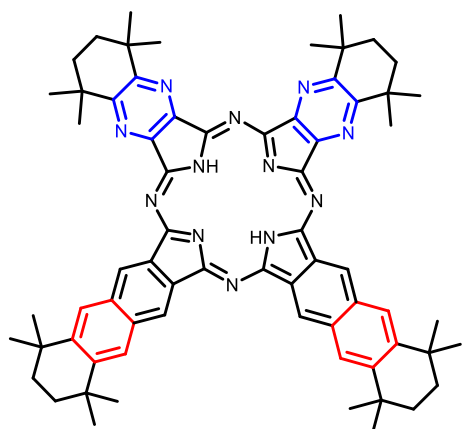
$A_4; Nc^*H_2$ [a]

Naphthalocyanine



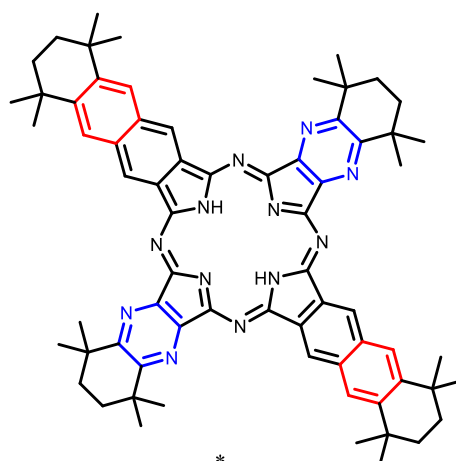
$A_3B; N_2\text{-Npz}^*H_2$ [b]

Bisazanaphthalocyanine



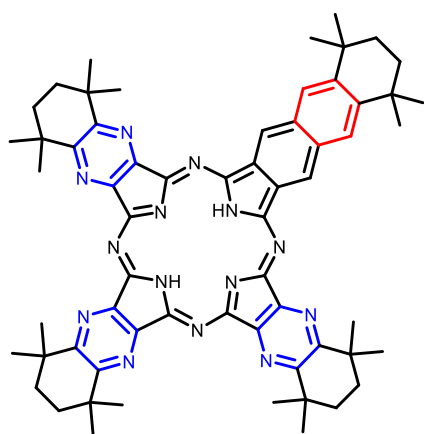
$A_2B_2; N_4\text{-Npz}^*H_2$ [b]

Tetraazaphthalocyanine



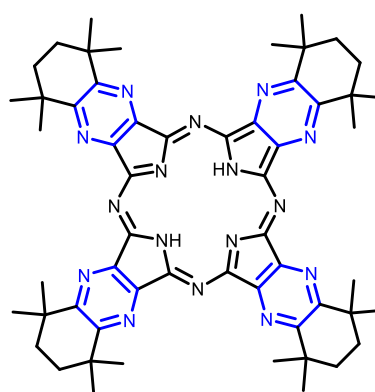
$ABAB; N_4\text{-Npz}^*H_2$

Tetraazaphthalocyanine



$AB_3; N_6\text{-Npz}^*H_2$ [b]

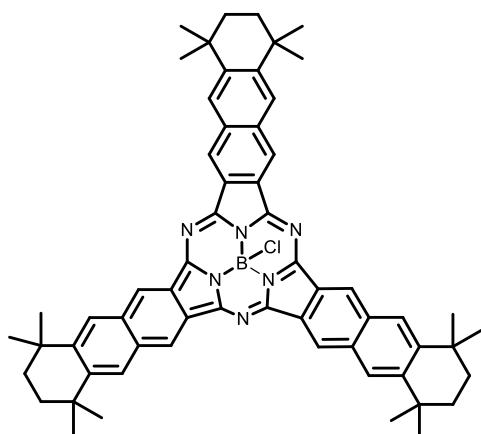
Hexaazaphthalocyanine



$B_4; N_8\text{-[Pc}^*M]$ [c]

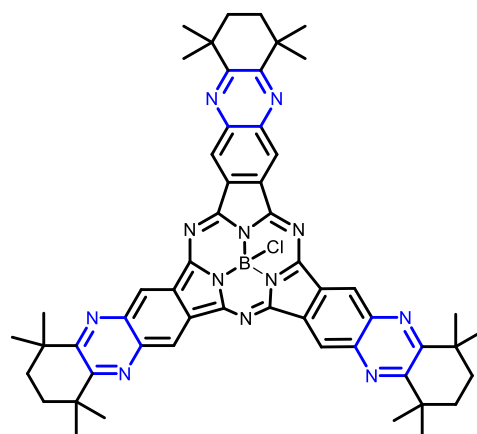
Octaazaphthalocyanine with $M = 2 H, Zn$
or Pyrazinoporphyrazine [Ppz^*M]

Subnaphthalocyanines



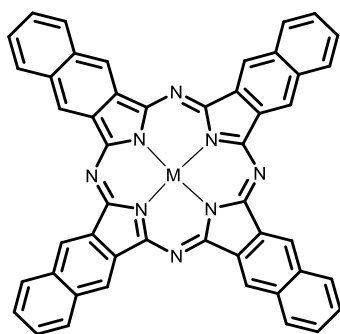
[SnC*BCl]* [a]

(* SnC*BCl is unstable)

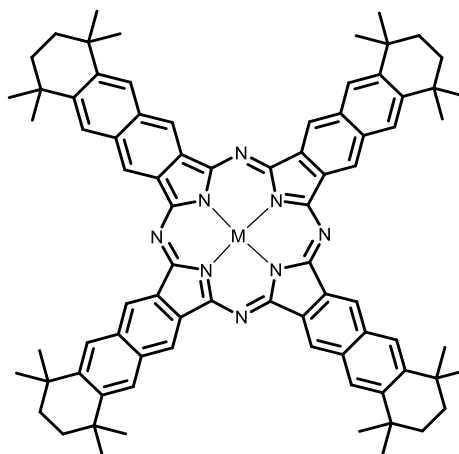


[Snpz*BCl]

Naphthalocyanines



[NcM] with M = 2H [b]



[Nc*M] [a, c]

with M = 2H

Zn

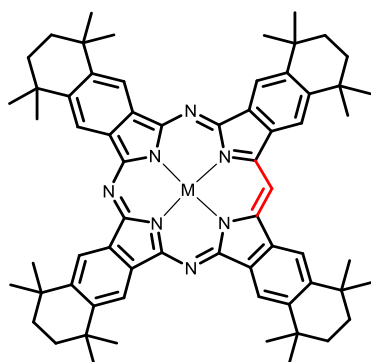
V=O

SiCl₂

TiCl₂

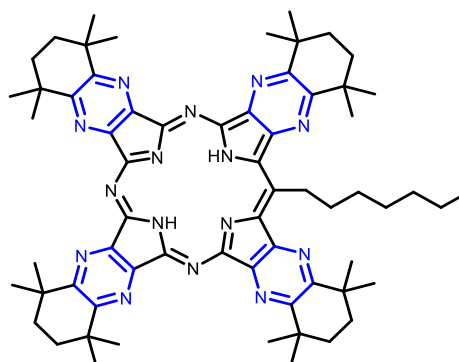
CrCl

Tetrabenzotriazaporphyrins TBTAP



[TBTAPM] [d]

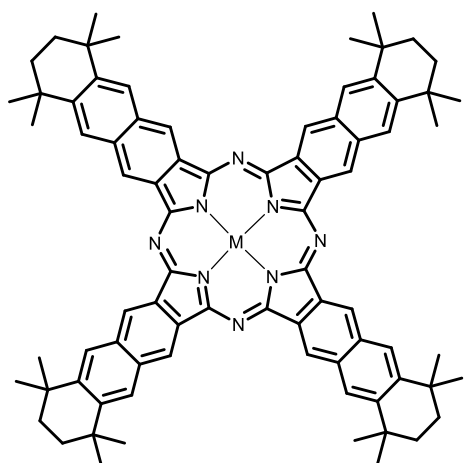
with M = 2 H, Mg



Ppz*H₂^{noctyl}

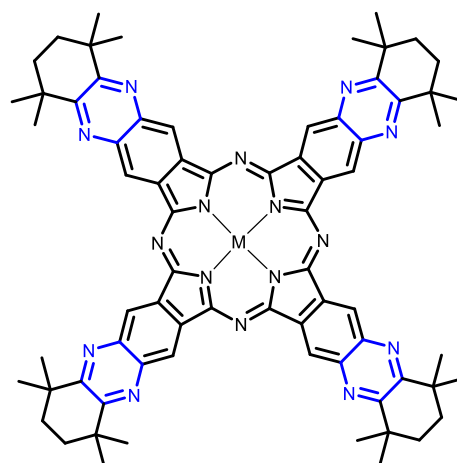
[a] T. Vollgraf, *Bachelorarbeit*, Philipps-Universität Marburg, **2014**. [b] S. A. Mikhalenko, E. A. Luk'yanets, *Zhurnal Obshchei Khimii* **1969**, 39 (11), 2554-2558. [c] S. A. Mikhalenko, L. I. Solov'eva, E. A. Luk'yanets, *J. Gen. Chem. USSR* **1988**, 58, 2618-2619. [d] N. Alharbi, A. Díaz-Moscoso, G. J. Tizzard, S. J. Coles, M. J. Cook, A. N. Cammidge, *Tetrahedron* **2014**, 70, 7370-7379.

Azanaphthalocyanines – $N_{x,y}$ -[NcM*]**



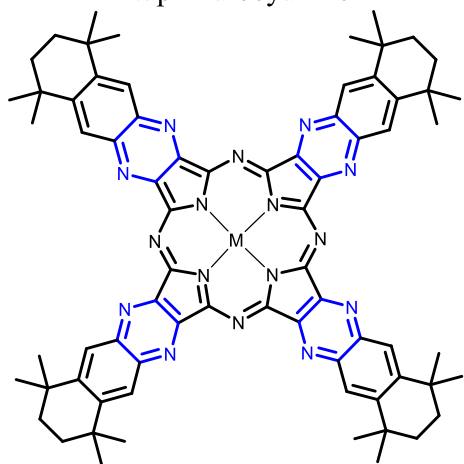
$N_{0,0}$ -[Nc**M*] [a]

Naphthalocyanine



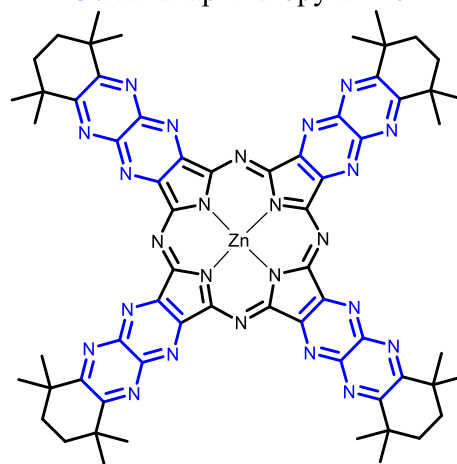
$N_{0,8}$ -[Nc**M*]

Octaazanaphthalopyrazine



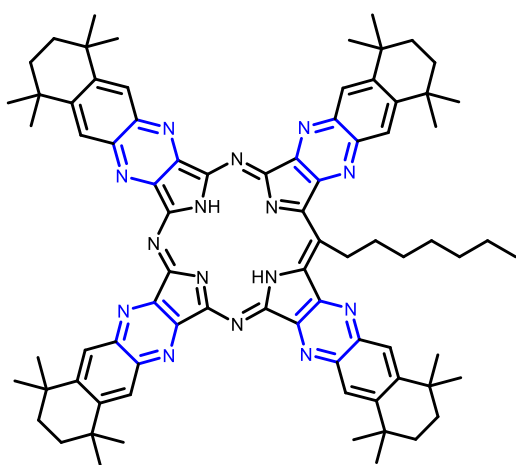
$N_{8,0}$ -[Nc**M*]

Octaazanaquinoxaline



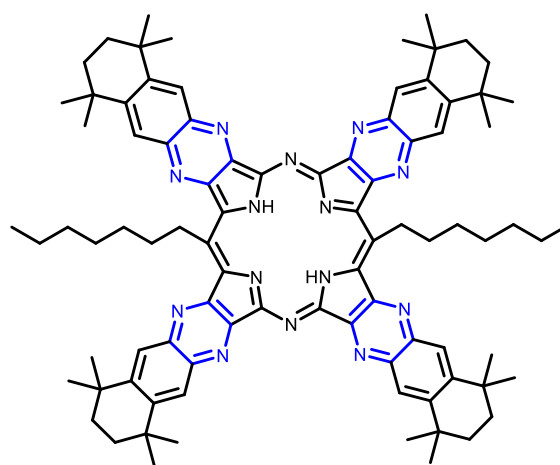
$N_{8,8}$ -[Nc**Zn*]

Hexadecanaphthalopyrazine
with *M* = 2 H, or Zn



(TQTAP) $Nqn^*H_2^{noctyl}$

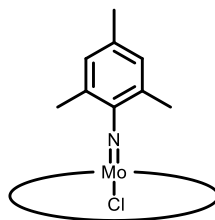
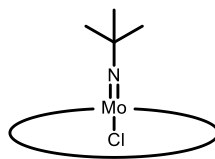
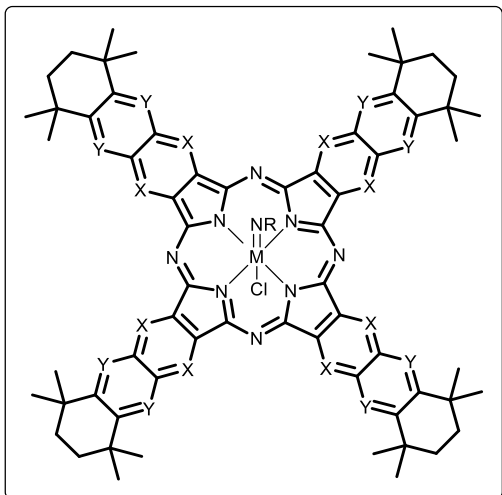
Tetraquinoxalintriazaporphyrin



TQDAP $Nqn^*H_2^{noctyl}$

Tetraquinoxalindisazaporphyrin

Azanaphthalocyanines Complexes with Molybdeneum and Tungsten



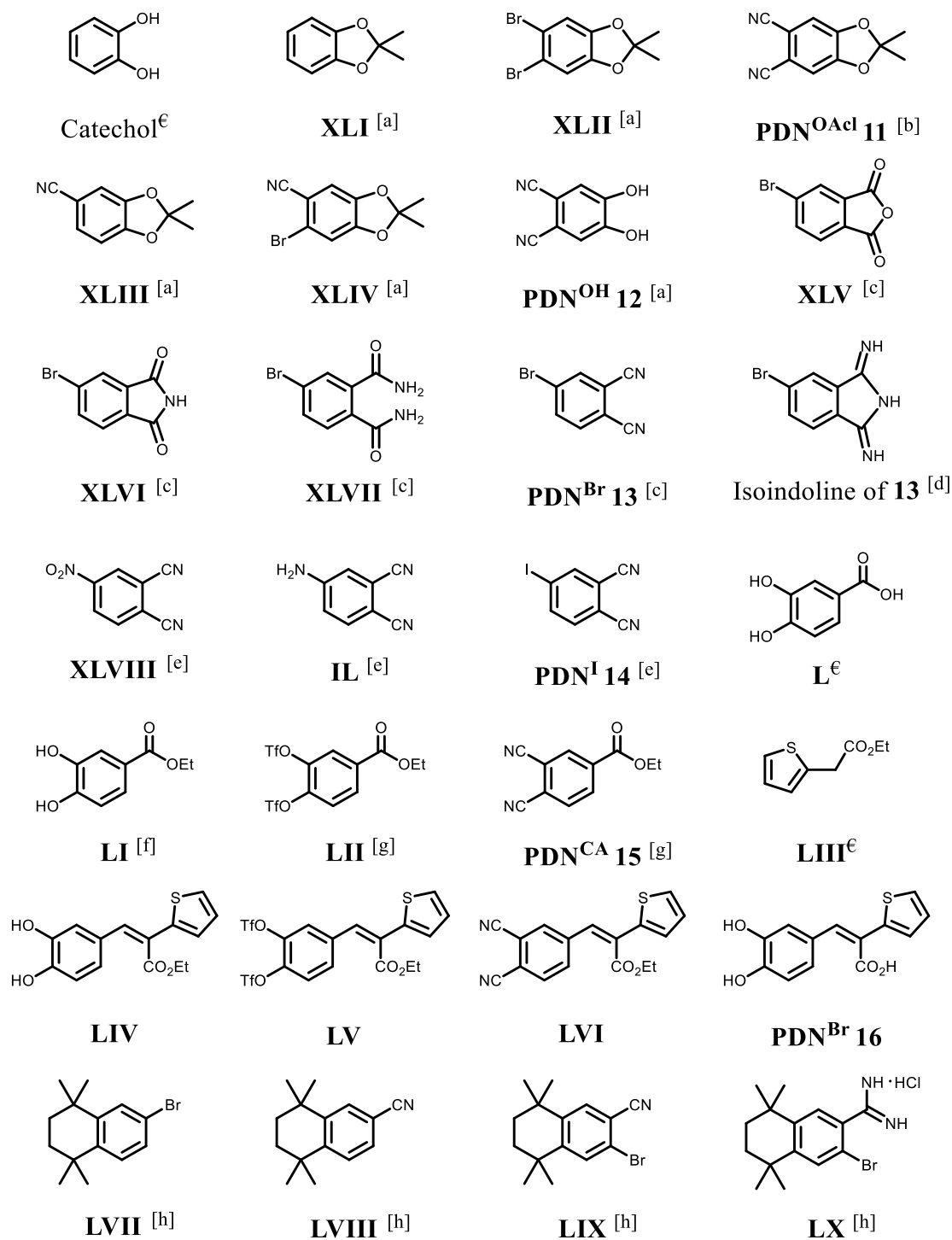
x, y = number of substituted [-CH=]
by [-N=] units at position X and Y

x = y = 0	$N_{0,0}$ -[Nc* $M(NR)Cl$]	with M = Mo, W and R = <i>t</i> Bu, Mes
x = 0, y = 8	$N_{0,8}$ -[Nc* $M(NR)Cl$]	with M = Mo and R = <i>t</i> Bu, Mes
x = 8, y = 0	$N_{8,0}$ -[Nc* $M(NR)Cl$]	with M = Mo and R = <i>t</i> Bu
x = y = 8	$N_{8,8}$ -[Nc* $M(NR)Cl$]	with M = Mo, (W) and R = <i>t</i> Bu, (Mes)

non-alkyl substituted naphthalocyanines:

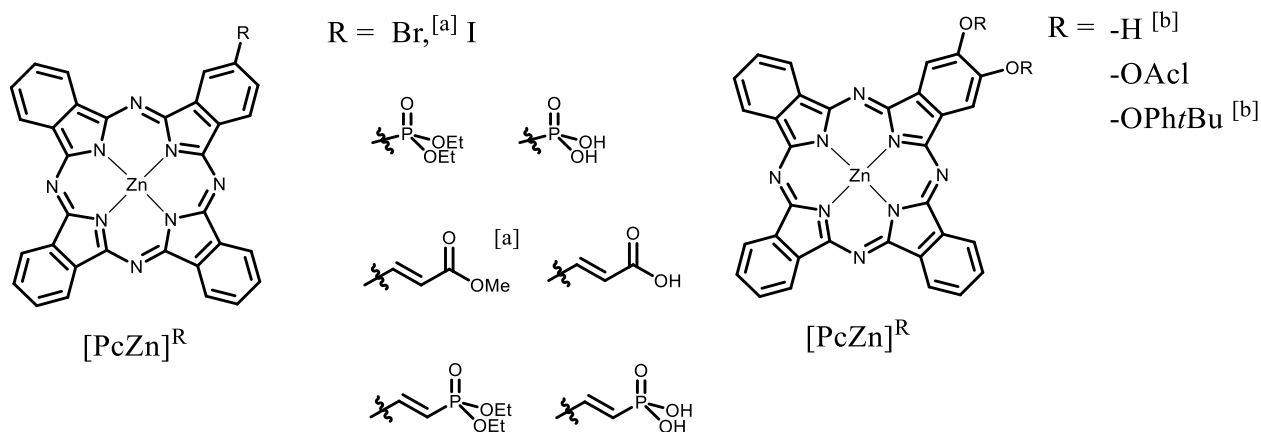


Functionalised Precursors

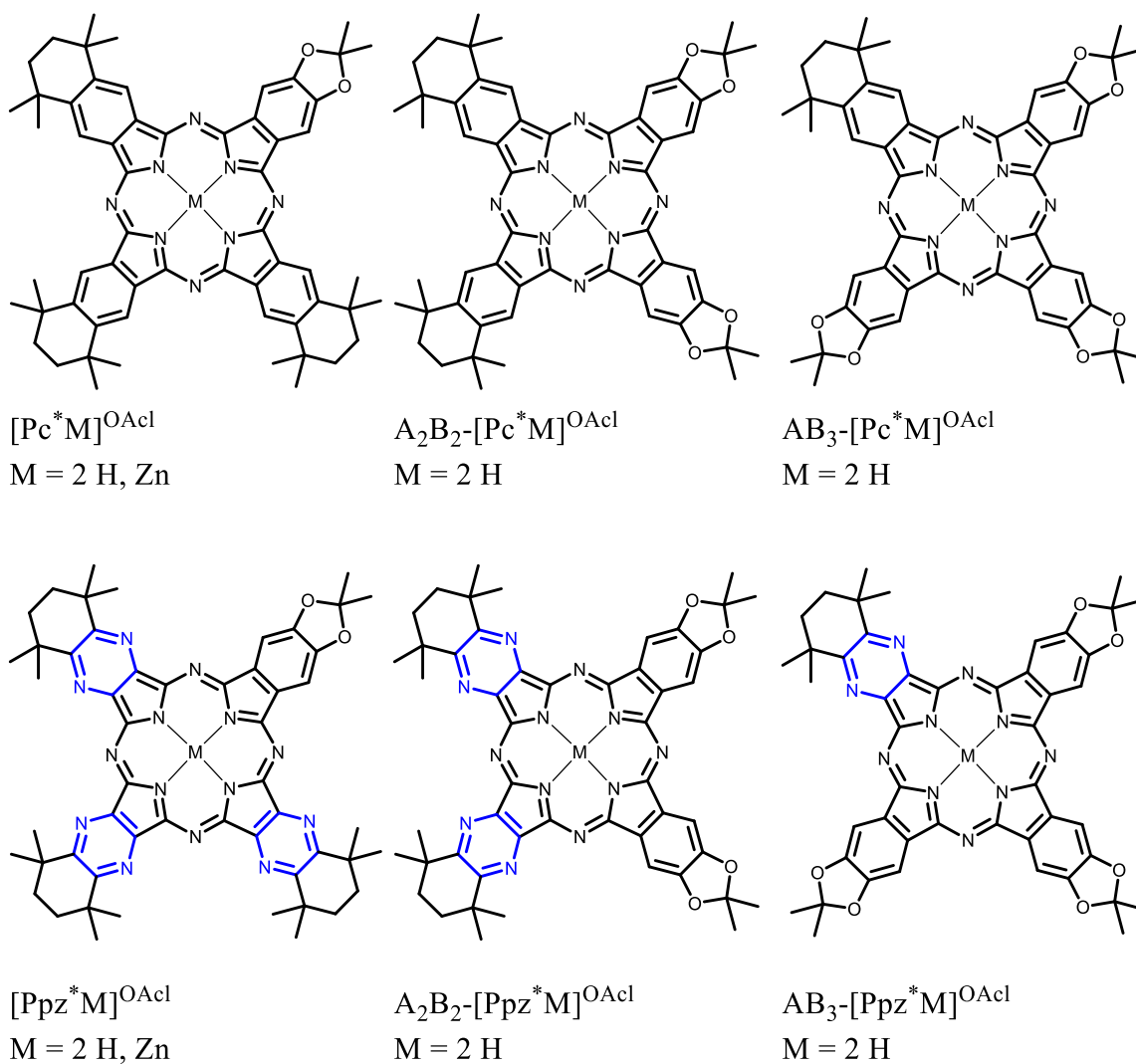


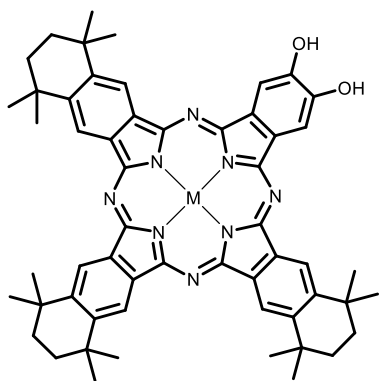
[a] A. V. Ivanov, P. A. Svinareva, L. G. Tomilova, N. S. Zefirov, *Russian Chemical Bulletin* **2001**, *50*, 919–920. [b] Z. Iqbal, A. Lyubimtsev, M. Hanack, *Synlett* **2008**, *2008*, 2287–2290. [d] G. Märkl, K. Gschwendner, I. Rötzer, P. Kreitmeyer, *HCA* **2004**, *87*, 825–844. [d] M. Liebold, *Master-Thesis*, Philipps-Universität Marburg, **2012**. [e] V. Aranyos, A. M. Castaño, H. Grennberg, M. F. Hawthorne, S. Sjöberg, A. Talec, T. Shono, H. Toftlund, *Acta Chem. Scand.* **1999**, *53*, 714–720. [f] E. Seraya, Z. Luan, M. Law, A. F. Heyduk, *Inorg. Chem.* **2015**, *54*, 7571–7578. [g] U. Drechsler, *Synlett* **1998**, *1998*, 1207–1208. [h] K. Pfaff, *Bachelorarbeit*, Philipps-Universität Marburg, **2014**.

Non-Alkyl Substituted Functionalised Phthalocyanines – [PcZn]^{FG}

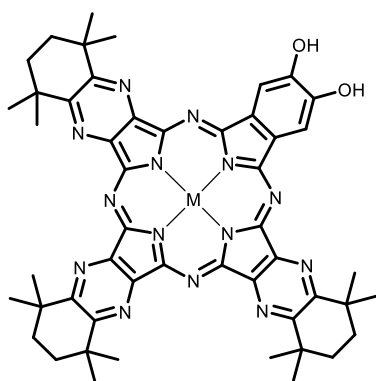


Alkyl Substituted Functionalised Phthalocyanines – [Pc*M]^{FG}

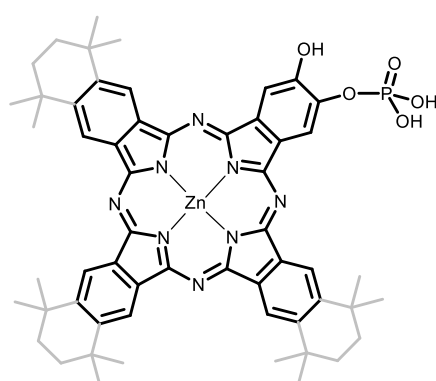




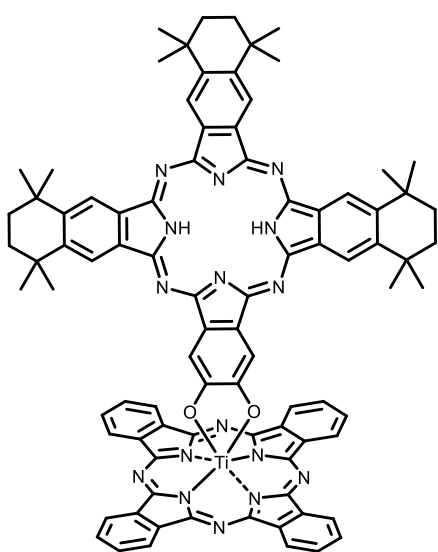
$[\text{Pc}^* \text{M}]^{\text{OH}}$
 $\text{M} = 2 \text{ H, Zn}$



$[\text{Pz}^* \text{M}]^{\text{OH}}$
 $\text{M} = 2 \text{ H, Zn}$

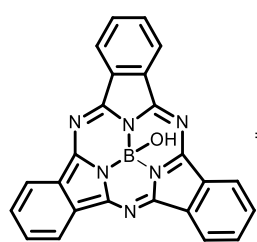


$[\text{Pc}^{(*)} \text{M}]^{\text{OPA}}$
 $\text{M} = \text{Zn}$

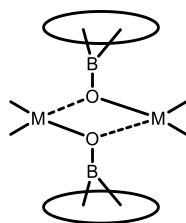
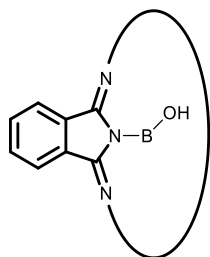


$[\text{PcTiOPc}^*]$

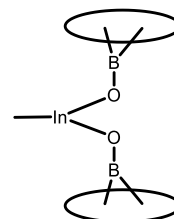
Subphthalocyanine Complexes



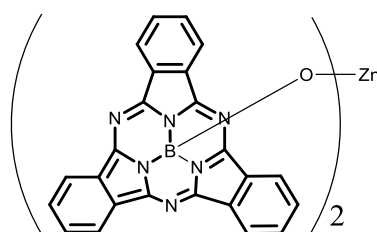
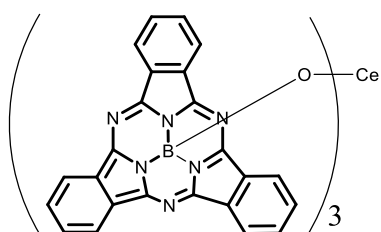
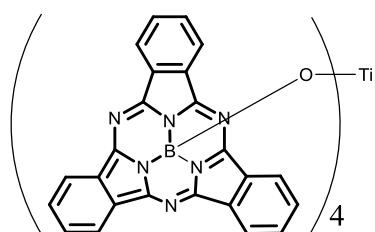
[SpcBOH] [a]



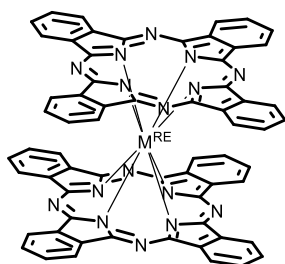
[Me₂M(μ-OBSpc)]₂
with M = Al,^[b] Ga, (In)



[MeIn(OBSpc)₂]



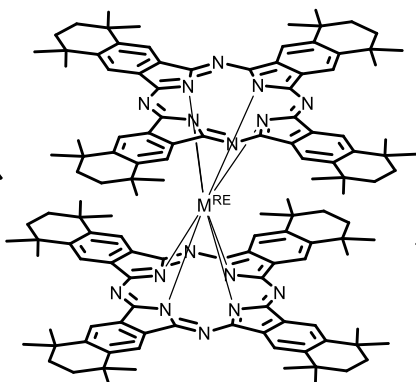
Rare Earth Metal Sandwich-Complexes – [Pc^(*)₂M^{RE}] and [Nc^{*}₂M^{RE}]



[Pc₂M^{RE}] [c]

with M = Eu, Tb

test reaction for Sm, Nd

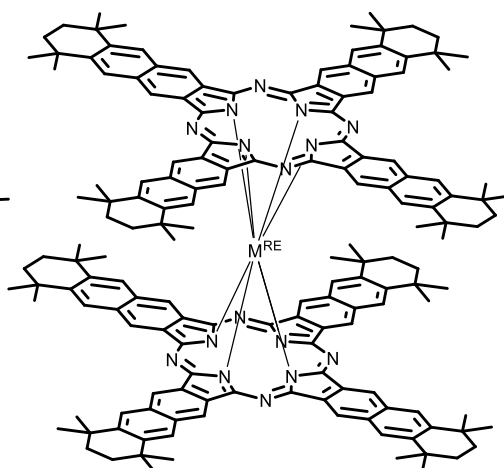


[Pc₂^{*}M^{RE}]

with M = Eu, Tb

test reaction for

Sc, Y, La, Ce, Nd, Sm, Gd, Lu



[Nc₂^{*}M^{RE}]

with M = Ce, Nd, Eu

test reaction for Pr, Tb, Dy

[a] J. Guilleme, D. González-Rodríguez, T. Torres, *Angew. Chem. Int. Ed.* **2011**, *50*, 3506–3509. [b] E. Sharikow, *Bachelorarbeit*, Philipps-Universität Marburg, **2013**. [c] prepared by literature known method: De Cian, A.; Moussavi, M.; Fischer, J.; Weiss, R. *Inorg. Chem.* **1985**, *24*, 3162-3167.

Table of Contents

1	Introduction	1
2	Theoretical Section.....	3
2.1	Structure and Properties of Phthalocyanines	3
2.1.1	Discovery of the Blue Dye	3
2.1.2	Properties of Phthalocyanines	4
2.1.3	Synthetic Strategy for the Synthesis of Phthalocyanines, Pyrazinoporphyrazines and Lower Symmetrical Azaphthalocyanines	8
2.1.4	Rare Earth Metal Complexes	14
2.1.5	Molybdenum and Tungsten Phthalocyanines	15
2.2	Applications of Phthalocyanines	17
2.2.1	Phthalocyanines in PDT	17
2.2.2	Phthalocyanines as Photosensitizers in DSSCs.....	19
2.2.3	Investigation of Single-Molecule Magnets (Ln-SMMs).....	27
2.2.4	Rare Earth Metal Phthalocyanines, [Pc ₂ M ^{RE}], applied in Gas Sensors.....	29
3	Purpose of the Work.....	31
4	Results and Discussion.....	35
4.1	Organic Precursors – Symmetrical Aza-/Dinitriles	35
4.1.1	Synthesis of Aza-/Dinitriles	36
4.1.2	Synthesis of Aza-/Naphthalonitriles.....	40
4.1.3	Synthesis of PzDN ^o	44
4.1.4	Synthesis of Thiophene Substituted PDNs.....	44
4.2	Synthesis of Azaphthalocyanines and Derivatives.....	46
4.2.1	Synthesis of Symmetrical Subphthalocyanines.....	46
4.2.2	NEXAFS and XPS Studies of [SpC*BCl].....	56
4.2.3	Synthesis of Phthalocyanines	57
4.2.4	Synthesis of Azaphthalocyanines	62
4.2.5	Photophysical Properties of Sub-/Azaphthalocyanines.....	82
4.2.6	Synthesis of Pyrazinonaphthalocyanines N _x -Npz*H ₂	92
4.2.7	Synthesis of Tetrabenzotriazaporphyrins (TBTAPs)	97
4.2.8	Meso Substituted Pyrazinoporphyrazines	101
4.2.9	Azanaphthalocyanine Complexes	104
4.2.10	Synthesis of New Alkyl Substituted Azanaphthalocyanines	106

4.3	Functionalised Phthalocyanines	122
4.3.1	General Introduction – Preliminary Work.....	122
4.3.2	Synthesis of Precursors	125
4.3.3	Synthesis of Unsubstituted Functionalised Phthalocyanines	127
4.3.4	Attempts to Form Ordered Mono-Layers.....	130
4.3.5	Attempts to Synthesise Soluble, Functionalised Phthalocyanines	131
4.3.6	Synthesis of Soluble, Functionalised Phthalocyanines	134
4.3.7	CV and UV-Vis Analysis of $[\text{Pc}^*\text{M}]^{\text{OH}}$ and $[\text{Ppz}^*\text{M}]^{\text{OH}}$	138
4.3.8	Application in DSSCs	141
4.3.9	Synthesis of Functionalised Subphthalocyanines	149
4.4	Metal Subphthalocyanine Complexes	154
4.4.1	Synthesis of Hydroxy Subphthalocyanine Precursor $[\text{SpCBOH}]$	154
4.4.2	Synthesis of Metal Subphthalocyanine Complexes	155
4.4.3	Synthesis of Hydroxy Subphthalocyanines $[\text{SpC}^*\text{BOH}]$	159
4.5	Rare Earth Metal Sandwich-Complexes	160
4.5.1	Introduction: Investigation of Rare Earth Metal Phthalocyanines	160
4.5.2	Synthesis of Non-Alkyl Substituted Rare Earth Metal Phthalocyanines	162
4.5.3	Preliminary Work: Synthesis of Half-Sandwich Complexes.....	163
4.5.4	Synthesis of Sandwich Complexes $[\text{Pc}^*_2\text{M}^{\text{RE}}]$	166
4.5.5	Synthesis of New Naphthalocyanine Sandwich Complexes.....	169
5	Zusammenfassung	173
6	Summary	183
7	Experimental Section	193
7.1	Methods	193
7.1.1	Solvents, Compounds and Starting Materials	193
7.1.2	Column Chromatography	193
7.1.3	MPLC: Sepacore System BÜCHI	194
7.1.4	Assembly of DSSCs	194
7.1.5	Autoclave Reactions.....	195
7.2	Analytical Methods	196
7.2.1	Elemental Analysis.....	196
7.2.2	NMR Spectroscopy	196
7.2.3	EPR Spectroscopy	197
7.2.4	IR Spectroscopy	197

7.2.5	UV-Vis Spectroscopy	197
7.2.6	Fluorescence Spectroscopy	198
7.2.7	Photophysical Measurements	198
7.2.8	Mass Spectrometry	199
7.2.9	Cyclic Voltammetry	200
7.3	Syntheses of Phthalonitrile Precursors	201
7.3.1	Synthesis of PDN*	201
7.3.2	Synthesis of PzDN*	204
7.3.3	Synthesis of PzDN ^o	205
7.4	Synthesis of Aza-/Naphthalonitriles	206
7.4.1	Synthesis of NDN and NDN*	206
7.4.2	Synthesis of NpzDN*	209
7.4.3	Synthesis of NqnDN*	212
7.4.4	Synthesis of NpyzDN*	220
7.5	Synthesis of Functionalised Precursors	221
7.5.1	Synthesis of PDN ^{OAcI}	221
7.5.2	Synthesis of PDN ^{O^{Ph}tBu}	221
7.5.3	Synthesis of PDN ^{Br}	221
7.5.4	Synthesis of PDN ^I	222
7.5.5	Synthesis of PDN ^{DI}	222
7.5.6	Synthesis of PzDN ^{Cl} and Precursors	222
7.6	Synthesis of QnDN ^{Tp} and PzDN ^{Tp}	223
7.6.1	Synthesis of QnDN ^{Tp} Precursor	223
7.6.2	Synthesis of QnDN ^{Tp}	223
7.6.3	Synthesis of PzDN ^{Tp}	224
7.7	Synthesis of Symmetrical Subphthalocyanines	225
7.7.1	Synthesis of [SpcBCI]	225
7.7.2	Synthesis of [SpcBF]	225
7.7.3	Synthesis of [SpcBOH]	226
7.7.4	Synthesis of [SpcB-Carbazole]	227
7.8	Synthesis of Substituted Subphthalocyanines	228
7.8.1	Synthesis of [Spc*BCI]	228
7.8.2	Synthesis of [Sppz*BCI]	229

7.8.3	Synthesis of [Sp ^{c*} BF]	229
7.8.4	Synthesis of [Sp ^{c*} BBr].....	230
7.8.5	Synthesis of [Sp ^{pz*} BF]	230
7.8.6	Synthesis of [Sp ^{pz*} BBr].....	231
7.8.7	Synthesis of [Sp ^{c*} BOH].....	232
7.8.8	Synthesis of [Sp ^{pz*} BOH].....	233
7.9	Synthesis of Azasubphthalocyanines	234
7.9.1	Synthesis of Azasubphthalocyanines N _x -[Sp ^{c*} BCl]	234
7.10	Synthesis of Symmetrical Phthalocyanines	235
7.10.1	Synthesis of Pc [*] H ₂	235
7.10.2	Synthesis of [Pc [*] Mg].....	235
7.10.3	Synthesis of [Pc [*] Pb]	236
7.10.4	Synthesis of Pc [*] H ₂ using [Pc [*] Pb].....	236
7.10.5	Synthesis of [Pc [*] Fe]	237
7.10.6	Synthesis of [Pc [*] Zn].....	237
7.10.7	Alternative Synthesis of [Pc [*] VO]	238
7.10.8	Synthesis of Ppz [*] H ₂	238
7.10.9	Isolation of Ppz [*] H ₂ ^{noctyl}	239
7.10.10	Synthesis of [Ppz [*] Zn].....	239
7.10.11	Attempt to Synthesise [Sp ^{pz°} BCl].....	240
7.10.12	Attempt to Synthesise Ppz [°] H ₂	240
7.10.13	Attempt to Synthesise [Ppz [°] Zn].....	241
7.11	Synthesis of Asymmetrical Phthalocyanines: N _x -Pc [*] H ₂	242
7.11.1	Synthesis of N _x -Pc [*] H ₂	242
7.11.2	Attempt to Synthesise ABAB N ₄ -Pc [*] H ₂ in a Ring-Expansion.....	245
7.11.3	Synthesis of ABAB N ₄ -Pc [*] H ₂	245
7.11.4	Synthesis of N _x -[Pc [*] Zn]	246
7.12	Synthesis of Asymmetrical Azanaphthalocyanines: N _x -Npz [*] H ₂	250
7.12.1	Synthesis of N _x -Npz [*] H ₂	250
7.12.2	Synthesis of N ₄ -Npz [*] H ₂	252
7.13	Synthesis of Naphthalocyanines.....	253
7.13.1	Synthesis of NcH ₂	253
7.13.2	Synthesis of Nc [*] H ₂	253
7.13.3	Attempt to Synthesise [NcV(NDip)Cl]	254

7.13.4	Synthesis of $[\text{Nc}^*\text{VO}]$	254
7.13.5	Synthesis of $[\text{Nc}^*\text{Zn}]$	255
7.13.6	Synthesis of $[\text{Nc}^*\text{TiCl}_2]$	256
7.13.7	Synthesis of $[\text{Nc}^*\text{SiCl}_2]$	256
7.13.8	Synthesis of $[\text{Nc}^*\text{CrCl}]$	257
7.13.9	Synthesis of $[\text{Snc}^*\text{BCl}]$	258
7.13.10	Attempt to Synthesise $[\text{Snpz}^*\text{BCl}]$	259
7.14	Synthesis of Azanaphthalocyanines	260
7.14.1	Synthesis of Npz^*H_2	260
7.14.2	Synthesis of $[\text{Npz}^*\text{Zn}]$	261
7.14.3	Synthesis of Nqn^*H_2	261
7.14.4	Synthesis of $[\text{Nqn}^*\text{Zn}]$	262
7.14.5	Attempt to Synthesise $[\text{Nppz}^*\text{M}]$	263
7.15	Azaphthalocyanine Complexes of Molybdenum and Tungsten.....	264
7.15.1	Synthesis of Precursors	264
7.15.2	Synthesis of $[\text{PcMo}(\text{N}t\text{Bu})\text{Cl}]$	264
7.15.3	Attempt to Synthesise $[\text{PcMoN}t\text{Bu}]$	264
7.15.4	Synthesis of $[\text{Pc}^{\text{F}}\text{Mo}(\text{N}t\text{Bu})\text{Cl}]$	265
7.15.5	Attempt to Synthesise $[\text{Ppz}^\circ\text{Mo}(\text{N}t\text{Bu})\text{Cl}]$	265
7.15.6	Attempt to Synthesise $[\text{Ppz}^\circ\text{Mo}(\text{NMes})\text{Cl}]$	265
7.15.7	Synthesis of $[\text{Pc}^{\text{OAc}}\text{Mo}(\text{N}t\text{Bu})\text{Cl}]$	265
7.15.8	Attempt to Synthesise $[\text{Pc}^*\text{Mo}(\text{Cp})\text{Cl}]$	266
7.15.9	Attempt to Synthesise $[\text{NcMo}(\text{N}t\text{Bu})\text{Cl}]$	266
7.15.10	Attempt to Synthesise $[\text{Pc}^*\text{Re}(\text{N}t\text{Bu})\text{Cl}]$	267
7.16	Azanaphthalocyanine Complexes of Molybdenum and Tungsten	
	$\text{N}_{x,y}[\text{Nc}^*\text{M}(\text{NR})\text{Cl}]$ with $\text{R} = t\text{Bu}, \text{Mes}$, and $\text{M} = \text{Mo}, \text{W}$	268
7.16.1	Synthesis of $[\text{NcW}(\text{N}t\text{Bu})\text{Cl}]$	268
7.16.2	Synthesis of $[\text{NcW}(\text{NMes})\text{Cl}]$	268
7.16.3	Synthesis of $\text{N}_{0,0}[\text{Nc}^*\text{Mo}(\text{N}t\text{Bu})\text{Cl}]$	269
7.16.4	Synthesis of $\text{N}_{0,0}[\text{Nc}^*\text{Mo}(\text{NMes})\text{Cl}]$	269
7.16.5	Synthesis of $\text{N}_{0,8}[\text{Nc}^*\text{Mo}(\text{N}t\text{Bu})\text{Cl}]$	270
7.16.6	Synthesis of $\text{N}_{0,8}[\text{Nc}^*\text{Mo}(\text{NMes})\text{Cl}]$	270
7.16.7	Synthesis of $\text{N}_{8,0}[\text{Nc}^*\text{Mo}(\text{N}t\text{Bu})\text{Cl}]$	271
7.16.8	Synthesis of $\text{N}_{8,8}[\text{Nc}^*\text{Mo}(\text{N}t\text{Bu})\text{Cl}]$	271

7.16.9	Attempt to Synthesise $N_{8,8}$ -[Nc*Mo(NMes)Cl].....	271
7.16.10	Attempt to Synthesise $N_{0,0}$ -[Nc*Mo(NTs)Cl]	272
7.16.11	Synthesis of $N_{0,0}$ -[Nc*W(NtBu)Cl]	272
7.16.12	Synthesis of $N_{0,0}$ -[Nc*W(NMes)Cl]	272
7.16.13	Synthesis of $N_{8,8}$ -[Nc*W(NtBu)Cl]	273
7.17	Functionalised Azasubphthalocyanines.....	274
7.17.1	Synthesis of N_x -[Spc*BCl] ^{Cl}	274
7.17.2	Synthesis of N_x -[Spc*BCl] ^I	275
7.17.3	Attempt of N_4 -[Spc*BCl] ^{vPA}	276
7.17.4	Synthesis of N_x -[Spc*BCl] ^F	276
7.17.5	Attempt to Synthesise F_x -[Spc*BCl] ^F	277
7.18	Synthesis of Non-Alkyl Substituted Phthalocyanines (of [PcM] ^{FG} -type)	278
7.18.1	Synthesis of [PcZn] ^{Br}	278
7.18.2	Synthesis of [PcZn] ^I	279
7.18.3	Synthesis of [PcZn] ^{vCA}	279
7.18.4	Synthesis of [PcZn] ^{PA}	280
7.18.5	Synthesis of [PcZn] ^{vPA}	282
7.18.6	Attempt to Synthesise PcH_2^{OAc} in a Cocyclisation.....	283
7.18.7	Synthesis of [PcZn] ^{OAc}	284
7.18.8	Synthesis of [PcZn] ^{O^{Ph}tBu}	284
7.18.9	Synthesis of [PcZn] ^{OH}	284
7.18.10	Attempt to Synthesise [PcZn] ^{OPA}	285
7.18.11	Attempt to Synthesise $PpzH_2^{OAc}$	285
7.19	Synthesis of Alkyl Substituted Functionalised Phthalocyanines.....	286
7.19.1	Attempts to Synthesise Soluble, Functionalised Phthalocyanines [PcM] ^{FG}	286
7.20	Synthesis of Alkyl Substituted Hydroxy Pc^*/Ppz^*	290
7.20.1	Attempt to Synthesise [Pc*Zn] ^{OH} in a Neat Reaction.....	290
7.20.2	Synthesis of $Pc^*H_2^{OAc}$	290
7.20.3	Synthesis of [Pc*Zn] ^{OAc}	291
7.20.4	Synthesis of $Pc^*H_2^{OH}$	292
7.20.5	Synthesis of [Pc*Zn] ^{OH}	293
7.20.6	Synthesis of $Ppz^*H_2^{OAc}$	294
7.20.7	Synthesis of [Ppz*Zn] ^{OAc}	294
7.20.8	Synthesis of [Ppz*Zn] ^{OH}	295

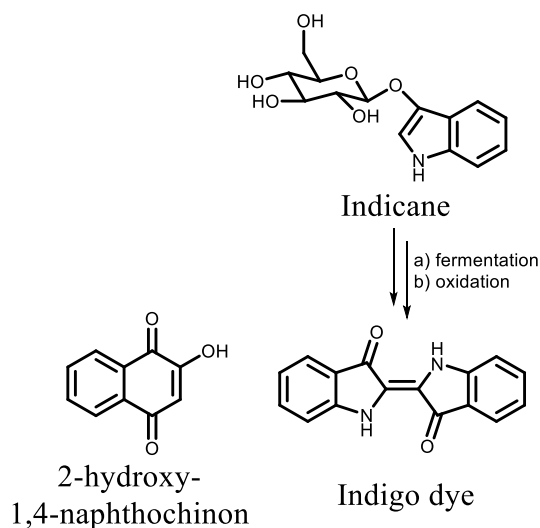
7.20.9	Attempt to Synthesise $\text{Ppz}^*\text{H}_2^{\text{OH}}$	296
7.20.10	Synthesis of $\text{Pc}^*\text{H}_2^{\text{OPA}}$	296
7.21	Synthesis of Lower Symmetric Naphthalocyanines	297
7.21.1	Attempt to Synthesise $\text{NcH}_2^{\text{OAcI}}$	297
7.21.2	Attempt to Synthesise $\text{Nc}^*\text{H}_2^{\text{OAcI}}$	297
7.21.3	Synthesis of <i>cis</i> -Bis(2,2'-bipyridine)diiodosilicium (IV) iodide	297
7.21.4	Synthesis of 4,5-Dihydroxyphthalonitrile	298
7.21.5	Attempt to Synthesise $[\text{NcSi}(\text{bipy})_2]$	298
7.21.6	Synthesis of $[\text{PcTi}(\text{Cat}^{\text{vinyl}}\text{CO}_2\text{H})]$	299
7.21.7	Synthesis of $[\text{PcTiPc}^*]$	299
7.21.8	Synthesis of New Catechol Substituted Titanylphthalocyanines	300
7.22	Synthesis of Tetrabenzotriazaporphyrins (TBTAP)	301
7.22.1	Synthesis of $[\text{TBTAP}^*\text{Mg}]$	301
7.22.2	Synthesis of TBTAP^*H_2	302
7.22.3	Attempt to Synthesise $[\text{TBTAP}^*\text{M}]^{\text{Ph}}$	303
7.22.4	Synthesis of $[\text{TBTAP}^*\text{M}]^{\text{PhOMe}}$ and Precursors	303
7.23	Synthesis of Precursors for a Selective Synthesis of TBTAP^*	306
7.23.1	Synthesis of 2,5-Dichloro-2,5-dimethylhexane	306
7.23.2	Synthesis of 6-Bromo-1,1,4,4-tetramethyltetralin	306
7.23.3	Synthesis of 6-Cyano-1,1,4,4-tetramethyltetralin	307
7.23.4	Synthesis of 5-Bromine-6-cyano-1,1,4,4-tetramethyltetralin	307
7.23.5	Synthesis of 3-Bromo-5,5,8,8-tetramethyl-5,6,7,8-tetrahydronaphthalene-2-carboximidamide	308
7.24	Synthesis of $[\text{Me}_2\text{M}(\mu\text{-OBSpc})]_2$ Complexes using $[\text{SpcBOH}]$	309
7.24.1	Synthesis of $[\text{Me}_2\text{Al}(\mu\text{-OBSpc})]_2$	309
7.24.2	Synthesis of $[\text{Me}_2\text{Ga}(\mu\text{-OBSpc})]_2$	309
7.24.3	Attempt to Synthesise $[\text{Me}_2\text{In}(\mu\text{-OBSpc})]_2$	310
7.24.4	Synthesis of $[(\text{SpcBO})_4\text{Ti}]$	310
7.24.5	Synthesis of $[\text{SpcBOZnhmids}]$	311
7.24.6	Synthesis of $[(\text{SpcBO})_3\text{B}]$	311
7.24.7	Attempts to Synthesise $[(\text{SpcBO})_3\text{M}^{\text{RE}}]$	312
7.25	Synthesis of Rare Earth Metal Phthalocyanines Sandwich-Complexes	313
7.25.1	General Procedure for Synthesis of $[\text{M}^{\text{RE}}(\text{hmids})_3]$	313
7.26	Synthesis of Known Phthalocyanine Precursors	314

7.26.1	Synthesis of [PcK ₂]	314
7.26.2	Synthesis of [Pc*Na ₂]	314
7.26.3	Synthesis of [Pc*K ₂]	314
7.27	Synthesis of Half-Sandwich-Complexes	315
7.27.1	Synthesis von [PcYOAc]	315
7.27.2	Synthesis of [PcYCp ^t Bu]	315
7.27.3	Synthesis of [PcYOAc]	316
7.28	Synthesis of New Soluble [Pc*M ^{RE} (R)]	317
7.28.1	Synthesis of [Pc*Sc(hmds)]	317
7.28.2	New Half Sandwich-Complexes of [Pc*M ^{RE} (OAc)]· <i>dbu</i> type	317
7.29	Synthesis of [Pc ₂ M ^{RE}]	320
7.29.1	Synthesis of [Pc ₂ Ce]	320
7.29.2	Synthesis of [Pc ₂ Sm]	320
7.29.3	Attempt to Synthesise [Pc ₂ Sm] in a Neat Reaction	321
7.29.4	Synthesis of [Pc ₂ Nd]	321
7.29.5	Synthesis of [Pc ₂ Eu]	321
7.29.6	Synthesis of [Pc ₂ Tb]	322
7.30	Synthesis of [Pc* ₂ M ^{RE}]	323
7.30.1	Synthesis of [Pc* ₂ Eu]	323
7.30.2	Synthesis of [Pc* ₂ Tb]	324
7.30.3	Synthesis of [Pc* ₂ Nd]	324
7.30.4	Attempt to Synthesise [Pc* ₂ Sm] ⁻ [CoCp ₂] ⁺	325
7.30.5	Attempt to Synthesise [Pc* ₂ Lu] ⁻ [TBA] ⁺	325
7.30.6	Attempt to Synthesise [Ppz* ₂ Nd]	325
7.30.7	Attempt to Synthesise [Ppz* ₂ Gd]	325
7.30.8	Attempt to Synthesise [Ppz* ₂ Gd]	326
7.30.9	Attempt to Synthesise [Ppz* ₂ Sm]	326
7.31	Attempted Synthesis of Heteroleptic Sandwiches [Pc*YPc], [Ppz*YPc]	327
7.31.1	Attempts for Heteroleptic Sandwiches using Pc*, Ppz* and Cp* as ligand	327
7.32	Synthesis of [Nc* ₂ M ^{RE}]	329
7.32.1	Attempt to Synthesise [Nc* ₂ La]	329
7.32.2	Synthesis of [Nc* ₂ Ce]	329
7.32.3	Synthesis of [Nc* ₂ Pr]	330
7.32.4	Synthesis of [Nc* ₂ Nd]	330

7.32.5	Synthesis of [Nc* ₂ Eu].....	330
7.32.6	Synthesis of [Nc* ₂ Tb].....	331
7.32.7	Synthesis of [Nc* ₂ Dy]	331
8	References	332
9	Crystal Structures	351
9.1.1	Crystal Structure of [Spc*BF]	352
9.1.2	Crystal Structure of [Spc*BCl]	353
9.1.3	Crystal Structure of N ₂ -Pc*H ₂	354
9.1.4	Crystal Structure of [Spc*BCl] ^{Cl}	355
9.1.5	Crystal Structure of A ₂ B ₂ N ₄ -[Pc*Zn·H ₂ O]	356
10	Supplement.....	357
10.1	Cyclovoltammetric Measurements of N _x -Pc*H ₂	357
10.2	Cyclovoltammetric Measurements of N _x -Nc*H ₂	358
10.3	UV-Vis, FS and Emission spectra of N _x -[Pc*M] and N _x -[Spc*BCl].....	359
10.4	Photophysical Measurements	360
10.5	Theoretical Calculations	361

1 Introduction

Dyes have fascinated and influenced human life and culture for centuries, probably since it exists. Natural dyes are quite impressive substances, in which a conjugated π -system causes an absorption in the visible spectrum. Most natural dyes are, in comparison to unnatural dyes or e. g. organic pigments, quite small molecules, but structural motifs are similar. A famous example for a natural dye is Indigo, first synthesised by the German chemist ADOLF VON BAEYER,^[1] or 2-hydroxy-1,4-naphthochinon, also known as *Lawson*, adapted from the henna plant "*Lawsonia inermis*",^[2] which is named after the scot ISAAC LAWSON. In the Middle East and parts of Africa, both dyes were traditionally mixed to obtain a black dyes colouring. Henna found application as a cosmetic,^[3] in medicine, as well as a continuing use in ceremonies.^[4] Indigo in comparison is mainly known for its purple colour. From the plant, only a



Scheme 1: Examples of famous natural dyes.

precursor", Indigane, can be isolated. After a fermentation process, cloth or any fabrics can be dyed with the indoxyl. After oxidation in air, Indigo is formed and the blue/purple colour becomes visible. But VON BAEYER did not only succeed in developing the synthesis of the Indigo dye (Scheme 1); besides the structure of Indigo and its precursors, VON BAEYER and his assistants could clarify the structure of Phenolphthalein and Fluorescein and were able to obtain Alizarin from an Anthrachinone precursors (Figure 1).^[5]

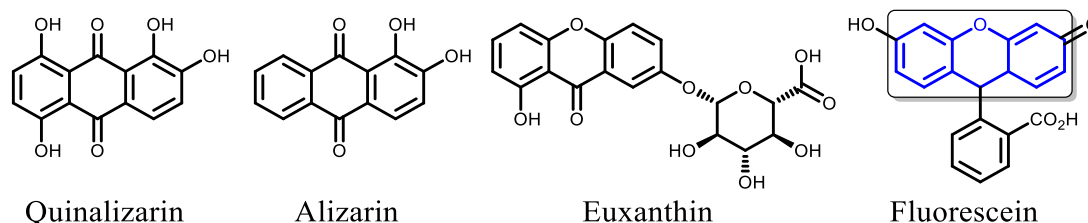


Figure 1: Examples of famous dyes, bearing a similar basic scaffold. Alizarin and Fluorescein were investigated by ADOLF VON BAEYER.

The basic scaffold of the Fluorescein dye is xanthene (tagged, in blue). This structural motif can be found in other dyes, such as Rhodamine B, or *Scheckfarbstoff AS*. Euxanthin (*Indian yellow*), was originally isolated from the urine of cows in India.^[6] Therefore, the cows were feed with leaves of the mango tree and received less water for drinking.^[7] Because of the



Figure 2: JOHANNES VERMEERS "Woman Holding a Balance", 1662-1663.^[9]

nutrient deficiency, the urine had a dark yellow colour. After evaporating the water, the dye could be obtained in the form of a dark yellow powder, and, pressed in the form of a sphere, it came to Europe with the name "*Piuri*". This way, about 50 g *Piuri*/cow per day were obtained.^[8]

The dye was used in Europe mainly for oil paintings.^[7] An examples, in which *Piuri* was found is shown on the left, in VERMEERS "*Woman Holding a Balance*" (Figure 2),^[9] or in VAN GOGHS "*The Starry Night*".^[10] On one hand, nowadays, some of the before mentioned dyes find application as *lacquers*. The word *lacquer*

is in industry mainly used for the salts of dyes. These salts of dyes are quite insoluble in common organic solvents in comparison to natural dyes, so called pigments. On the other hand, some of the classical dyes of industrial production, such as Indigo or Alizarin, are replaced by others. In the beginning of the 20th century, Euxanthin for example was prohibited because the process was declared as inhuman.^[8]

In the 19th century, these dyes used in oil paintings, such as *Piuri*, were mainly identified by using UV-Vis spectroscopy. The dye shows a strong fluorescence emission when it is excited at 365 nm. Another method to differentiate it from other dyes such as Quinalizarin is IR spectroscopy. Today, the origin of oil paintings is determined with more modern methods such as X-ray fluorescence analysis (RFA). One co-founder of the X-ray investigation on paintings was KURT WEHLTE.^[11] The analysis of dyes by UV-Vis and IR spectroscopy became routine analysis for chemists. X-ray analytical methods are also common methods for investigation of surfaces in physics and chemistry. Total reflection X-ray fluorescence (TRFA), micro X-ray fluorescence (μ -RFA) and X-ray absorption spectroscopy (XAS) methods are used. In XAS methods, the fine structure of surfaces can be investigated. Two known methods are the extended X-ray absorption fine structure spectroscopy (EXAFS) and the near-edge X-ray absorption spectroscopy (NEXAFS). With this method, the orientation of molecules on surfaces as well as their chemical composition can be analysed.

2 Theoretical Section

2.1 Structure and Properties of Phthalocyanines

2.1.1 Discovery of the Blue Dye

Phthalocyanines (Pcs) (the name is derived from phthalic acid and the Greek word: cyanos, κυανός; blue),^[12,13] or *29H,31H*-tetrabenzob[*b,g,l,q*][5,10,15,20]tetraazaporphyrins,^[14] are 42 π -electron HÜCKEL-aromatic (planar, $4n+2$) heterocycles. In 1907, the first phthalocyanine was observed as a by-product by BRAUN and TCHERNIAC, in the form of a blue powder in the filter paper, when they melted *o*-cyanobenzimide.^[15] In 1928, the Scottish company *Scottish Dyes* observed a blue-greenish powder within the reaction of phthalic acid anhydride with ammonia and enamel. An [PcFe] was formed. In following work, the structure of phthalocyanines was determined by LINSTEAD and ROBERTSON.^[12] This led to the start of the industrial production of phthalocyanines, already in 1935; since then the worldwide production of [PcCu] increased to an amount of 80,000 t per year.^[12]

The Pc is structurally related to the porphyrin (Por), which is the basic scaffold of haemoglobin and chlorophyll. The structural relationship is obvious when looking at the structural formula (Figure 3). In comparison, the Pc has four [-N=] units substituting the [-CH=] units in the meso position, and it is annulated with four benzene units. The annulation leads to an increased structural variability, offering eight additional positions.

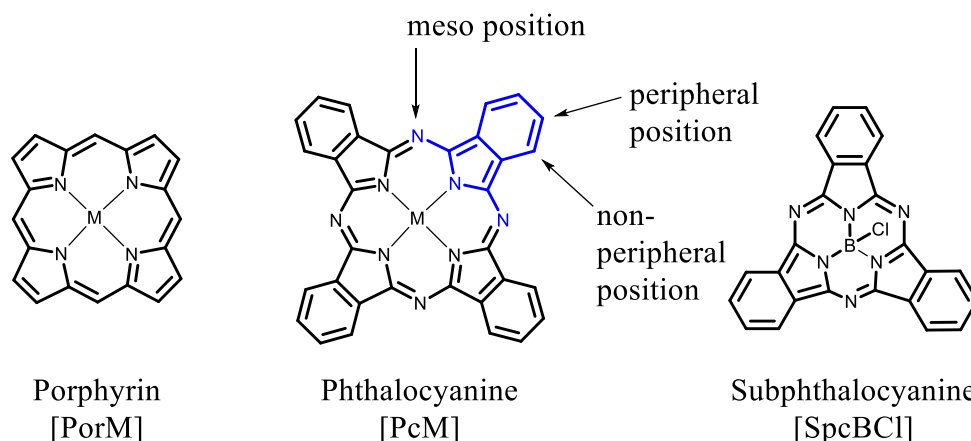


Figure 3: Structure of a porphyrin, a phthalocyanine and a subphthalocyanine in comparison.

This unit of a Pc is called isoindoline, as shown in Figure 3 in blue. A Pc contains four phthalonitrile (PDN) units, the ring contracted subphthalocyanine (SpcBCl) consist of only three PDN units, caused by the smaller radius of the templating boron atom B^{3+} of 23 pm. In

Theoretical Section

contrast, a larger U^{4+} ions leads to the so-called superphthalocyanine (Superpc) consisting of five PDN units. The phthalocyanine ligand itself is a dianionic ligand. Besides the protonated form, coordination to over 66 central atoms is known:^[12] see Table 1.^[16,17]

Table 1: Part of a periodic table, showing literature described complexes of [PorM] and [PcM].

Li												B	C		
Na	Mg											Al	Si	P	
K	Ca	Sc	Ti	V	Cr	Mn	Fe	Co	Ni	Cu	Zn	In	Ge	As	
Rb	Sr	Y	Zr	Nb	Mo	Tc	Ru	Rh	Pd	Ag	Cd	Ga	Sn	Sb	
Cs	Ba	La	Hf	Ta	W	Re	Os	Ir	Pt	Au	Hg	Tl	Pb	Bi	
		An													

Nowadays, the most common way to synthesise Pcs is a cyclotetramerisation reaction. The mechanism was i. a. investigated by CHRISITE and DEANS.^[18] Here, phthalonitriles or isoindoline precursors are used. The synthesis is possible in a neat reaction, using only the PDN and a metal acetate, an ammonia source, such as urea or ammonium heptamolybdate, and high temperatures of 300 °C. For the synthesis of free Pc ligands PcH_2 , long-chain alcohols in presence of a strong bases such as DBU or DBN are commonly used for the initiation of the cyclisation and redox reaction. The synthesis of Pc is also possible using the typical precursors of PDN, namely phthalic acid, its anhydride, imide, or amide. In this instance, PDN or isoindoline derivatives are formed *in situ*.^[19]

2.1.2 Properties of Phthalocyanines

Pcs are thermally and chemically very stable compounds. The purification can be done by recrystallization in conc. sulfuric acid,^[20] or by sublimation of e. g. [PcCu] at >500 °C.^[21] In addition to the thermal and chemical stability of Pcs, as dyes, their optical properties of course are important. In a UV-Vis spectrum of a Pc, at first the strong absorption maximum in the visible light region attracts attention. This absorption band is called the Q-band. The Q-band is a π - π^* transition from the HOMO to the LUMO (Figure 4). Another characteristic, weaker absorption is found in the higher energetic area, the B- or SORET-band. The Q-band is characteristically located at 660-690 nm, and the B-band at ~350 nm. The main disadvantage of Pcs is also caused by the large π -system, which not only gives the dye its intense colour, but results in a strong π -stacking as well. Nonetheless, the extinction coefficient of

$3 \cdot 10^5 \text{ L mol}^{-1} \text{ cm}^{-1}$ is very high and explains the intense colour.^[12] Aggregation is typical for metal containing Pcs. Unsubstituted Pcs are almost insoluble in common organic solvents. However, by introducing sterically demanding groups in one of the peripheral or non-peripheral positions, or even in the axial position, the aggregation decreases while solubility increases. By substitution of the Pc, the Q-band can be bathochromically shifted by introducing auxochromes (such as $-\text{OH}$, $-\text{NH}_2$), and hypsochromically by introducing anti-auxochromes (such as $-\text{NO}_2$), respectively.^[22] Substitution in the peripheral position has a weaker influence on the

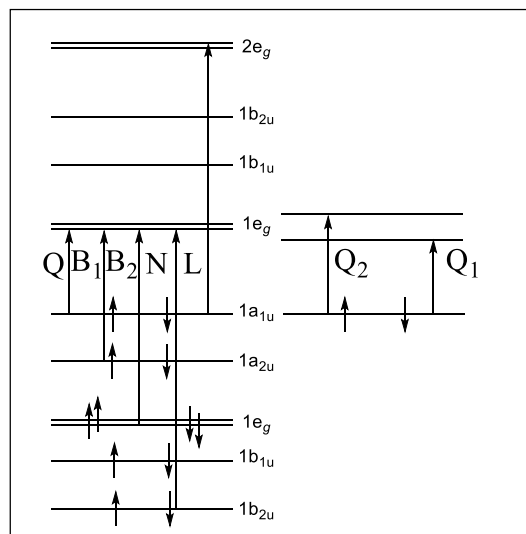


Figure 4: Molecular orbitals of a D_{4h} symmetrical phthalocyanine. Adapted from literature.^[25]

π -system (and therefore on the position of the Q-band) compared to substitution in the meso position and the non-peripheral position.^[23] In Figure 5, a peripherally alkyl substituted phthalocyanine is shown, bearing an annulated 2,2,5,5-tetramethylcyclohexane system in the peripheral position. This causes a red shift of the Q-band to 711 nm.^[24,25] In case of this C_{2v} -symmetrical molecule, the degeneracy of the $1e_g$ orbitals is lifted.^[26] This is in contrary to the [PcM] shown on the left, where only one sharp peak is visible. In UV-Vis spectroscopy of Pcs, the chosen solvent is also important. The spectra shown below were measured in DCM.

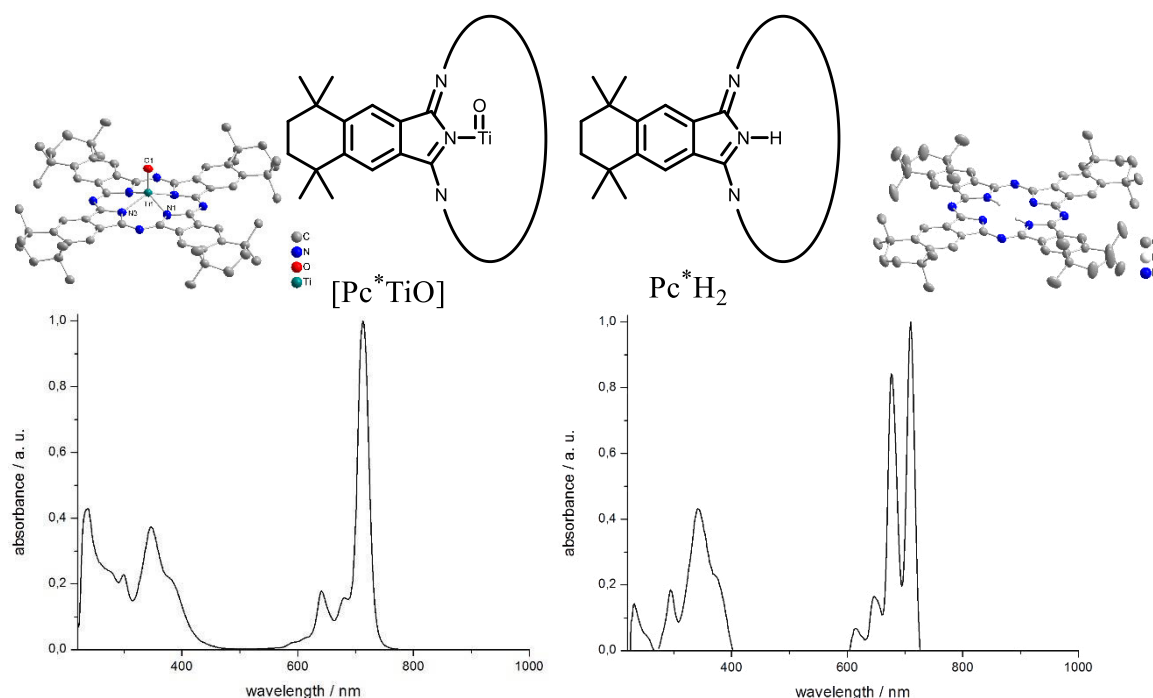


Figure 5: An example for an UV-Vis absorption spectrum of a D_{4h}/C_{4v} - and a D_{2h} - symmetrical molecule. On the left side: $[\text{Pc}^*\text{TiO}]$, on the right side: Pc^*H_2 .^[25]

Theoretical Section

Another polar solvent such as pyridine or other bases would interact with the protons of the inner ring of a PcH₂, raise the symmetry so that the orbitals are once again degenerate, and one Q-band peak is visible.^[27] In addition, different substitution patterns are reported in literature, using besides alkyl groups, alkoxy groups or imides. Here, a non-linear trend of the shift of the Q-band could be observed with the number and the position of the moiety.^[28] The annulation (with four additional benzene units) of a Pc leads to the so called naphthalocyanines (Nc). The unsubstituted [NcM]s are bathochromically shifted to ~760 nm in comparison to the Pcs.

In addition to the UV-Vis absorption, Pcs are often discussed with regard to their fluorescence behaviour. A high fluorescence quantum yield, Φ_F , is needed, if the substances are to be used in OLEDs;^[29] however, Pcs are, due to their small STOKES shift, not promising OLED candidates. The fluorescence of Pcs is more in focus in discussions of their application in photodynamic therapy (PDT). Here, emission is avoided as much as possible, because it is inversely correlated to the production of singlet oxygen (Figure 6). A dependence of singlet-oxygen quantum yields (Φ_Δ) and fluorescence quantum yields (Φ_F) on the size of the Pc and its symmetry was proved for [PcZn] and derivatives. When the size is increased, or the symmetry lowered, the Φ_F decreases.^[30] This appears to be inverse for Φ_Δ . The correlation between Φ_F and Φ_Δ can be rationalised with the help of a JABLONSKI diagram, as shown in Figure 6.^[31,32] It summarizes the electron transfer processes and possible photoreactions of dyes.

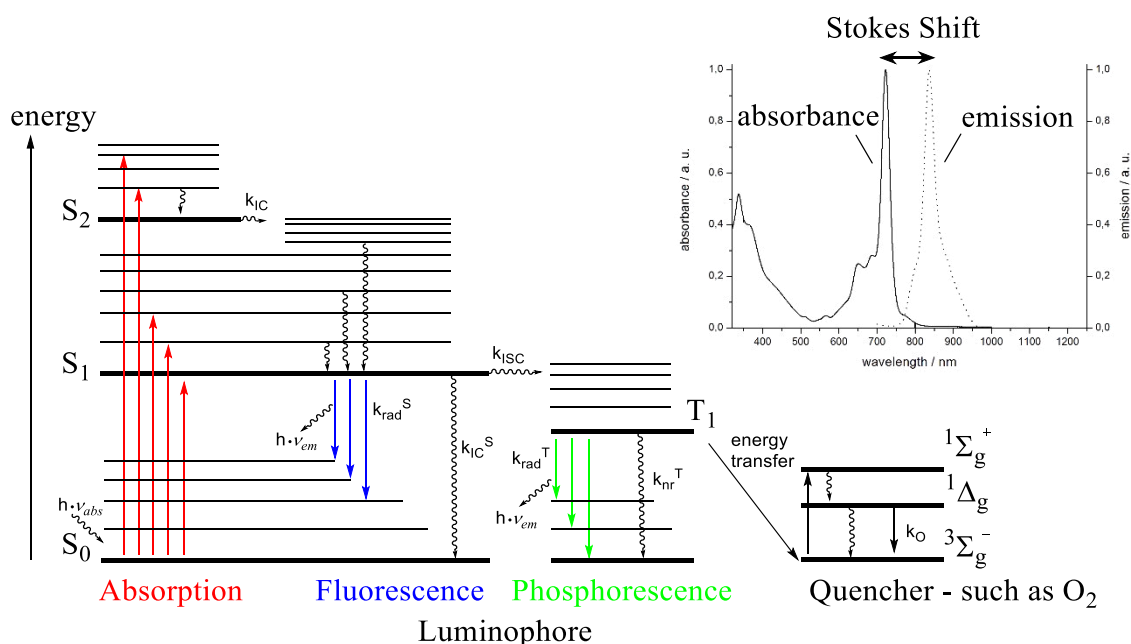


Figure 6: JABLONSKI diagram for illustration of electron processes within a molecule. Adapted from literature.^[32]

When electromagnetic radiation is absorbed by a photosensitizer, an electron can get excited into excited states S_1 , S_2 and their vibrational levels. After excitation, different processes can take place:

- IC (Internal conversion) occurs: transition of the electron from a higher into a lower state, without emission of a photon. "Vibrational deactivation" – translational, vibrational, rotational states.
- ISC (Inter system crossing): the electron is transferred to another MO with a simultaneous spin inversion, thus changing the multiplicity from a singlet to a triplet state.
- Charge transfer to a semiconductor
- The energy can be transferred to a "quencher" such as $^3O_2 \rightarrow ^1O_2$.

This is given by the significant value of singlet oxygen quantum yield (Φ_Δ)

The electron can also "drop down" in the form of light emitting relaxation from the excited state, S_1 , into the ground state, what is called fluorescence (FS). After ISC, the relaxation process from a T_1 state is called phosphorescence; phosphorescence processes have a longer lifetime, due to IC and the spin-forbidden $T_1 \rightarrow S_0$ transition. The emitted light is of a lower energy, and therefore at a longer wavelength, compared to FS.

2.1.3 Synthetic Strategy for the Synthesis of Phthalocyanines, Pyrazinoporphyrazines and Lower Symmetrical Azaphthalocyanines

In this work, "symmetrical Pcs" name Pcs with a D_{4h} -symmetry, as well as the protonated forms of A_4 -type, [PcM], or B_4 -type, [PpzM]. Consequently, lower symmetry Pcs (sometimes found as asymmetrical Pcs) describe mixed Pcs, or so-called azaphthalocyanines, N_x -[PcM] (Figure 7). The access to these lower symmetrical N_x -[PcM] is possible by different reported methods, described below.^[33]

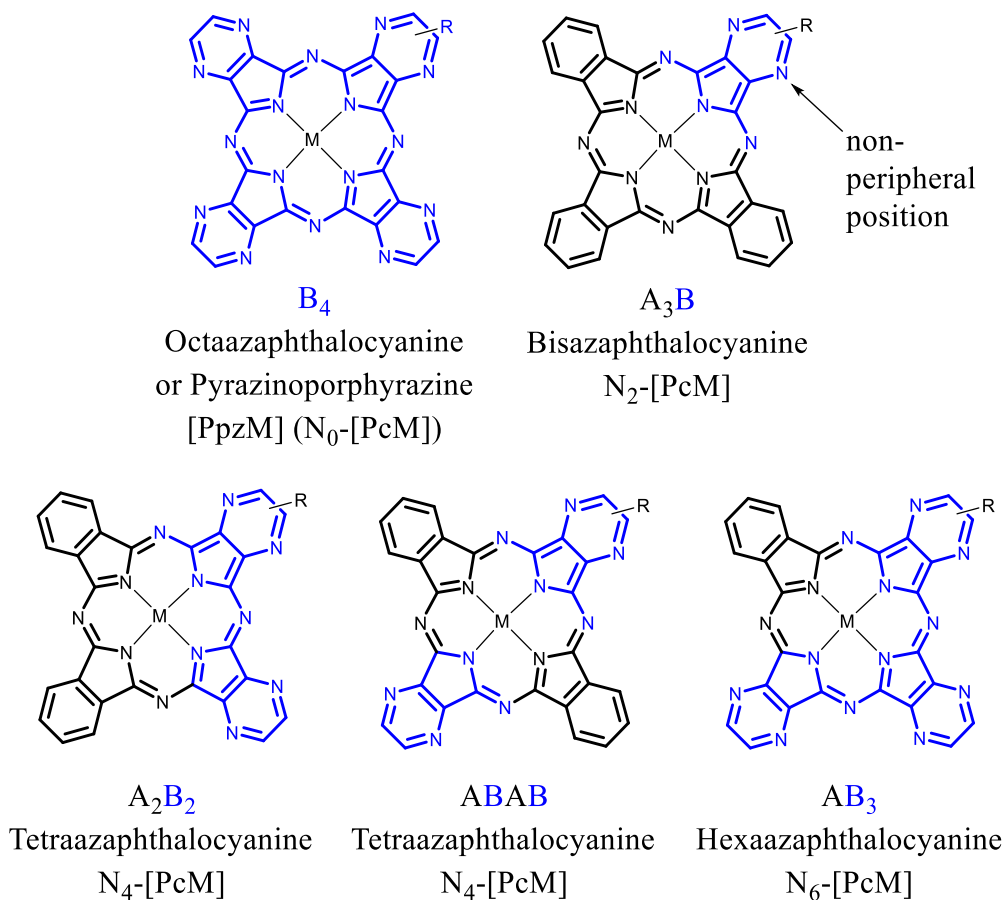
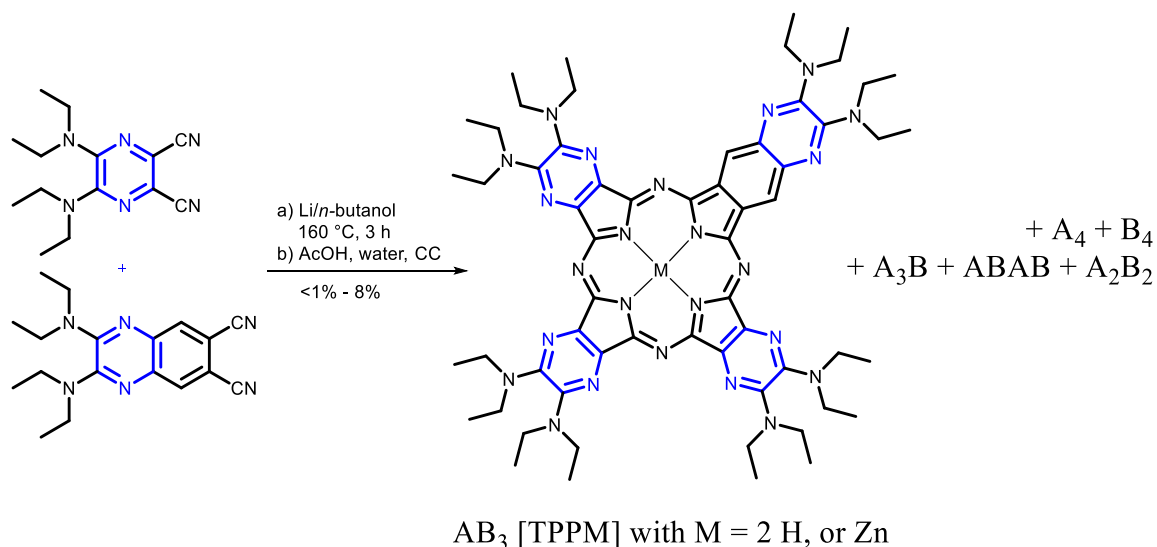


Figure 7: Schematic structures of a pyrazinoporphyrazine (PpzM) and azaphthalocyanines (N_x -[PcM]).

Cocyclisation. The oldest reported, and most obvious, synthesis uses the same conditions as known from homocyclisation, except that two dinitriles are used in various ratios instead of just one dinitrile.^[34] Depending on the reactivity, the cocyclisation follows a statistic distribution of the used ratio of both PDN. The main problem with this synthesis is the separation of the resulting products, which is usually done by column chromatography (CC), and the limited yields caused by the statistic product distribution. As a result of π -stacking, the chromatographic separation is, in most cases, very challenging, if at all possible. One example was carried out by MUSIL, who inserted stepwise phenyl-units into a pyrazinoporphyrazine, [TPPM] (Scheme 2).^[35] The synthesis was carried out in a cyclotetramerisation reaction using

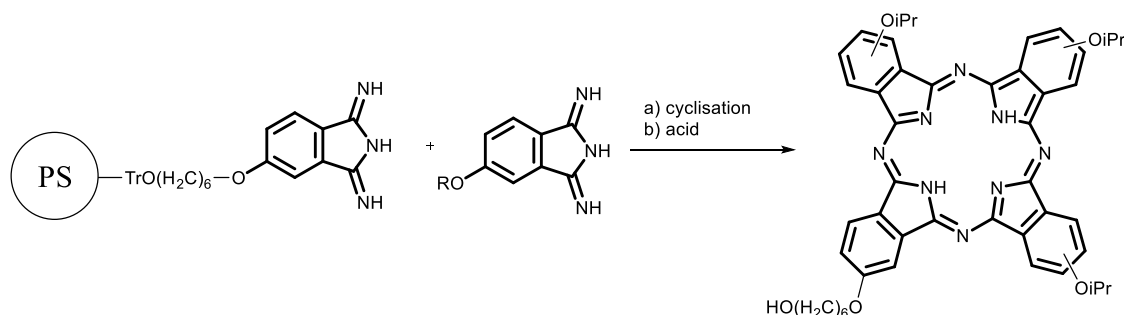
both dinitriles in a ratio of 1:1. As result of π -system enlargement, a stepwise linear increase of the Q-band by 22 nm per inserted arene unit was observed.



Scheme 2: Synthesis of lower symmetrical azaphthalocyanines [TPPM].^[35]

Alternatively, the cocyclisation can be sterically driven, as for when one dinitrile has bulky rigid groups, favouring one product.^[36] Besides the more selective synthesis, the highest reported yield of one isomer is about 36%,^[37] but in most cases only <math><1\% - 5\%</math> of each compound is obtained.

Polymer Support. Another method that at first view appears much easier is the synthesis of A₃B phthalocyanines using a polymer support (Scheme 3). The synthesis was developed by LEZNOFF.^[38,39] In this synthesis, one 1,3-diminoisodindole bears a functional group and is coupled to a polymer support. Then, the other soluble 1,3-diminoisodindole is added, and a cyclisation is carried out. After completed cyclisation, the excess of the second 1,3-diminoisodindole is washed off, and the phthalocyanine is removed from the support by acids.

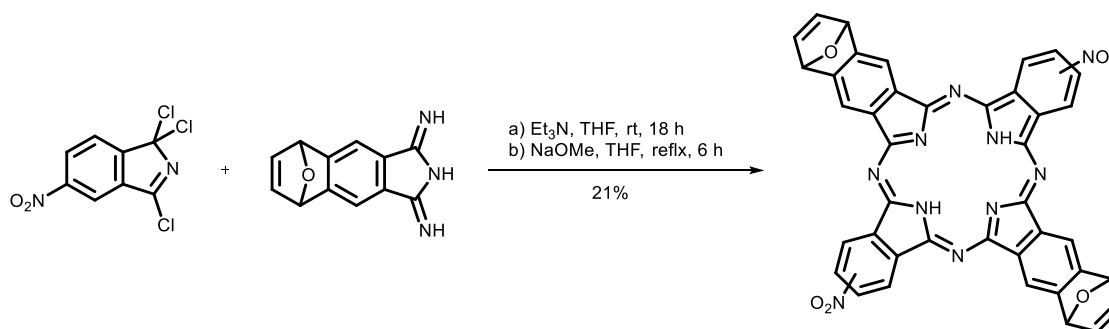


Scheme 3: Example of a synthesis of an A₃B phthalocyanine using a polymer support.
(Tr = trityl, polymer-bound trityl ether)

Theoretical Section

The main advantage is that no CC has to be carried out. The polymer support method was further developed by WÖHRLE, who tried to use functionalised silica gel supports.^[40] While the synthesis and the workup is easy, the polymer based synthesis is limited due to a reported maximum yield of 20%. Further limitations are commercially available polymer supports, functional linker groups, which have to be bound on the support and easily removed, as well as the stability of the second PDN.

Crossed Condensation. Another interesting method to obtain lower symmetry Pcs is the crossed condensation. It is used for the selective synthesis of ABAB non-uniformly substituted phthalocyanines.^[41,42] It is mainly based on a strong, selective reactivity of the two different building blocks (Scheme 4).



Scheme 4: Selective synthesis of a lower symmetrical ABAB Pc.

The reported reaction conditions appear to be quite mild in comparison to the, in general, harsh conditions in the regular synthesis of Pcs. This is caused by the labile character of the 1,3,3-trichloroisindoline, which is also reflected in the poor yields of 21% of the resulting ABAB Pc. Other crossed condensations also use the reactivity and rigidity of dinitriles. LEZNOFF synthesised cofacial dimeric Pcs, whereby one PDN is a bridged dinitrile B-B, linked over an alkyl/ alkenyl group (Figure 8). When using a 1,3-diiminoisindoline, "A", in excess, of course the A₄ isomer is formed, but an A₃B-BA₃ linked Pc is obtained in reasonable yields of 7%.^[43]

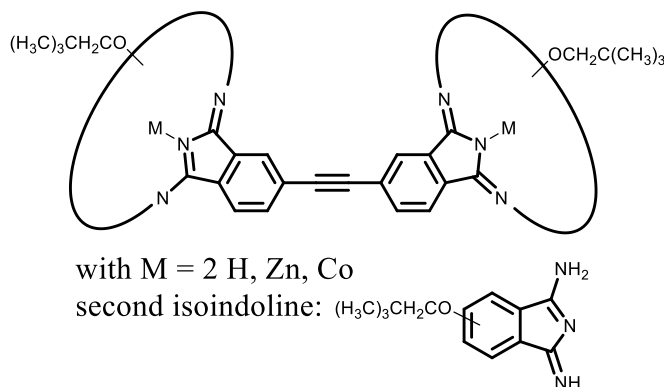
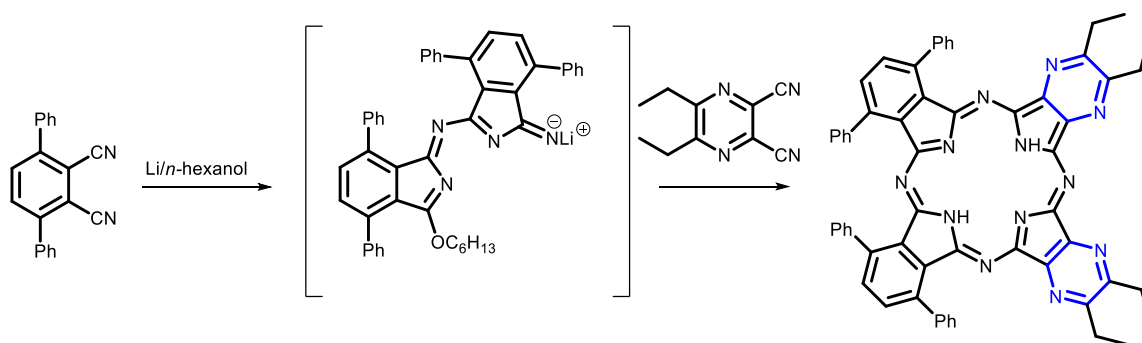


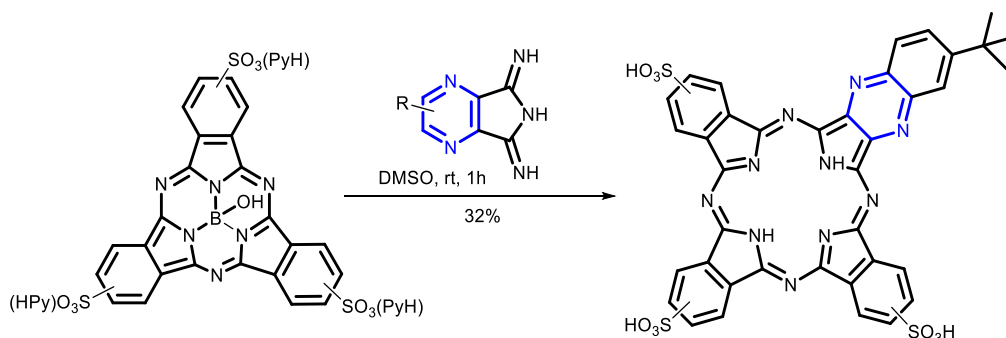
Figure 8: Co-facial dimeric Pc synthesised by LEZNOFF.^[43]

KOBAYASHI reported on the favoured synthesis of A_2B_2 Pcs. In this synthesis, one dinitrile A reacts to an A_2 dimer in a "precyclisation" under mild reaction conditions. After addition of a second PDN, A_2B_2 Pcs can be obtained in comparably good yields of 20%.^[44] In this reaction, the steric demand of the phenyl-substituted PDN used in the "precyclisation" is very high. The electronic properties of PDN differs from PyzDN, caused by the electron withdrawing character of the nitrogens, which makes the latter more reactive towards nucleophilic attack.



Scheme 5: Synthesis of an A_2B_2 Pc using a preformed half-Pc as precursor, by KOBAYASHI.^[44]

Subphthalocyanine Ring Expansion. The last method that will be discussed in this work is the ring expansion of a subphthalocyanine using e. g. a 1,3-diiminoisoindoline. The Spc ring expansion is also named KOBAYASHI ring expansion.^[45] In the shown example (Scheme 6), the photodynamic activity of novel trisulfonated A_3B zinc azaphthalocyanines is discussed.^[46]



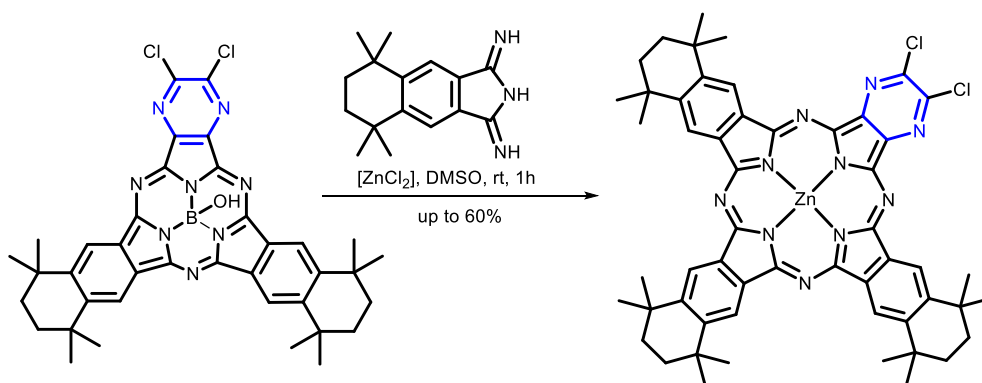
Scheme 6: Synthesis of an asymmetrical, sulfonated A_3B azaphthalocyanine for the investigation of photodynamic activities of azaphthalocyanines.

The selectivity of the ring expansion is controversially discussed in literature. Yields of 90% were reported for the A_3B phthalocyanine,^[45] but also mixtures of all possible cocyclised products have been observed.^[47] In the second case, probably a degradation of the subphthalocyanine occurs, and the so formed PDN/isoindoline species cocyclises. Besides the fact that the synthesis to the A_3B Pc can be very selective, the synthesis of the Spc is often combined with poor yields and purification by CC is necessary. In the example shown above

Theoretical Section

(Scheme 6), a selective conversion of A₃B Pc was found, which is quite appealing.^[46] However, the synthesis of the subphthalocyanine using a sulfonic acid substituted PDN precursor was possible in 60% yields. In such cases, this method is then of comparable efficiency to the cocyclisation method.

In our group, a KOBAYASHI ring expansion was previously used for the expansion of a hybrid azasubphthalocyanine A₂B N₂-[Spc*BCl]^{Cl}.^[13] These azasubphthalocyanines were obtained in a cyclotrimerisation reaction of two dinitriles with up to 24% yield. It was observed, that a cyclotrimerisation of a PDN and a PzDN leads to higher yields and simplifies the chromatographic separation of the resulting isomeric mixture in comparison to the reaction of a pure PDN or two different PDN units. By insertion of an electron rich isoindoline into an electron poor A₂B N₂-[Spc*BCl] the corresponding A₃B N₂-[Pc*M]^{Cl} was obtained in 60% yield (Scheme 7).



Scheme 7: Synthesis of an A₃B azaphthalocyanine N₂-[Pc*M]^{Cl}.

In summary, the synthesis of azaphthalocyanines is possible using different routes. Most methods, such as crossed condensation and polymer support based synthesis, are limited due to the labile character of the precursors or due to the requirements described above. In several cases, the ring expansion may lead quite selectively to an A₃B product. A systematic study of all compounds appears to be only possible using the cocyclisation method, when all products are obtained. However, a ring expansion seems to be a good compromise, when A₃B Pcs bearing an anchor group are target compounds.

A Systematic Study of azaphthalocyanines is not often found in literature, because of the poor yields and difficulties in purification by using CC, and in general nitrile units with very different physical properties, e. g. solubility, are used for a simplified separation. Nevertheless, some known series are shown in Figure 9.^[48]

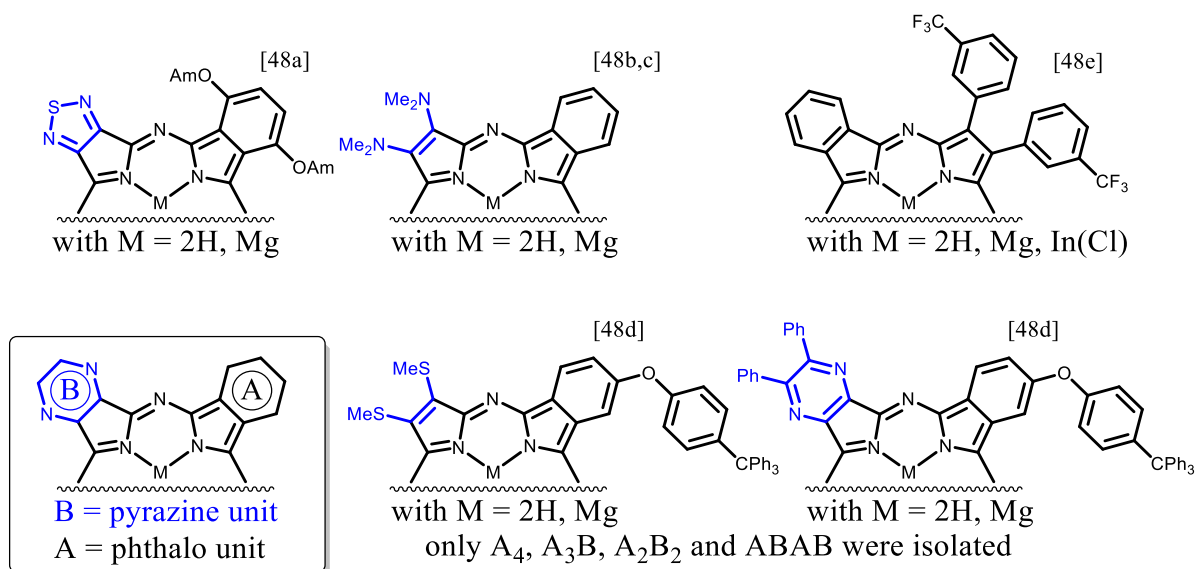


Figure 9: Some selected literature described aza-Pc series.

A change of spectroelectronic properties of azaphthalocyanine series is controversially discussed. But in all examples, an exchange of [-CR=] building blocks by [-NR=] in the non-peripheral or meso-position shifts the Q-band hypsochromically due to the electron withdrawing character of the inserted nitrogen atoms.

KOBAYASHI reported on a linear dependence of the Q-band shift, when a systematic substitution of [-CH=] by [=CPh] units in the peripheral positions (α -phenylation) of a Pc was done.^[30,49] With increasing α -phenylated [PcZn] the HOMO increases, while the LUMO was found to be relatively stable. The results observed in cyclovoltammetric measurements mirror the shift of the Q-band in UV-Vis spectroscopy.^[49] The main problem found in this study is the break of the linear dependence when a distortion of the molecule is observed. The Pc gets distorted when two phenyl-groups are located on neighbouring isoindoline units.

A linear dependence of a Q-band shift was also found by MUSIL, systematically inserting a benzene unit into a porphyrin derivative (Scheme 2).^[35] By annulation of a Pc, Ppz or a Pz, the Q-band is red shifted. In all cases reported here, a split of the Q-band was found when the symmetry of the compounds is lowered. The ABAB compounds, especially ABAB azaphthalocyanines, were described as most attractive for photodynamic therapy (PDT), and are discussed in more detail in section 2.2.1.^[30]

2.1.4 Rare Earth Metal Complexes

Rare earth metal phthalocyanines were described in literature, for the first time about 40 years ago. But still they are in focus in current research, as a first example of a mixed sandwich complex of PLATEL demonstrated, in 2015 (Figure 10).^[50] Here, the, in general, quite insoluble Pc ligand was converted

"via detour" over an intermediate

[PcScCl·LiCl]·thf

complex, which appears to be very soluble in THF, that finally leads to the desired products

[PcScCp*] and

[PcScCp].^[50] With this, not only the first Sc complex was crystallised, but a new class of metallophthalocyanine-ocenes was synthesised. Other rare earth metal phthalocyanines were mainly investigated with regards to their physical properties to apply them as single-molecule magnets (SMM). SMMs have the ability to be a magnet themselves after magnetisation, when the external magnetic field is turned off. The first and most prominent SMM is a manganese complex: $[\text{Mn}_{12}(\text{OAc})_{16}\text{O}_{12}(\text{H}_2\text{O})_4] \cdot 2\text{AcOH} \cdot 4\text{H}_2\text{O}$. Owing to the magnetic coupling, this complex possesses a total spin of $S = 4 (4 \text{ Mn}^{4+}, S = 3/2) \cdot 3/2 - 8 (8 \text{ Mn}^{3+}, S = 2) \cdot 2 = 10$.^[51-53] Different classes of SMMs are described in reviews.^[54,55] In the present work, the focus is on rare earth metal phthalocyanine complexes discussed in more detail in section 2.2.3.

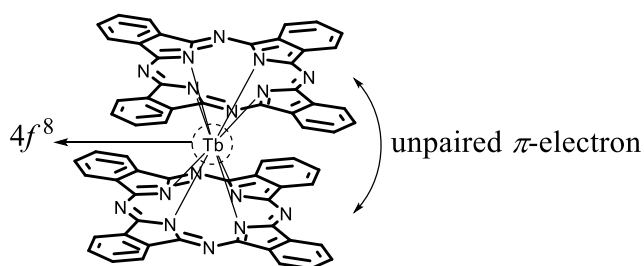


Figure 11: Example of a rare earth metal phthalocyanine complex $[\text{Pc}_2\text{M}^{\text{RE}}]$.

In comparison to the shown Sc complex (Figure 10), rare earth metals, M^{RE} , have the ability to form sandwich complexes with phthalocyanines.^[56,57] One advantage of these complexes is their stability, while all described organometallic SMMs are sensitive to oxygen and moisture.^[54] A

[Pc₂Tb] for example is stable enough to be sublimed in vacuum (Figure 11). A more detailed discussion of the properties of these sandwich-complexes with regard to their application as SMMs is presented in section 2.2.3 and the synthesis and the nature of this complex is discussed in section 4.5.

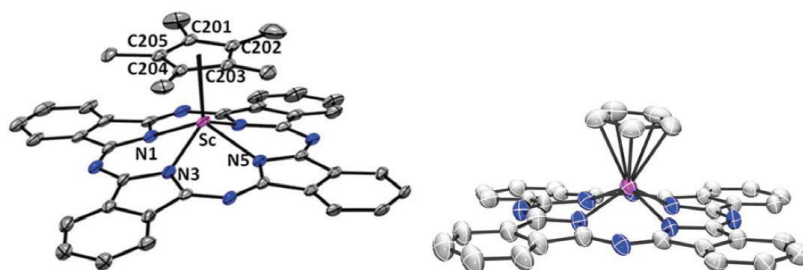
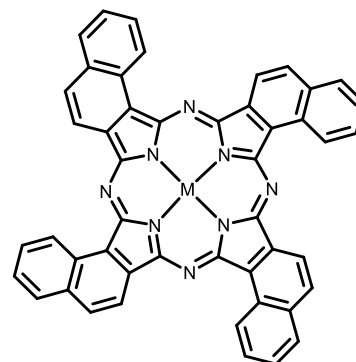


Figure 10: First "metallophthalocyanine-ocenes" and first crystallized [PcSc]-complex. Adapted from literature.^[50]

2.1.5 Molybdenum and Tungsten Phthalocyanines

Molybdenum phthalocyanines are mainly found in the oxidation state +IV or +V. In analogy to porphyrins [PorMo]* (such as [PorMo^{+V}(O)(OH)],^[58] [PorMo^{+IV}O] or [PorMo^{+IV}Cl₂],^[59] and [PorMo^{+V}N]^[60]), they are handled as interesting materials for O₂ reduction.^[61] When Mo-complexes are applied as catalysts in redox reactions, the enhanced electron density of a naphthalocyanine complex (Figure 13), in comparison to the smaller phthalocyanine complex, leads to an activation of ligand metal oxygen electron transfer.^[62] Furthermore, [PcMo] complexes were investigated with regard to epoxidation of olefins by using a molybdenum phthalocyanine as catalyst.^[63]



with M = Fe, Mo

Figure 13: Example of an investigated molybdenum naphthalocyanine complex applied in redox reactions, by DIENG.^[62]

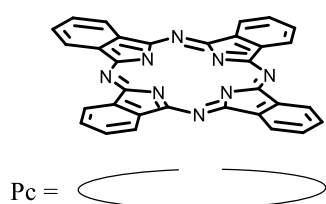
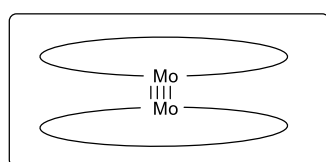


Figure 12: A reported bisphthalocyanine molybdenum complex [(PcMo^{+II})₂].^[64]

Similar to [Pc₂M^{RE}], bisphthalocyanine complexes, [PcMMPc] with M = Mo, Re, or Ir

(Figure 12) are described with a fourfold bond between the central atoms, e. g. [(Pc²⁻Mo)₂]; which is also in analogy to porphyrin molybdenum complexes.^[64] Oxido (e. g. [PcMoO],^[65] or [Pc^tBuMO], with M = Mo, W),^[66] nitrido (e. g. [Pc^tBuMN], with M = Mo, W, [Pc^{alkyl-chain}ReN],^[66,67] and halogenido (^{trans}[PcMo(Br₂)⁻]^[68] or cyano ([PcMo(CN)₂])^[64] as axial ligands are described.

*Note: here, the abbreviation [PorM] is used for any kind of porphyrin derivative, such as phenyl-porphyrins, tolyl-porphyrins or mesityl-porphyrins.

2.2 Applications of Phthalocyanines

Because of interesting properties of Pcs, including their electronic absorption spectra and high extinction coefficients, as well as their photophysical properties such as fluorescence and sensitising ability to form singlet oxygen, there are numerous applications for Pcs. Of course, as dyes, similar to the compounds described in section 1, they were traditionally applied as dye ingredient in paints,^[72] lacquers, and, nowadays, in catalysis^[73] and plastics.^[12] Their application, as photosensitizer (PS) in dye sensitized solar cells (DSSCs),^[74-77,78,79] as semiconductor in organic field effects transistors (OFETs),^[74] or photoconductors in laser printers was described.^[80] In addition, they are used as colour filters in liquid crystal displays.^[12] In applications, such as DSSCs, an efficient electron transfer to a semiconductor is needed, while in others, described photophysical processes, as shown in the JABLONSKI diagram (Figure 6), are of interest. Some examples are fluorescent markers,^[81,82] and sensitizers in photodynamic therapy (PDT).^[83] In 2012, the number of publications and patents on phthalocyanines increased to over 50,000.^[84] In this work, the "State of the Art" is described as best as possible proceeding the relevant section in the "Results and Discussion" section. The main focus is the systematic investigation of azaphthalocyanines. Therefore, the application for PDT is of interest, in specific the UV-Vis, FS and CV properties. In addition, phthalocyanines used as photosensitizers in DSSCs are discussed.

2.2.1 Phthalocyanines in PDT

Besides photodynamic therapy (PDT), surgical removal of tumour cells, as well as radio- and chemotherapy, are techniques for cancer treatment. The most famous substance applied in the chemotherapy is probably cisplatin, or chemically named *cis*-diamminedichloridoplatinum(II). In general, in chemotherapy, a lot of side effects with the healthy human tissue can occur. This is why PDT has gained more interest in recent years in research. The principle is quite simple: a photosensitizer (PS) is needed (absorbing at a wavelength between 600-800 nm), as well as oxygen and visible light. Owing to the limited penetration depth of visible light the cancer tissue should not be deeper than 2-3 mm. The PS should show a low dark toxicity and a high phototoxicity. In comparison to chemotherapeutic drugs, the phototherapeutic drugs (here, the PS) are less toxic.^[84,85] The goal of PDT is to selectively accumulate PSs in the tumour tissue, which becomes toxic upon illumination. Photofrin[®] and Photosan[®] are well known PSs of the first generation in PDT.^[85] One of the active compounds, dihaematoporphyrinether, is shown in Figure 15.

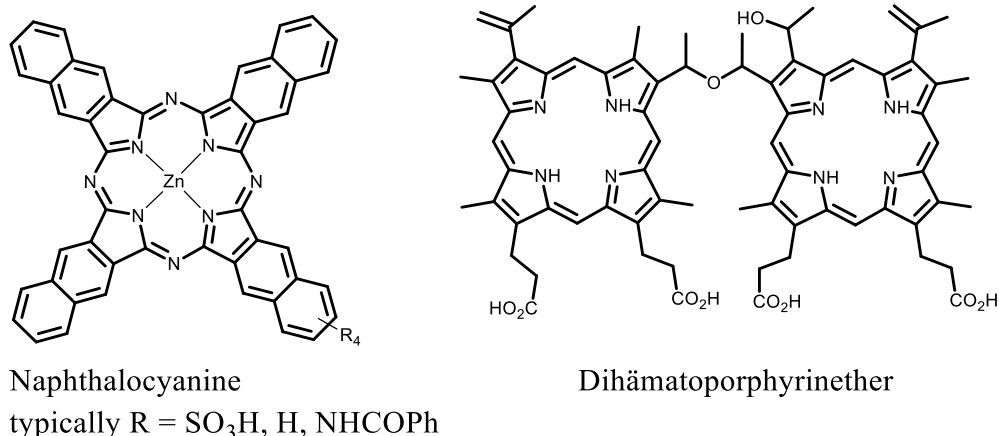
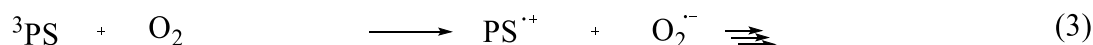


Figure 15: Typical photosensitizers (PS) in PDT. On the right side: dihämatoporphyrin, an active PS of the first generation of PDT. On the left side: a naphthalocyanine, second generation of PDT.

Typical representatives of the second generation are naphthalocyanines (Figure 15, left). Besides an absorbance >680 nm, the properties of a PS should be a high singlet oxygen quantum yield, Φ_{Δ} , which is in correlation to a low fluorescence quantum yield, Φ_F , and a high absorption coefficient, ε . It is important, because the higher ε is, the more photons are absorbed. By decreasing energy of the light (which correlates with the higher wavelength), the penetration depth into the tissue increases. As described in the JABLONSKI diagram (Figure 6), the following equations are possible after the absorption of a photon and were summarized by HIRTH:^[85]



Scheme 9: Possible pathways leading to a tissue damaging. Adapted from literature, by HIRTH and WÖHRLE.^[85]

After light absorption, the photosensitizer can get excited from a ground state, S_0 (PS), into an excited singlet-state, ${}^1\text{PS}^*$, (1). After an intersystem-crossing, the photosensitizer is in a triplet-state, ${}^3\text{PS}^*$. The excited ${}^3\text{PS}^*$ can react within radical reactions or in reductive reactions with biomolecules (2) or in an oxidative reaction with oxygen (3). The processes are called *reductive quenching* (2) or *oxidative quenching* (3), respectively.^[86] Predominantly, an energy transfer from the ${}^3\text{PS}^*$ to triplet-oxygen, ${}^3\text{O}_2$, occurs (4). This leads to the formation of singlet-oxygen, ${}^1\text{O}_2$. The so-generated ${}^1\text{O}_2$ can easily react with biomolecules in the cell interior. Typical reactions are common reactions, such as [2+2]- or [4+2]-cycloaddition, of ALDER en-reaction type. It is these reactions that make the PS cytotoxic.^[85]

As already mentioned, naphthalocyanine is a PS of the second generation.^[85] While the Q-band wavelength shifts to red from porphyrins > phthalocyanines > naphthalocyanines, and the extinction coefficient increases the same way $<10^4 \rightarrow <10^5$, the stability decreases with the enlargement of the π -system from Por < Pc < Nc. A more detailed investigation of naphthalocyanines seems to be obvious.^[85] However, the more photolabile character of Ncs has to be taken into consideration, because the PS concentration in the tumour tissue has to be high enough and almost constant for the time of illumination. The non-polar character, when looking at the structure of the Nc, is not so problematic. In these cases, the PS can be enclosed in liposomes when introducing them into the cancer cell. Especially in the treatment of pigmented melanomas, the Nc have been much more efficient in comparison to their smaller homologues Por and Pc. Taking this into consideration, less investigated azanaphthalocyanines, in which [-CH=] building blocks are exchanged by [-N=], are interesting compounds for application in PDT.^[87] The third generation of PS combines the advantages of the second generation, but the aim is a more targeted drug delivery.

In summary, Pcs are interesting compounds for application as PS in PDT.^[88] The azaphthalocyanines in section 2.1.3 can be taken into consideration now. In comparison to Pcs, the Q-bands of Ppzs are more blue shifted, whereby the Q-bands of Ncs are red shifted. In literature, lower symmetric Ncs have shown a maximum of singlet oxygen quantum yield, Φ_{Δ} , for the ABAB compounds.^[30] It also differs strongly from its regioisomer A₂B₂, which makes the systematic investigation of a series of azaphthalocyanines and azanaphthalocyanines unavoidable and even more interesting.^[30]

2.2.2 Phthalocyanines as Photosensitizers in DSSCs

During the last years, there has been an increasing demand for renewable energies. Since the '90s, in Germany, renewable energy production increase from about 20 to almost 160 billion kWh per year.^[89] The "renewable energy mix" includes on- and offshore wind parks, solar energy, biomass, and water power. In 2014, from this "renewable energy mix", photovoltaics produced almost 50 billion kWh. It was also the first year, in which more renewable energy was produced than energy obtained from the polluting combustion of brown coal. With a capacity of over 2.3 GW/year in 2010, China became world leader in the production of silicon based solar cells.^[90] However, the irony is that the *Kreditanstalt für Wiederaufbau* in Germany

Theoretical Section

supports, with the help of a subsidiary bank, different coal projects abroad.^[91] In 2015, at the Expo, in Mailand, the German pavilion possessed an organic photovoltaic membrane rooftop.^[92] After the last United Nations Climate Change Conference, it is obvious that the demand for renewable energies will continually increase in the next centuries to reach the set climate goals.

In 1883, the first solar cell was developed by FRITTS.^[93] It took more than 70 years to raise the efficiency of these silicon based solar cells up to $\eta = 6\%$.^[94] In 2001, silicon based crystalline solar cells could yield an efficiency of 24%, multicrystalline silicon 18% and amorphous silicon still 13%.^[95] Considering the cost-benefit factor, the amorphous solar cell gained the largest share of the market. Besides the fact that silicon is the eighth most common element by mass in the universe and the second most abundant, the purification of silicon for use in a crystalline solar cell is very energy consuming. Another problem is the weight of these solar cells, whereby the amorphous silicon solar cell is only a thin layer cell. Known alternatives to the silicon based cells are solar cells based on semiconductor materials such as GaAs, CdTe, or CuInSe₂ reaching 41%, 16%, and 20% solar efficiency, respectively. By trying to avoid these toxic materials, TANG constructed a bilayer solar cell, based on [PcCu] and a perylene derivative.^[96] With a price of 7-15 euros per kilogram [PcCu], a worldwide production of >80,000 t per year and a value of more than one billion US\$, the use of these materials is much more attractive.^[12] Based on this preliminary work, another solar cell was developed by GRÄTZEL and O'REGAN. The dye-sensitized solar cell (DSSC), also known the GRÄTZEL cell, is based on a semiconductor, on which a dye or photosensitizer is bond. An electrolyte and a transparent conducting oxide (TCO) coating are also applied. In contrast to the electron transfer processes, described in previous sections, in DSSCs the electron should be transferred into a conduction band, instead of FS processes or an ISC (Figure 16).

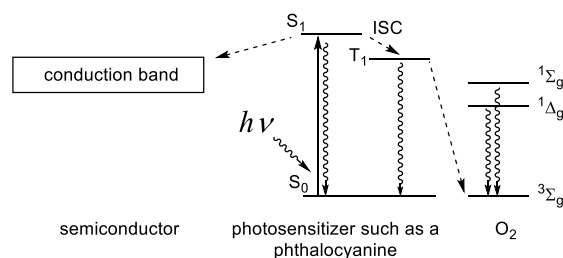


Figure 16: Possible energy transfers of a PS. Compare to JABLONSKI diagram (Figure 6).
Adapted from literature.^[25]

The assembly of a DSSC is shown in Figure 17,^[97] and the principle in Figure 18, below.^[95]

Principle.^[97,98] On top of the DSSC is a transparent glass or plastic, and a photoanode. As photoanode, a transparent conducting oxide (TCO) such as fluorine doped tin oxide (FTO) or indium tin oxide (ITO) is common. The light passes through the glass and is absorbed by a PS, such as a Pc. The PS itself is adsorbed or chemisorbed on the semiconductor, which is commonly a mesoporous TiO₂ or a ZnO material (as alternatives also SnO₂ or perovskites are known).

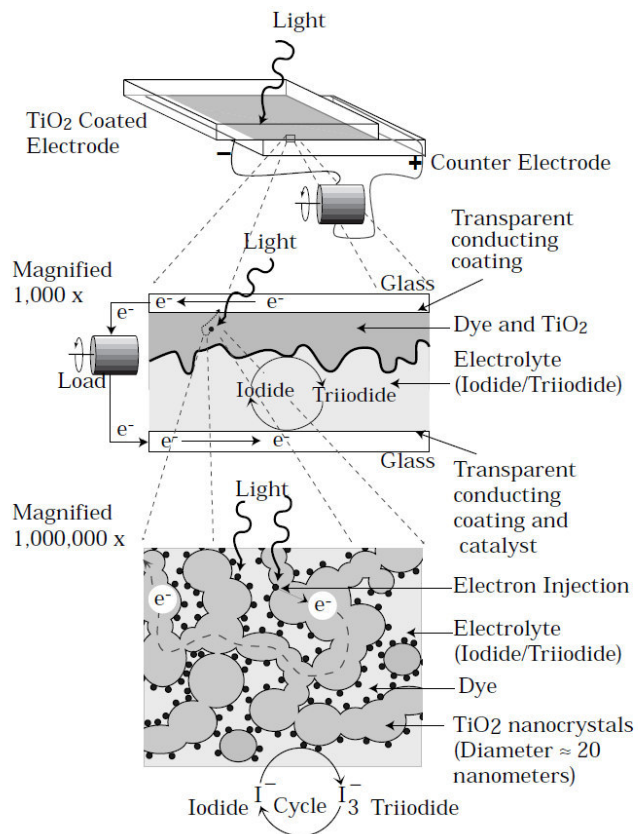
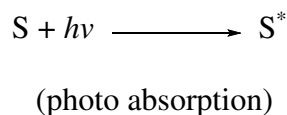


Figure 17: Assembly of a DSSC. Adapted from literature.^[97]



As visible in Figure 16, the excited electron can be transferred either into a triplet state, relax in form of FS or it is transferred to the conduction band (CB).

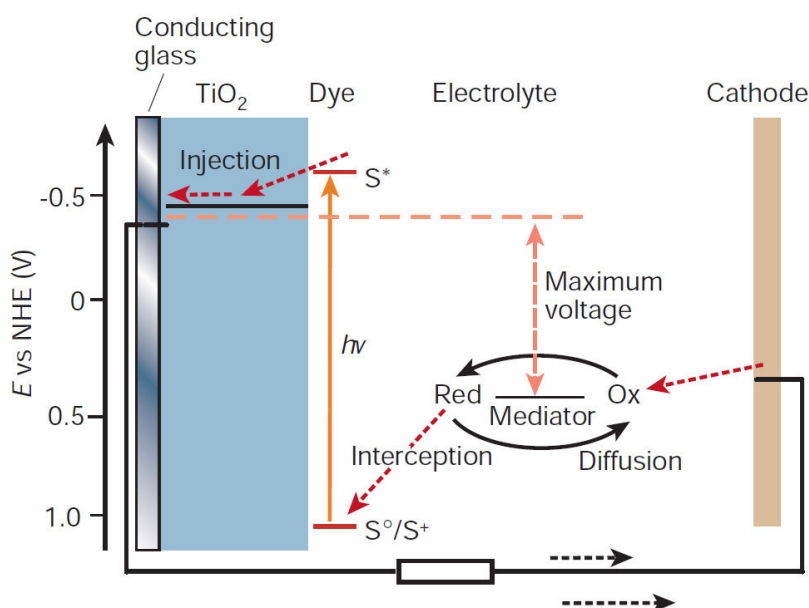
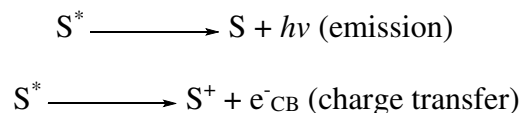


Figure 18: Principles of a dye-sensitized solar cell (DSSC), developed by GRÄTZEL. Adapted from literature.^[95]

In the case of a charge transfer to the CB, the electron is in the LUMO of the semiconductor. After electron injection into the CB and charge separation, the dye is in an oxidised form. The electron passes through the mesoporous material until it reaches the photoanode. Meanwhile, the dye is reduced by a redox mediator, which is

Theoretical Section

typically iodide/triiodide. The triiodide is reduced at the counter electrode to iodide. The electrochemical cycle is thus completed. An alternative to iodide/triiodide is, for example, an ionic liquid (ferrocene derivative), or a $\text{Co}^{3+}/\text{Co}^{2+}$ couple. The maximum voltage is the difference between the potential of the redox mediator and the conduction band of the semiconductor.^[13,97,98]

Analysis of DSSCs. Some significant values for the evaluation of the performance of a DSSC are discussed below. Therefore, the DSSC is measured in the dark and then illuminated. The current density is measured as dependence on the potential. The values obtained in the measurement are shown in Figure 19. The efficiency η of a DSSC is given by following equation:^[94]

$$\eta = \frac{I_{SC} V_{OC} FF}{P_{in}}$$

with:

FF = fill factor

P_{in} = incident light

P_{max} = maximum power

I_{SC} = short circuit current density; $V = 0$

V_{OC} = open circuit potential; $I = 0$

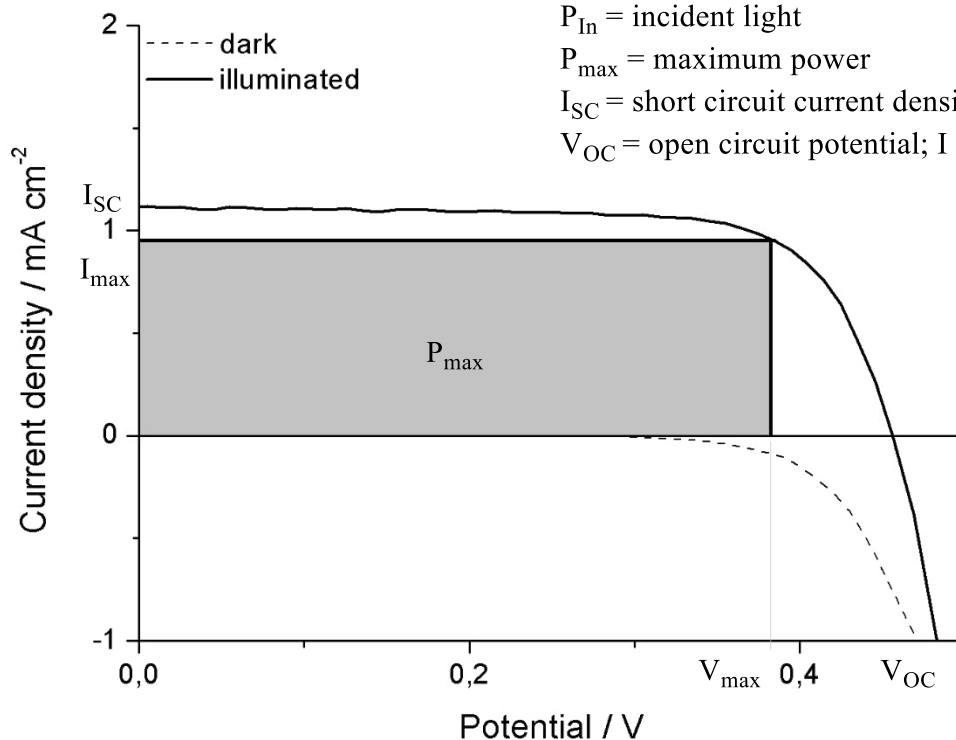


Figure 19: Current-voltage characteristic (I-U curve) of a dye sensitized solar cell.

Besides the electric power of the light, P_{in} (incident light), used to illuminate the cell, the efficiency of a solar cell depends on two values: I_{SC} and V_{OC} . The value obtained of the ordinate is the current density I_{SC} and I_{max} . SC stands for short circuit with $V = 0$. Of the abscissa, the potential is obtained: V_{OC} and V_{max} . OC stands for open circuit with $I = 0$. V_{OC} is obtained from the potential difference of the dye and the redox mediator and can be varied by changing them.

I_{max} and V_{max} are the values for which the product $I_{max} \cdot V_{max}$ reaches its maximum: P_{max} the maximum power. The relation between $I_{max} \cdot V_{max} = P_{max}$ and $I_{sc} \cdot V_{oc}$ give the fill factor, FF, by their division:

$$FF = \frac{P_{max}}{I_{sc} V_{oc}}$$

Therefore, the FF can assume a value between 0 and 1.

Finally, the incident photon-to-electrical-conversion efficiency, IPCE, is an important value, giving information about the quantum yield of the charge transfer, when the cell is illuminated. It is sometimes referred to quantum efficiency (QE).^[99] QE can be differentiated into two types:^[99] external (EQE) and internal

quantum efficiency (IQE). EQE is determined by illuminating the cell (or sample) with changing monochromatic light. The electric current is determined and the frequency of the light is varied. A curve of the current is plotted vs the wavelength (Figure 20). The area under the curve represents the total number of carriers while illuminating the sample with the full light spectrum, what corresponds to the current density. IQE considers only the absorbed light, excluding e. g. reflected light. Therefore, IQE is higher than EQE and both values may give useful information about possible side processes or loss mechanisms. IPCE is often used to study degradation mechanisms of cells.

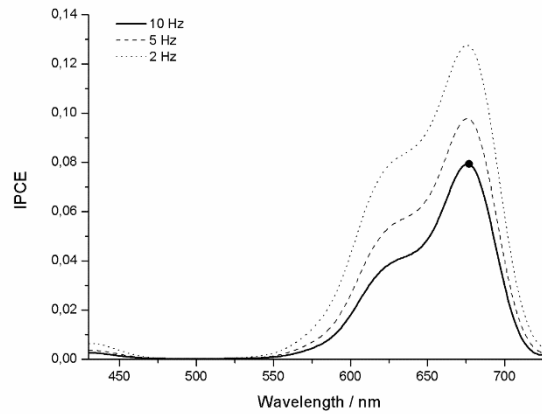


Figure 20: Determination of incident photon-to-electrical-current-conversion efficiency (IPCE) vs wavelength.

The IPCE is defined by the equation shown below:

$$IPCE = \frac{h\nu \cdot I_{sc}(\lambda)}{\lambda \cdot e \cdot I_o(\lambda)}$$

with: I_{sc} = short circuit current and I_o = monochromatic light flux

(h = Planck's constant, c = speed of light, e = charge of an electron)

Theoretical Section

Photosensitizers (PS). The dyes, or the PSs, have to fulfil some requirements for application in DSSCs:

- Of course a strong absorbance in the visible light area should be present
- The PS should be stable, also when it is adsorbed on a semiconductor
- The energy levels of the LUMO of the PS and CB of the conductor material (above the Fermi level) should align

Of course more problems may occur when looking at the DSSC more intensely: there are deactivation processes for the dye. Radiationless deactivation, e. g. vibronic deactivation, or excitonic charge recombination. The dye should not only align with the Fermi level, it should also bind strongly on the surface without destroying or modifying it and should have the ability to inject the electron into the semiconductor CB after the absorption.

Since the development of DSSCs, a huge number of PSs have been developed and described in literature.^[90] A lot of dyes are derivatives of the "black dye", which yielded an efficiency of 10.4%, in 2001.^[100] With this efficiency, this anionic Ru(II)terpyridine complex based dye is still one of the "leaders" of PSs. Other examples are porphyrin based dyes. A push-pull pattern leads to better charge separation and higher efficiencies for these dyes (Figure 21).^[76]

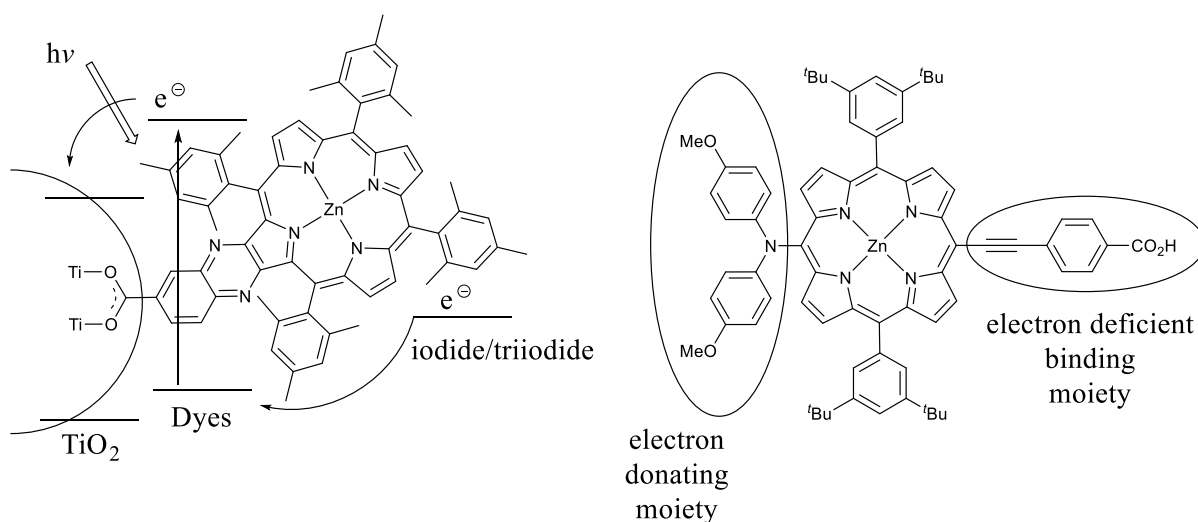
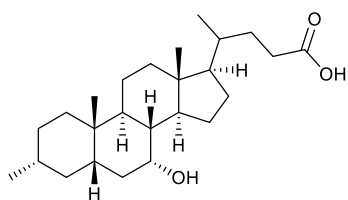


Figure 21: Push-pull porphyrin dyes used as PS in DSSCs.

Also purely organic dyes have been published, leading to a remarkable efficiency of 7.5% by replacing also the electrolyte redox couple with ferrocene/ferrocenyl.^[101] Here, "cheno" was used as a co-adsorbent (Figure 22), which is typical for highly aggregating compounds, such as



"cheno"
or chenodeoxycholic acid

Figure 22: One example for a co-adsorbent, used to lower aggregation and raise absorbance.

phthalocyanines. While "cheno" is the most employed co-adsorbent, other examples are octanol derivatives, diphenylphosphinic acid (DPPA) or cyclopentylacetic acid (CPEAA).^[102]

Porphyrins (Figure 21) are well established dyes with reasonably good cell performances.^[103,104] An advantage of Pcs is the absorbance of the Q-band in the red and NIR region, which is in comparison to Por red-shifted to the visible light area.^[76,104]

Furthermore, they show "*transparency over a large portion of the visible spectrum*" and Pc are quite stable compounds.^[12,104] To gain a maximum of orbital overlapping of the Pc and the semiconductor, the Pcs can be tuned by substitution in different positions. Furthermore, a separation of the charge in the molecule can occur, which is present in the push-pull systems shown above.

To bind phthalocyanines onto a semiconductor interface, different binding modes are possible. The phthalocyanine can be directly bound via axial substituents, or with a linker, see Figure 23 on the left and in the middle.

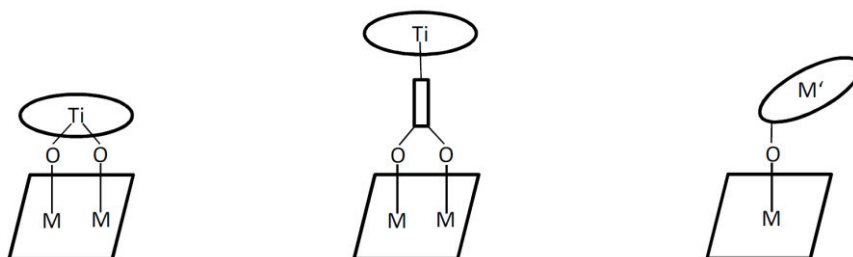


Figure 23: Possible binding modes of a Pc adsorbed onto a semiconductor such as ZnO or TiO₂. Adapted from literature.^[25]

The other possibility is a bond to a semiconductor using an anchor in the peripheral or the non-peripheral position. The different binding modes are discussed in literature.^[105] Apparently, the axial anchors are inefficient, because of the large separation of the Pc orbitals from the semiconductor band structure.^[25] The dye TT40 (Figure 24) is an example of an equatorially linked phthalocyanine.^[104,106] Since 2013, it is the most efficient Pc based PS with an efficiency of 6.1% using cheno as additive.

Theoretical Section

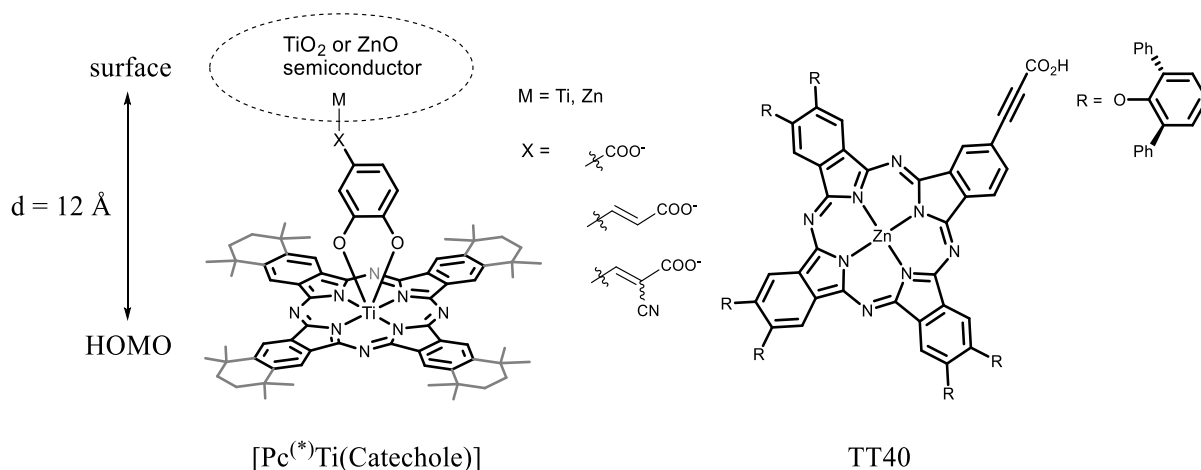
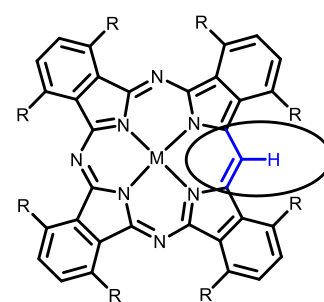


Figure 24: Examples for Pcs as PS in DSSCs. Left hand: axial bonded Pc. Right hand: Equatorial bonded Pc bearing an carboxylic acid as anchor moiety.

Furthermore, $[-\text{N}=\text{C}=\text{N}-]$ units in the meso position in Pcs can be functionalised (Figure 25). The exchange of meso $[-\text{CH}=\text{C}=\text{CH}-]$ by $[-\text{N}=\text{C}=\text{N}-]$ units leads to a strong blue shift of the Q-band from the Pc (733 nm) to the tetrabenzoporphyrin (TBP, 677 nm) over the tetrabenzotriazaporphyrin (TBTAP) and derivatives.^[107] Recently, these compounds with Ni as central metal atom, $[\text{TBTAP}^R\text{Ni}]$, were investigated in organic thin film transistors (OTFT).^[108] A functionalisation with an anchor moiety, such as carboxylic acid, in the meso position is in focus on current research.



Tetrabenzotriazaporphyrin
[TBTAPM]
with $R = \text{hexyl or decyl}$

Figure 25: A tetrabenzotriazaporphyrin (TBTAP).

Nowadays, the best type of a solar cell seems to be a solid state solar cell, developed by GRÄTZEL, in 2013.^[109] He developed a perovskite sensitised solar cells with efficiencies reaching up to 15%. Just recently, tandem solar cells were reported, yielding an efficiency of $>25\%$ by combination of a silicon based solar cell and perovskite solar cells.^[110]

2.2.3 Investigation of Single-Molecule Magnets (Ln-SMMs)

Single-Molecule Magnets (SMM) possess the ability to maintain magnetic properties, even after removing a previously applied magnetic field. Up to now, this magnetic behaviour is only observed at quite low temperatures (~liquid-helium temperatures). The reasons for the temperature dependence will be presented in this section, when looking at the requirements that have to be fulfilled by an SMM. SMMs show interesting magnetic behaviour, of which, especially in the organometallic chemistry, the number of developments is underexploited. Therefore, different classifications according to various criteria are described: ^[54]

- Block of periodic table
- Number of metal centres in molecular structure
- Type of ligands in SMM

Properties. Up to now, the phenomenon of SMM properties is mainly empirically studied and not based on theoretical predictions. But besides the difficulty in predicting the structural motif of a SMM, some requirements have to be realised: ^[111]

- 1) In the very beginning of investigating SMMs, the focus was put on the high spin ground state, S_t , which is for $Mn_{12}OAc$: $S_t = 10$. *"The normal trend for the molecular state is the pairing of electrons [...] with a cancellation of the electron spins. The design of a molecule-based magnet requires that this trend be successfully opposed"*.^[112]
- 2) Besides S_t , the easy-axis magnetic anisotropy, D_{st} , is seen as a crucial value in designing SMMs.^[54] While *"all SMMs contain metal ions with anisotropic electronic structure; however the presence of anisotropy is still no guarantee of SMM properties"*.^[54] The SMM needs a preferred orientation of the magnetic moment, independent of the external magnetic field.
The property of being a good SMM is given by the anisotropy barrier, U_{eff} ; *"the bigger the barrier, the more prominent the [...] properties at higher temperatures"* of the SMM are.^[54]
- 3) A SMM should show hysteresis behaviour, displayed in plots of magnetisation (M) vs magnetic field (H).
- 4) A dependence of the magnetic anisotropy of the symmetry was proposed: for high, as well as low, symmetrical molecules, quantum tunnelling (quantum tunnelling of magnetisation (QTM)) is observed, leading to an isotropic system. Therefore, lower than cubic, but at least a C_3 symmetry is suggested when designing a SMM.^[54]

Theoretical Section

Another important value in the requirements is the blocking temperature, T_B , giving the highest temperature at which the SMM still shows hysteresis behaviour. The hysteresis is dependent on the sweep rate of the magnetic field.^[55] After this brief summary of the requirements of SMMs, the next section summarises achievements of phthalocyanine based SMMs.

Complexes. The most famous transition-metal SMM is the manganese(III)/manganese(IV) cage complex, introduced in section 2.1.4.^[52,53] Just six years ago, in 2010, the first organometallic SMM was reported:^[54,113] it is a benzotriazole-bridged dimer dysprosium complex. The most studied and prominent lanthanide phthalocyanine complex is the terbium(III) salt, $[\text{Bu}_4\text{N}][\text{Pc}_2\text{Tb}]$.^[114] One main advantage of using phthalocyanines as coordinating ligand is, besides the number of possible lanthanides in $[\text{Pc}_2\text{M}^{\text{RE}}]$ complexes and their structural variability, the redox state: the $[\text{Pc}_2\text{M}^{\text{RE}}]^-$ can be oxidised once or twice and form a neutral $[\text{Pc}_2\text{M}^{\text{RE}}]$ complex or $[\text{Pc}_2\text{M}^{\text{RE}}][\text{X}]$, with X = anion. Investigations about the nature of $[\text{Pc}_2\text{M}^{\text{RE}}]$ are discussed more in detail in section 4.5.1. The well-studied $[\text{Bu}_4\text{N}][\text{Pc}_2\text{Tb}]$ complex demonstrated several remarkable physical properties of rare earth metal phthalocyanine sandwich complexes:^[54]

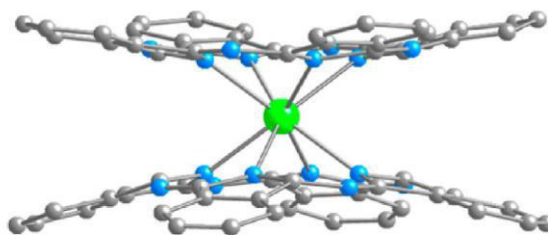


Figure 26: Structure of the terbium (III) phthalocyanine anion $[\text{Pc}_2\text{Tb}]^-$. Adapted from literature.^[54] Tb in green, N in blue.

- $[\text{Bu}_4\text{N}][\text{Pc}_2\text{Tb}]$ contains only one single paramagnetic centre
- With $U_{\text{eff}} > 230 \text{ cm}^{-1}$, the complex underlined the importance of the anisotropy barrier, compared to previously reported transition-metal SMMs
- The origin of SMM properties could be further investigated and understood by "*eliminating any cooperative intermolecular interaction*".^[54]

Further investigations led to a large number of Ln-SMMs $[\text{Pc}_2\text{M}^{\text{RE}}]$ -type complexes with even more remarkable physical properties.^[56,57] In 2014, a heteroleptic terbium (III) phthalocyanine complex, $[\text{Pc}^{\text{OC}_6\text{H}_4\text{-}i\text{Bu}}\text{PcTb}]$, held the record for an anisotropy barrier of $U_{\text{eff}} > 652 \text{ cm}^{-1}$. Anyway, up to now it is difficult to predict the behaviour of molecules with regard to their single-ion anisotropy by structural motif.^[115] Empirically, dysprosium (III) and terbium (III) with axial ligands show a high anisotropy, while for erbium (III) an equatorial ligand field is preferable.^[54]

2.2.4 Rare Earth Metal Phthalocyanines, $[\text{Pc}_2\text{M}^{\text{RE}}]$, applied in Gas Sensors

As a result of their physical properties, $[\text{Pc}_2\text{M}^{\text{RE}}]$ were studied with regard to their application in gas sensors: ^[116]

Resistive gas sensors are based on conductivity measurements, carried out by a thin phthalocyanine film deposited on microelectrodes. The measurements have a detection selectivity in ppb range. While the electronic conductivity change of $[\text{PcM}]$ is quite slow (within 20 min), halogen gases,^[117] nitrogen gases ^[118] or ozone ^[119] can be detected. In comparison, $[\text{Pc}_2\text{M}^{\text{RE}}]$ deposited films show a drastic decrease in conductivity, caused by its oxidation to a $[\text{Pc}_2\text{M}^{\text{RE}}]^+$ with $\text{M}^{\text{RE}} = \text{Ce}, \text{Lu}, \text{or Pr}$, when gases such as NO_2 are present.^[120] Furthermore, halogen gases,^[121] ammonia,^[122] and others can be detected.^[116]

Optical gas sensors detect a shift of the Q-band of $[\text{Pc}_2\text{M}^{\text{RE}}]$. An exposure of the sensor, for example to NO_x gas, shifts the Q-band to lower energies and a change in colour of the deposited film from green to red can be observed.^[116] This reversible process is also visible for electron donating gases such as ammonia, while here, in contrast, the Q-band is shifted hypsochromically, what explains why the film appears blue.^[116]

These optical gas sensors can also detect vibrational changes in IR or Raman spectroscopy.^[123] By applying deposited $[\text{PcPb}]$ or $[\text{Pc}_2\text{Y}]$ films, a change of diagnostic IR bands can be observed at $\sim 1400 \text{ cm}^{-1}$, as it will be discussed in more detail in section 4.5. Especially for $[\text{Pc}_2\text{M}^{\text{RE}}]$ sandwich complexes, the IR band indicates the nature of the complex (section 2.2.3) and can therefore be used in the mentioned application.^[116,124]

Electrochemical sensors measure a cyclic voltammogram, based on the redox-properties of $[\text{Pc}_2\text{M}^{\text{RE}}]$. These electrochemical sensors are discussed as potential "electronic tongues",^[125] because they may distinguish between different solutions.^[125] This is due to a characteristic electrochemical behaviour of the solutions investigated. Different $[\text{Pc}_2\text{M}^{\text{RE}}]$ with $\text{M}^{\text{RE}} = \text{Eu}, \text{Gd}, \text{Lu}$ and a substituted $[\text{Pc}_2\text{Pr}]$ are described.^[125]

3 Purpose of the Work

In 2015, the United Nations Climate Change Conference was held in Paris. For the first time, about 190 states, including industry- and emerging nations summarised plans to keep the global warming below a 2 °C level.^[126] This also includes financial aids for developing countries.^[126] Since the abandonment of nuclear energy, other energy sources have become more important. Brown coal and hard coal dominate the market of the German "Energy mix".^[89] In 2014, the amount of energy produced using brown coal was surpassed for the first time by renewable energies including wind, sun and biogas produced energy. However, in 2013, the per capita consumption of CO₂ in Germany lies with 10.2 t, in front of China with 7.4 t, and behind the USA with 16.5 t.^[127] With the CO₂ emission climatic extremes are increasing: e.g. heat waves, hurricanes, or flood-like rain falls are occurring more frequently. In summary, the increasing importance of renewable energies and, with this, the need for innovative technologies becomes clear.

Because of their interesting optoelectronic properties, structural diversity, and number of possible substitution pattern, phthalocyanines (Pcs) are in focus in research with regard to their application in OFETs,^[108] PDT,^[85] electronic switches, or DSSCs.^[105] A tuning of HOMO/LUMO levels is possible by decreasing the size of the chromophore to a 14 π -/32 π -electron aromatic subphthalocyanine (Spc, Figure 27).^[128] These non-planar cone shaped subphthalocyanines differ strongly in photophysical and structural properties compared to their larger homologues, the phthalocyanines (Figure 28). The planar, metal free ligand, PcH₂, with an 18 π -/42 π -electron system can be additionally benzannulated to an 18 π -/58 π -electron naphthalocyanine (Nc, Figure 29).

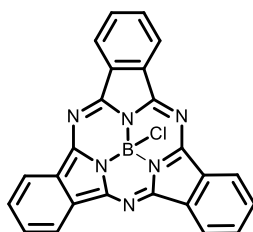


Figure 27: A subphthalocyanine [SpcBCl].

This work is focussed on a collaborative investigation of charge transfer processes, exciton dynamics and photoluminescence (PL) analysis within the SFB1083. Therefore, the aim is to investigate the influence of a gradual substitution of [-CH=] by [-N=] units (shown in blue, Figure 28) in phthalocyanines ((N₀)-[PcM], left side) and azaphthalocyanines (N_x-[Pc**M*]) on fundamental physical properties such as absorption and emission, PL, HOMO/LUMO levels, reduction potentials, singlet oxygen quantum yields (Φ_{Δ}) and fluorescence quantum yields (Φ_F), as well as fluorescence lifetimes (τ_F). The systematic exchange of two [-CH=] by [-N=] units of a phthalocyanine finally leads to a so called pyrazinoporphyrazine ((N₈)-[PpzM], right side).

Purpose of the Work

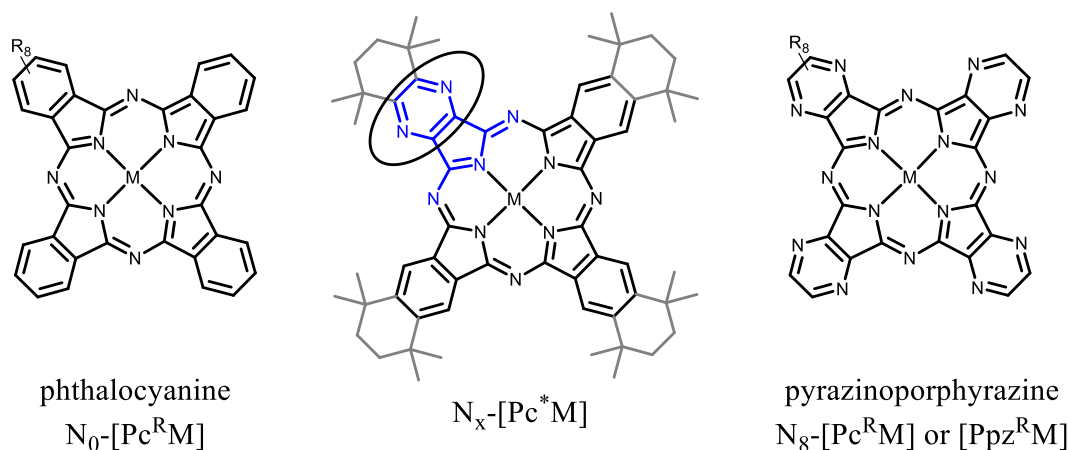


Figure 28: A systematic investigation of a gradual exchange of [-CH=] by [-N=] units; - from a phthalocyanine (N_0 -[PcM]) over azaphthalocyanines (N_x -[PcM]) to pyrazinoporphyrazines (N_8 -[PcM]).

Furthermore, the influence of extending the π -system on these physical properties was investigated (Figure 29). Therefore, a ring extension (shown in red) of an azaphthalocyanine N_x -[Pc^{*}M] with regard to a benzannulation (by one benzene unit per isoindoline unit) should be tested to give the so-called naphthaloporphyrazines N_x -[Npz^{*}M].

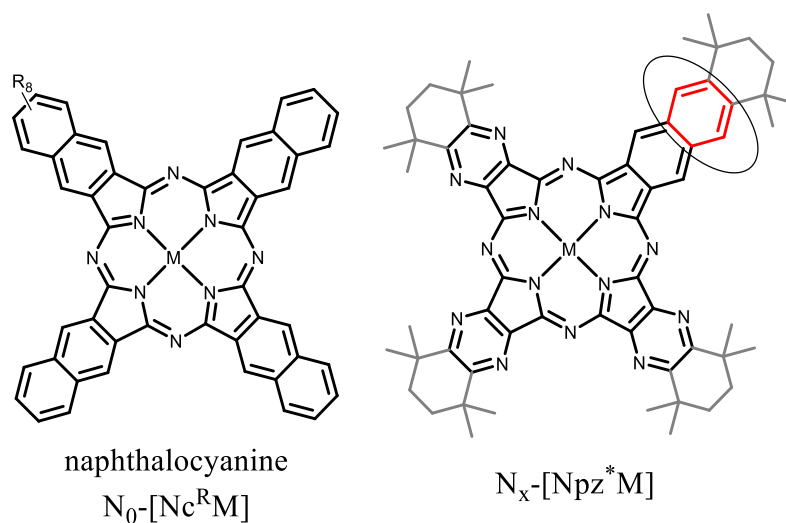
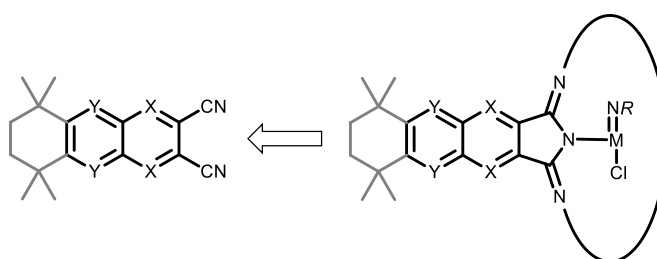
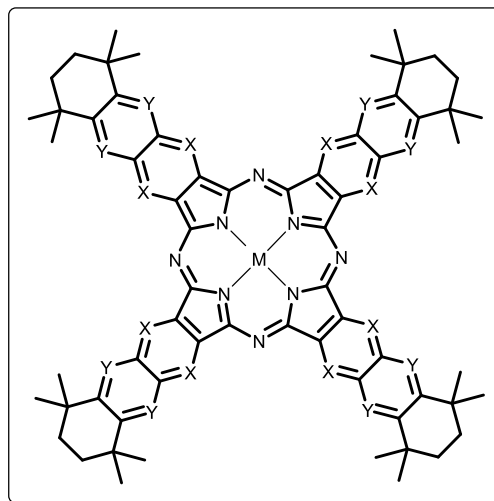


Figure 29: The expansion of an azaphthalocyanine N_x -[Pc^{*}M] by benzannulation may lead to a N_x -[Npz^{*}M].

The systematic investigation of phthalocyanines is, in general, limited due to their low solubility and corresponding high aggregation effects. The advantage of the here shown compounds (Figure 28) is their lowered aggregation caused by sterically demanding alkyl groups in the peripheral position. This alkyl substitution pattern was first described by MIKHALENKO.^[24] These alkyl groups were chosen, not only because of the increased solubility, but the symmetry of the molecule is maintained, which simplifies purification, analysis and crystallisation of these molecules.

Besides the lower symmetrical N_x -[Pc**M*], the larger homologues, specifically a series of C_{4v} -symmetrical azanaphthalocyanines, $N_{x,y}$ -[Nc**M*], bearing alkyl groups in the peripheral position, is not yet described in literature. Diverse applications, caused by the interesting properties of these alkyl substituted azanaphthalocyanines, are discussed.^[129] Similar to the compounds shown in Figure 28, the [-CH=] units of a naphthalocyanine $N_{x,y}$ -[Nc**M*] with $x = y = 0$ should be exchanged by [-N=] (X or Y, or both) in N_8 -steps in each position (Scheme 10). These compounds are interesting because of the strong influence on the Q-band by axial substitution, described in previous work.^[69,70] The axial ligands were exchanged for smaller homologues [PcMo(NR)Cl] with $R = tBu, Mes, Ts$.^[70] The electronic properties should be determined and, if possible, compared to theoretical EPR calculations, TD-DFT calculations, and more simple HÜCKEL calculations, done by the group of BERGER (Department of Chemistry of the Philipps-Universität Marburg).



X and Y = [-N=] or [-CH=] units
x,y give the number of [-N=] units

Scheme 10: Investigation of $N_{x,y}$ -[Nc**M*] with *M* = group 6 metal with a d^1 -configuration.

Purpose of the Work

Meanwhile, in our group, the axial functionalisation of Pcs was investigated in previous work.^[25,130] Here, catechol derivatives were axially bonded on phthalocyanines (Figure 30, left side). Those catechol moieties were substituted with an anchor so that the complexes could be successfully bonded onto common surfaces, such as ZnO and TiO₂, and were tested as photosensitizers in DSSCs.^[25] Synthetically more challenging experiments for a peripheral functionalisation of a Pc bearing the mentioned alkyl moieties were planned to be carried out.

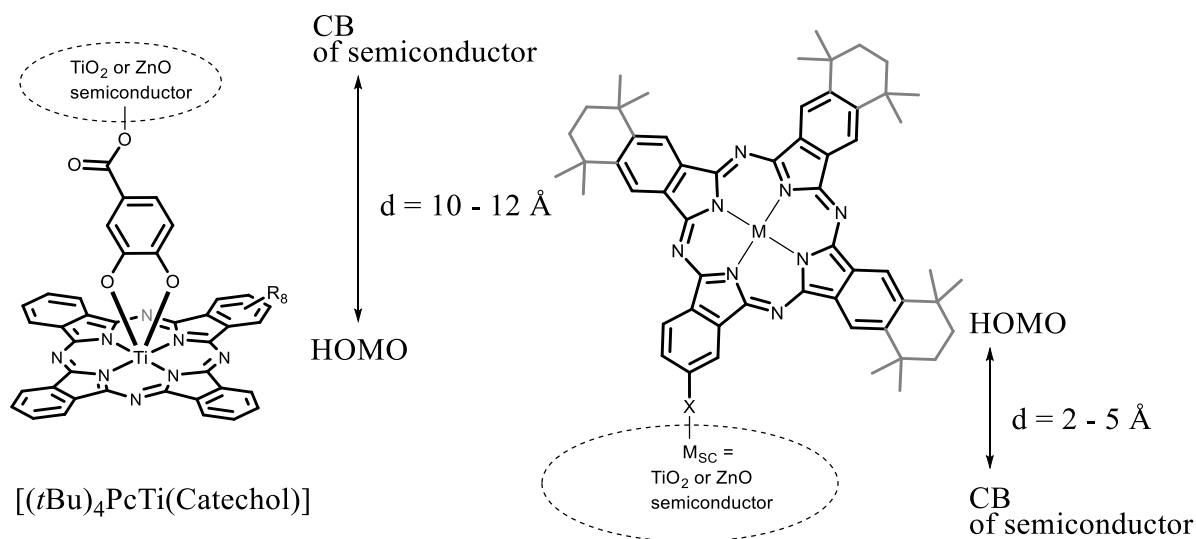


Figure 30: Investigated functionalisation modes of Pcs for possible application in DSSCs.

In this work, the focus was on literature described carboxylic acid anchors,^[105] as well as on phosphonic acids and catechol-like anchors, of which a strong bond affinity on ZnO and TiO₂ surfaces is expected.^[131,132] Within the SFB1083, a Pc without sterically demanding alkyl groups and with a phosphonic acid anchor is of interest, because of a better comparability to the well investigated [PcCu] and the easier formation of a monolayer. As central metal atom, these molecules in general have a Zn atom, which is electrochemically inert and does not interfere with electron transfer processes to a semiconductor surface, in analogy to metal free PcH₂. The main goal was, after synthesis and full characterisation of these molecules, testing the binding to a semiconductor surface, and, if possible, the application as a photosensitizer in DSSCs. With a successful electron transfer and application in a DSSC, the efficiency of the charge transfer would have to be proved by further incident photon-to-electrical-conversion efficiency (IPCE) and photoluminescence (PL) measurements.

4 Results and Discussion

The section "Results and Discussion" is subdivided into several subsections. The first section is about the synthesis of organic dinitrile precursors, which are further used for cyclisation to a corresponding macrocycle. The second section is about the synthesis of azaphthalocyanines, related azasubphthalocyanines, and azanaphthalocyanines. The section is mainly focused on the investigation of absolute and relative HOMO/LUMO levels as well as optoelectronic properties of these compounds, and their interest in physics for use as semiconductors. In the third section, functionalised phthalocyanines for use as dyes in DSSCs will be discussed. Finally, studies about subphthalocyanines used as borato ligand and syntheses of rare earth metal compounds have been carried out, as described in the fourth and fifth section.

4.1 Organic Precursors – Symmetrical Aza-/Dinitriles

The focus of the first part of this work was the synthesis of new soluble azaphthalocyanines and azanaphthalocyanines in order to determine and to tune the before mentioned relative and absolute HOMO/LUMO level alignment. Therefore, different dinitriles were targeted. Organic precursors with functional groups are described in the following section 4.3.2. On one hand, PDN* **1** and PyzDN* **2** have been synthesised. Both compounds **1** and **2** are well established in our group and have been described in literature before.^[24,70] On the other hand, the known NDN* **3** was synthesised as well as azanaphthalonitriles **4-6**.^[24] The NpzDN* **4** and NqnDN* **5**, as well as the NpyzDN* **6** were synthesised for the first time.

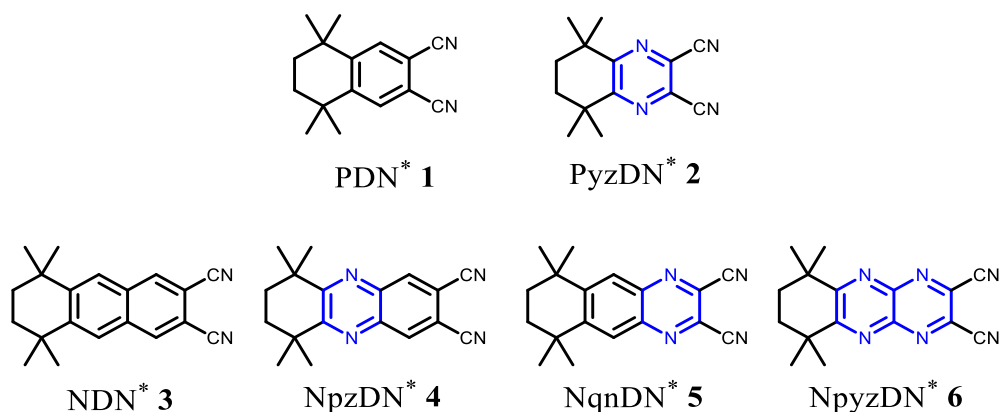
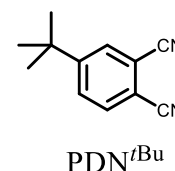


Figure 31: Structures of C_{2v} -symmetrical dinitrile precursors: 2,2,5,5-tetramethylcyclohexane annulated phthalonitrile (**1**), pyrazinenitrile (**2**), naphthalonitrile (**3**), 2,2,5,5-tetramethylated tetrahydropyridazine (**4**), 2,2,5,5-tetramethylcyclohexane annulated quinoxaline (**5**) and pyrazinopyridazine (**6**).

The advantage of the mentioned dinitriles **1-6** is an increase in solubility of the resulting phthalocyanines and azaphthalocyanines in common organic solvents, due to the sterically demanding alkyl groups in the peripheral position. With an increase in solubility, a decrease of

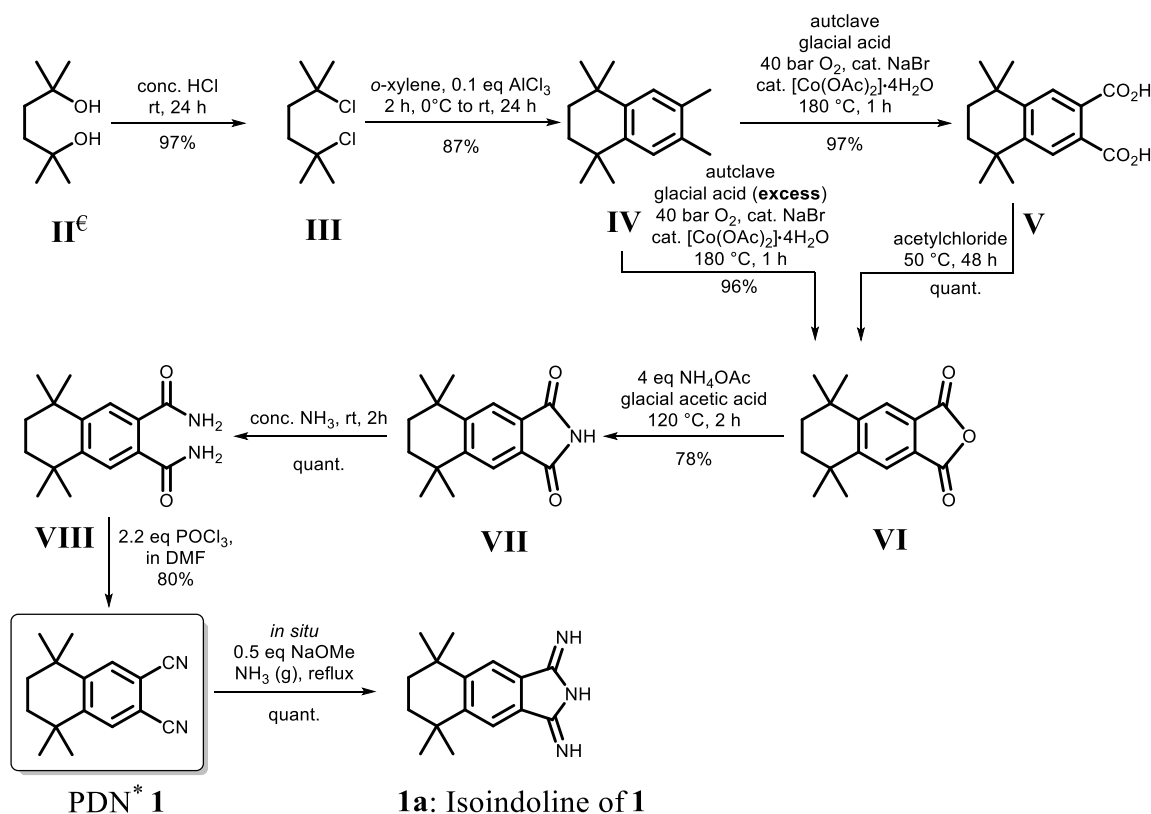
Results and Discussion

aggregation effects might be observed, while the symmetry of the phthalocyanines is maintained. Compared to the commercially available PDN^{tBu} (shown on the right), the symmetry of compounds **1-6** leads to only one diastereoisomer after cyclisation, which simplifies the analysis of NMR spectra and favours crystallisation. For application in DSSCs, the alkyl groups have a +I effect, which makes them even more attractive for electron transfer into a semiconductor's conduction band.



4.1.1 Synthesis of Aza-/Dinitriles

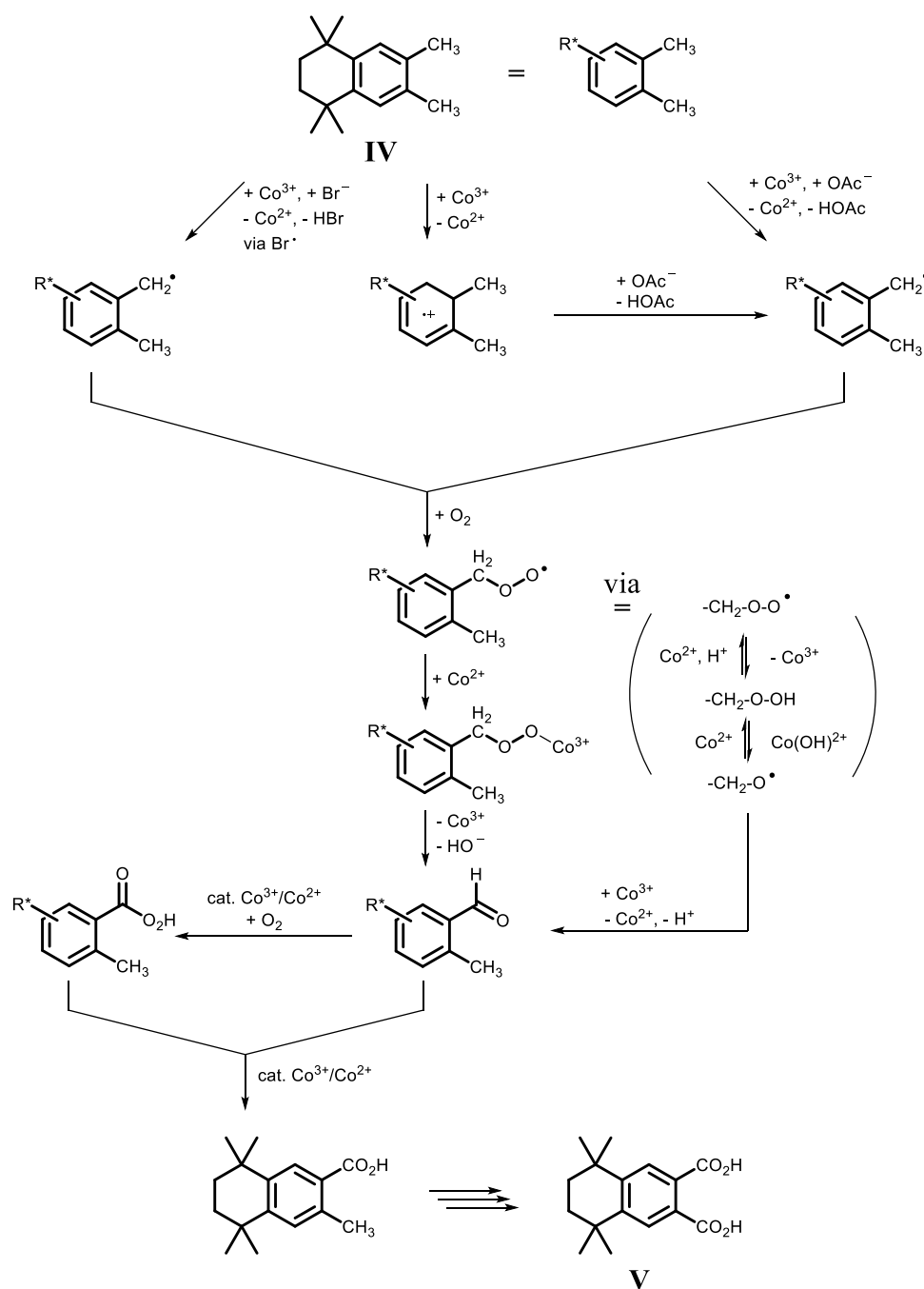
In 1988, MIKHALENKO *et al.* described PDN^* **1** for the first time. The synthesis was varied and optimised by SEIKEL.^[24,25] In this work, we followed and optimised the synthesis of MIKHALENKO *et al.*, because of its high yields >30% over seven steps and easy, straightforward syntheses. In comparison to other syntheses described in literature,^[133] no column chromatography is needed. The seven step synthesis of the PDN^* **1** is shown in Scheme 11.



Scheme 11: Synthesis of PDN^* **1** according to MIKHALENKO.^[24,25]

The synthesis starts with the commercially available 2,5-dimethylhexane-2,5-diol **II**. Protolysis with HCl yields the dichloride **III**. In the FRIEDEL-CRAFT alkylation using *o*-xylene as both solvent and reagent, the basic tetraline scaffold **IV** is formed. The key-step in

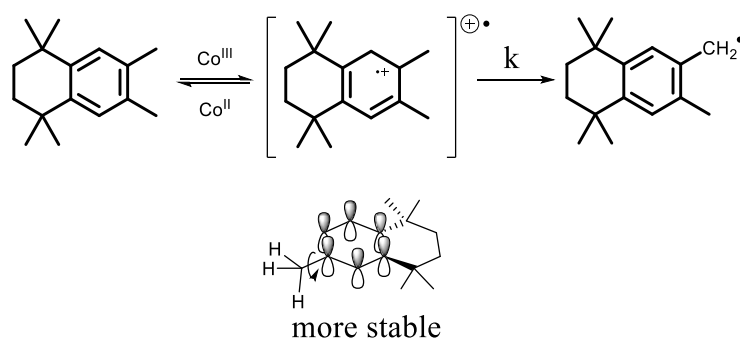
the synthesis is the following oxidation of this tetraline **IV**. Up to now, the side chain oxidation was limited by low yields of <54%, and it was quite uneconomical as well as environmentally unfriendly because an excess of potassium permanganate in aq. pyridine is needed. For the synthesis of the dicarboxylic acid **V** a catalytic procedure applying literature known conditions for the industrial *p*-xylene oxidation processes to terephthalic acid was used.^[134] The reaction was carried out in glacial acid, with NaBr and $[\text{Co}(\text{OAc})_2] \cdot 4\text{H}_2\text{O}$ as catalyst, at 180 °C and 40 bar O_2 . In Scheme 12, the suggested radical mechanism is displayed.



Scheme 12: Suggested mechanism: radical oxidation of tetraline **IV**.

Results and Discussion

Depending on the amount of glacial acetic acid, the anhydride **VI** will be obtained when it is used in excess. In this case, the glacial acetic acid is acting as a water scavenger. It was possible to obtain the dicarboxylic acid **V** in 97% yield, when 15 g tetraline **IV** was used. In literature, the mechanism is mainly discussed as a radical chain reaction. Here, the most important and rate determining step is the reversible formation of Ar-CH₂[•] and Co(III) via electron transfer.^[135] The arene radical cation forms a thermodynamically favoured benzylic radical by elimination of a proton. The transition state (Scheme 13) explains the selectivity of the reaction. The abstraction of the proton is additionally accelerated by the presence of radicals like Br[•], R[•] or RO[•]. The Ar-CH₂[•] is trapped by oxygen and forms finally peroxides and peroxy radicals for further reaction, until the dicarboxylic acid is finally formed by loss of 1 eq of water. The remaining steps were carried out according to MIKHALENKO.^[24] The reaction path is typical for the synthesis of phthalonitriles. At first, an anhydride **VI** is formed, followed by the imide **VII**, the diamide **VIII** and its dehydration to dinitrile PDN* **1**. In summary, the overall yield over seven steps was raised from 30% to >50%, so the reaction is much more feasible for technical application of phthalocyanines in DSSCs.

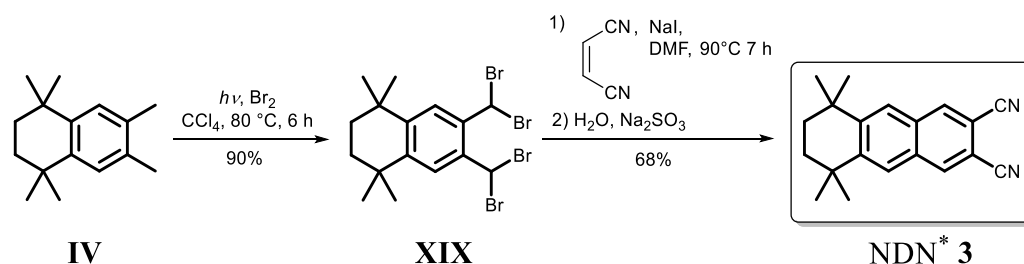


Scheme 13: Rate determining intermediate compound.^[135]

For high purity, PDN* **1** was finally sublimed in vacuum. Two other synthetic routes to compound **1** should be mentioned. One route starts from compound **III** and benzene. The aromatic system of the resulting tetrahydronaphthalene scaffold is brominated with 2 eq of bromine, and can then be converted to the dinitrile.^[133,136] The disadvantages of this route, compared to the one shown in Scheme 11, are not only the toxic substances, but also more laborious workup because column chromatography is needed. A second synthesis is a direct FRIEDEL-CRAFT alkylation of phthalonitrile **I** with **III** as described only recently.^[137] Despite the fact that no experimental description is given, a FRIEDEL-CRAFT alkylation of such electron poor aromatic systems seems to be unlikely. This is due to the electronic properties of the electron withdrawing nitrile groups, so no electrophilic attack of **III** is possible.

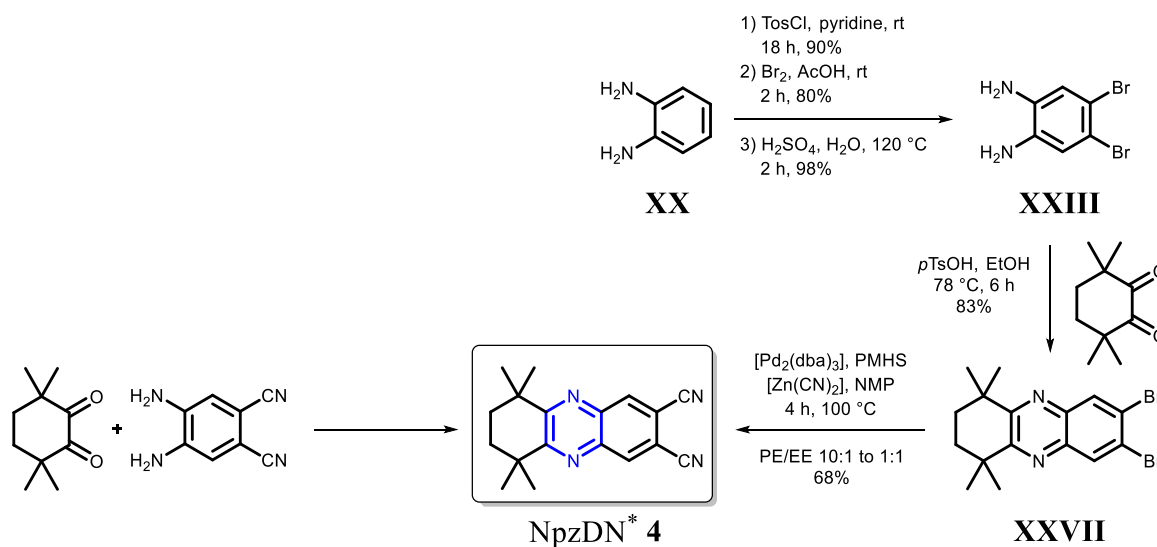
4.1.2 Synthesis of Aza-/Naphthalonitriles

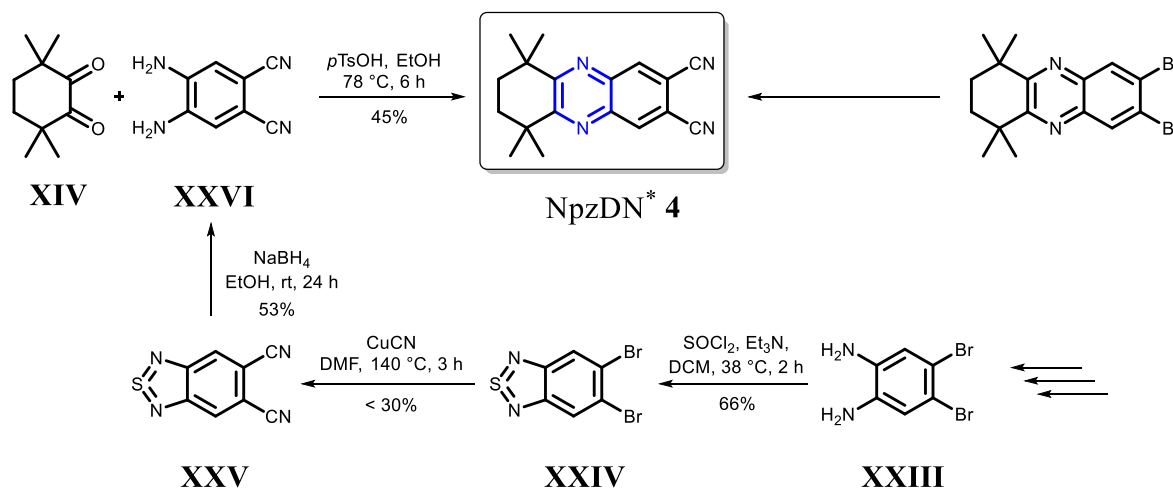
In addition to PDN* **1** and PyzDN* **2**, the annulated derivative NDN* **3** and its analogues NpzDN* **4** and NqnDN* **5** and NpyzDN* **6** (Figure 31) were synthesised. The NDN* **3** was synthesised according to the description of MIKHALENKO *et al.*^[24] following the reaction conditions described for the unsubstituted 2,3-dicyanonaphthalonitrile NDN.^[140,141] In the first step, the tetraline ligand **IV** is brominated at the side chain with 2 eq bromine per methyl group under light induced radical conditions (Scheme 15).

Scheme 15: Synthesis of NDN* **3**.

The $\alpha, \alpha, \alpha', \alpha'$ -tetrabromide-*o*-xylene **XIX** was converted with fumaronitrile in DMF at 90 °C to the NDN* **3**. NaI was used as scavenger for released bromine. As a mechanism, a DIELS-ALDER reaction or nucleophilic attack of the brominated methyl groups may occur, but is not yet completely elucidated. The synthesis could be reproduced with yields of up to 68% according to literature.^[24]

The new developed synthesis of the analogue NpzDN* **4** is possible via two routes. The first synthesis has the formation of the dibromide **XXVII** as key-step, which can be obtained starting with *o*-phenylene diamine (**XX**) (Scheme 16, on the right side).

Scheme 16: Different syntheses of NpzDN* **4**.

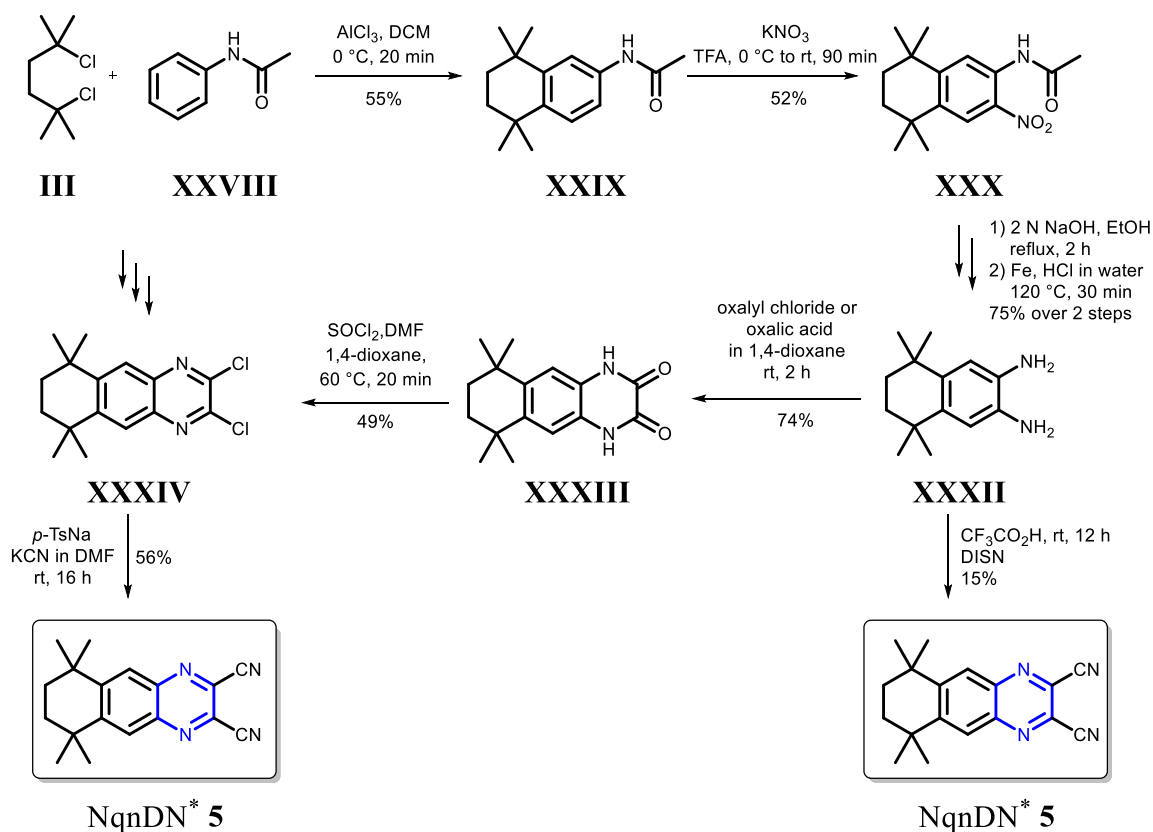


Scheme 17: Different syntheses of NpzDN* 4.

The dibromide **XXVII** could be obtained with 83% yield, using 3,3,6,6-tetramethylcyclohexane-1,2-dione (**XIV**) in a condensation reaction as described in the synthesis of PyzDN* 2, above. The NpzDN* 4 could be finally obtained in yields of 68% by using the conditions described by HANACK *et al.*^[136] The second synthesis, on the left side in Scheme 17, is a condensation of 3,3,6,6-tetramethylcyclohexane-1,2-dione with 4,5-diaminophthalonitrile (**XXVI**). The disadvantage of this synthesis is the synthesis of the 4,5-diaminophthalonitrile (**XXVI**), the yield of which is mainly limited by the low yield in the ROSENMUND-VON-BRAUN reaction of **XXIV** to **XXV**. To sum up, the reaction path shown on the right side in Scheme 16 offers better yields of 40% over 5 steps of NpzDN* 4, compared to less than 7% over 7 steps.

The analogue to NpzDN* 4, NqnDN* 5, was prepared starting with a derivate of paracetamol and phenacetin – acetanilide **XXVIII**. The first 4 steps are already literature known and have been described by SHUDO *et al.*^[142] In the first step, the acetanilide is converted with the dichloride **III** in a FRIEDEL-CRAFT alkylation to compound **XXIX**. The purification could not be accomplished as described in literature. Instead of column chromatography or recrystallization in EtOH/H₂O 1:1 mixture, the product was washed with hexane and finally recrystallized in EA. After the brown slurry was macerated several times, a white powder could be obtained. After nitration of **XXIX** using KNO₃ in TFA, compound **XXX** gets deprotected and reduced with Fe and HCl to form the diamine **XXXII**. The diamine **XXXII** might be converted directly to NqnDN* 5, or treated with oxalyl chloride and thionyl chloride to form the precursor **XXXIV**. Using a literature known method with sodium *p*-toluenesulfinate (*p*-TsNa) and KCN in DMF, the dichloride **XXXIV** can be converted to NpzDN* 5 in 30% yield (Scheme 18).^[87] An alternative reagent, NH₄CN, is reported.^[143]

Results and Discussion

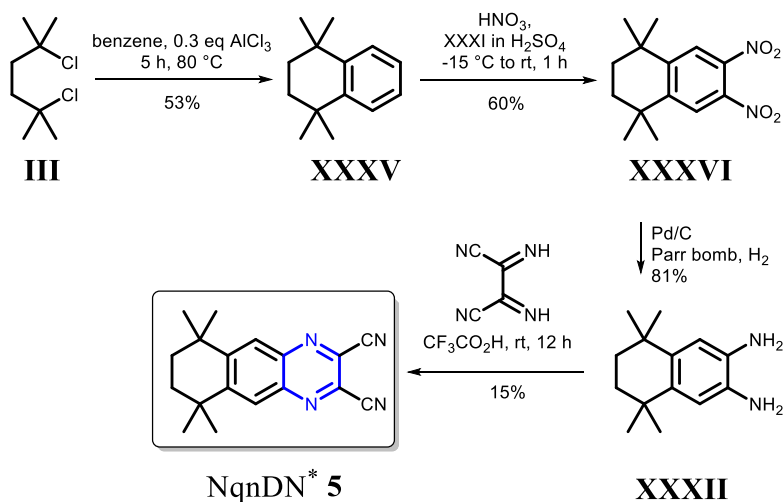


Scheme 18: Two literature adapted syntheses to new NqnDN* 5.

For direct synthesis of NqnDN* 5, diiminosuccinonitrile (DISN) is converted with the amine **XXXII** under acidic conditions, using $\text{CF}_3\text{CO}_2\text{H}$ as solvent.^[144] DISN was freshly prepared by the oxidation of DAMN using DDQ, but maximum yields of 15% were obtained.^[145] In the same way, the analogue of **5**, the non-alkyl substituted azanaphthalonitrile NqnDN, was synthesised in literature.^[146,147] In the reaction of **XXXII** with DISN, a cyclic intermediate is formed by the elimination of two equivalents of ammonia to yield the substituted 2,3-dicyanoquinoxaline NqnDN* 5. Under neutral conditions, hydrogen cyanide is the better leaving group, forming another 2,3-diaminoquinoxaline. This compound could be used as a precursor for anthracene derivatives.

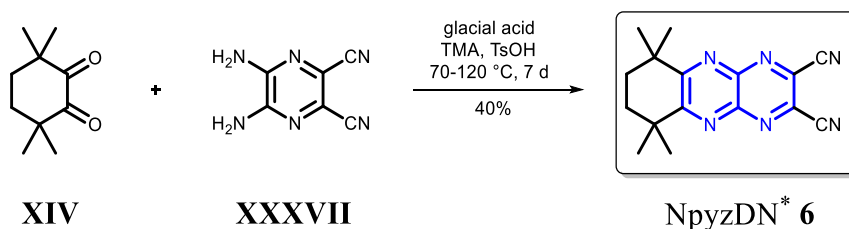
Because of the unsatisfying overall yield, toxic reagents, and partly expensive synthesis, a different route was attempted (Scheme 19). 1,1,4,4-tetramethyltetraline (**XXXV**) is formed in a FRIEDEL-CRAFT alkylation in benzene with 53% yield. After nitration with HNO_3 in H_2SO_4 , the dinitrated product **XXXVI** is formed, which can be reduced with H_2 over Pd/C in a Parr bomb.^[148] The nitration of **XXXV** was also carried out in glacial acid anhydride, but here only the mono-nitrated product was obtained. Compared to the reduction with Fe/HCl (Scheme 18), the reduction with H_2 is much more efficient with >81% yield, and workup is easier. Compound **XXXII** can be converted to NqnDN* 5 using both reaction pathways described above, pictured

in Scheme 18. In summary, the second route to NqnDN* **5** is much easier and better yields of the diamine of >25% over 4 steps were obtained. An upscaling of the reaction is also possible.



Scheme 19: Alternative synthesis of NqnDN* **5**.

The most electron deficient naphthalopyrazinoporphyrazinenitrile, NpyzDN* **6**, was prepared by using the commercially available 5,6-diaminopyrazine-2,3-dicarbonitrile (**XXXVII**). In a first attempt, 5,6-diaminopyrazine-2,3-dicarbonitrile (**XXXVII**) was converted with 3,3,6,6-tetramethylcyclohexane-1,2-dione (**XIV**) in glacial acetic acid (Scheme 20), similar to the synthesis of PyzDN* **2**.



Scheme 20: Synthesis of NpyzDN* **6**.

The yield of 17% indicates an incomplete conversion of the dione **XIV**. By addition of triethyl orthoformate (TEA) and longer reaction times of 7 d at 120 °C, the yield could finally be increased to 40%. TEA was added to the reaction to act as a water scavenger. Caused by a protonation at the nitrogen atoms, 5,6-diaminopyrazine-2,3-dicarbonitrile (**XXXVII**) is a weak nucleophile. Nevertheless, an incomplete reaction of the dione **XIV** was detected using NMR spectroscopy. Longer reaction times and autoclave conditions using higher temperatures may improve the conversion to NpyzDN* **6**. However, both educts could be recovered: the diamine **XXXVII** by filtration after the reaction, the dione **XIV** was macerated with hexane and separated by extraction (in hexane) from the NpyzDN* **6**. Complete conversion can be

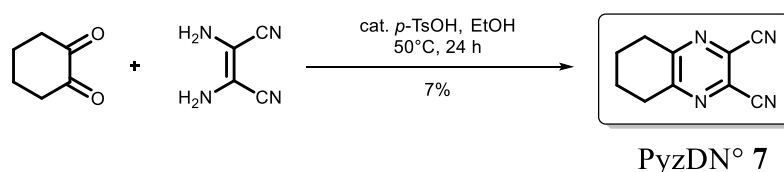
Results and Discussion

monitored by TLC by stirring both **XIV** and **XXXVII** in a 1:1 ratio for 10 d at 120 °C in glacial acid. But the yield could not be increased.

In this section, the first complete series of C_{2v} symmetrical azanaphthalonitriles, bearing alkyl groups in the peripheral position is described. Three new azanaphthalonitriles NpzDN* **4** and NqnDN* **5**, and NpyzDN* **6** were synthesised and characterized.

4.1.3 Synthesis of PyzDN°

In addition to the 2,2,5,5-tetramethylcyclohexane annulated azanitrils, a cyclohexane substituted pyrazine precursor **7** was synthesised (Scheme 21).^[149] The precursor was chosen because it should result in complexes with similar optical properties to complexes of PyzDN* **2** by virtue of its symmetry advantages.

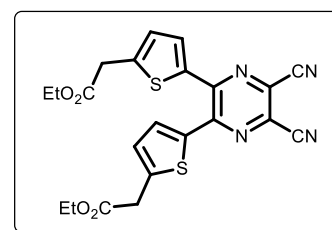


Scheme 21: Synthesis of PyzDN° 7.

Although the synthesis of PyzDN° **7** appears rather straightforward, in comparison to the condensation for PyzDN* **2**, the yield of 7% after column chromatography and recrystallization from DEE was quite low. Not many complexes have been reported in literature after the first synthesis by POPP.^[150] So far, only phthalocyanines derived from PyzDN° **7** specifically [Ppz°M] with M = Mg, Cu and Co are known, but none of these complexes were characterized sufficiently, because of the described low solubility in common organic solvent.^[133,149]

4.1.4 Synthesis of Thiophene Substituted PDNs

In an early stage of this thesis, it was attempted to reproduce the bithiophene substituted PDN^{TP} **8** for further cyclisation to a pyrazinoporphyrazine. The synthesis was previously described, but several attempts at cyclisation were unsuccessful.^[25] Interestingly, PDN^{TP} **8** shows by addition of a base a strong hypsochromic shift of the Q-band into the visible light area

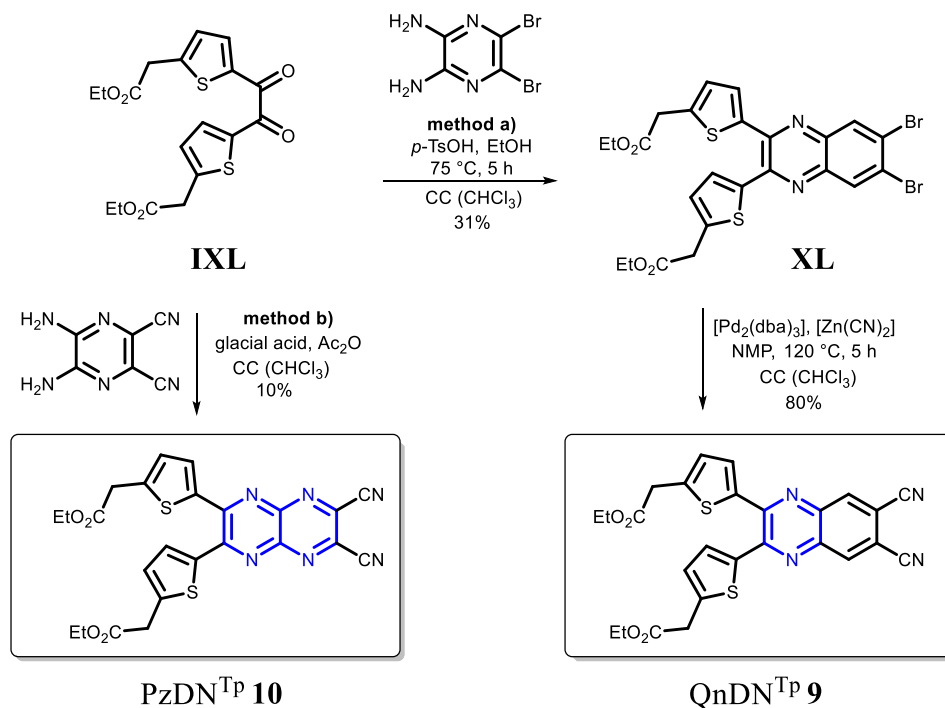


PDN^{TP} **8**

Figure 32: Literature known PDN^{TP} **8**.^[25]

(612 nm). The shift and strong colour is caused by the push-pull system after deprotonation of one of the acidic methylene groups.^[25]

The same was observed for its new larger homologues, QnDN^{Tp} **9** and PzDN^{Tp} **10**. According to the known procedure,^[25] thiophene dione **IXL**, obtained in a FRIEDEL-CRAFTS alkylation, reacts in a condensation reaction to the corresponding dinitrile **10**. Similar to the NpyzDN* **6**, PzDN^{Tp} **10** was obtained in lower yields of 10%. QnDN^{Tp} **9** was obtained in a palladium catalysed reaction of **XL** with [Zn(CN)₂] with yields of 25% over two steps.



Scheme 22: Synthesis of new thiophene substituted naphthalonitriles QnDN^{Tp} **9** and PzDN^{Tp} **10**.

In the UV-Vis spectrum of QnDN^{Tp} **9** and PzDN^{Tp} **10** a similar behaviour was observed, as for the smaller homologue: After addition of a drop dbu, a bathochromic shift from 416 nm to 627 nm for QnDN^{Tp} **9**, and from 322 nm to 572 nm for PzDN^{Tp} **10** was observed.

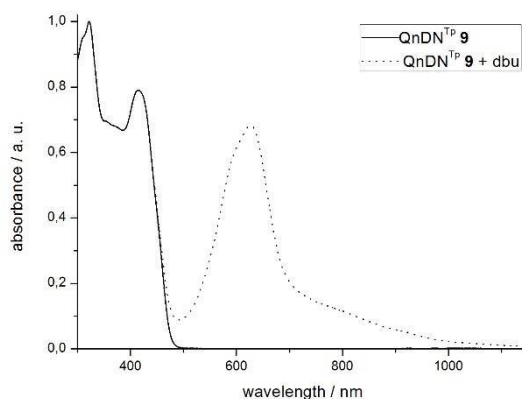


Figure 33: UV-Vis absorption spectra of QnDN^{Tp} **9** (straight line) and the spectrum after addition of a drop dbu (dotted line), measured in DCM, at rt.

4.2 Synthesis of Azaphthalocyanines and Derivatives

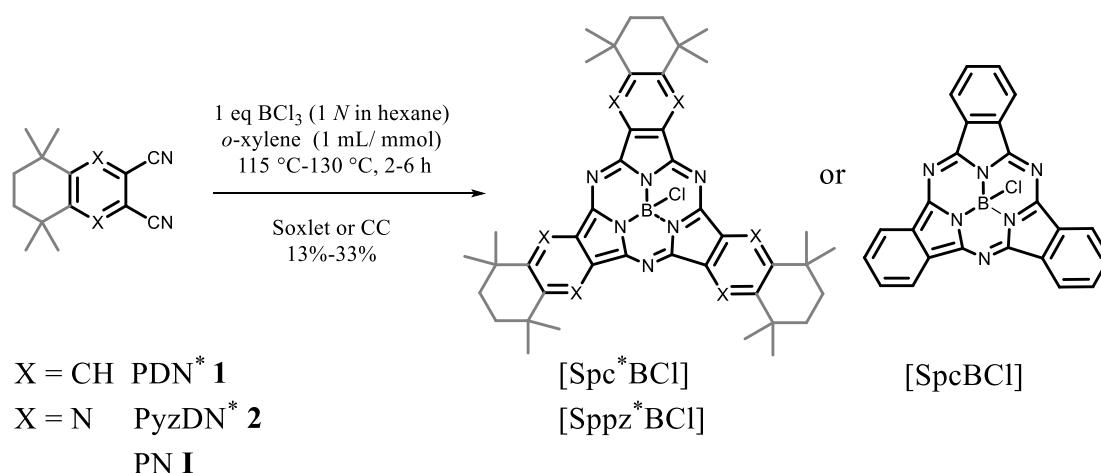
The general topic of this section is about symmetrical azaphthalocyanines, and their derivatives, such as azasubphthalocyanines and the larger azanaphthalocyanines. In addition, symmetrical subphthalocyanines and axially substituted subphthalocyanines are discussed.

4.2.1 Synthesis of Symmetrical Subphthalocyanines

4.2.1.1 Synthesis and Structural Properties of [Spc*BCl] and [Sppz*BCl]

Phthalocyanines [PcM] are one of the most investigated class of synthetic dyes.^[12,128] In recent years, research was also focussed on the investigation of the smaller ring-contracted phthalocyanines with only three isoindoline units, the so-called subphthalocyanines (Spcs). Because of different optoelectronic properties, these compounds are used for more than just ring expansion to obtain phthalocyanines in synthesis.^[45] Described applications^[128] range from light emitting diodes (LEDs),^[151-155] sensors,^[156] organic field effect transistors (OFETs),^[157] solar cells,^[158,159,160] and others. Just recently, a fullerene-free bilayer solar cell with 8.4% efficiency was described, using a subnaphthalocyanine/subphthalocyanine mixture as donor material.^[161]

[SpcBCl] was first described by MELLER and OSSKO in 1972 when they tried to synthesise a boron(II)phthalocyanine.^[162] Years after, the synthesis is still quite similar, using BCl₃ in a high boiling solvent such as CNP – see Scheme 23. In 2007, CLAESSENS *et al.* described the mechanism of the subphthalocyanine formation by isolating a trimeric boron(III)-intermediate and by performing quantum-chemical computations.^[163] In this work, the synthesis was carried out with the substituted dinitriles PDN* **1** and PYZDN* **2**.^[25]



Scheme 23: Synthesis of [SpcBCl], [Spc*BCl], or [Sppz*BCl].

Both compounds, [Sp^c*BCl] and [Sp^z*BCl], were synthesised in a similar way to the reaction described in literature, however, profiting from the solubility and symmetry advantages described in section 4.1.^[13] The high boiling solvent CNP was substituted with toluene or *o*-xylene. A similar aromatic solvent with high boiling point was chosen to prevent light induced molecular chlorination of the product in a FRIEDEL-CRAFTS type reaction.^[163] Reaction conditions were not optimised, but adjusted to literature recommended conditions for synthesis of [Sp^cBCl]. The solutions were stirred at about 130 °C in a Teflon valve equipped flask with 3 eq BCl₃ per intended Sp^c.^[164] Yields of up to 13% for [Sp^c*BCl] and 33% for [Sp^z*BCl] could be obtained.

In the ¹H NMR spectra of [Sp^c*BCl] (Figure 34) the typical low-field shifted aromatic protons at 8.84 ppm are visible, which is caused by the electronic conjugation, and electron density of the π -ring.

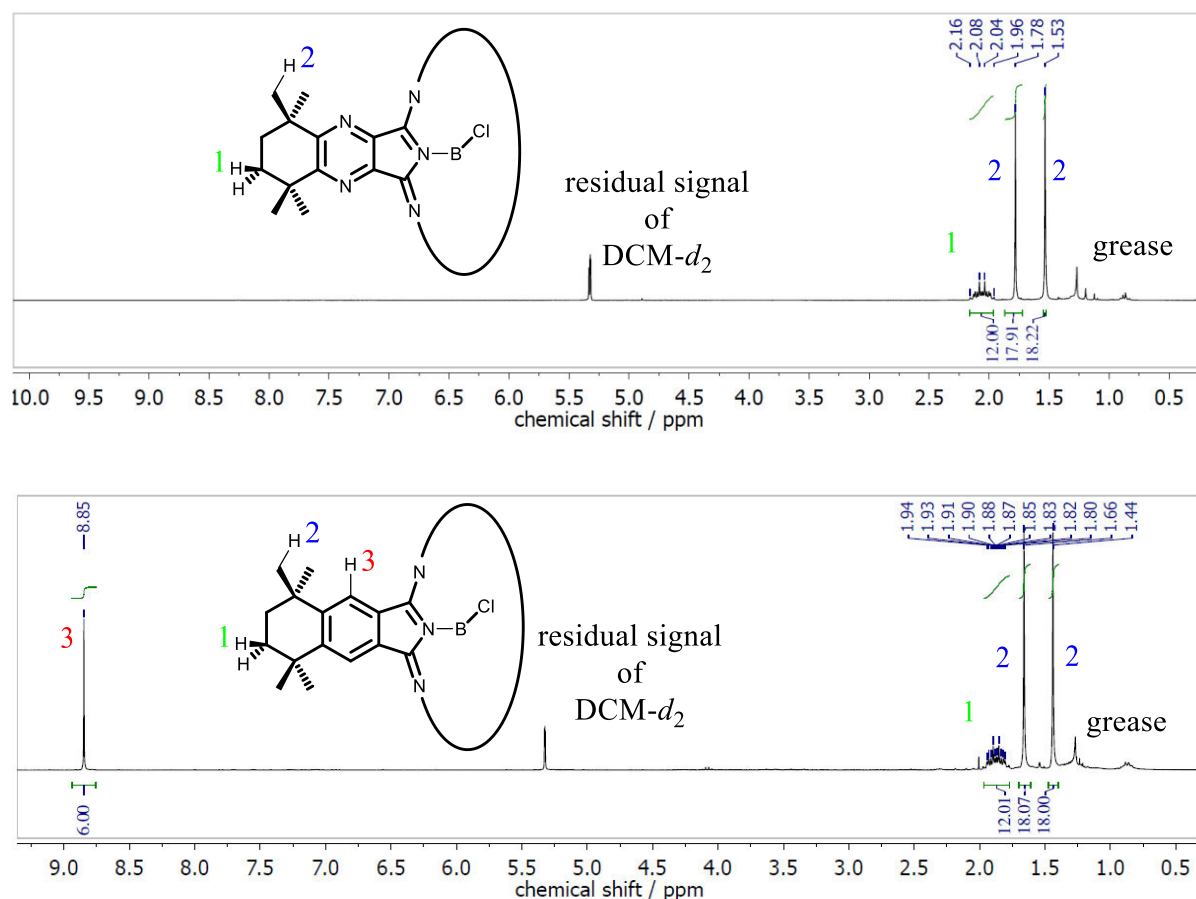


Figure 34: ¹H NMR spectrum of [Sp^z*BCl] (upper) and [Sp^c*BCl] (lower), in DCM-*d*₂ (300 MHz).

The low-field shift of the aromatic protons is not so strong compared to other known phthalocyanines, e. g. Pc^{*}H₂ with about 9.98 ppm, shown in section 4.2.3.1. Furthermore, the

Results and Discussion

alkyl groups of $[\text{Sp}^*\text{BCl}]$ are split, and the methylene groups show a multiplet at 1.80-1.94 ppm. The same was observed for $[\text{Sp}^*\text{pzBCl}]$, shown in the upper spectrum (Figure 34). In comparison, a low-field shift of methylene and methyl groups can be clearly seen. The split of the alkyl groups is caused by the concave shape of the $[\text{Sp}^*\text{BCl}]$ and $[\text{Sp}^*\text{pzBCl}]$, respectively, evident in the crystal structure of $[\text{Sp}^*\text{BCl}]$.

Crystals for X-ray analysis were obtained from a saturated DCM- d_2 solution. The result of XRD analysis is shown in Figure 35. The crystal structure verifies the cone shaped form of these subphthalocyanines, as well as the distorted chair conformation of the 2,2,5,5-tetramethylcyclohexane rings. The sp^3 -boron atom of $[\text{Sp}^*\text{BCl}]$ is (almost undistorted) tetrahedrally surrounded by three nitrogen atoms of the isoindoline units, and one axial chlorine atom. Considering this, the methylene groups

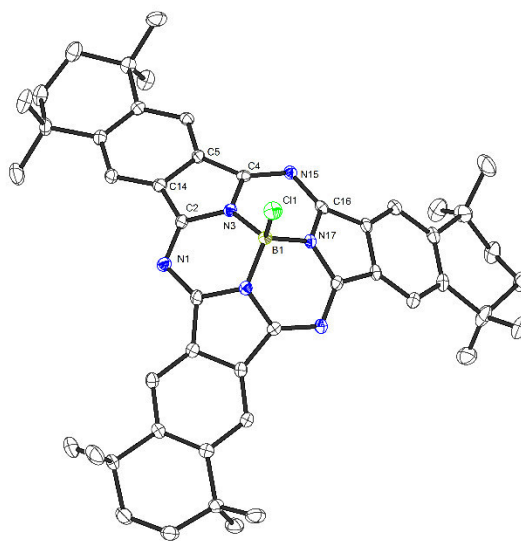


Figure 35: Molecular structure of $[\text{Sp}^*\text{BCl}]$ in crystal.

can be split in an upper and a lower group, while the lower one faces into the ‘inner sphere’ of the core, and the other is above, or on the ‘outer sphere’ of the core, visible in Figure 36 B.

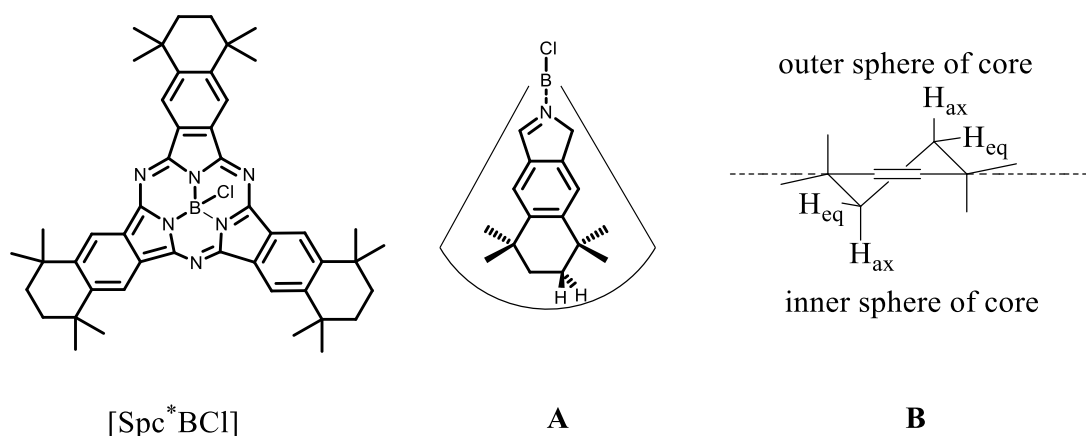


Figure 36: Structure of $[\text{Sp}^*\text{BCl}]$. Adapted from literature.^[13]

With this, both methyl groups have a different electronic surrounding, which explains the splitting of the signals in the ^1H NMR spectrum. The distorted, annulated 2,2,5,5-tetramethylcyclohexane ring in chair conformation splits the methylene protons additionally.

Selected crystallographic data are collected in Table 2 and compared to the known [SpcBCl]. Owing to symmetry reasons, the carbon atoms of one pyrrole unit are given with only 50% probability. Apart from the fact that the 2,2,5,5-tetramethylcyclohexane rings have a chair conformation, [Spc*BCl] has a 3m symmetry, whereby the B-Cl vector is the rotation axis of the molecule. The B-Cl bond matches quite well with other literature known B-Cl single bonds (1.87 Å)^[165] or with the distance of dimeric [BCl₂(NMe₂)] (1.83 Å),^[166] as described by KIETAIBL.^[167] The cone shaped structure is contrary to the aromatic system, but the conjugated 14 π -electron HÜCKEL system still shows a quasi-aromatic character.

Table 2: Selected bond length (Å) and -angles (°) of [Spc*BCl] and [SpcBCl].^[167]

	[Spc*BCl]	[SpcBCl] ^[167]
B1-Cl1	1.853(4)	1.863(7)
B1-N1	1.480(3)	1.466(8)
B1-N3	1.479(4)	1.468(5)
B1-N5	1.480(3)	1.466(8)
N1-B1-Cl1, N3-B1-Cl1, N5-B1-Cl1	112.2(2), 115.7(2), 112.2(2)	113.8(1), 112.8(1), 113.8(1)
N1-B1-N3, N3-B1-N5, N1-B1-N5	105.4(2), 105.0(3), 105.4(2)	105.1(1), 105.3(0), 105.3(0)
φ_{pyrrole}	44.2	43.1-44.3

φ_{pyrrole} : angle between inclined planes of pyrrole units.

The cone shaped structure only leads to a weaker overlapping of the p-orbitals. The large π -system also explains the shortened B-N bonds of the pyrrole unit, which normally are in the range of about 1.56-1.64 Å.^[166,168] A larger B-N bond would lead to a higher distortion of the aromatic system, but this would be sterically more hindered. In Figure 37, the molecular arrangement of the [Spc*BCl] is shown. Alternating stacks of two different orientations allows for the maximum amount of interaction between the π -system of the Spcs.

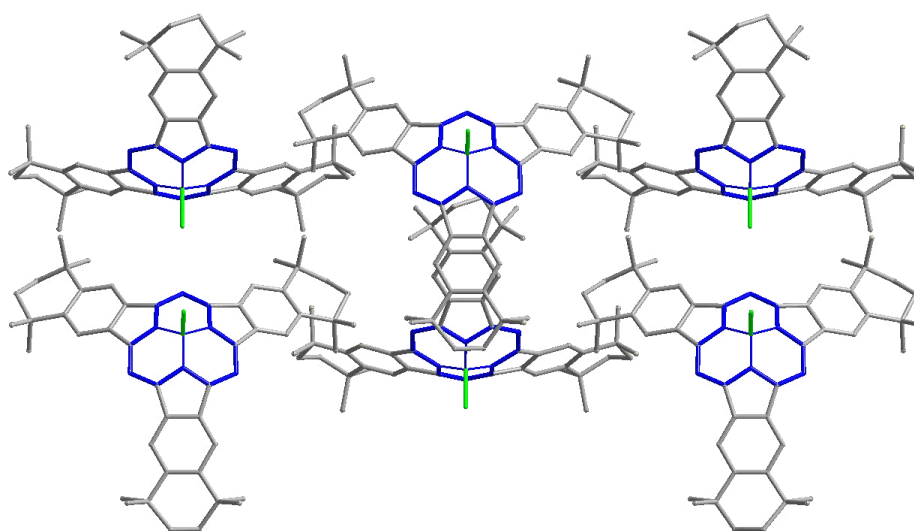


Figure 37: Molecular arrangement of [Spc*BCl]. Solvent molecules and disordered mesityl groups are omitted for clarity.

Results and Discussion

In Figure 38, literature known molecular arrangements of Spcs in the solid state are shown.^[128]

In comparison to these observed molecular packing motifs, the [Spc*BCl] has an, up to now, unknown arrangement, probably caused by the sterically demanding alkyl groups, minimizing the π - π interaction of the isoindoline units. As Figure 37 illustrates, the [Spc*BCl] has a head to head orientation regarding the mutual arrangement of isoindoline units in space.^[128] In contrast to the

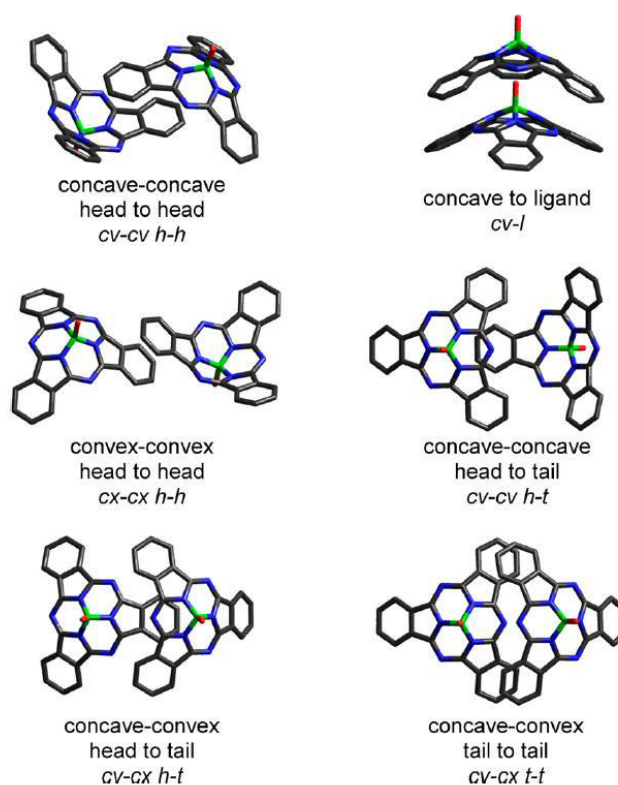
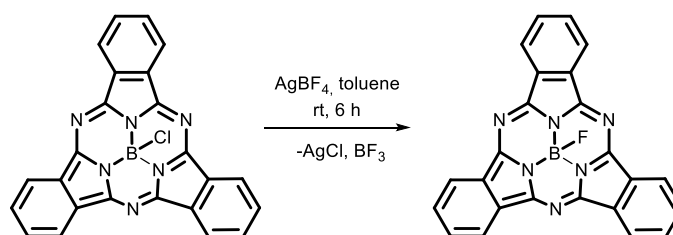


Figure 38: Observed arrangements of Spcs in the solid state. Adapted from literature.^[128]

head to head formations (Figure 38) cv-cv and cx-cx, [Spc*BCl] seems to form a concave-convex pair. It is important to investigate subphthalocyanines, and phthalocyanines in general, with regard to their lattice structure, to optimise physical applications (Introduction 2.2).

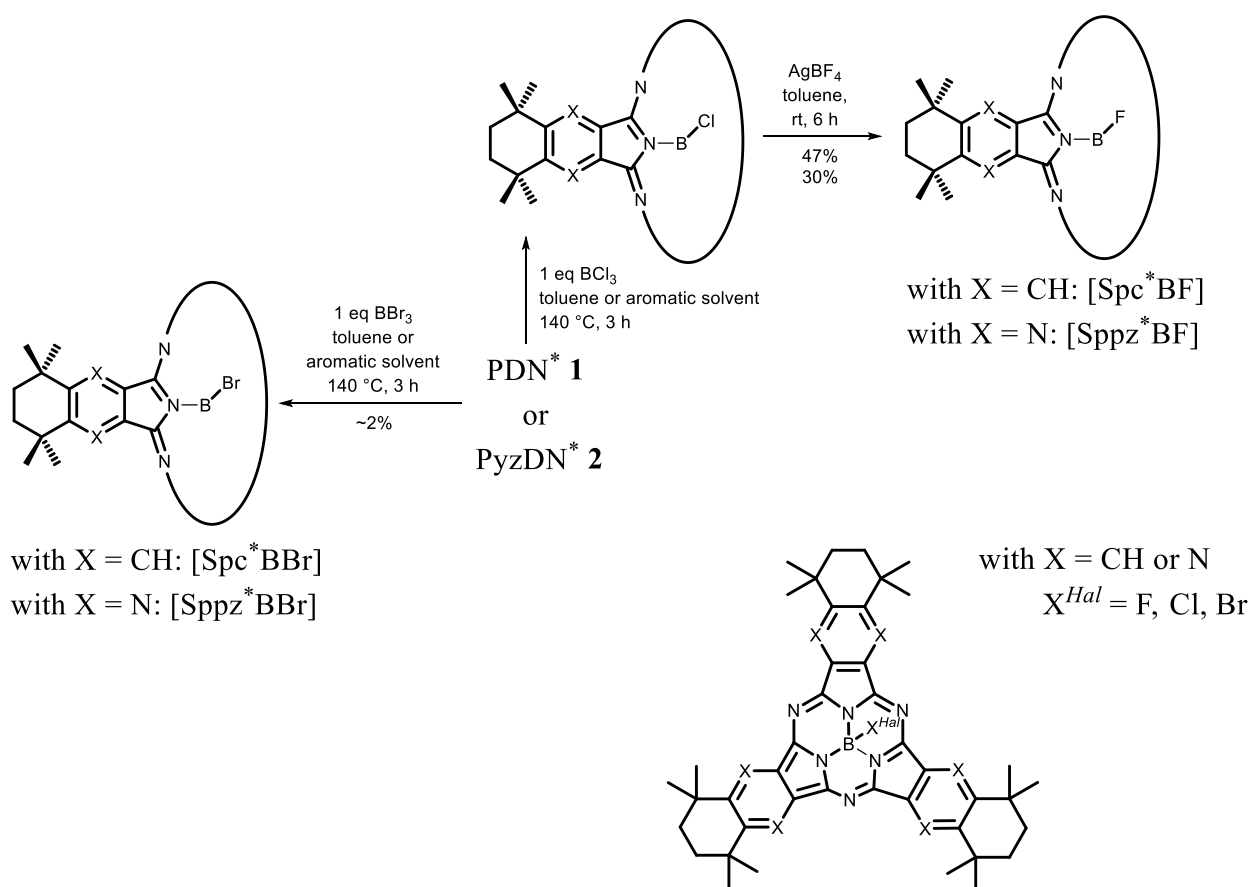
4.2.1.2 Halogen Substituted Subphthalocyanines [Spc*BX] and [Sppz*BX]

In addition to the known [Spc*BCl] and [Sppz*BCl], axial halogen substituted analogues were synthesised. The axial substitution of subphthalocyanines is interesting because of the effect this has in altering the materials dipole behaviour on different semiconductor surfaces. With the axial substituent, a fine tuning of the Q-band can be accomplished, because of its weak influence on the π -system and subsequently the Q-band position.^[169,170] The halogen substituted analogues were obtained following the synthesis of TORRES *et al.*: [SpcBF] was synthesised from [SpcBCl] using AgBF_4 (Scheme 24).^[169,170]



Scheme 24: Synthesis of [SpcBF].^[169,170]

In literature, the synthesis of [SpcBBr] was carried out similarly to the synthesis of [SpcBCl] using 1 eq of PDN **1** and 1 eq BBr₃.^[171] Following these synthetic strategies, the two axially equatorially alkyl substituted subphthalocyanines, [Spc*BF] and [Spc*BBr], were obtained in 47%, starting from [Spc*BCl], and in 2% yield starting from PDN* **1** and BBr₃. The length of the B-halogen bonds of [SpcBX^{Hal}] increases constantly as the size of the halogen atom increases, from B-F (1.39 Å)^[172] to B-Br (2.05 Å).^[173] As expected, the B-Br bond is the weakest bond, which explains the low yields, caused by a decrease in the stability of [Spc*BX^{Hal}] with X^{Hal} = F → Br. In mass spectrometry, no high resolution mass spectrum of [Spc*BBr] was obtained. Here, only the fragments [Spc*B]⁺ and methoxy compound [Spc*BOMe]⁺ were observed. The synthesis of a [Spc*BI] could not be accomplished. All structures were identified by using ¹H and ¹¹B NMR spectroscopy. In addition, subpyrazinoporphyrazines [Sppz*BX^{Hal}] with X^{Hal} = F, Cl, Br were synthesised in yields of 30%, 35% and 2% following the same synthetic strategies as mentioned above. In comparison to [Spc*BCl], [Sppz*BCl] was crystallized by SEIKEL in a concave to ligand cv-*I* arrangement (Figure 38). It is the first XRD structurally characterised subpyrazinoporphyrazine, [SppzBCl].^[25] All synthesised compounds are summarised in Scheme 25.



Scheme 25: Synthesised Spcs and Sppzs with different axial halogen atoms.

Results and Discussion

Besides the crystal structure of [Sp^c*B^{Cl}] and NMR experiments, all obtained [Sp^c*B^{X^{Hal}}] and [Sp^{pz}*B^{X^{Hal}}] were characterized by UV-Vis and FS spectroscopy. Similar to phthalocyanines, these complexes have a significant Q-band, which is hypsochromically shifted compared to the one of Pcs. This hypsochromic shift is caused by the non-planar π -system of the [Sp^cB^{Cl}]. Compared to [Sp^cB^{Cl}] (565 nm), the substituted [Sp^c*B^{X^{Hal}}] show a bathochromic shift, while [Sp^{pz}*B^{X^{Hal}}] are hypsochromically shifted. In comparison to Sp^cs, the subpyrazinoporphyrazines (Sp^{pz}s) do not show any shift of the Q-band when the axial halogen atom is exchanged, as summarised in Table 3. This may result from the more electron deficient π -system of the porphyrazine.

Table 3: UV-Vis absorption of [Sp^c*B^{X^{Hal}}] with X^{Hal} = F, Cl, Br in comparison (measured in DCM).

	Q-band / nm	B-band / nm
[Sp ^c *B ^F]	577	320
[Sp ^c *B ^{Cl}]	582	318
[Sp ^c *B ^{Br}]	578	319
[Sp ^{pz} *B ^F]	534	333
[Sp ^{pz} *B ^{Cl}]	534	334
[Sp ^{pz} *B ^{Br}]	534	313

Further optical and photophysical properties will be discussed in section 4.2.4.1, where azasubphthalocyanines are described. But the similarity of the UV-Vis absorptions of axial functionalised subphthalocyanines and subpyrazinoporphyrazines might be explained when the crystal structures of [Sp^c*B^{Cl}] is compared with analogues, such as [Sp^c*B^F].

4.2.1.3 Molecular Structure of [Spc*BF] in Comparison of [Spc*BCl]

Suitable X-ray crystals of [Spc*BF] were obtained from a saturated DCM- d_2 solution. The molecular structure is shown in Figure 39. Besides the reaction progress monitored by using TLC, ^{19}F NMR spectroscopy was used to observe the exchange of Cl by F with AgBF_4 . Similar to the structure of [Spc*BCl], the three pyrrole units show a cone shaped form. [Spc*BF] shows the same molecular arrangement and 3m symmetry as [Spc*BCl]. The space group $\text{Cmc}2_1$ is the same. Both compounds are isostructurally related.

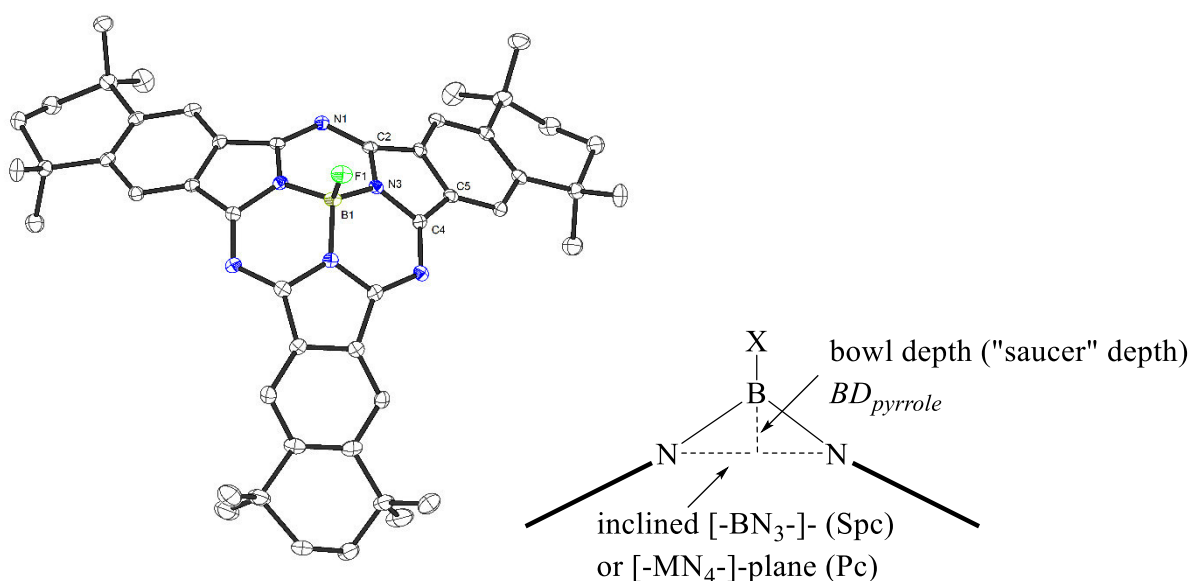


Figure 39: Molecular structure of [Spc*BF] in crystal.

In Table 5, selected crystallographic data of both crystal structure analyses of [Spc*BCl] and [Spc*BF] are compared, in Table 4 bond length and relevant determined values. The average B-X^{Hal} bond distance of [Spc*BX^{Hal}] is lengthened from $\text{B-X}^{\text{Hal}} = \text{F}$ (1.397 Å) to Cl (1.853 Å).

Table 4: Selected bond length (Å) and -angles (°) of [Spc*BCl], [Spc*BF] and [SpcBCl].^[167]

	[Spc*BCl]	[Spc*BF]	[SpcBCl] ^[167]
B1-X1	1.853(4)	1.396(6)	1.863(7)
B1-N1	1.480(3)	1.487(4)	1.466(8)
B1-N3	1.479(4)	1.478(6)	1.468(5)
B1-N5	1.480(3)	1.487(4)	1.466(8)
N1-B1-C11, N3-B1-C11, N5-B1-C11	112.2(2), 115.7(2), 112.2(2)	113.6(2), 113.6(2), 113.6(2)	113.8(1), 112.8(1), 113.8(1)
N1-B1-N3, N3-B1-N5, N1-B1-N5	105.4(2), 105.0(3), 105.4(2)	104.8(3), 105.2(4), 104.8(3)	105.1(1), 105.3(0), 105.3(0)
BD_{pyrrole}	0.56	0.60	0.57
φ_{pyrrole}	44.2	45.2	43.1-44.3

φ_{pyrrole} : angle between inclined planes of pyrrole units.

For all three compounds, the values obtained for the angles of inclined planes of pyrrole units, φ_{pyrrole} are comparable, with $\varphi_{\text{pyrrole}} = 45^\circ$.

Results and Discussion

φ_{pyrrole} is an important value for the deviation of the planarity resulting from the sum of all three N-B-N angles, which are about 105° each. The bowl depth (sometimes known as "saucer" depth, Figure 39), BD_{pyrrole} , was determined as a value for the distance of the central boron(III) atom to the pyrrole plane $[-\text{BN}_3-]_{\text{pyrrole}}$. For subphthalocyanines, as well as for phthalocyanines, it is a significant value to determine variations of the central metal atom compared to the aromatic system $[-\text{BN}_3-]_{\text{pyrrole}}$, or $[-\text{MN}_4-]_{\text{isoindoline}}$, respectively. Therefore, the central metal atom is shifted "out-of-plane". All BD_{pyrrole} are, with $BD_{\text{pyrrole}} \sim 0.59$, in the expected range for subphthalocyanines.^[174] Both values, BD_{pyrrole} and φ_{pyrrole} , give useful information about the concave nature of the phthalocyanine relative, as a deviation of the planarity, which is, in case of these subphthalocyanines, quite distinctive. The average value for C-C bonds in the annulated aromatic benzene rings is within the expected length for a benzene ring of 1.395 \AA .^[167,175]

Table 5: Selected crystallographic data for $[\text{Sp}^*\text{BCl}]$ and $[\text{Sp}^*\text{BF}]$.

Formula	C48 H54 B1 Cl1 N6	C48 H54 B1 F1 N6
Formula weight	726.26	829.70
Crystal system	Orthorhombic	Orthorhombic
Space Group	Cmc ₂₁	Cmc ₂₁
Unit cell dimensions		
a / \AA	24.8236(10)	24.5288(15)
b / \AA	16.3090(6)	15.7219(8)
c / \AA	10.9728(4)	11.4144(6)
α / deg	90	90
β / deg	90	90
γ / deg	90	90
Volume / \AA^3	4442.3(3)	4401.8(4)
Z	4	4
Density (calc.) / mg/m^3	1.265	11.252
Absorption coef. / mm^{-1}	0.22 x 0.22 x 0.09	0.16 x 0.14 x 0.12
Reflections collected	28577	22775
Independent reflections	4177	3922
R(int)	0.0342	0.0792
wR ₂ (all data)	0.0754	0.0845
R ₁ (I > 2 σ (I))	0.0293	0.0386

4.2.1.4 Synthesised Subnaphthalocyanines

While the synthesis and electrochemical properties of azasubporphyrins, subphthalocyanines and subnaphthalocyanines, their fused dinuclear species and mixed complexes are well known in literature,^[176] no examples are given in which the nitrogen atoms are systematically exchanged. In addition to the discussed and previously described subphthalocyanines, $[\text{Sp}^*\text{BCl}]$ and $[\text{Sp}^*\text{BF}]$, a first attempt was carried out to synthesise larger homologues, using the same literature known conditions. Also, PyzDN° **7** was tested in a cyclotrimerisation reaction with BCl_3 , but no formation of a subphthalocyanine could be observed either in

UV-Vis spectroscopy or mass spectrometry. In case of the subnaphthalocyanines, a $[\text{Snc}^*\text{BCl}]$ and $[\text{Snpz}^*\text{BCl}]$ complex could be obtained using the π -system extended azanaphthalonitriles **3** and **5** (Figure 40). Thereby, in the synthesis of $[\text{Snc}^*\text{BCl}]$, a change in colour to violet could be observed as it is typical for ring contracted subphthalocyanines.^[162] Different attempts of purification were carried out, but always a loss of colour and a degradation of $[\text{Snc}^*\text{BCl}]$ was observed, even by filtration under an inert atmosphere. In contrast, $[\text{Snpz}^*\text{BCl}]$ seems to be reasonably stable and was purified by column chromatography.

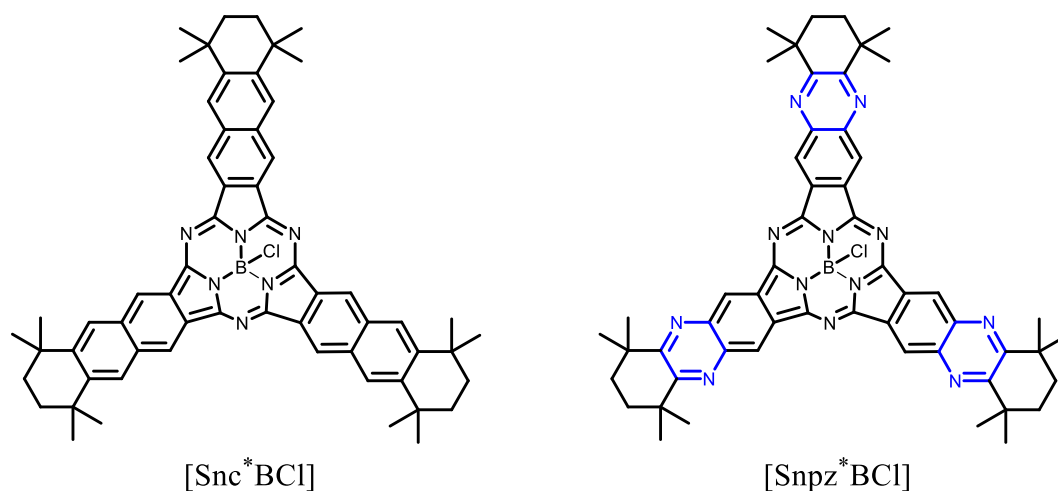


Figure 40: New subnaphthalocyanines $[\text{Snc}^*\text{BCl}]$ and azasubnaphthalocyanine $[\text{Snpz}^*\text{BCl}]$.

Compared to the other subphthalocyanines described in the preceding section, the Q-band is hypsochromically shifted to >700 nm, which is why the compound appears green. While the methylene and methyl protons have a comparable shift and splitting, the aromatic protons of $[\text{Snpz}^*\text{BCl}]$ (9.65 ppm) are low-field shifted compared to $[\text{Spc}^*\text{BCl}]$ (8.91 ppm), as visible in ^1H NMR spectrum (in C_6D_6 , 300 MHz). This is caused by the enlarged π -system of the subnaphthalocyanine. The shifted Q-band, the stability and solubility makes the $[\text{Snpz}^*\text{BCl}]$ an attractive compound with regard to its use in bulk heterojunction solar cells. Even in combination with other introduced subphthalocyanines, the compound is interesting as a donor material. One example is the before mentioned communication of 2014 by HEREMANS *et al.*, who described the application of $[\text{SpcBCl}]$ and $[\text{SncBCl}]$ in solar cells.^[161]

4.2.2 NEXAFS and XPS Studies of [Spc*BCl]

The physical properties of [Spc*BCl] were further investigated by KOTHE (Department of Physics of the Philipps-Universität Marburg) by using AFM, XRD, NEXAFS and XPS experiments.^[177] [Spc*BCl] thin layer films were prepared on a β -quartz and a TiO₂ (rutile) surface at 322 K or 473 K. The obtained layers were assessed using UV-Vis spectroscopy and compared to solution UV-Vis spectra. In both preparations, in the beginning of the sublimation an impurity was observed. This is probably caused by the stability of the [Spc*BCl], which slowly degraded by oxidation to its derivatives, as described by WÖHRLE.^[85] The impurities did not show a high content of nitrogen, according to the suggested degradation mechanism. The impurities could be excluded by preparation of the layers at higher temperatures in the KNUDSEN cell.

The first layer, prepared at lower temperatures (substrate temperature of 322 K), did not show a higher crystalline order. In the case of preparing the sample at a higher temperature (473 K), angles of 28.1° and 28.4° were observed on quartz in XPS measurements (Figure 41). This indicates a lying orientation of [Spc*BCl] on the quartz. Higher order is visible in the AFM measurements, but compared to known Pcs, the crystallinity of the [Spc*BCl] is still low.

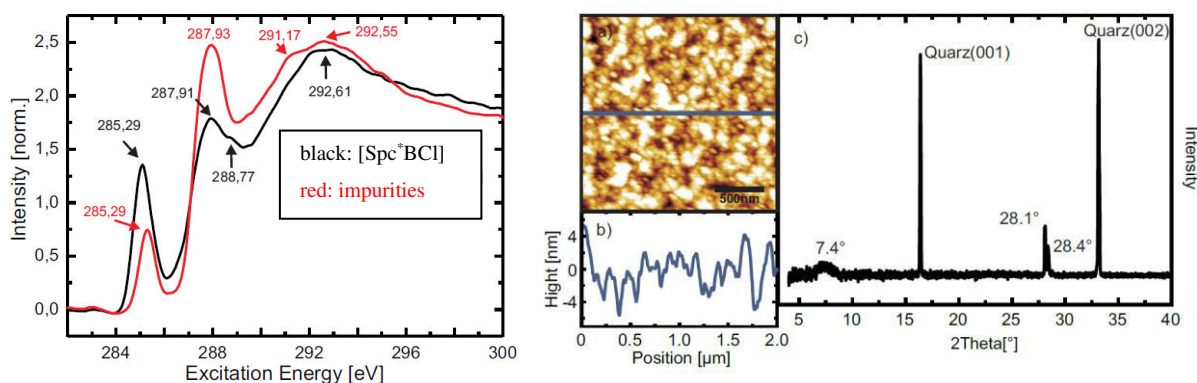


Figure 41: NEXAFS spectrum of [Spc*BCl] (left side), thin layer on quartz, 2 x 2 μm AFM measurement (a), right side) of evaporated layer. b) line scan of a). c) XPS measurement: peaks at 28.1° and 28.4° due to the thin film layer of [Spc*BCl].

Further investigation by XPS and NEXAFS measurements show quite a good carbon/nitrogen content with a 7.18:1 ratio, compared to the theoretical value of 8:1. After inelastic mean free path (IMFP) calculations, the value increases to a ratio of 7.53:1. On the quartz surfaces, boron and chlorine were observed in the sublimed layer, which additionally proves the intact formation of a [Spc*BCl] layer after sublimation. For further investigations, [Spc*BCl] will be characterized by the group of CHATTERJEE with a focus on the optical properties, as well as [SpcBOH] with a focus on PL properties in the group of HEIMBRODT.

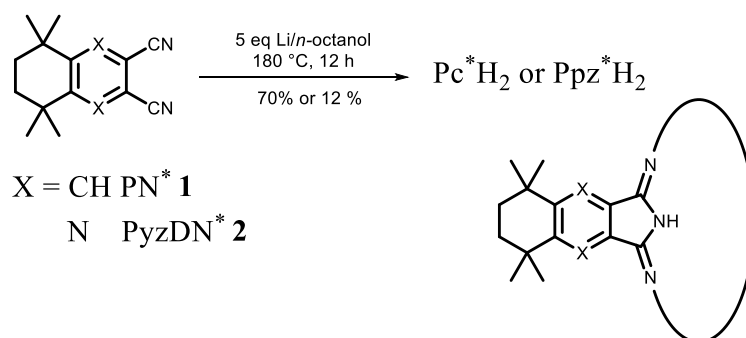
4.2.3 Synthesis of Phthalocyanines

In the first part of this main section, the synthesis of symmetrical A₄-type phthalocyanines is described. A more detailed description of synthetic strategies for lower symmetrical phthalocyanines is given in the theoretical section 2.1.3. Their synthesis is discussed in the second part of this section. These compounds were first described in the thesis of SEIKEL,^[25] but in order to understand the optical properties of these compounds, they were synthesised and isolated in larger amounts for additional analytic and spectroscopic investigations. For reasons of completeness and a better understanding, properties of these [A_nB_m]-type of azaphthalocyanines are discussed, following the preliminary work.

4.2.3.1 General Synthesis of Symmetrical Phthalocyanine Ligands and Metal Pcs

In comparison to subphthalocyanines, the phthalocyanine synthesis is in general easier and offers higher yields of up to 90%.^[12] Metallised phthalocyanines have in most cases a planar π -system, except when larger metal atoms are coordinated. If the metal cation does not fit into the ligand cavity, another effect is observed: the cation is coordinated with a characteristic distance d to the 4 N-plane, while the 4 isoindoline units are still almost coplanar, with respect to each other. In the case of phthalocyanines, this bowl depth, $BD^{\text{isoindoline}}$, is less distinctive than for subphthalocyanines (compare to 4.2.1.3, Figure 39). In some cases, a weak concave distortion, similar to [SpcBCl] derivatives, is observed (compare to section 4.5). Similar to the described subphthalocyanine [Spc*BCl] and its analogue subpyrazinoporphyrazine [Sppz*BCl], it is the electron density of the π -system that is the main difference of the phthalocyanine Pc*H₂ and the pyrazinoporphyrazine Ppz*H₂. This results in a hypsochromic shift of the pyrazinoporphyrazine Ppz*H₂ compared to the phthalocyanine Pc*H₂. Pc*H₂ was first described by MIKHALENKO *et al.*,^[24] and the electron poor Ppz*H₂ analogue by SEIKEL.^[70] MIKHALENKO *et al.* also described different metal phthalocyanines [Pc*M] with M = VO, Co, Zn, 2 H for the first time.^[24] The general synthesis of the two metal-free ligands Pc*H₂ and Ppz*H₂ is carried out at high temperatures using the respective dinitrile **1** or **2** at 180 °C in a Li/*n*-octanol solution (Scheme 26).

Results and Discussion



Scheme 26: Synthesis of Pc*H₂ and Ppz*H₂ ligands.

The nucleophilic alcohol attacks at the first dinitrile unit and an isoindoline scaffold is formed, further PDN is inserted until the dihydro-Pc precursor is completed. After the redox reaction, Li-phthalocyanine gets protonated by using H₃PO₄. Li₃PO₄, the solvent and by-products can be easily removed by macerating (washing) the phthalocyanine/pyrazinoporphyrazine with MeOH, or by column chromatography using PE/DCM. In comparison to the ¹H NMR spectrum of [Spc*BCl] (Figure 34), the ¹H NMR spectrum of Pc*H₂ (Figure 42) is easier to analyse: because of the planarity of Pc*H₂, the C₄ symmetry of the molecule is maintained, so only one singlet can be observed for the methyl and methylene protons. The aromatic protons are low-field shifted to 9.90 ppm, typical for phthalocyanines. Furthermore, the NH protons are influenced by the ring-current and appear high-field shifted at 0.00 ppm.

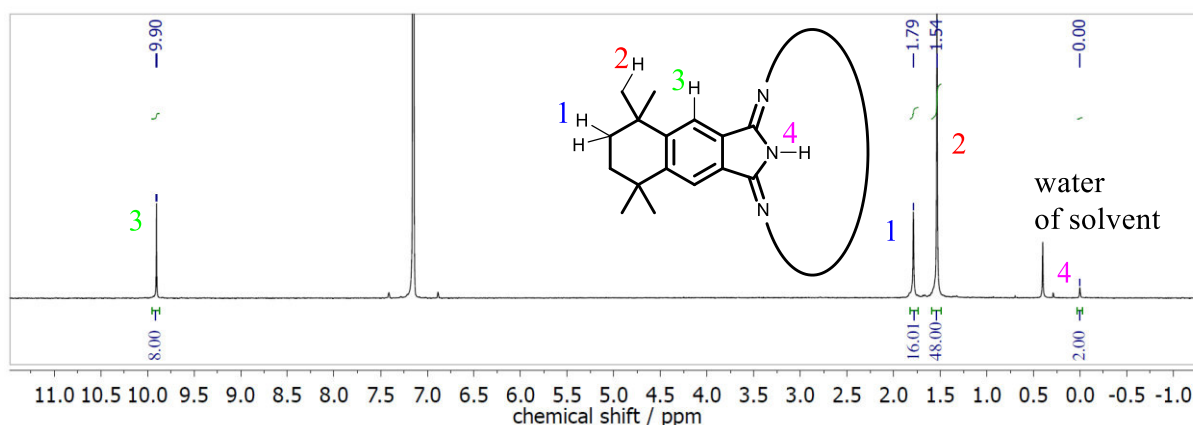


Figure 42: ¹H NMR spectrum of Pc*H₂, in C₆D₆ (300 MHz).

For the isolation of high purity samples, Pc*H₂ can be sublimed in vacuum without degradation whereas Ppz*H₂ decomposes at <400 °C. In an ongoing project, the cyclisation of NppzDN* **6** (Figure 31), after subliming it on a semiconductor surface, is investigated by the group of GOTTFRIED (Department of Chemistry of the Philipps-Universität Marburg) and compared to NDN* **3**. In contrast to already formed azanaphthalocyanines and pyrazinoporphyrazines, the sublimation of all dinitriles **1-6** is possible. With this, highly ordered films of Nppzs might be obtained, even if the on the surface formed [Nppz*M] is not sublimable.

In order to better understand the degradation point of these phthalocyanines, a TGA-DSC measurement of Pc^*H_2 (Figure 43) was carried out. It can be clearly seen how stable even alkyl substituted phthalocyanines are: the inflection point lies at almost 500 °C.

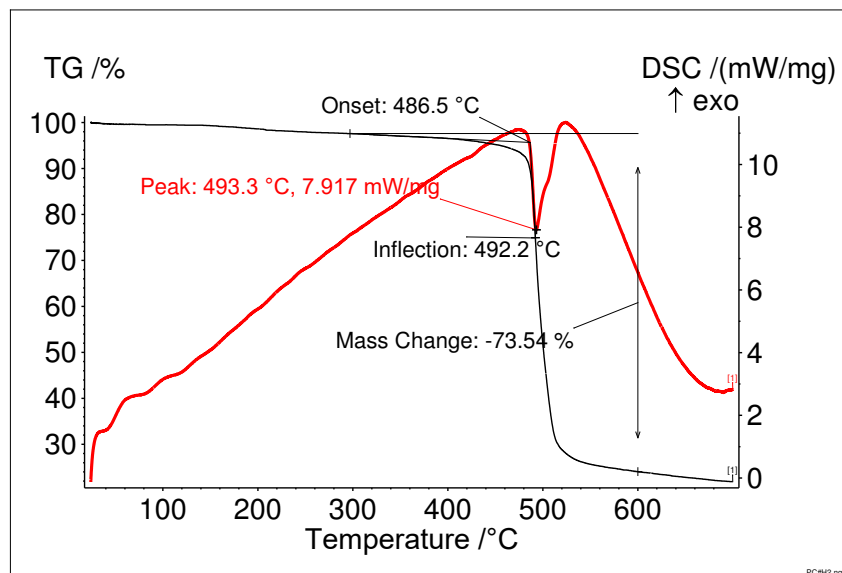
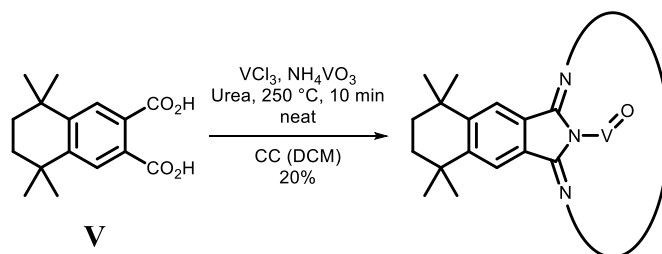


Figure 43: TGA-DSC measurement of Pc^*H_2 .

Access to symmetrical A_4 metal phthalocyanines of the $[\text{Pc}^*\text{M}]$ type is even simpler. In the theses of SEIKEL and BAYOUMI, the axially substituted $[\text{Pc}^*\text{TiCl}_2]$ was functionalised using catechol derivatives; other 3 *d* - metal complexes from Ti-Zn were also synthesised.^[25,133] In the synthesis of $[\text{Pc}^*\text{M}]$, a conversion of dicarboxylic acid **V** to the dinitrile $\text{PDN}^* \mathbf{1}$ is not needed, as described in section 4.1.1. The dicarboxylic acid **V** can be obtained in >80% over 3 steps. Using literature known procedures, compound **V** can be directly converted to a $[\text{Pc}^*\text{VO}]$, in only 4 steps, the last of which is shown in Scheme 27.^[178] Therefore, VCl_3 was used with an excess of NH_4VO_3 as “nitrogen source”.



Scheme 27: Synthesis of $[\text{Pc}^*\text{VO}]$.

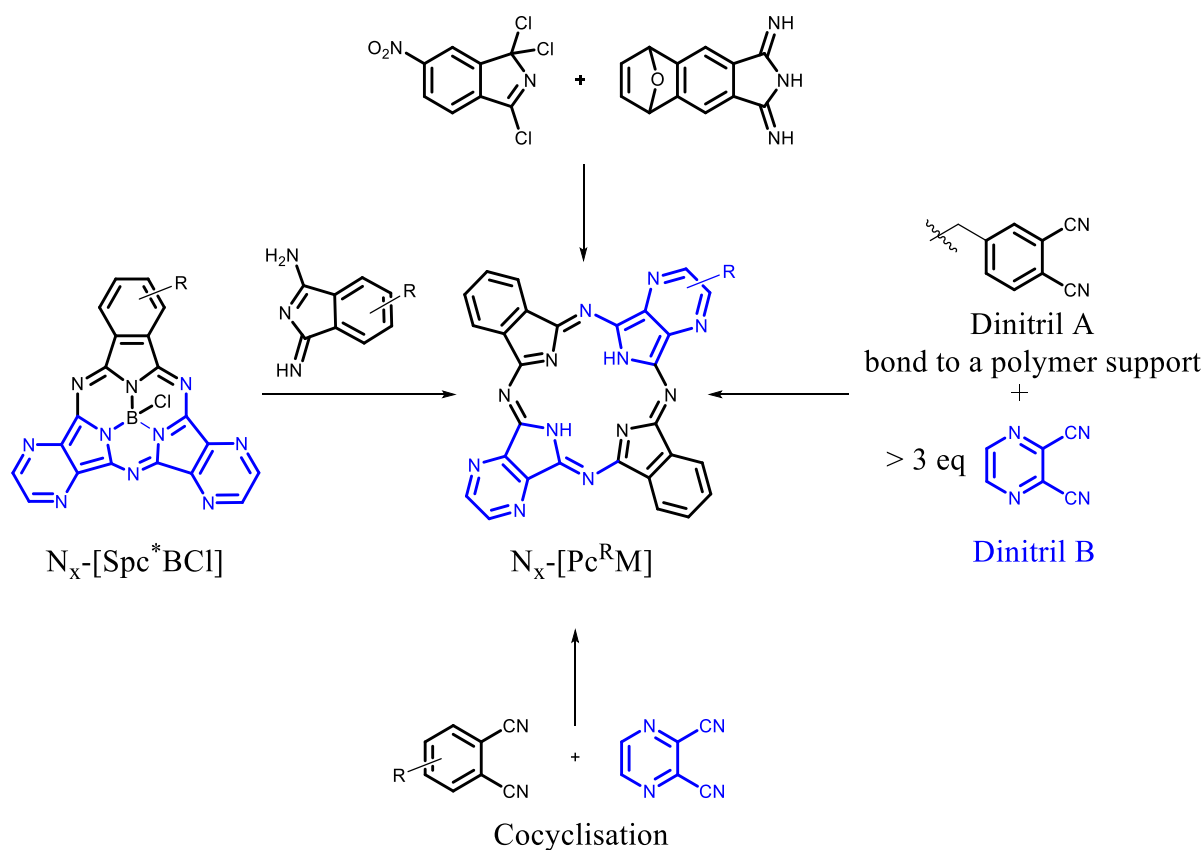
With regards to the yields of only 50%, obtained by BAYOUMI using $\text{PDN}^* \mathbf{1}$,^[133] this synthesis simplifies not only the access to $[\text{Pc}^*\text{VO}]$ but also the access to imido complexes of the type $[\text{Pc}^*\text{V}(\text{NR})]$. After filtration through silica, the $[\text{Pc}^*\text{VO}]$ was obtained in better CHN-purity as

Results and Discussion

described before. When the amount of glacial acid in the synthesis of **V** is increased, the anhydride **VI** is obtained. **VI** can also be used as a precursor for metal complexes. Other [Pc**M*] phthalocyanines and their syntheses are summarised in the work of BAYOUMI.^[133]

4.2.3.2 Synthesis of $[A_nB_m]$ -Type Azaphthalocyanines

In recent years, a huge number of symmetrical A_4 phthalocyanines has been described.^[12] Furthermore, the number of porphyrazine compounds is high, as well.^[161] More difficult is the synthesis of lower symmetrical phthalocyanines, visible in the limited number of publications (section 2.1.3).^[81,179] However, these compounds are interesting with regard to photophysical and optical properties when they are systematically studied. In literature, not many publications are found investigating the optical properties of azaphthalocyanine series and their larger homologues (Introduction 2.1.3).^[35,87] We were interested in the optical properties of azaphthalocyanines of lower symmetry of the type N_x -[Pc^{*}M] with M = 2 H, or Zn.



Scheme 28: Different accesses to $[A_nB_m]$ -type hybrid phthalocyanines.

Top: crossed condensation, right: polymer support based synthesis, left: KOBAYASHI ring expansion, bottom: cocyclisation.

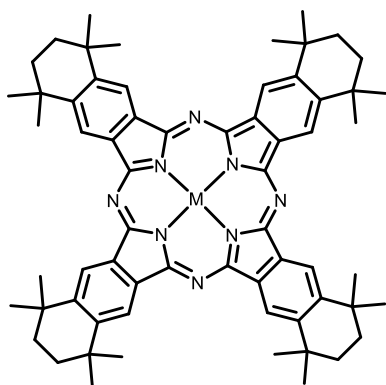
Different synthetic approaches (Scheme 28) of synthesising lower symmetrical Pcs of an $[A_nB_m]$ -type, are literature known.^[178,180] For the synthesis of A_3B phthalocyanines by using a polymer support, a functional group is needed, as shown on the right side (Scheme 28).^[38,39,181]

Access to ABAB phthalocyanines is possible by using two different dinitriles with contrary reactivity.^[42,182] However, there is controversy surrounding the discussions in recent literature concerning the described selectivity.^[180] The synthesis of A₂B₂ phthalocyanines is observed when one dinitrile preforms a dimeric species.^[30] On the left side in Scheme 28, a KOBAYASHI ring expansion is shown, using an asymmetrical subphthalocyanine to yield an ABAB phthalocyanine.^[45] The disadvantages of this method are generally low yields in the synthesis of subphthalocyanines, and their low stability, so isoindoline units of the degraded Spc may insert in a subphthalocyanine again and a product mixture is obtained. On the bottom, a random cocyclisation is shown. Here, a separation of sometimes more than 6 isomers has to be carried out depending on the substituents and the reactivity of the dinitriles.

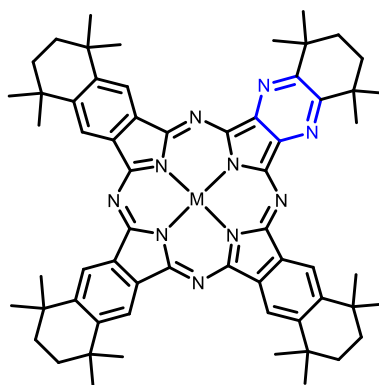
4.2.4 Synthesis of Azaphthalocyanines

To obtain azaphthalocyanines N_x-[Pc**M*] with M = 2 H or Zn, SEIKEL could synthesise the corresponding zinc-/azaphthalocyanines in a cocyclisation, using both dinitriles PDN* **1**/PyzDN* **2** in ratio 1:1, in a high boiling solvent such as CNP or quinoline.^[25] In this random cocyclisation, all compounds N_x-[Pc**M*] with x = 0, 2, 4, 6 and 8 (Figure 44) were obtained in a mixture excepted for the ABAB N₄-[Pc**M*]. As these compounds were not fully analysed previously, it was attempted to follow the synthetic strategy and to reproduce the N_x-[Pc**M*] series for complete characterisation and a more detailed photophysical investigation.

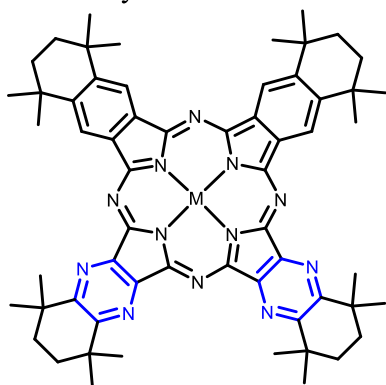
Therefore, N_x-Pc*H₂ and separately its A₄, and B₄ system, respectively, were synthesised. After gradient column chromatography, A₄Pc*H₂, A₃BN₂-Pc*H₂, A₂B₂N₄-Pc*H₂, AB₃N₆-Pc*H₂ and B₄Ppz*H₂ could be obtained in yields of 3-20%. Depending on the ratio of dinitriles, the yield can be "shifted" to the desired product. But in general, a favoured formation of A₂B₂N₄-Pc*H₂ was observed. All compounds were characterized by using ¹H and ¹³C NMR, IR, UV-Vis, FS spectroscopy, APCI-HR spectrometry and cyclic voltammetry (CV). Additionally, the compounds were investigated concerning their photophysical properties in cooperation with the group of ZIMČÍK and NOVÁKOVÁ (Department of Pharmacy at the Charles University of Prague). The results of singlet oxygen quantum yield, Φ_Δ, and fluorescence quantum yields, Φ_F, are discussed in the last part of this section.



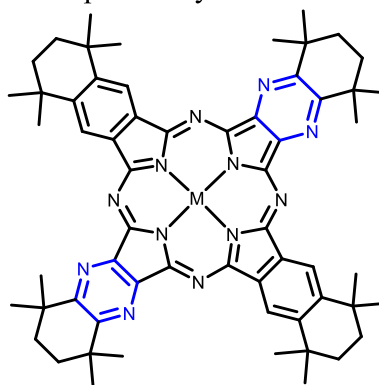
A_4 ; $[Pc^*M]$
Phthalocyanine with $M = 2 H, Zn$



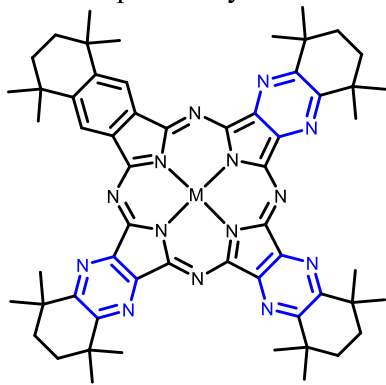
A_3B ; N_2 - $[Pc^*M]$
Diazaphthalocyanine with $M = 2 H, Zn$



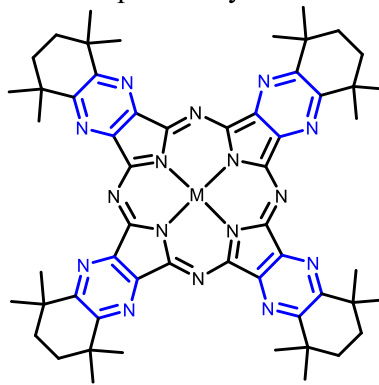
A_2B_2 ; N_4 - $[Pc^*M]$
Tetraazaphthalocyanine with $M = 2 H, Zn$



$ABAB$; N_4 - $[Pc^*M]$
Tetraazaphthalocyanine with $M = 2 H, Zn$



AB_3 ; N_6 - $[Pc^*M]$
Hexaazaphthalocyanine with $M = 2 H, Zn$



B_4 ; N_8 - $[Pc^*M]$
Octaazaphthalocyanine with $M = 2 H, Zn$
or Pyrazinoporphyrazine $[Ppz^*M]$

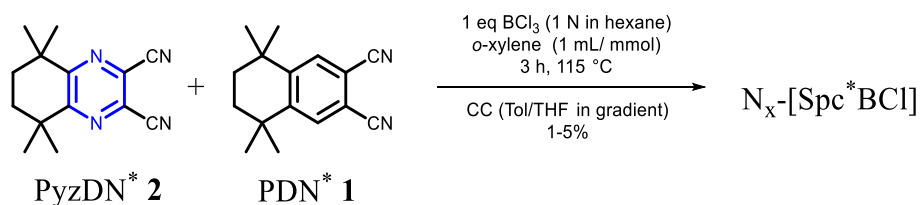
Figure 44: Synthesised azaphthalocyanines and zinc-azaphthalocyanines: N_x - $[Pc^*M]$ with $M = 2 H$ or Zn .

To obtain the A_3B/AB_3 and the $ABAB/A_2B_2$ derivatives in a more selective way, a synthesis involving a ring-expansion of the relevant compounds was attempted.

4.2.4.1 Synthesis of Azasubphthalocyanines N_x -[Spc*BCl]

To obtain the N_x -[Pc*M] (Figure 44) in a more selective way as from a cyclotetramerisation, it was attempted to synthesise them via a KOBAYASHI ring-expansion (Scheme 28, left side). The ring expansion of a [Sppz*BCl] with a PDN* **1** or **1a** to N_6 -[Pc*M] with $M = 2\text{ H or Zn}$, respectively, has been described elsewhere.^[25] This synthetic strategy, and the ring expansion of lower symmetrical A_2B azasubphthalocyanines, was tested in preliminary work of our group.^[13]

To selectively yield ABAB N_4 -Pc*H₂, a ring expansion of a N_4 -[Spc*BCl] with the isoindoline of PDN* **1** should be attempted. Therefore, a new azasubphthalocyanine series (Figure 45) was synthesised in a cyclotrimerisation reaction using both dinitriles in ratio 1:1.



Scheme 29: Synthesis of azasubphthalocyanines N_x -[Spc*BCl].

After separation by column chromatography using Tol/THF in gradient, [Spc*BCl] was eluted first, followed by N_x -[Spc*BCl] with increasing pyrazine character, $x = 2 \rightarrow 6$.

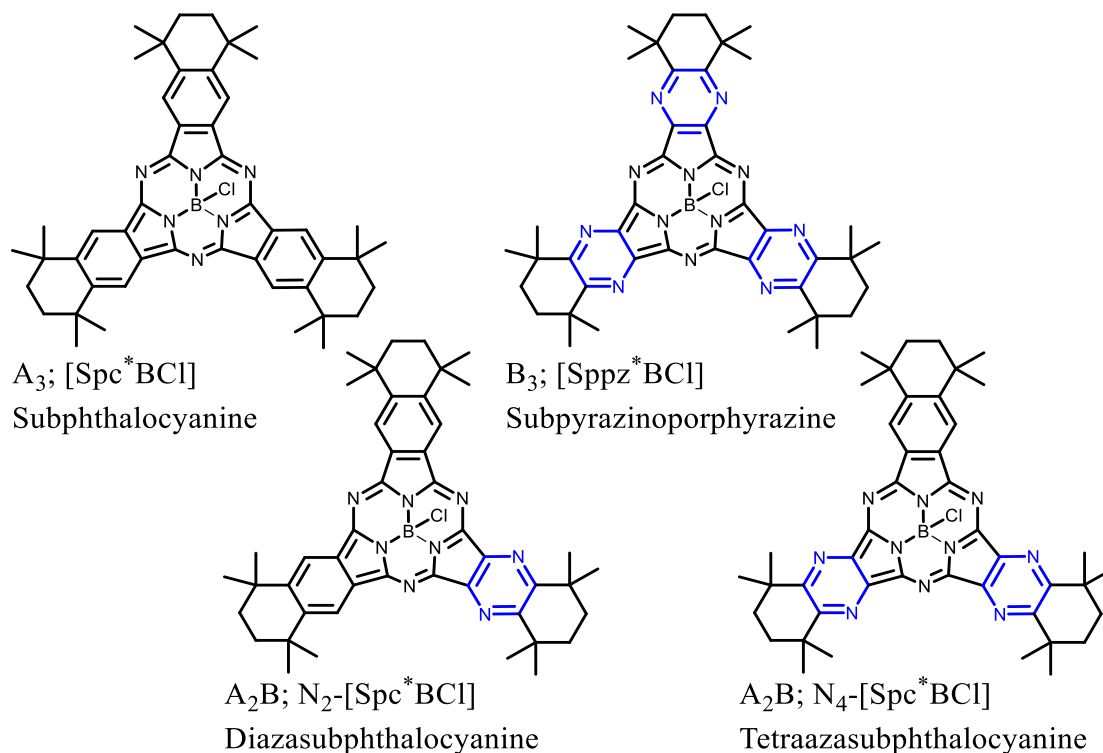


Figure 45: C_{3v} symmetrical and new lower symmetrical aza-Spcs: N_2 -[Spc*BCl] and N_4 -[Spc*BCl].

Because of the low overall yield in this reaction of <15%, A₃ and B₃ were only identified by UV-Vis spectroscopy and MS. Anyway, for full characterisation [Sp^{*}c*BCl] and [Sppz^{*}BCl] were synthesised in separate "selective" reactions using only one PDN^{*} **1**, or PyzDN^{*} **2**, respectively (section 4.2.1.1). [Sp^{*}c*BCl], [Sppz^{*}BCl], N₂-[Sp^{*}c*BCl] as well as the N₄-[Sp^{*}c*BCl] could be isolated in 1-5% yield. The main problem in the separation of the products, N_x-[Sp^{*}c*BCl], is the removal of ligand traces, or unreacted educt. The best method to obtain these compounds is by preparative TLC using Tol/THF 20:1.

Similar to the ¹H NMR spectrum of [Sp^{*}c*BCl] (Figure 34, chapter 4.2.1) the non-peripheral aromatic protons of the azasubphthalocyanines are low-field shifted. All four ¹H NMR spectra of N₀-[Sp^{*}c*BCl], N₂-[Sp^{*}c*BCl], N₄-[Sp^{*}c*BCl] and [Sppz^{*}BCl] are shown in Figure 46 in comparison. Here, the more electron deficient character is very noticeable. The more pyrazine units there are in the molecule, the more electron deficient the aromatic protons of the azasubphthalocyanine are. Similar to (N₀)-[Sp^{*}c*BCl], all methylene units show a multiplet. The methyl groups of the N₂- and N₄-[Sp^{*}c*BCl] show additional signals in the form of six singlets, caused by the lowered symmetry and different chemical surrounding. For [Sppz^{*}BCl], again, two signals for the methyl groups, and a multiplet for the methylene are observed. The compounds are further discussed in the section of optical and theoretical properties (p. 75).

Results and Discussion

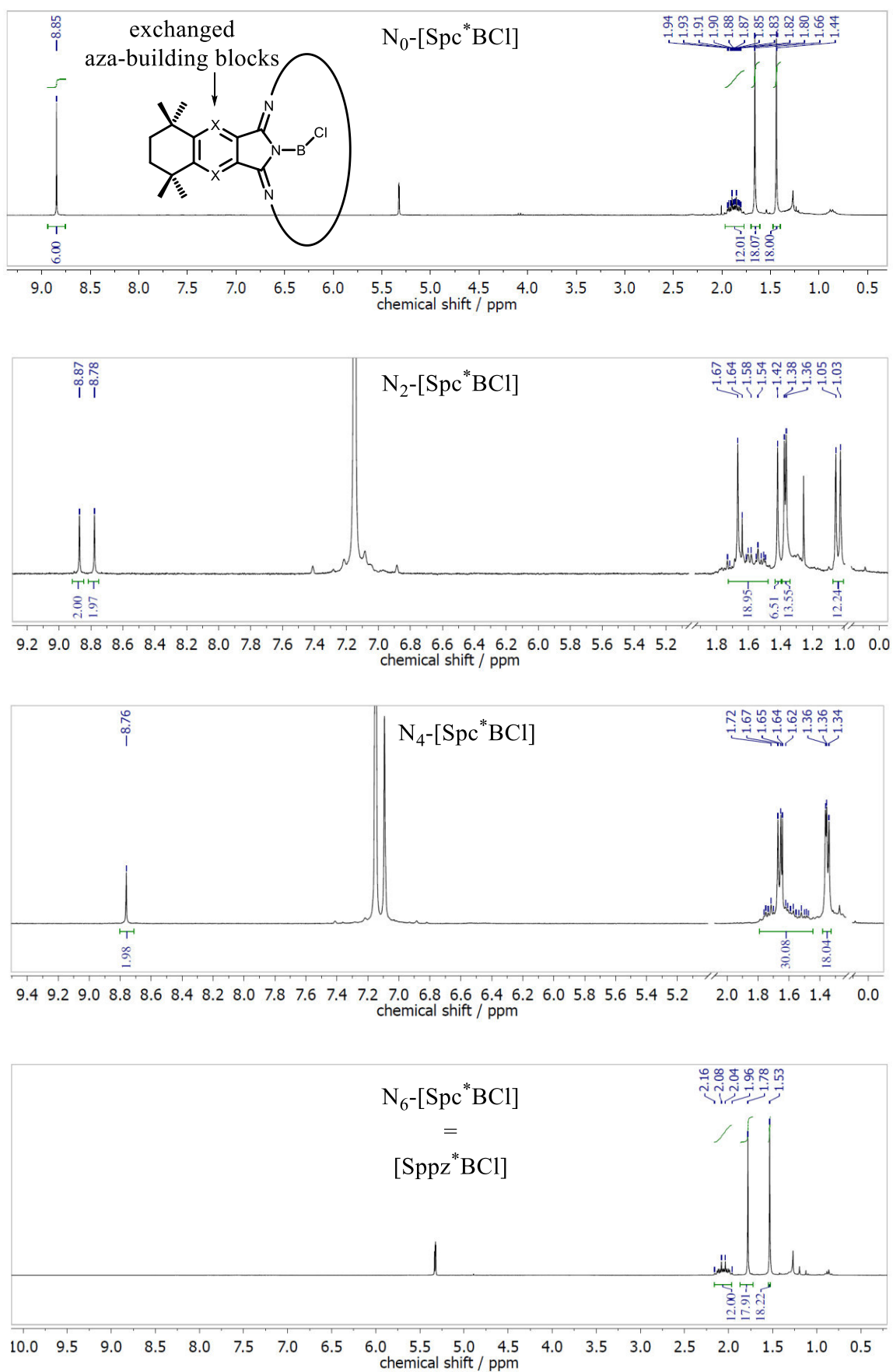
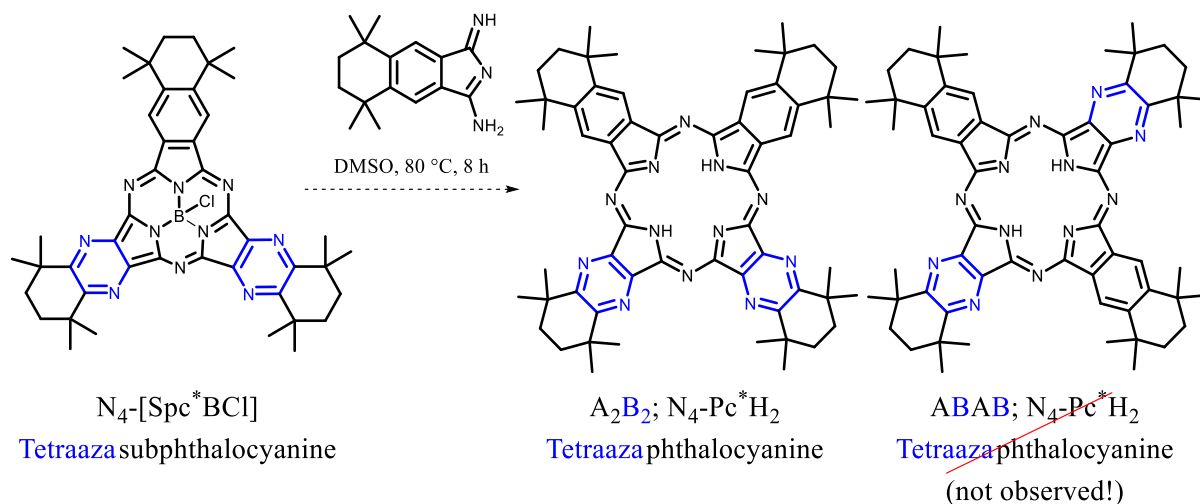


Figure 46: Parts of ^1H NMR spectra: azasubphthalocyanines $\text{N}_x\text{-}[\text{Spc}^*\text{BCl}]$, in C_6D_6 or DCM-d_2 (300 MHz).

4.2.4.2 Attempt to Synthesise ABAB N₂-Pc*H₂ in a Ring Expansion

A ring expansion was carried out for two different systems. For the first system, [Sppz*BCl] was expanded with one PDN* 1 unit to give N₂-Pc*H₂.^[25] For the second system, the discussed N₄-[Spc*BCl] was expanded to give the ABAB and A₂B₂ systems in a ratio of 1:2 (Scheme 30).



Scheme 30: Synthesis of a N₂-Pc*H₂, following the synthesis strategy of KOBAYASHI *et al.* by ring-expansion of a azasubphthalocyanine.

The synthesis of N₄-Pc*H₂ was carried out in a DMSO solution at 80 °C. The isoindoline of the PDN* 1 was freshly prepared and added to a solution of the N₄-[Spc*BCl]. The raw product was analysed by UV-Vis spectroscopy and ¹H NMR spectroscopy, but no product mixture was observed. In contrast, the expansion of azasubphthalocyanines N₄-[Spc*BCl] seems to be quite selective to yield the A₂B₂ system in a 5% yield after column chromatography. This might be caused by the electron deficient character of the pyrazine units, as well. But a yield of 5% makes it difficult to discuss the selectivity of the reaction when a ratio of A₂B₂/ABAB of 2:1 is statistically expected.

It was observed that a ring expansion is favoured for electron deficient subphthalocyanines, such as subpyrazinoporphyrazines, with an electron rich PDN. In the case of the ring expansion of [Spc*BCl], no insertion of PyzDN* 2 or its isoindoline 2a was observed.

Anyway, if only one product is accessible through this route described above, a more selective route to A₂BC-type systems is obvious and should be investigated in more detail in future. The electron deficient character of the pyrazine units effects an additional hypsochromic shift of the azaphthalocyanines, compared to its phthalocyanine derivatives. Additional azasubphthalocyanine complexes substituted with halogen atoms in the non-/peripheral position are discussed in section 4.3.9.

4.2.4.3 Molecular Structure of $N_2\text{-Pc}^*\text{H}_2$

An X-ray analysis of $N_2\text{-Pc}^*\text{H}_2$ was carried out, after receiving crystals from a saturated DCM solution. The molecular structure is shown in Figure 47. The $N_2\text{-Pc}^*\text{H}_2$ is the first crystallized 2,2,5,5-tetramethylcyclohexane annulated, lower symmetrical phthalocyanine.

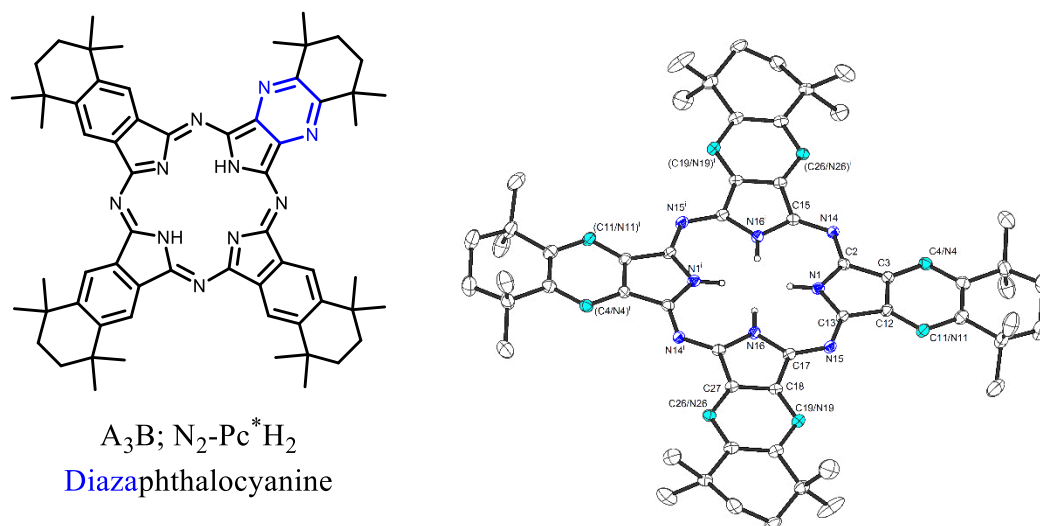


Figure 47: Molecular structure of $N_2\text{-Pc}^*\text{H}_2$ in crystal.

Selected crystallographic data are listed in Table 6 in comparison to Pc^*H_2 crystallized by SEIKEL and solved by OELKERS.^[25] All bond lengths are quite similar. The asymmetric A₃B system crystallizes in a monoclinic crystal system in space group P2_{1/c}, in comparison to triclinic R3 for Pc^*H_2 . The crystal is disordered, so that the [-N=]/[-CH=] units in the non-peripheral position cannot be differentiated using X-ray diffraction techniques. All non-peripheral [-CH=] positions are partly occupied by [-N=] to 25% (shown in light blue). A less disordered crystal might be obtained by recrystallization from toluene. The molecular structure and the crystal packing for $N_2\text{-Pc}^*\text{H}_2$ are shown in Figure 47 and Figure 48, respectively.

Table 6: Selected bond length (Å) and -angles (°) of $N_2\text{-Pc}^*\text{H}_2$ and Pc^*H_2 .^[167]

	$N_2\text{-Pc}^*\text{H}_2$	Pc^*H_2 [167]
C1-N1	1.363(3)	1.369(6)
N3-H1N	0.8800	0.95(5)
N1-H1N		2.07(6)
N1-C2	1.371(3)	1.383(6)
C4-N4	1.328(3)	1.326(6)
C2-N2	1.330(3)	1.339(6)
N4-C1a	1.336(3)	1.347(6)
N2-C3	1.323(3)	1.320(6)
C3-N3	1.374(3)	1.392(7)
N3-C4	1.362(3)	1.353(6)
C3-N3-H1N	125.6	112(4)
C4-N3-H1N		136(4)

For both compounds, Pc^*H_2 and $\text{N}_2\text{-Pc}^*\text{H}_2$, $\nu_{\text{isoindoline}}$ is with $\nu_{\text{isoindoline}} \sim 2^\circ$ very low, verifying the planarity of the compounds. The molecular packing of phthalocyanines is an important feature with respect to the conductivity in solid state. Similar to the literature described structure of Pc^*H_2 , here, the molecular packing of $\text{N}_2\text{-Pc}^*\text{H}_2$ differs from the known molecular packings of Pc^*H_2 , which is commonly a *herringbone* type.^[183] Each molecule of $\text{N}_2\text{-Pc}^*\text{H}_2$ is alternately tilted to the next one, and not organised in staples as in Pc^*H_2 . This is caused by the sterically demanding alkyl groups. Similar structural motifs, as observed in $\text{N}_2\text{-Pc}^*\text{H}_2$, are in general, only observed in the polymorphic structures of e.g. $[\text{PcGe}(\text{OH})_2]$, whereby the molecules are connected via hydrogen bonds of the non-peripheral aromatic protons to the axial oxygen atoms of the neighbouring phthalocyanines.^[184]

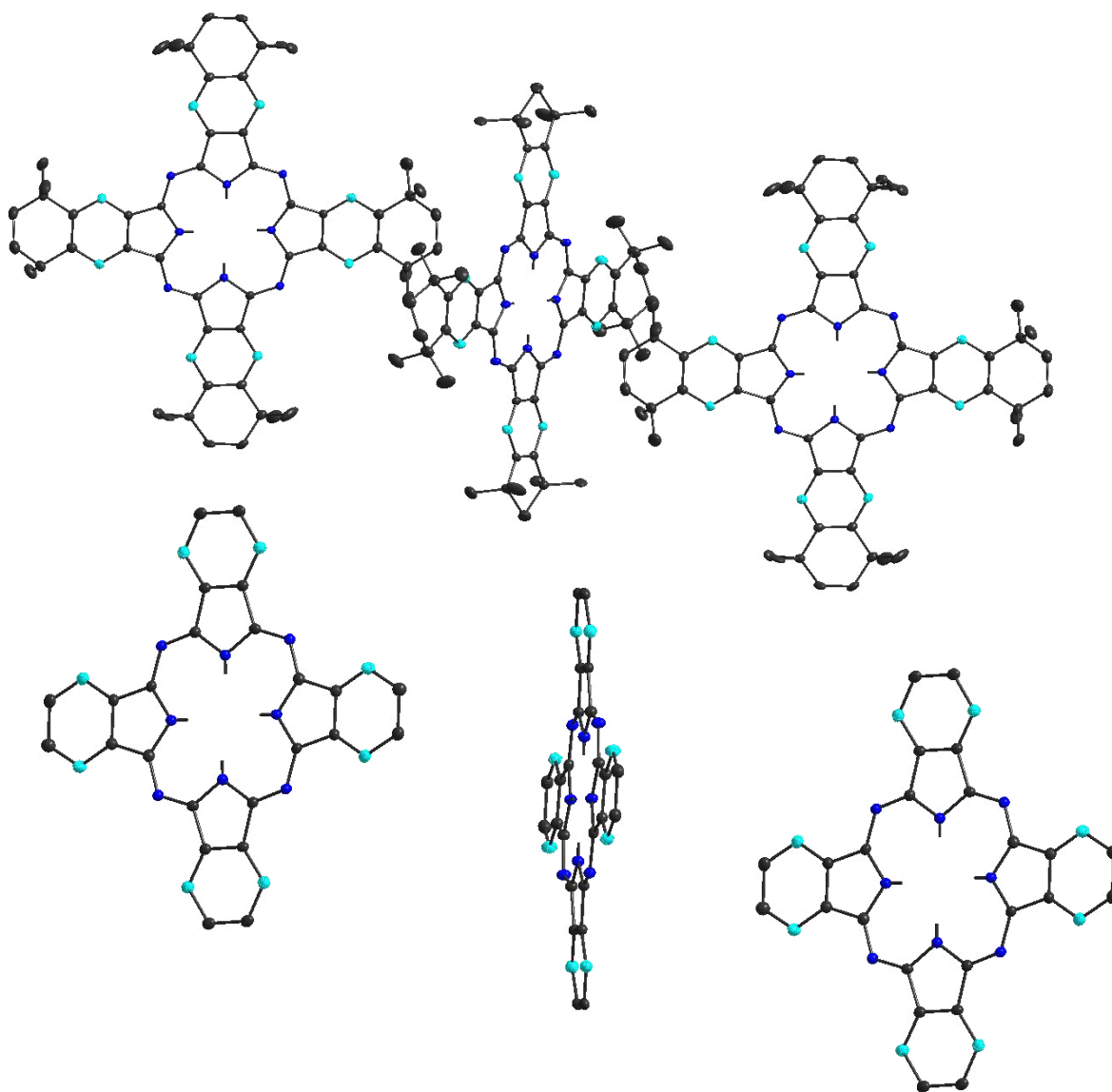


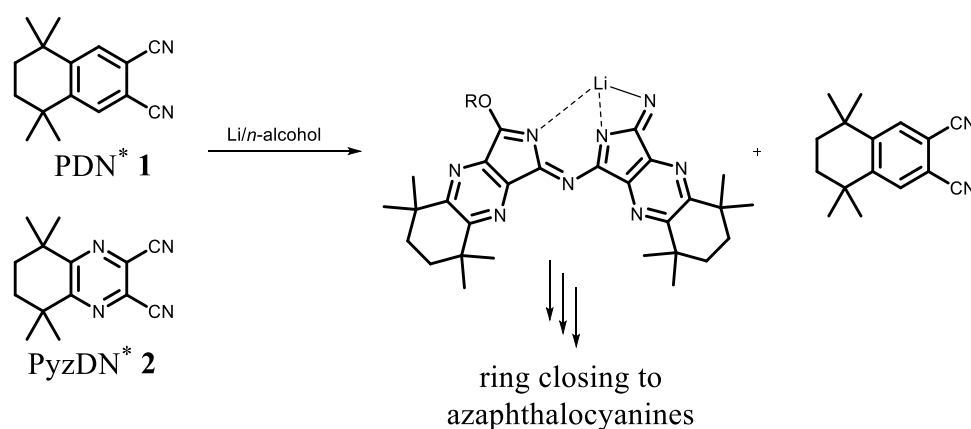
Figure 48: Molecular arrangement of $\text{N}_2\text{-Pc}^*\text{H}_2$ in crystal. Above: with methylated cyclohexane ring in peripheral position; - Below: inner phthalocyanine core. Solvent molecules, protons and disordered methyl groups are omitted for clarity.

Results and Discussion

In addition, suitable crystals for X-ray analysis could be obtained of $A_2B_2 N_4-[Pc^*Zn]$. In comparison to the planar $N_2-Pc^*H_2$, in the resolved structure of $A_2B_2 N_4-[Pc^*Zn]$, the strong influence of axial ligands on the position of the central metal atom in the $[-ZnN_4-]$ cavity is visible. Here, water is coordinated at the Zn atom, leading to an increased distance between the Zn metal and the $[-N_4-]$ plane, $d_{out-of-plane} = 0.59$.

4.2.4.4 Synthesis of ABAB N₄-Pc*H₂

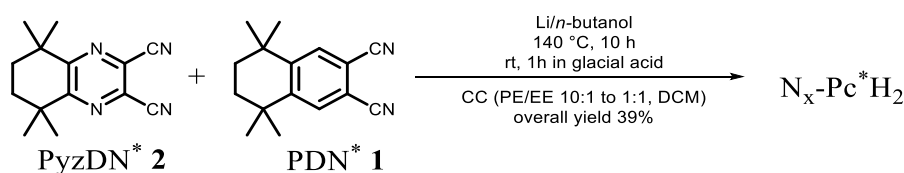
In the ring expansion of electron deficient [Sppz*BCl] and N₄-[SpC*BCl] with **1** or **1a**, AB₃ N₆-[Pc*M] and A₂B₂ N₄-[Pc*M] with M = 2 H, Zn were obtained, but (in the second synthesis) not the ABAB N₄-[Pc*M] derivative. As previously described for Li/*n*-octanol cocyclisations with azaphthalonitriles (see section 4.2.4),^[25] again, only the A₂B₂ N₄-Pc*H₂, and not its ABAB N₄-Pc*H₂ derivative was obtained. However, the AB₃ N₆-Pc*H₂ was obtained, because of a favoured ring formation of the pyrazine units.^[30] The favoured formation of the A₂B₂ N₄-Pc*H₂, and AB₃ N₆-Pc*H₂ respectively, may be explained by a preformed dimeric isoindoline species (Scheme 31).



Scheme 31: Formation of a N₄-Pc*H₂ in a Li/*n*-octanol cyclisation.^[25]

MACK and KOBAYASHI explained this phenomenon with steric reasons.^[30] However, the formation of only the preformed half-ring of PyzDN* **2** cannot be explained with steric reasons, as there is a similar steric demand of both dinitriles **1** and **2**.

So, further attempts to obtain the ABAB N₄-Pc*H₂ system were carried out. To yield ABAB N₄-Pc*H₂, a neat reaction of PDN* **1** and PyzDN* **2** with [Pb(OAc)₂] in a WOOD metal bath at 280 °C was carried out. After demetallation of the phthalocyanine using aq. HCl in pyridine, followed by CC, the same compounds were obtained in lower yields, as from Li/*n*-octanol cyclisation method. Therefore, an alternative synthetic route was carried out (Scheme 32) using larger amounts of **1** and **2**, of almost 2 g in total. After CC using PE/EA 4:1, ABAB N₄-Pc*H₂ was obtained in ~1% yield, eluted right after Pc*H₂ and A₃B N₂-Pc*H₂.



Scheme 32: Synthesis of ABAB N₄-Pc*H₂.

Results and Discussion

The A_2B_2 $N_4\text{-Pc}^*H_2$ can be differentiated from its derivative $ABAB$ $N_4\text{-Pc}^*H_2$ via UV-Vis spectroscopy (Figure 53, section 4.2.4.6), and by 1H NMR spectroscopy (Figure 49). The aromatic protons of $ABAB$ $N_2\text{-Pc}^*H_2$ in the non-peripheral position, as tagged on the right side below, are chemically equivalent.

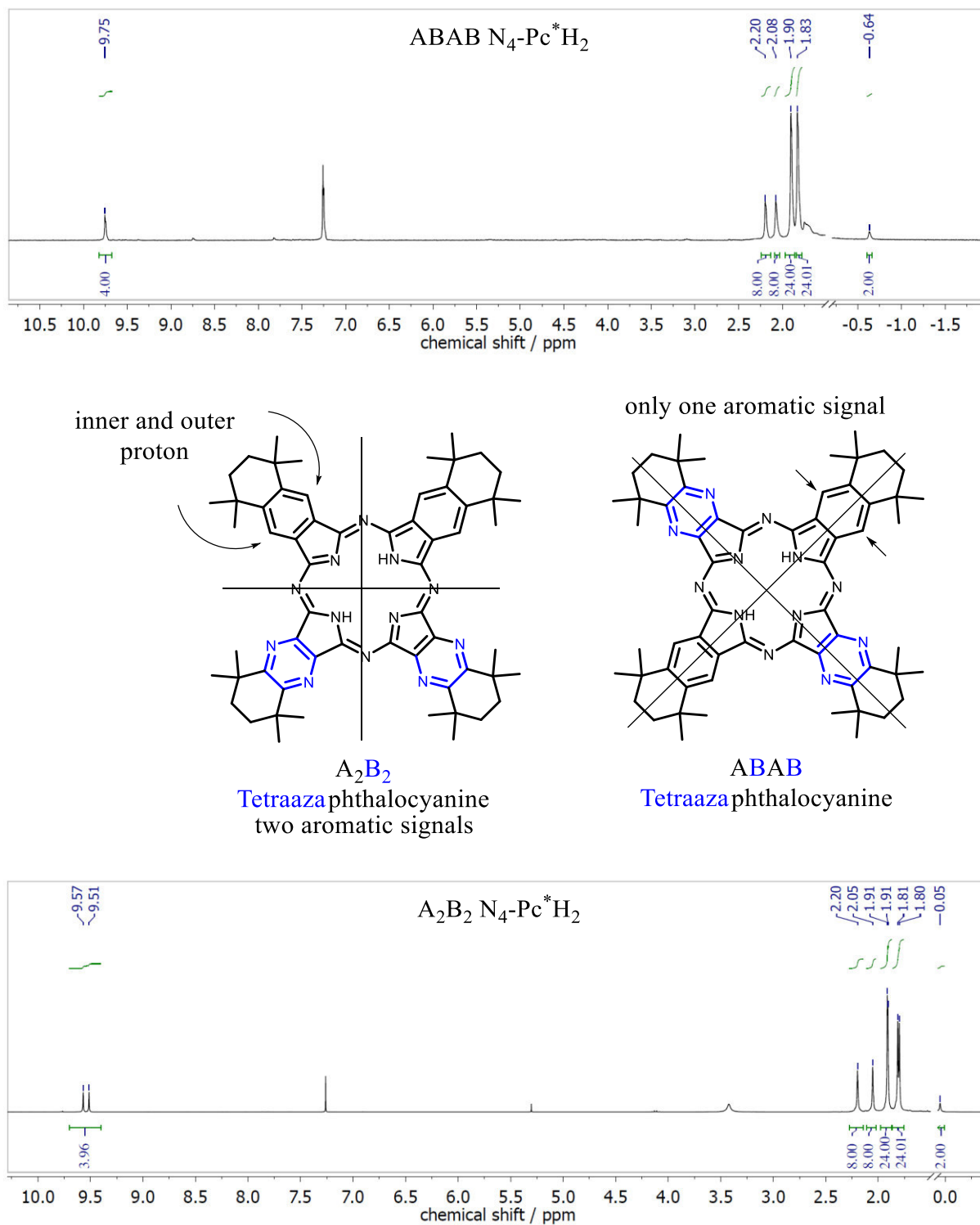


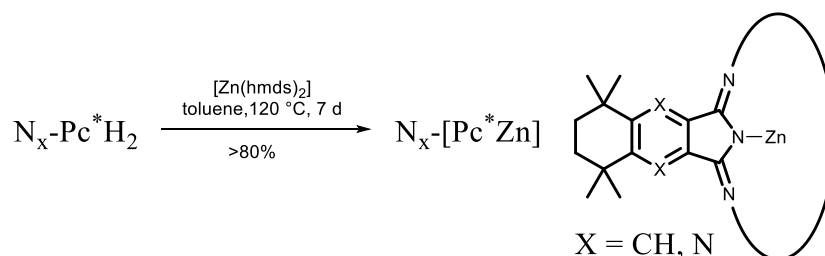
Figure 49: 1H NMR spectra of $ABAB$ (above) and A_2B_2 (below) $N_4\text{-Pc}^*H_2$, in $CDCl_3$ (300 MHz).

In the case of $A_2B_2 N_4\text{-Pc}^*H_2$, two inner and two outer aromatic protons are present, so two signals should be present, as visible in the 1H NMR spectrum on the bottom. The same is valid for the methyl protons. Because of the more electron deficient character of the pyrazine units, the high-field shifted protons of the methyl and methylene groups correspond to the pyrazine isoindoline units. With this, a D_{2h} symmetry of the phthalocyanine $A_2B_2 N_4\text{-Pc}^*H_2$ is confirmed. In contrast, $ABAB N_4\text{-Pc}^*H_2$ is more symmetrical and with this only two signals for the methyl/methylene protons are visible. It is interesting to observe the more electron rich character for the $ABAB N_4\text{-Pc}^*H_2$, as seen by the larger low-field shift of the aromatic CH , and a larger high-field shift for the inner NH protons.

Similar to the $N_4\text{-Pc}^*H_2$ isomers, $A_3B N_2\text{-Pc}^*H_2$ and $AB_3 N_6\text{-Pc}^*H_2$ can be assigned for certain not only by UV-Vis spectroscopy, but also by 1H NMR spectroscopy, giving either three aromatic signals or one, respectively. The shift of the aromatic CH and the inner NH protons is also in correlation with the electron density of the π -system.

4.2.4.5 Synthesis of Zinc-Azaphthalocyanines $N_x\text{-[Pc}^*Zn]$

As described before, it was attempted to yield the $N_x\text{-[Pc}^*Zn]$ compounds via cocyclotetramerisation. In a direct cocyclisation with a zinc precursor in a high boiling solvent, the formation of all possible derivatives could be observed. However, in column chromatography, a higher tendency to peak tailoring/broadening was observed. The products could not be completely separated from each other. So, the synthesis of zinc-azaphthalocyanines $N_x\text{-[Pc}^*Zn]$ was carried out using $[Zn(hmnds)_2]$ in toluene for the metalation of the more easily separated $N_x\text{-Pc}^*H_2$ species. Excess of $[Zn(hmnds)_2]$ (>5 eq) was used to yield quantitative conversion to the corresponding zinc-azaphthalocyanines after stirring for 7 d at 120 °C. The resulting product was purified by washing with DEE.



Scheme 33: Synthesis of zinc-azaphthalocyanines, using $[Zn(hmnds)_2]$.

Results and Discussion

The conversion was monitored with ^1H NMR spectroscopy in an NMR-experiment. Already 1 min after addition of the $[\text{Zn}(\text{hmds})_2]$, a conversion to the $\text{N}_x\text{-}[\text{Pc}^*\text{Zn}]$ could be observed. The ^1H NMR spectrum of the purified $\text{A}_2\text{B}_2 \text{N}_4\text{-}[\text{Pc}^*\text{Zn}]$ in $\text{DCM-}d^2$ solution is shown in Figure 50.

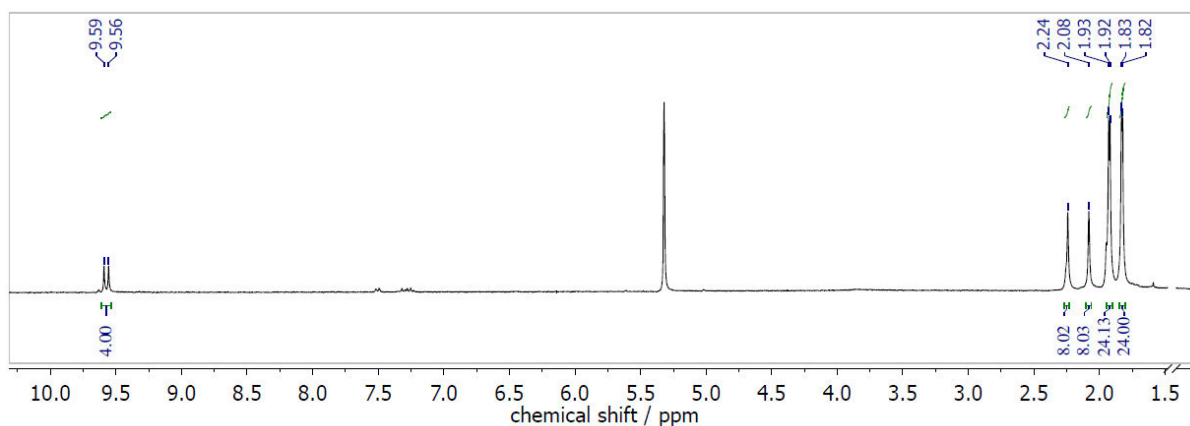


Figure 50: ^1H NMR spectrum of $\text{A}_2\text{B}_2 \text{N}_4\text{-}[\text{Pc}^*\text{Zn}]$, in $\text{DCM-}d_2$ (300 MHz).

The complete conversion to $\text{N}_x\text{-}[\text{Pc}^*\text{Zn}]$ was verified with mass-spectrometry by the absence of free ligand, $\text{N}_x\text{-Pc}^*\text{H}_2$. If necessary, additional purification by preparative TLC was done. In the following section, a more detailed property discussion of the $\text{N}_x\text{-}[\text{Pc}^*\text{Zn}]$ in comparison to $\text{N}_x\text{-Pc}^*\text{H}_2$ is given.

4.2.4.6 Optical Properties of Azaphthalocyanines and Azasubphthalocyanines

UV-Vis Spectroscopy. The optoelectronic properties of the synthesised compounds were studied by using UV-Vis spectroscopy and cyclic voltammetry (CV). In UV-Vis spectroscopy, the energy difference between the HOMO and the LUMO can be determined when an electron is excited. The Q-band, as the most important and most intense band of the phthalocyanines, relates to a π - π^* transition.^[12] In CV, the HOMO is determined by removing an electron, and the LUMO by introducing one. In comparison to theoretical calculations, the determination of HOMO/LUMO levels by using CV neglects the exchange integral and the COULOMB interaction integral. In Figure 52, the UV-Vis spectra of N_x -Pc*H₂ and N_x -[Pc*Zn] are shown and in Figure 54 compared to N_x -[Spc*BCl]. All measurements were carried out in a DCM or in a MeOH solution (SI). The bathochromic shift of the Q-band with decreasing number of [-N=] (exchange of [-N=] by [-CH=]) in the N_x -Pc*H₂ and N_x -[Pc*Zn] is clearly seen. A hypsochromic shift is observed by introducing zinc into the metal free N_x -Pc*H₂ ligands. The Q-band is hypsochromically shifted from [Spc*BCl] (582 nm) to [Sppz*BCl] (534 nm), from Pc*H₂ (711 nm) to Ppz*H₂ (655 nm), and from [Pc*Zn] (692 nm) to [Ppz*Zn] (638 nm), respectively.

All synthesised aza-analogues, such as azasubphthalocyanines N_x -[Spc*BCl] and azaphthalocyanines N_x -Pc*H₂, show the same trends between the two A₃/B₃ or A₄/B₄ systems of the corresponding dinitrile. As can be seen in Figure 51, the increase of the energy gap does not show perfectly linear behaviour by stepwise exchange of the [-CH=] units by [-N=] units. Additionally, in Figure 52, the degenerate nature of the orbitals is easily seen for the A₄ and B₄ system, as well as for A₂B₂ N_4 -Pc*H₂. For A₃B N_2 -Pc*H₂ and AB₃ N_6 -Pc*H₂, only broadened Q-bands were observed. The Q-band splitting of A₃B N_2 -Pc*H₂ and AB₃ N_6 -Pc*H₂ is almost undetectable, but is visible as broadened signals (Figure 52) for a DCM solution and in the Supplement 10.3 for MeOH solutions. According to the UV-Vis spectra shown in Figure 53, the decreased symmetry of the Pc is shown by a split of the Q-band, as is visible on the right side for A₂B₂ N_4 -Pc*H₂. The splitting of the Q-band is caused by the "asymmetrical nature" of the N_x -[Pc*M], which is either present due to the exchanged [-CH=] units by [-N=] ones, or by the inner protons.

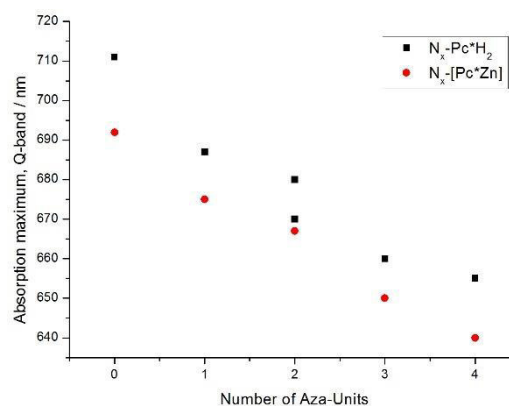


Figure 51: Decrease of the Q-band absorption maximum plotted vs the number of substituted aza-units in the phthalocyanine core N_x -Pc*H₂ and N_x -[Pc*Zn], in DCM at rt.

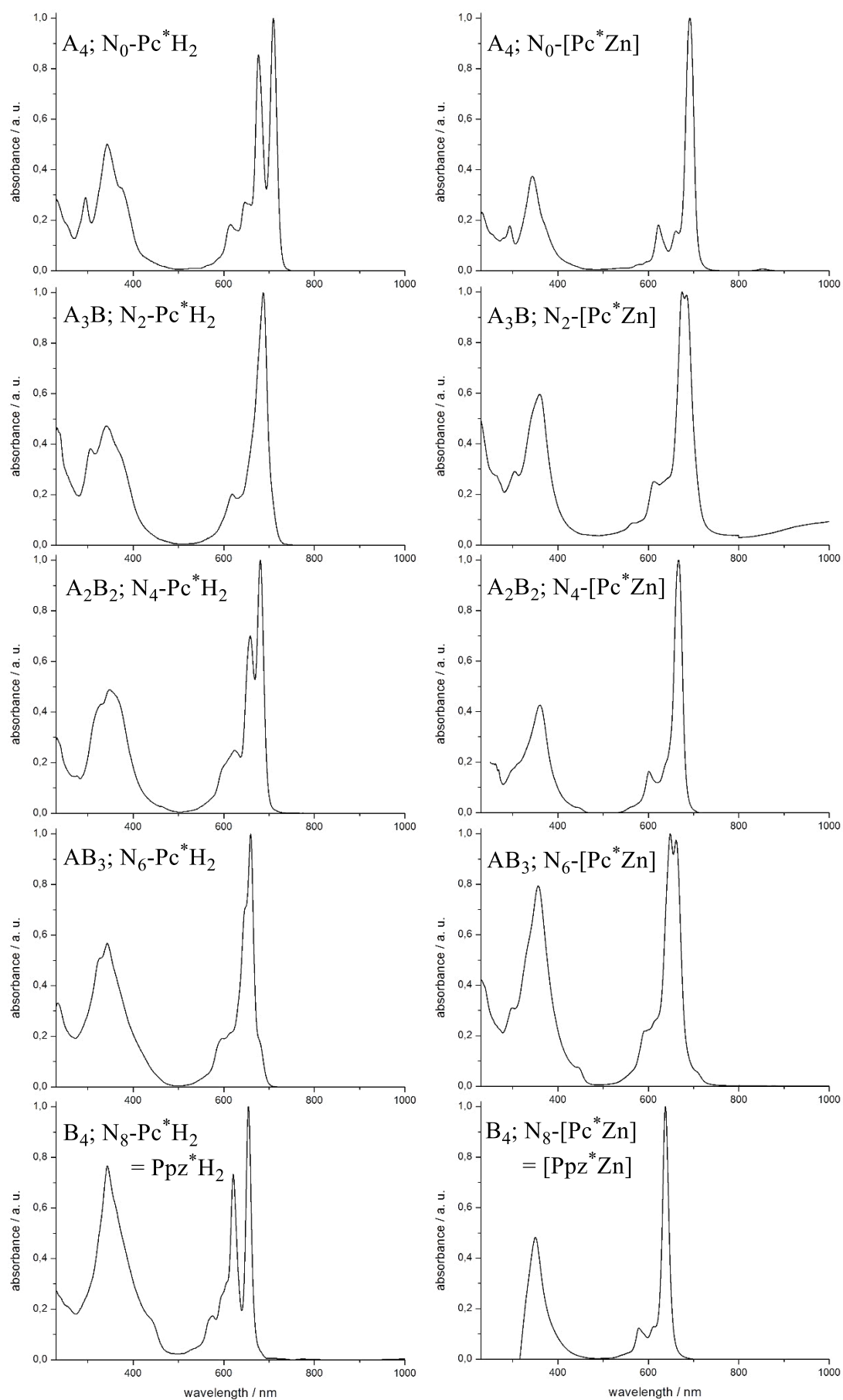


Figure 52: UV-Vis spectra of $N_x\text{-Pc}^*\text{H}_2$ and $N_x\text{-[Pc}^*\text{Zn]}$, in DCM at rt.

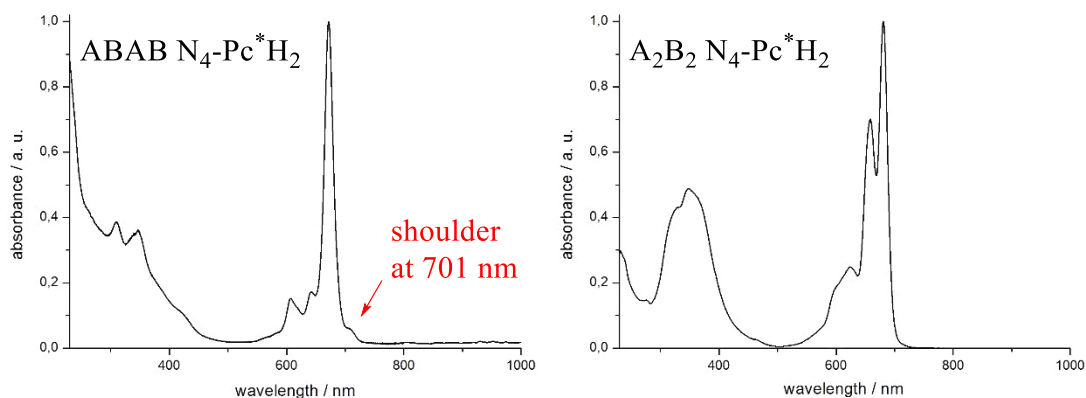


Figure 53: UV-Vis spectra of ABAB $N_4\text{-Pc}^*\text{H}_2$ and $A_2B_2 N_4\text{-Pc}^*\text{H}_2$ in comparison, in DCM at rt.

The UV-Vis spectra additionally verify the two different structural types of $N_4\text{-Pc}^*\text{H}_2$: ABAB and A_2B_2 , as was already proved by the ^1H NMR spectrum (Figure 49). While at first glance, only one sharp Q-band is observed in the spectrum of ABAB $N_4\text{-Pc}^*\text{H}_2$ (Figure 53), a smaller shoulder is visible at 701 nm. This shoulder is even better resolved in the UV-Vis spectrum measured in a MeOH solution (SI).

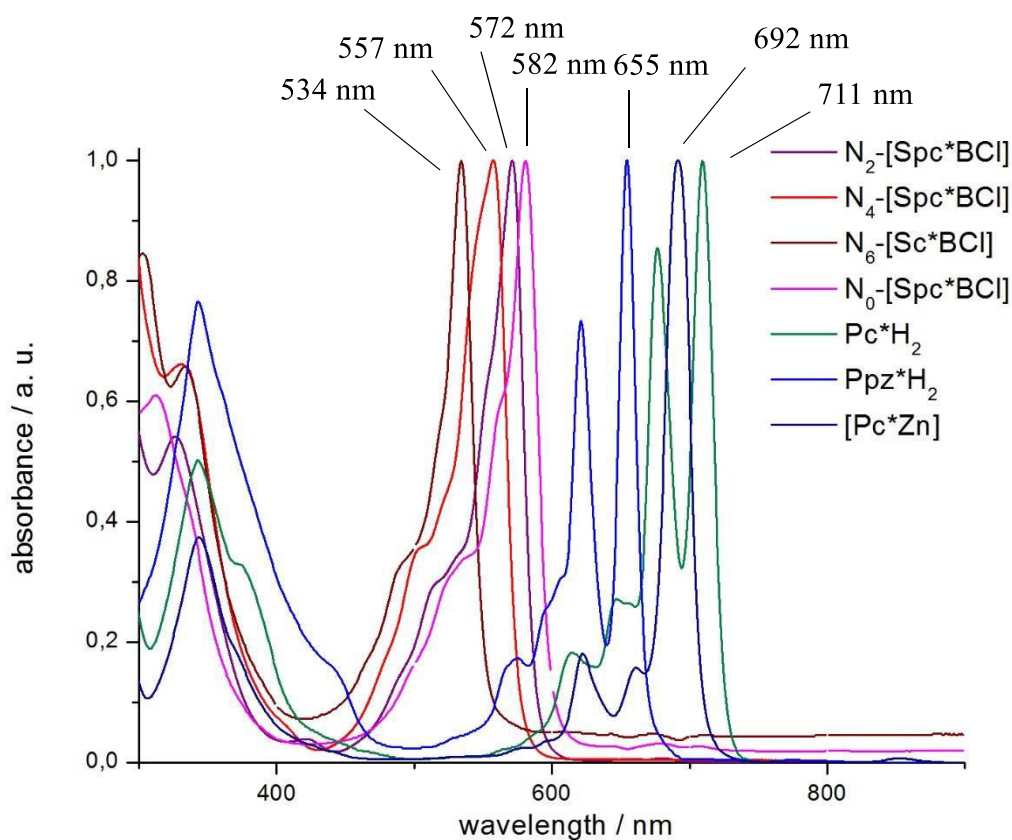


Figure 54: UV-Vis spectra of aza-Spcs $N_x\text{-[Spc}^*\text{BCl]}$ in comparison to Pc^*H_2 , $[\text{Pc}^*\text{Zn}]$ and Ppz^*H_2 , in DCM at rt.

Results and Discussion

Considering this band, at 701 nm, as a split of the Q-band, the strongest splitting is observed for ABAB $N_4\text{-Pc}^*\text{H}_2$, which is in accordance with literature expectations.^[30] The Q-band pendant to 701 nm is also visible in fluorescence measurements, described in section 4.2.5. All $N_x\text{-[Spc}^*\text{BCl]}$ show only one Q-band peak in UV-Vis spectra. This is caused by the previously discussed cone-shape of the complexes, which results in a distorted π -system of the subphthalocyanine in general and the "quasi-aromatic" character caused by the weaker overlapping of the p-orbitals, discussed before.

Cyclovoltammetric Measurements and Calculations All $N_x\text{-Pc}^*\text{H}_2$ were additionally characterized with CV and the results were compared to UV-Vis measurements and to time dependent density functional theory (TD-DFT) calculations. CV measurements were carried out in DCM solution, except $N_8\text{-Pc}^*\text{H}_2$ (Ppz^*H_2), which was measured in THF because of its low solubility in DCM. For measurements, a glassy carbon working electrode was used, because of its greater surface area compared to Pt. Because of the greater surface area, current flows more efficiently, and with this, a better resolution of the electrical potentials was observed. Additionally, a Pt electrode was used as pseudo reference, and a Pt electrode as counter electrode. All measurements were carried out with ferrocene/ferrocenyl as internal reference added in the last measurement. The collected electrochemical data and Q-band absorption energies are listed in Table 7.

An example of the analysis of electrochemical data is given in the chapter on functionalised phthalocyanines, section 4.3.7. In CV, $N_x\text{-Pc}^*\text{H}_2$ show in general one reversible oxidation process and one irreversible oxidation process at higher potentials, as well as two reversible reduction processes (Figure 55). All six cyclovoltammetric measurements can be found in the Supplement 10. In both techniques, UV-Vis spectroscopy and CV, with an increase of pyrazine units ($-N=$) in $N_x\text{-Pc}^*\text{H}_2$, the energy of the HOMO-LUMO gap increases. This is seen in UV-Vis spectroscopy as a decrease of the Q-band absorption wavelength, i. e. an increase of

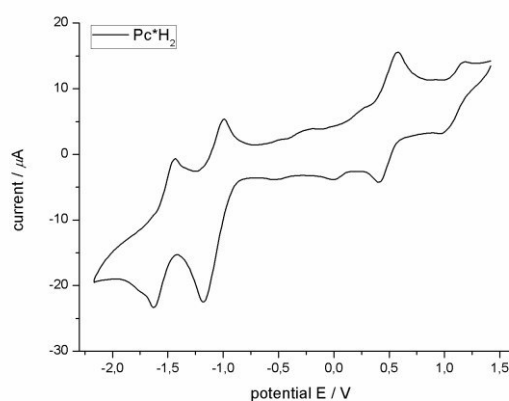


Figure 55: Exemplary CV measurement of Pc^*H_2 , carried out in DCM, ferrocene/ferrocenyl was used as reference, at 25 °C.

the excitation energies. Similar to the increase of the Q-Band, the HOMO-LUMO gap determined by CV increases not-perfectly linearly.

The calculations were done by TROMBACH (AK TONNER at the Department of Chemistry of the Philipps-Universität Marburg). Experimental and theoretical results are compared in Figure 56. The electronic structures of the metal free $N_x\text{-Pc}^*\text{H}_2$ ligands and zinc azaphthalocyanines, $N_x\text{-[Pc}^*\text{Zn}]$, were calculated by density functional theory, using PBE and B3LYP exchange correlation functional. B3LYP, used as density functional, was found to provide results which are in good agreement with experimental values.^[185] For $N_x\text{-Pc}^*\text{H}_2$ ligands, different tautomers and regioisomers can be described (Supplement 10.3, Table SI-2). Therefore, it was found that, depending on the position of the inner hydrogen atoms, the molecules have different stabilities. Especially for ABAB $N_4\text{-Pc}^*\text{H}_2$, the tautomer with the hydrogens coordinated at the pyrazine units shows a significantly lower stability ($\Delta E = 56.4$ kJ/mol) compared to its other tautomer. In comparison to A_2B_2 $N_4\text{-Pc}^*\text{H}_2$, its regioisomer ABAB is only 5.6 kJ/mol separated, for $N_4\text{-[Pc}^*\text{Zn}]$ only 1.6 kJ/mol. All other tautomers, such as A_3B and AB_3 , show a quite small energy differences ($\Delta E = 4.0$ kJ/mol) and, therefore, in experiments all tautomers should lie in equilibrium.

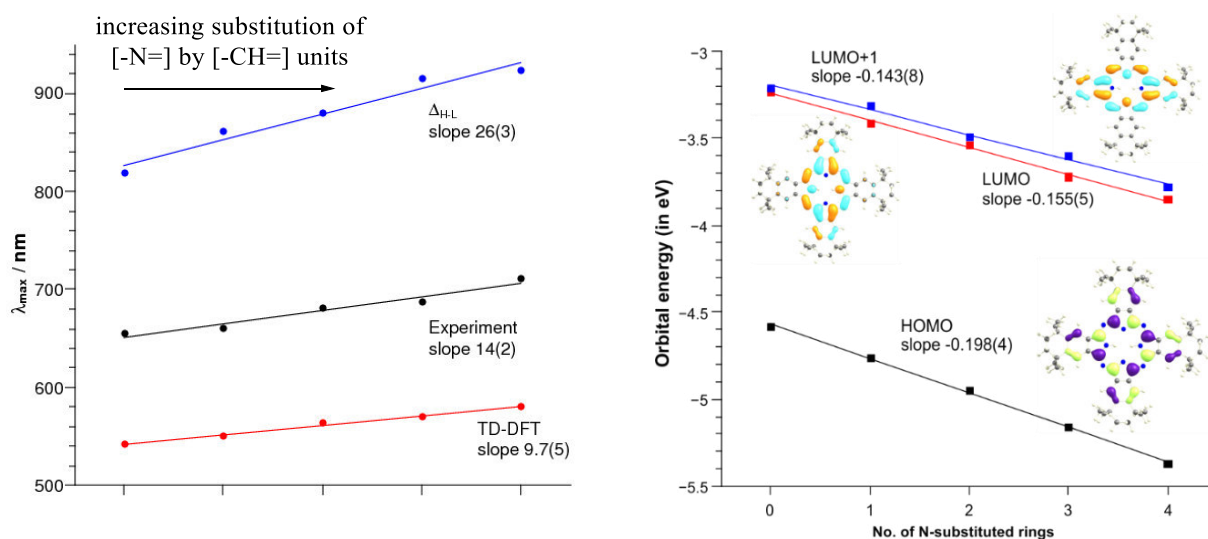


Figure 56: Left side: Trend of experimental UV-Vis Q-band absorption maxima (black), results of TD-DFT (red) and $\Delta_{\text{H-L}}$ (blue) absorption maxima with linear regression curves for $N_x\text{-Pc}^*\text{H}_2$. Right side: Orbital energies for HOMO (black), LUMO (red) and LUMO+1 (blue) for varying [-N=]-unit content of $N_x\text{-Pc}^*\text{H}_2$. Orbitals for $N_0\text{-Pc}^*\text{H}_2$ are depicted.

The electronic structure of all isomers was analysed. In TD-DFT calculations, it was found that electronic excitations were dominated by HOMO \rightarrow LUMO or the HOMO \rightarrow LUMO+1 transition for electronic excitations. These excitations form the Q-band of the phthalocyanine. The small differences of the energetic levels of the LUMO and LUMO+1 are in accordance

Results and Discussion

with the small differences between the absorption maxima in UV-Vis spectroscopy. An increase of the HOMO-LUMO gap was observed by increasing the number of [-N=] units in the azaphthalocyanines, by substitution of [-CH=] building blocks. This correlates with the experimental data obtained by UV-Vis spectroscopy and CV measurements. From calculations, it is clearly seen that the HOMO levels are less stabilised compared to the LUMO/LUMO+1 levels (Figure 56, on the right side), when the number of [-N=] units increases. This can be seen in a quicker decrease of the HOMO levels.

Frontier orbital energies (Figure 56, in blue) indicate much higher excitation energies as computed and experimental results. Nevertheless, the trend of all values is the same, but quantitative reproduction fails and has to be further improved.

Table 7: Electrochemical data of $N_x\text{-Pc}^*\text{H}_2$ in comparison.^[a]

	$N_8\text{-Ppz}^*\text{H}_2$	AB_3 $N_6\text{-Pc}^*\text{H}_2$	$ABAB$ $N_4\text{-Pc}^*\text{H}_2$	A_2B_2 $N_4\text{-Pc}^*\text{H}_2$	A_3B $N_2\text{-Pc}^*\text{H}_2$	$N_0\text{-Pc}^*\text{H}_2$
$E_{\text{ox}}^1 / \text{V}$	0.87	0.35	0.28	0.36	0.43	0.67
$E_{\text{red}}^1 / \text{V}$	-1.05	-1.47	-1.47	-1.37	-1.23	-0.91
$E_{\text{red}}^2 / \text{V}$	-1.37	-1.82	-1.79	-1.77	-1.65	-1.36
$E_g^{\text{CV}} / \text{V}$	1.92	1.82	1.75	1.73	1.67	1.58
$\lambda_{\text{max}} / \text{nm}$	655	660	670	680/656	687	711

[a] Measurements were carried out in DCM, E_{red} and E_{ox} are expressed as $E_{1/2}$, ferrocene/ferrocenyl was used as reference. Glassy carbon working electrode, Pt counter electrode, Ag reference electrode, at 25 °C. The potential difference, E_g^{CV} , was calculated as the difference between the first oxidation and the first reduction peak.

Surprisingly, the observed trend of $N_x\text{-Pc}^*\text{H}_2$ seen in CV does not correlate with the expected trend observed for other [PcZn] and [PpzZn] in literature.^[87] Other [PcZn] should be comparable, because zinc as central atom is electrochemically inert. As mentioned earlier, the increase of the HOMO-LUMO gap, $(E_{\text{LUMO}} - E_{\text{HOMO}})^{\text{redox}}$, is according to the increase of the hypsochromic Q-band shift, which is in correlation to calculations. In contrast, the first oxidation, E_{ox}^1 , and reduction, E_{red}^1 , of $N_x\text{-Pc}^*\text{H}_2$ decrease with increasing number of x from x = 0 ($E_{\text{ox}}^1 = 0.67$, $E_{\text{red}}^1 = -0.91$) \rightarrow x = 4 ($E_{\text{ox}}^1 = 0.28$, $E_{\text{red}}^1 = -1.41$), while for x = 8 ($E_{\text{ox}}^1 = 0.87$, $E_{\text{red}}^1 = -1.05$) an increase of E_{ox}^1 was found (Table 7). The increase of E_{ox}^1 from x = 0 \rightarrow 8 is in accordance with literature known species such as Pc and Ppz derivatives, but contrary for their more lower symmetrical derivatives $N_x\text{-Pc}^*\text{H}_2$, with x = 2, 4 and 6. In literature, for [PcZn] and [PpzZn] with an increasing red-shift, an increase of HOMO and LUMO levels, and E_{ox}^1 as well as E_{red}^1 was found by experimental measurements such as CV, or DPV, as visible for $N_x\text{-Pc}^*\text{H}_2$ with x = 0 compared to x = 8.^[30,87] Furthermore, for aza-[PcZn], a stronger decrease of the HOMO was found, combined with a weaker decrease of the LUMO (Figure 56).

In addition, the dipole moment, μ , and polarizability, α , were calculated for a better understanding of electronic processes on surfaces and semiconductors (Supplement 10.3, Table SI-2). A good accordance with the rational evaluation of the dipole moment was observed. The polarizability increases for both series N_x -[Pc**M*] with *M* = 2 H, Zn by increasing substitution of [-CH=] units by more polarizable [-N=] units.

In summary, calculations and experimental results are in good accordance with each other, when looking at the trend of Q-band absorptions of N_x -[Pc**M*]. The qualitative data of excitation energies determined in experimental UV-Vis spectra or CV measurements compared to those from calculations are different, but observed trends are the same. In Table 8, different excitation energies of the azaphthalocyanines N_x -Pc**H*₂ with *x* = 0 → 8 are summarised. Experimental values obtained from UV-Vis spectroscopy are listed, as well as the potential difference, E_g^{CV} , determined by CV. Calculated values for the UV-Vis absorption and the transition are also given. For a better understanding of observed trends, the photophysical properties of the series N_x -[Spc**B*Cl] and N_x -[Pc**M*] were investigated.

Table 8: Excitation energies: calculated, and optical vs redox potentials.

	δ (Ar-CH) / ppm [a]	B-band / nm [b]	Q-band / nm [b]	Calc. / nm [c]	(HOMO- LUMO) ^{optical} / eV [d]	E_g^{CV} / V [e]	$\Delta_{HL}^{calc.}$ / eV [f]	$\Delta_{HL+1}^{calc.}$ / eV [f]
N_6 -[Spc* <i>B</i> Cl]	-	334	534					
N_4 -[Spc* <i>B</i> Cl]	8.76	331	558					
N_2 -[Spc* <i>B</i> Cl]	8.87/8.78	327	571					
N_0 -[Spc* <i>B</i> Cl]	8.91	312	581					
N_8 -Pc* <i>H</i> ₂	-	341	655	541	1.89	1.92	1.52	1.59
N_6 -Pc* <i>H</i> ₂	9.75	342	660	550	1.88	1.81	1.44	1.56
N_4 -Pc* <i>H</i> ₂ ABAB	9.79	343	672	561	1.85	1.75		
N_4 -Pc* <i>H</i> ₂ A ₂ B ₂	9.56/9.50	347	680	563	1.82	1.73	1.41	1.46
N_2 -Pc* <i>H</i> ₂	9.69-9.42	341	687	569	1.80	1.67	1.35	1.45
N_0 -Pc* <i>H</i> ₂	9.91	343	710	580	1.74	1.58	1.35	1.37

[a] ¹H NMR shift of aromatic protons (Ar-H) of N_x -Pc**H*₂ in non-peripheral position of residual [-CH=]-units, substituted by [-N=], in C₆D₆ (300 MHz). [b] B-band / Q-band maximum of N_x -Pc**H*₂, measured in DCM or MeOH. [c] Calculated Q-band maximum using TD-DFT. [d] From experimental UV-Vis measurements: from Q-band ([b]) maxima calculated optical HOMO-LUMO gap. [e] The potential difference, E_g^{CV} , was calculated as the difference between the first oxidation and the first reduction peak (Table 7). [f] absorption maximum from B3LYP/def2-TZVPP. For details, compare to supplement for computational results.

4.2.5 Photophysical Properties of Sub-/Azaphthalocyanines

As described in the introduction 2.2.1, Pcs are interesting compounds for application as photosensitizer (PS) in photodynamic therapy (PDT).^[88] Therefore, a low light emission, i. e. fluorescence, is needed, so that a crossing from the excited singlet to the triplet state is obtained. In literature, a quite small STOKES shift is described for Pc. While several Pcs and Ppzs, as well as larger homologues, were investigated in literature,^[179] and their singlet oxygen quantum yield, Φ_{Δ} , and fluorescence quantum yield, Φ_F , was determined, the systematic investigation by stepwise exchange of [-CH=] with [-N=] is lacking. Therefore, in addition to the electrochemical properties of N_x -[Pc**M*] with *M* = 2 H, Zn (Figure 44), the photophysical properties were investigated in cooperation with the group of ZIMČÍK and NOVÁKOVÁ (Department of Pharmacy at the Charles University of Prague).

Preparation of the Samples. In the following part, the preparation of the samples N_x -[Spc*BCl] and N_x -[Pc**M*] with *M* = 2 H, or Zn for UV-Vis absorption and fluorescence emission measurements, fluorescence quantum yield, Φ_F , as well as for singlet oxygen quantum yield, Φ_{Δ} , measurements, is described. Therefore, all compounds were synthesised and purified immediately before measurement by using preparative TLC (TLC plates on glass with silica gel 60 F₂₅₄ MERCK company). Pc*H₂ and Ppz*H₂ were synthesised using the Li/*n*-octanol method (see section 4.2.3, Scheme 26), and purified by preparative TLC in DCM and DCM/EA 6:1, respectively. For separation of A₃B N₂-Pc*H₂, ABAB and A₂B₂ N₄-Pc*H₂, and AB₃ N₆-Pc*H₂ DCM was used. N₀-[Pc*Zn] and N₈-[Pc*Zn] ([Ppz*Zn]) were synthesised in a neat reaction, and could be used without any further purification by TLC. N_x -[Pc*Zn] were synthesised by treatment of the chromatographically separated N₂-Pc*H₂, ABAB and A₂B₂ N₄-Pc*H₂, and N₆-Pc*H₂ in toluene with [Zn(hmds)₂] or in pyridine using [Zn(OAc)₂]. N_x -[Pc*Zn] were purified by TLC using Tol/THF 20:1. A mixture of CHCl₃/EA 20:1 can alternatively be used. Similarly, symmetrical A₃/B₃ subphthalocyanines/subpyrazinoporphyrazine were synthesised separately, and A₂B and AB₂ N_x -[Spc*BCl] in a random cyclotrimerisation as a mixture. [Spc*BCl] and N₂-[Spc*BCl], N₄-[Spc*BCl] were purified by TLC using toluene; [Sppz*BCl] in DCM. Images of TLC plates are shown in the experimental section. After separation, the products were scratched off the TLC plates and washed off the silica by using a CHCl₃/MeOH 3:1 mixture. The resulting blue/purple solutions were concentrated under reduced pressure.

Fluorescence measurements were carried out by using the diluted N_x -[Pc^{*}M] in THF and N_x -[Spc^{*}BCl] in MeOH. The absorption was adjusted in UV-Vis spectroscopy to a relative absorption of ~ 0.1 . For all five compounds, electronic absorption spectra, fluorescence spectra and excitation spectra were measured. N_x -Pc^{*}H₂ and N_x -[Pc^{*}Zn] were measured using [PcZn] as reference, for both singlet oxygen and absorption/emission measurements. N_x -[Spc^{*}BCl] were measured using rhodamine G6 as reference. The estimated error of this measurement is $\pm 10\%$.

Fluorescence and absorption measurements were carried out in the same cuvette. Impurities or aggregation phenomena can be determined by performing a fluorescence emission measurement right after the fluorescence measurement, as shown on the right side in Figure 57. As usual, for all samples a baseline was measured and the obtained spectra were corrected. For the measurements of the emission spectra, the phthalocyanines were excited at 350 nm and 598 nm, and the subphthalocyanines at a wavelength of 490 nm.

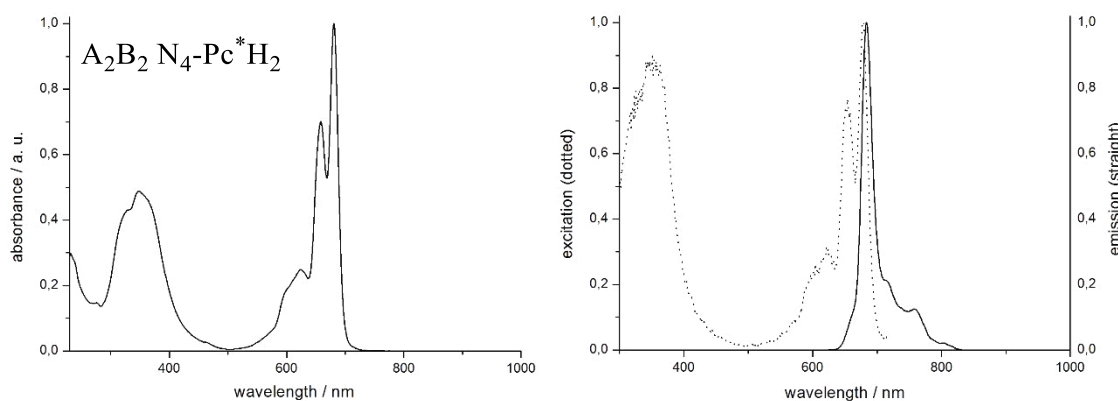


Figure 57: Normalised UV-Vis absorption measurement of $A_2B_2 N_4$ -Pc^{*}H₂ (left) vs FS (solid, straight line) of $A_2B_2 N_4$ -Pc^{*}H₂ and corrected fluorescence emission spectra (excitation, dotted line), in THF at rt.

An in-depth theoretical discussion of how the Φ_F is obtained can be found in literature.^[186] Here, the absolute fluorescence quantum yield, Φ_F , was finally calculated using the reference and its known effective quantum yield in comparison to the integral of the sample, as shown in the equation below:^[187]

$$\phi_F^S = \phi_F^{Ref} \left(\frac{F^S}{F^{Ref}} \right) \left(\frac{1 - 10^{-A^{Ref}}}{1 - 10^{-A^S}} \right)$$

Results and Discussion

In the equation, the fluorescence quantum yield, Φ_F , is obtained from the area under the emission curve, F , in which S indicates the sample and Ref indicates the reference, and A the absorption at the excitation wavelength. The absorption at the excitation wavelength, A , can be calculated with the BOUGUER-LAMBERT-BEER law (see section on singlet oxygen) and the known wavelength mentioned above (aza-Pcs at 350 nm and 598 nm, aza-Spcs at 490 nm). All determined values of Φ_F are summarised in Table 9 for N_x -[Pc^{*}M] and in Table 10 for N_x -[Spc^{*}BCl].

In measurements, the absorption and excitation spectra match perfectly to each other, confirming the monomeric form of the compounds in solution; aggregation can therefore be excluded. Aberrations of the fluorescence emission spectra were observed only for Ppz^{*}H₂, indicating the presence of another species, such as a partially deprotonated ligand-species.^[188] However, Φ_F of Ppz^{*}H₂ appears very weak. The fluorescence spectra show an expected small STOKES shift, which can be finely tuned by the number of pyrazine units within the N_x -[Pc^{*}M] and N_x -[Spc^{*}BCl]. Visible to the unaided eye is the aza-fine tuning of these compounds in the fluorescence-emission based on the macrocycle core of the samples, when the samples are illuminated with light of $\lambda = 365$ nm. In Figure 58, the cuvettes of the azasubphthalocyanines N_x -[Spc^{*}BCl] and a zinc-pyrazinoporphyrazine are shown.



Figure 58: Cuvettes of a [PpzZn] (left) in THF and N_x -[Spc^{*}BCl] in MeOH, with increasing number of [-N=] in N_x -[Spc^{*}BCl] from $x = 0, 2, 4, \text{ to } 6$ (left to right). Samples are illuminated with light at $\lambda = 365$ nm.

Singlet oxygen quantum yield, Φ_{Δ} , was determined using the experimental setup of the group of ZIMČÍK and NOVÁKOVÁ. A schematic illustration of the device is shown in Figure 59. For N_x -[Pc**M*], [PcZn] was used as reference, for N_x -[SpC**BCl*], Bengal Rose was used. Different filters for azaphthalocyanines and azasubphthalocyanines were used, as described in the experimental section. The filter prevents excessive heating of the sample while only transmitting light above a desired wavelength.

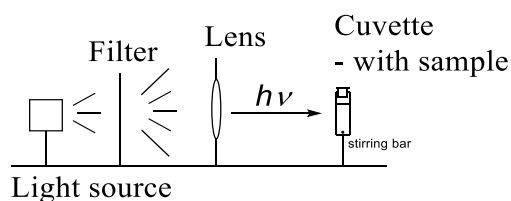
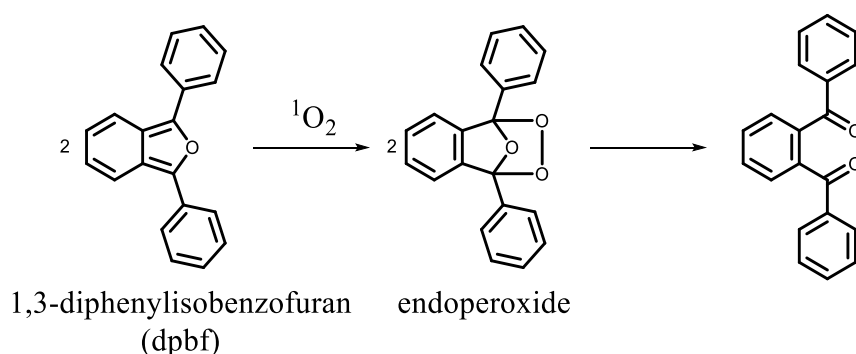


Figure 59: Schematic measurement setup for determination of singlet oxygen production.

In this method, the singlet oxygen yield, Φ_{Δ} , was determined by the decomposition of 1,3-diphenylisobenzofuran (dpbf) in THF, with the respective sample. The reaction of the decomposition is shown in Scheme 34. The dpbf forms as intermediate an endoperoxide, which is finally oxidised to dibenzophenone, which causes the UV-Vis absorption at about 410 nm to decrease.^[179] For better comparability, the measurements of all samples were carried within one series of measurements. A $\sim 5 \cdot 10^{-5}$ N stock solution of dpbf in THF was prepared. The intensity of the respective dye was adjusted to a relative absorbance of 0.1 before the measurement. The estimated error of this method is $\pm 10\%$.



Scheme 34: Formation of dibenzophenone from dpbf, induced by formation of singlet oxygen when N_x -[Pc**M*]/ N_x -[SpC**BCl*] was illuminated.

For the measurements, first a UV-Vis spectrum of the singlet oxygen scavenger dpbf was measured in a 10 x 10 mm quartz cuvette and the baseline was set, after saturation of the solution with oxygen, for 1 min.^[189,190] Then, the pure sample was added and measured in the dark (Figure 60).

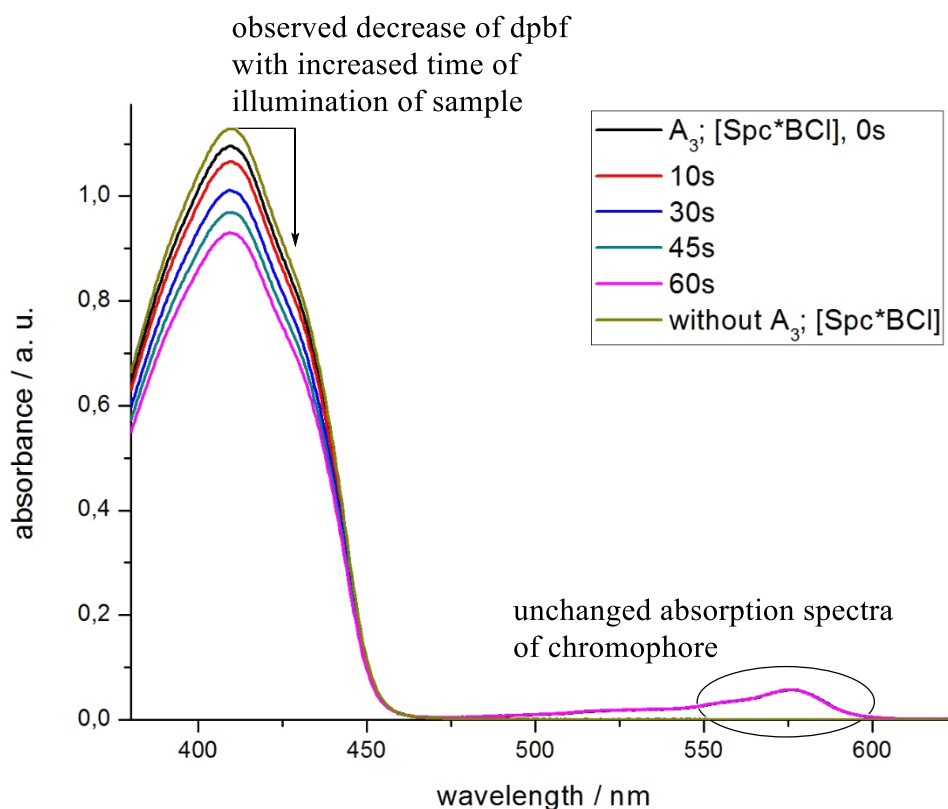
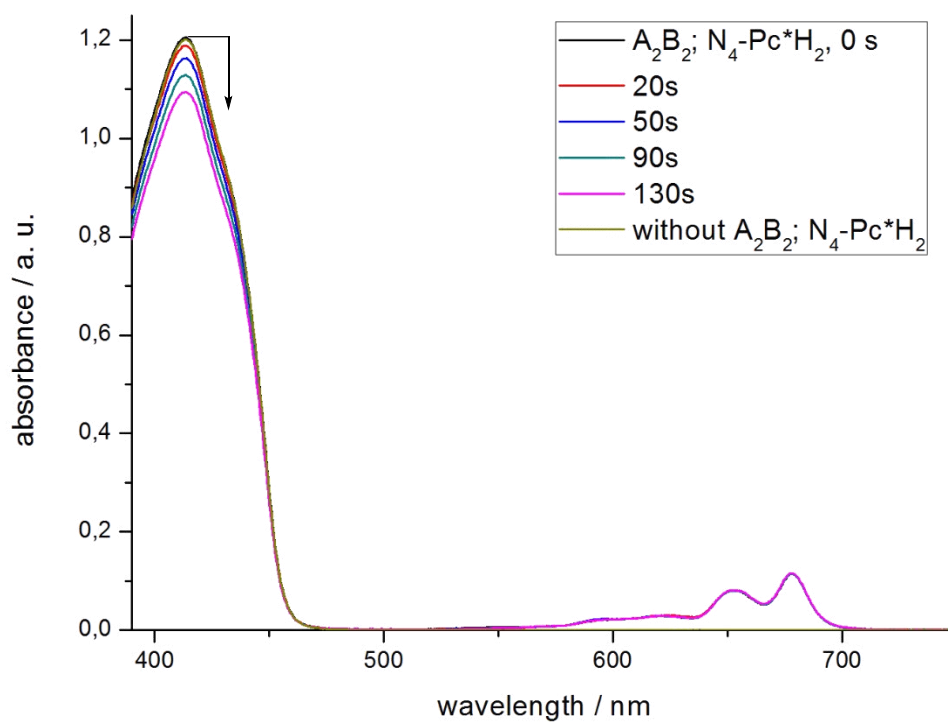


Figure 60: Measurements for determination of singlet oxygen production. Examples are shown for chromophores $A_2B_2; N_4-Pc^*H_2$ and $[Spc^*BCI]$, measured vs decreasing intensity of the indicator, dpbf, with the time of illumination of the sample.

After this "second baseline" was set, the sample was illuminated for at least 5 separate intervals in the shown setup (see again in Figure 59). For illumination, a xenon lamp was used (100 W, ozone free XE DC short arc lamp, Newport). The time of illumination was adjusted in correlation to the decrease of dpbf (Figure 60). The intensity of the singlet oxygen scavenger, dpbf, should not decrease by more than 15% from its initial intensity. The absorption spectrum of the investigated compounds should not change at all. Two example spectra for Φ_{Δ} determination are shown in Figure 60. On the top, the spectrum of $A_2B_2 N_4\text{-Pc}^*\text{H}_2$ is shown and that for $[\text{Sp}^*\text{BCl}]$ is shown on the bottom. It is visible that the absorption spectra of the sample did not change while measuring.

The decrease in intensity of the reference compounds was determined and plotted versus the time of irradiation of the sample. The slope of the resulting linear function $f = k \cdot x + c$ was determined, and the singlet oxygen yield, Φ_{Δ} , was estimated by comparative method using [PcZn] or Bengal Rose as reference. The singlet oxygen quantum yield is finally calculated using the following equation: ^[179]

$$\phi_{\Delta}^S = \phi_{\Delta}^{Ref} \frac{k^S \cdot I_{aT}^{Ref}}{k^{Ref} \cdot I_{aT}^S}$$

In the equation, k is the slope, determined by the decrease of dpbf, in dependence of $\ln(A_0/A_t)$. A_0 is the measured absorption at the initial time $t = 0$ and A_t the absorption after illuminated time t . I_{aT} is the intensity of total absorbed light by the compound while illuminated. It is calculated as the sum of intensities I_a . In the case of $N_x\text{-[Pc}^*\text{M]}$, the filter cuts-off the light under 523 nm, and above 750 nm, no absorption was observed. Then, I_{aT} is the sum between 523 nm and 750 in e. g. 0.5 nm measured steps.

The absorbed light at a specific wavelength I_a is given by the BOUGUER-LAMBERT-BEER law:

$$I_a = I_0 \cdot (1 - e^{-2,3A}) \text{ and } A = \lg\left(\frac{I_0}{I_a}\right) = \varepsilon cd$$

Furthermore, *Ref* indicates the measured reference compound, and *S* the measured sample.^[191]

Results and Discussion

Obtained values for $\Phi_{\Delta} + \Phi_{\text{F}}$ are summarised in Table 9 for $N_x\text{-[Pc}^*\text{M]}$ and in Table 10 for $N_x\text{-[Spc}^*\text{BCl]}$. All values for fluorescence quantum yield and singlet oxygen yield, are plotted in Figure 61. It is evident that values of $N_x\text{-[Pc}^*\text{Zn]}$ obtained for $\Phi_{\Delta} + \Phi_{\text{F}}$ are approximately 0.9, which are reasonably close to the ideal value of 1. The singlet oxygen quantum yield, Φ_{Δ} , of a useful and efficient species for application in PDT is in general >0.6 .^[87] The sum of the $\Phi_{\Delta} + \Phi_{\text{F}}$ should lie >0.75 . If the sum is lower, then in general internal conversion or "quenching processes" of the macrocycles are occurring.

According to other examples described in literature, the highest singlet oxygen quantum yield, Φ_{Δ} , could be observed for ABAB $N_4\text{-[Pc}^*\text{Zn]}$, which is also significantly higher than the one for the corresponding A_2B_2 derivative.^[30]

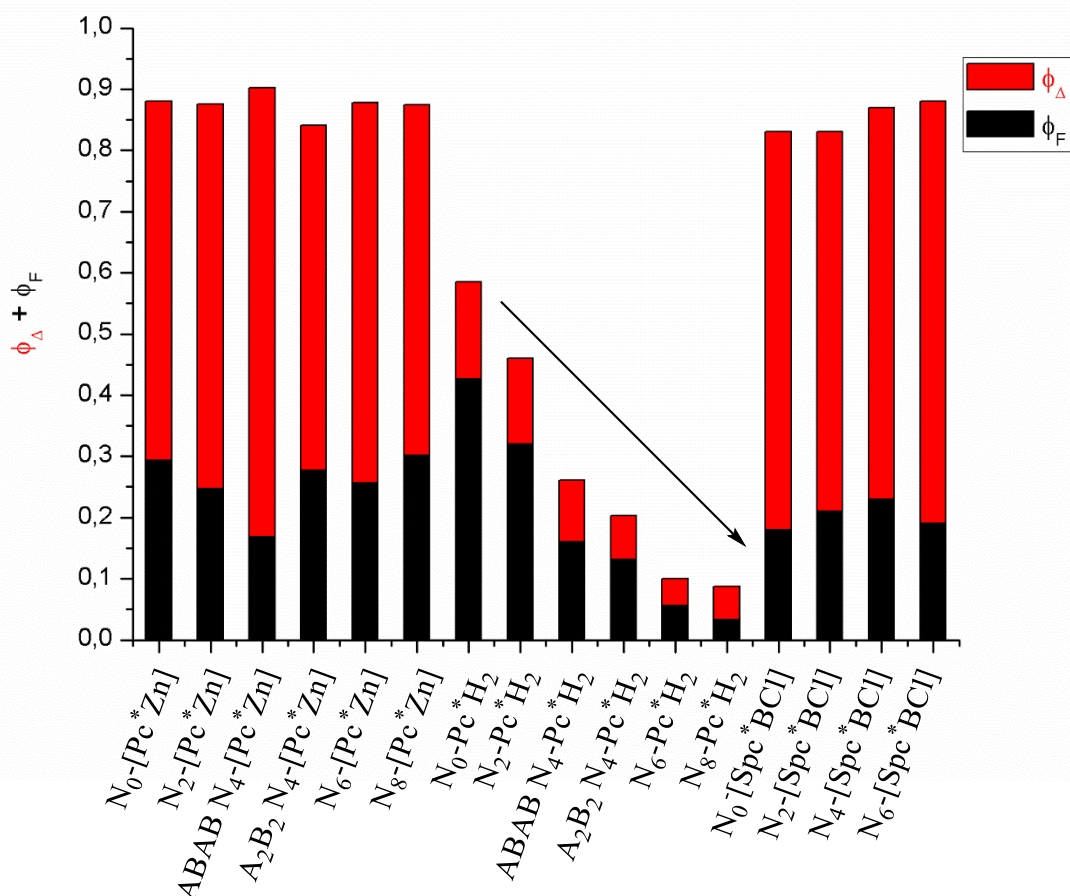


Figure 61: Obtained values for fluorescence quantum yield, Φ_{F} , and singlet oxygen quantum yield, Φ_{Δ} , of $N_x\text{-[Pc}^*\text{M]}$ with $M = 2 \text{ H or Zn}$ and $N_x\text{-[Spc}^*\text{BCl]}$.

The opposite of that is visible for the fluorescence quantum yield, Φ_{F} ; a significantly higher value was found for $A_2B_2 N_4\text{-[Pc}^*\text{Zn]}$ in comparison to the ABAB derivative. Φ_{F} of $A_2B_2 N_4\text{-[Pc}^*\text{Zn]}$ shows similar values as the A_4 and B_4 systems, $N_0\text{-}$ and $N_8\text{-[Pc}^*\text{Zn]}$. In contrast

to N_x -[Pc*Zn], N_x -Pc*H₂ shows a strong decrease of both Φ_Δ and Φ_F . Such a trend has not been observed before. Only strong differences between free ligands of phthalocyanines and pyrazinoporphyrazines are known, but no systematic investigation by increasing the number of nitrogen atoms, [-N=] units, has ever been carried out. The previously described trend for benzo-fused porphyrazines,^[192] that Φ_F decreases with increasing size of the molecule and when the symmetry of the molecule is lowered,^[30] is not found for the N_x -Pc*H₂ series. In addition, ABAB N_4 -Pc*H₂ does not show the highest Φ_Δ , as observed for ABAB N_4 -[Pc*Zn] in the N_x -[Pc*Zn] series. In the case of the protonated series, both Φ_Δ and Φ_F seem to almost perfectly decrease with an increasing number of x of N_x -Pc*H₂, from $x = 0 \rightarrow 8$. The decrease of the sum of Φ_Δ and Φ_F can be explained by the previously mentioned internal conversion within the macrocycles. Spin orbit coupling (SOC) of central zinc can be taken into consideration as well; it facilitates ISC.

Table 9: Obtained values for fluorescence quantum yield, Φ_F , and singlet oxygen quantum yields, Φ_Δ , of N_x -[Pc*M] with $M = 2$ H or Zn, measured in THF.

	Exc. / 350 nm	Exc. / 598 nm	Φ_F ^[a]	Φ_F ^[b] [Lit] ^[25]	Φ_Δ ^[a]	$\Phi_F + \Phi_\Delta$
N_0 -[Pc*Zn]	0.275	0.310	0.29	0.13	0.59	0.88
N_2 -[Pc*Zn]	0.241	0.253	0.25		0.63	0.88
ABAB N_4 -[Pc*Zn]	0.159	0.177	0.17		0.73	0.90
A ₂ B ₂ N_4 -[Pc*Zn]	0.261	0.351	0.28		0.64	0.91
N_6 -[Pc*Zn]	0.242	0.271	0.26		0.62	0.88
N_8 -[Pc*Zn]	0.272	0.302	0.22	<0.05	0.57	0.80
N_0 -Pc*H ₂	0.435	0.453	0.444	0.14	0.159	0.603
N_2 -Pc*H ₂	0.308	0.332	0.320		0.140	0.460
ABAB N_4 -Pc*H ₂	0.159	0.163	0.161		0.100	0.261
A ₂ B ₂ N_4 -Pc*H ₂	0.126	0.137	0.132		0.071	0.203
N_6 -Pc*H ₂	0.052	0.059	0.056		0.044	0.100
N_8 -Pc*H ₂	0.037	0.029	0.033	0.48	0.054	0.087

[a] Φ_Δ measured in an oxygen saturated solution of THF using [PcZn] as reference, dpbf as scavenger and indicator. Φ_F was measured in THF using [PcZn] as reference. Excitation was done at 350 nm and 598 nm. [b] previously determined values for selected substances.^[25]

Results and Discussion

N_x -[Sp c^* BCl] show a similar behaviour as reported for other examples for substituted Sp c s.^[193] Here, the sum of $\Phi_\Delta + \Phi_F$ is also ~ 0.9 . Both Φ_Δ and Φ_F , of all N_x -[Sp c^* BCl] show comparable values of $\Phi_\Delta = 0.7$ and $\Phi_F = 0.2$, whereby a weak increase of Φ_Δ from N_0 -[Sp c^* BCl] ($\Phi_\Delta = 0.64$) to N_6 -[Sp c^* BCl] ($\Phi_\Delta = 0.88$) can be observed.

Table 10: Obtained values for fluorescence quantum yield, Φ_F , and singlet oxygen quantum yield, Φ_Δ , of N_x -[Sp c^* BCl], measured in MeOH.

	Φ_F [a]	Φ_Δ [a]	[Lit] ^{[25],[b]}	$\Phi_F + \Phi_\Delta$
N_0 -[Sp c^* BCl]	0.176	0.643	0.21	0.819
N_2 -[Sp c^* BCl]	0.215	0.654		0.868
N_4 -[Sp c^* BCl]	0.237	0.668		0.905
N_6 -[Sp c^* BCl]	0.191	0.881	0.18	1.07

[a] Φ_Δ measured in an oxygen saturated solution of MeOH using Rose Bengal as reference. Φ_F was measured in MeOH using Rhodamine as reference. Excitation was done at 490 nm. [b] previously determined values for selected substances.

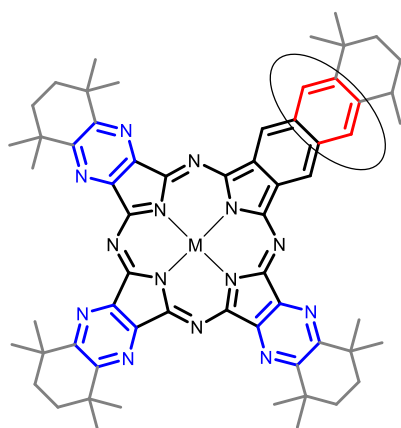
In Table 9 for N_x -[Pc * M] and in Table 10 for N_x -[Sp c^* BCl], previously determined values of fluorescence quantum yields, Φ_F , are also shown, which differ strongly from values determined in this work.^[25] This shows the importance of measuring the samples together (within one series of measurements) to obtain comparable values. To give comparable examples of literature described values for Φ_F , similar compounds were chosen: Φ_F (PcH $_2$) = 0.77,^[194] Φ_F ([PcZn]) = 0.23,^[111] Φ_F ([Sp c BCl]) = 0.25,^[193] and Φ_F (substituted [PpzZn]) = <0.23 .^[195] Almost all literature reported compounds show higher values, but the trends seen are all comparable.

Fluorescence lifetime, τ_F , was determined by ZIMČÍK and NOVÁKOVÁ. Determined values for τ_F are in correlation with Φ_F ; for $AB_3 N_6\text{-Pc}^*\text{H}_2$ and Ppz^*H_2 , the decay curves were biexponential with increased contribution. Owing to the small sum of $\Phi_\Delta + \Phi_F$ and small lifetime τ_F , another relaxation pathway can be proposed for increasing number of pyrazine units x in $N_x\text{-Pc}^*\text{H}_2$. In Table 11, all values obtained in photophysical measurements are summarized and compared.

Table 11: Electronic and photophysical data of $N_x\text{-[Pc}^*\text{M]}$ in THF and $N_x\text{-[Spc}^*\text{BCl]}$ in MeOH.^[a]

	λ_{max} (Q-band) / nm	λ_F / nm	STOKES-Shift / nm	τ_F / ns ^[b]	Φ_F ^[c]	Φ_Δ ^[d]	$\Phi_F + \Phi_\Delta$
$N_0\text{-Pc}^*\text{H}_2$	707, 673	711	4	5.52	0.42	0.16	0.58
$N_2\text{-Pc}^*\text{H}_2$	686	692	6	3.45	0.33	0.14	0.47
$N_4\text{-Pc}^*\text{H}_2$	678, 653	684	6	1.62	0.14	0.07	0.21
$N_4\text{-Pc}^*\text{H}_2$	668, (701)	674	6	1.79	0.16	0.10	0.26
$N_6\text{-Pc}^*\text{H}_2$	658, 643	664	6	3.92 (26%), 0.63 (74%)	0.06	0.04	0.10
$N_8\text{-Pc}^*\text{H}_2$	652, 623	658	6	2.15 (29%), 0.36 (71%)	0.03	0.05	0.08
$N_0\text{-[Pc}^*\text{Zn]}$	683	689	6	3.31	0.31	0.59	0.90
$N_2\text{-[Pc}^*\text{Zn]}$	679, 668	686	7	2.69	0.25	0.63	0.88
$N_4\text{-[Pc}^*\text{Zn]}$	658	667	9	3.08	0.35	0.56	0.91
$N_4\text{-[Pc}^*\text{Zn]}$	679, 651	687	8	1.98	0.18	0.73	0.91
$N_6\text{-[Pc}^*\text{Zn]}$	648	663	15	2.69	0.27	0.62	0.89
$N_8\text{-[Pc}^*\text{Zn]}$	633	642	9	2.98	0.30	0.57	0.87
$N_0\text{-[Spc}^*\text{BCl]}$	575	587	12	2.04	0.18	0.65	0.82
$N_2\text{-[Spc}^*\text{BCl]}$	566	577	11	2.19	0.21	0.62	0.82
$N_4\text{-[Spc}^*\text{BCl]}$	555	567	12	2.85	0.23	0.64	0.87
$N_6\text{-[Spc}^*\text{BCl]}$	533	546	13	2.98	0.19	0.69	0.87

[a] absorption maximum (λ_{max}), fluorescence emission maximum (λ_F), fluorescence lifetime (τ_F), fluorescence quantum yield (Φ_F), singlet oxygen quantum yield (Φ_Δ). [b] $\lambda_{\text{exc}} = 371$ nm or 634 nm. [c] with [PcZn] ($\Phi_{F(\text{THF})} = 0.32$, $\lambda_{\text{exc}} = 598$ nm) and rhodamin G6 ($\Phi_{F(\text{EtOH})} = 0.94$, $\lambda_{\text{exc}} = 490$ nm) as reference for $N_x\text{-[Pc}^*\text{M]}$ and $N_x\text{-[Spc}^*\text{BCl]}$, respectively. [d] with [PcZn] ($\Phi_{\Delta(\text{THF})} = 0.53$) and bengal rose ($\Phi_{\Delta(\text{MeOH})} = 0.76$) as reference for $N_x\text{-[Pc}^*\text{M]}$ and $N_x\text{-[Spc}^*\text{BCl]}$, respectively.

4.2.6 Synthesis of Pyrazinonaphthalocyanines $N_x\text{-Npz}^*\text{H}_2$ 

$$N_x\text{-}[Npz^*M]$$

N = Naphthalocyanine units

pz = pyrazine units

x = number of [-N=] building blocks in $[Npz^*M]$

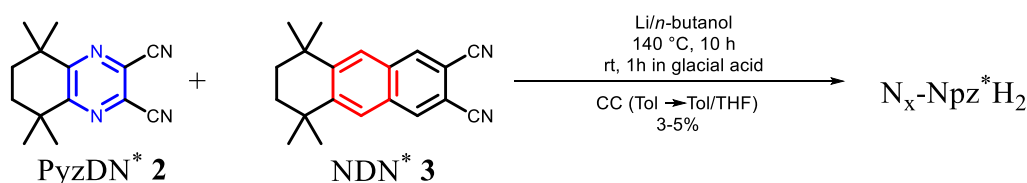
Figure 62: $N_x\text{-Npz}^*\text{H}_2$ compounds, synthesised by LANGE.

Additional benzannulation of $N_x\text{-Pc}^*\text{H}_2$ was carried out.

In addition to the synthesised azaphthalocyanine series $N_x\text{-}[Pc^*M]$, LANGE attempted to synthesise a series of naphthaloporpyrazines $N_x\text{-Npz}^*\text{H}_2$.^[196] The difference of $N_x\text{-Npz}^*\text{H}_2$ to the compounds described in the previous section, $N_x\text{-Pc}^*\text{H}_2$, is the additional benzannulation, shown on the left in red. Mixed soluble pyrazinoquinoxalino-porphyrazines are already described in literature (compare to section 2.1.3).^[35] Thereby, similar conditions were chosen, using *n*-BuOH and 10 eq of Li. In this

bachelor thesis, for the first time, the influence of additional annulated benzene units should be studied and compared to the completed aza-series $N_x\text{-Pc}^*\text{H}_2$. LANGE was able to synthesise a new series of azanaphthalocyanine hybrid compounds $N_2\text{-Npz}^*\text{H}_2$, A_2B_2 $N_4\text{-Npz}^*\text{H}_2$ and $N_6\text{-Npz}^*\text{H}_2$ using $PDN^* 1$ and $NDN^* 3$ in a 1:1 ratio (Figure 63). The ABAB $N_4\text{-Npz}^*\text{H}_2$ could be isolated in later work, for completeness of the series $N_x\text{-Npz}^*\text{H}_2$ with $x = 0 \rightarrow 8$.

The synthesis was carried out as described before, with the Li/*n*-butanol method. All $N_x\text{-Npz}^*\text{H}_2$ could be obtained in yields of 2-5% after CC (gradient Tol \rightarrow Tol/THF 10:1).



Scheme 35: Synthesis of $N_x\text{-Npz}^*\text{H}_2$ described in the bachelor thesis of LANGE.

Similarly, compared to the $N_x\text{-Pc}^*\text{H}_2$ series, here, first $Nc^*\text{H}_2$ was eluted, and then azacompounds $N_x\text{-Npz}^*\text{H}_2$ with increasing pyrazine character (exchange of [-CH=] units by [-N=]) from $x = 2 \rightarrow 8$. All of the compounds were characterized by ^1H NMR, UV-Vis, FS spectroscopy and APCI-HR mass spectrometry.

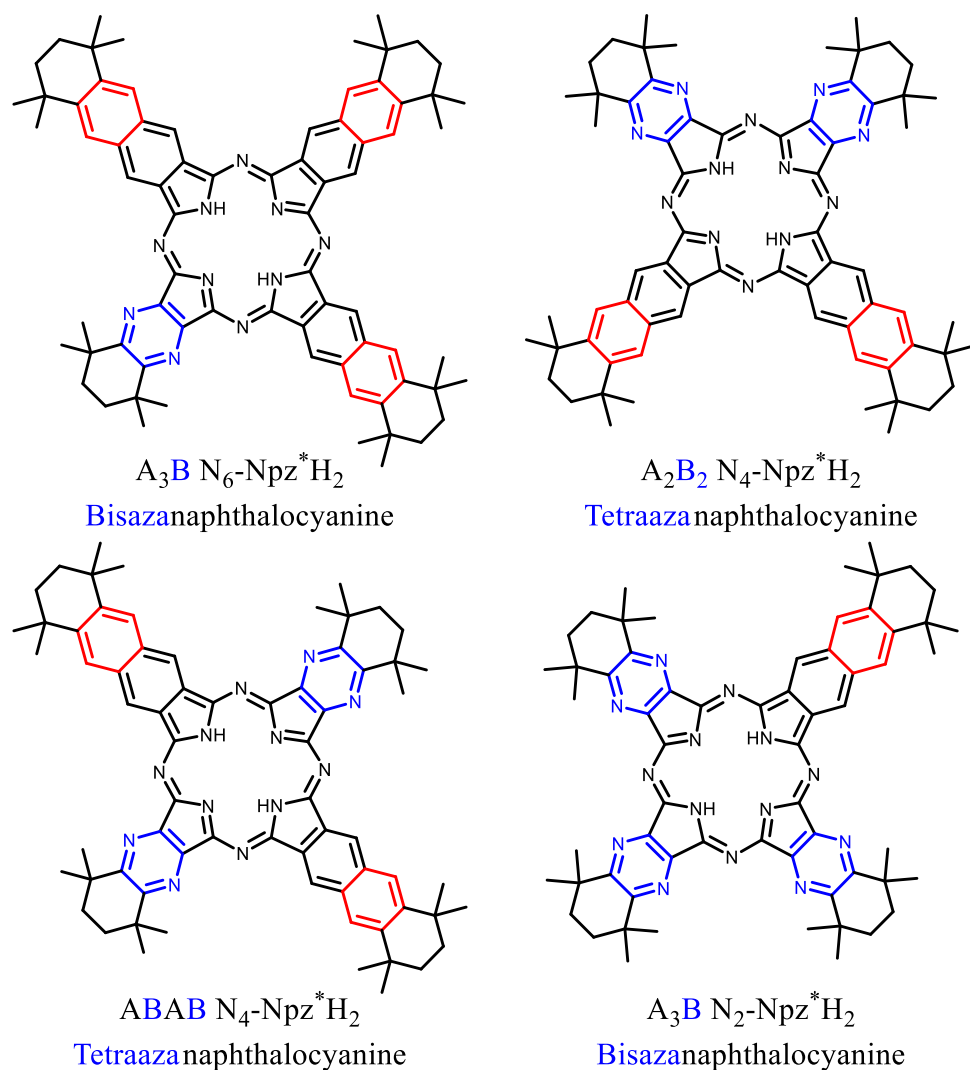


Figure 63: Synthesised $N_x-Npz^*H_2$ by LANGE.^[196]

The UV-Vis absorption and FS spectra were measured in DCM and are shown in Figure 64 besides the UV-Vis spectra of the $N_x-Pc^*H_2$ series. All obtained values of UV-Vis data and FS are collected in Table 12. Similar to $N_x-Pc^*H_2$, these compounds show a hypsochromical shift of the Q-band from that of Nc^*H_2 (797 nm) to Ppz^*H_2 (655 nm) with increasing number of [-N=] units in $N_x-Npz^*H_2$: $x = 0 \rightarrow 8$. Here again, a non-linear increase of the band gap was observed. N_2 - and $N_6-Npz^*H_2$ show a lower Stokes shift of ~10 nm in comparison to 14 nm for $A_2B_2 N_4-Npz^*H_2$.

In comparison to the UV-Vis spectrum of $ABAB N_4-Pc^*H_2$, $ABAB N_4-Npz^*H_2$ does show an intense splitting of the Q-band peaks, as it is typical for these ABAB compounds. Here, the degenerate orbitals are split quite clearly, and the highest STOKES shift of ~31 nm was observed, which is in accordance with comparable literature described compounds.^[30]

Results and Discussion

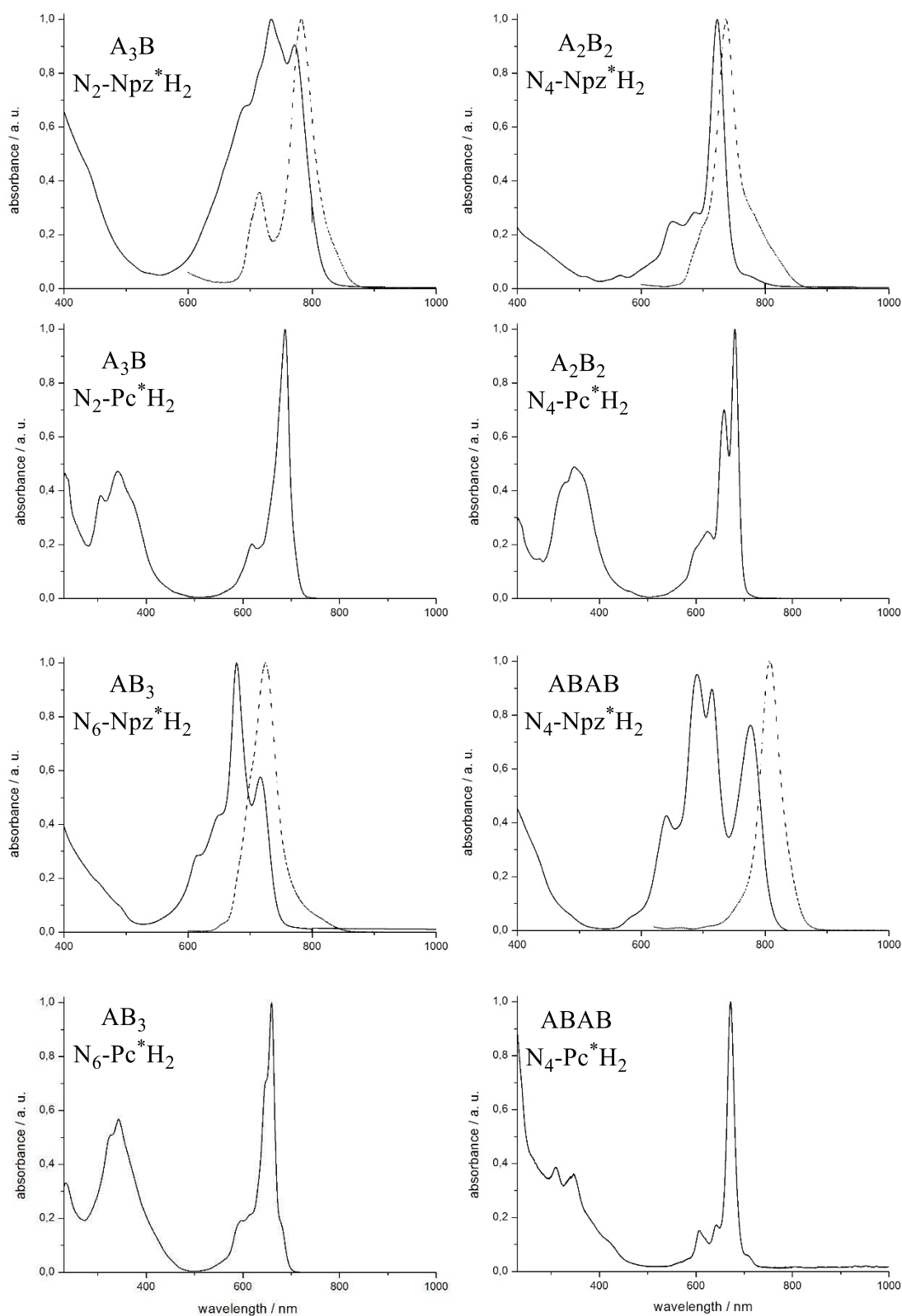


Figure 64: Measured UV-Vis (straight lines) and FS (dotted lines) spectra of $N_x\text{-Npz}^*\text{H}_2$ (upper) compared to UV-Vis spectrum of $N_x\text{-Pc}^*\text{H}_2$ (lower spectrum), in DCM at rt.^[196] Influence of benzannulation and symmetry of the respective molecule is visible.

(In FS measurements, the additional peak observed at ~700 nm is caused by an error of the device)

Table 12: UV-Vis absorption and FS of N_x -Npz^{*}H₂ series compared to N_x -Pc^{*}H₂ series, measured in DCM. The influence of the benzannulation is given by $\Delta\lambda$, as well as the STOKES shift of the N_x -Npz^{*}H₂ series.

	B-Band / nm	Q-Band Nc / nm	Q-Band Pc / nm	$\Delta\lambda$ / nm	Emission / nm	STOKES Shift / nm
N_0 -Nc [*] H ₂ / N_0 -Pc [*] H ₂	327	797	710	87	805	8
N_2 -Npz [*] H ₂ / N_2 -Pc [*] H ₂	331	772, 738	687	51	782	10
A ₂ B ₂ N_4 -Npz [*] H ₂ / N_4 -Pc [*] H ₂	337	723	680	43	737	14
ABAB N_4 -Npz [*] H ₂ / N_4 -Pc [*] H ₂	342	777, 690	672	18	808	31
N_6 -Npz [*] H ₂ / N_6 -Pc [*] H ₂	342	717, 678	660	18	724	8
N_8 -Ppz [*] H ₂	342	655	655	-	758	3

In cyclic voltammetry (CV), because of their lower solubility compared to N_x -Pc^{*}H₂, a weaker intensity of the peaks with increasing $x = 0 \rightarrow 8$ was observed. The CV spectra are attached as SI to this thesis. In summary, a decreasing HOMO-LUMO gap from Ppz^{*}H₂ to N_2 -Npz^{*}H₂ was observed; compare Table 13 below. Similar to N_x -Pc^{*}H₂, a reverse trend to literature expectations with decreasing oxidation and reduction potentials was observed. Once more E_{ox1} and E_{red1} potentials are decreasing as the number of pyrazine units increases. In all CV measurements, the first oxidation peak appears broadened. It seems that two oxidation peaks are laying beside each other.

Table 13: Electrochemical data of N_x -Npz^{*}H₂ in comparison.^[a]

	Ppz [*] H ₂	N_6 -Npz [*] H ₂	ABAB ^[b] N_4 -Npz [*] H ₂	A ₂ B ₂ N_4 -Npz [*] H ₂	N_2 -Npz [*] H ₂	Nc [*] H ₂ ^[b]
E_{ox}^2 / V	-	-	-	0.16	0.29	0.15
E_{ox}^1 / V	0.87	0.02	0.34	-0.25	-0.32	-0.11
E_{red}^1 / V	-1.05	-1.79	-1.14	-1.74	-1.69	-1.35
E_{red}^2 / V	-1.37	-2.26	-1.52	-2.11	-2.02	-1.74
E_g^{CV} / V	1.92	1.81	1.48	1.49	1.37	1.25
λ_{max} / nm	655	678	690	723	738	797

[a] CV and UV-Vis measurements were carried out in DCM. In CV, E_{red} and E_{ox} are expressed as $E_{1/2}$, ferrocene/ferrocenyl was used as reference. Glassy carbon working electrode, Pt counter electrode, Ag reference electrode, at 25 °C. The potential difference, E_g^{CV} , was calculated from the difference between the first oxidation and the first reduction peak. [b] because of the low solubility of ABAB N_4 -Npz^{*}H₂ and Nc^{*}H₂ in DCM, the CV results are given from measurements in THF.

In both CV and UV-Vis spectroscopy, a decrease of the HOMO-LUMO band gap with increasing benzannulation of N_x -Pc^{*}H₂ was observed. The Q-bands of N_x -Npz^{*}H₂ are additionally shifted bathochromically in comparison to their smaller homologues N_x -Pc^{*}H₂. The shift is not increasing in a linear fashion with respect to the amount of annulation.

In ¹H NMR spectroscopy, A₂B₂ and ABAB isomers of N_4 -Npz^{*}H₂ (Figure 65) can be identified in the same way as done for the N_4 -Pc^{*}H₂ compounds (see section 4.2.4.1).

Results and Discussion

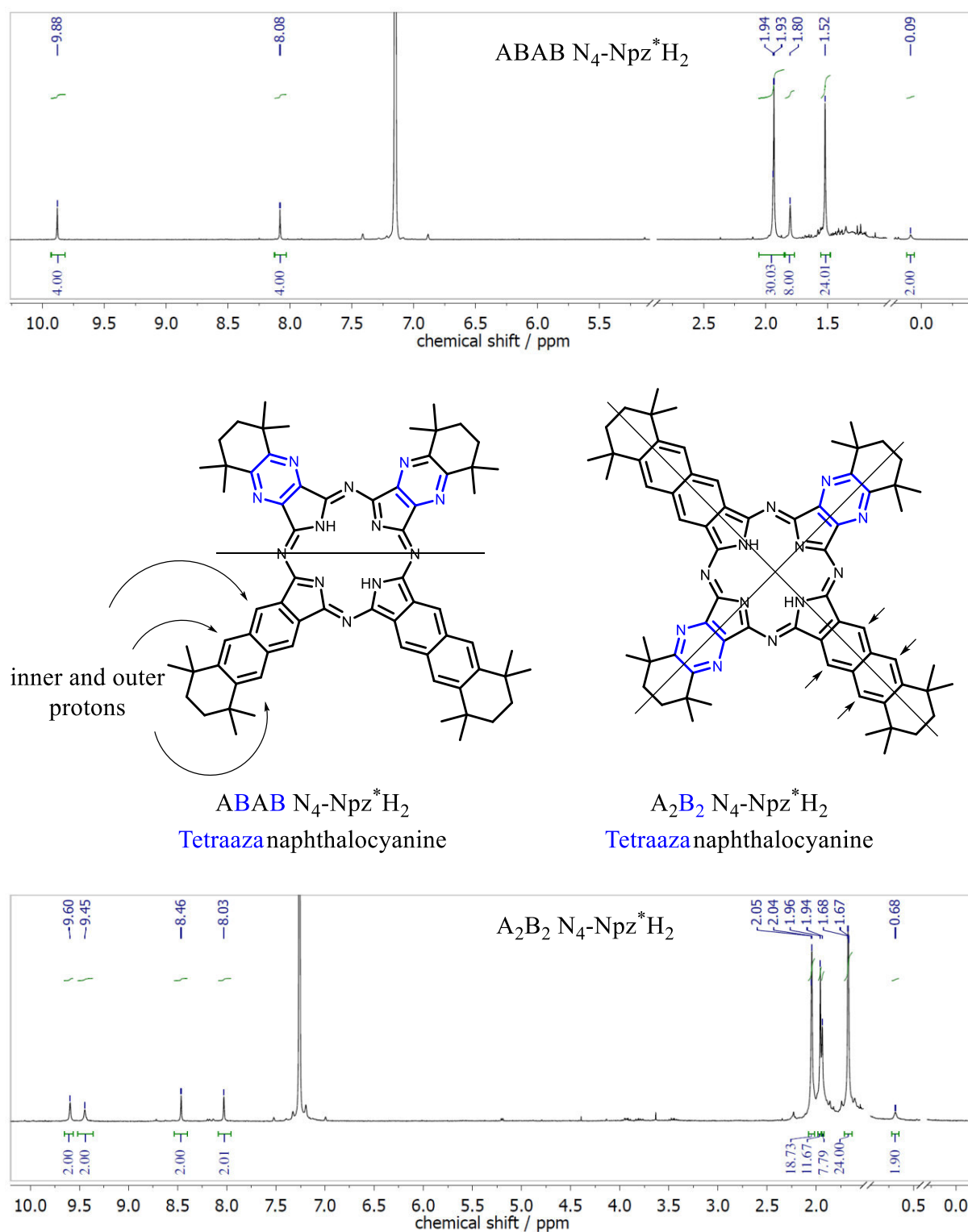


Figure 65: ^1H NMR spectrum of ABAB (upper) and A_2B_2 (lower) $\text{N}_4\text{-Npz}^*\text{H}_2$, in $\text{CDCl}_3/\text{C}_6\text{D}_6$ (300 MHz).

For ABAB/ A_2B_2 $\text{N}_4\text{-Npz}^*\text{H}_2$, one or two additional signals compared to ABAB/ A_2B_2 $\text{N}_4\text{-Pc}^*\text{H}_2$ are visible at 8.08 ppm or 8.46 ppm and 8.03 ppm, respectively. These signals are due to the outer aromatic protons of the annulated benzene rings. Conversely, the inner NH protons are low-field shifted to 0.09 and 0.68 ppm, caused by the electron rich π -system.

In future, Φ_{Δ} and Φ_F of these compounds should be determined, as the lower symmetrical naphthalocyanine units appear to have a positive influence with regards to their potential PDT applications.^[84] Therefore, especially the trend of Φ_{Δ} and Φ_F of the protonated species $N_x-Nc^*H_2$ would be of interest. Φ_{Δ} and Φ_F of the corresponding metalated analogues $N_x-[Npz^*Zn]$ should be in accordance with data of comparable compounds described in literature.^[30] We expect that with an annulation of $N_x-[Pc^*Zn]$, Φ_F of $N_x-[Npz^*Zn]$ decreases compared to $N_x-[Pc^*Zn]$, while the highest Φ_{Δ} will be expected for ABAB $N_4-[Nc^*Zn]$.

4.2.7 Synthesis of Tetrabenzotriazaporphyrins (TBTAPs)

The synthesis of tetrabenzotriazaporphyrins (TBTAP, Figure 66) and derivatives has been described several times in literature: just recently, a selective synthesis of unsubstituted TBTAPs with yields of 40% was described by the group of CAMMIDGE.^[197,198] The structural difference to $N_x-Pc^*H_2$ is the systematic exchange of [-N=] building blocks by [-CH=] in the meso positions of the Pc, instead of the non-peripheral position.

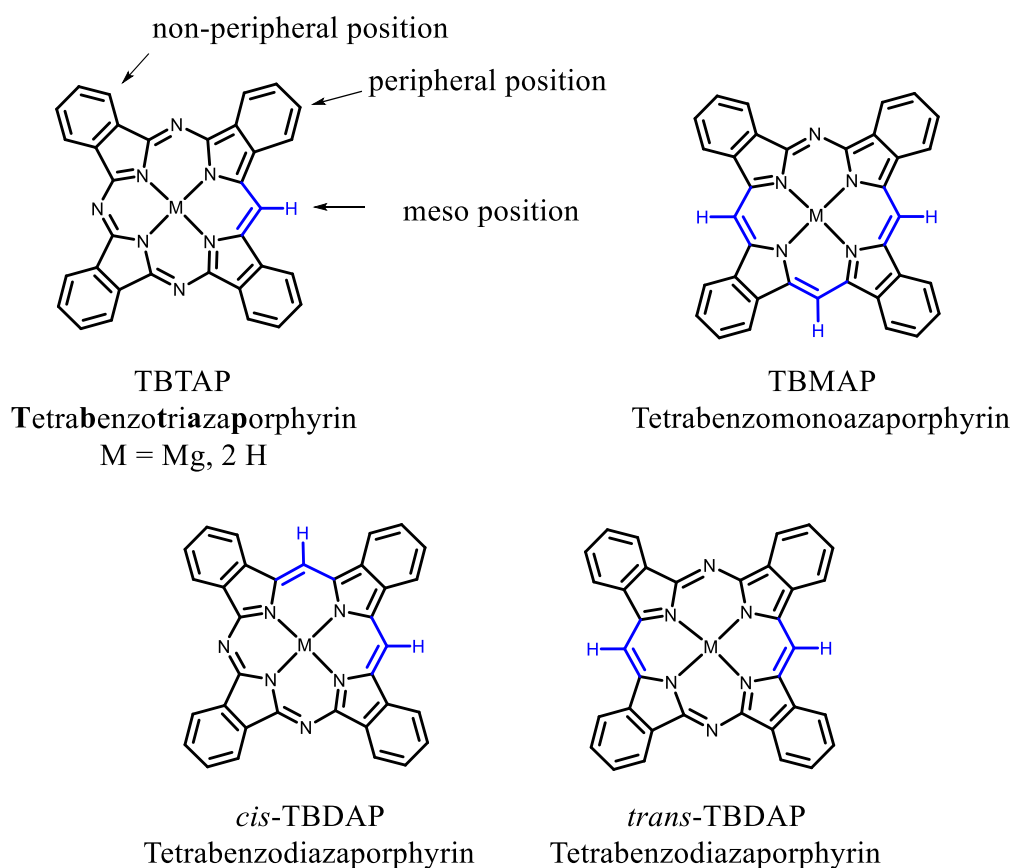
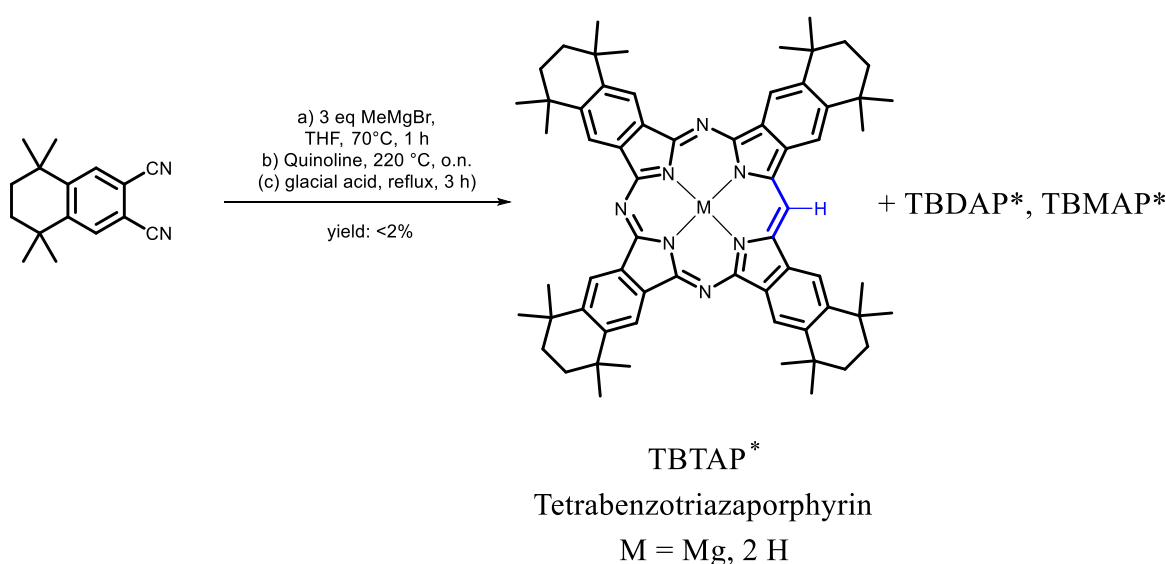


Figure 66: Structures of TBTAP, TBDAP and TBMAP.

Results and Discussion

In the selective synthesis by the group of CAMMIDGE, an unsubstituted aminoisoindoline is preformed in a SONOGASHIRA coupling, which is then reacted with 3 eq of PDN to form the porphyrin ring.^[197,198] The synthesis of TBTAP and derivatives using peripheral alkyl substituted phthalonitriles is still not so far investigated. Complicated synthetic routes using GRIGNARD reagents are the most common. The main disadvantage of these syntheses are the low yields. In these reactions, the phthalonitrile is attacked by the GRIGNARD reagent as nucleophile, so the aminoisoindoline is formed *in situ*. At high temperatures a mixture of tetrabenzotriazaporphyrin (TBTAP), tetrabenzodiazaporphyrin (TBDAP) and tetrabenzomonoazaporphyrin (TBMAP) and the corresponding phthalocyanine is formed. A separation by column chromatography leads to the products in low yields <10%. The first synthesis applying PDN* 1 and a phenyl- GRIGNARD was also described by CAMMIDGE, in 2014.^[137] However, no analysis data and spectra of the synthesised compound were given. In this chapter, the UV-Vis spectra and NMR spectra are described. The reaction was carried out according to the literature known conditions (Scheme 36). The formation of the cyclised product [TBTAP*Mg] was controlled by UV-Vis spectroscopy and MS. The Mg-cation was directly removed with glacial acid by refluxing the solution for 1-3 h, because an easier separation of the free ligands was expected. After removing the solvents, the products TBTAP*, TBDAP* and TBMAP* were separated by column chromatography, yielding up to 2% of each compound depending on the used amount of MeMgBr. The *meso*-position substituted TBTAP* was characterized by using ¹H NMR and UV-Vis spectroscopy and APCI-HRMS.



Scheme 36: Synthesis of a soluble tetrabenzotriazaporphyrin (TBTAP*) and its derivatives TBDAP and TBMAP.

TBTAP* could be differentiated in high-resolution mass spectrometry from its derivatives TBDAP* and TBMAP*. Both TBDAP* and TBMAP* were only observed in mass spectroscopy,

for further analysis, not enough substance was obtained. Therefore, more equivalents of MeMgBr might be used to shift the formation towards TBMAP*.

In comparison to the Pc^*H_2 , the TBTAP* shows an expected hypsochromic shift of the Q-band in UV-Vis spectroscopy. Pc^*H_2 has its $\pi-\pi^*$ transition at 710 nm and 677 nm, the TBTAP at 701 nm and 661 nm. In both compounds, the degeneracy of $1e_g$ orbitals is lifted. In the $^1\text{H NMR}$ spectrum of TBTAP*, the aromatic proton in the *meso*-position is easily assigned because it is additionally low-field shifted in comparison to the non-peripheral CH protons. It appears at 10.75 ppm.

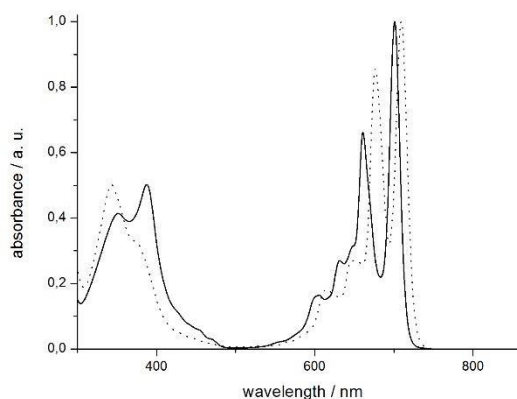


Figure 67: UV-Vis spectrum of TBTAP* (straight line) in comparison to Pc^*H_2 (dotted line), in DCM at rt.

In addition to TBTAP*, the synthesis of different derivatives with a functional group in the *meso*-position was attempted. Different literature known substituted phenyl-GRIGNARD reagents were used, summarised in Figure 68. But in all syntheses, the obtained yields were too low. In some cases, the formed TBTAP* could be detected by MS and UV-Vis spectroscopy.

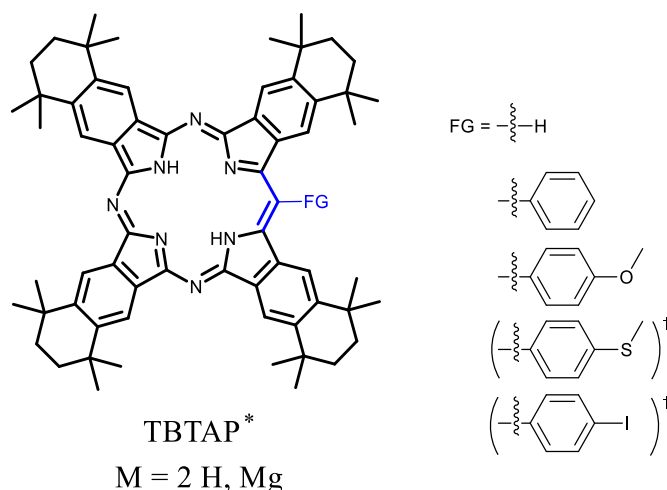


Figure 68: Attempted synthesis of TBTAP* derivatives with functional groups in *meso*-position.

In Table 14 different approaches are summarized. All GRIGNARD reagents were freshly prepared and Mg activated by using $\text{TMSCl}/i\text{PrOH}$ in THF. But in the case of MeSArMgBr

Results and Discussion

and IArMgCl , no conversion was observed at all. Again, conversion was controlled using UV-Vis spectroscopy and APCI-MS experiments.

Table 14: Attempted syntheses to obtain functionalised $\text{TBTAP}^{\text{*FG}}$.

GRIGNARD	Isolated	UV-Vis	MS	$^1\text{H NMR}$	Isomer detected
MeMgBr	+ (<2%)	+	+	+	+
ArMgBr	+ (<1%)	+	+	-	-
MeOArMgBr	+ (mixture with Pc^*H_2)	(+)	(+)	(+)	-
MeSArMgBr	-	-	-	-	-
IArMgCl	-	-	-	-	-

In the synthesis of TBTAP^* derivatives, using a MeOArMgBr -GRIGNARD, a change in colour to green was observed at 220 °C. After column chromatography, a $^1\text{H NMR}$ spectrum (Figure 70) was measured: it is quite evident that the $\text{TBTAP}^{\text{*PhOMe}}$ could not be separated from Pc^*H_2 . Different approaches for an ether cleavage of $\text{TBTAP}^{\text{*PhOMe}}$ to $\text{TBTAP}^{\text{*PhOH}}$ were carried out, using LEWIS acid such as AlCl_3 , MgI_2 and were stirred at rt-170 °C for up to 48 h, but in no case was a deprotection observed, neither in UV-Vis, nor in MS.

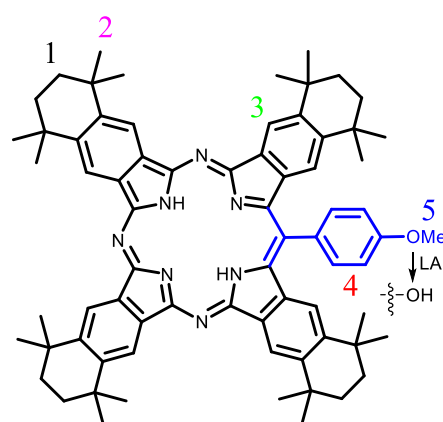


Figure 69: Attempted *meso*-substituted TBTAP^* .

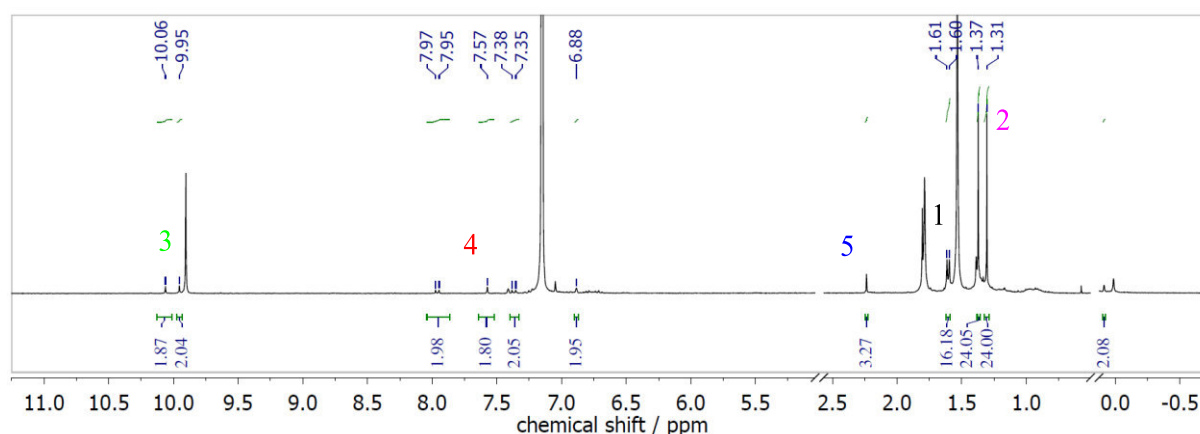
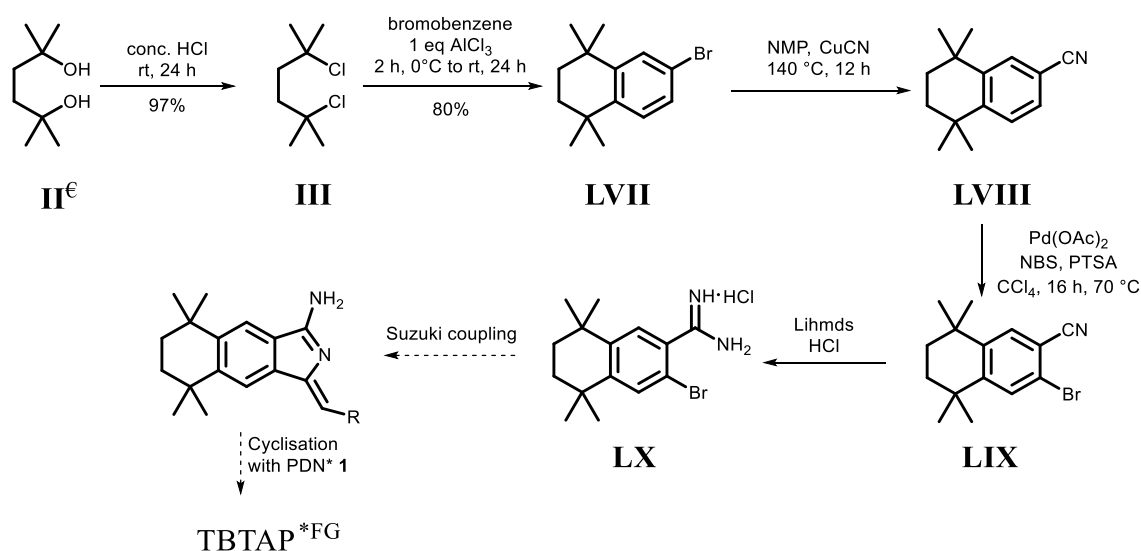


Figure 70: $^1\text{H NMR}$ spectrum of $\text{TBTAP}^{\text{*ArOMe}}$ after CC, in C_6D_6 (300 MHz).

In UV-Vis spectroscopy, the Q-band of the impure $\text{TBTAP}^{\text{*ArOMe}}$ shows only a weak hypsochromic shift into the near IR-region. An additional hypsochromic shift might be caused by introducing a second carbon into the phthalocyanines, giving it a push-pull character as is known for the porphyrin derivative.

Because of the low yields and difficulties in the separation, no more attempts were carried out to synthesise *meso*-substituted TBTAP* via GRIGNARD reagents. A selective synthesis of a TBTAP* derivative was developed in the Bachelor-Thesis of PFAFF (Scheme 37).^[199] There, an HCl salt of a bromoamidine **LX** could be synthesised with the 2,2,5,5-tetramethylcyclohexane annulated alkyl groups. In a next step, a functionalisation can be attempted using any alkynes with literature known SUZUKI reaction conditions in a microwave reaction. The obtained precursor and 3 eq of PDN* **1** may lead to a functionalised substituted TBTAP in higher yields as described for the GRIGNARD method used in this section, according to the procedure described by CAMMIDGE.^[197,198]



Scheme 37: Attempt for a selective synthesis of a TBTAP*^{FG} following CAMMIDGE *et al.*^[192]

4.2.8 Meso Substituted Pyrazinoporphyrazines

Similar to meso substituted phthalocyanines, it was attempted to synthesise pyrazinoporphyrazines in a GRIGNARD reaction. Here, neither a change in colour to green could be observed, nor could any product be identified by using MALDI-ToF. But in comparison to phthalocyanine analogues,^[200] in the Li/*n*-octanol synthesis of Ppz*H₂, described in section 4.2.3.1, additional spots were observed on TLC plates. With our cooperation partner, the product could be identified as a meso-C^{noctyl} substituted pyrazinoporphyrazine (Figure 71), here, named as tetrapyrazinotriazaporphyrin (TPTAP) or Ppz*H₂^{noctyl}.^[201]

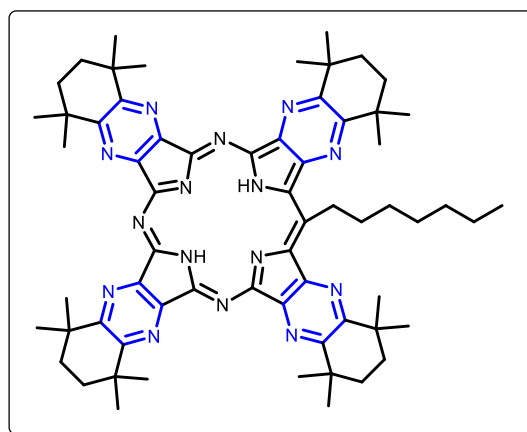
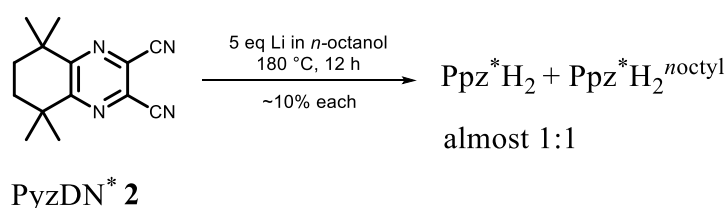


Figure 71: Characterized by-product in the synthesis of Ppz*H₂: meso-substituted Ppz*H₂^{noctyl}.



Scheme 38: Synthesis of Ppz*H₂ and identified by-product Ppz*H₂^{noctyl}.

In addition, a third green spot was observed on the TLC plate, probably tetrapyrazinodiazaporphyrin (TPDAP). The by-products might be formed in a condensation reaction of one nitrile unit with *n*-octanal, which is formed within the redox reaction of this cyclotetramerisation. The proposed mechanism has to be further investigated in following studies. In Figure 72, the ¹H NMR spectrum of Ppz*H₂^{noctyl} is shown.

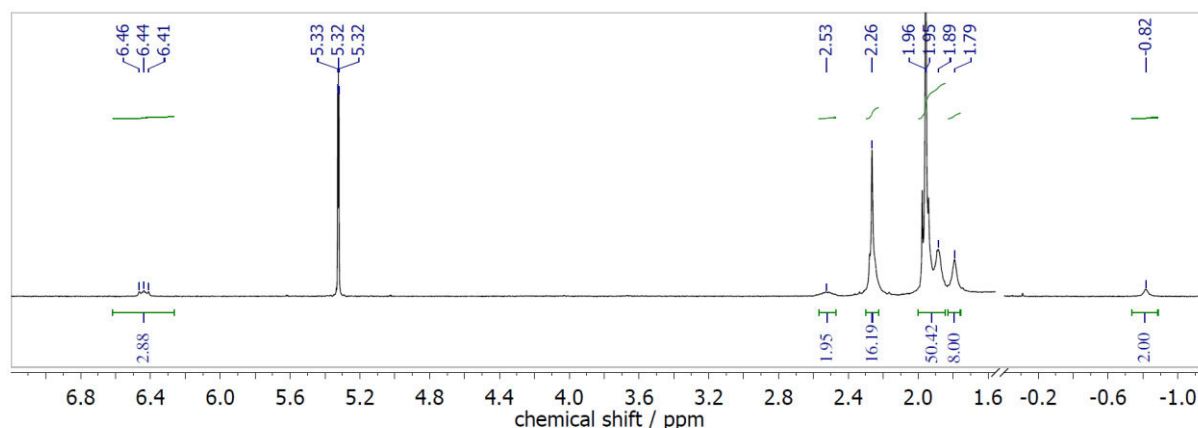


Figure 72: ¹H NMR spectrum of Ppz*H₂^{noctyl}, in DCM-*d*₂ (300 MHz).

In contrast to TBTAP* described in the section before, here no splitting of the methyl/methylene proton signals could be observed. More highly resolved spectra might show the splitting of these signals. But the proton signals of the *n*-octyl group are visible. These signals are mainly

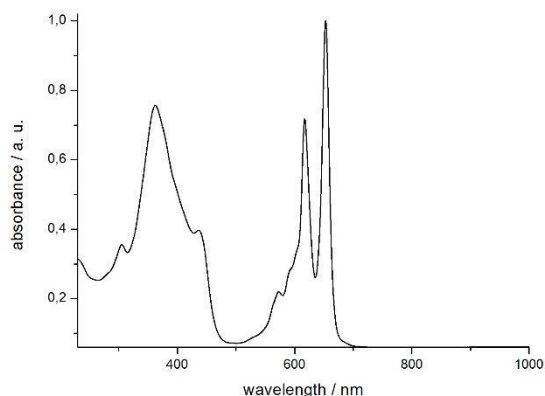


Figure 73: UV-Vis spectrum of Ppz*H₂^{noctyl}, in DCM.

observed as broadened singlets or multiplets. Ppz*H₂^{noctyl} was further analysed by using APCI-HRMS and UV-Vis spectroscopy. The UV-Vis spectrum (Figure 73, on the left) shows only a weak hypsochromic shift of the Q-band to 653 nm compared to the Ppz*H₂ ligand (655 nm). The splitting of the Q-band is still present as it was also observed for TBTAP* (see section 4.2.7,

Figure 67). A more detailed investigation of this compounds with regard to Φ_{Δ} and τ_F would be interesting as well. Interestingly, neither the Q-band of TBTAP* nor the one of Ppz*H₂^{noctyl} displays a larger splitting in measured UV-Vis spectra, compared to Pc*H₂ and Ppz*H₂, respectively. In future, a systematic study of these compounds and their photophysical properties is essential.

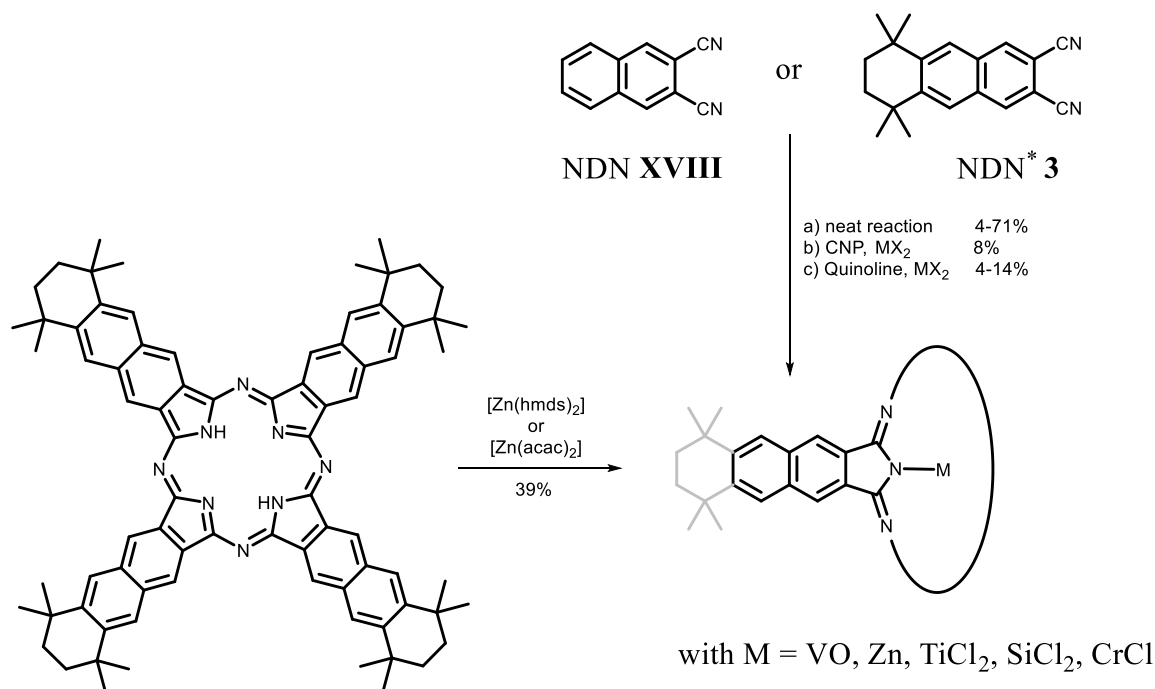
4.2.9 Azanaphthalocyanine Complexes

Naphthalocyanines, especially the free ligands, are of recent interest in physical investigations with regard to self-assembling monolayers on Au(111) and Ag(111) surfaces.^[16,202] In a recent surface science report by GOTTFRIED,^[16] it is obvious that the research concerning properties of naphthalocyanines on surfaces is lacking. Pyrazinoporphyrazines and naphthalopyrazinoporphyrazines are almost completely uninvestigated.^[129] Some studies of pyrazinoquinoxaline porphyrins in PDT are known.^[203] In general, naphthalocyanines show interesting properties in singlet oxygen production. However, systematic studies of photophysical properties of azanaphthalocyanines and azanaphthalocyanines are rare,^[87] and for alkyl substituted naphthalocyanines a series is not yet described. In most cases, only $[\text{Nc}^*\text{M}]$ with $\text{M} = \text{2 H, Zn}$ are described, while other inorganic central metals and the influence of axial ligands are almost completely ignored. An example of such a complex is $[\text{Fe(III)naphthaloporphyrin}]$, coordinated by two pyridine units, applied in oxygen reduction.^[204] In this section, the focus is on the synthesis of new metal-free and metalated naphthalocyanines $[\text{Nc}^*\text{M}]$ and its aza-complexes $\text{N}_{x,y}\text{-}[\text{Nc}^*\text{M}]$ using dinitriles **3-6** as building blocks introduced in the beginning of this work (section 4.1.2).

4.2.9.1 Synthesis of Free Naphthalocyanine Ligands and its Metal Complexes

MIKHALENKO described $\text{PDN}^* \mathbf{1}$ and $\text{NDN}^* \mathbf{3}$ in previous work.^[24] Starting with $\text{NDN}^* \mathbf{3}$, the protonated naphthalocyanine Nc^*H_2 and the metal complexes $[\text{Pc}^*\text{M}]$ with $\text{M} = \text{Cu, Zn, Co, VO}$ were synthesised.^[24] In our group, VOLLGRAFF could reproduce the synthesis of Nc^*H_2 , $[\text{Nc}^*\text{VO}]$ and $[\text{Nc}^*\text{Zn}]$ and complete missing characterisation data including FS and IR spectroscopy, as well as MS. Furthermore, a ^1H NMR spectrum of Nc^*H_2 could be obtained. The described UV-Vis data of VOLLGRAFF are in accordance with the results of MIKHALENKO. In addition, VOLLGRAFF was able to test different literature known methods for the synthesis of $[\text{Nc}^*\text{M}]$.^[140] The most efficient method to synthesise the naphthalocyanine complexes seems to be either in a melt of reaction partners using 4 eq $\text{NDN}^* \mathbf{3}$ and 1 eq of the corresponding metal cation precursor with yields of up to 71%, or by metalation of preformed Nc^*H_2 . For more sensitive complexes with axial ligands, other methods have to be used. VOLLGRAFF characterized these complexes by using NMR (only for Nc^*H_2 and $[\text{Nc}^*\text{Zn}]$), UV-Vis, FS and IR spectroscopy, MALDI-ToF and elemental analysis.

The solubility of Nc^*H_2 and $[\text{Nc}^*\text{Zn}]$ was sufficient to obtain ^1H NMR spectra. In the case of $[\text{Nc}^*\text{Zn}]$, a drop of pyridine was added to minimize aggregation effects and increase the solubility in benzene- d_6 .



Scheme 39: Overview to the syntheses of Nc complexes by VOLLGRAFF.^[140]

The influence of exchanging the central metal atom can be observed in UV-Vis spectroscopy. VOLLGRAFF described a bathochromic shift of the Q-band from $[\text{Nc}^*\text{Zn}]$ (792 nm) to $[\text{Nc}^*\text{SiCl}_2]$ (851 nm). In UV-Vis spectroscopy, the Q-band of the free Nc^*H_2 ligand itself is bathochromically shifted compared to all Pc-complexes mentioned in the sections before. The shift of the Q-band of Sppz, Spc, Ppz, Pc to Nc is visible in the UV-Vis spectra in Figure 74.

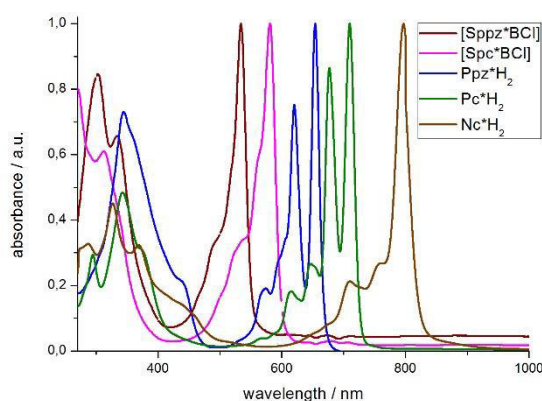


Figure 74: UV-Vis spectrum of Nc^*H_2 in comparison to $[\text{Pc}^*\text{M}]$ and $[\text{Spz}]$, in DCM.

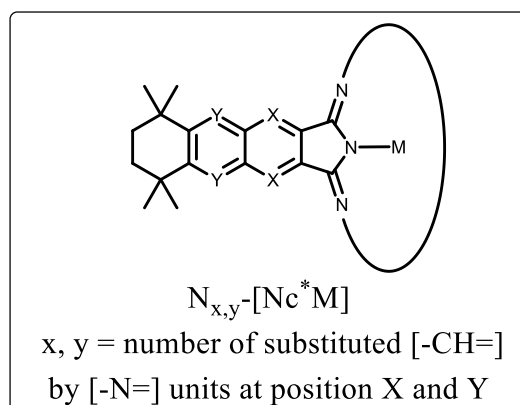
In addition to the metal complexes, subnaphthalocyanine $[\text{Snc}^*\text{BCl}]$ was synthesised for the first time, as already mentioned in section 4.2.1.4. The $[\text{Snc}^*\text{BCl}]$ appears to be unstable in the

Results and Discussion

presence of air and light. It could be characterized by UV-Vis, MS and ^1H NMR spectroscopy, but degradation was observed. It could not be purified sufficiently for full analysis by using CC, or filtration under inert gas. A bleaching of the colour was always observed, which indicates a degradation of $[\text{Sn}^*\text{BCl}]$ of the macrocycle.

4.2.10 Synthesis of New Alkyl Substituted Azanaphthalocyanines

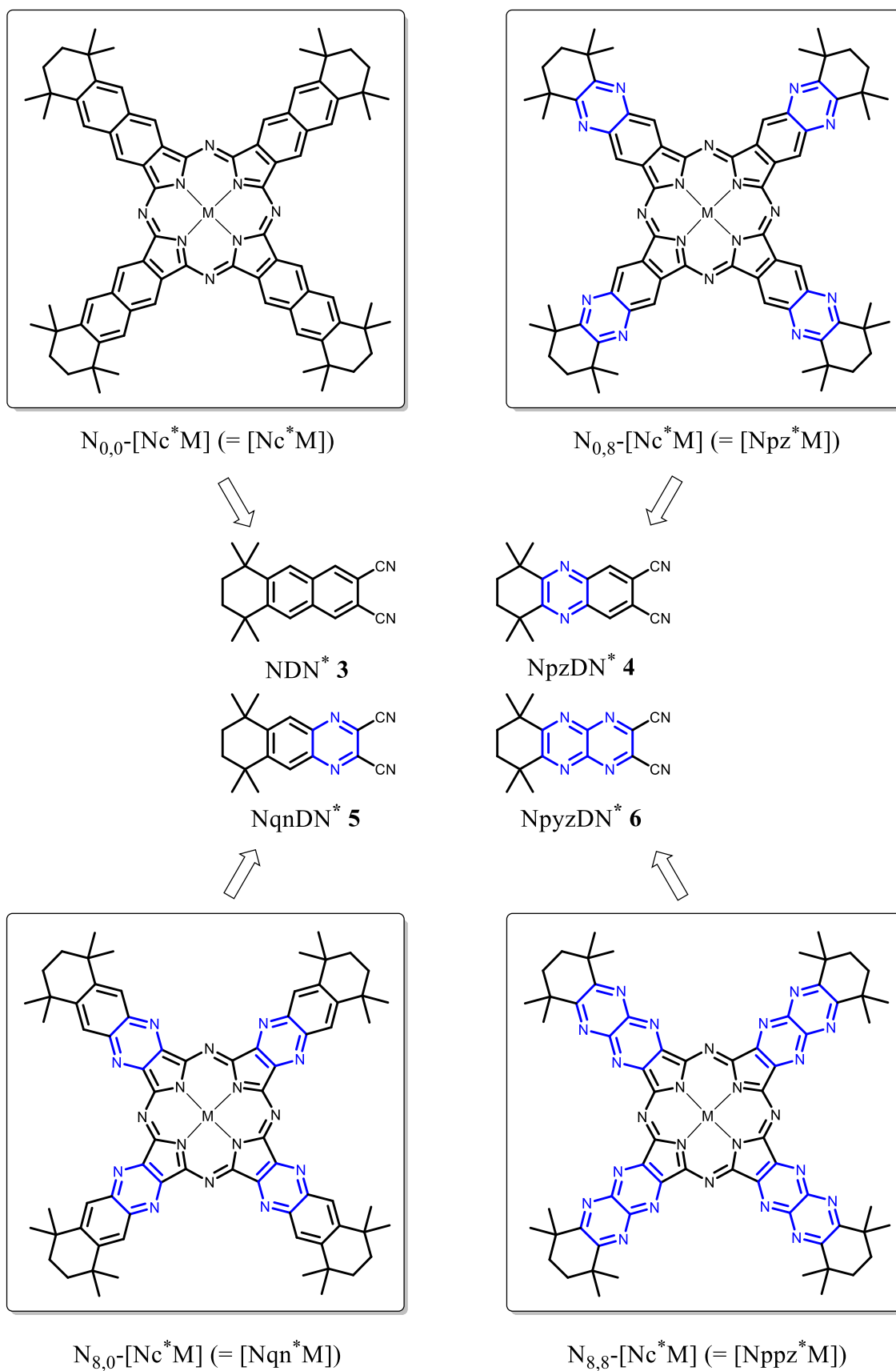
In the final stages of this thesis, first attempts were carried out to synthesise a new series of azanaphthalocyanines of the developed dinitriles **4-6**. An overview for naming these complexes and their structural formulas, is shown in Figure 75 and Scheme 40. Firstly, the metal-free ligands and their complexes $\text{N}_{x,y}\text{-}[\text{Nc}^*\text{Zn}]$ should be synthesised. Secondly, group 6, d^1 -metal complexes $\text{N}_{x,y}\text{-}[\text{Nc}^*\text{M}(\text{R})]$ with $\text{M} = \text{Mo}, \text{W}$ and $\text{R} =$ axial ligands are described in the second part of this chapter.



$x = y = 0$	$\text{N}_{0,0}\text{-}[\text{Nc}^*\text{M}] = [\text{Nc}^*\text{M}]$	annulated n aphthalocyanine
$x = 0, y = 8$	$\text{N}_{0,8}\text{-}[\text{Nc}^*\text{M}] = [\text{Npz}^*\text{M}]$	methylated tetrahydro p henazine
$x = 8, y = 0$	$\text{N}_{8,0}\text{-}[\text{Nc}^*\text{M}] = [\text{Nqn}^*\text{M}]$	annulated q uinoxaline
$x = y = 8$	$\text{N}_{8,8}\text{-}[\text{Nc}^*\text{M}] = [\text{Nppz}^*\text{M}]$	annulated p yrazinopyrazine

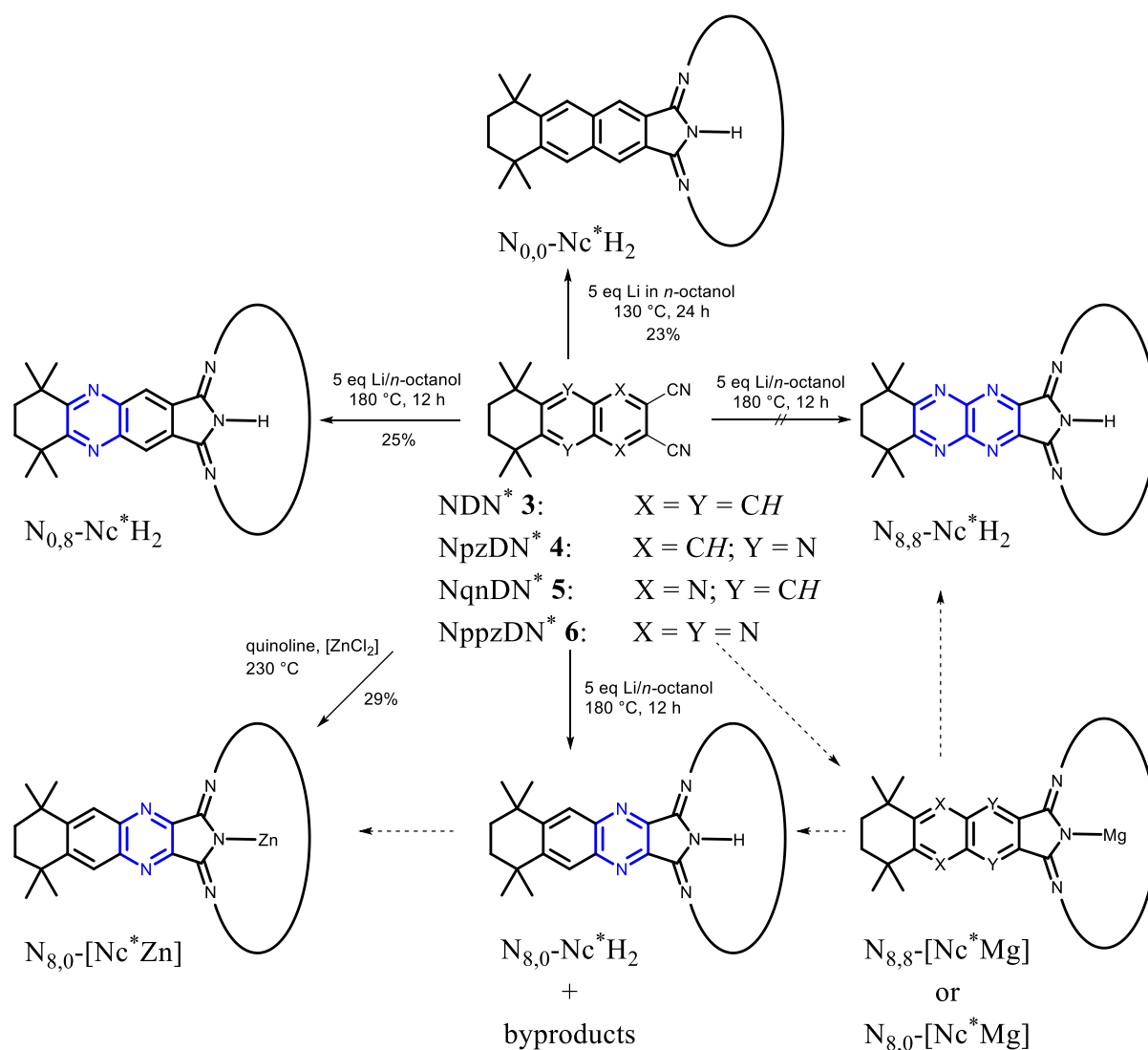
Figure 75 : Nomenclature of synthesised azanaphthalocyanine complexes.

Based on the preliminary work of VOLLGRAFF, octaazanaphthalocyanine, $\text{N}_{0,8}\text{-Nc}^*\text{H}_2$ (bearing the $[-\text{N}]=$ units in the outer positions), was synthesised in up to 25% yield using the established Li/n -octanol method (Scheme 41). Similar to $\text{N}_{0,0}\text{-Nc}^*\text{H}_2$, the solubility of $\text{N}_{0,8}\text{-Nc}^*\text{H}_2$ is very low in common organic solvents. Nevertheless, it was possible to obtain a ^1H NMR spectrum of the compound in d_5 -bromobenzene (Figure 76). The inner aromatic protons in the non-peripheral position of the $\text{N}_{0,8}\text{-Nc}^*\text{H}_2$ are low-field shifted to 9.55 ppm in comparison to $\text{N}_{0,0}\text{-Nc}^*\text{H}_2$ (9.43 ppm); the same applies for the NH -protons at 0.43 ppm.



with M = a central metal atom or 2 H

Scheme 40: Nomenclature of azanaphthalocyanine complexes.



Scheme 41: Syntheses of $N_{x,y}$ - Nc^*H_2 ligands and their Zn complexes $N_{x,y}$ -[Nc^*Zn].

The shift is caused by the electron poor/electron withdrawing annulated pyrazine units. Here, the same advantages as discussed for Pc^*H_2 are visible: solubility is increased while the symmetry is maintained. So, only one signal is observed for the methyl groups and one for the methyl/methylene protons.

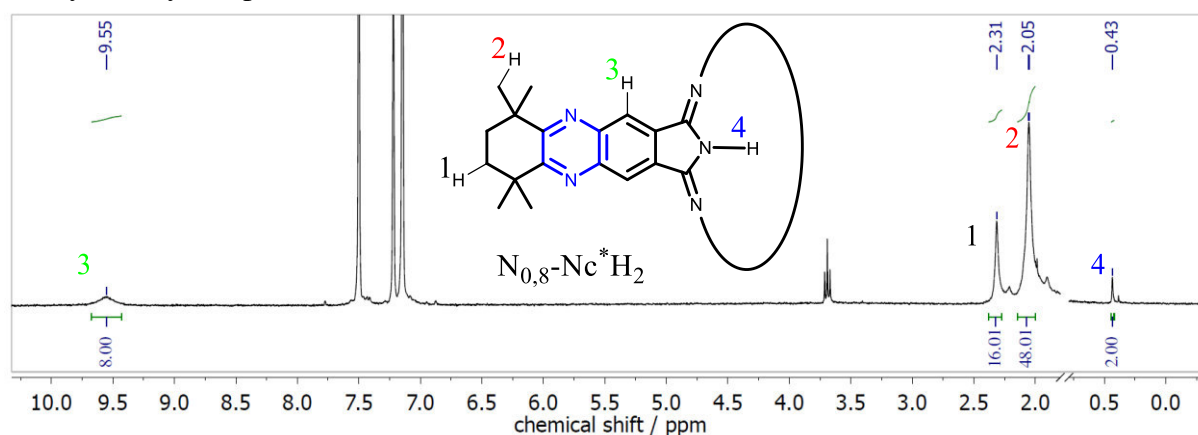


Figure 76: 1H NMR spectrum of $N_{0,8}$ - Nc^*H_2 , in bromobenzene- d_5 (300 MHz).

The octaazanaphthalocyanine derivative $N_{8,0}\text{-Nc}^*\text{H}_2$ could not be obtained using dinitrile **5** in Li/*n*-octanol conditions. In the synthesis of $N_{8,0}\text{-Nc}^*\text{H}_2$ (Scheme 41), after deprotonation, a change in colour from brown to green was observed. The green powder was washed with MeOH and hexane. The resulting product was analysed by using UV-Vis spectroscopy and MALDI-ToF. In UV-Vis

spectroscopy, more than one Q-band was found: a strong absorption at 729 nm, 706 nm and 671 nm, with decreasing intensity. While the UV-Vis spectrum already indicated a product mixture, in MS (Figure 77) a mixture of meso- $C^{n\text{octyl}}$ substituted $N_{8,0}\text{-Nc}^*\text{H}_2$ derivatives $N_{8,0}\text{-Nc}^*\text{H}_2^{n\text{octyl}}$ and $N_{8,0}\text{-Nc}^*\text{H}_2^{2x\ n\text{octyl}}$ was detected. It is quite interesting that the intensity of the signals in MS increase with number of meso- $C^{n\text{octyl}}$ groups in the meso position. The proposed structures of the compounds are shown below (Figure 78). Next to the new structural type of meso alkyl substituted Ppz's, $\text{Ppz}^*\text{H}_2^{n\text{octyl}}$, reported in section 4.2.8, these structures are completely new structural motifs as well. In comparison to $\text{Ppz}^*\text{H}_2^{n\text{octyl}}$, here, $N_{8,0}\text{-Nc}^*\text{H}_2^{2x\ n\text{octyl}}$ was obtained as the major product, suggesting a similar tendency of ionisation in the MALDI-ToF measurement.

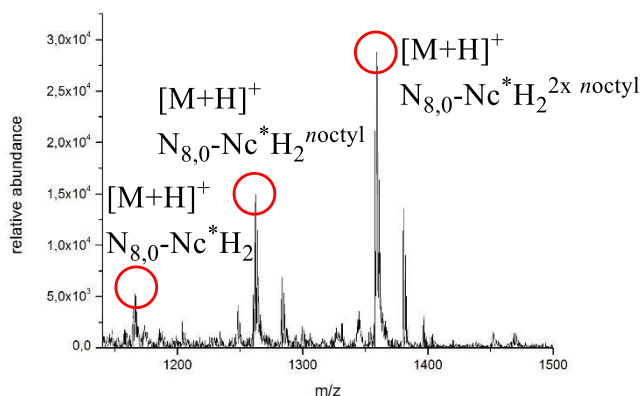


Figure 77: MALDI-ToF of $N_{8,0}\text{-Nc}^*\text{H}_2$ ($N_{8,0}\text{-Nc}^*\text{H}_2$) and by-products.

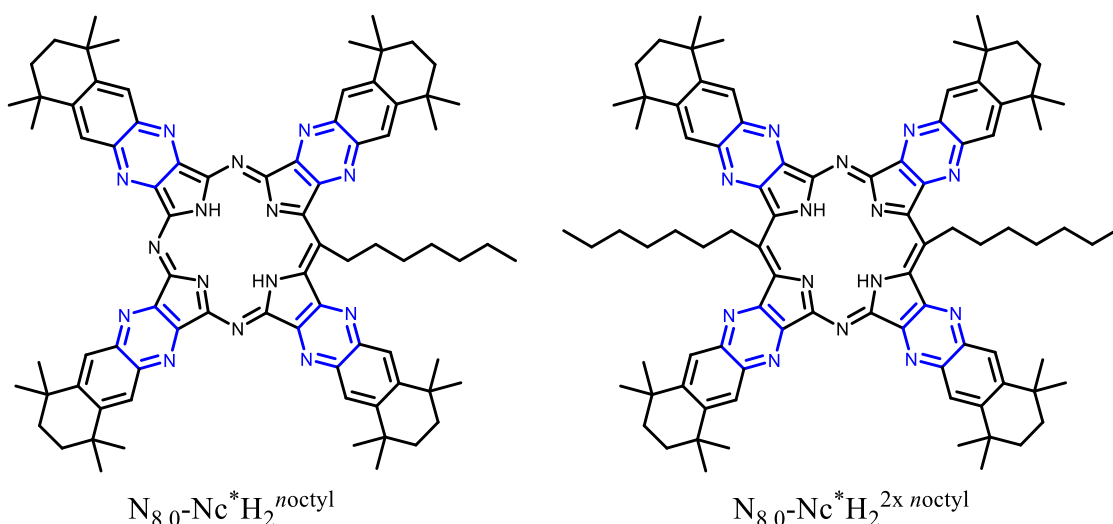
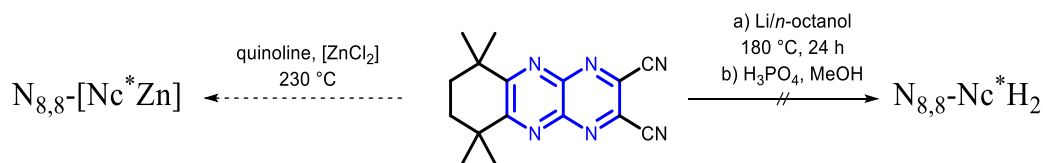


Figure 78: New meso-substituted octaazanaphthalocyanines bearing *n*-octyl groups in the meso position.

The here shown trend of by-product formation obtained in the Li/*n*-octanol synthesis, also explains why $N_{8,8}\text{-Nc}^*\text{H}_2$ could not be obtained in this way (Scheme 41). When dinitrile **6** was dissolved in a Li/*n*-octanol solution, a change in colour to black was observed. After protonation

Results and Discussion

with H_3PO_4 , no change in colour to green could be observed, and neither in UV-Vis spectroscopy nor in MS were any traces of expected product found.



Scheme 42: Attempt to synthesise $\text{N}_{8,8}\text{-}[\text{Nc}^*\text{M}]$ with $\text{M} = 2 \text{ H, Zn}$.

Therefore, in future, the synthesis has to be carried out on a larger scale, to separate the desired product from possible meso substituted by-products. Another route to obtain the metal-free $\text{N}_{8,8}\text{-Nc}^*\text{H}_2$ might be the synthesis over a $\text{N}_{8,8}\text{-}[\text{Nc}^*\text{Mg}]$ precursor, which could be demetallated in an acidic pyridine solution afterwards (Scheme 41).

In addition, the more selective synthesis of corresponding zinc complexes $\text{N}_{x,y}\text{-}[\text{Nc}^*\text{Zn}]$ was attempted. $\text{N}_{0,8}\text{-Nc}^*\text{H}_2$ could be converted into the zinc complex $\text{N}_{0,8}\text{-}[\text{Nc}^*\text{Zn}]$ by using $[\text{Zn}(\text{hmds})_2]$ in toluene or $[\text{Zn}(\text{acac})_2]\cdot 2\text{H}_2\text{O}$ in pyridine. In comparison to the free ligand, $\text{N}_{0,8}\text{-}[\text{Nc}^*\text{Zn}]$ shows an intense pink colour as is typical for subphthalocyanines.^[162] $\text{N}_{8,0}\text{-}[\text{Nc}^*\text{Zn}]$ and $\text{N}_{8,8}\text{-}[\text{Nc}^*\text{Zn}]$ were observed in a cyclotetramerisation reaction using quinoline, $[\text{ZnCl}_2]$ and **5** or **6**, respectively. $\text{N}_{8,8}\text{-}[\text{Nc}^*\text{Zn}]$ could not be obtained in sufficient amounts for full analysis. However, it could be observed in MS and UV-Vis spectroscopy. The zinc complexes $\text{N}_{0,0}\text{-}[\text{Nc}^*\text{Zn}]$, $\text{N}_{0,8}\text{-}[\text{Nc}^*\text{Zn}]$ and $\text{N}_{8,0}\text{-}[\text{Nc}^*\text{Zn}]$ could be further analysed and show a decreased solubility in common organic solvents used in NMR spectroscopy such as CDCl_3 or benzene. It was possible to dissolve the compounds sufficiently for a ^1H NMR spectrum by the addition of a drop of pyridine- d_5 . In UV-Vis spectroscopy, a hypsochromic shift of the Q-band by inserting zinc into the metal-free ligand is, according to the expected trends ($\text{N}_x\text{-}[\text{Pc}^*\text{M}]$, section 4.2.4.6), observed for $\text{N}_{x,y}\text{-}[\text{Nc}^*\text{Zn}]$. The hypsochromic shift of the Q-band from the naphthalocyanine $\text{N}_{0,0}\text{-}[\text{Nc}^*\text{Zn}]$ (797 nm) to the naphthalopyrazinoporphyrazine $\text{N}_{8,8}\text{-}[\text{Nc}^*\text{Zn}]$ (712 nm) is also in accordance with expectations. The Q-band of $\text{N}_{8,0}\text{-}[\text{Nc}^*\text{Zn}]$ (729 nm) is stronger blue-shifted compared to the one of $\text{N}_{0,8}\text{-}[\text{Nc}^*\text{Zn}]$ (754 nm), because of the proximity of the exchanged $[-\text{CH}=\text{C}-]$ building blocks by $[-\text{N}=\text{C}-]$ to the metal-centre $[-\text{MN}_4-]$. For the synthesis of $\text{N}_{8,8}\text{-}[\text{Nc}^*\text{Zn}]$, optimization of the reaction was attempted, using common literature known methods, summarised in the experimental section.

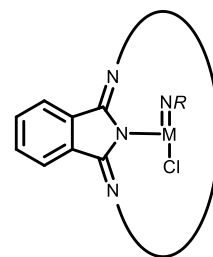
In summary, two new series of azanaphthalocyanines have been reported here bearing alkyl groups in the peripheral position. All obtained $N_{x,y}[\text{Nc}^*\text{Zn}]$ were synthesised either in quinoline solution using a zinc metal cation precursor and the respective building block **3-6** or via metalation of $N_{x,y}\text{-Nc}^*\text{H}_2$. The compounds were characterised by using MALDI-ToF and UV-Vis spectroscopy, and where possible, by ^1H NMR and IR spectroscopy and elemental analysis. The expected hypsochromic shift of the Q-band was observed while increasing the number of [-N=] units and their proximity to the inner [-MN₄-] unit from $N_{0,0}[\text{Nc}^*\text{Zn}]$ (797 nm), $N_{0,8}[\text{Nc}^*\text{Zn}]$ (754 nm), $N_{8,0}[\text{Nc}^*\text{Zn}]$ (729 nm) to $N_{8,8}[\text{Nc}^*\text{Zn}]$ (712 nm). Owing to the low yields in the synthesis of NppzDN^* **6** and $N_{8,8}[\text{Nppz}^*\text{Zn}]$, the analysis is lacking and has to be completed in following work.

Furthermore, it was attempted to synthesise metal-free $N_{x,y}\text{-Nc}^*\text{H}_2$ ligands. Besides the isolation of $N_{0,0}\text{-Nc}^*\text{H}_2$ and $N_{0,8}\text{-Nc}^*\text{H}_2$, however, a new series of compounds was found, bearing C^{noctyl} -groups in the meso position of $N_{8,0}\text{-Nc}^*\text{H}_2$. The substitution of the meso-[-N=] units by meso- C^{noctyl} was observed when NqnDN^* **5** was cyclised under *Li/n*-octanol conditions. The synthesis of $N_{8,8}\text{-Nc}^*\text{H}_2$ was not successful. In both reactions, a cyclisation with NqnDN^* **5** and NppzDN^* **6** has to be carried out on a larger scale to ensure a separation of all compounds and for full characterisation of the formed meso substituted by-products. Both series, $N_{x,y}[\text{Nc}^*\text{M}]$ and meso- $C^{\text{noctyl}} N_{x,y}[\text{Nc}^*\text{M}]$, are interesting series for further investigations of their HOMO-LUMO level alignment and band gap following synthetic procedures reported here.

In the following research, the focus was placed on the investigation of different group 6 organoimido complexes of d^1 electronic configuration. Such species $[\text{PcMo}(\text{NR})\text{Cl}]$, $[\text{Pc}^*\text{Mo}(\text{NR})\text{Cl}]$ and $[\text{Ppz}^*\text{Mo}(\text{NR})\text{Cl}]$ were already described by our group.^[70,205]

4.2.10.1 Synthesis of Group 6 – Azanaphthalocyanine Metal Complexes

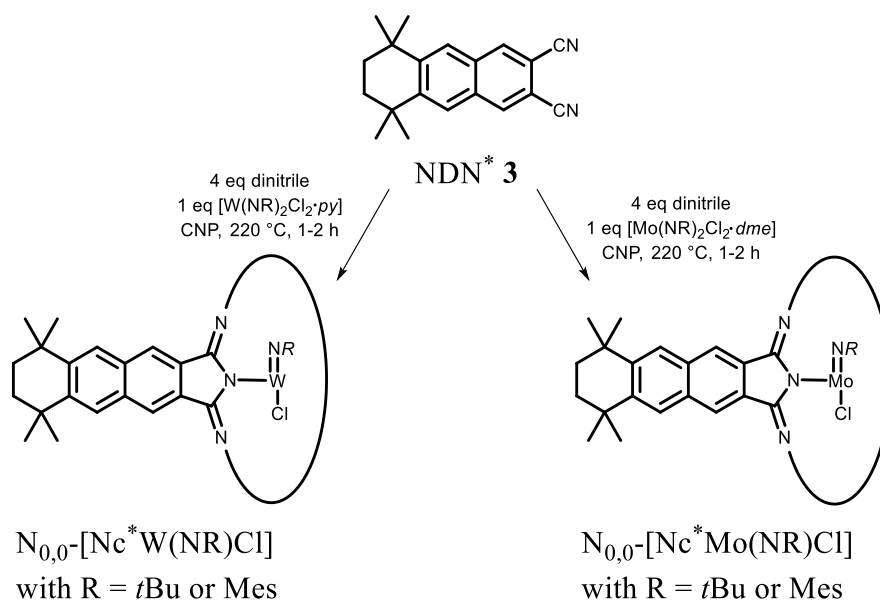
In 2011, our group described for the first time organoimido functionalised phthalocyanines of the type $[\text{PcM}(\text{NR})\text{Cl}]$ with $\text{M} = \text{Mo}$, W , Re and $\text{R} = t\text{Bu}$, Mes , Ts (Figure 79).^[205] In addition to these rather poorly soluble (in common organic solvents) Pc complexes, the less aggregating alkyl substituted Pc^* and Ppz^* were synthesised by SEIKEL.^[70] These thermostable dyes are not only interesting because of their use in optoelectronic devices such as photosensitizer or photoanodes,^[70] but electron transfer to semiconductor surfaces might be studied if these complexes are further functionalised. It is expected that the HOMO-LUMO gap and absolute HOMO-LUMO levels might be tuned when different aza-aromatic dinitriles **3-6** are used in the cyclotetramerisation.



with $\text{M} = \text{Mo}$, W , Re
 $\text{R} = t\text{Bu}$, Mes

Figure 79: Described metal complexes of a $[\text{PcM}(\text{NR})\text{Cl}]$ -type.

The aim of this section was the synthesis of a new series of azanaphthalocyanines of the type $\text{N}_{x,y}\text{-}[\text{Nc}^*\text{M}(\text{NR})\text{Cl}]$ type with $\text{M} = \text{Mo}$, W and $\text{R} = t\text{Bu}$, Mes . Optical and magnetic properties using UV-Vis or EPR spectroscopy, respectively, are compared. The synthesis of these azanaphthalocyanines was carried out by the established method of DARWISH, applying CNP at 220 °C. As metal precursors, $[\text{Mo}(\text{NR})_2\text{Cl}_2 \cdot dme]$ with $\text{R} = t\text{Bu}$, Mes or $[\text{W}(\text{NR})_2\text{Cl}_2 \cdot py]$ with $\text{R} = t\text{Bu}$, Mes were used and converted with 4 eq of the corresponding azanaphthalocyanine. The general procedure is shown below (Scheme 43), as an example for the synthesis of $\text{N}_{0,0}\text{-}[\text{Nc}^*\text{Mo}(\text{NR})\text{Cl}]$ and $\text{N}_{0,0}\text{-}[\text{Nc}^*\text{W}(\text{NR})\text{Cl}]$ with $\text{R} = t\text{Bu}$ or Mes .



Scheme 43: Synthesis of new $\text{N}_{0,0}\text{-}[\text{Nc}^*\text{M}(\text{NR})\text{Cl}]$ with $\text{R} = t\text{Bu}$ or Mes and $\text{M} = \text{Mo}$ or W .

As a mechanism, DARWISH expected a "homolytic cleavage and a loss of a nitrene diradical and a chlorine",^[69] which would explain the start of a redox reaction and the origin of the two required electrons for the ring formation of the phthalocyanine. The resulting low concentration of chlorine radicals leads to a formation of the $N_{x,y}-[Nc^*M(NR)Cl]$, whereby Mo or W has an oxidation state +V. For all four dinitriles **3-6** the corresponding molybdenum compound $N_{x,y}-[Nc^*Mo(NtBu)Cl]$ was synthesised using $[Mo(NtBu)_2Cl_2 \cdot dme]$ as metal precursor, following the procedure shown in Scheme 43. All synthesised compounds are summarised in Figure 80.

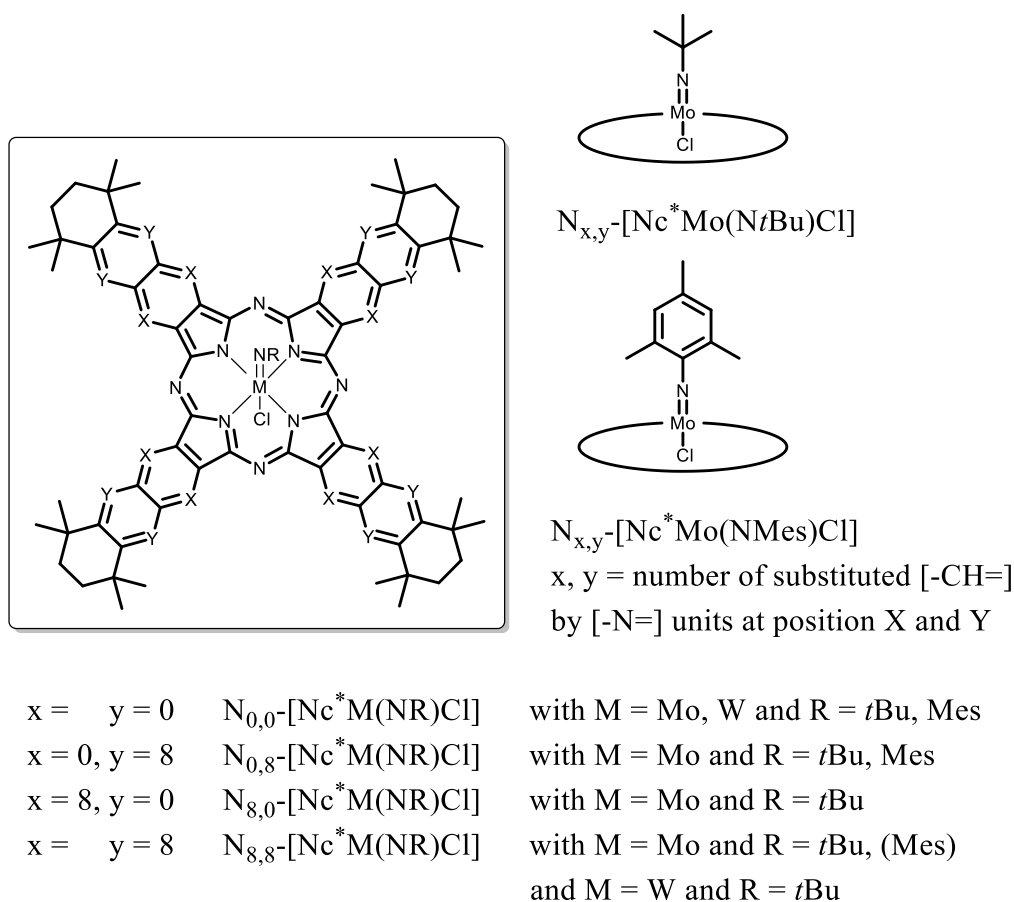


Figure 80: Synthesised new $N_{x,y}-[Nc^*M(NR)Cl]$ of molybdenum and tungsten with different axial ligands.

The synthesis of some molybdenum complexes was limited by low yields, varying between 2-52%. Better yields of up to 82% yield were obtained in case of tungsten complexes, and -NMe₃ as axial ligand. All compounds were characterized by using at least UV-Vis, IR spectroscopy, MALDI-ToF mass spectrometry and elemental analysis. Higher aberrations in elemental analysis can be explained with the formation of molybdenum and tungsten carbides or nitrides, respectively, in thermal combustion. Impurities of other paramagnetic metal complexes would be quite clearly visible in EPR spectroscopy and could be excluded.

Results and Discussion

The formation of the corresponding complex was monitored by using UV-Vis spectroscopy and MS. In MALDI-ToF mass spectroscopy, the chlorine atom is lost when the molecule gets ionised, even by its soft laser ionisation. The same phenomena were observed for other $[\text{PcM}(\text{NR})\text{Cl}]$ complexes with $\text{M} = \text{Mo}, \text{W}$ in APCI-HRMS measurements. Here, APCI-HRMS could not be used because of the device's limitation to about $m/z = 1000$. Some of the complexes were characterized by using softer FD measurements, and for the first time it was possible to obtain a high resolution mass spectrum of these complexes. As representative a LIFDI spectrum of $\text{N}_{0,0}\text{-}[\text{Nc}^*\text{W}(\text{NtBu})\text{Cl}]$ is shown in Figure 81.

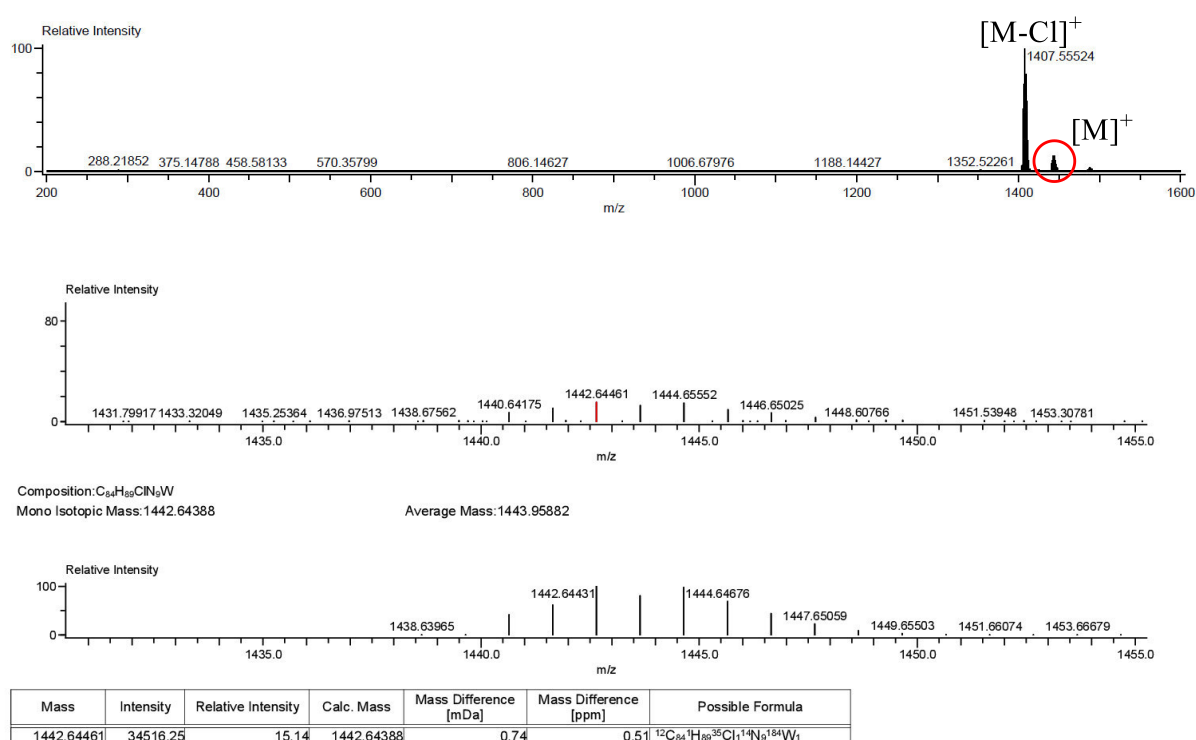


Figure 81: FD spectrum of $\text{N}_{0,0}\text{-}[\text{Nc}^*\text{W}(\text{NtBu})\text{Cl}]$, measured from a toluene solution. Top: Full measured spectrum. Middle: High resolution mass spectrum of $[\text{M}]^+$, 100% isotope in red. Bottom: Calculated spectrum.

The peak found at $m/z = 1407.5552$ corresponds to the fragment $[\text{M}-\text{Cl}]^+$ and is still the signal with a relative abundance of 100% in this measurement, because of the labile bonding of the chloro ligand. The large mass difference between the experimental and theoretical peaks is caused by the evaluation of the mass spectrum, which has to be calibrated with an internal standard that seems to be problematic at the point of measurements.

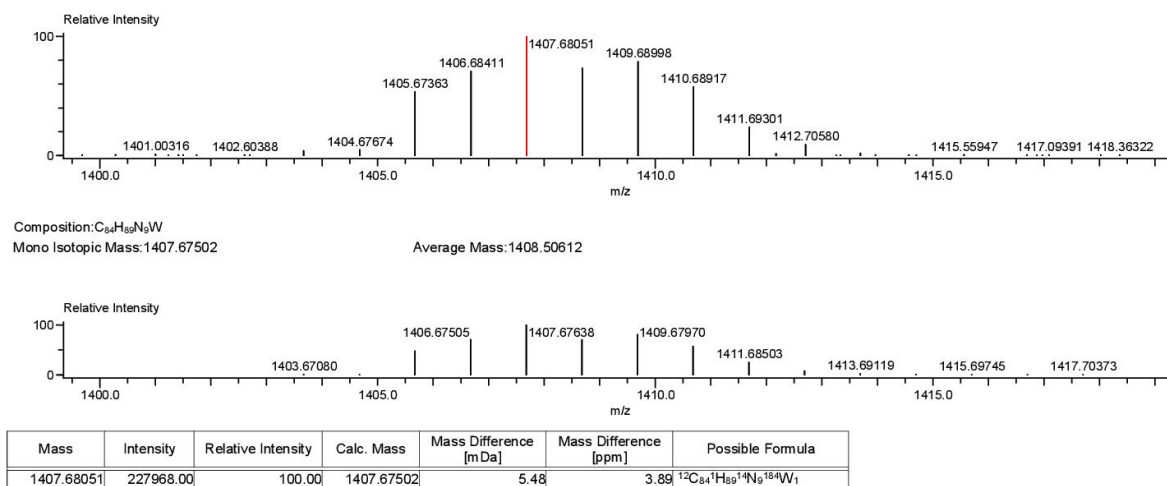


Figure 82: Second FD-HRMS spectrum of $[\text{Nc}^*\text{W}(\text{NtBu})\text{Cl}]$, measured in a toluene solution. Top: High resolution MS of $[\text{M}-\text{Cl}]^+$. Bottom: Calculated spectrum.

However, besides the shown LIDFI measurements, in MALDI-ToF spectra the isotopic pattern of the ionised complexes is very clear as well. A spectrum of $\text{N}_{8,8}-[\text{Nc}^*\text{Mo}(\text{NtBu})\text{Cl}]$ is shown in Figure 83. Here, also additional fragments at $m/z = 1218.410$ of $[\text{M}-\text{Cl},-\text{Mes}]^+$ can be observed.

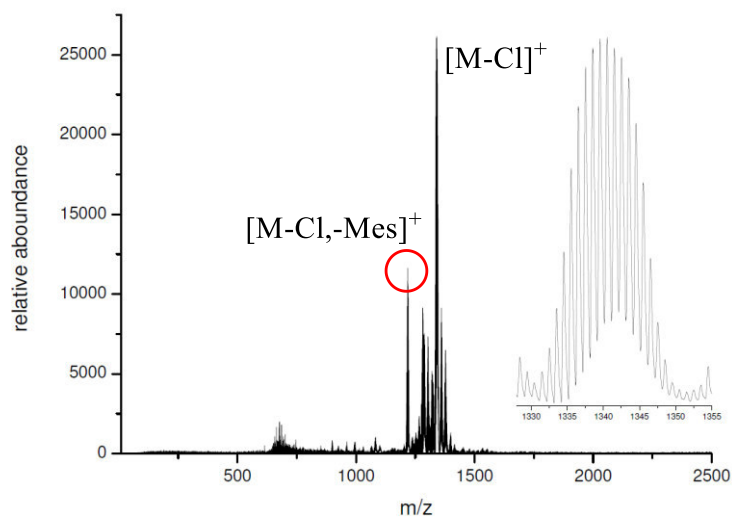


Figure 83: MALDI-ToF spectrum of $\text{N}_{8,8}-[\text{Nc}^*\text{Mo}(\text{NMes})\text{Cl}]$, measured from a toluene solution.

4.2.10.2 UV-Vis and Magnetic Properties of Azanaphthalocyanines

UV-Vis spectra of $N_{x,y}$ -[Nc*Mo(NtBu)Cl] are shown in Figure 84, measured in chlorobenzene, at rt. The B-band is excluded for clarity. A hypsochromic shift of the Q-band from $N_{0,0}$ -[Nc*Mo(NtBu)Cl] (869 nm) to $N_{8,8}$ -[Nc*Mo(NtBu)Cl] (729 nm) is observed in UV-Vis spectroscopy. The bathochromic shift of the Q-band of $N_{0,0}$ -[Nc*Mo(NtBu)Cl] (869 nm) and $N_{0,8}$ -[Nc*Mo(NtBu)Cl] (812 nm) explains why they appear brown, in comparison to the hypsochromically shifted green $N_{8,8}$ -[Nc*Mo(NtBu)Cl] (729 nm) and the greyish-green $N_{8,0}$ -[Nc*Mo(NtBu)Cl] (761 nm). An increase of the B-band intensity was observed, the more electron deficient the naphthalocyanine is, and the higher the pyrazine character (number of [-N=] units in the complex) of $N_{x,y}$ -[Nc*Mo(NtBu)Cl] is. In addition, a stronger shift of the Q-band was observed by exchanging the inner ($N_{8,0}$ -[Nc*Mo(NtBu)Cl]) [-CH=] units by [-N=] compared to the outer ($N_{0,8}$ -[Nc*Mo(NtBu)Cl]) ones, due to their proximity to the central [-MN₄-] unit.

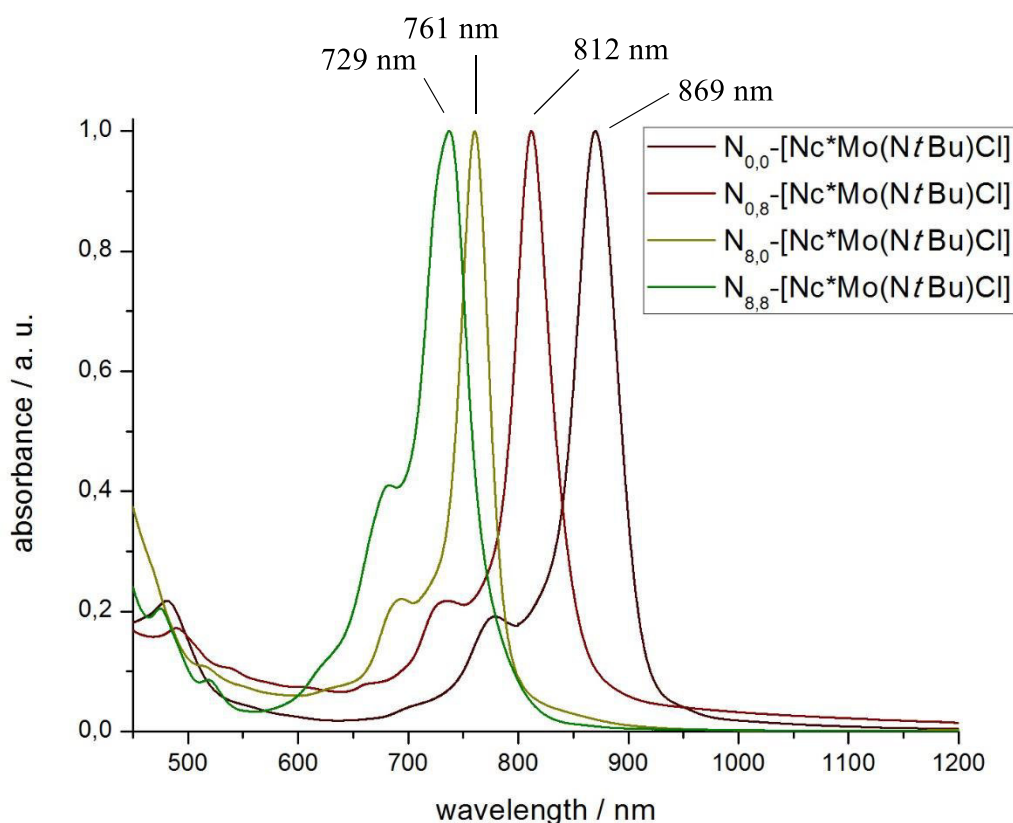


Figure 84: UV-Vis absorption, Q-band of synthesised $N_{x,y}$ -[Nc*Mo(NtBu)Cl], in CB at rt.

In Figure 85, Nc^*H_2 ($N_{0,0}$ - Nc^*H_2) is compared to $N_{0,0}$ -[Nc*Mo(NtBu)Cl] and $N_{0,0}$ -[Nc*Mo(NMes)Cl], respectively. Comparing the Q-band shift of $N_{0,8}$ - Nc^*H_2 and $N_{0,8}$ -[Nc*Mo(NtBu)Cl] (48 nm) with Nc^*H_2 ($N_{0,0}$ - Nc^*H_2) and $N_{0,0}$ -[Nc*Mo(NtBu)Cl] (72 nm) a stronger bathochromic shift of the Q-band can be observed by metalation of the free ligands

with decreasing number of [-N=] building blocks. It can be concluded, that the influence on the Q-band by axial substitution or metalation of a free phthalocyanine ligand is lower for electron poor Ppz (increasing [-N=] units) than for electron rich Pcs ([-CH=] units). This is in accordance with the axial substitution of Spcs, the equatorial functionalisation of Pc (N_x -[Pc^{*}M]), and the substitution in the meso position (TBTAP) described in the previous sections 4.2.1.2, 4.2.4.6 and 4.2.7.

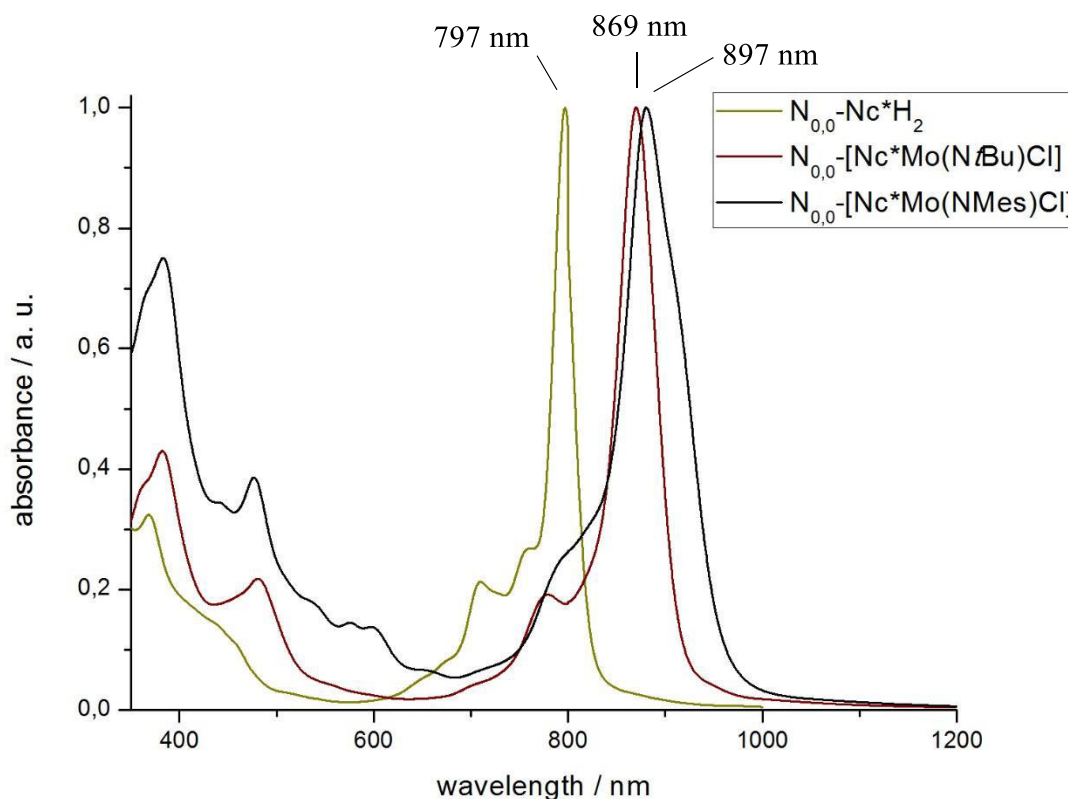


Figure 85: Free $N_{0,0}$ -Nc^{*}H₂ ligand in comparison to new synthesised molybdenum complexes $N_{0,0}$ -[Nc^{*}Mo(N*t*Bu)Cl] and $N_{0,0}$ -[Nc^{*}Mo(NMes)Cl].

EPR measurements. Of the naphthalocyanine complexes $N_{0,0}$ -[Nc^{*}Mo(N*t*Bu)Cl] and $N_{0,0}$ -[Nc^{*}Mo(NMes)Cl] EPR spectroscopic measurements were carried out, to explain the strong shift of the Q-band caused by axial N-imido substituents. The complexes are adequately soluble in toluene; - less polar solvents are better for EPR measurements so toluene was used rather than a CNP/toluene mixture. The X-band EPR spectrum of $N_{0,0}$ -[Nc^{*}Mo(N*t*Bu)Cl] is shown in Figure 86 on the bottom, and the one of $N_{0,0}$ -[Nc^{*}Mo(NMes)Cl] above. In both spectra, the five signals besides the main relaxation are visible and prove the oxidation state of the Mo^{+V}. The super hyperfine structure of the main signals is highly resolved, as shown on the right hand side.

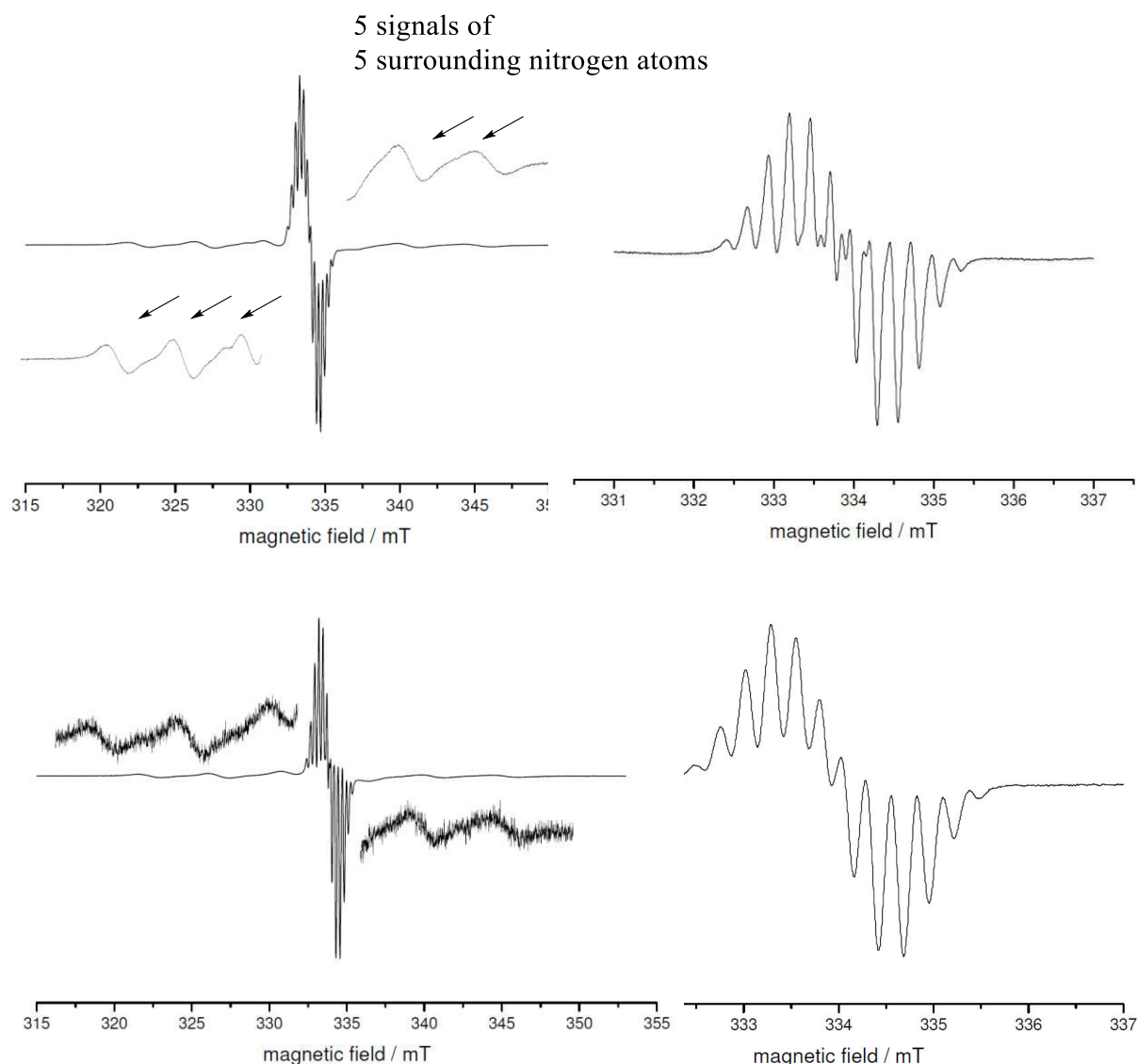


Figure 86: X-band EPR measurements of $N_{0,0}$ -[Nc*Mo(NMe)Cl] (upper spectra) and of $N_{0,0}$ -[Nc*Mo(NtBu)Cl] (lower spectra), 1 N in toluene at rt. Left hand side: hyperfine structure. Right hand side: Resolved super hyperfine structure of molybdenum and 5 N atoms (4 equal ones, 1 axial).

The X-band measurement shows a weak ZEEMAN interaction compared to the anisotropic hf interaction. The line aberration shows a central isotropic GAUß form. For each compound, $N_{0,0}$ -[Nc*Mo(NtBu)Cl] and $N_{0,0}$ -[Nc*Mo(NMe)Cl], twelve shf lines are visible, and an empty centre. These signals can be assigned to shf couplings of the ^{14}N ($I = 1$), and not to a further split by the $^{35/37}\text{Cl}$, as incorrectly described in previous work.^[25,205] The symmetry of both could additionally be verified by Q-band EPR measurements (Figure 87), which is orthorhombic and axial symmetric, respectively. In this work, only $N_{0,0}$ -[Nc*Mo(NtBu)Cl] and $N_{0,0}$ -[Nc*Mo(NMe)Cl] were characterized by Q-band EPR measurements, because the influence of the exchange of [-CH=] by [-N=] is negligible for the paramagnetic behaviour of the Mo^{+V} , as visible when comparing [Pc*Mo(NR)Cl] and [Ppz*Mo(NR)Cl] with $R = t\text{Bu}$ or Me s (Table 15).

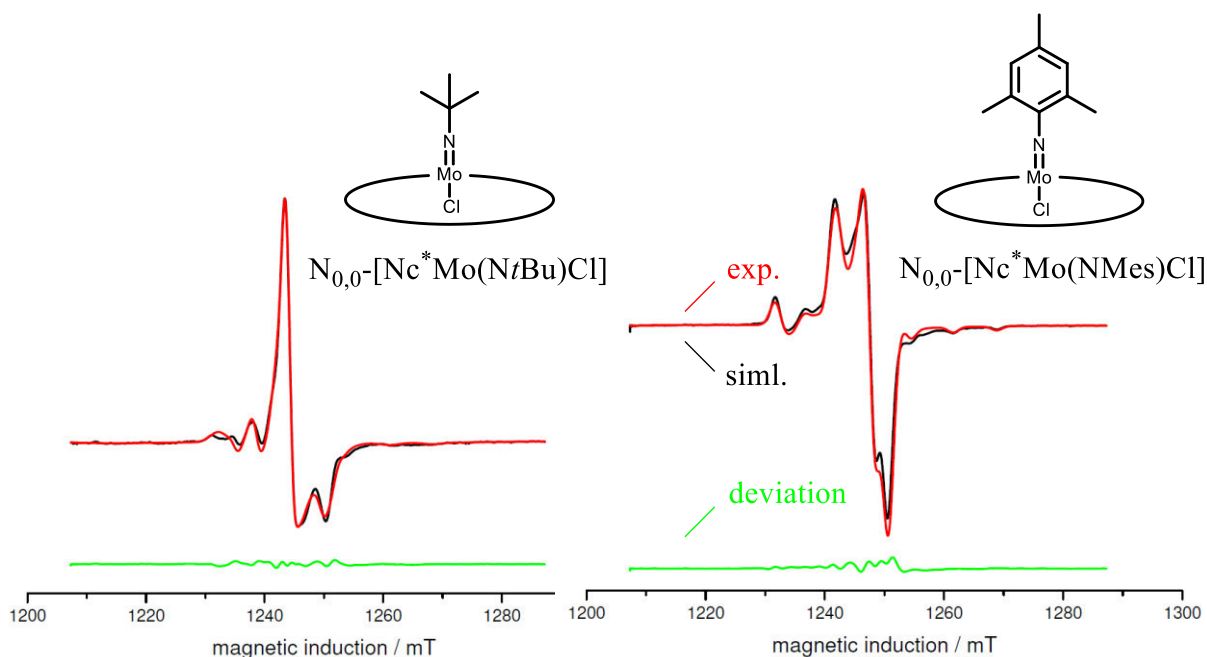


Figure 87: Q-Band measurement of $N_{0,0}$ -[Nc*Mo(NtBu)Cl] (left hand side), $N_{0,0}$ -[Nc*Mo(NMes)Cl] (right hand side) 100 K, toluene. Axial, orthorhombic splitting and differences between g_{iso} -values. In black: simulation. In red: measurement of sample. In light green: deviation.

For the Q-band measurements (Figure 87), a 2 N solution of $N_{0,0}$ -[Nc*Mo(NR)Cl] in toluene was used. Measurements were carried out at a temperature of 100 K or at rt. The experimental results (red) and simulations (black) as well as the deviations (green) are shown. In Table 15, the g_{iso} values are summarised.

Table 15: g_{iso} values obtained in Q-band measurements, in toluene (100 K).

	g_{iso}		g_{iso}
[PcMo(NtBu)Cl]	1.984 ^[205]	[PcMo(NMes)Cl]	1.980 ^[205]
[Pc*Mo(NtBu)Cl]	1.9810 ^[70]	[Pc*Mo(NMes)Cl]	1.9789 ^[70]
[Ppz*Mo(NtBu)Cl]	1.9808 ^[70]	[Ppz*Mo(NMes)Cl]	1.9789 ^[70]
$N_{0,0}$ -[Nc*Mo(NtBu)Cl]	1.9788	$N_{0,0}$ -[Nc*Mo(NMes)Cl]	1.9779

The weak influence of the π -system (and its increasing or decreasing electronic character) on the g_{iso} value is visible. For $N_{0,0}$ -[Nc*Mo(NtBu)Cl], a $g_{iso} = 1.9788$ and for $N_{0,0}$ -[Nc*Mo(NMes)Cl] a $g_{iso} = 1.9779$ was determined. The isotropic hf constants, a_{iso} , were determined. For $N_{0,0}$ -[Nc*Mo(NtBu)Cl], $a_{iso} = 4.63$ mT at 34.523 GHz was determined, for $N_{0,0}$ -[Nc*Mo(NMes)Cl], $a_{iso} = 4.58$ mT, at 34.524 GHz. The isotropic spectra are not influenced by the hf interaction of the magnetic Mo. The mentioned mistake described in previous work is the splitting of the signal into 5 lines, caused by the surrounding of four Pc-ligand N-atoms. It was supposed that one line is caused by the axial $^{35/37}\text{Cl}$ -atom ($I = 3/2$). In these spectra, it is quite clear that all splits do come from axial N^R -atoms, with $R = t\text{Bu}$ or Mes . The better resolution might be caused by the solvent, here toluene instead of a more polar solvent mixture of CNP/toluene 2:1 was used.

Results and Discussion

In Figure 88, an axial symmetry for $N_{0,0}$ -[Nc*Mo(NtBu)Cl] is visible. The molecule has C_{4v} symmetry. In the case of $N_{0,0}$ -[Nc*Mo(NMes)Cl], a decrease of symmetry to C_{2v} is visible. The lower symmetry explains the, in comparison to other axial ligands, strong shift of the Q-bands. The d_{xz} and d_{yz} orbitals of the C_{4v} symmetrical compounds $N_{0,0}$ -[Nc*Mo(NMes)Cl] are increased in comparison to the octahedral C_{2v} compound $N_{0,0}$ -[Nc*Mo(NtBu)Cl]. In Figure 88, an orbital scheme of the degenerate orbitals is shown.^[25] In the case of the C_{4v} axial symmetry, the orbitals are degenerate. In case of a mesityl substitution, the degeneracy is lifted, and the d_{yz} orbital is increased. Calculations about the nature of the axial -NMes ligand could give us more information about the overlapping of Mo-N_{imido} π -orbitals Mo(d_{xz})-N(p_x) or Mo(d_{yz})-N(p_y), and are actually carried out by AG BERGER (Department of Chemistry at the Philipps-Universität Marburg).

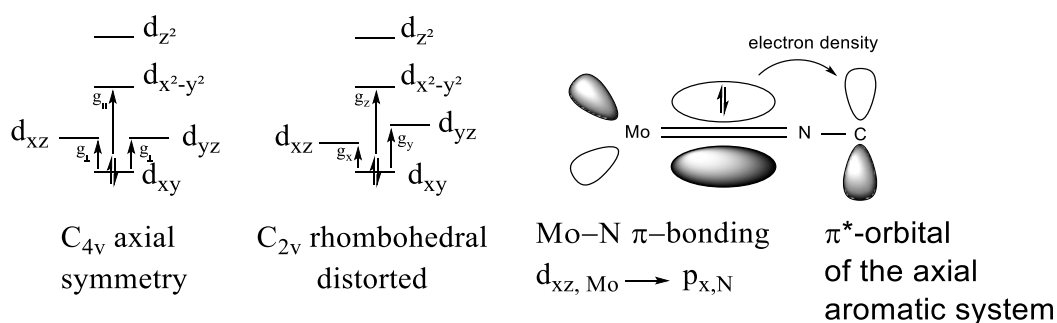


Figure 88: Orbital scheme of axially symmetrical and rhombohedral distorted molybdenum Pc complexes. Adapted from literature.^[25]

In addition to the molybdenum complexes, the naphthalocyanine tungsten complex $N_{0,0}$ -[Nc*W(NtBu)Cl] was analysed by EPR spectroscopy. In comparison to the spin of d^1 -Mo with $5/2$, d^1 -W has a spin of $1/2$. This is reflected in the EPR spectrum within only one signal in X-band measurements (Figure 89).

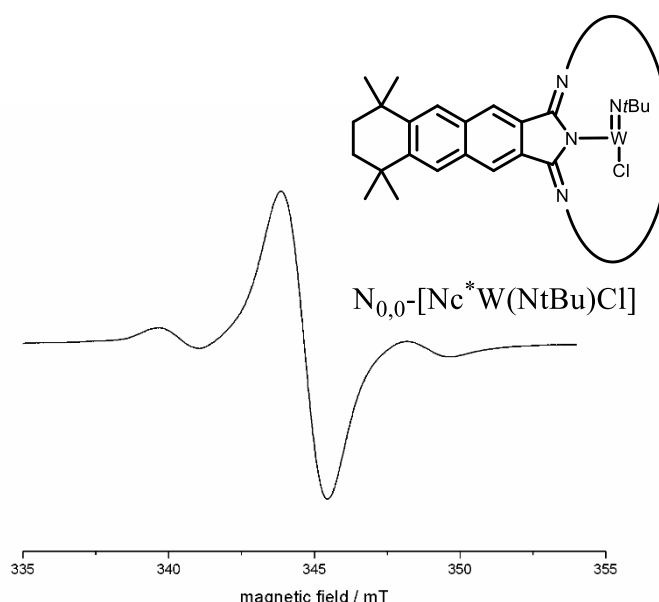
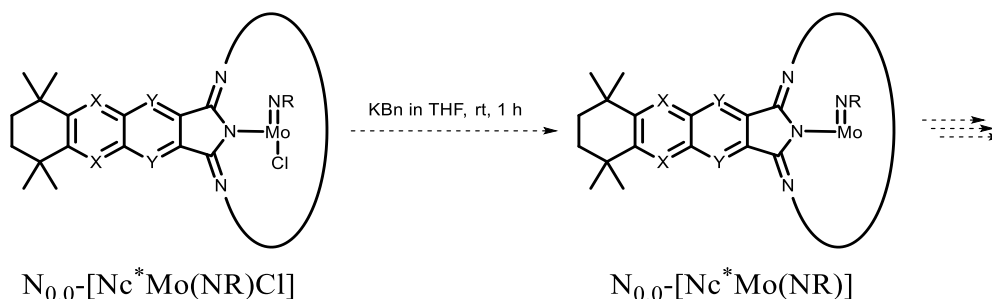


Figure 89: X-band EPR measurement of $N_{0,0}$ -[Nc*W(NtBu)Cl], in toluene at rt. Only one signal of the spin $1/2$ visible.

For further investigations, the azanaphthalonitriles might be easily converted into the corresponding d^2 -molybdenum and d^2 -tungsten oxo-complex $N_{0,0}$ -[Nc^{*}Mo(O)], by first reducing the Mo/W to oxidation number +IV with KBn, and then stirring in aq. THF solution. These oxo-complexes may bind differently to TiO₂ or ZnO surfaces.



Scheme 44: Further possible functionalisation of $N_{x,y}$ -[Nc^{*}Mo(*Nt*Bu)Cl] complexes.

In summary, the first series of azanaphthalocyanines bearing alkyl groups in the peripheral position has been presented within the preceding chapters. While an azanaphthalocyanine series of $N_{x,y}$ -[Nc^{*t*Bu}M], bearing alkyl groups in the peripheral position, has been patented, and their synthesis has been announced, no characterisation was described up to the time of writing this thesis.^[129] Several applications for these compounds were proposed.^[129] In addition, their smaller homologues, namely azasubnaphthalocyanines $N_{x,y}$ -[Snc^{*}BCl], bearing these alkyl group were not systematically studied and a synthesis of a $N_{8,0}$ -[Snc^{*}BCl] is described in section 4.2.1.4. Here, the series of azanaphthalocyanines has the same advantages as their smaller azaphthalocyanine series: the alkyl groups decrease aggregation effects and raise the solubility of the resulting azanaphthalocyanine while a C_{4v} -symmetry of $N_{x,y}$ -[Nc^{*}Mo(*Nt*Bu)Cl] is maintained.

It was observed that the synthesis applying Li/*n*-octanol conditions is favoured for dinitrile precursors of $N_{0,0}$ -[Nc^{*}M] and $N_{0,8}$ -[Nc^{*}M], while meso-substituted by-products^[200] were observed for $N_{8,0}$ -[Nc^{*}M] and only a poor formation of $N_{8,8}$ -[Nc^{*}Zn], with M = 2 H, Zn. In contrast, higher yields were obtained for $N_{8,0}$ -[Nc^{*}M(NR)Cl] and $N_{8,8}$ -[Nc^{*}M(NR)Cl] with M = Mo, W and R = *t*Bu, Mes in quinoline conditions at 230 °C with the respective imido precursor [Mo(NR)₂Cl₂·*sol*v]. All obtained C_{4v} -symmetrical $N_{x,y}$ -[Nc^{*}Mo(*Nt*Bu)Cl] were analysed by using MALDI-ToF or LIFDI-MS, elemental analysis, UV-Vis and IR spectroscopy, and some selected examples with EPR spectroscopy. In EPR measurements, the structure and the symmetry of these compounds could additionally be proved, which is orthorhombic or axial symmetric for R = Mes or *t*Bu in $N_{x,y}$ -[Nc^{*}Mo(NR)Cl].

4.3 Functionalised Phthalocyanines

The section "Functionalised Phthalocyanines" is divided in several subsections. The first section addresses the synthesis of phthalonitrile precursors bearing a functional group. The following sections describe the synthesis of functionalised phthalocyanines, $[\text{PcM}]^{\text{FG}}$, and soluble alkyl substituted derivatives, $[\text{Pc}^*\text{M}]^{\text{FG}}$. Both types were designed for bonding of the phthalocyanines as a photosensitizer (PS) onto semiconductor surfaces, such as TiO_2 or ZnO . $[\text{PcM}]^{\text{FG}}$ type Pcs were mainly synthesised to test if bonding via the functional group occurs and to investigate the form of the resulting interface. Within the SFB1083, the aim was a better understanding of electron processes at semiconductor surfaces using different anchor moieties. Using this knowledge, the synthesis of new soluble phthalocyanines for their application as PS in DSSC is optimised. By exchanging $[-\text{CH}=\text{N}-]$ units with $[-\text{N}=\text{C}=\text{N}-]$, the HOMO-LUMO gap can be tuned so as to adjust it to the conduction band of the semiconductor (level alignment). The construction of DSSCs gives useful information about charge-transfer processes, which should be further compared to photoluminescence (PL) measurements.

4.3.1 General Introduction – Preliminary Work

The syntheses of Pcs bearing a functional group are widely discussed in literature. In recent years, several reviews were published discussing them as PS in DSSCs. In 2013, RAGOUSI compared different phthalocyanines with anchor groups.^[105] To absorb a Pc in a specific mode onto a semiconductor, the anchor of the phthalocyanines can be added at different positions, as shown in the sketch below (Figure 90).^[25] There are axial anchors, or functional groups, directly bound at the metal of the phthalocyanine such as in $[\text{Pc}^*\text{TiS}_2]$, or cross-linked, i.e. catechol derivatives (Figure 91). In the first case, the phthalocyanine seems to be bound almost coplanar ("flat") to the surfaces. In addition, 16 peripheral positions or four meso-positions of a Pc can be used for equatorial functionalisation.

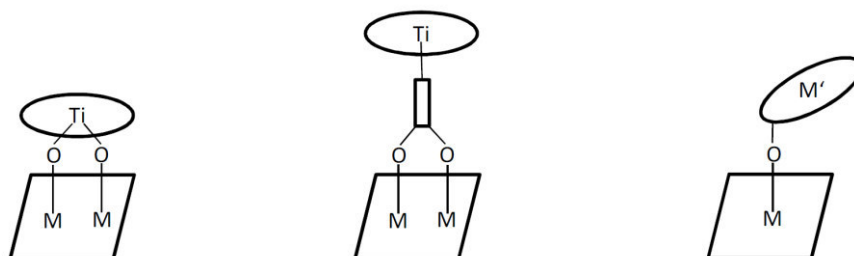


Figure 90: Binding modes of phthalocyanines. Adapted from literature.^[25]
a) direct bonding b) axial anchor such as catechol c) equatorial anchor.

When the equatorially functionalised Pc is bound onto a surface, different competing orientations of the phthalocyanine are possible (Figure 90). It may stand vertically to the

surfaces, lie flat on it, similar to the axial anchors, or be orientated at any angle between 0° and 90° . These orientations may be influenced by additional axial ligands, sterically demanding groups in the periphery of the phthalocyanine or the metal core. Also, the length of the anchor may influence the orientations.^[105] In preliminary work of our group, SEIKEL synthesised different axially substituted phthalocyanines, soluble and less soluble ones, of the type $[\text{Pc}^{(*)}\text{Ti}(\text{Cat})]$ (Figure 91) with catechol derivatives (Cat) as anchor moiety. The advantage of these compounds is that the sterically demanding axial anchor decreases aggregation effects of the π -systems so that better injection of electrons with less recombination of the exciton pairs between the dyes is expected.^[77,206] Axially substituted $[\text{PcTi}(\text{Cat})]$ were reported by HANACK.^[207] In Figure 91, on the hand side, a $[\text{Pc}^{(*)}\text{Ti}(\text{Cat})]$ type is shown; on the right side the axially substituted $[\text{Pc}^{\text{tBu}}\text{Ti}(\text{Cat})]$ analogues previously described by TORRES are shown.^[77]

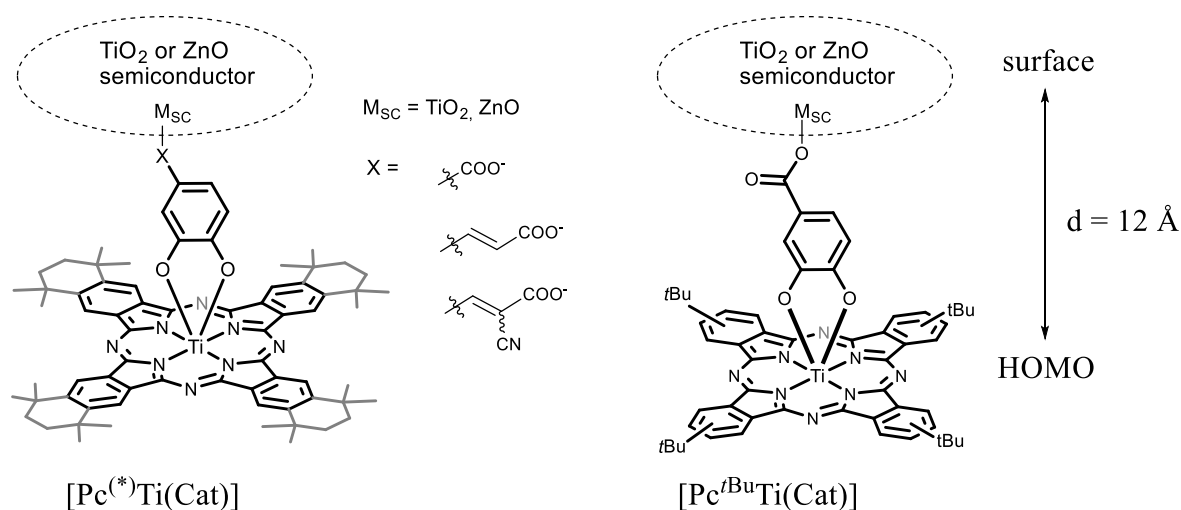


Figure 91: Different known axial functionalised phthalocyanines.^[25,77]

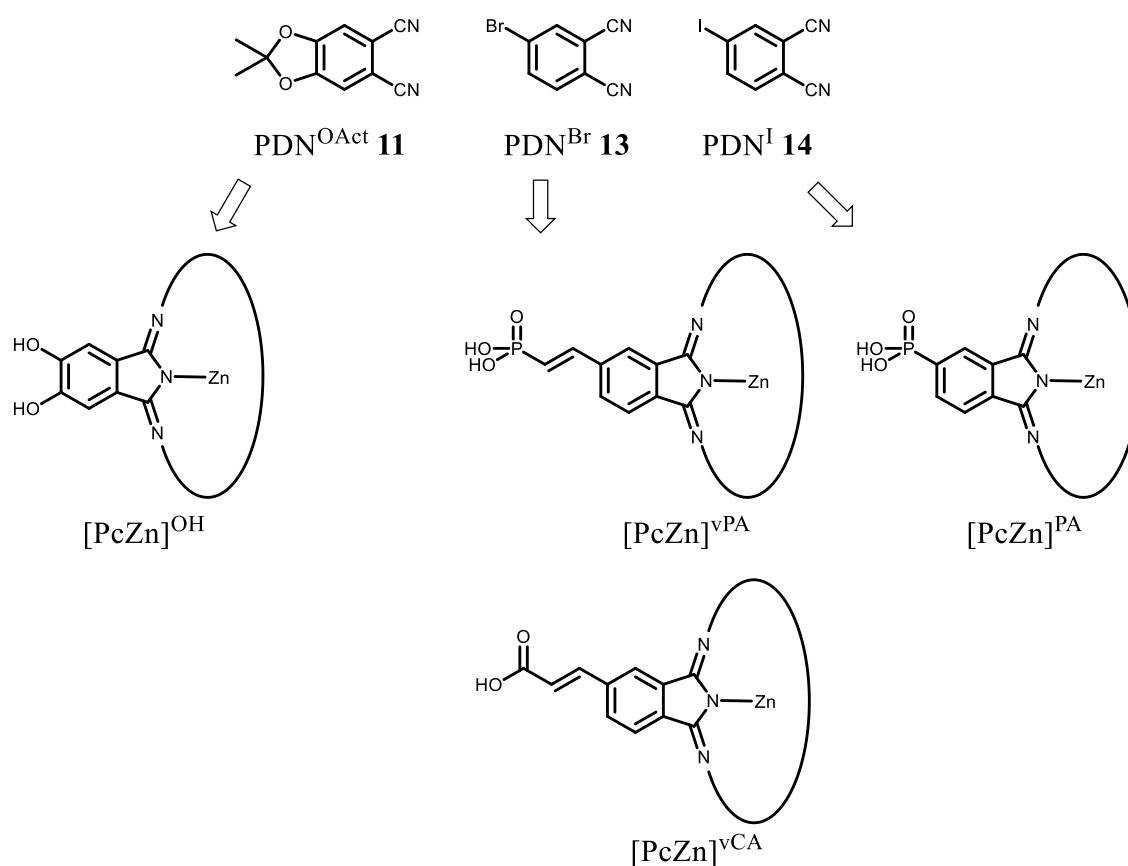
The main disadvantage of these compounds is the distance of the dye to the semiconductor, because of the large axial spacer. The distance of about 12 \AA was given in literature.^[25] Therefore, an effective electron transfer from the dye to the semiconductor is not possible, so efficiencies of $<0.023\%$ were determined, when applying Pcs of a $[\text{Pc}^{(*)}\text{Ti}(\text{Cat})]$ type as PS in DSSCs.

However, in this work, the investigation was more focused on equatorially functionalised phthalocyanines (right side, Figure 90). The aggregation of these compounds can be minimized by the addition of sterically demanding groups in the peripheral position. In 2013, the most efficient A_3B phthalocyanine TT40 on TiO_2 was reported, as shown in the introduction 2.2.2 (Figure 24).^[104,106]

Results and Discussion

TT40 uses a carboxylic acid as anchor moiety and is substituted with *push*-ligands in the peripheral positions leading to a remarkable efficiency of $\eta = 6.13\%$ when applied in a DSSC. Other anchors are also reported, such as a phosphinic acid, yielding $\eta = 3.24\%$.^[75,79] Here, a strong bonding of the phosphinic acid moiety was observed, as well as a greater photostability compared to carboxylic anchors.^[75,79] Nitrogen substituents in the peripheral position were calculated to be promising candidates for *push*-ligands.^[208] Best calculated results were obtained for moieties such as $-\text{NR}_2$ with R = alkyl groups. An attractive alternative appears to be guanidine as *push* ligand.^[13]

The main disadvantage of equatorially functionalised phthalocyanines reported so far is that they were obtained as isomeric mixture, which makes them useless for better understanding of physical processes on molecular level taking place at interfaces. Taking this into consideration, it was attempted to synthesise new equatorially functionalised phthalocyanines, bearing only one functional group in the peripheral position.

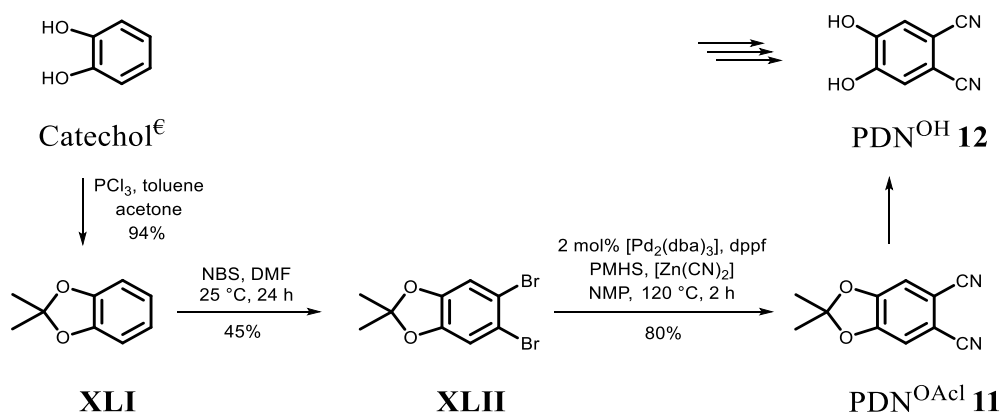


Scheme 45: Structural motifs of target functionalised phthalocyanines $[\text{PcZn}]^{\text{FG}}$.

At first, the synthesis of phthalocyanines without alkyl groups in peripheral positions, $[\text{PcZn}]^{\text{FG}}$, was carried out (Scheme 45). Most of the equatorial anchor functionalities were already described either in literature or previously in our group, e.g. the carboxylic acid.^[13] Phosphonic acid as anchor moiety was chosen because a strong bond to TiO_2 is reported.^[131,132] After this, the more synthetically challenging alkyl substituted $\text{Pc}^*\text{H}_2^{\text{FG}}$ and $[\text{Pc}^*\text{Zn}]^{\text{FG}}$ were investigated. As alkyl substituted dinitriles, the previously used precursors $\text{PDN}^* \mathbf{1}$ and $\text{PyZDN}^* \mathbf{2}$ (section 4.1) were chosen.

4.3.2 Synthesis of Precursors

In order to synthesise the target compounds (Scheme 45), the precursor 5,6-dicyano-2,2-dimethyl-1,3-benzodioxole ($\text{PDN}^{\text{OAcI}} \mathbf{11}$), 4-bromophthalonitrile ($\text{PDN}^{\text{Br}} \mathbf{13}$) and 4-iodophthalonitrile ($\text{PDN}^{\text{I}} \mathbf{14}$) were synthesised to obtain the corresponding phthalocyanines either via ring expansion or by cyclotetramerisation. All precursors are known from literature. The $\text{PDN}^{\text{I}} \mathbf{11}$ and $\text{PDN}^{\text{Br}} \mathbf{13}$ were synthesised to add other functional groups, such as phosphonate and carboxylate anchors, after cyclisation.

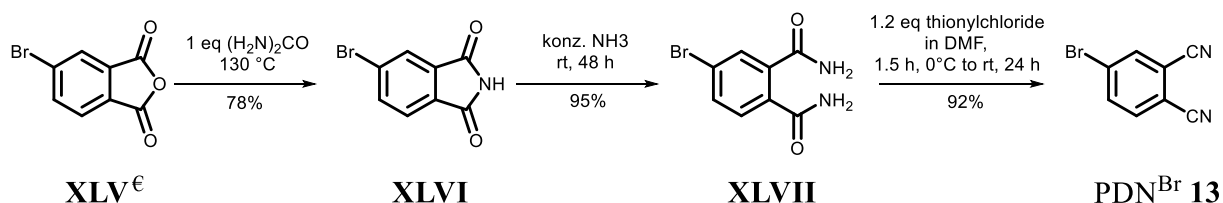


Scheme 46: Synthesis of 5,6-dicyano-2,2-dimethyl-1,3-benzodioxole (**11**).

The PDN^{OAcI} was synthesised to investigate a possible bonding of the resulting catechol phthalocyanine to a semiconductor.^[131,132] The synthesis of the $\text{PDN}^{\text{OAcI}} \mathbf{11}$ is shown in Scheme 46; it has been described several times in literature.^[136,209–211] In the first step, the pyrocatechol was protected by forming an acetal **XLI**.^[209] Compound **XLI** is then converted to the dibromide **XLII** using NBS,^[211] and finally converted with a yield of 80% to the $\text{PDN}^{\text{OAcI}} \mathbf{11}$ in a palladium catalysed coupling, using a method reported by HANACK.^[136] The last step is also possible using ROSENMUND VON BRAUN reaction conditions, but a much lower yield of only about 30% is achieved, while the workup is more complicated.

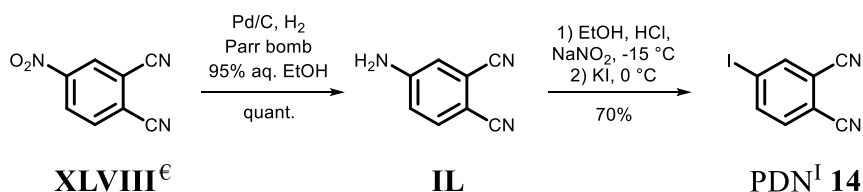
Results and Discussion

4-Bromophthalonitrile (**13**) was already known in our group. It was synthesised according to procedures described before.^[13,212] The synthesis of PDN^{Br} is feasible in overall yields of 68% in 3 steps, starting from the commercially available 4-bromophthalanhydride (**XLV**).



Scheme 47: Synthesis of 4-bromophthalonitrile (**13**).

PDN^I **14** was synthesised in addition to the PDN^{Br} **13** to test its reaction towards different Pd catalysed coupling reactions and to compare yields, because the C-I bond is more reactive. The procedure of the synthesis of PDN^I **14** is literature known, since 1985. It was described by LEZNOFF and TOMER (Scheme 48).^[213] PDN^I **14** is often used in recent literature to functionalise different lower symmetrical phthalocyanines.^[214]

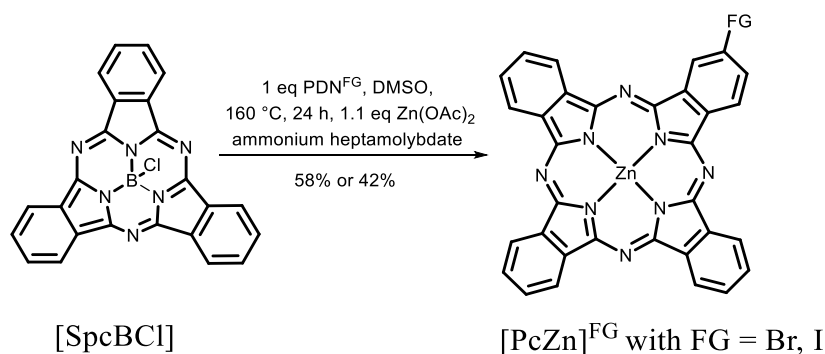


Scheme 48: Synthesis of 4-iodophthalodinitrile (**14**).

In the first step, the commercially available 4-nitrophthalonitrile **XLVIII** is reduced in a heterogeneous catalysis H₂ over Pd/C. After filtration and removing the solvent, 4-aminophthalonitrile (**II**) is obtained in quantitative yields and sufficient purity. The amine **II** can be converted to PDN^I **14** in a SANDMEYER reaction, using NaNO₂ and KI. The dark yellow powder was obtained in yields of 70%.

4.3.3 Synthesis of Unsubstituted Functionalised Phthalocyanines

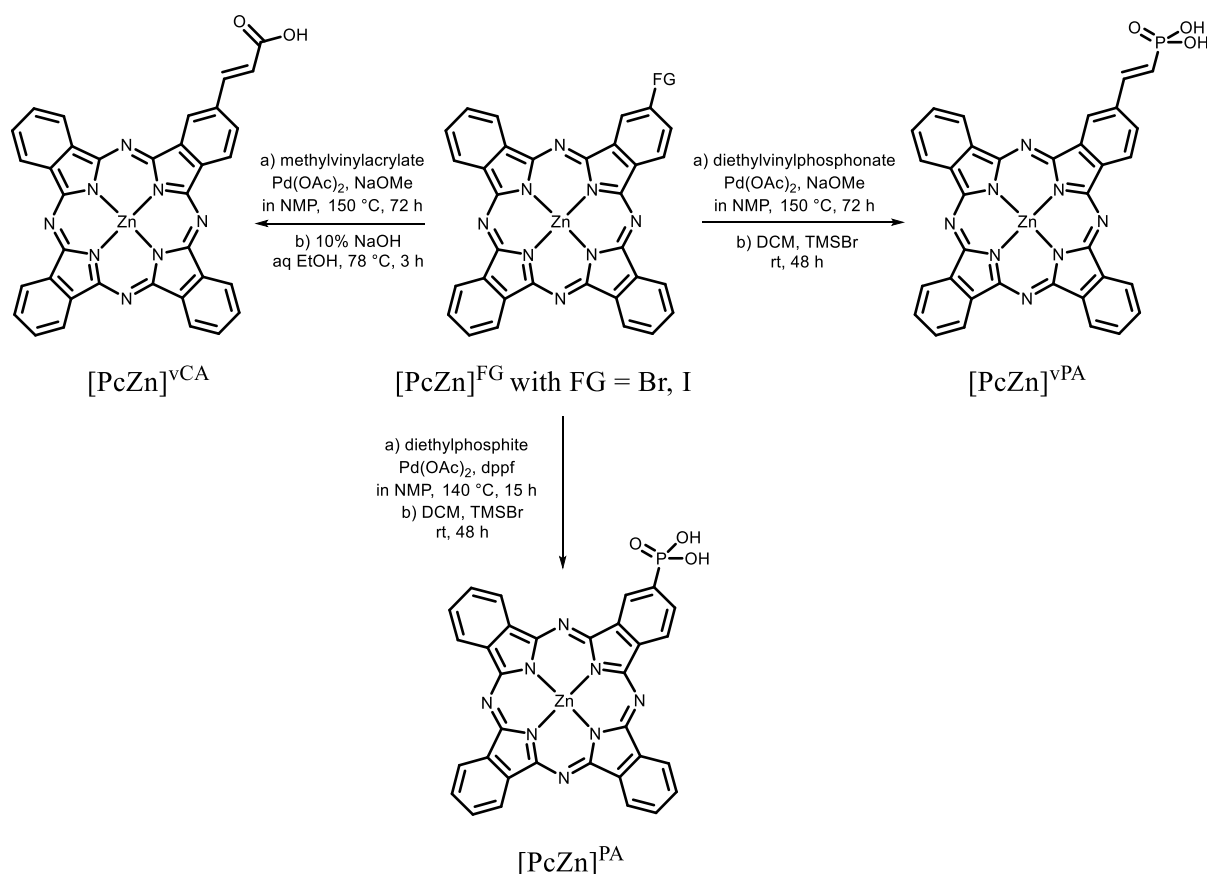
In literature, a synthesis for a mono-functionalised bishydroxy-phthalocyanine $[\text{PcZn}]^{\text{OH}}$ was described before.^[105] Several cross couplings in peripheral positions, such as SONOGASHIRA,^[215,216] HECK,^[216] and STILLE,^[217] reactions are literature known, using soluble phthalocyanine derivatives. In most of these examples, with an increase in solubility in water or common organic solvents, the symmetry of the Pcs is lowered because of additional moieties in the peripheral position.^[215,218] In our group, the synthesis of $[\text{PcZn}]^{\text{vCA}}$ (Scheme 50) was described before, using $[\text{SpCBCl}]$ as starting material, which might be extended by using the corresponding isoindoline of a dinitrile PDN^{FG} (compare to section 4.2.4.2).^[13] The mono-functionalised phthalocyanines, bearing only one functional group in the peripheral position, were synthesised using the KOBAYASHI ring expansion. Cocyclisations are also described, but a difficult separation of the isomers by CC was avoided.^[219] A ring expansion of a $[\text{SpCBCl}]$ (Scheme 49) was possible using the isoindolines of PDN^{Br} **13** and PDN^{I} **14** in yields of 58% and 42%, respectively.



Scheme 49: Synthesis of mono-functionalised Pcs $[\text{PcZn}]^{\text{Br}}$,^[13] and $[\text{PcZn}]^{\text{I}}$ via ring expansion.

Both compounds, $[\text{PcZn}]^{\text{Br}}$ and $[\text{PcZn}]^{\text{I}}$, were characterized by using ^1H NMR, IR, UV-Vis spectroscopy, MALDI-ToF, APCI-HR mass spectrometry, and elemental analysis. The Br, I moieties were further substituted by functional groups, applying known cross-coupling methods.^[13,220,221] After deprotection of the resulting esters,^[221,222] the functionalised zinc phthalocyanines with a phosphonic acid as anchor $[\text{PcZn}]^{\text{PA}}$, vinyl phosphinic acid $[\text{PcZn}]^{\text{vPA}}$, and vinyl carboxylic acid $[\text{PcZn}]^{\text{vCA}}$ were obtained (Scheme 50). The solubility of the protected compounds was sufficient for column chromatography using a Tol/THF gradient. After deprotection, the target compounds were washed several times with hexane/MeOH.

Results and Discussion

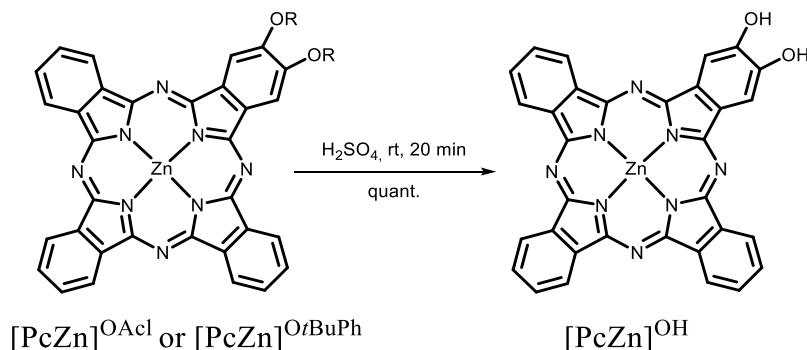


Scheme 50: Synthesised mono functionalised [PcZn]^{FG}.

In all cases, the synthesis is quite straightforward, while the purification of the resulting phthalocyanines was quite difficult. Yields of <10% reflect the problematic nature of these syntheses. All compounds were characterized by MALDI-ToF mass spectrometry, while under APCI conditions, a loss of the phosphonate anchor occurred. In comparison to all other [PcZn]^{FG}, the carboxylate anchor of [PcZn]^{vCA} seems to be more stable for APCI. ³¹P NMR and/or ¹H NMR measurements of the compounds were carried out, but in the case of the phosphonate substituted phthalocyanine, it was difficult to detect the ³¹P nucleus. Only very weak and broad signals could be found, even by ¹H-³¹P coupled measurements. In IR measurements, typical phthalocyanine fingerprint and $\nu(\text{OH})$ stretching vibrations are clearly visible.

In literature, [PcZn]^{OH} was synthesised in a cyclotetramerisation using the PDN^{OrBuPh} and PDN **I** in a 1:3 ratio, by LEZNOFF *et al.*^[219] After column chromatography, the [PcZn]^{OrBuPh} was obtained, deprotected with sulfuric acid and compared to its cocyclisation A₂B₂ derivative with regard to their application in photodynamic therapy. For reasons of completeness, it should be

mentioned that an A_2B_2 diol species appears more active in *in vivo* tests than its A_3B derivative $[PcZn]^{OH}$, contrary to Φ_{Δ} determined for compounds described in section 4.2.4.6 (p. 75).



Scheme 51: Synthesis of $[PcZn]^{OH}$ by deprotection of the corresponding A_3B Pc.^[219]

In this work, the reactions were carried out using PDN^{OAc} or PDN^{OBuPh} to insert into $[SpcBCl]$. After successful insertion and a short column chromatography, both complexes, $[PcZn]^{OAc}$ and $[PcZn]^{OBuPh}$, could be successfully deprotected by stirring the A_3B phthalocyanine in conc. H_2SO_4 for several minutes. In cooperation with KOTHE (WITTE group at the Department of Physics of the Philipps-Universität Marburg), and SFB1083, $[PcZn]^{vPA}$ and $[PcZn]^{OH}$ were further investigated by X-ray absorption spectroscopy methods such as XPS and NEXAFS. Therefore, both compounds were bound onto a ZnO surface. The results are briefly summarised in the following section 4.3.4. However, both compounds show a high aberration of the C/N ratio, but the phosphoric anchor to ZnO was detected in XPS measurements. In similar experiments, the 2-phenylvinylphosphinic acid was used to test a bonding of the compound on ZnO. In those experiments, a decomposition of the ZnO surface by the phosphonic acid was observed. Anyway, a new series of unsubstituted phthalocyanines bearing one equatorial anchor is presented. This series offers the possibility to investigate and determine a systematic structure-property correlation with regard to electron transfer processes onto semiconductor surfaces (section 4.3.8).

4.3.4 Attempts to Form Ordered Mono-Layers ^[177]

In cooperation with KOTHE (WITTE group at the Physics Department of the Philipps-Universität Marburg), within the SFB 1083, non-alkyl substituted zinc phthalocyanines, $[\text{PcZn}]^{\text{vPA}}$ and $[\text{PcZn}]^{\text{OH}}$, were investigated more precisely with regard to their bonding on semiconductor surfaces. First, investigations with benzylvinylphosphonic acid were carried out, as well as with catechol (Figure 92). The ZnO surfaces were coated using 0.05-0.5 mmol dye suspended in DMF with the respective substance, for 5 d. The absorption of the adsorbed dye was monitored with TDS and UV-Vis spectroscopy.

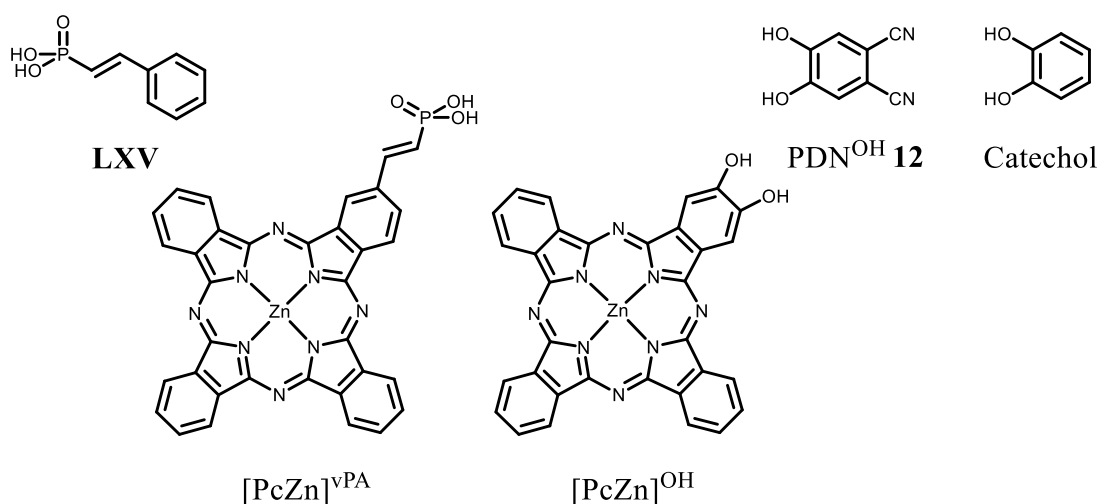


Figure 92: Investigated Pcs and precursor studies by the Physics Department of Chemistry at the Philipps-Universität Marburg.

In UV-Vis spectra, a weak shift to higher energies of the solid UV-Vis spectrum was found, in comparison to the UV-Vis measurement in DMF. But only a weak absorption was found for the solid state measurement. The thin film shows no excitonic structure, which might be caused by a low order of the Pc on the surface. In AFM measurements, only a weak stepwise increase of 5 Å was found. Here already, impurities could be observed. In photoelectronic measurements, e. g. XPS, different element signals were compared. In Figure 93 on the top, an overview is shown, whereby no phosphorous could be detected at all. On the bottom the Zn3s and P2p region is high resolved. Anyway, only a weak phosphor signal was found and a P/Zn ratio of 0.098 was found. In comparison to the benzyl vinylphosphonic acid with a ratio 3.5, this value is far too low. Similar values were obtained for the C/N ratio, whereby C/N = 1263 was found, compared to a theoretical value of C/N = 4.25. To confirm that $[\text{PcZn}]^{\text{vPA}}$ was successfully bonded to the surface, NEXAFS measurements were carried out and compared to

[PcZn]. In case of the [PcZn]^{vPA} only weak signatures were observed, which are similar to [PcZn]. Because the electronic properties of both compounds are quite similar, it was concluded that the sample is dominated by impurities. To sum up, neither any order of a phthalocyanine could be found, nor any proof of the formation of a monolayer of the covalently bonded [PcZn]^{vPA}.

The results of the dihydroxy-phthalocyanine [PcZn]^{OH} are quite similar, while the C/N values fit a bit better. Here, an amount of 20% [PcZn]^{OH} on the surface was found. The NEXAFS signature shows a weak upright standing position of [PcZn]^{OH}.

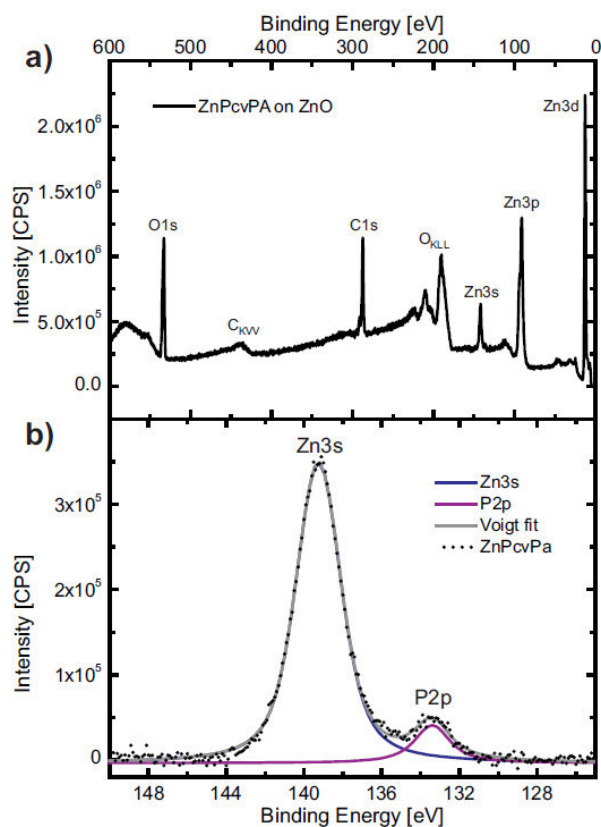
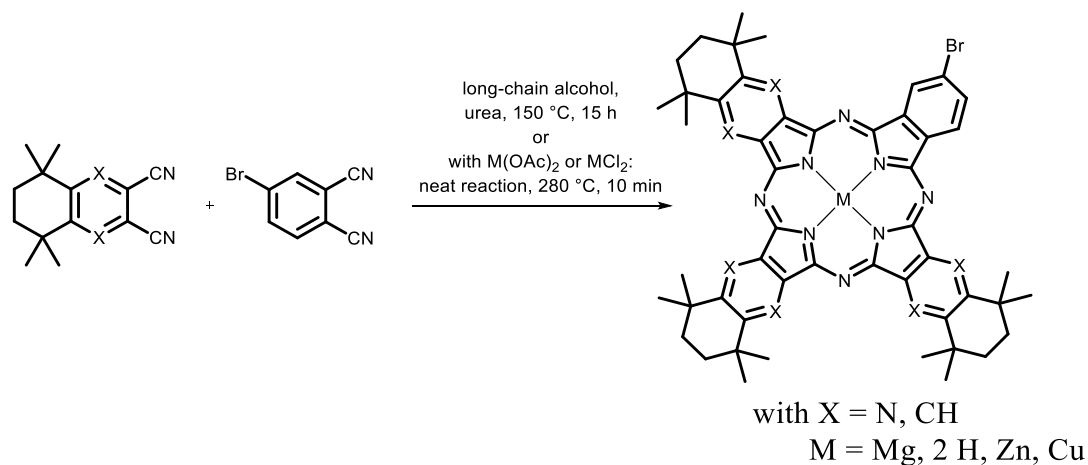


Figure 93: XPS measurements carried out by KOTHE (Physics Department of Chemistry of the Philipps-Universität Marburg).

In future, TGA measurements would help to gain information about the stability of [PcZn]^{vPA}, so gradient sublimation may be carried out to get the phthalocyanines in higher purity. It could not be explained where the high carbon values come from, because elemental analysis suggests a higher metal value in the sample. The pale colour and weak absorption spectra indicate a degradation of the phthalocyanines within the preparation of the samples. This might be caused by the high temperatures used in deposition of >70 °C, 5 d. In later studies, described in 4.3.7, different solvents and adsorption times were tested to optimize the absorption of the dye, when applying them in DSSCs. Furthermore, a high dependence of the stability of dyes was found when different substrates, such as ZnO or TiO₂, were used. Other A₃B phthalocyanines with thiol anchors linked to a Au surface are part of actual ongoing investigations by BARTLETT, and appear to be more promising candidates.

4.3.5 Attempts to Synthesise Soluble, Functionalised Phthalocyanines

Several attempts to obtain lower symmetrical phthalocyanines are summarised in section 4.2.3.2. Most syntheses follow a cocyclisation method using two dinitriles A and B. Depending on their reactivity, a 1:3 ratio of both dinitriles A/B is most common. In this section, several syntheses were carried out to functionalise phthalocyanines with an anchor in the peripheral position. Because of similar retention factors, a separation of molecules bearing Br and I instead of alkyl groups appears rather difficult. In previous work in our group, a similar synthesis was attempted, and a separation of the resulting phthalocyanines was not successful.^[13] In this work, it was attempted to functionalise the isomeric mixture (obtained from a cyclisation) in a HECK coupling first and to separate the mixture afterwards. For cocyclisation, two routes were applied (Scheme 52): in the first route, the two respective dinitriles were heated in a long-chain alcohol such as *n*-octanol in a ratio of 3:1, using a base such as DBU to initiate the reaction, to finally obtain the metal free phthalocyanines. In comparison to previously described procedures, here, no Li/*n*-octanol solution can be used, because the halogen atom is exchanged by a nucleophile and LiX salts with X = Br, I precipitate. In the second route, the dinitriles were converted in a neat reaction to the phthalocyanines at 280 °C in a 1:2 ratio. In neat reactions, only metalated phthalocyanines [Pc**M*]^{Br/I} were obtained.

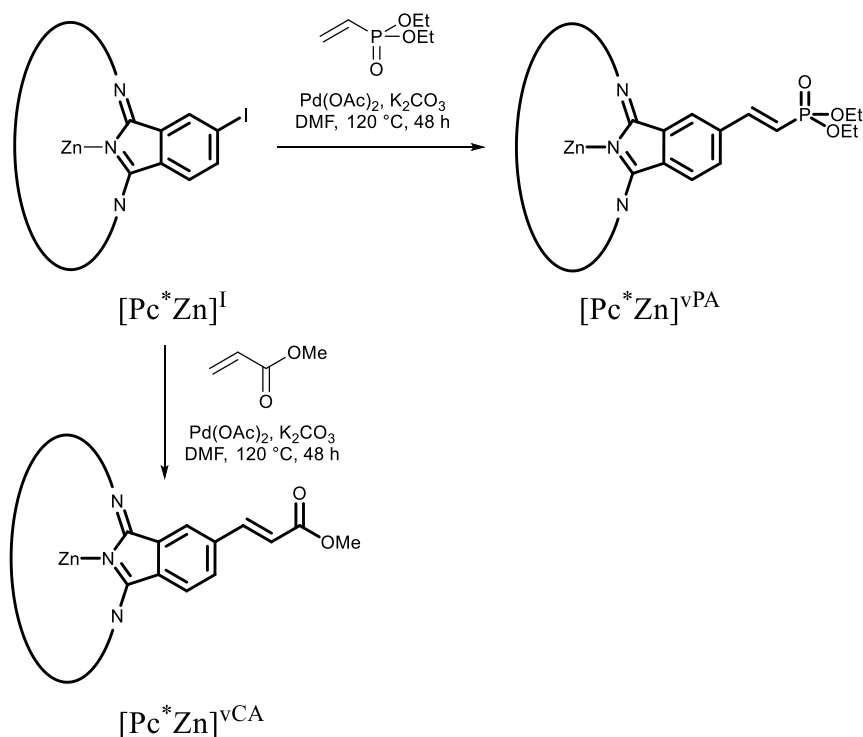


Scheme 52: Synthesis of soluble alkyl substituted phthalocyanines with a functional group for modification.

After cyclotetramerisation and purification via a short silica column, the obtained mixtures were analysed by using UV-Vis spectroscopy and MS to confirm the formation of Pc. The protonated form Pc*H₂^{Br/I} cannot be used for further coupling reactions, because a palladation of Pc*H₂^{FG} occurs, i. e. Pd inserts into the Pc cavity. In the neat reactions, different product mixtures were identified, containing the desired A₃B product [Pc*Mg]^{Br}, [Pc*Zn]^{Br/I} and [Pc*Cu]^{Br} as main product. The obtained mixtures were directly converted with a vinylcarboxylester or a vinylphosphonic diethyl ester to the respective functionalised phthalocyanines. The reactions

were carried out using typical HECK conditions (Scheme 53), a high boiling solvent such as NMP or DMF, a Pd catalyst such as $[\text{Pd}(\text{OAc})_2]$, and the respective vinyl functional group. The reactions were monitored using TLC and NMR experiments. In the case of $[\text{Pc}^*\text{Mg}]^{\text{Br}}$ and $[\text{Pc}^*\text{Cu}]^{\text{Br}}$, a demetallation was observed under the chosen conditions, and a mixture including $[\text{Pc}^*\text{Pd}]^{\text{R}}$ was observed.

The most promising results were obtained in the coupling reactions of vinylphosphonic and vinylcarboxylic acid esters at $[\text{Pc}^*\text{Zn}]^{\text{I}}$ (Scheme 53).



Scheme 53: Synthesis of $[\text{Pc}^*\text{Zn}]^{\text{vPA}}$.

In the synthesis of $[\text{Pc}^*\text{Zn}]^{\text{vPA}}$, after preparative TLC, the formed species were identified in UV-Vis measurements. Sharp Q-bands could be observed. In ^{31}P NMR spectroscopy, the expected broadened signals were observed, at 27.59 ppm. But in APCI-MS and MALDI-ToF experiments, the product could not be identified, which might be caused by the labile character of the phosphonic acid under chosen conditions.

Results and Discussion

In several attempts, separation by preparative CC was unsuccessful, regardless of the solvent used. Always a deep green powder was obtained, but no pure NMR spectrum was obtained. $[\text{Pc}^*\text{Zn}]^{\text{vCA}}$ was synthesised and it was attempted to isolate the pure A_3B Pc by CC. A typical MALDI-ToF spectrum is shown in Figure 94. In most cases, a mixture of the desired A_3B phthalocyanine and the A_4 system (or other isomers) was obtained.

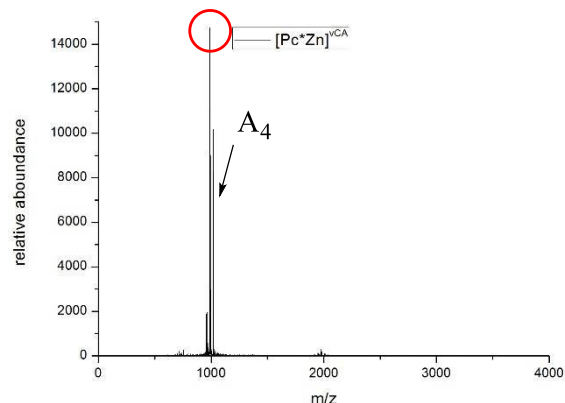


Figure 94: MALDI-ToF of $[\text{Pc}^*\text{Zn}]^{\text{vCA}}$. Attempt to separate a functionalised $[\text{Pc}^*\text{Zn}]^{\text{FG}}$.

In summary, protonated $\text{Pc}^*\text{H}_2^{\text{Br}, \text{I}}$ could not be converted via Pd catalysis to $\text{Pc}^*\text{H}_2^{\text{FG}}$ without $[\text{Pc}^*\text{Pd}]^{\text{FG}}$ complex formation under the chosen conditions. Because of an increased π -stacking and peak tailoring, functionalised metal $[\text{Pc}^*\text{M}]^{\text{FG}}$ could not be yielded in a sufficient amount and purity for full characterisation. Therefore, a different route was attempted using PDN^{OAcI} as precursor to yield $[\text{Pc}^*\text{M}]^{\text{OAcI}}$, described in the following section.

4.3.6 Synthesis of Soluble, Functionalised Phthalocyanines

Comparing the compounds described in the previous section 4.3.1 (Scheme 45), in UV-Vis spectroscopy, $[\text{PcZn}]^{\text{OH}}$ has shown the highest tendency to aggregate (as will be shown in section 4.3.8). With this, the excited electrons are quenched in between the phthalocyanines instead of being transferred to the semiconductor conduction band when applied in DSSCs. But because the catechol substituted phthalocyanine $[\text{PcZn}]^{\text{OH}}$ showed the highest tendency to be chemisorbed on a ZnO surface (described in the following section 4.3.8.2), the substituted analogues $[\text{Pc}^*\text{Zn}]^{\text{OH}}$, and $[\text{Ppz}^*\text{Zn}]^{\text{OH}}$ were chosen as target compounds. In addition, aggregation effects should decrease with the introduction of the sterically demanding alkyl groups. Furthermore, a functionalisation of $[\text{Pc}^*\text{Zn}]^{\text{OH}}$ to $[\text{Pc}^*\text{Zn}]^{\text{FG}}$ might be possible. The substituted Pcs, $\text{Pc}^*\text{H}_2^{\text{OAcI}}$,

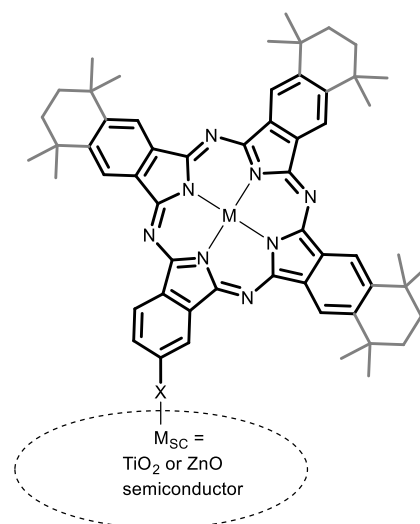
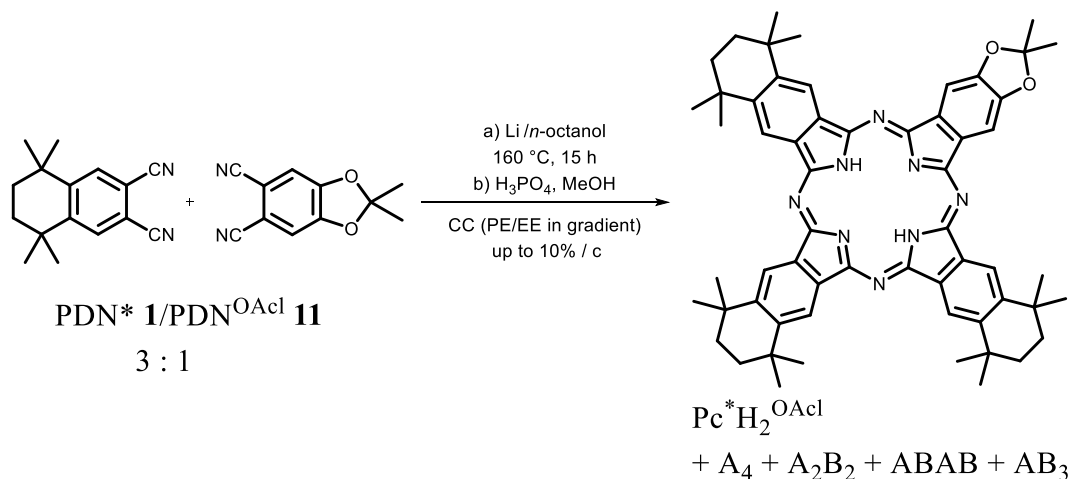


Figure 95: Equatorial bonded Pc on semiconductor surface.

were synthesised in a cocyclisation, because purification of [Spc*BCI] is tedious and only possible in low yields. Because of the described problems with the separation of the [PcZn] mixtures, caused by a higher tendency of π -stacking and accompanying peak tailoring in CC, at first the free ligands $\text{Pc}^*\text{H}_2^{\text{OAcI}}$, and $\text{PpZ}^*\text{H}_2^{\text{OAcI}}$ were synthesised. The $\text{Pc}^*\text{H}_2^{\text{OAcI}}$ was synthesised using the established Li/*n*-octanol method (Scheme 54).



Scheme 54: Synthesis of $\text{Pc}^*\text{H}_2^{\text{OAcI}}$.

Both dinitriles $\text{PDN}^* \mathbf{1} / \text{PDN}^{\text{OAcI}} \mathbf{11}$ were reacted in a 3:1 ratio, to finally obtain the A_3B phthalocyanine $\text{Pc}^*\text{H}_2^{\text{OAcI}}$ as main product with 10% yield after CC. Besides the A_3B product, $\text{Pc}^*\text{H}_2^{\text{OAcI}}$, the other isomers of the cyclotetramerisation were obtained. At first, Pc^*H_2 was eluted, followed by $\text{Pc}^*\text{H}_2^{\text{OAcI}}$, the A_2B_2 and ABAB as an isomeric mixture, and finally the AB_3 compound. Here, both compounds, A_2B_2 and ABAB , were observed. The isomers could not be separated from each other in one CC, but the aromatic signals can be differentiated in ^1H NMR spectroscopy. $\text{Pc}^*\text{H}_2^{\text{OAcI}}$ was characterised using ^1H and ^{13}C NMR spectroscopy, IR and UV-Vis spectroscopy, APCI-HRMS and elemental analysis.

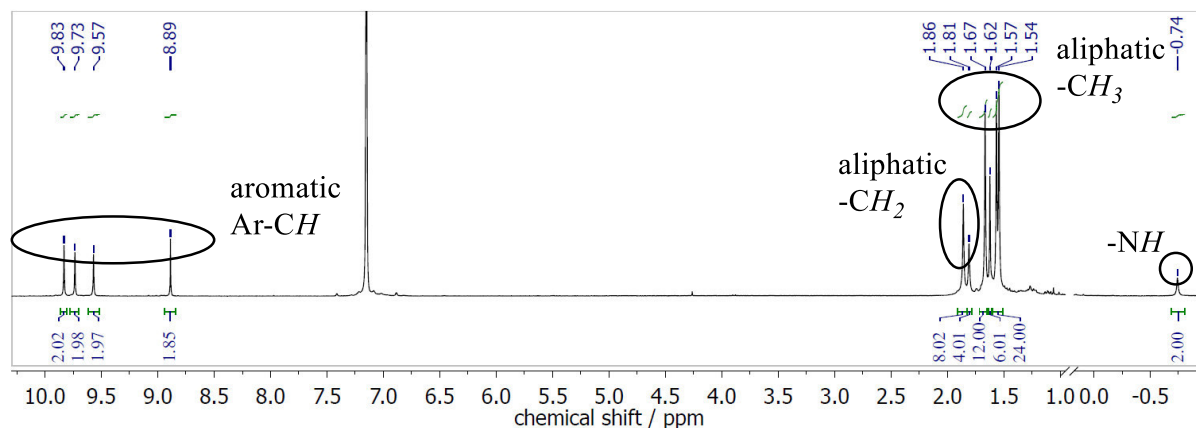
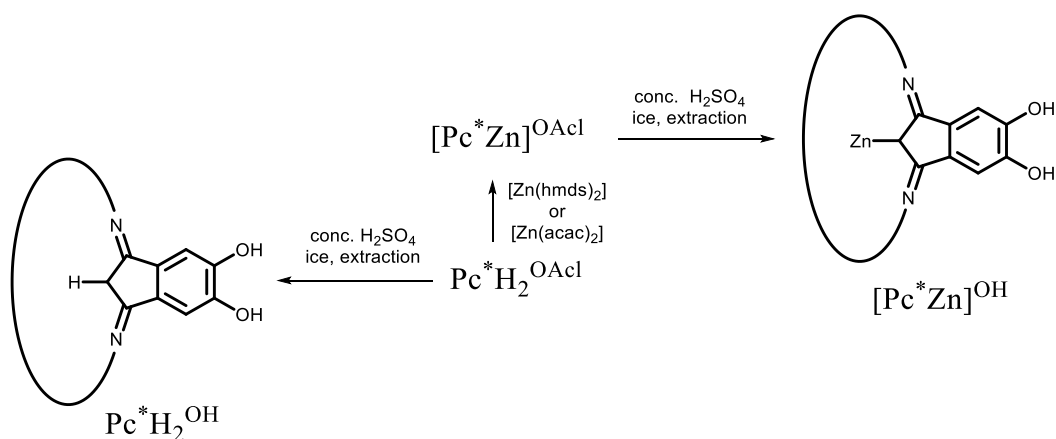


Figure 96: ^1H NMR spectrum of A_3B $\text{Pc}^*\text{H}_2^{\text{OAcI}}$, in C_6D_6 (300 MHz).

Results and Discussion

Cyclic voltammetry measurements of target compounds, $\text{Pc}^*\text{H}_2^{\text{OAc}}$ and $[\text{Pc}^*\text{Zn}]^{\text{OAc}}$, were carried out, as described below. Because of a lower symmetry of the molecule compared to Pc^*H_2 , the ^1H NMR spectrum shows four signals for the aromatic protons (Figure 96). The same is observed for the aliphatic protons. In UV-Vis spectroscopy, the Q-band of $\text{Pc}^*\text{H}_2^{\text{OAc}}$ is 4 nm hypsochromically shifted to $\lambda = 707$ nm, in comparison to Pc^*H_2 (711 nm). The AB_3 system has its main absorption at 694 nm. As expected, the influence on the Q-band caused by exchanging the peripheral substituents is weak, because of its distance to the centre of the phthalocyanine.

After obtaining $\text{Pc}^*\text{H}_2^{\text{OAc}}$, zinc was inserted, using $[\text{Zn}(\text{hmds})_2]$ or $[\text{Zn}(\text{acac})_2]$. The insertion was possible in good yields of >90%, using the metalating reagent in excess. The excess was finally removed by sonication in DEE and washing/filtering the compound. In the last step, the phthalocyanines $[\text{Pc}^*\text{M}]^{\text{OAc}}$ with $\text{M} = 2 \text{ H}$ or Zn were deprotected using conc. H_2SO_4 : Both Pcs were completely dissolved in the acid, while a change in colour to violet/brown was observed. After complete dissolution, the mixture was stirred for another 5 min and poured onto ice to regain a green powder. After workup, the corresponding hydroxy phthalocyanines $\text{Pc}^*\text{H}_2^{\text{OH}}$ and $[\text{Pc}^*\text{Zn}]^{\text{OH}}$ were obtained. The insertion of a metal atom as well as the deprotection to $[\text{Pc}^*\text{Zn}]^{\text{OH}}$ can be carried out in yields >90% over 2 steps (Scheme 55). Less harsh conditions were attempted using aq. TFA, or AcOH. The reaction solution was stirred for several days and the temperature was increased, but no reaction, just degradation, was observed by decolouration of the solution.

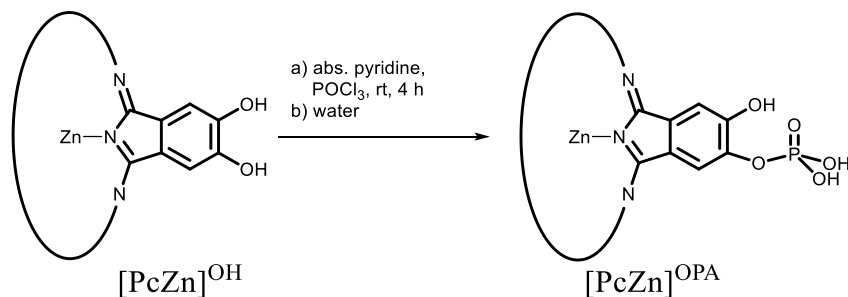


Scheme 55: Synthesis of final catechol functionalised Pcs $\text{Pc}^*\text{H}_2^{\text{OH}}$ and $[\text{Pc}^*\text{Zn}]^{\text{OH}}$.

In UV-Vis spectroscopy, the Q-band of $[\text{Pc}^*\text{Zn}]^{\text{OH}}$ appears blue-shifted (686 nm) compared to $\text{Pc}^*\text{H}_2^{\text{OH}}$ (707 nm), which is unshifted compared to its protected analogue $\text{Pc}^*\text{H}_2^{\text{OAc}}$ (707 nm).

The synthesis of $\text{Ppz}^*\text{H}_2^{\text{OH}}$ and $[\text{Ppz}^*\text{Zn}]^{\text{OH}}$ was carried out in a similar way (Scheme 54 and Scheme 55). The separation of the $\text{Ppz}^*\text{H}_2^{\text{OAc}}$ appeared to be more difficult, but still yields of 8% were obtained. Here, only the A_2B_2 aza-Pc^{OH} derivative (no ABAB) and traces of AB_3 were observed after column chromatography. In UV-Vis spectroscopy, after deprotection of $[\text{Ppz}^*\text{Zn}]^{\text{OAc}}$ to $[\text{Ppz}^*\text{Zn}]^{\text{OH}}$, a Q-band blue-shift of 14 nm was observed, while the Pc* analogues ($[\text{Pc}^*\text{M}]^{\text{OAc}}$ to $[\text{Pc}^*\text{M}]^{\text{OH}}$) are only shifted 1 nm. The Q-band of $\text{Ppz}^*\text{H}_2^{\text{OAc}}$ at 674 nm is hypsochromically shifted after insertion of Zn to 654 nm, and to 640 nm for $[\text{Ppz}^*\text{Zn}]^{\text{OH}}$, respectively. Again, a weaker shift of the Q-band by metalation of the electron poor free PpzH_2 ligand was observed, compared to a metalation of PcH_2 . $\text{Ppz}^*\text{H}_2^{\text{OH}}$ could not be completely characterised, because mainly degradation was observed, visible by decolouration of the solution. After pouring the dissolved $\text{Ppz}^*\text{H}_2^{\text{OAc}}$ onto water, only traces of $\text{Ppz}^*\text{H}_2^{\text{OH}}$ were observed. Anyway, a mass spectrum, as well as ¹H NMR and UV-Vis spectra were accomplished. In future, this catechol ligand might be synthesised from the demetalation of a less stable $[\text{Ppz}^*\text{Pb}]^{\text{OAc}}$ precursor, or from a less harsh deprotection of $\text{Ppz}^*\text{H}_2^{\text{OPhrBu}}$ as was already successfully tested in this work.

Using the catechol derivatives as precursor, another functional moiety, not yet described in literature, was observed.



Scheme 56: Synthesis of a new structural motif for binding Pcs on semiconductor surfaces.

Therefore, $[\text{PcZn}]^{\text{OH}}$ and $\text{Pc}^*\text{H}_2^{\text{OH}}$, respectively, was dissolved in pyridine, POCl_3 was added and stirred at rt. To the reaction, water was added to yield a phosphate anchor in the peripheral position of the Pc (Scheme 56). Both compounds, $[\text{PcZn}]^{\text{OPA}}$ and $\text{Pc}^*\text{H}_2^{\text{OPA}}$ were identified by using MS and UV-Vis spectroscopy. The advantage of this kind of functional group is the number of ZnO bonds potentially being formed to the ZnO semiconductor.

4.3.7 CV and UV-Vis Analysis of $[\text{Pc}^*\text{M}]^{\text{OH}}$ and $[\text{Ppz}^*\text{M}]^{\text{OH}}$

For application in DSSCs, the HOMO and LUMO levels, and the efficiency of the compounds when used in DSSCs should be determined. Therefore, the examples $[\text{Pc}^*\text{M}]^{\text{OH}}$ and $[\text{Ppz}^*\text{M}]^{\text{OH}}$ were chosen as representatives. For interest, $\text{Pc}^*\text{H}_2^{\text{OH}}$ was tested as well, to give comparable values as observed in the $\text{N}_x\text{-Pc}^*\text{H}_2$ series and for their investigation of electron transfer processes and photoluminescence. In addition, the free ligands show better solubility, compared to their zinc analogues, but have comparable HOMO-LUMO levels as visible in the electronic absorption spectra (compare to section 4.2.4.6).

In contrast to the $\text{N}_x\text{-Pc}^*\text{H}_2$ series, $\text{Pc}^*\text{H}_2^{\text{OH}}$ was measured in THF because of solubility reasons. The measurements were carried out under an inert atmosphere. For the measurements, a 100 mM stock solution of THF with $[\text{TBA}]\text{PF}_6$ was prepared. Out of the solution, a 0.1 mM solution of Fc in the respective solvent was prepared as standard. For measurements, a glassy carbon working electrode ($d = 3 \text{ mm}$) was used. Additionally, a Pt electrode or a silver-silver sulfide was used as pseudo reference, and a Pt electrode as counter electrode. For some first examples, different scan rates were tested. Before the measurement of the sample, the electrochemical window of the solvent was determined. In Figure 97, an uncalibrated CV spectrum of $\text{Pc}^*\text{H}_2^{\text{OH}}$ before Fc addition is shown. As useful scan rate, 10 mV/s was chosen, because, despite the low solubility of $\text{Pc}^*\text{H}_2^{\text{OH}}$, the best peak resolution was observed at this scan rate.

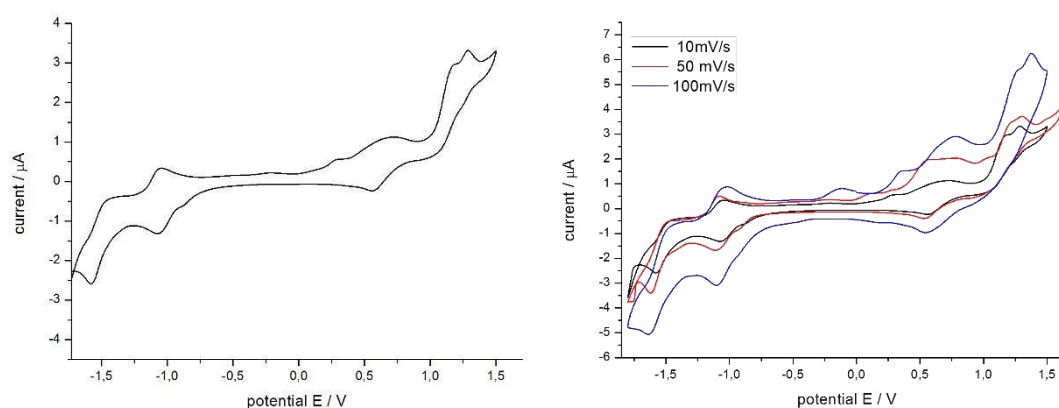


Figure 97: Cyclic voltammetric measurement of $\text{Pc}^*\text{H}_2^{\text{OH}}$ in 10 mM $[\text{TBA}]\text{PF}_6$ in THF solution. Left hand: first measurement with a scan rate of 10 mV/s. Right hand: Different scan rates of 10 mV/s, 50 mV/s and 100 mV/s.

Furthermore, the scan rate of 10 mV/s could be applied for spectroelectronic measurements. After the measurements, the spectra were calibrated with ferrocene/ferrocenyl as reference (Figure 98). Therefore, to each measurement 0.1 mL of the Fc stock solution was added after the measurement of the potential-current curve.

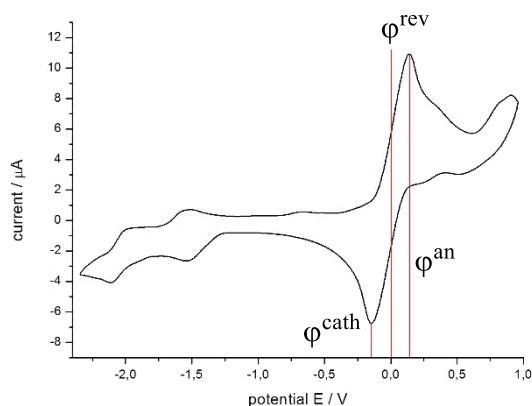


Figure 98: CV measurement calibrated vs added ferrocene/ferrocenyl.

If appropriate, differential pulse voltammograms (DPV) were measured, in some cases, these were additionally monitored by using square wave voltammetry. In DPV experiments, the

oxidation and reduction potentials could be determined more easily (Figure 99). In summary, for $\text{Pc}^*\text{H}_2^{\text{OH}}$ comparable potentials to Pc^*H_2 could be observed, which is also in accord with the weakly shifted Q-band from 711 to 707 nm, respectively. The increased potential difference, E_g^{CV} , of $\text{Pc}^*\text{H}_2^{\text{OH}}$ (1.68 V) in comparison to Pc^*H_2 (1.58 V) might be caused by the different solvent (THF and DCM): For Pc^*H_2 , a potential difference, E_g^{CV} , between the first oxidation and the first reduction peak of 1.65 V was observed in THF.

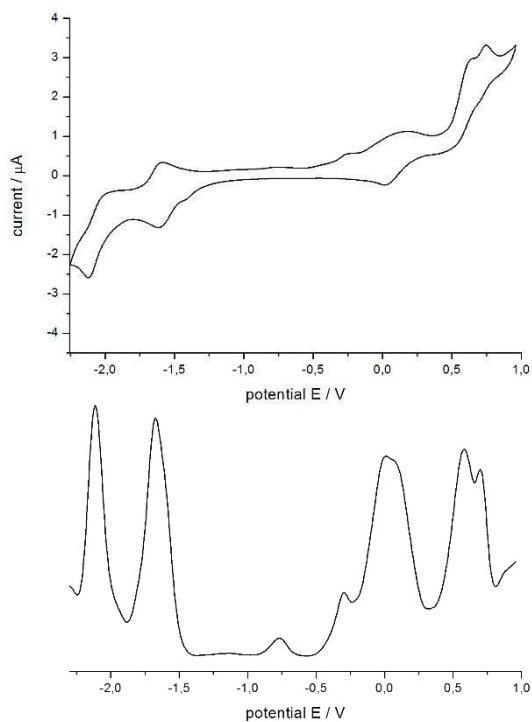


Figure 99: Calibrated CV and DPV of $\text{Pc}^*\text{H}_2^{\text{OH}}$ in comparison. Spectrum calibrated vs ferrocene/ferrocenyl.

Results and Discussion

The HOMO and LUMO energy levels can be calculated by the following equations: ^[191]

$$E_{HOMO} = -[(E_{ox} - E_{1/2(Fc)} + 4.8)]$$

$$E_{LUMO} = -[(E_{red} - E_{1/2(Fc)} + 4.8)]$$

A more detailed discussion about possible electron processes is given in the introduction (section 2.2). Photophysical and electrochemical properties of an azaphthalocyanine series were also investigated in literature. ^[87]

In Figure 100, measured UV-Vis spectra of $Pc^*H_2^{OH}$ and $[Pc^*Zn]^{OH}$ are shown in comparison and obtained data in UV-Vis spectroscopy and CV are summarized below (Table 16). Here, the Q-band of the $[Pc^*Zn]^{OH}$ is also not split, caused by the annulment of the degeneracy when a central metal atom is inserted. Similar effects should be visible by choosing different solvents, such as pyridine. ^[27] The values obtained by CV for $[Pc^*Zn]^{OH}$ have to be tentatively assessed, because of the low solubility of the substance in THF. Here, pyridine could be used as an alternative solvent for following measurements.

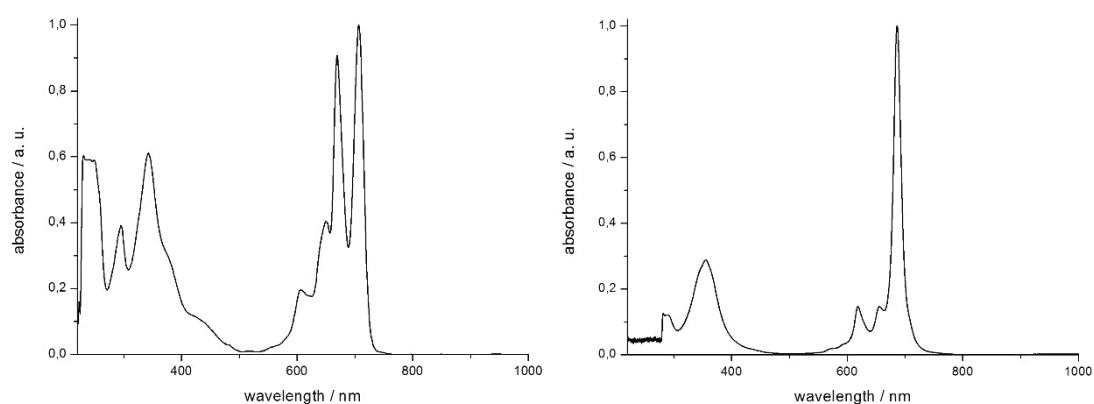


Figure 100: UV-Vis spectra of $Pc^*H_2^{OH}$ (left) and $[Pc^*Zn]^{OH}$ (right) in comparison, in DCM at rt.

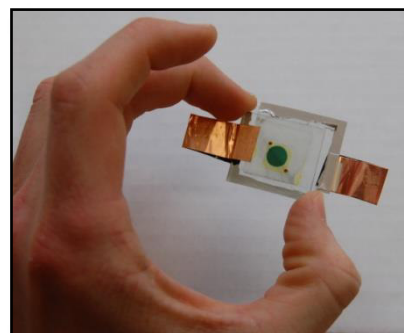
Table 16: Electrochemical data of $Pc^*H_2^{OH}$ and $[Pc^*Zn]^{OH}$, measured in THF and calibrated vs Fc. UV-Vis measurements were carried out in DCM at rt.

	$[Pc^*Zn]^{(OH)}$	$Pc^*H_2^{OH}$
E_{ox}^1 / V	-0.64	0.00
E_{red}^1 / V	-2.62	-1.68
E_{red}^2 / V	-3.02	-2.11
E_g^{CV} / V	1.98	1.68
λ_{max} / nm	686	707
(Q-band)		

4.3.8 Application in DSSCs

4.3.8.1 Investigations of ZnO-based DSSCs

To use Pcs as PSs in dye sensitized solar cells (DSSCs), firstly, their bonding onto the respective surfaces has to be investigated. Within the SFB1083, the compounds should not only be tested with respect to their efficiency. If any efficiency was observed, a charge-transfer process is proved, which makes the compounds useful for further studies of photoluminescence measurements (PL). For the



construction of DSSCs, two semiconductor substrates are quite well established: one is ZnO and the other that is most commonly used as a semiconductor for DSSCs is TiO₂.^[223] Both surfaces have comparable wide band gaps, while the FERMI level should lay in the area of 1.5 eV below the LUMO of the chromophore. Band gaps of both semiconductor surfaces are literature known: TiO₂ (Anatas): 3.2 eV,^[90] TiO₂ (Rutile): 3.0 eV,^[90] and for ZnO: 3.37 eV.^[224] The main advantage of ZnO in comparison to TiO₂ is the electromobility of the material, given by the Wurzit structure of the semiconductor.^[225] Both materials are quite stable towards various environmental conditions, such as solvents and pH, whereby the pH of ZnO should not be >10.5, which leads to a disruption of the lattice structure of the material.

According to the discussed excitation processes of a dye, the JABLONSKI diagram can display possible paths of relaxation (see section 2.2.2). In contrast to the previously discussed inter system crossing (ISC) of an electron, an injection into the conduction band is desired. MORANDEIRA *et al.* described possible loss paths as shown below (Figure 101, right), which have to be avoided if possible.^[206]

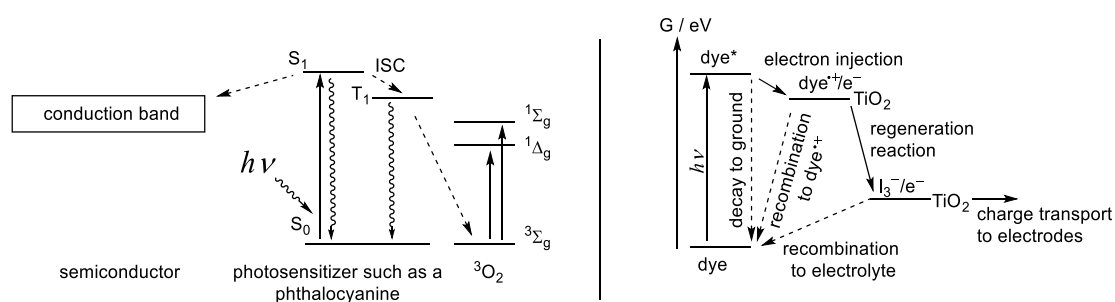


Figure 101: Literature described, possible electron transfer processes of an excited PS (left),^[25] and beneficial paths (straight arrow) and loss paths (dotted arrow, right).^[206]

Results and Discussion

MORANDEIRA categorised into beneficial and loss paths to understand and optimise DSSCs: beneficial paths are electron injection from an excited dye into the CB of a semiconductor, electron migration to the external circuit and a successful dye regeneration by the electrolyte. Loss paths are excited state decays, such as radiationless decay, electron recombination with the dye cation or the used electrolyte.^[206]

We can conclude that radiationless decay processes, as they were observed in photophysical measurements (section 4.2.5) of the metal free azaphthalocyanine series, $N_x\text{-Pc}^*\text{H}_2$, do not favour the transfer of an electron to the conduction band. This makes metal-free ligands, such as PcH_2^{FG} , unusable for application as PS in DSSCs.

4.3.8.2 DSSCs using Unsubstituted Phthalocyanine Dyes

In cooperation with FALGENHAUER and TINZ (SCHLETTWEIN group at the Department of Physics of the Justus-Liebig-Universität Gießen) in a first attempt, the dyes shown in Figure 102 were bonded onto ZnO surfaces.

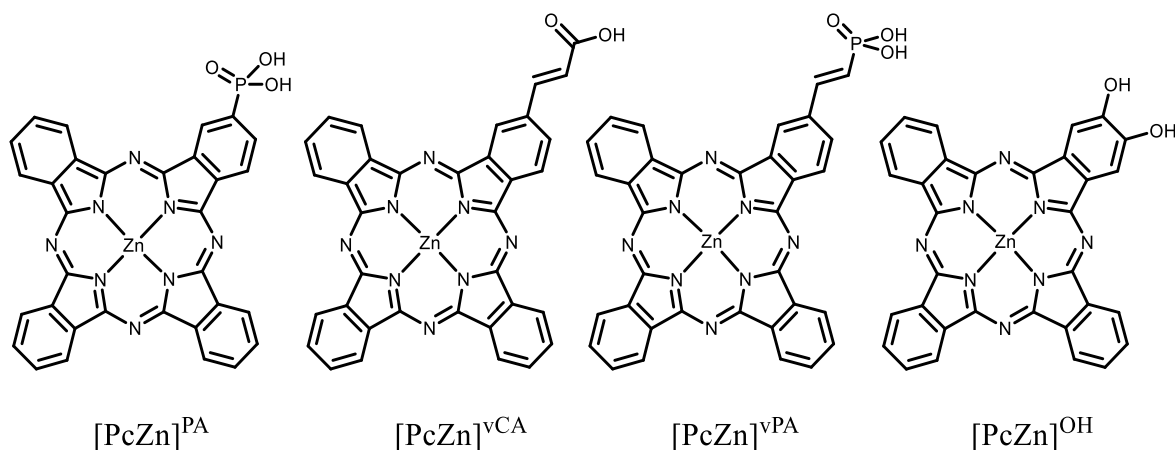


Figure 102: Functionalised [PcZn]^{FG} investigated with regard to their bonding to ZnO.

The ZnO surface, provided by FALGENHAUER and TINZ, was prepared according to a method, first developed by YOSHIDA *et al.*,^[226] whereby the ZnO is electrochemically precipitated on fluorine doped tin oxide (FTO). The intact surface was determined with methods such as AFM and laser microscopy. A laser microscope picture of mesoporous ZnO is shown in Figure 103. To bind the shown phthalocyanines on the surface, at first, different solvents were tested, the time was varied and different anchors of the non-alkyl substituted Pc were compared. The absorption of the Pc was controlled with an ULBRICHT Kugel. In first attempts, Pcs were bonded from a DMF solution, because of solubility reasons. In all cases, an absorption of the dye onto the surface was observed, after leaving the ZnO target for 24 h in the 1-2 mmolar DMF solution with the respective dye. A change in colour of the ZnO was visible, turning from almost transparent into a deep blue/green colour. In UV-Vis measurements a strong aggregation could be observed, which was clearly visible by the broadening of the absorption maxima, especially for non-alkyl annulated phthalocyanines.

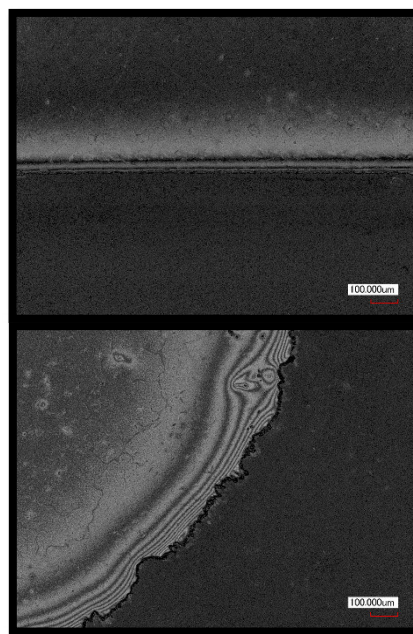
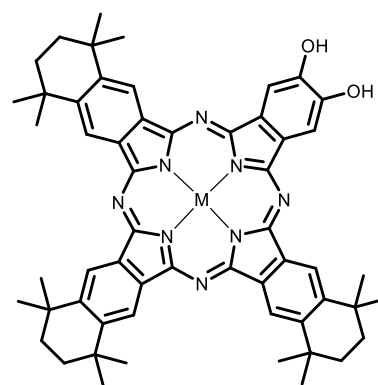


Figure 103: Mesoporous ZnO on FTO in lasermicroscope.

Results and Discussion

In addition to non-alkyl substituted phthalocyanine dyes, alkyl substituted phthalocyanines were tested (Figure 104). Therefore, the catechol derivatives were chosen for the absorption tests, because of their observed strong bonding to the ZnO surface. $\text{Pc}^*\text{H}_2^{\text{OH}}$, $[\text{Pc}^*\text{Zn}]^{\text{OH}}$ and $[\text{Ppz}^*\text{Zn}]^{\text{OH}}$ were compared applying three different solvents: DMF, because of the high solubility of all compounds in it, toluene and MeCN. Toluene was chosen because it may lower π -stacking of the phthalocyanines and MeCN is an established solvent for these dyes and it is also used for dissolving I_2/I_3^- as redox mediator.

With all solvents, 10 mL of a 1 mmolar dye-solution was prepared. In the case of the MeCN solution, an incomplete suspension was obtained, even after sonication for several minutes. The ZnO targets were added to the solution overnight, but a colouration of the ZnO surface was



with $\text{M} = 2\text{H}$, or Zn

Figure 104: Catechol like Pc.

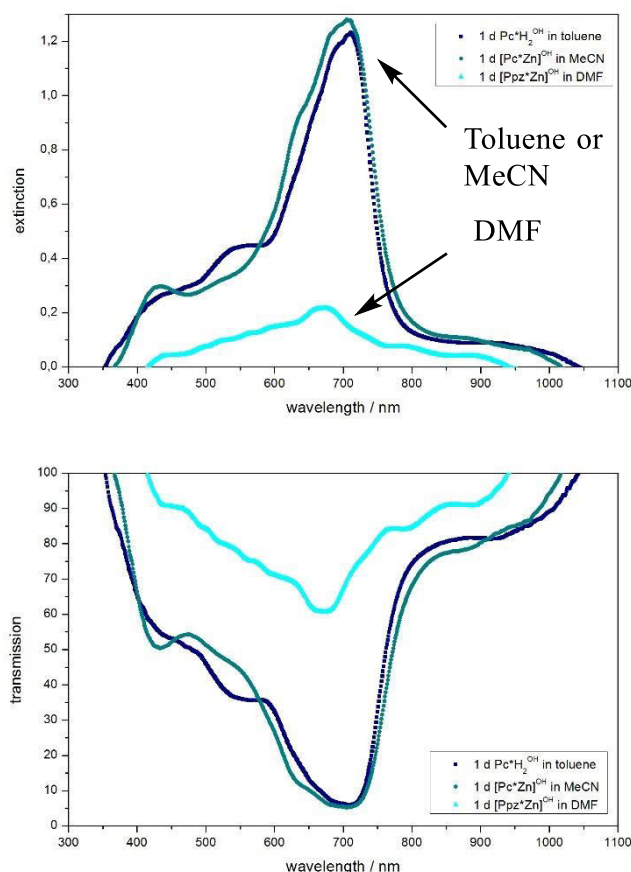
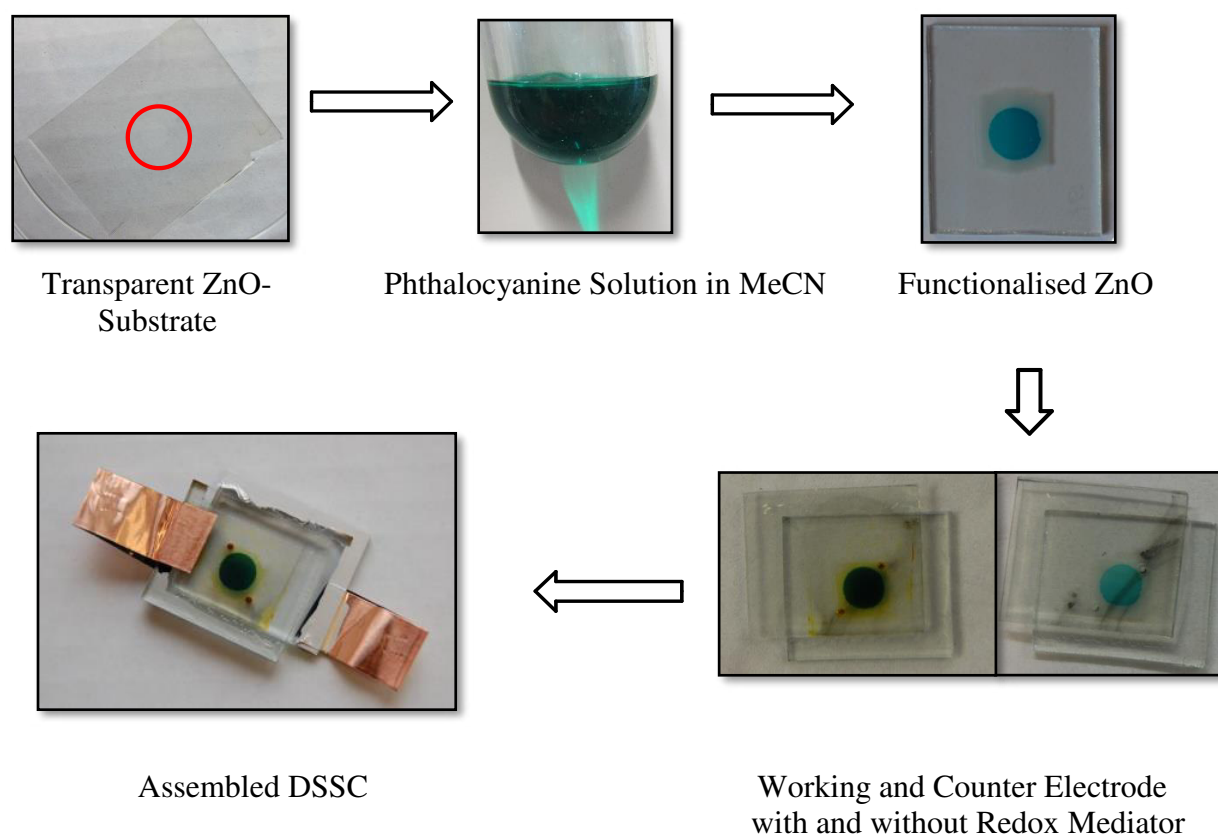


Figure 105: Transmission and extinction spectra of $\text{Pc}^*\text{H}_2^{\text{OH}}$, $[\text{Pc}^*\text{Zn}]^{\text{OH}}$ and $[\text{Ppz}^*\text{Zn}]^{\text{OH}}$ in comparison. Measured in solid state. For absorption, coated glass was added for 24 h at rt in a solution of the Pc using different solvents. Measurements were carried out using an ULBRICHT Kugel in cooperation with the Physics Department of the Justus-Liebig Universität Gießen.

already visible after only a few minutes. The formation of the layer was controlled with the above mentioned ULBRICHT Kugel. The UV-Vis absorptions and transmissions are shown in Figure 105.

In both spectra it is visible that the best results could be obtained from MeCN solutions or toluene solutions. In DMF, only a low dye density on the surface was observed. For the DSSCs, MeCN was chosen as solvent because of its mentioned use in the electrolyte solution. It appears to be the best compromise between “solubility and insolubility”, so the dye has a higher tendency to be absorbed from the solution onto the ZnO semiconductor. While the absorption spectra of $\text{Pc}^*\text{H}_2^{\text{OH}}$ and $[\text{Pc}^*\text{Zn}]^{\text{OH}}$ look quite similar, it was observed that $\text{Pc}^*\text{H}_2^{\text{OH}}$ on ZnO is light green, compared to the dark green $[\text{Pc}^*\text{Zn}]^{\text{OH}}$.

With all useful targets, closed DSSCs were constructed. Therefore, the substrates were fixed together with another FTO layer. On this layer, the counter electrode, Pt, was deposited. In the layer, two holes were added, which were used for filling the the cell with the electrolyte solution. After addition of the electrolyte (see yellow solution in Scheme 57, (bottom, right hand side), containing MeCN with 0.05 N Imidazole and 0.5 N I₂), the holes were sealed with a soldering iron, so no electrolyte solution could evaporate while measuring the cells. The completely constructed cell was connected with two copper wires, used to facilitate the electron flow. A silver paste was added on the top of the cell to prevent a short circuit. The finished solar cell and the steps of construction are summarised in Scheme 57.



Scheme 57: Steps of construction of a DSSC in summary.

The measurements were carried out by illumination of the DSSC with a Xenon-*Bogenlampe* (light intensity $P_{\text{int}} = 100 \text{ mW/cm}^2$). In all cases, a current-voltage characteristic (I-U curve) was obtained, and the significant values, I_{SC} and U_{OC} , were determined. The measurements were analysed according to theoretical section 2.2.2. In the case of $[\text{PcZn}]^{\text{OH}}$, a high aggregation was already detected in the electronic absorption spectra. This is also visible in the low

Results and Discussion

efficiency of the constructed cell. In the case of $[\text{PcZn}]^{\text{PA}}$, a short-circuit was observed, but all necessary values could be determined. The obtained values were calculated and give reasonable and comparable values. A high dependence of the absorption of the dye on the ZnO semiconductor was observed, so first correct solvent and conditions for the deposition have to be chosen. All obtained values are listed in Table 17, examples of the I-U curves are shown in Figure 106.

Table 17: Determined efficiency for non-alkyl substituted $[\text{PcZn}]^{\text{FG}}$.

Film	Area / cm^2	I_{sc} / mA/cm^2	V_{oc} / V	FF	Efficiency / %
$[\text{PcZn}]^{\text{vPA}}$	0.445641	1.7417	0.49	0.65	0.55
$[\text{PcZn}]^{\text{PA}}$	0.450473	1.2882	0.45	0.73	0.42
$[\text{PcZn}]^{\text{vCA}}$	0.445246	0.6432	0.37	0.67	0.16
$[\text{PcZn}]^{\text{OH}}$	0.406794	0.0328	0.10	0.31	0.001056

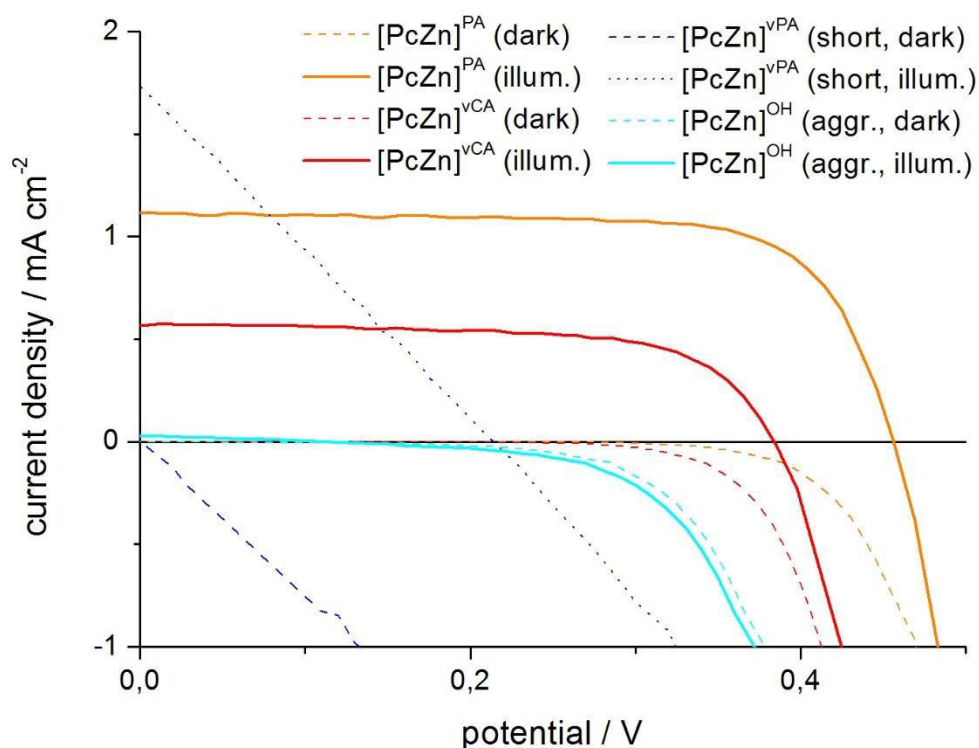


Figure 106: Current-voltage characteristic (I-U curve) of different $[\text{PcZn}]^{\text{FG}}$. $[\text{PcZn}]^{\text{vPA}}$ shows a short circuit, $[\text{PcZn}]^{\text{OH}}$ showed a strong aggregation in UV-Vis absorption.

The achieved efficiencies are low (Table 17), but for non-alkyl substituted Pcs and their high tendency to aggregate, the data are quite remarkable. The trend observed by varying the anchor moiety is nicely visible: the most promising anchor moiety appears to be the phosphonic acid of $[\text{PcZn}]^{\text{vPA}}$ ($\eta = 0.5\%$), followed by the carboxylic acid $[\text{PcZn}]^{\text{vCA}}$ ($\eta = <0.2\%$) and the catechol $[\text{PcZn}]^{\text{OH}}$ ($\eta \sim 0.001\%$), when correct solvent and conditions for the deposition are

chosen. In addition to the I-U curves, incident photon-to-electron conversion efficiencies (IPCEs) were determined. Because the wavelength is not proportional to the current, a correlation between the wavelength and the current can be associated with the illumination of the DSSC. In all constructed DSSCs, an increase of the current was observed in the absorption regions of the PSs. An IPCE measurement of $[\text{PcZn}]^{\text{vPA}}$ is shown in Figure 107. It is clear that the relative IPCE increases with the intensity of illumination and the absorbed wavelength of the dye.

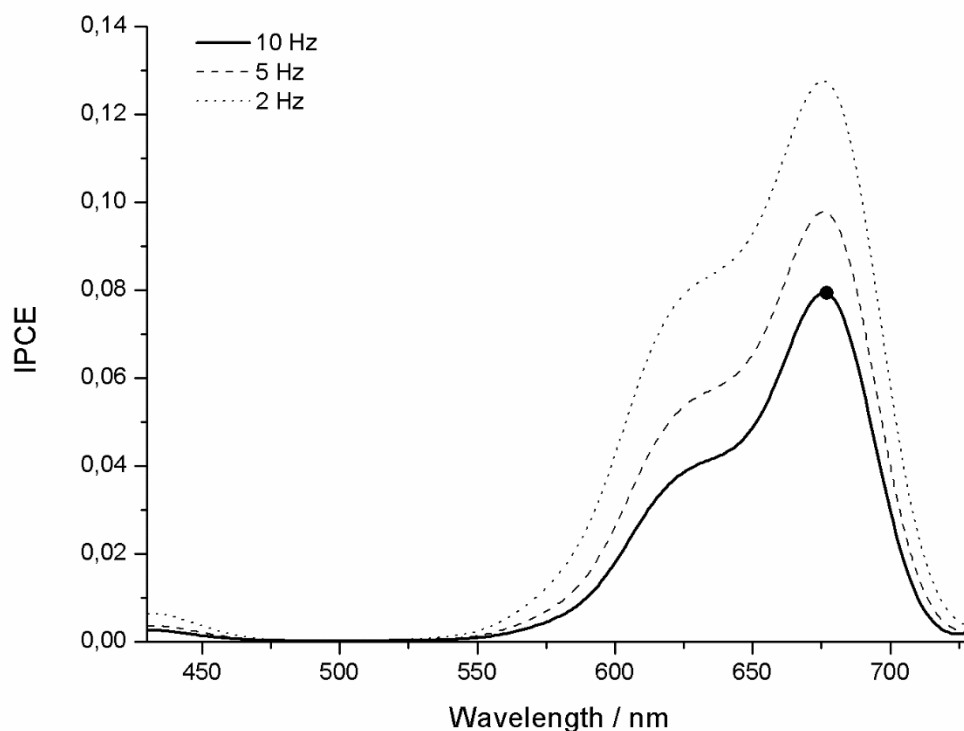


Figure 107: Incident photon-to-electron conversion efficiency (ICPE) curves of $[\text{PcZn}]^{\text{vPA}}$.

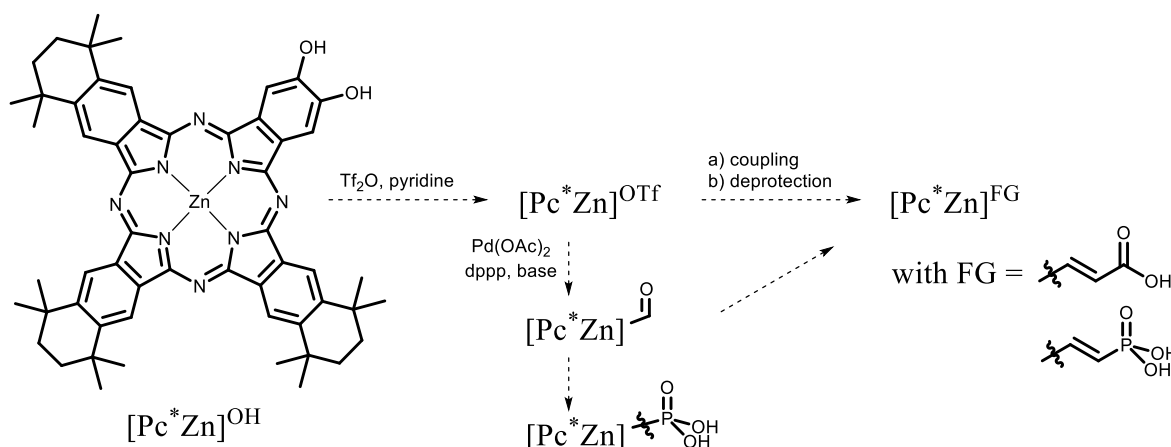
In order to get higher efficiencies in DSSCs, in a next step, the better soluble and lower aggregating alkyl substituted phthalocyanine derivatives $\text{Pc}^*\text{H}_2^{\text{OH}}$ and $[\text{Pc}^*\text{Zn}]^{\text{OH}}$ were compared. While the catechol anchor of $[\text{PcZn}]^{\text{OH}}$ does not seem to be good for electron transfer onto the semiconductor, the differences between the metal-free $\text{Pc}^*\text{H}_2^{\text{OH}}$ and $[\text{Pc}^*\text{Zn}]^{\text{OH}}$ are present in I-U curves. Comparing $[\text{PcZn}]^{\text{OH}}$ and $[\text{Pc}^*\text{Zn}]^{\text{OH}}$, a great increase in electron transfer efficiency with the alkyl substitution is visible. This proves that alkyl groups increase the electron donation and decrease the aggregation effects. The efficiency could be increased by a factor of 10 with annulation of alkyl groups. In addition, PL measurements might be used to confirm the charge-transfer process and are in progress, being carried out by MEYENBURG (HEIMBRODT group at the Department of Physics of the Philipps-Universität Marburg).

Results and Discussion

The bonding of soluble phthalocyanines onto TiO_2 surfaces was tested as well, in cooperation with WALLAUER (ROLING group of the Department of Chemistry at the Philipps-Universität Marburg). In a first attempt, phthalocyanines were absorbed from a 2 mmolar THF solution. Here, a fast degradation and an incomplete bonding of the phthalocyanine was observed in the form of a decolouration of the TiO_2 surface. In a second attempt, MeCN, toluene and DCM were tested. Despite the fact that the phthalocyanines were not completely dissolved in MeCN, it shows the best absorption, but decolouration also occurred within a couple of hours. The efficiencies of $[\text{Pc}^*\text{Zn}]^{\text{OH}}$ were quite low (<0.01) and were not further investigated.

Summary and Outlook. In this section, a series of non-alkyl substituted A_3B phthalocyanines, $[\text{PcZn}]^{\text{FG}}$ with FG = vinylphosphonic acid, phosphonic acid, carboxylic acid and catechol, was applied in DSSCs and compared to more soluble, less aggregating alkyl substituted phthalocyanines, $[\text{Pc}^*\text{M}]^{\text{OH}}$ with $\text{M} = 2 \text{ H or Zn}$. The most efficient dye in ZnO based DSSCs appears to be the vinylphosphonic acid $[\text{PcZn}]^{\text{vPA}}$ ($\eta = 0.5\%$), followed by vinylcarboxylic acid $[\text{PcZn}]^{\text{vCA}}$ ($\eta = <0.2\%$) and the catechol $[\text{PcZn}]^{\text{OH}}$ ($\eta \sim 0.001\%$). In comparison to $[\text{PcZn}]^{\text{OH}}$, $[\text{Pc}^*\text{M}]^{\text{OH}}$ with $\text{M} = 2 \text{ H or Zn}$ ($\eta > 0.01\%$) shows a better efficiency by a factor of 10. This proves the electron donating character (+I-effect) of the alkyl moieties as well as their effect in minimizing aggregation. In good correlation to the $\text{N}_x\text{-}[\text{Pc}^*\text{M}]$ series, a more efficient electron transfer was found for the metalated compound $[\text{Pc}^*\text{Zn}]^{\text{OH}}$ in comparison to $\text{Pc}^*\text{H}_2^{\text{OH}}$.

Taking the structural-property correlation obtained from the $[\text{PcZn}]^{\text{FG}}$ series and $[\text{Pc}^*\text{M}]^{\text{OH}}$ into consideration now, in future, soluble Pc^* derivatives should be further investigated.



Scheme 58: Synthetic options to further functionalise the synthesised A_3B $[\text{Pc}^*\text{Zn}]^{\text{OH}}$.

Despite the quite poor efficiency of the diol $[\text{Pc}^*\text{Zn}]^{\text{OH}}$, in following work the easily accessible A_3B $[\text{Pc}^*\text{Zn}]^{\text{OH}}$ can be further converted to a $[\text{Pc}^*\text{Zn}]^{\text{OTf}}$. The bistriflate might be converted to

an aldehyde functionality by using a palladium catalysed reductive carbonylation conditions (Scheme 58).^[227] The aldehyde serves as starting material for a phosphinic acid,^[228] or vinyl functionalised phthalocyanine $[\text{Pc}^*\text{Zn}]^{\text{FG}}$ with $\text{FG} = \text{vCA}$ or vPA . Furthermore, HECK and SONOGASHIRA coupling chemistry might be accomplished via the triflates.

In this section, different A_3B -type functionalised Pcs $[\text{Pc}^{(*)}\text{Zn}]^{\text{FG}}$ were compared in DSSCs. A synthesis plan for A_3B -type $[\text{Pc}^*\text{Zn}]^{\text{FG}}$ was successfully developed (Scheme 58) and first insight into structure-property relationships will allow for further tuning and optimising of these chromophores with regard to their efficiency for charge separation at the organic/inorganic interface.

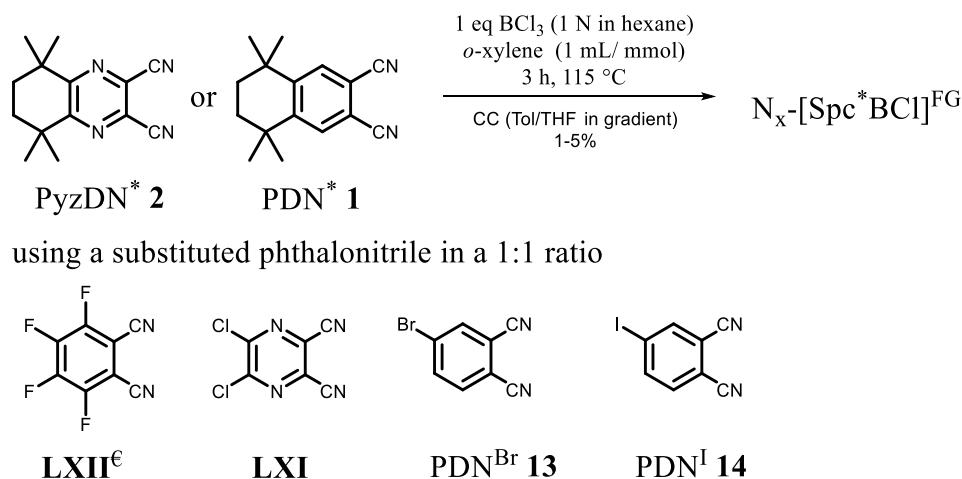
4.3.9 Synthesis of Functionalised Subphthalocyanines

This section reports on attempts to find a more straightforward synthetic strategy to vinylphosphonic acid substituted phthalocyanines and offers a strategy to even lower symmetry A_2BC -type phthalocyanines. The first selective access to an ABAC -type phthalocyanine was described by DUMOULIN *et al.*^[33] With the knowledge obtained in the previous section 4.2.4.2, a selective ring expansion of an A_2B -type subphthalocyanine precursor seems to be possible.

Furthermore, fluorinated subphthalocyanines by itself can easily be functionalised with axial anchors, such as $[\text{Spc}^{\text{F}}\text{BOArCO}_2\text{H}]$, and were studied as PSs in DSSCs.^[229] In addition, in the peripheral position, substituted halogen subphthalocyanines $[\text{SpcBCl}]^{\text{FG}}$ are remarkable compounds with described applications in organic photovoltaics (OPVs).^[230] In recent literature, the interface energy gap was studied and compared for $\text{FG} = \text{F}, \text{Cl}, \text{H}$.^[230] Because structural investigations of subpyrazinoporphyrazines are almost completely unknown,^[13,25] here, a new series of azasubphthalocyanines $\text{N}_x\text{-}[\text{Spc}^*\text{BCl}]^{\text{FG}}$ is reported, of which HOMO-LUMO levels can be aligned for their application in OPVs. Therefore, the synthesis of $[\text{Spc}^*\text{BCl}]^{\text{Cl}}$ and other functionalised azasubphthalocyanines ($\text{N}_x\text{-}[\text{Spc}^*\text{BCl}]^{\text{FG}}$) was carried out in a cyclotrimerisation reaction, as described in section 4.2.4.1.

Results and Discussion

In Scheme 59, the schematic synthesis to N_x -[Spc*BCI]^{FG} is shown. The complete series of isolated compounds is displayed in Figure 108. The bromine and chlorine substituted subphthalocyanines, N_x -[Spc*BCI]^{Br} and N_x -[Spc*BCI]^{Cl}, have been described before.^[13]



Scheme 59: Synthesis of substituted boron-(III)-subpyrazines (N_x -[Spc*BCI]^{FG}).

All A₂B and AB₂ products were obtained using two dinitriles A/B in a 1:1 ratio in a cyclotrimerisation reaction. As described in literature, depending on the position of the functional group, the ratio is statistical or can depend on the reactivity of the dinitriles.^[231,232] Because the electronic character of the here used dinitriles is quite similar, A₂B N₂-[Spc*BCI]^{FG} and AB₂ N₄-[Spc*BCI]^{FG} were obtained as main products in an almost 1:1 ratio. In all cases, the AB₂ N₄-[Spc*BCI]^{FG} system could be separated from A₂B N₂-[Spc*BCI]^{FG}, but no further separation of isomers of lower symmetrical AB₂ N₄-[Spc*BCI]^{FG} with FG = Br, I was carried out. A separation of C₃ and C₁ isomers of [Spc^{tBu}BCI] was described in previous work by HANACK.^[231] The advantage of these aza-Spcs is not only their stability: they are stable over months when stored in air at rt and even in solution, but also yields are high, up to 24%.

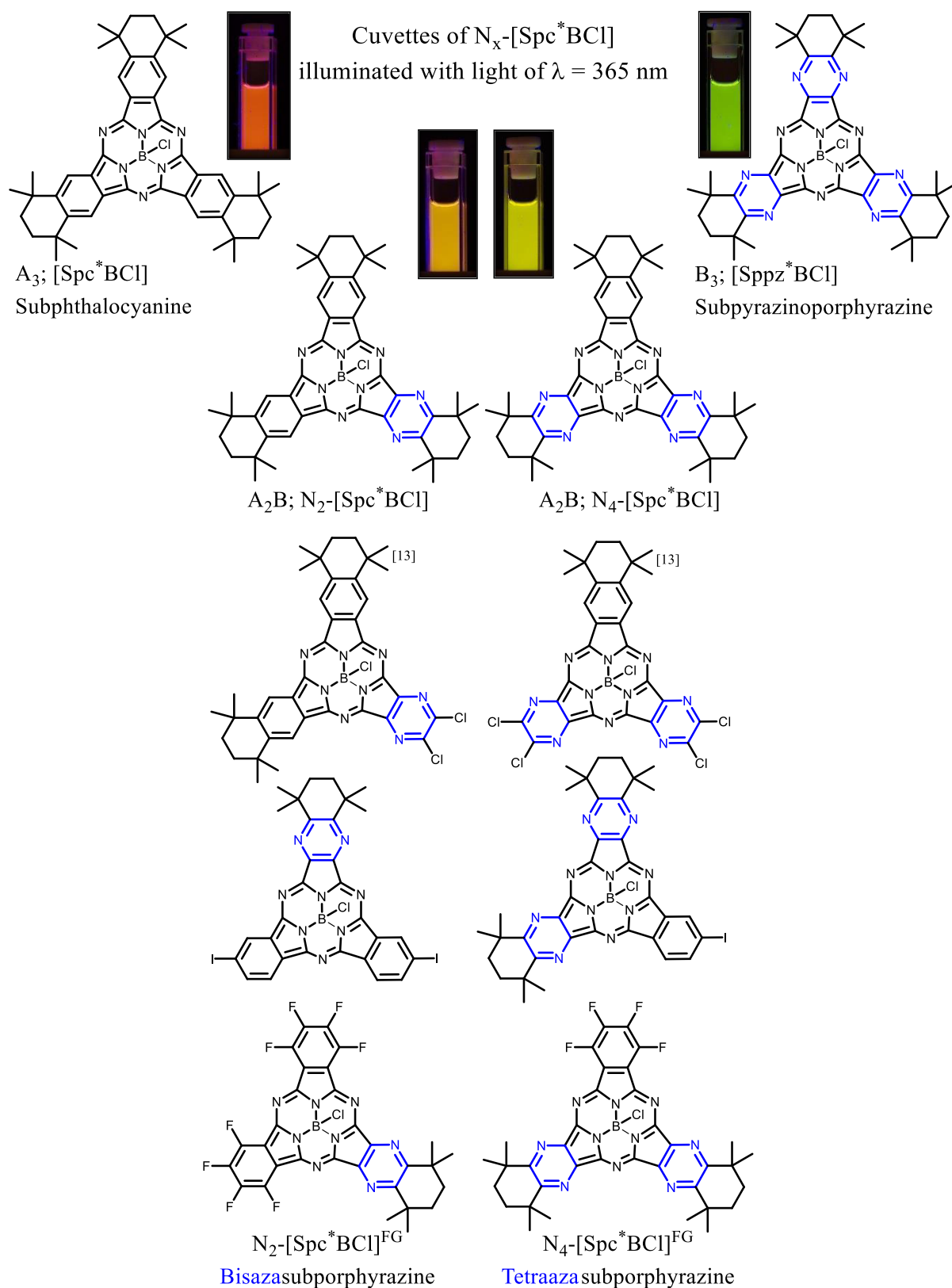
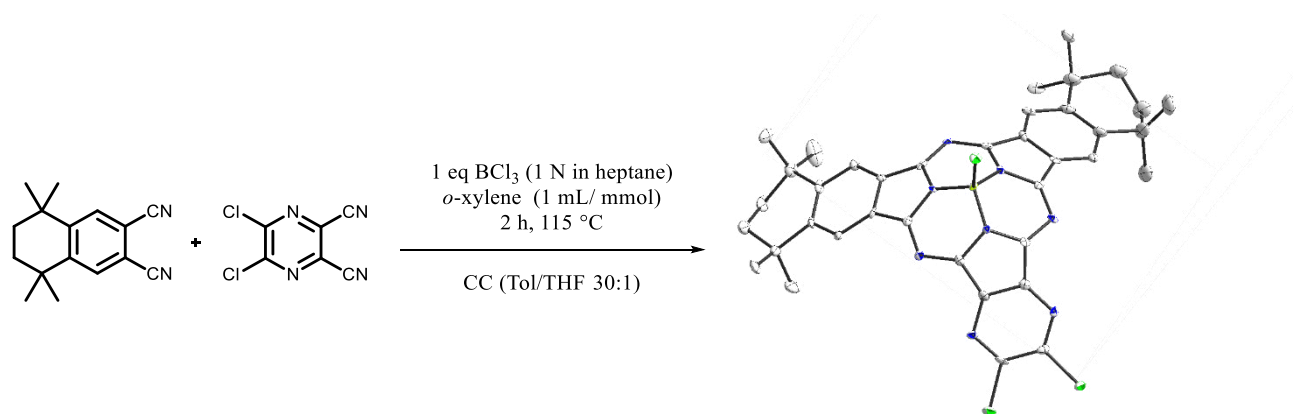


Figure 108: Synthesised series of alkyl substituted N_x -[Sp^{*}BCl] complexes, incorporating different halogen substituents. On the top: Cuvettes of N_x -[Sp^{*}BCl] in MeOH, with increasing number of [-N=] in N_x -[Sp^{*}BCl] from $x = 0, 2, 4$, to 6 (left to right). Samples are illuminated with light of $\lambda = 365$ nm.

Results and Discussion

All shown compounds were characterized by using ^1H NMR, UV-Vis, FS spectroscopy and mass spectrometry. Besides the isolation of the first crystallographically characterised $[\text{Sppz}^*\text{BCl}]$,^[25] it was possible to synthesise the first aza-Spcs series and even to obtain single crystals of N_2 - $[\text{Spz}^*\text{BCl}]^{\text{Cl}}$ from dichloromethane (Scheme 60).



Scheme 60: Synthesis of $[\text{Spz}^*\text{BCl}]^{\text{Cl}}$.

The molecular arrangement is shown in Figure 109. The molecular structure was solved by squeezing disordered solvent molecules.^[233,234,234] The areas, in which the solvent was squeezed, are shown in grey.

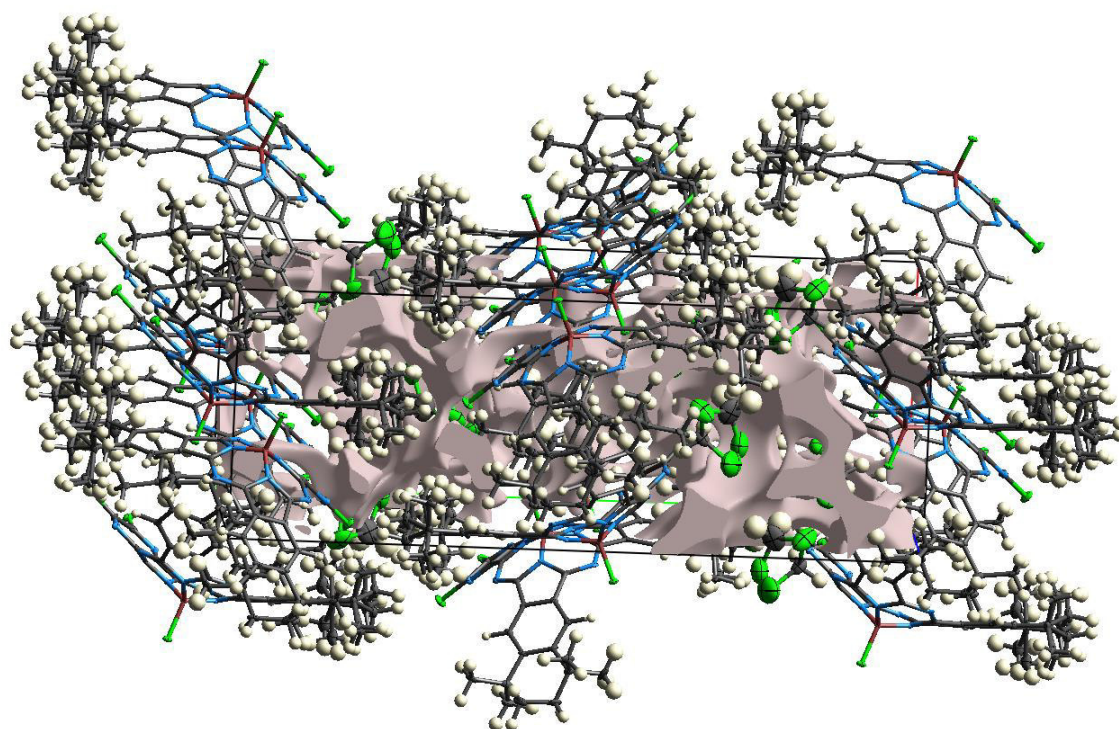
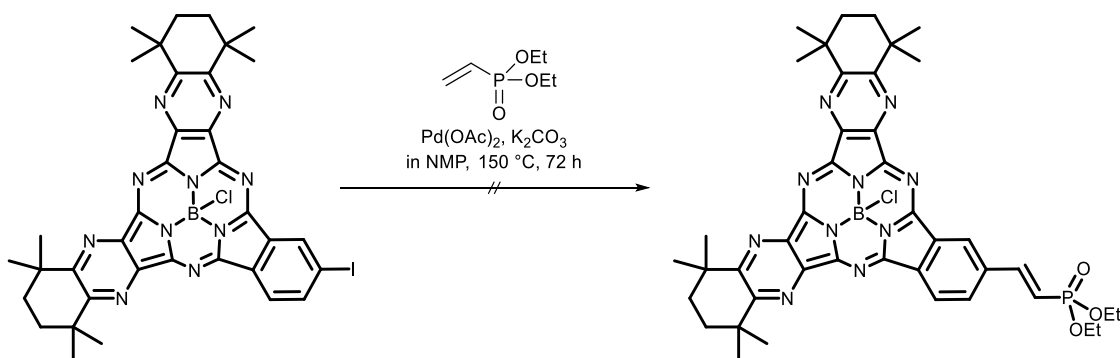


Figure 109: Lattice structure of the first described aza-Spcs N_2 - $[\text{Spz}^*\text{BCl}]^{\text{Cl}}$. The XRD analysis was refined by squeezing disordered dichloromethane molecules (grey area).

The functionalisation of subphthalocyanines is known from literature, and was previously described in our group as well.^[13] A HECK coupling to functionalise N_4 -[Spc*BCl]^I was attempted (Scheme 61). Product formation could be monitored by TLC, but in workup, a fast decolouration was observed. In future, similar reactions with axially substituted aza-Spcs, such as N_4 -[Spc*BOPh]^I, might be carried out.^[164]



Scheme 61: Attempt to functionalise a N_4 -[Spc*BCl]^I.

In the electronic absorption spectra of the N_x -[Spc*BCl]^{FG} series, a strong hypsochromic shift of the Q-band by increasing the number of [-N=] units can be observed. All Q-band maxima are compared in Table 18. Regardless of the position, peripheral or non-peripheral, the substitution of an alkyl group of an isoindoline unit by a halogen atom leads to a 10 nm hypsochromic shift of the Q-band. This is in contrast to a pyrazine unit, where a bathochromic shift was observed, when N_x -[Spc*BCl]^{Cl} is compared to N_x -[Spc*BCl], with $x = 2$ or 4 (Table 18). The size and number of the halogen atoms do not lead to a strong shift of the Q-band.

Table 18: Measured Q-bands of N_x -[Spc*BCl], in DCM, rt.

Q-band / nm	N_x -[Spc*BCl]	N_x -[Spc*BCl] ^F	N_x -[Spc*BCl] ^{Cl}	N_x -[Spc*BCl] ^{Br}	N_x -[Spc*BCl] ^I
N_2 -[Spc*BCl] ^{FG}	572	563	580	558	561
N_4 -[Spc*BCl] ^{FG}	557	550	576	546	548

Here, a simple but effective synthesis of N_x -[Spc*BCl]^{FG} is described, by varying the number and type of halogen substituent from F → I in the peripheral position. These compounds could be extended with a PDN* unit to an A_3B type,^[13] or even lower symmetrical A_2BC phthalocyanine. Strong nitrogen donor substituents could lead to a relatively efficient electron transfer, according to theoretical calculations of recent literature.^[105,208] Therefore, here, guanidine as substituent is proposed.^[13] Furthermore, the HOMO-LUMO gap of this new azasubphthalocyanine series can be tuned and adjusted to the semiconductors CB for application in OPVs.

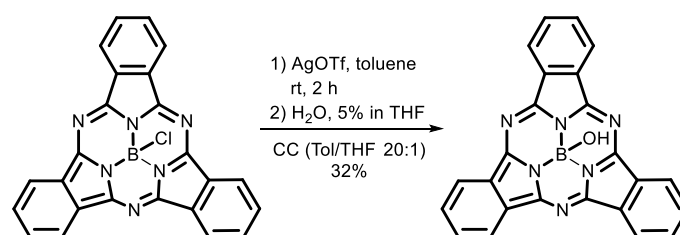
4.4 Metal Subphthalocyanine Complexes

Besides the synthesis of axial halogen substituted subphthalocyanines and azasubphthalocyanines and its hybrid compounds, N_x -[Sp c^* BCl], subphthalocyanines are interesting compounds with regard to their application in semiconductors,^[161] or LEDs.^[151–155] In this section, the functionalisation of [Sp c BCl] is described, and first attempts to synthesise metal subphthalocyanine complexes were carried out using [Sp c BO]⁻ as anionic borato ligand.

4.4.1 Synthesis of Hydroxy Subphthalocyanine Precursor [Sp c BOH]

The synthesis of [Sp c BOH] was described several times in literature.^[169,170,235,236] Most syntheses start with the [Sp c BCl], which is commercially available or easy to obtain from PDN and BCl₃. XRD structural investigations of [Sp c BOH] were carried by POTZ.^[236]

Here, the synthesis was attempted using different routes, the one described by POTZ, applying aq. pyridine and [Sp c BBr], and the one by YAMASAKI, applying an acid-pasting method with H₂SO₄.^[235,236] In both cases, only traces and mixtures of the product were observed. Another synthesis described in literature, is the synthesis by GUILLEME of the TORRES group.^[169,170] In this synthesis, triflate is used as leaving group after addition of AgOTf to [Sp c BCl] and removing precipitated AgCl. Different nucleophiles were tested for triflate substitution at the intermediate [Sp c BOTf].^[169,170] Aq. THF solution led to the hydroxy subphthalocyanine [Sp c BOH] (Scheme 62). The synthesis could not be reproduced in reported 83% yield, here, only 32% were obtained. This might be caused by the side reaction, a condensation of 2 eq of formed [Sp c BOH], when the solution was stirred too long. The reaction was monitored by TLC.



Scheme 62: Synthesis of [Sp c BOH].

The main disadvantage of this synthesis is the extensive workup. Separation via column chromatography was carried out, using toluene/THF 20:1. At first, [Sp c BCl] was eluted, followed by [(Sp c B)₂O] and finally [Sp c BOH] was obtained. It was also attempted to convert [(Sp c B)₂O] into the monomers using KOH solution, but only an incomplete conversion was observed making the CC unwarranted. The main advantage of subphthalocyanines, from the

synthetic point of view, is their high solubility in common organic solvents, caused by the "umbrella like" structure, described in the previous section 4.2.1.1. The solubility of the non-alkyl substituted [SpcBOH] for example is high enough to obtain ^1H NMR spectra in benzene (Figure 110).

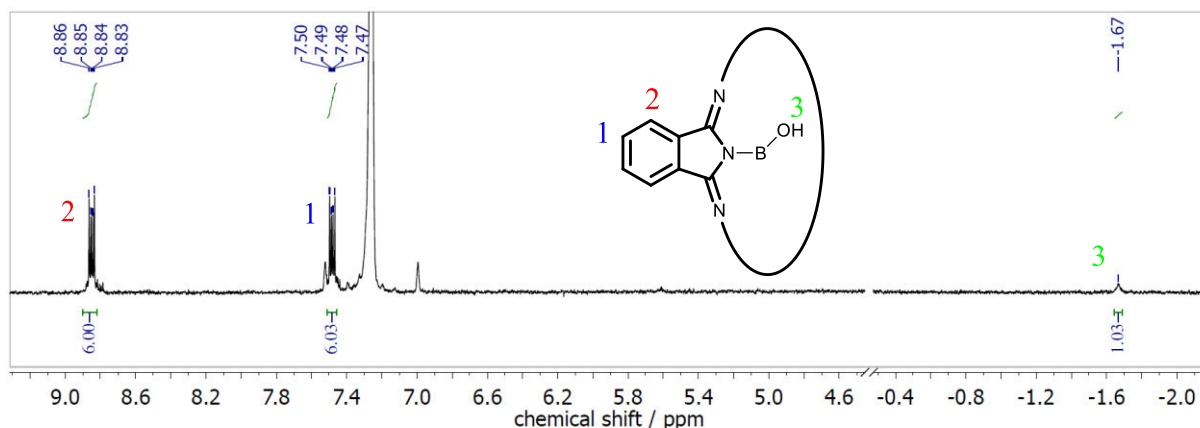


Figure 110: ^1H NMR spectrum of [SpcBOH], in C_6D_6 (300 MHz).

The low-field shift of the non-peripheral aromatic protons is characteristic for the subphthalocyanines. The hydroxy signal $-\text{OH}$ can be observed as a broadened signal, high-field shifted to -0.5 - (-2.0) ppm. In ^{11}B NMR spectroscopy, the inner boron (III) nucleus is shifted to -15.5 ppm. In addition, UV-Vis and FS spectroscopy and mass spectrometry were carried out.

4.4.2 Synthesis of Metal Subphthalocyanine Complexes

While a lot of fused dimeric boron subphthalocyanines,^[159,235,237] axial functionalised subphthalocyanines,^[169,170] alkyl bridged compounds, ring contracted and annulated extended derivatives are described in literature,^[160,238] the number of studies regarding subphthalocyanines as borato ligand to metals is limited.^[239] There are ferrocene or ruthenocene complexes bonded in axial or in non-/peripheral positions.^[240] Subphthalocyanines were coupled by alkyl bridges to phthalocyanines.^[128] Biomimetic models using coupled subphthalocyanine-[FeFe] hydrogenases were described.^[241] However, no coordination of subphthalocyanines as anionic borato ligand in metal complexes has been described before. Templating several [SpcBOH] at one metal centre forces the π -system of the isoindoline units to interaction. Therefore, these compounds may show interesting physicochemical or magnetic behaviour. Rare earth metal complexes with [SpcBO] $^-$ ligands might be used as single molecule magnets (SMM).

Results and Discussion

At first, the reactivity of [SpCBOH] towards highly reactive organo-triols such as [MMe₃] with M = Al, Ga, In was studied. On one hand, these compounds were chosen because of their high reactivity, on the other hand because of an increase in solubility caused by the methyl groups. To obtain [Me₂Al(μ-OBSpc)]₂ complexes, a [SpCBOH] solution was added dropwise to a solution of AlMe₃ at low temperatures of -78 °C. When the violet subphthalocyanines solution was added, a change in colour to deep light blue was observed. After warming up to rt, the colour appeared purple again. The solvent and the excess of AlMe₃ were removed in vacuum. The formation of the respective metal complexes can be monitored by ¹H NMR or ¹¹B NMR experiments. In ¹H NMR spectroscopy, the typical methyl signals of AlMe₃ are high-field shifted, because of their proximity to the π-system, [-BN₃-], respectively. In the case of a degradation of Spc, the dinitrile or similar by-products can be identified by high-field shifted multiplets, but in this reaction, [SpCBOH] appeared to be stable enough.

Following this method, the reaction was carried out for GaMe₃ and InMe₃. In the ¹H NMR spectrum (Figure 111) the methyl groups of [Me₂Ga(μ-OBSpc)]₂ are visible at -0.56 ppm. The aromatic protons are additionally high-field shifted in a 0.1 ppm range. In comparison to shifts induced by central metal atoms, it is only a small shift, but a significant one. The outer, peripheral protons are less strongly high-field shifted. In all NMR spectra, a shift of the two methyl protons of the central metal atom from -1.20 ppm (Al), via -0.56 ppm (Ga) to 0.16 ppm (In) can be observed. This is in accordance with the size and acidity of the metal.

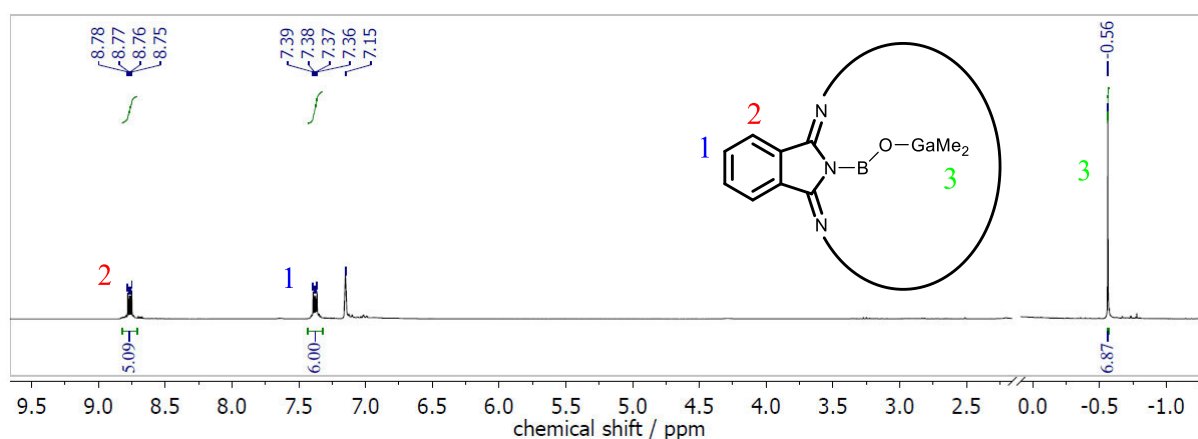


Figure 111: ¹H NMR spectrum of [Me₂Ga(μ-OBSpc)]₂, in C₆D₆ (300 MHz), grease impurities are removed for clarity.

In addition to ¹H NMR spectroscopy, MALDI-ToF was carried out under inert gas. The best results were obtained measuring the MALDI-ToF without matrix. The ionisation by laser light absorption of the π-system is sufficient. An example of a MALDI-ToF spectrum is shown in Figure 112.

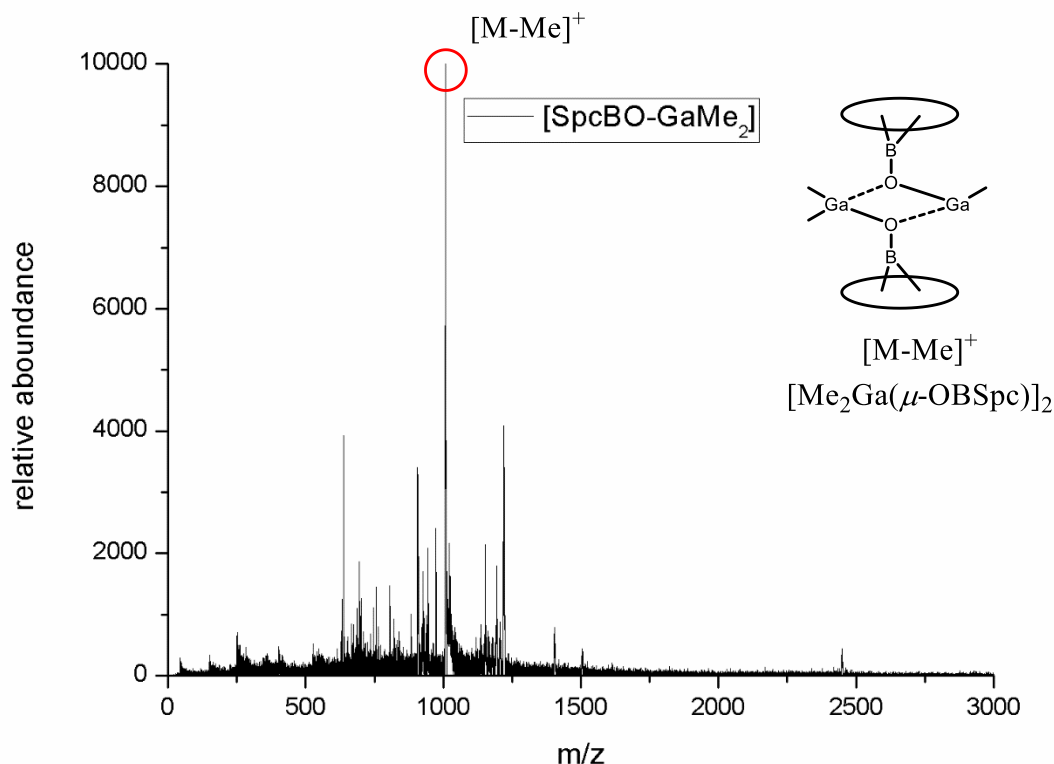


Figure 112: Inert gas MALDI-ToF spectrum of $[\text{Me}_2\text{Ga}(\mu\text{-OBSpc})]_2$.

In the MALDI-ToF measurement, a dinuclear species was observed. It is common that a methyl group is lost while ionising the compounds in measurement. The 100% peak at 1008.736 could be assigned to $[\text{Me}_3\text{Ga}_2(\mu\text{-OBSpc})_2]$, $[\text{M-Me}]^+$. The lower peaks could be assigned to fragments, such as 906.369 for $[\text{M-GaMe}_2]^+$. In UV-Vis spectroscopy, the influence on the Q-band is very weak, about 1 nm. This is in accordance with the weak shift observed in ^1H NMR spectroscopy.

Dinuclear species $[\text{Me}_2\text{M}(\mu\text{-OBSpc})]_2$ could be synthesised and characterized for icosagens, $\text{M} = \text{Al}, \text{Ga}$. For $\text{M} = \text{In}$, based on the higher basicity of the second methyl group, only a mixture of $[\text{Me}_2\text{In}(\mu\text{-OBSpc})]_2$ and $[\text{MeIn}(\text{OBSpc})_2]$ was found, in a ratio of 2:1, which was determined by ^1H NMR spectroscopy. It was attempted to vary the temperature and to use InMe_3 in a large excess of more than 20 eq, but always $[\text{MeIn}(\text{OBSpc})_2]$ was identified in ^1H NMR spectroscopy. In comparison to $[\text{Me}_2\text{M}(\mu\text{-OBSpc})]_2$, the three methyl protons of $[\text{MeIn}(\text{OBSpc})_2]$ could be assigned by integration and additionally by a greater high-field shift to -0.52 ppm.

Results and Discussion

Based on these results, the synthesis of other metal complexes was tested. Because it is essential to verify the structure of the above mentioned metal complexes by an X-ray structural analysis, it was intended to promote a crystallisation using more symmetrical complexes, such as $[(\text{SpCBO})_x\text{M}]$ with $\text{M} = \text{Ti}, \text{B}, \text{M}^{\text{RE}}$ and $x = 4, \text{ or } 3$, respectively. These tests were carried out within the Bachelor-Thesis by SHARIKOW.^[242] SHARIKOW was able to synthesise a $[(\text{SpCBO})_4\text{Ti}]$ complex, using $[\text{Ti}(\text{NMe}_2)_4]$ and added it dropwise to a solution of 4 eq of $[\text{SpCBOH}]$. In accordance with previously observed trends, a weak shift of the non-peripheral protons into the low-field was observed in the ^1H NMR spectrum. The elemental analysis shows higher deviations of calculated expected values, but the complex could be characterized by MALDI-ToF and UV-Vis spectroscopy. In UV-Vis spectroscopy, a weak broadening of the signal in comparison to the $[\text{SpCBOH}]$ was observed.

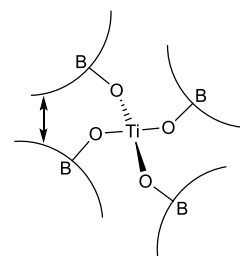
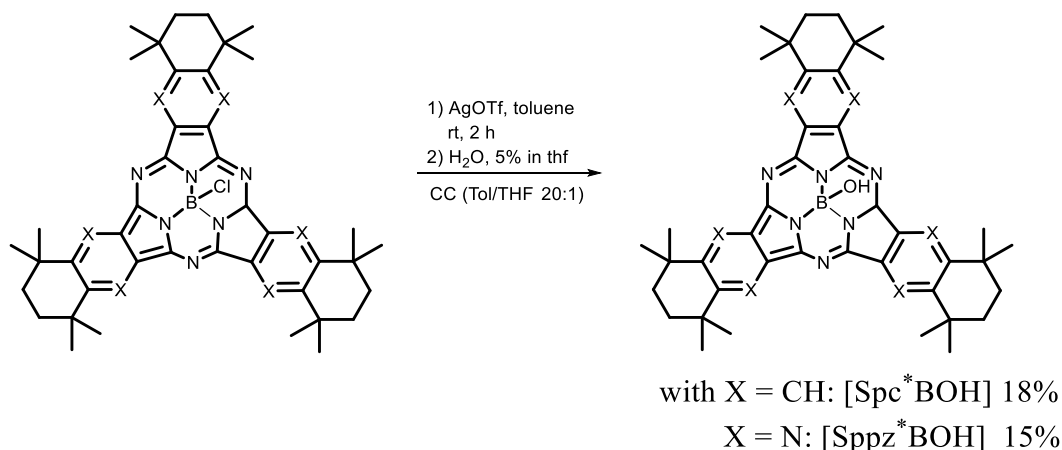


Figure 113: Attempt to synthesise $[(\text{SpCBO})_4\text{Ti}]$.

Summary. In this chapter, first metal subphthalocyanine complexes of the $[(\text{SpCBO})_x\text{M}]$ type were described, using $[\text{SpCBO}]^-$ as anionic borato ligand. Dinuclear triel complexes $[\text{Me}_2\text{M}(\mu\text{-OBSpc})]_2$ with $\text{M} = \text{Al}, \text{Ga}$ could be synthesised and characterized. Under inert atmosphere, these complexes are stable enough for complete analysis even for mass spectrometry. It could be shown that $[\text{SpCBOH}]$ is able to coordinate more than just once to a metal. Here, further analysis by using magnetic circular dichroism (MCD) experiments would be of interest to gain more information about the electronic behaviour of the complexes.

4.4.3 Synthesis of Hydroxy Subphthalocyanines [Sp^c*BOH]

In addition, SHARIKOW could demonstrate that similar boron acids [Sp^c*BOH] and [Sp^{pz}*BOH], can be synthesised for less aggregating systems (Scheme 63).^[169,170,242]



Scheme 63: Synthesis of axial functionalised subphthalocyanine [Sp^c*BOH] and -porphyrine [Sp^{pz}*BOH].

Besides their interesting absorption and emission properties, these phthalocyanines can be used to synthesise "umbrella-like complexes", as described in chapter 4.4.2. In Figure 114, cuvettes (UV-Vis and FS) of the synthesised [Sp^{pz}*BOH] and [Sp^c*BOH] are shown. Here, again, visible to the unaided eye is the aza-fine tuning of these compounds in the fluorescence emission based on the macrocycle core of the samples, when the samples are illuminated with light of $\lambda = 365$ nm.

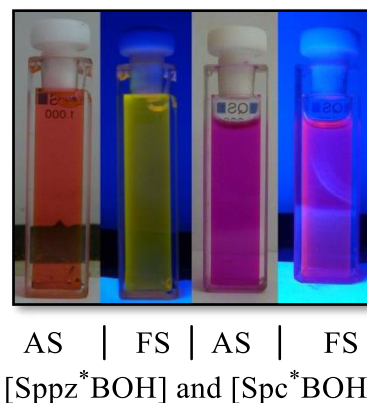


Figure 114: Cuvettes of [Sp^{pz}*BOH] and [Sp^c*BOH] in DCM. UV-Vis (AS = absorbance, left) and FS by irradiating the sample with 365 nm light (right).

The fluorescence and absorption behaviour of [Sp^{pz}*BOH] and [Sp^c*BOH] is very interesting and the B-OH functionalities of these soluble chromophores might be very useful for binding subphthalocyanines to ZnO or TiO₂ interfaces or via H-bonding to purine bases of DNA stands. Therefore, in cooperation with MEYENBURG (HEIMBRODT group at the Department of Physics of the Philipps-Universität Marburg), time-resolved photoluminescence (TRPL) measurements are carried out, using [Sp^c*BOH] adsorbed on different TiO₂ surfaces. In recent results, an acceleration of the PL could be observed, applying different [Sp^c*BOH]/TiO₂ interfaces. This indicates a successful charge-transfer from the molecule to the semiconductor when the substance is soaked on the surface.

4.5 Rare Earth Metal Sandwich-Complexes

The last section is about the synthesis of phthalocyanine and naphthalocyanine sandwich-complexes of rare earth metals (M^{RE}). These sandwich-complexes play an important role in surface science, where a specific magnetism is of interest, which might be influenced by a rare earth metal complex. Phthalocyanine sandwich-complexes, such as $[\text{Pc}_2\text{Sn}]^{[243]}$ or $[\text{Pc}_2\text{U}]^{[244]}$, are literature known, as well as sandwich complexes with rare earth metals in the centre of two Pc-ligands $[\text{Pc}_2M^{\text{RE}}]$. In recent investigations in designing single molecular magnets (SMM), it is of utmost importance to understand the molecule-metal interface and resolve the spin character of molecular orbitals interacting with a ferromagnetic surface, as was carried out recently by WIESENDANGER and RUBEN.^[245] The main focus was on the two rare earth metals Eu and Tb. First, it was attempted to reproduce literature known simple phthalocyanine sandwich-complexes, such as $[\text{Pc}_2M^{\text{RE}}]$. Second, knowledge gained from reproducing literature results was used in the sandwich complex synthesis with the more soluble ligands $\text{Pc}^{*(2-)}$ and $\text{Nc}^{*(2-)}$. In the periodic table, both metals, Eu and Tb, are on the right or left side of Gd. f^7 -Gd has the highest spin of the rare earth metals. That makes them interesting, because it may give the surface an additional spin, for the reason that it has exactly one azimuthal quantum number +1 or -1. A more detailed discussion of $[\text{Pc}_2M^{\text{RE}}]$ applied in SMMs is given in the Introduction 2.2.3.

4.5.1 Introduction: Investigation of Unsubstituted Rare Earth Metal Phthalocyanines

In a first attempt, the already literature described unsubstituted phthalocyanine sandwich-complexes $[\text{Pc}_2M^{\text{RE}}]$, with a focus on $M^{\text{RE}} = \text{Eu}$ and Tb, were synthesised (Figure 115).^[246] For more than 40 years, these $[\text{Pc}_2\text{Ln}]$ have been controversially discussed in literature. This due to the diprotic and non-innocent ligand, which is typically Pc^{2-} and the rare earth metal, which is mainly in an oxidation state of +3 as $M^{\text{RE}}(\text{III})$. In the following, the structures of such a complex are outlined using the example of $[\text{Pc}_2\text{Tb}]$ and $[\text{Pc}_2\text{Lu}]$. WEIS summarised the proposed nature of these molecules:^[246]

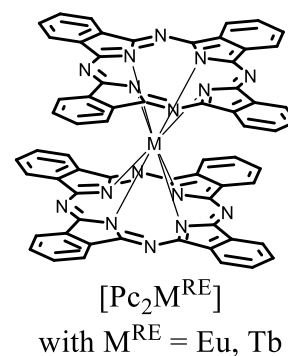


Figure 115: Structure of a $[\text{Pc}_2M^{\text{RE}}]$.

- (i) The phthalocyanine has an ionized double decker sandwich complex form, whereby a $[\text{Pc}_2M^{\text{RE}}]^-$ is present, in a protonated form, such as $[\text{Pc}_2M^{\text{RE}}\text{H}]$ with $M^{\text{RE}} = \text{Lu}(\text{III})$

- (ii) The complex is protonated, while one phthalocyanine ligand forms a one electron oxidised form such as $[\text{Pc}^{(2-)}\text{Pc}^{(\cdot-)}\text{M}^{\text{RE}}\text{H}]^+$ with $\text{M}^{\text{RE}} = \text{Lu(III)}$
- (iii) Or a reduced form is present such as $[\text{Pc}_2\text{M}^{\text{RE}}]^-$, or a one-ligand oxidised form is present such as $[\text{Pc}^{(2-)}\text{Pc}^{(\cdot-)}\text{M}^{\text{RE}}]$

MOSKALEV and KIRIN reported about the first synthesis of $[\text{Pc}_2\text{Lu}]$ using $[\text{Lu}(\text{OAc})_3] \cdot \text{H}_2\text{O}$ and PDN, in 1965, decades after the first synthesis of Pc.^[247] Using PDN and the $[\text{M}^{\text{RE}}(\text{OAc})_3]$ in a 10:1 ratio in a neat reaction and after separation by column chromatography, they observed a blue and a greenish powder. They supposed that the blue spot is a $[\text{Pc}_2\text{LnH}]$ sandwich-complex, while the green powder is a half-sandwich type by-product such as $[\text{PcLnCl}]$, despite an unsatisfying elemental analysis.^[247,248] MACKAY instead indicated that both structures correspond to a double-decker type, whereby the blue spot may interconvert to the green one.^[249] WEIS combined the work of CORKER *et al.*^[250], who showed that an unpaired electron is present in the green $[\text{Pc}^{(2-)}\text{Pc}^{(\cdot-)}\text{M}^{\text{RE}}\text{H}^+]\text{A}^-$ (whereby A^- is an unidentified anion) by magnetic susceptibility measurements, and of MARCHON *et al.*^[251], who determined the presence of an unpaired electron in a phthalocyanine ligand by EPR spectroscopy.^[246]

WEIS concluded for this synthesis the up-to-now accepted nature of $[\text{Pc}^{(2-)}\text{Pc}^{(\cdot-)}\text{M}^{\text{RE}}]$: a non-protonated one-electron ligand-oxidised structure.^[246] The proton was "excluded" by magnetic and optical measurements, while anion exchange should be visible in IR. Meanwhile, WEIS could not differentiate if the one electron is delocalized on (i) one Pc ligand or (ii) is delocalized over both Pc ligands, by analysing the crystal structure. Under the described reaction conditions, a $[\text{Pc}_2\text{M}^{\text{RE}}]^-$ complex is formed, which gets oxidised in air to the neutral $[\text{Pc}^{(2-)}\text{Pc}^{(\cdot-)}\text{M}^{\text{RE}}]$

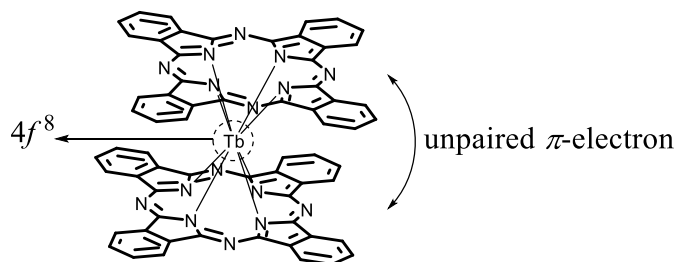


Figure 116: Discussed $[\text{Pc}_2\text{Tb}]^0$ complex by ISHIKAWA.

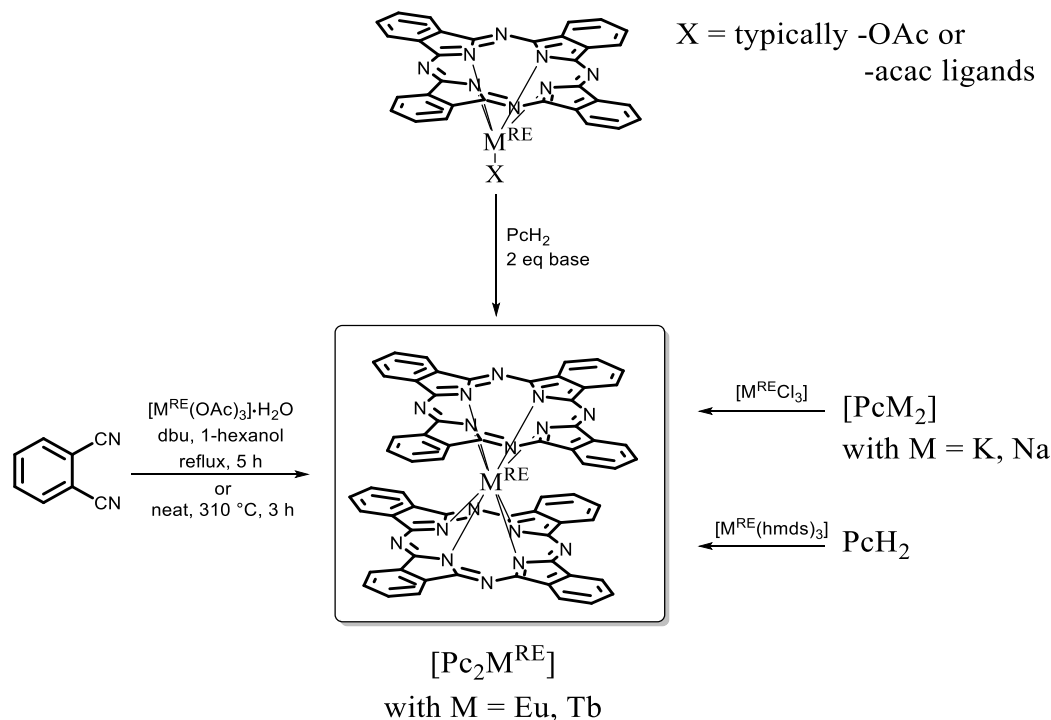
species.^[246] ISHIKAWA was able to demonstrate experimentally by use of absorption and MCD spectra a delocalisation of the unpaired π -electron over both ligands.^[252,253] He accomplished this by comparing not

only double-decker Pcs, but mixed $[\text{PcNcTb}]$, which had properties in UV-Vis spectroscopy and in theoretical calculations that were in between $[\text{Pc}_2\text{Tb}]$ and $[\text{Nc}_2\text{Tb}]$.^[252] As intuitively proposed, theoretical calculations do show a favoured localisation of the π -electron of $[\text{PcNcTb}]$ on the Nc ligand. In comparison to anionic complexes, such as $[\text{Pc}_2\text{Tb}]^- \text{TBA}^+$, $[\text{Pc}_2\text{Tb}]^0$ is an interesting complex for SMM. Not only does it possess a total angular momentum

quantum number $J = 6$ (while J is obtained from the total orbital angular momentum quantum number L and the total spin angular momentum S) similar to its anionic brother, it was also proved to have a spin of $S = 1/2$, using alternating current susceptibility measurements.^[254,255] The $[\text{Pc}_2\text{Tb}]^0$ showed a significantly higher temperature for the magnetisation lag to alternating current magnetic field. As visible in Figure 116, the f - π interaction should be studied to explain this phenomenon. In summary, in the discussed neutral oxidised complexes $[\text{Pc}_2\text{Tb}]^0$, terbium has an oxidation number of +3. One ligand is present as $\text{Pc}^{(2-)}$, the second as $\text{Pc}^{(-)}$. Both ligands are weakly twisted, but cannot be differentiated. WIESENDANGER and previous reports concluded a central $J = 6$ Ising-type high-spin system.^[245] The Tb^{3+} has a $4f^8$ -electron conformation and the peripheral $S = 1/2$ π electron is delocalized over two Pc ligands.^[254]

4.5.2 Synthesis of Non-Alkyl Substituted Rare Earth Metal Phthalocyanines

The synthesis of $[\text{Pc}_2\text{M}^{\text{RE}}]$ was carried out according to previously described reactions using $[\text{M}^{\text{RE}}\text{Cl}_3]$ and $[\text{PcK}_2]$ or in a neat reaction using $[\text{M}^{\text{RE}}(\text{OAc})_3]$ and PDN.^[246,247] Both syntheses require a more complicated work up with column chromatography or filtration over alumina, because PcH_2 is formed as well. As alternative synthesis, $[\text{PcK}_2]$ was used, which was freshly prepared by using KBN and PcH_2 . The rare earth metalation was carried out with the obtained $[\text{PcK}_2]$ precursor and $[\text{M}^{\text{RE}}\text{Cl}_3] \cdot \text{solv}$ with $\text{M} = \text{Eu}, \text{Tb}$ in THF.



Scheme 64: Summary of different literature described synthetic approaches to $[\text{Pc}_2\text{M}^{\text{RE}}]$.^[246,247,257]

Both compounds, $[\text{Pc}_2\text{M}^{\text{RE}}]$ with $\text{M} = \text{Eu}, \text{Tb}$ could be obtained from $[\text{PcK}_2]$ and $[\text{M}^{\text{RE}}\text{Cl}_3]\cdot\text{solv}$ with $\text{M} = \text{Eu}, \text{Tb}$ or via metalation of PcH_2 with $[\text{M}^{\text{RE}}(\text{hmds})_3]$, respectively. The complexes were analysed by routine analysis, such as MS, UV-Vis and IR. In ^1H NMR spectroscopy, a low-field shift of the aromatic protons of $[\text{Pc}_2\text{Eu}]$ to 11.39 ppm and 9.09 ppm, respectively, was observed. In the UV-Vis spectra, a hypsochromic shift of the Q-band of both compounds in comparison to PcH_2 can be observed. The Q-band of $[\text{Pc}_2\text{Tb}]$ (666 nm) is also hypsochromically shifted about 2 nm compared to $[\text{Pc}_2\text{Eu}]$ (668 nm). The 2 nm shifts are in accord with literature, whereby a bathochromic shift with the decreasing size of the central metal atom is expected.^[124] E. g. $[\text{Pc}_2\text{Lu}]$ has a literature Q-band absorption of 658 nm.^[252] Even if the compounds are handled under an inert atmosphere, an oxidation of the anionic ligand may occur on the silica gel during filtration. $[\text{Pc}_2\text{Tb}]$ and $[\text{Pc}_2\text{Eu}]$ have additionally the advantage of being sublimable in vacuum.^[245]

4.5.3 Preliminary Work: Synthesis of Half-Sandwich Complexes

In the context of this work, SWOLANA and PFAFF carried out several attempts to obtain mixed phthalocyanine sandwich-complexes.^[199,256] SWOLANA reproduced the $[\text{PcYOAc}]$ following the synthesis of PUSHKAREV *et al.* (Figure 117).^[257] Therefore, PcH_2 was metalated by using 2.1 eq of DBU and $[\text{Y}(\text{OAc})_3]$ in toluene. Following PUSHKAREV *et al.*, SWOLANA tried to convert $[\text{PcYOAc}]$ into double-decker sandwich complexes (Scheme 66).

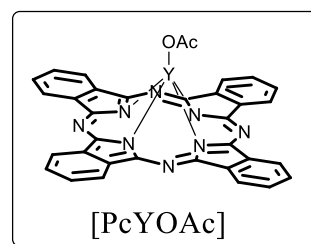
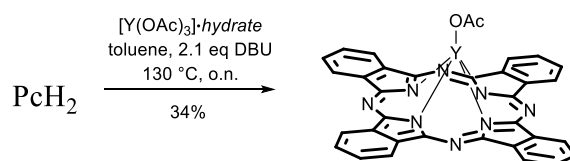
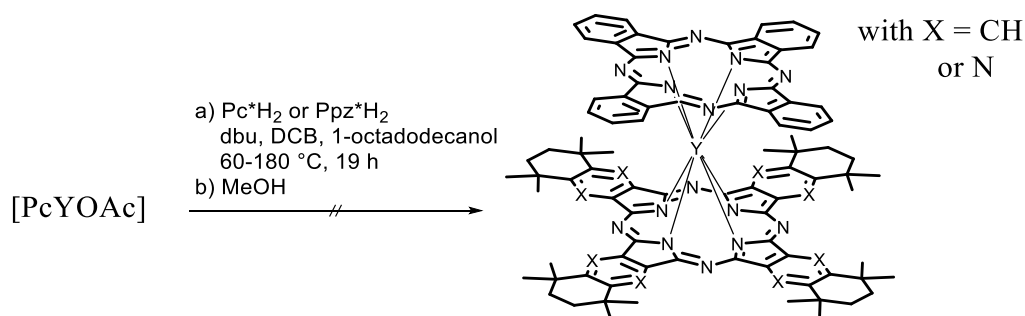


Figure 117: Synthesised $[\text{PcYOAc}]$ half sandwich-complex.



Scheme 65: Synthesis of $[\text{PcYOAc}]$ following PUSHKAREV.^[256,257]

Under the chosen conditions (Scheme 66), as main product, Pc^*H_2 was observed in MALDI-ToF, whereby measurements were carried out under inert atmosphere. A formation to $[\text{PcPc}^*\text{Y}]$ was detected in MALDI-ToF $m/z = 1544.218$, and in UV-Vis spectroscopy, a weak shift was observed.



Scheme 66: Attempt to form double-decker sandwich-phthalocyanines of $[\text{PcPc}^*\text{Y}]$ or $[\text{PcPpz}^*\text{Y}]$ type.

PFAFF observed increased solubility of $[\text{PcYOAc}]$ when residual DBU was present. This is no new phenomena and was already described in literature by JANCZAK,^[258] who could prove that DBU is present as a common impurity in commercially available $[\text{PcZn}]$.

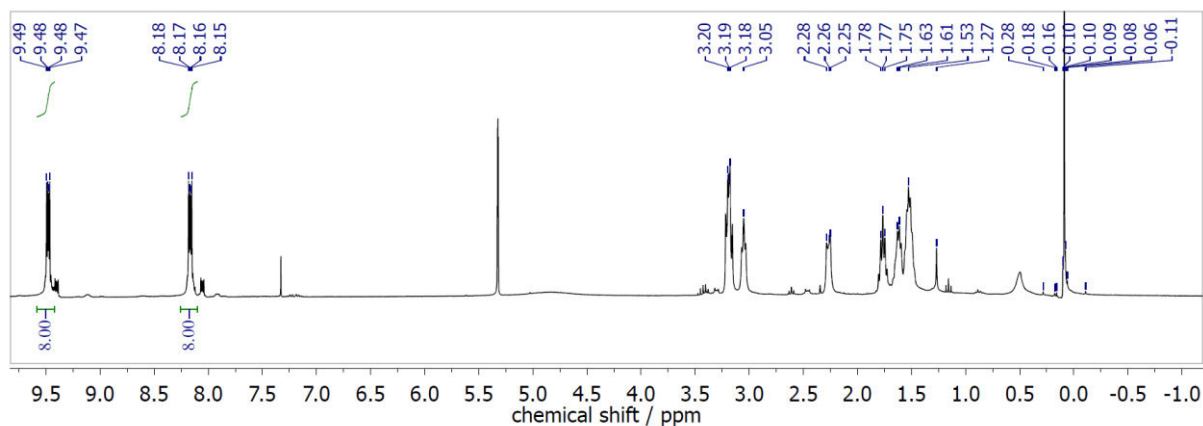


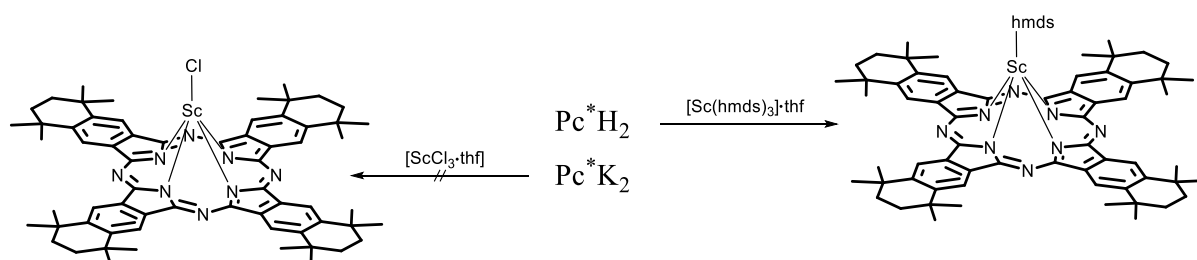
Figure 118: ^1H NMR spectrum of $[\text{PcYOAc}\cdot\text{dbu}]$, in $\text{CDCl}_3/\text{CD}_2\text{Cl}_2$ (300 MHz).

DBU, as a strong base, forms an adduct with $[\text{PcZn}]$, viz. $[\text{PcZn}\cdot\text{dbu}]$, which has an increased solubility caused by a weaker π - π stacking.^[258] By using HCl or acidic solvents like CDCl_3 , DBU can be protonated and the ligand releases the coordinated DBU. In comparison to $[\text{PcZn}\cdot\text{dbu}]$, $[\text{PcYOAc}\cdot\text{dbu}]$ was not soluble enough in toluene to better resolve the axially coordinated DBU ligand in the high-field shifted area between 0.5 and -1.0 ppm. COSY and TOCSY spectra were measured in pyridine- d_5 to prove the bonding. But here, mainly the literature mentioned high-field shifts prove the axial coordination of DBU in $[\text{PcYOAc}\cdot\text{dbu}]$.

PFAFF extended the series with the soluble Pc^* to $[\text{Pc}^*\text{M}^{\text{RE}}\text{OAc}]$ and attempted different metals, such as $\text{M}_{\text{RE}} = \text{Gd}$ and Tb . For Gd and Tb , a less selective conversion to the product $[\text{Pc}^*\text{M}^{\text{RE}}\text{OAc}]$ was observed, compared to $[\text{PcM}^{\text{RE}}\text{OAc}]$; by-product traces of the sandwich complex $[\text{Pc}^*_2\text{M}^{\text{RE}}]$ $\text{M}_{\text{RE}} = \text{Gd, Tb}$ and the free ligand Pc^*H_2 were observed. The purification of

$[\text{Pc}^*\text{M}^{\text{RE}}\text{OAc}]$ can be done by CC. It is remarkable that in MALDI-ToF spectrometry only the DBU formed complexes $[\text{M}-(\text{OAc})]^+$ were detected $[\text{Pc}^*\text{M}^{\text{RE}}\cdot\text{dbu}]$.

In addition, the synthesis of $[\text{Pc}^*\text{M}]$ with $\text{M} = \text{metal of group 3}$ was described before.^[133] The whole series of $[\text{Pc}^*\text{M}]$ complexes with $\text{M} = 3d\text{-metals}$ was described by BAYOUMI, with the exception of the most sensitive compound: $[\text{Pc}^*\text{Sc}^{3+}\text{Cl}]$. On ^1H NMR scale, $[\text{Pc}^*\text{Sc}^{3+}\text{Cl}]$ and -hmds substituted complex $[\text{Pc}^*\text{Sc}(\text{hmds})]$ could be synthesised. The synthesis was carried out in C_6D_6 using $[\text{Sc}(\text{hmds})_2\text{Cl}]$ or $[\text{Sc}(\text{hmds})_3]$ (Scheme 67). When $[\text{Pc}^*\text{K}_2]$ and $[\text{ScCl}_3]$ were used instead, no reaction was observed.



Scheme 67: Synthesis of $[\text{Pc}^*\text{Sc}(\text{hmds})]$ (right) out of Pc^*H_2 and attempt using $[\text{Pc}^*\text{K}_2]$ (left).

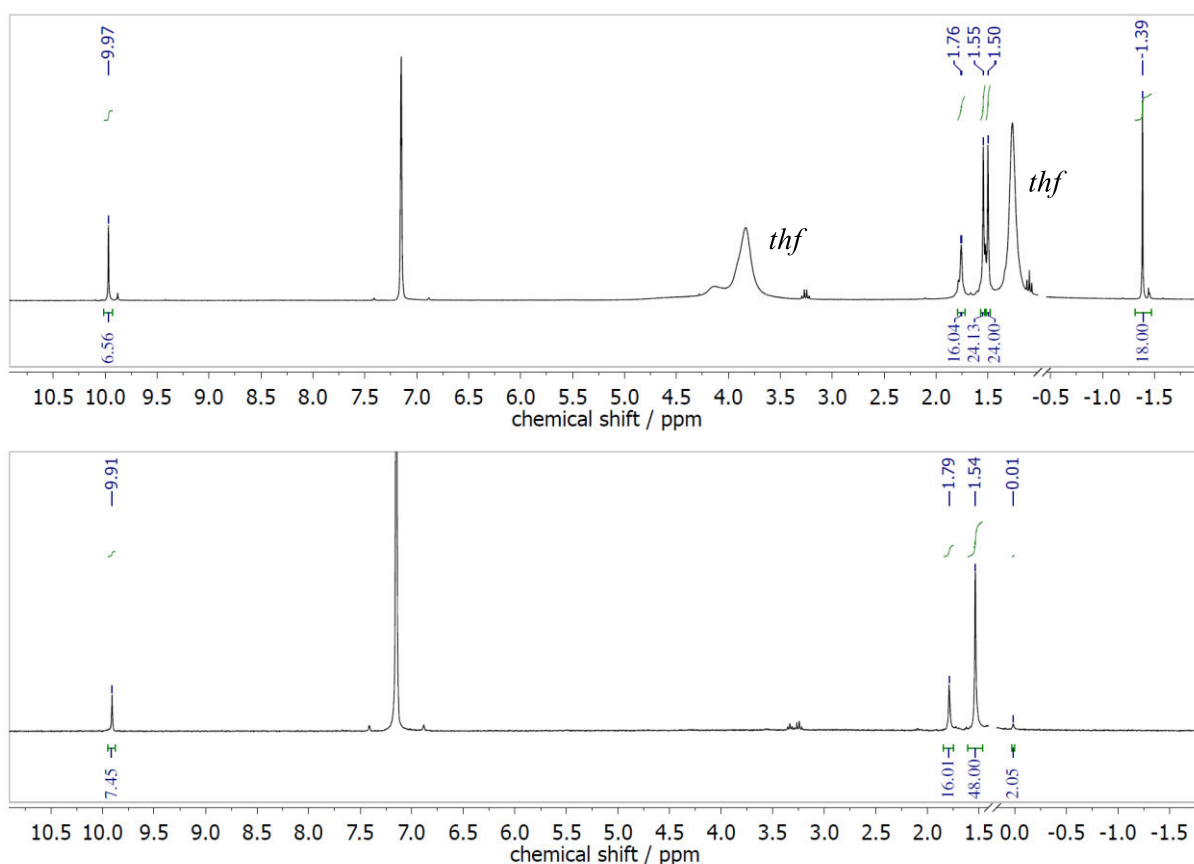
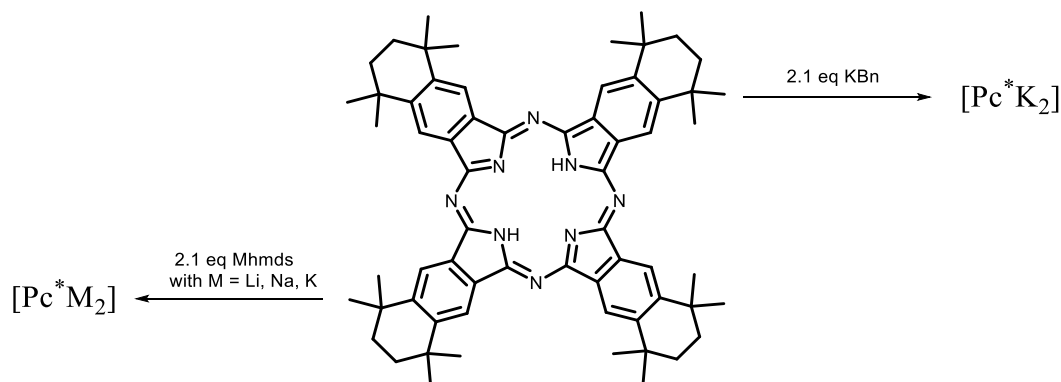


Figure 119: ^1H NMR experiment for the synthesis of $[\text{Pc}^*\text{Sc}(\text{hmds})]$, in C_6D_6 (300 MHz). $[\text{Sc}(\text{hmds})_3]$ has been cut off for clarity.

As is shown in Figure 119, the initially observed singlet of the methyl protons is split into two signals as the reaction proceeds. The initially electronically identical methyl protons now have a different chemical surrounding. Because of the size of Sc, it is not coordinated within the ligand plane, but above. The axial ligand additionally pulls the metal out of plane. The aromatic protons of $[\text{Pc}^*\text{Sc}(\text{hmds})]$ compared to Pc^*H_2 are only weakly low-field shifted by 0.06 ppm. The axial -hmds methyl protons instead are high-field shifted to -1.39 ppm, as is typical for axially substituted phthalocyanine ligands influenced by the ring current effect.^[259]

4.5.4 Synthesis of Sandwich Complexes $[\text{Pc}^*_2\text{M}^{\text{RE}}]$

As $[\text{PcK}_2]$ was used as a precursor for the synthesis of $[\text{Pc}_2\text{M}^{\text{RE}}]$, the precursors $[\text{Pc}^*\text{Li}_2]$, $[\text{Pc}^*\text{Na}_2]$ and $[\text{Pc}^*\text{K}_2]$ are known and reproduced as previously described by our group.^[260] Therefore, the symmetrical free ligands Pc^*H_2 and Nc^*H_2 , described in section 4.2.3.1 (p. 57), were synthesised. The conversion to the corresponding alkali salts was carried out by using LiHMDS, NaHMDS, KHMDS or KBn, respectively (Scheme 68).

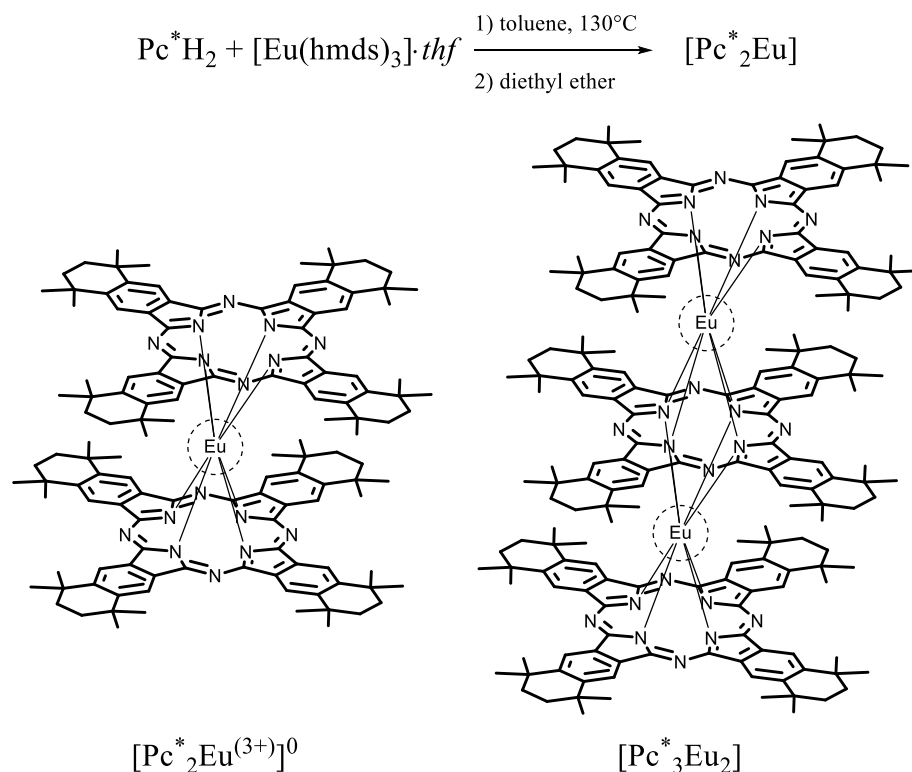


Scheme 68: Synthesis of group 1 metal phthalocyanines $[\text{Pc}^*\text{M}_2]$.

In the case of the synthesis of potassium phthalocyanine $[\text{Pc}^*\text{K}_2]$ from Pc^*H_2 using KHMDS, longer reaction times of >24 h were needed. The easier way to obtain $[\text{Pc}^*\text{K}_2]$ is when KBn is used. $[\text{Pc}^*\text{K}_2]$ was characterized by using ^1H NMR spectroscopy and UV-Vis spectroscopy. From $[\text{Pc}^*\text{Na}_2]$, an APCI-HR mass spectrum could be obtained. In UV-Vis spectroscopy, the difference between the Q-band absorption is clearly visible: while the Q-band of Pc^*H_2 is split, the Q-band of $[\text{Pc}^*\text{M}_2]$ with $\text{M} = \text{Na}, \text{K}$ shows only one sharp signal.

Several attempts were carried out to convert $[\text{Pc}^*\text{K}_2]$ to rare earth metal complexes $[\text{Pc}^*_2\text{M}^{\text{RE}}]$ (compare to Scheme 64, right side), but in most cases no selective reaction was observed. Here, the products were separated by column chromatography, giving the complexes in quite low yields. Furthermore, a direct synthesis using the $\text{PDN}^* \mathbf{1}$ with $[\text{M}^{\text{RE}}(\text{OAc})_3]$ was attempted

(compare to Scheme 64, left side), but the synthesis does not appear to be more selective. This might be due to described problems towards a change of solvent.^[124] Therefore, an alternative method was applied using $[M^{RE}(hmds)_3]$ and Pc^*H_2 (Scheme 69). In first attempts, almost no conversion was observed. After increasing the reaction time and temperature, after several days, a complete conversion was observed for $[Pc^*_2Eu]$ and $[Pc^*_2Tb]$ complexes. In test reactions, a complete formation of $[Pc^*_2M^{RE}]$ was observed for $M^{RE} = Sc, Y, La, Ce, Nd, Sm, Gd$ and Lu , using MALDI-ToF and UV-Vis spectroscopy.



Scheme 69: Synthesis of $[Pc^*_2Eu(3+)]^0$ using $[Eu(hmds)_3]$. Observed double-decker and triple-decker sandwich-complexes.

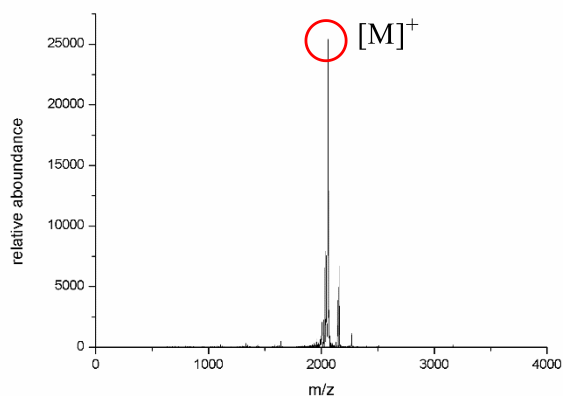
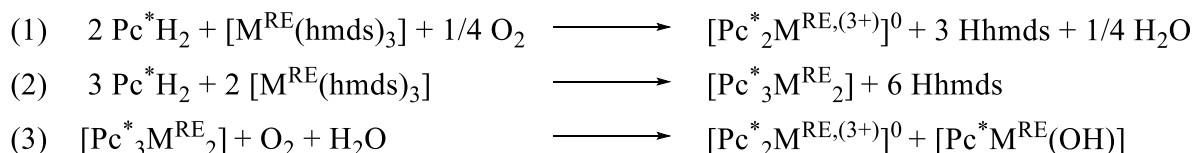


Figure 120: MALDI-ToF spectrum of $[Pc^*_2Eu]^0$.

The workup was carried out by washing the products with DEE to remove remaining traces of the $[M^{RE}(hmds)_3]$. Filtration through a short column of silica gave the pure complexes in the reported form $[Pc^*_2M^{RE}]^0$. In MALDI-ToF, full conversion of Pc^*H_2 to $[Pc^*_2Eu]$ was found (Figure 120).

Results and Discussion

In some cases, for other rare earth metals, the formation of triple-decker (Scheme 69) and quadru-decker complexes were observed. Then, the sandwich complexes were additionally purified using CC. Up to now, it can not be predicted when only double-decker and how only triple-decker complexes can be obtained, but a nice alternative synthetic route for $[\text{Pc}^*_2\text{M}^{\text{RE}}]$ was established and optimised. We propose that different reactions are taking place:



Via oxidation on air $[\text{Pc}^*_2\text{M}^{\text{RE}}]^0$ is formed (1), as it was observed in a similar literature known synthesis of $[\text{Pc}_2\text{M}^{\text{RE}}]^0$ complexes.^[246] When the reaction is carried out under inert atmosphere, the double-decker and triple-decker formation are competing processes (1+2). When a triple-decker is formed as main product, it can decompose to $[\text{Pc}^*_2\text{M}^{\text{RE}}]^0$ and $[\text{Pc}^*\text{M}^{\text{RE}}(\text{OH})]$ by oxidation in the presence of water (3). $[\text{Pc}^*\text{M}^{\text{RE}}(\text{OH})]$ may now degrade to the free ligand, which was observed in some cases. This is in accord with the observation that $[\text{Pc}^*_2\text{M}^{\text{RE}}]^0$ is obtained in higher yields of >40% when $[\text{M}^{\text{RE}}(\text{hmds})_3]$ is used in excess (~5 eq).

In UV-Vis spectroscopy, these $[\text{Pc}^{(2-)}\text{Pc}^{(-)}\text{M}^{\text{RE},3+}]^0$ show an intense Q-band and an additional broadened B-band/SORET band between 320 nm to 380 nm. Furthermore, shoulders of the Q-band and diagnostic radical bands are described, at about 500 nm.^[261] In comparison, neutral complexes of $[\text{Pc}_3\text{M}^{\text{RE}}_2]$ should show a sharp B-band and no absorption at 480-490 nm.^[261] In

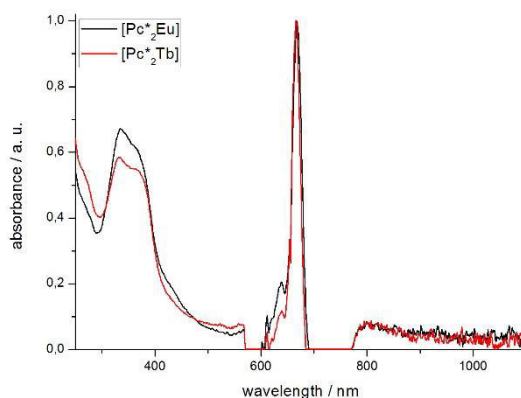


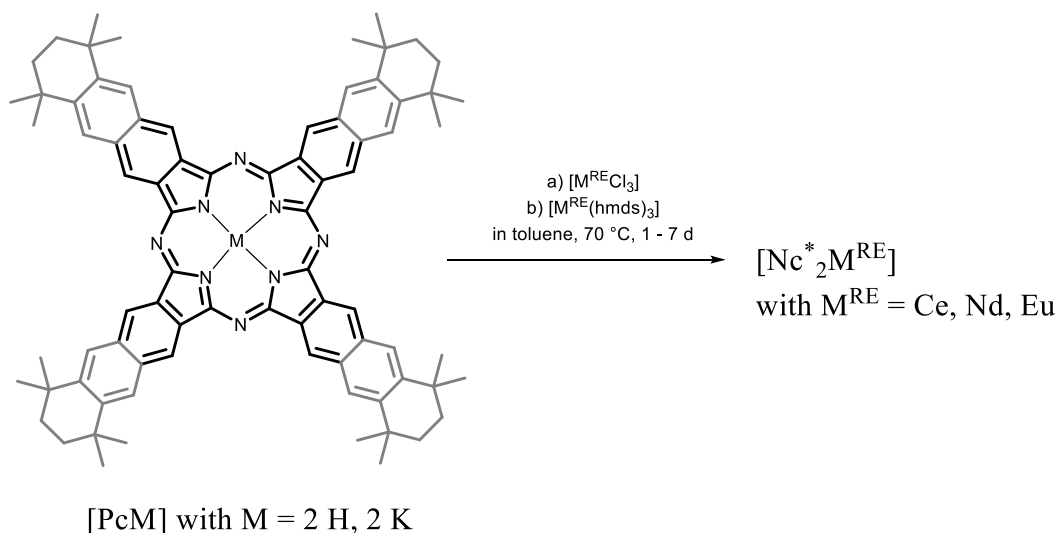
Figure 121: UV-Vis spectra of new rare earth metal complexes $[\text{Pc}^*_2\text{M}^{\text{RE}}]$ with $\text{M}^{\text{RE}} = \text{Eu}, \text{Tb}$.

both UV-Vis spectra, $[\text{Pc}^*_2\text{Eu}]$ and $[\text{Pc}^*_2\text{Tb}]$ (Figure 121), because of the noise of the UV-Vis device, the radical bands are poorly detected, but the shoulders of the Q-band at about 626 nm as well as the broadened B-bands are clearly visible. In addition, the absence of a bathochromically shifted band, which is expected for reduced complexes, is not observed.^[261]

4.5.5 Synthesis of New Naphthalocyanine Sandwich Complexes

Finally, the largest phthalocyanine homologue of this work Nc^*H_2 was tested in the synthesis of $[\text{Nc}^*_2\text{M}^{\text{RE}}]$. It is literature known that yields in the synthesis of $[\text{Pc}_2\text{M}^{\text{RE}}]$, using a respective phthalonitrile (PDN) and a rare earth metal salt, gradually depend on the size of the central metal atom, as well as on the targeted chromophore: Por,^[262] Pc,^[261] or Nc.^[124] Furthermore, the choice of the right solvent appears to be important and a separation of the side products, PcH_2 or NcH_2 , complicates the purification.^[124] A systematic study of rare earth metal naphthalocyanines was carried out by JIANG, investigating a $[\text{Nc}_2^{\text{tBu}}\text{M}^{\text{RE}}]$ series with $\text{M} = \text{La}, \text{Ce}, \text{Pr}, \text{Nd}, \text{Eu}, \text{Gd}, \text{Tb}, \text{Y}, \text{or Er}$ spectroscopically and electrochemically.^[124]

The first pure naphthalocyanine sandwich-complex in our group was synthesised by VOLLGRAFF.^[140] VOLLGRAFF was able to use the precyclised Nc^*H_2 and $[\text{Ce}(\text{hmds})_3]$ to obtain $[\text{Nc}^*_2\text{Ce}]$ (Scheme 70). The reaction takes quite a long time, >72 h, caused by the low basicity of the *hmds* compared to the strongly bonded protons in the $[-\text{N}_4-]$ core of the ligand. But compared to a reaction of $[\text{Nc}^*\text{K}_2]$ with $[\text{M}^{\text{RE}}\text{Cl}_3]$, it appears more straight forward and less harsh. The main advantage in the developed synthesis was the complete conversion to $[\text{Nc}^*_2\text{M}^{\text{RE}}]$ complexes when $[\text{M}^{\text{RE}}(\text{hmds})_3]$ is used in excess. After washing several times with DEE and filtration through a short column of silica the oxidised complex, $[\text{Nc}^*_2\text{Ce}]^0$, was obtained.



Scheme 70: Synthesis of naphthalocyanine complexes $[\text{Nc}^*_2\text{M}^{\text{RE}}]^0$.

La	Ce	Pr	Nd	Pm	Sm	Eu	Gd	Tb	Dy	Ho	Er	Tm	Yb	Lu
----	----	----	----	----	----	----	----	----	----	----	----	----	----	----

Red: Attempted, but not observed; - blue: synthesised complexes $[\text{Nc}^*_2\text{M}^{\text{RE}}]$; - white: not attempted.

With the exception of $[\text{La}(\text{hmds})_3]$, in which case only decolouration was observed, several metals formed a $[\text{Nc}^*_2\text{M}^{\text{RE}}]$ complex with $\text{M}^{\text{RE}} = \text{Ce}, \text{Pr}, \text{Nd}, \text{Eu}, \text{Tb}$ and Dy . Of $[\text{Nc}^*_2\text{M}^{\text{RE}}]$

Results and Discussion

complexes with $M = \text{Ce}, \text{Nd}, \text{Eu}$, a sufficient amount for complete analysis was isolated. In Figure 122, the obtained MALDI-ToF spectrum of $[\text{Nc}^*_2\text{Ce}]$ is shown, as well as the isotopic pattern. In Figure 123, the UV-Vis spectrum of $[\text{Nc}^*_2\text{Ce}]$ is shown, representing a typical spectrum for $[\text{Nc}^*_2\text{M}^{\text{RE}}]$.^[124]

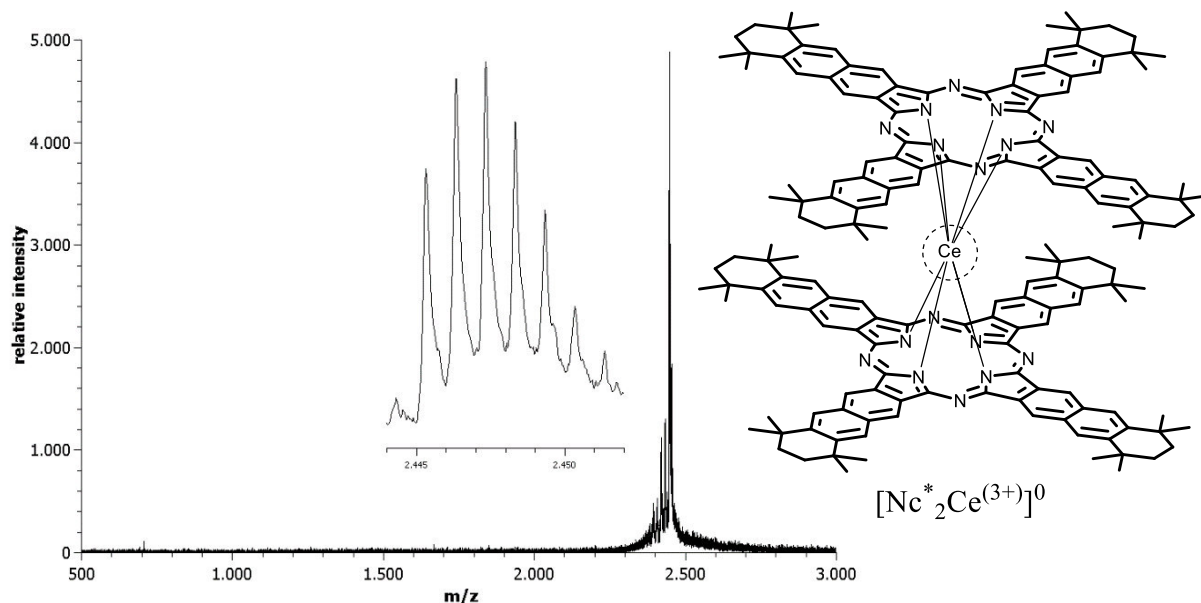


Figure 122: MALDI-ToF spectrum of $[\text{Nc}^*_2\text{Ce}]$. In the separated window the isotopic pattern is resolved.

UV-Vis spectra of investigated metal complexes $[\text{Nc}^*_2\text{M}^{\text{RE}}]$, with $\text{M}^{\text{RE}} = \text{Ce}, \text{Pr}, \text{Nd}, \text{Eu}, \text{Tb}$ and Dy , show the expected behaviour: a hypsochromic shift of the Q-band when the ionic radius of the central metal ion increases.^[124] Here, from about 800 nm ($[\text{Nc}^*_2\text{Ce}]$) to 778 nm ($[\text{Nc}^*_2\text{Eu}]$). In comparison to all the other spectra shown in this work, the UV-Vis spectrum of $[\text{Nc}^*_2\text{Ce}]$ shows two

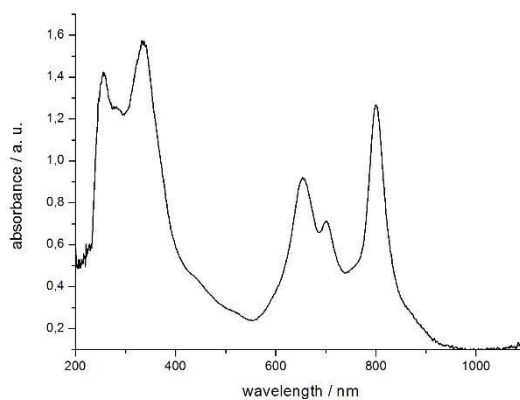


Figure 123: UV-Vis spectrum of $[\text{Nc}^*_2\text{Ce}]$ complex, in DCM at rt.

additional bands at 701 nm and 656 nm. These signals can be assigned to the one-electron ligand-oxidised structure.^[124] In literature, reduction experiments of $[\text{Nc}^{t\text{Bu}}_2\text{M}^{\text{RE}}]$ have been carried out using NaBH_4 , ending up in the formation of an anionic complex $[\text{Nc}^{t\text{Bu}}_2\text{M}^{\text{RE}}]^-$.^[124] A faster/easier reduction of the metal centre was observed, the larger the M^{RE} in the centre is. A reduction with NaBH_4 took for $[\text{Nc}^{t\text{Bu}}_2\text{Ce}]$ just a view minutes, while the smaller metal ion Lu in $[\text{Nc}^{t\text{Bu}}_2\text{Lu}]$ needed several hours. In a first attempt to reduce $[\text{Nc}^*_2\text{Ce}]$, after 10 min no change in the UV-Vis spectrum was observed, which might be caused by the even more sterically demanding alkyl substitution pattern.

Not only the UV-Vis spectra, but also the IR spectra are significant for these compounds. In the case of the $[\text{Nc}^*{}_{2}\text{M}^{\text{RE}}]$, signals at about $1313\text{-}1329\text{ cm}^{-1}$ are diagnostic for the radical ligand $\text{Nc}^{\cdot-}$ (Figure 124).^[124] The band at 1316 cm^{-1} , shown in the example of $[\text{Nc}^*{}_{2}\text{Nd}]$ of the Bachelor-Thesis of SWOLANA, indicates the radical nature of the ligand.

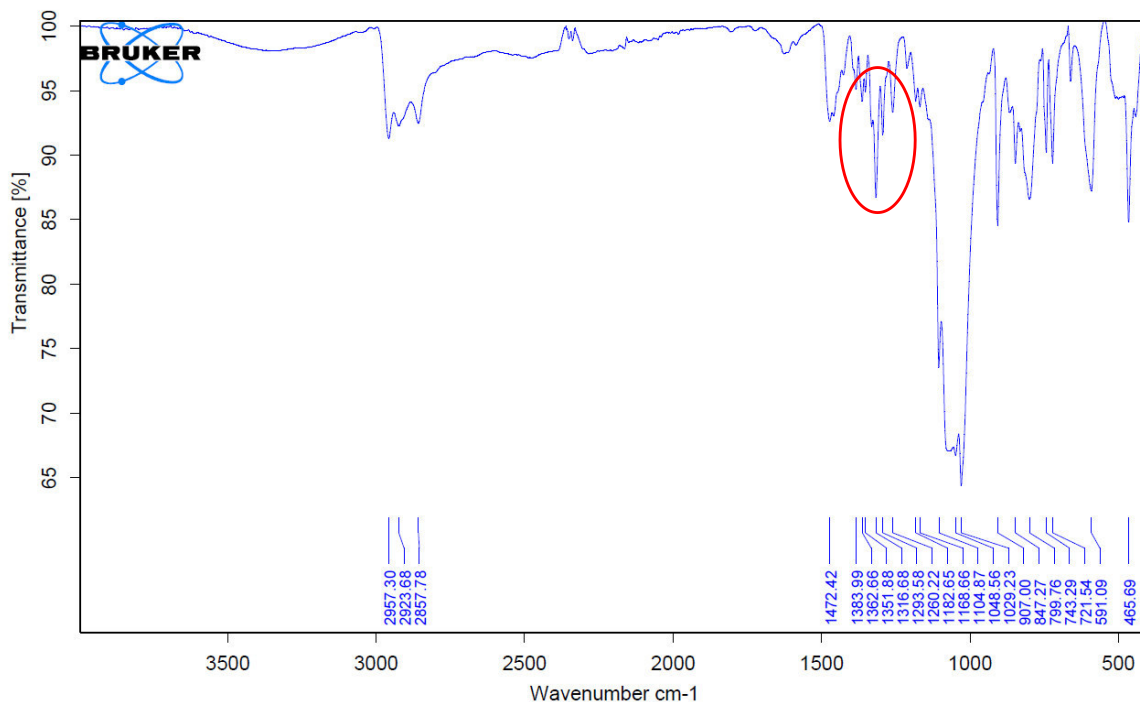


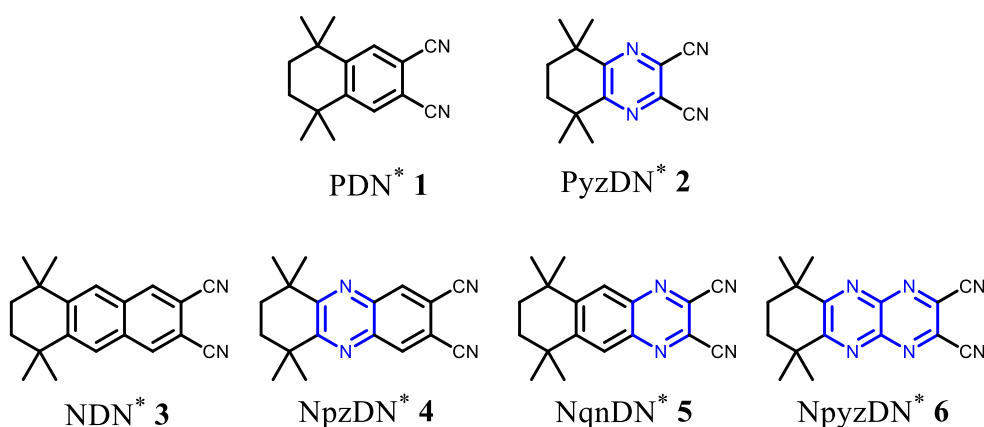
Figure 124: ATR-IR spectrum of $[\text{Nc}^*{}_{2}\text{Nd}]$, indicating the radical character of one ligand in the $[\text{Nc}^{(2-)}\text{Nc}^{(-)}\text{Nd}]$ one-electron ligand-oxidised structure.

Summary. In the last chapter of this work, several rare earth metal complexes were synthesised, using $[\text{M}^{\text{RE}}(\text{hmds})_3]$ as metal precursor and the free ligand Pc^*H_2 or Nc^*H_2 . The advantage of this developed synthetic route is the complete conversion to a $[\text{Pc}^{(*)}{}_{2}\text{M}^{\text{RE}}]$ or $[\text{Nc}^*{}_{2}\text{M}^{\text{RE}}]$ complex, so no separation of residual ligand $\text{Pc}^{(*)}\text{H}_2$ or Nc^*H_2 has to be carried out by CC. The most selective synthesis was observed using Nc^*H_2 , yielding only $[\text{Nc}^*{}_{2}\text{M}^{\text{RE}}]$. In the case of $[\text{Pc}^*{}_{2}\text{M}^{\text{RE}}]$, some triple-, besides the double-decker, sandwich complexes could be observed, so further purification by column chromatography was obligatory. In future, these reaction parameters could be optimised for a more detailed prediction of the reaction products. In addition, TGA/DSC measurements should be carried out for following physical investigations with our cooperation partners from the Department of Physics at the Philipps-Universität Marburg. In accordance with other literature described complexes, the one-electron ligand-oxidised form $[\text{Nc}^{(2-)}\text{Nc}^{(-)}\text{M}^{\text{RE}}]$ could be proved by using UV-Vis and IR spectroscopy as well as MS. Complexes of $[\text{Pc}^{(*)}{}_{2}\text{M}^{\text{RE}}]$ with $\text{M}^{\text{RE}} = \text{Eu}, \text{Tb}$ and $[\text{Nc}^*{}_{2}\text{M}^{\text{RE}}]$ with $\text{M}^{\text{RE}} = \text{Ce}, \text{Nd}$ and Eu were synthesised and characterised.

5 Zusammenfassung

Ziel dieser Arbeit, die im Rahmen des SFB1083 durchgeführt wurde, war die Synthese und Charakterisierung von Phthalocyaninen (Pc) und Pyrazinoporphyrazinen (Ppz) sowie deren Hybridverbindungen, sogenannten Azaphthalocyaninen (N_x -[PcM] mit M = zentrales Metallatom oder 2 H), und höheren Homologen, den Naphthalocyaninen (Nc). Fokus der Arbeit war, neben der optoelektronischen Anwendung ausgewählter Verbindungen in Farbstoffsolarzellen (DSSCs), die systematische Untersuchung der Verbindungen in Bezug auf ihre optische Anregung im UV-Vis-Bereich im Vergleich zu zykovoltammetrischen Messungen sowie die Korrelation der photophysikalischen Eigenschaften, wie Singulett-Sauerstoff-, Fluoreszenz-Quantenausbeuten und Fluoreszenzlebenszeit.

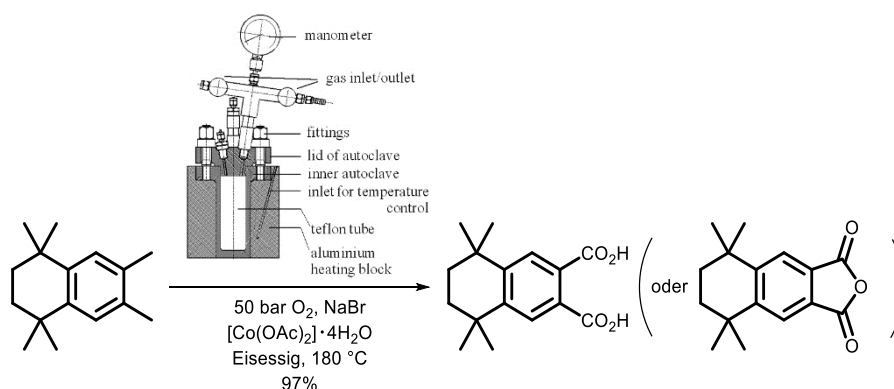
Organische Vorläufer: Neben den literaturbekannten Verbindungen PDN* 1, PyzDN* 2 und NDN* 3 wurden erstmalig die nächst größeren azasubstituierten Homologen NpzDN* 4, NqnDN* 5 und NppzDN* 6 dargestellt. Die in Kapitel 4.1 vorgestellten Verbindungen stellen die erste vollständige Serie an C_{2v} -symmetrischen Naphthalonitrilen mit Alkylgruppen in den peripheren Positionen dar, bei der systematisch die [-CH=]-Baugruppen der Aromaten gegen [-N=]- ausgetauscht wurden.



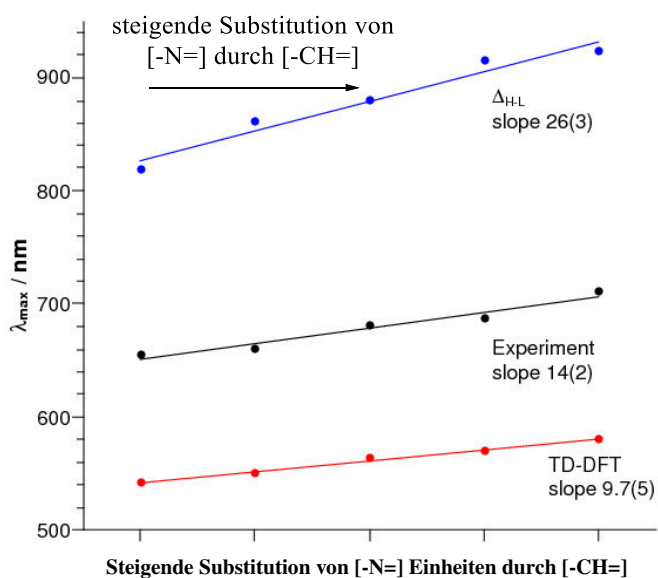
Vorteil dieser Verbindungen gegenüber dem kommerziell erhältlichen PDN^{tBu} ist die Annelierung eines 2,2,5,5-Tetramethylcyclohexanringes. Zum einen wird dadurch die für Pc typische Aggregation minimiert und deren Löslichkeit in gängigen organischen Lösungsmitteln erhöht, zum anderen bilden sich bei der Zyklisierung von C_{2v} -symmetrischen Phthalonitrilen zum A₄-Typ-Chromophor im Vergleich zum [Pc^{tBu}M] keine 4 Regioisomere aus. Durch die Symmetrie der A₄-Moleküle wird die Analyse der Verbindungen deutlich vereinfacht und die Einkristall-Röntgenstrukturanalyse begünstigt.

Zusammenfassung

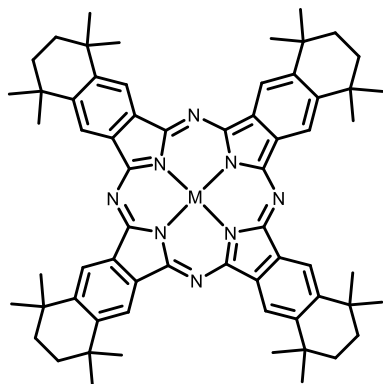
Der Schlüsselschritt in der Synthese von PDN* **1** ist die Oxidation des Tetralinsystems zur Dicarbonsäure. Die Gesamtausbeute in der von MIKALENKO entwickelten Synthese war, aufgrund der gewählten Bedingungen in diesem Oxidationsschritt, mit 30% über sieben Stufen bisher vergleichsweise niedrig. Als Oxidationsmittel diente ein Überschuss an Kaliumpermanganat in Pyridin. Dabei wurde eine mäßige Ausbeute von unter 60% erhalten. Die Seitenkettenoxidation wurde in Anlehnung an bekannte Industrieprozesse, etwa der aeroben *p*-Xylol zu Terephthalsäure-Oxidation, zu einem katalytischen Verfahren mit 97% Ausbeute ausgearbeitet.



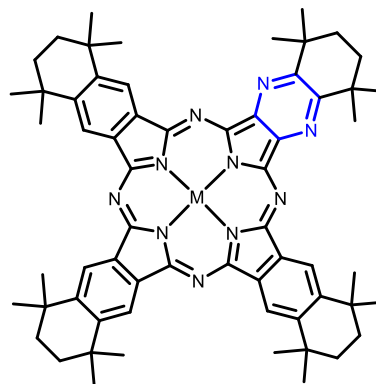
Azaphthalocyanine des Typs N_x-[Pc* M] mit M = 2 H oder Zn wurden aus der Cozyklisierung der Dinitrile PDN* **1** und dem PyzDN* **2** bzw. durch anschließende Metallierung der chromatographisch separierten Verbindungen N_x-Pc*H₂ mit [Zn(hmds)₂] oder [Zn(OAc)₂] dargestellt. Die Azaphthalocyanine N_x-[Pc* M] mit x = 0, 2, 4, 6 oder 8 N-Atomen werden in Kapitel 4.2 beschrieben und diskutiert. Dabei konnte die Serie um die noch unbekannt Verbindung vom ABAB-Typ N₄-[Pc* M] mit M = 2 H, Zn ergänzt und erstmals vollständig mittels NMR-, FS- und UV-Vis-Spektroskopie und Massenspektrometrie charakterisiert werden. Die beiden Strukturisomere A₂B₂ und ABAB konnten dabei eindeutig über ¹H-NMR- und UV-Vis-Spektroskopie zugeordnet werden. Neben der Cozyklisierung konnten die Verbindungen A₂B₂ N₄-[Pc* M] und A₃B N₂-[Pc* M] auch über eine KOBAYASHI-Ringerweiterung aus dem



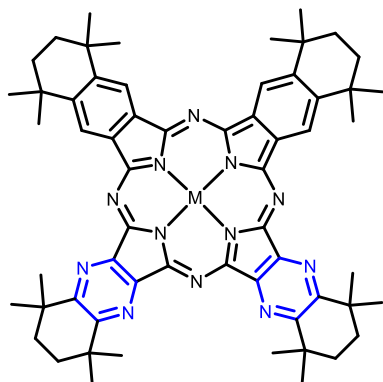
jeweiligen Subphthalocyanin $AB_2 N_4$ -[Sp c^*BCl] bzw. $A_2B N_2$ -[Sp c^*BCl] und dem Isoindolin des PDN * **1** dargestellt werden. Das HOMO-LUMO *gap* der Verbindungen N_x -Pc *H_2 wurde mittels zyklischer Voltammetrie ermittelt.



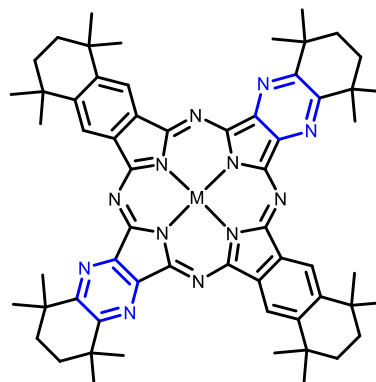
A_4 ; [Pc *M]
Phthalocyanin mit $M = 2 H, Zn$



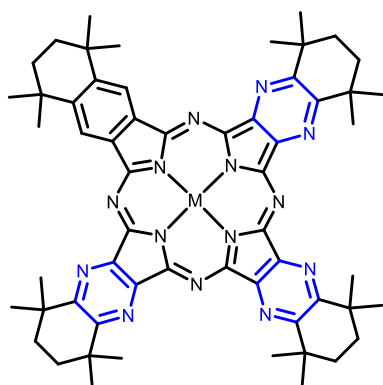
A_3B ; N_2 -[Pc *M]
Diazaphthalocyanin mit $M = 2 H, Zn$



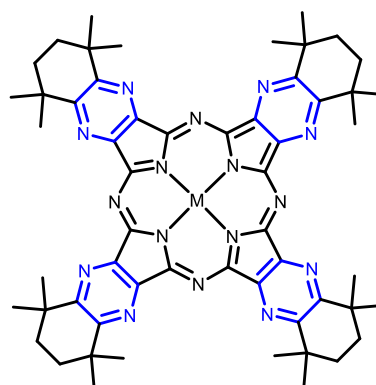
A_2B_2 ; N_4 -[Pc *M]
Tetraazaphthalocyanin mit $M = 2 H, Zn$



$ABAB$; N_4 -[MPc *M]
Tetraazaphthalocyanin mit $M = 2 H, Zn$



AB_3 ; N_6 -[Pc *M]
Hexaazaphthalocyanin mit $M = 2 H, Zn$

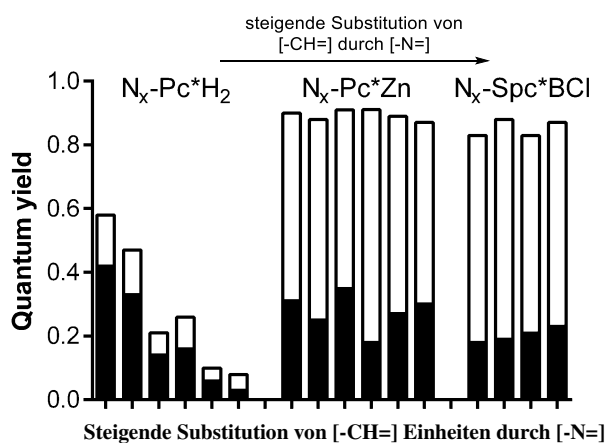


B_4 ; N_8 -[Pc *M]
Octaazaphthalocyanin mit $M = 2 H, Zn$
oder Pyrazinoporphyrazine [Ppz *M]

Zusammenfassung

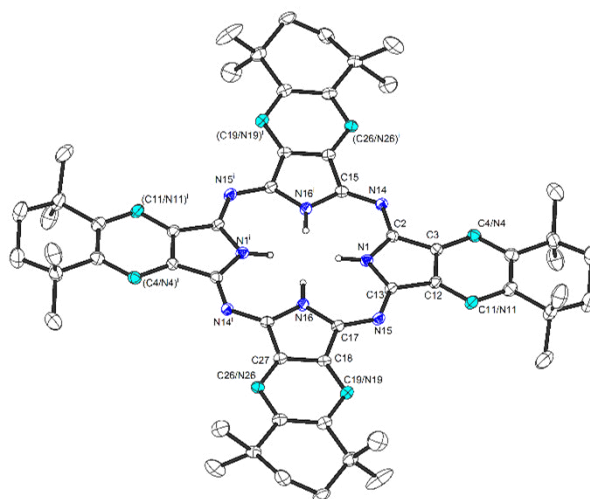
Die experimentell ermittelten Daten der UV-Vis-Spektroskopie und CV wurden mit Ergebnissen von TD-DFT-Rechnungen in Kooperation mit der AG TONNER (Fachbereich Chemie der Philipps-Universität Marburg) verglichen. Dabei wurde ein nicht perfekt linearer Trend der hypsochromen Verschiebung der Q-Bande sowie eine Vergrößerung des HOMO-LUMO *gaps* mit steigender Substitution der [-CH=]-Einheiten durch [-N=]- in den nicht-peripheren Positionen beobachtet. Ursache der Zunahme ist die stärkere energetische Absenkung des HOMOs relativ zu der des LUMOs mit zunehmender Zahl an N-Atomen im Azaphthalocyanin $N_x-[Pc^*M]$.

Weiteren wurden die Verbindungen auf ihre photophysikalischen Eigenschaften hin untersucht. Die Singulett-Sauerstoff-Quantenausbeuten (Φ_Δ , schwarze Balken) sowie Fluoreszenz-Quantenausbeuten (Φ_F , weiße Balken) und -Lebenszeiten (τ_F) wurden in Kooperation mit ZIMČÍK und NOVÁKOVÁ (Fachbereich Pharmazie der



Charles-University in Prague) bestimmt. In der Verbindungsserie $N_x-[Pc^*Zn]$ wurde die höchste Singulett-Sauerstoff-Quantenausbeute für die Verbindung des ABAB-Typs $N_4-[Pc^*Zn]$ beobachtet. Alle $N_x-[Pc^*Zn]$ weisen in Summe $\Phi_\Delta + \Phi_F$ Werte von ~ 0.9 auf. Einen bisher noch nicht beschriebenen Trend zeigt im Vergleich dazu die Verbindungsserie $N_x-Pc^*H_2$ auf, wobei die Werte $\Phi_\Delta + \Phi_F$ mit steigender [-N=]-Substitution deutlich absinken.

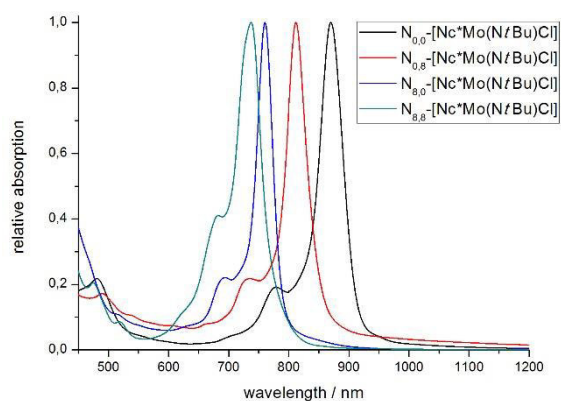
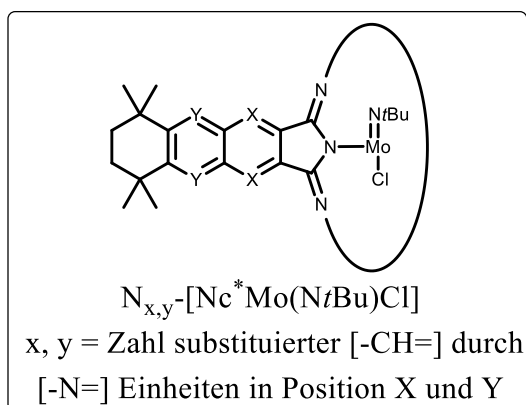
Erstmalig konnte in dieser Arbeit ein asymmetrisches 2,2,5,5-tetramethylcyclohexanringssubstituiertes Azaphthalocyanin des A_3B -Typs $N_2-Pc^*H_2$ röntgenographisch untersucht werden. Wie bei peripher-substituierten Phthalocyaninen häufiger beobachtet, sind die Moleküle in ihrer kristallinen Packung im Gegensatz zu unsubstituierten Phthalocyaninen



gegeneinander verkippt. Aufgrund der charakteristischen statistischen Fehlordnung ließen sich weder in dieser noch in der Struktur des A_2B_2 -Typs $N_4-[Pc^*Zn]$ die [-CH=]- und [-N=]-Gruppen eindeutig zuordnen. Im A_3B -Typ $N_2-Pc^*H_2$ weisen sie zu 25% eine berechnete Besetzung der

[-CH=]- durch [-N=]-Einheiten auf. Wie in Kapitel 4.2.6 diskutiert, wurden im Rahmen der Bachelorarbeit von LANGE die Azaphthalocyanin-Serie $N_x\text{-Pc}^*\text{H}_2$ um eine weitere Benzoleinheit zu sogenannten Azanaphthalopyrazinen $N_x\text{-Npz}^*\text{H}_2$ anneliert. Auch hier konnte die Serie um das ABAB $N_4\text{-Npz}^*\text{H}_2$ ergänzt und von dem strukturellen Isomer A_2B_2 über $^1\text{H-NMR}$ - und UV-Vis-Spektroskopie differenziert werden.

Azanaphthalocyanine des Typs $N_{x,y}\text{-[Nc}^*\text{M(NR)Cl]}$ mit $M = \text{Mo, W}$ und $R = t\text{Bu, Mes}$ mit dem beschriebenen annelierten 2,2,5,5-Tetramethylcyclohexanring konnten erstmals mit Metallen der Gruppe 6 (W, Mo) aus den Dinitrilen **3-6** dargestellt werden.

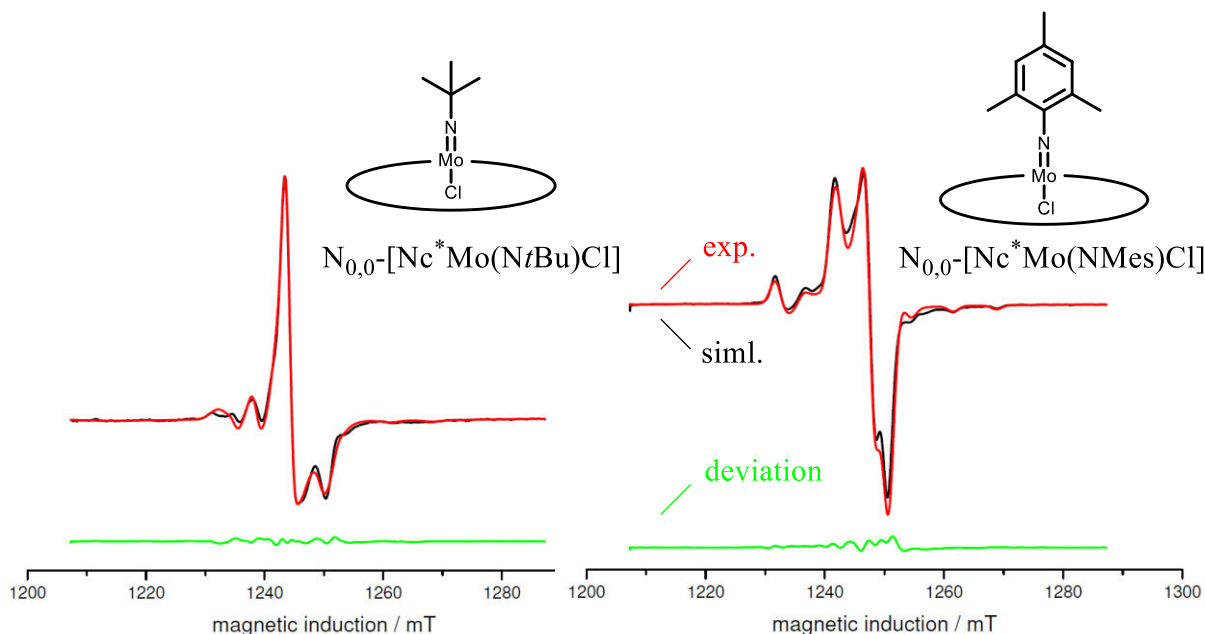


$x = y = 0$	$N_{0,0}\text{-[Nc}^*\text{Mo(N}t\text{Bu)Cl]} = [\text{Nc}^*\text{M}]$	anelliertes Naphthalocyanin
$x = 0, y = 8$	$N_{0,8}\text{-[Nc}^*\text{Mo(N}t\text{Bu)Cl]} = [\text{Npz}^*\text{M}]$	methyliertes (tetrahydro)Phenanzin
$x = 8, y = 0$	$N_{8,0}\text{-[Nc}^*\text{Mo(N}t\text{Bu)Cl]} = [\text{Nqn}^*\text{M}]$	anelliertes Quinoxalin
$x = y = 8$	$N_{8,8}\text{-[Nc}^*\text{Mo(N}t\text{Bu)Cl]} = [\text{Npz}^*\text{M}]$	anelliertes Pyrazinopyrazin

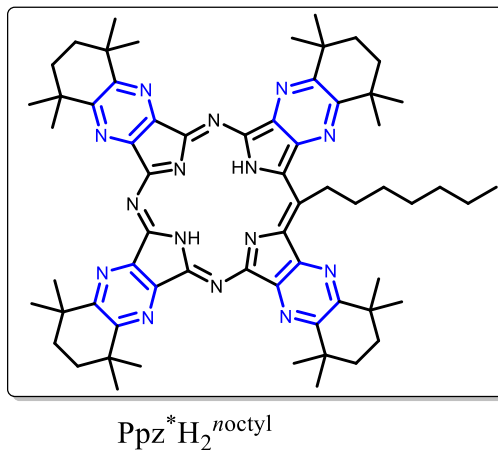
Die Reihe der Verbindungen $N_{x,y}\text{-[Nc}^*\text{M(NR)Cl]}$ mit $M = \text{Mo}$ und $R = t\text{Bu}$ stellt dabei die erste bekannte C_{4v} -symmetrische Azanaphthalocyanin-Serie mit Alkylresten in den peripheren Positionen dar (Kapitel 4.2.9). Die Q-Banden der Verbindungen $N_{0,0}\text{-[Nc}^*\text{Mo(N}t\text{Bu)Cl]}$, $N_{0,8}\text{-[Nc}^*\text{Mo(N}t\text{Bu)Cl]}$, $N_{8,0}\text{-[Nc}^*\text{Mo(N}t\text{Bu)Cl]}$ und $N_{8,8}\text{-[Nc}^*\text{Mo(N}t\text{Bu)Cl]}$ weisen im UV-Vis-Spektrum mit steigender [-N=]-Substitution und Nähe zum Metallzentrum [-MN₄-] eine hypsochrome Verschiebung von 900 nm nach 700 nm auf. Die Verbindungen wurden über UV-Vis-Spektroskopie, Elementaranalyse sowie massenspektrometrische Methoden, wie LIFDI oder MALDI-ToF, charakterisiert. Die Verbindungen $N_{0,0}\text{-[Nc}^*\text{Mo(NR)Cl]}$ mit $R = t\text{Bu, Mes}$ wurden zusätzlich mittels EPR-Spektroskopie analysiert. Dabei ist der strukturelle Unterschied des orthorhombischen $N_{0,0}\text{-[Nc}^*\text{Mo(NMes)Cl]}$ zum axialsymmetrischen $N_{0,0}\text{-[Nc}^*\text{Mo(N}t\text{Bu)Cl]}$ deutlich sichtbar. Dies kann auch eine Erklärung für die starke

Zusammenfassung

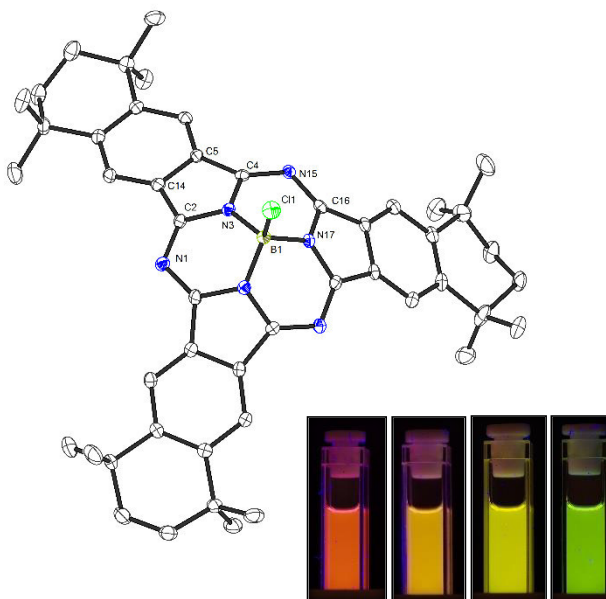
Verschiebung der Q-Banden von 27 nm sein. DFT-Rechnungen der Arbeitsgruppe BERGER sollen dies zukünftig belegen.



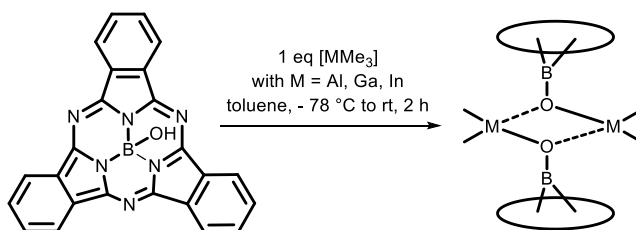
Neben der Synthese der Gruppe 6 d^1 -Metall-Naphthalocyaninkomplexe wurde ein Zugang zu den freien Liganden $N_{x,y}-Nc^*H_2$ und deren Zinkkomplexen $N_{x,y}-[Nc^*Zn]$ getestet. Die Verbindungen $N_{0,0}-Nc^*H_2$, $N_{0,8}-Nc^*H_2$ sowie $N_{0,0}-[Nc^*Zn]$ bzw. $N_{0,8}-[Nc^*Zn]$ konnten in Analogie zu literaturbekannten Synthesen (Kapitel 4.2.10) dargestellt werden. $N_{8,0}-[Nc^*Zn]$ konnte aus dem Dinitrilpräkursor **5** und $[ZnCl_2]$ in Chinolin bei 230 °C nach 12 h in 29% Ausbeute erhalten werden. Bei den Versuchen die Verbindungen $N_{8,0}-Nc^*H_2$ bzw. $N_{8,8}-Nc^*H_2$ darzustellen, konnte in Analogie zur Synthese des Ppz^*H_2 eine erhöhte Tendenz zur Bildung eines meso-substituierten Komplexes $Ppz^*H_2^{noctyl}$ bzw. $N_{8,0}-Nc^*H_2^{noctyl}$ gefunden werden. Der genaue Bildungsmechanismus sowie die Isolierung der Reinverbindungen muss in Folgestudien durchgeführt werden. $N_{8,0}-Nc^*H_2$ konnte per DC isoliert und massenspektrometrisch und UV-Vis-spektroskopisch untersucht werden. Bei dem Versuch der Zyklisierung von Verbindung **6** zum $N_{8,8}-[Nc^*Zn]$ -Komplex konnte per Massenspektrometrie und UV-Vis-Spektroskopie die Bildung des Naphthalopyrazinoporphyrzins belegt werden.



Subphthalocyanine (SpC) der 2,2,5,5-Tetramethylcyclohexanringsysteme konnten reproduziert und axial funktionalisiert werden. Dabei wurde eine Serie der ringkontrahierten regenschirmartigen Phthalocyanin-homologen [SpC*BR] sowie die erste Serie von Subpyrazinoporphyrazinen [Sppz*BR] mit R = F, Cl, Br, OH dargestellt und charakterisiert. SpC absorbieren in ihrer Q-Bande durch das kleinere π -System im höher energetischen Bereich von 580 nm die elektronenärmeren Sppz bei 534 nm. Die rechts abgebildeten Küvetten (FS, beleuchtet bei $\lambda = 365$ nm) der neu dargestellten



Azasubphthalocyanin Serie, N_x -[SpC*BCl] mit $x = 0, 2, 4$ und 6 (von links nach rechts), verdeutlichen die Unterschiede im Absorptions- und Emissionsverhalten durch Austausch der [-CH=]- durch [-N=]-Baugruppen. Die Molekülstruktur des [SpC*BCl] stellt eine der wenigen röntgenkristallographisch untersuchten alkylsubstituierten SpC dar. Des Weiteren wurden erste Metall-Boratkomplexe des Typs $[Me_2M(\mu-OBSpc)]_2$ mit $M = Al, Ga$ erfolgreich aus $[MMe_3]$ und [SpCBOH] dargestellt. Die Charakterisierung der Verbindungen erfolgte mittels 1H -NMR-, IR-, UV-Vis- und FS-Spektroskopie. Aufgrund von massenspektrometrischen Experimenten, wie MALDI-ToF, wurde auf eine dinukleare Struktur geschlossen. Wie bei axialen Substitutionen von Phthalocyaninen konnte auch bei den Subphthalocyaninkomplexen $[Me_2M(\mu-OBSpc)]_2$ mit $M = Al, Ga$ im UV-Vis-Spektrum nur eine geringe Verschiebung der Q-Bande von 1 nm im Vergleich zum [SpC*BOH] beobachtet werden.



Im Anschluss wurden erste Versuche der Synthese von mehrfach borato-koodinierten Metallkomplexen durchgeführt. Dabei konnten $[(SpCBO)_4Ti]$ und $[(SpCBO)_3B]$ beobachtet und charakterisiert werden.

Die Anwendung als Photosensitizer in Dye Sensitized

Solar Cells (DSSC) konnte für äquatorial funktionalisierte

Verbindungen getestet werden. Die Synthese der

funktionalisierten Pc ist in Kapitel 4.3 besprochen. Dabei

wurden zum einen unsubstituierte A₃B-Pc des [PcZn]^{FG}-

Typs mit diversen Ankergruppen (FG =

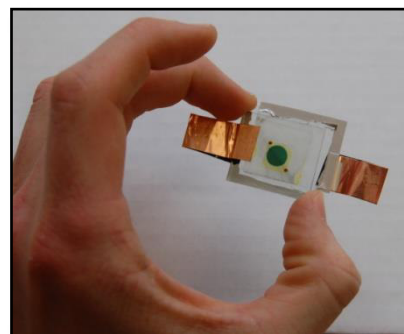
Vinylphosphonsäure, Vinylcarbonsäure, Phosphonsäure

oder Catecholat-Gruppen) über eine KOBAYASHI-Ringerweiterungsreaktion dargestellt, zum

anderen 2,2,5,5-tetramethylcyclohexanringsubstituierte Verbindungen mit Catecholatgruppen

als Anker, [Pc^{*}M]^{OH} mit M = 2 H, Zn, über eine Cozyklisierung mit bis zu 10% Ausbeute

erhalten.



Die Verbindungen konnten erfolgreich

auf mesoporösen ZnO-

Halbleiterschichten verankert werden

und es konnten Strom-Spannungs-

kennlinien- sowie IPCE-Messungen

durchgeführt werden. Die Messungen

wurden in Kooperation mit der AG

SCHLETTWEIN (Fachbereich Physik

der Justus-Liebig-Universität Gießen)

durchgeführt. Die beste Ankergruppe, in Bezug auf den damit verbundenen Elektronentransfer

zum Halbleiter ZnO, stellt der Phosphonsäureanker der Verbindung [PcZn]^{vPA} ($\eta = 0.5\%$) dar,

gefolgt von der Vinylcarbonsäure [PcZn]^{vCA} ($\eta = <0.2\%$) und dem 1,2-Diol [PcZn]^{OH}

($\eta \sim 0.001\%$). Im Vergleich dazu konnte für das alkylsubstituierte [Pc^{*}Zn]^{OH} ein deutlich

verbesserter Elektronentransfer gegenüber dem [PcZn]^{OH} beobachtet werden. Die Effizienz des

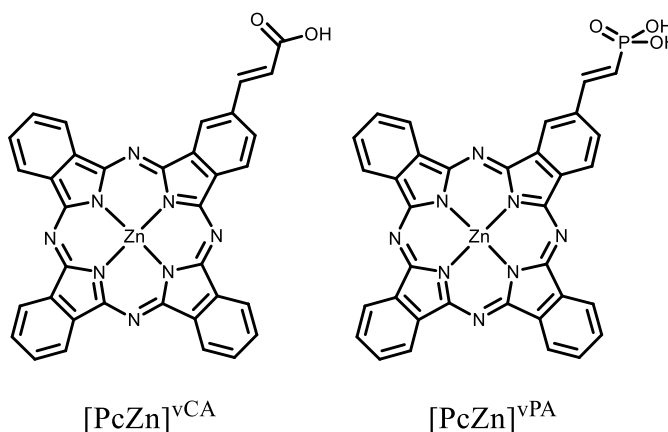
[Pc^{*}Zn]^{OH} konnte durch die Substitution mit Alkylresten um einen Faktor 10 verbessert werden,

liegt aber dennoch bei $\eta \sim 0.01-0.02\%$. Dies belegt unter anderem die Rekombinations-/

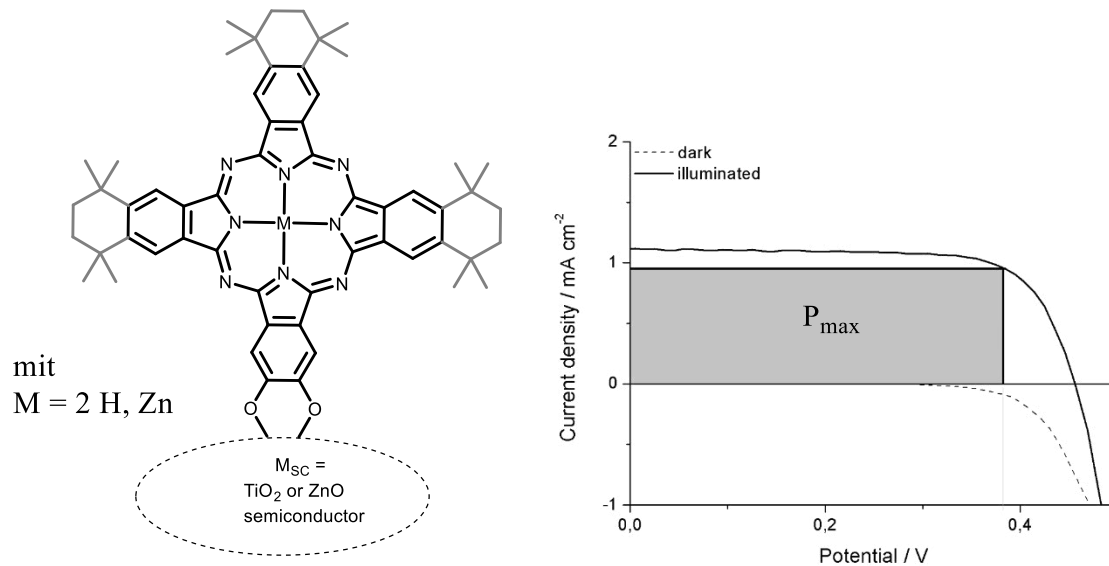
Desaktivierungsprozesse, die durch die starke Aggregation der unsubstituierten Pc bedingt sind,

aber auch den effizienten elektronenschiebenden Charakter der Alkylreste. Im Vergleich zum

[Pc^{*}Zn]^{OH} wurde auch das metallfreie Pc^{*}H₂^{OH} vermessen. In Analogie zu der Serie der



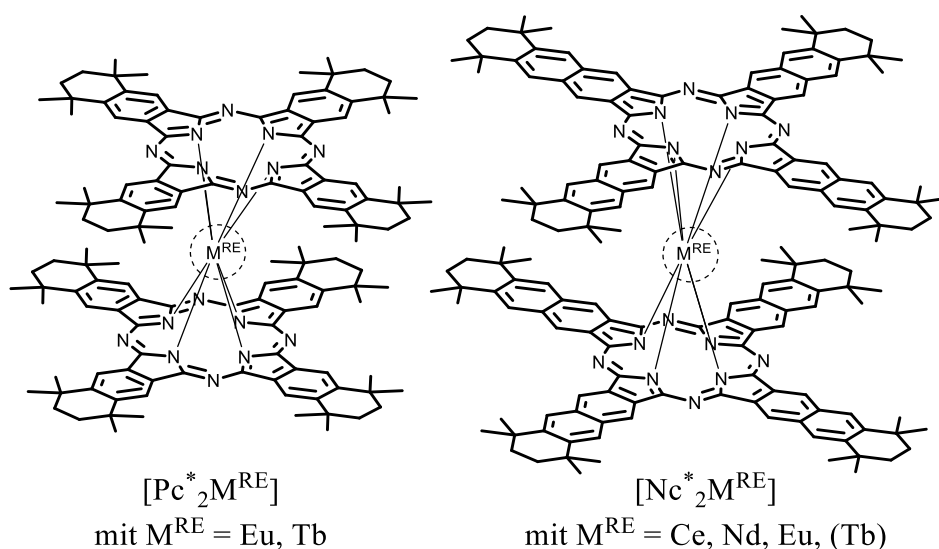
N_x -[Pc* M] mit $M = 2 H, Zn$ konnten zunehmende "Quenching"-Prozesse und somit geringere Effizienzen für die metallfreien Liganden beobachtet werden.



In aktuell laufenden Messungen werden die gebauten Messzellen auf ihre Photolumineszenz hin untersucht. Hierbei konnte bereits jetzt ein schneller Ladungstransfer zum Halbleiter hin beobachtet werden, jedoch ebenso eine schnelle Rekombination, wodurch nur ein schlechter Elektrontransfer und somit die niedrigen Effizienzen der Zellen erklärt werden können. In Zukunft wäre eine weitere Modifikation des oben dargestellten, gut zugänglichen $[Pc^*Zn]^{OH}$ zu einem mit Vinylphosphonsäureanker substituierten A₃B-Typ Phthalocyanins $[Pc^*Zn]^{vPA}$ oder $[Pc^*Zn]^{vCA}$ denkbar.

Phthalocyanin-Sandwich-Komplexe des Typs $[\text{Pc}^*_2\text{M}^{\text{RE}}]$ bzw. $[\text{Nc}^*_2\text{M}^{\text{RE}}]$ konnten für die Seltenerdmetalle des $\text{M}^{\text{RE}} = \text{Eu}, \text{Tb}, \text{Ce}$ und Nd erhalten werden. Die Seltenerdmetalle Eu^{3+} und Tb^{3+} wurden aufgrund des zum $f^7\text{-Gd}^{3+} +/ - 1/2$ veränderten Spins in Anlehnung an die vielfach untersuchten Gd-Phthalocyaninkomplexe gewählt.

Der einfachste Zugang zu $[\text{Pc}^*_2\text{M}^{\text{RE}}]$ und $[\text{Nc}^*_2\text{M}^{\text{RE}}]$ erfolgte durch die Umsetzung der freien Liganden Pc^*H_2 bzw. Nc^*H_2 mit $[\text{M}^{\text{RE}}(\text{hmds})_3]$. Für eine vollständige Bildung der entsprechenden $[(\text{Pc})^-(\text{Pc}')^{2-}\text{M}^{\text{RE},3+}]^0$ -Komplexe wurden Reaktionszeiten von bis zu 7 d bei $110\text{ }^\circ\text{C}$ in Toluol gewählt. Die Sandwich-Komplexe weisen eine typische Aufspaltung der B-Bande im UV-Vis-Spektrum bei 323-331 nm und bei 341-352 nm auf. Sowohl die Naphthalocyaninkomplexe als auch die Phthalocyaninkomplexe weisen eine mit abnehmendem Radius des zentralen $\text{M}^{\text{RE},3+}$ korrelierende zunehmende hypsochrome Verschiebung der Q-Bande von 800 nm ($[\text{Nc}^*_2\text{Ce}]$) nach 778 nm ($[\text{Nc}^*_2\text{Eu}]$) bzw. vom metallfreien Liganden bei 711 nm (Pc^*H_2) über 694 nm ($[\text{Pc}^*_2\text{Eu}]$) nach 692 nm ($[\text{Pc}^*_2\text{Tb}]$) auf. Des Weiteren konnten die typischen $\nu(\text{C}=\text{N})$ -Valenzschwingungen der Nc-Radikalanion-Liganden im IR-Spektrum von $[\text{Nc}^*_2\text{Ce}]$ bei 1361 cm^{-1} und 1314 cm^{-1} beobachtet werden.

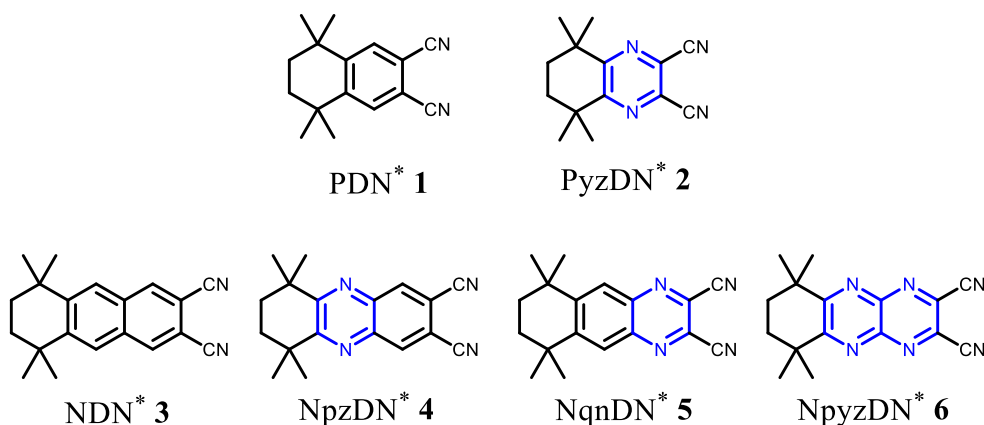


Die vorliegende Arbeit hat die facettenreiche Chemie und die Möglichkeit von Struktur-Eigenschaftskorrelationen der Phthalocyanin- und Naphthalocyanin-Metallverbindungen und ihrer azaanalogen Verbindungen unter Beweis gestellt.

6 Summary

The aim of this work, which was carried out within the SFB1083, was the synthesis and characterisation of phthalocyanines (Pc), pyrazinoporphyrazines (Ppz), their hybrid compounds, the so called azaphthalocyanines (Pz, N_x -[Pc**M*] with *M* = central metal or 2 H) and larger homologues, the naphthalocyanines (Nc). The focus was, besides their optoelectronic application in dye sensitized solar cells (DSSCs), the systematic investigation of selected compounds, frontier MOs using electronic absorption spectroscopy and in cyclic voltammetry. In addition, photophysical properties of these compounds were investigated, in particular their ability to form singlet oxygen; their fluorescence quantum yields and the fluorescence lifetimes were also determined.

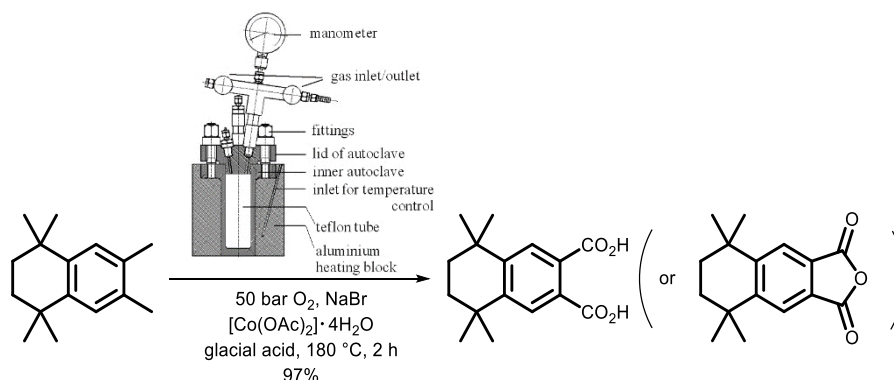
Organic precursors. Firstly, the literature known compounds PDN* **1**, PzDN* **2** and NDN* **3** were reproduced; the series was then completed by the synthesis of compounds NpzDN* **4**, NqnDN* **5** and NppzDN* **6**. Besides their synthesis and characterisations discussed in section 4.1, compound **3-6** are a novel series of C_{2v} -symmetrical naphthalonitriles bearing alkyl groups in the peripheral position, while [-CH=] building blocks are systematically exchanged by [-N=] units.



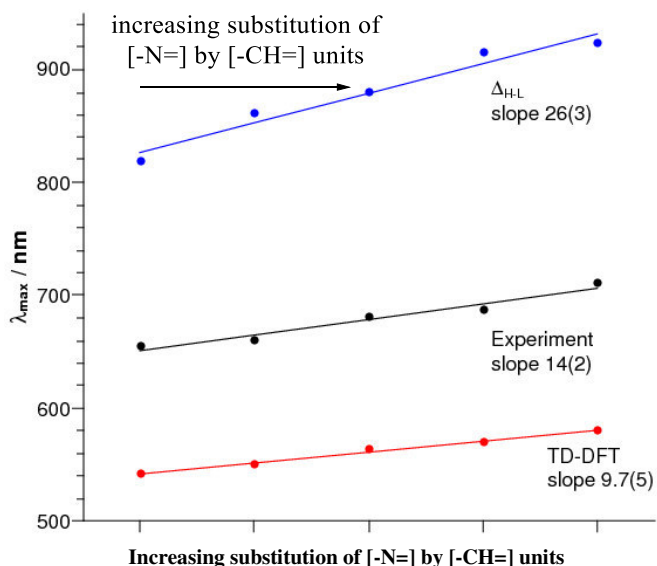
In comparison to the commercially available Pc^{tBu} , the advantages of these 2,2,5,5-tetramethylcyclohexane annulated compounds are the increased solubility in common organic solvents due to the reduced aggregation of the Pc caused by sterically demanding alkyl groups. Furthermore, in cyclotetramerisation of C_{2v} -symmetrical phthalonitriles no mixture of 4 regioisomers is obtained, in contrast to $[Pc^{tBu}M]$. Owing to the symmetry of the A_4 -type molecules resulting from a cyclisation of **1-6**, the analysis in NMR spectroscopy is simplified, crystallisation of these compounds is favoured, and, therefore, an X-ray analysis is possible.

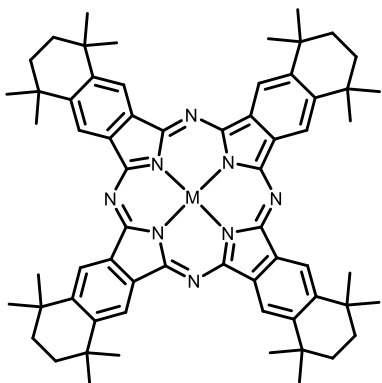
Summary

The key-step in the synthesis of PDN* **1** is the oxidation of the tetraline system to a dicarboxylic acid. The synthesis of PDN* **1** was firstly reported by MIKHALENKO. Up to now, the overall yield of ~30% over seven steps was limited due to the chosen conditions in the oxidation step. As oxidant potassium permanganate was used in excess in aq. pyridine. Following famous industrial processes, such as the aerobic oxidation of *p*-xylene to terephthalic acid, the side chain oxidation of tetraline was optimized in a catalytic procedure, increasing the yield up to 97%.

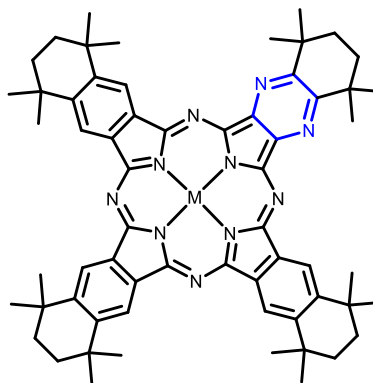


Azaphthalocyanines (of N_x-[Pc**M*] type with M = 2 H, Zn) were synthesised in a cocyclisation of two dinitriles PDN* **1** and PyzDN* **2**, followed by metalation of chromatographically separated N_x-Pc*H₂ using [Zn(hmds)₂] or [Zn(OAc)₂], respectively. Azaphthalocyanines N_x-[Pc**M*] with x = 0, 2, 4, 6, or 8 are discussed and described in section 4.2. All N_x-[Pc**M*] were characterized by using NMR, UV-Vis, FS spectroscopy, cyclic voltammetry, mass spectrometry and photophysical experiments. First synthesised ABAB N₄-[Pc**M*] with M = 2 H, Zn completed the up-to-now unfulfilled series. Both structural isomers ABAB and A₂B₂ could be clearly identified by using ¹H NMR spectroscopy and UV-Vis spectroscopy. Besides the cocyclisation, A₂B₂ N₄-Pc*H₂ and AB₃N₆-Pc*H₂ could be synthesised in a KOBAYASHI ring expansion of an AB₂N₄-[Sp^{c*}BCl] or [Sp^{pz*}BCl], respectively, using the isoindoline of PDN* **1**.

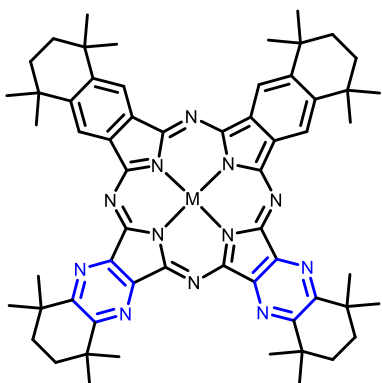




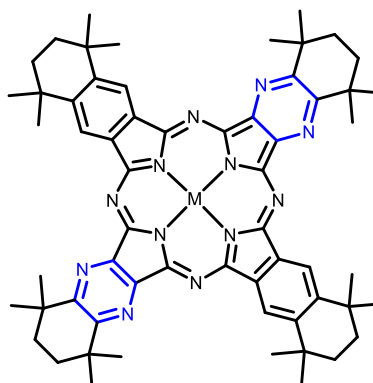
A_4 ; $[Pc^*M]$
Phthalocyanine with $M = 2 H, Zn$



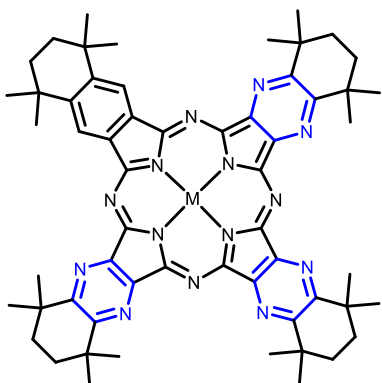
A_3B ; N_2 - $[Pc^*M]$
Diazaphthalocyanine with $M = 2 H, Zn$



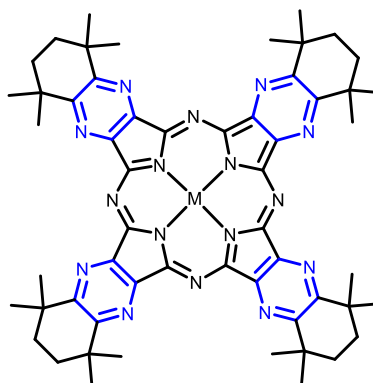
A_2B_2 ; N_4 - $[Pc^*M]$
Tetraazaphthalocyanine with $M = 2 H, Zn$



$ABAB$; N_4 - $[MPc^*M]$
Tetraazaphthalocyanine with $M = 2 H, Zn$



AB_3 ; N_6 - $[Pc^*M]$
Hexaazaphthalocyanine with $M = 2 H, Zn$

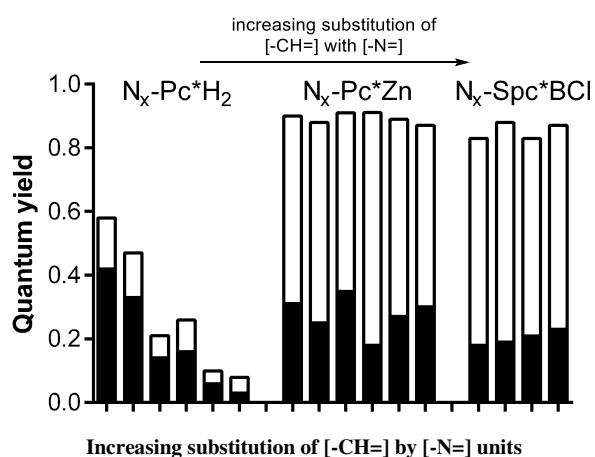


B_4 ; N_8 - $[Pc^*M]$
Octaazaphthalocyanine with $M = 2 H, Zn$
or Pyrazinoporphyrazine $[Ppz^*M]$

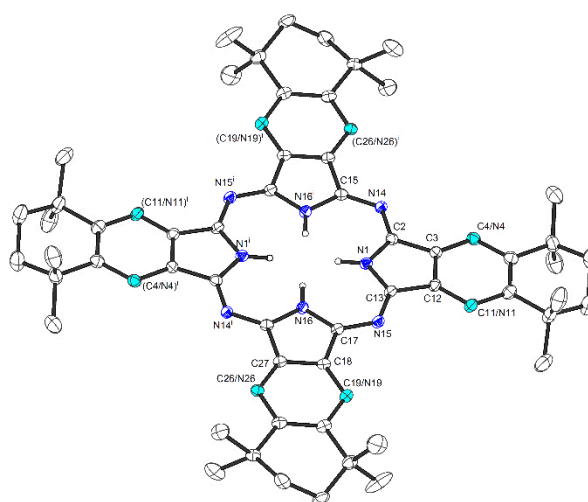
Summary

The values obtained by UV-Vis spectroscopy and CV were compared to TD-DFT calculations in cooperation with the TONNER group (Department of Chemistry of the Philipps-Universität Marburg). In both experimental data and theoretical calculations, a non-perfect linear trend of the hypsochromic shift of the Q-band was found when the HOMO-LUMO gap is increased with the increasing number of substitution of [-CH=] by [-N=] in the non-peripheral position. The reason for the HOMO-LUMO gap increase is the stronger decrease of the HOMO level relative to the one of the LUMO with increasing number of [-N=] units in N_x -[Pc**M*].

In addition, photophysical properties were investigated. Singlet oxygen quantum yields (Φ_Δ), fluorescence quantum yields (Φ_F) and fluorescence lifetimes (τ_F) were determined for both series of N_x -[Spc*BCl] and N_x -[Pc**M*] in cooperation with ZIMČÍK and NOVÁKOVÁ (Department of Pharmacy of the Charles-University in Prague). The highest value for singlet oxygen quantum yield was observed for ABAB N_4 -[Pc*Zn]. The sum of $\Phi_\Delta + \Phi_F$ values is for both N_x -[Pc*Zn] and N_x -[Spc*BCl] ~ 0.9 . In comparison, a trend, not yet described in literature, was found for N_x -Pc* H_2 , which shows a significant decrease of $\Phi_\Delta + \Phi_F$ with increasing number of [-N=] units.

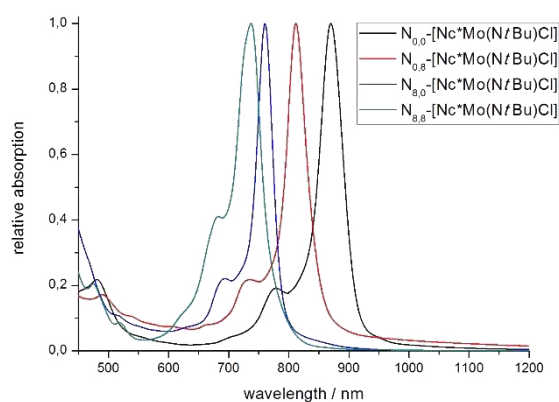
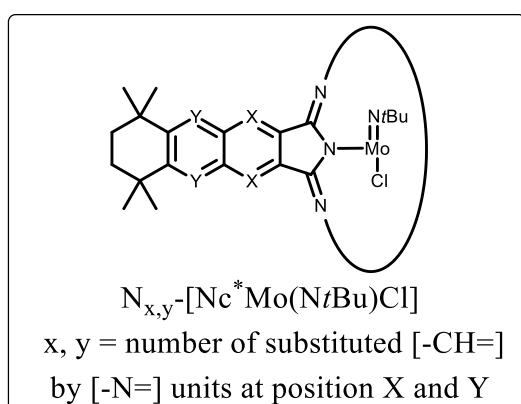


For the first time, an asymmetrical 2,2,5,5-tetramethylcyclohexane substituted aza-phthalocyanine N_2 -Pc* H_2 was analysed by X-ray diffraction. In contrast to the *herringbone* pattern of unsubstituted Pcs, N_2 -Pc* H_2 units are twisted almost 90° in their lattice structure. Similar to other obtained structures, such as A_2B_2 N_4 -[Pc*Zn], substituted [-CH=] and [-N=] units cannot be differentiated by X-ray analysis. In both structures, a characteristic statistical disorder is observed, in which the [-CH=] units are partly



occupied by [-N=], to 25%, or 50%, respectively. Within the bachelor thesis of LANGE, the isoindoline units of the azaphthalocyanine series $N_x\text{-Pc}^*\text{H}_2$ were annulated with a benzene unit. These $N_x\text{-Npz}^*\text{H}_2$ are discussed in section 4.2.6. The series was also completed with the ABAB $N_4\text{-Npz}^*\text{H}_2$ and differentiated from its A_2B_2 isomer by using $^1\text{H NMR}$ and UV-Vis spectroscopy.

Azanaphthalocyanines ($N_{x,y}\text{-[Nc}^*\text{M(NR)Cl]}$ with $M = \text{Mo}, \text{W}$ and $R = t\text{Bu}, \text{Mes}$) were synthesised using 2,2,5,5-tetramethylcyclohexane annulated dinitriles **3-6** and group 6 metal precursors ($[\text{M(NR)}_2\text{Cl}_2\cdot\text{solv}]$ with $M = \text{Mo}, \text{W}$, $R = t\text{Bu}, \text{Mes}$ and $\text{solv} = \text{py}$ or dme).

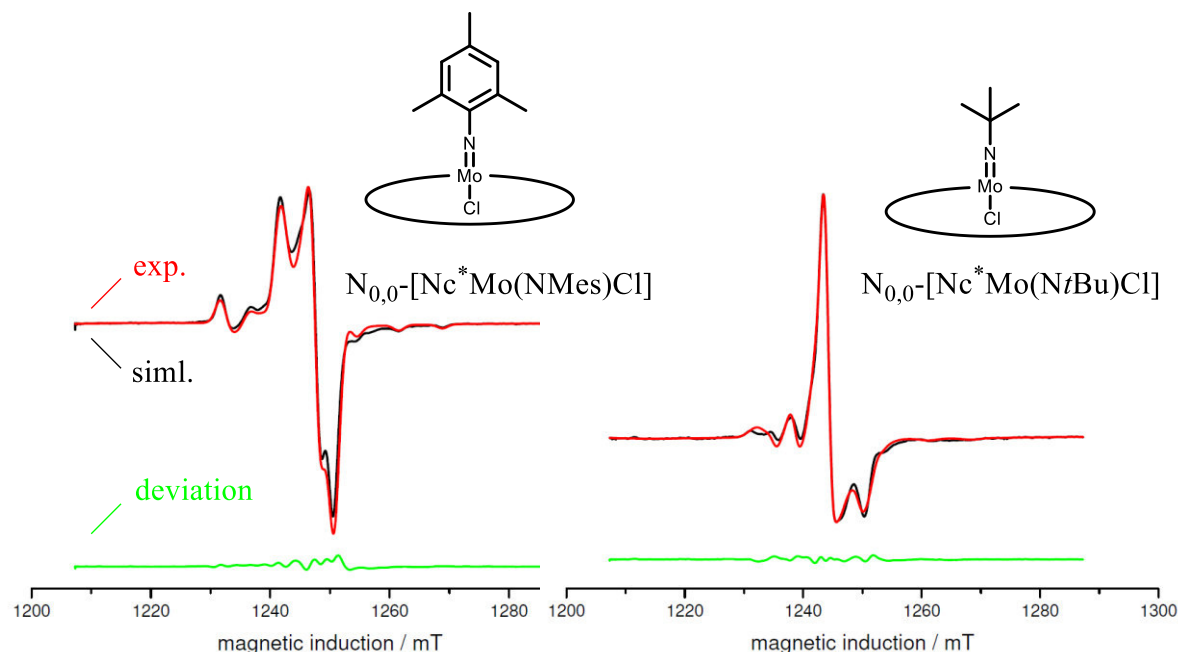


$x = y = 0$	$N_{0,0}\text{-[Nc}^*\text{Mo(N}t\text{Bu)Cl]}$	$= [\text{Nc}^*\text{M}]$	annulated n aphthalocyanine
$x = 0, y = 8$	$N_{0,8}\text{-[Nc}^*\text{Mo(N}t\text{Bu)Cl]}$	$= [\text{Npz}^*\text{M}]$	methylated tetrahydro p henazine
$x = 8, y = 0$	$N_{8,0}\text{-[Nc}^*\text{Mo(N}t\text{Bu)Cl]}$	$= [\text{Nqn}^*\text{M}]$	annulated q uinoxaline
$x = y = 8$	$N_{8,8}\text{-[Nc}^*\text{Mo(N}t\text{Bu)Cl]}$	$= [\text{Nppz}^*\text{M}]$	annulated p yrazin p yrazine

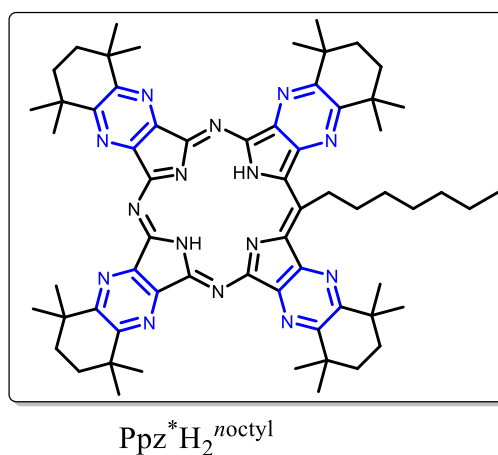
This is the first described series of azanaphthalocyanines (section 4.2.9) bearing alkyl groups in the peripheral position. The compounds were analysed using at least UV-Vis and IR spectroscopy, elemental analysis and mass spectrometric methods, such as MALDI-ToF or LIFDI. The Q-bands of the compounds $N_{0,0}\text{-[Nc}^*\text{Mo(N}t\text{Bu)Cl]}$, $N_{0,8}\text{-[Nc}^*\text{Mo(N}t\text{Bu)Cl]}$, $N_{8,0}\text{-[Nc}^*\text{Mo(N}t\text{Bu)Cl]}$ and $N_{8,8}\text{-[Nc}^*\text{Mo(N}t\text{Bu)Cl]}$ show a hypsochromic shift from 900 nm to 700 nm with increasing substitution of [-CH=] units by [-N=] and proximity to the central [-MN₄-] unit. The Q-band is uncommonly strongly shifted by a substitution of the axial ligand of $N_{0,0}\text{-[Nc}^*\text{Mo(NR)Cl]}$ with $R = t\text{Bu}$ or Mes : for $N_{0,0}\text{-[Nc}^*\text{Mo(N}t\text{Bu)Cl]}$ and $N_{0,0}\text{-[Nc}^*\text{Mo(NMes)Cl]}$ a shift of 27 nm was observed. Both compounds, $N_{0,0}\text{-[Nc}^*\text{Mo(N}t\text{Bu)Cl]}$ and $N_{0,0}\text{-[Nc}^*\text{Mo(NMes)Cl]}$, were analysed by EPR spectroscopy.

Summary

In EPR measurements, the structural differences between the orthorhombic $N_{0,0}$ -[Nc*Mo(NMes)Cl], contrary to the axially symmetric $N_{0,0}$ -[Nc*Mo(N*t*Bu)Cl], is clearly visible. Calculations of orbital interaction with our cooperation partner BERGER (Department of Chemistry of the Philipps-Universität Marburg) are in progress.

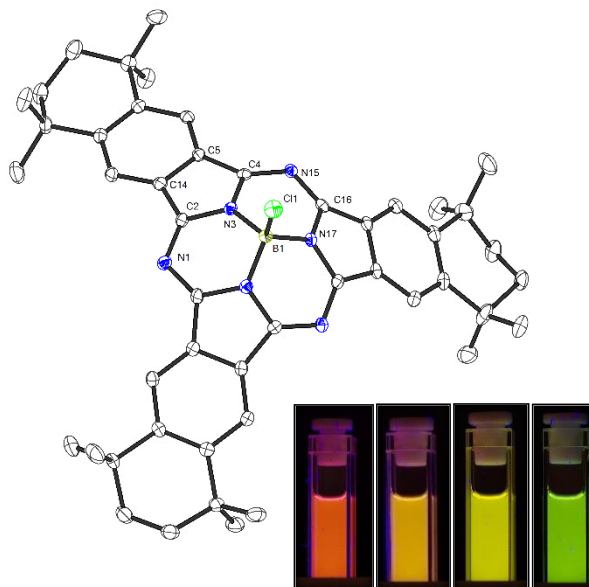


Besides the synthesis of group 6 d^1 -metal naphthalocyanine complexes, the access to metal-free $N_{x,y}$ -Nc*H₂ ligands was attempted in a final stage of this work. $N_{0,0}$ -Nc*H₂ and $N_{0,8}$ -Nc*H₂ as well as their Zn-complexes, $N_{0,0}$ -[Nc*Zn] and $N_{0,8}$ -[Nc*Zn], were synthesised according to literature known methods (section 4.2.10). $N_{8,0}$ -[Nc*Zn] was obtained in 29% yield from compound **5** and [ZnCl₂] in quinoline after 12 h at 230 °C. In first attempts to synthesise $N_{8,0}$ -Nc*H₂ and $N_{8,8}$ -Nc*H₂, similar to the synthesis of Ppz*H₂, a higher tendency to form meso-C^{noctyl}-substituted complexes Ppz*H₂^{noctyl} or $N_{8,0}$ -Nc*H₂^{noctyl} was observed. The mechanism, as well as the isolation of the pure $N_{8,0}$ -Nc*H₂^{noctyl}, has to be carried out in future studies. $N_{8,0}$ -Nc*H₂ could be isolated by preparative TLC and was analysed by using mass spectrometry and UV-Vis spectroscopy. In the synthesis of $N_{8,8}$ -[Nc*Zn], no pure product could be isolated, but a cyclotetramerisation was proven by mass-spectrometry and UV-Vis spectroscopy.

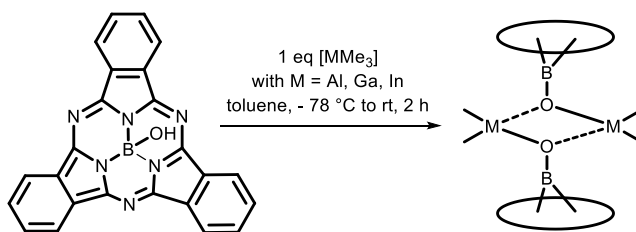


Subphthalocyanines (Spc) and Subpyrazinoporphyrazines (Sppz) bearing the annulated 2,2,5,5-tetramethylcyclohexane ring could be reproduced and axially substituted with halogen atoms. A series of these smaller, ring contracted, "umbrella-like", distorted Pc homologues [Spc*BR] and the first series of [Sppz*BR] with R = F, Cl, Br and OH were synthesised and characterized.

Spcs (N₀-[Spc*BCl]) absorb light in the higher energetic area at about 580 nm and electron deficient Sppzs (N₆-[Spc*BCl]) at 534 nm. On the right side, cuvettes of a new N_x-[Spc*BCl] series with X = 0, 2, 4 and 6 are shown (FS, illuminated at $\lambda = 365$ nm). Visible to the



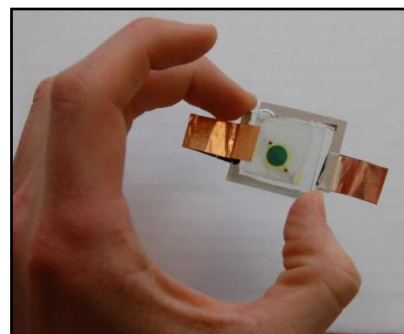
unaided eye is the change of the absorbance and emission behaviour, by exchanging [-CH=] by [-N=] building blocks. The structure of [Spc*BCl] is one example for the rare, substituted Spcs that was analysed by X-ray diffraction. In addition, first attempts were carried out to synthesise surrounded metal-complexes of [Me₂M(μ -OBSpc)]₂ type with M = Al, Ga using [MMe₃] as metal precursor and [SpcBOH]. The synthesis of these compounds was monitored by ¹H NMR spectroscopy and the resulting [Me₂M(μ -OBSpc)]₂ characterised by using UV-Vis, FS and IR spectroscopy. According to mass spectrometric results from MALDI-ToF, a dinuclear structure is proposed. Compared to axial substitution of phthalocyanines, the UV-Vis spectra of subphthalocyanine complexes [Me₂M(μ -OBSpc)]₂ with M = Al, Ga show a slight shift of the Q-band of about 1 nm in comparison to [SpcBOH].



In following experiments, the synthesis of numerous borato coordinated metal complexes was attempted, whereby [(SpcBO)₄Ti] as well as [(SpcBO)₃B] were observed and characterised. These metal complexes show a weak broadening of the Q-band in UV-Vis spectroscopy, because the π -systems are forced into physical proximity.

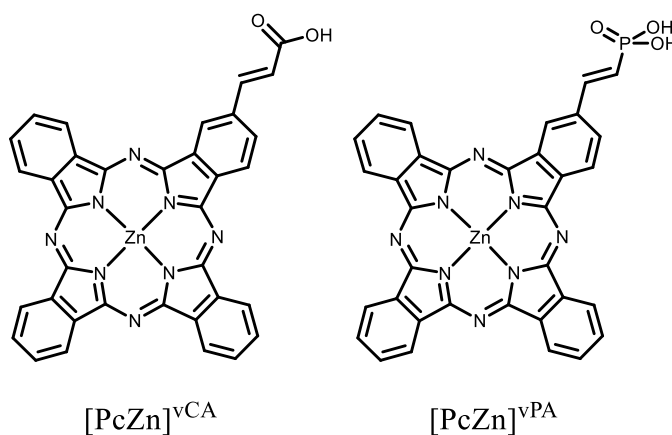
Summary

Application as Photosensitizer in Dye Sensitized Solar Cells (DSSCs) was carried out for equatorially functionalised compounds. Their synthesis is discussed in section 4.3. Unsubstituted Pc, $[\text{PcZn}]^{\text{FG}}$, with different anchors were synthesised (FG = vinylphosphonic acid, phosphonic acid, vinylcarboxylic acid, or catechol) using a KOBAYASHI ring-expansion.

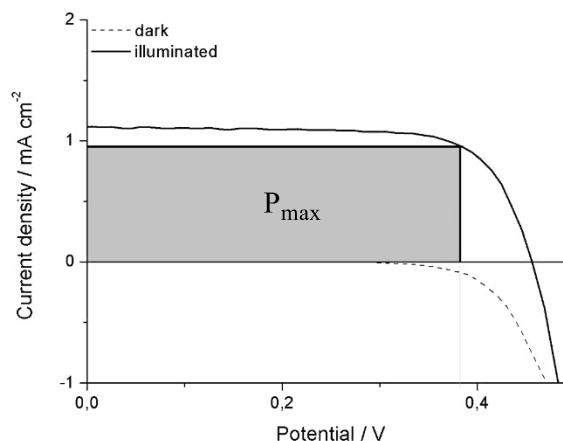
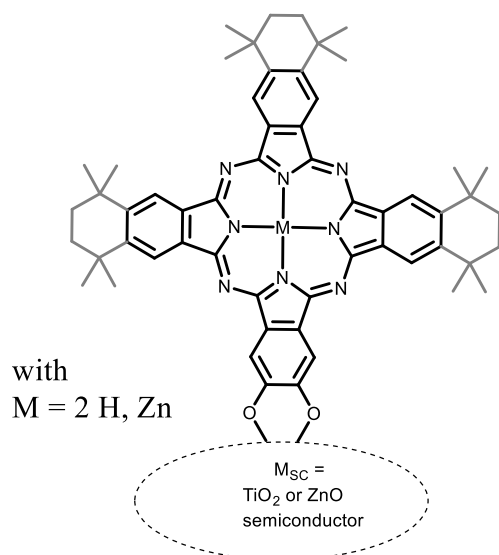


In addition, 2,2,5,5-tetramethylcyclohexane annulated Pcs ($[\text{Pc}^*\text{M}]^{\text{OH}}$ with $\text{M} = 2 \text{ H, Zn}$) with a catechol anchor were synthesised in yields of up to 10% in a cocyclisation.

All compounds were successfully bonded to ZnO semiconductor surfaces. Current-voltage characteristic (I-U curve) and IPCE measurements were carried out in collaboration with AG SCHLETTWEIN (Department of Physics of the Justus-Liebig-Universität Gießen). The most promising anchor moiety appears to be the phosphonic



acid of $[\text{PcZn}]^{\text{vPA}}$ ($\eta = 0.5\%$), followed by the carboxylic acid $[\text{PcZn}]^{\text{vCA}}$ ($\eta = <0.2\%$) and the catechol $[\text{PcZn}]^{\text{OH}}$ ($\eta \sim 0.001\%$), when correct solvent and conditions for the deposition are chosen. In comparison to the unsubstituted compound $[\text{PcZn}]^{\text{OH}}$, the alkyl substituted $[\text{Pc}^*\text{Zn}]^{\text{OH}}$ shows a higher efficiency in DSSCs by a factor 10, and with this, a better electron transfer to the semiconductor. This clearly shows how the electron donating and sterically demanding alkyl groups decrease aggregation and recombination processes. However, in accordance with the $\text{N}_x\text{-}[\text{Pc}^*\text{M}]$ series with $\text{M} = 2 \text{ H, Zn}$, lower efficiencies were measured for $\text{Pc}^*\text{H}_2^{\text{OH}}$ compared to $[\text{Pc}^*\text{Zn}]^{\text{OH}}$, which is caused by increased "quenching" processes taking place when the central metal atom is removed.

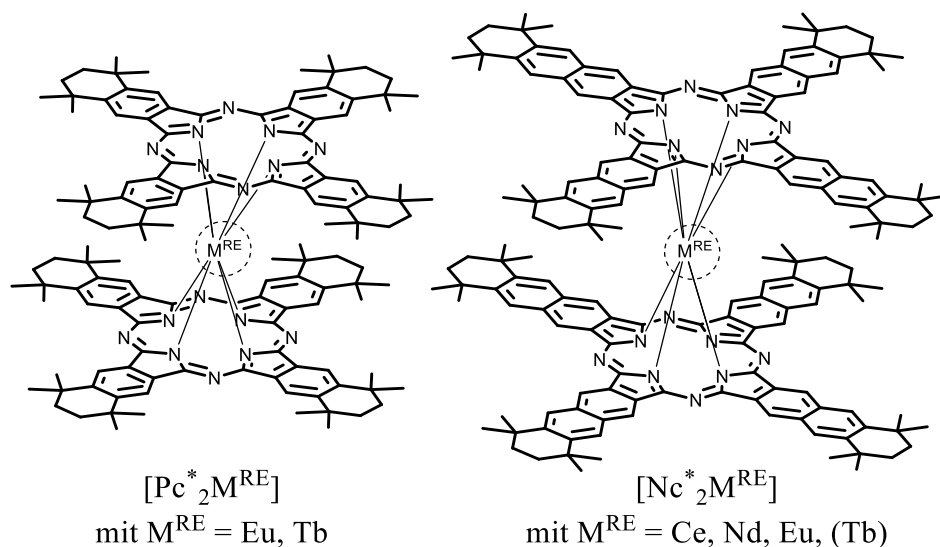


Currently, photoluminescence measurements are being carried out for constructed cells. A fast electron transfer to the semiconductor was observed, but also a fast recombination process, which might explain the low electron transfer to the semiconductor and the low cell efficiencies. However, a favoured electron transfer from the dye to a semiconductor by using an equatorial anchor in comparison to previously described axial anchor moieties was proven. In future work, the described structure-property correlation obtained from previous sections can be used to design and modify equatorially functionalised Pcs. The readily accessible $[\text{Pc}^*\text{Zn}]^{\text{OH}}$ can be converted into a vinylphosphonic acid substituted A₃B type Pc, such as $[\text{Pc}^*\text{Zn}]^{\text{vPA}}$ or $[\text{Pc}^*\text{Zn}]^{\text{vCA}}$. Furthermore, the complexes should be tested with additives such as cheno or axially coordinating moieties such as guanidine; meso-C^{FG} Pc and derivatives could also be investigated.

Summary

Phthalocyanine Sandwich-Complexes of a $[\text{Pc}^*_2\text{M}^{\text{RE}}]$ and $[\text{Nc}^*_2\text{M}^{\text{RE}}]$ type were synthesised for $\text{M}^{\text{RE}} = \text{Eu}, \text{Tb}, \text{Ce}$ and Nd . The main focus was on the rare earth metals Eu^{3+} and Tb^{3+} , because of their different spin of $\pm 1/2$ in comparison to the quite well investigated $f^7\text{-Gd}^{3+}$ phthalocyanine complexes, of a $[\text{Pc}_2\text{Gd}]$ type.

In this work, the easiest synthetic access to $[\text{Pc}^*_2\text{M}^{\text{RE}}]$ and $[\text{Nc}^*_2\text{M}^{\text{RE}}]$ was found to be the reaction of the free ligand Pc^*H_2 and Nc^*H_2 in presence of the respective $[\text{M}^{\text{RE}}(\text{hmds})_3]$. For a complete formation to the $[(\text{Pc})^-(\text{Pc}')^{2-}\text{M}^{\text{RE}, 3+}]^0$ complex reaction times of up to 7 d at 110°C in toluene were necessary. The obtained sandwich complexes show a split of the B-band in the UV-Vis spectrum at 323-331 nm and at 341-352 nm. In addition, both naphthalocyanine and phthalocyanine complexes show, with a decreasing radius of the central metal ion $\text{M}^{\text{RE}, 3+}$, an increasing hypsochromic shift of the Q-band from 800 nm ($[\text{Nc}^*_2\text{Ce}]$) to 778 nm ($[\text{Nc}^*_2\text{Eu}]$) and from the metal free ligand at 711 nm (Pc^*H_2) over 694 nm ($[\text{Pc}^*_2\text{Eu}]$) to 692 nm ($[\text{Pc}^*_2\text{Tb}]$). Furthermore, typical $\nu(\text{C}=\text{N})$ valence vibrations in the IR spectrum of $[\text{Nc}^*_2\text{Ce}]$ were observed at 1362 cm^{-1} and 1314 cm^{-1} .



The presented work displayed multi-faceted chemistry of phthalocyanines, naphthalocyanines and their aza-analogue complexes. Within a set of selected examples, the prediction of optoelectronic properties using structure-property correlations has been demonstrated.

7 Experimental Section

7.1 Methods

All reactions with hydrolysis- and/or oxidation-sensitive compounds were carried out under argon or nitrogen atmosphere using SCHLENK techniques and absolute solvents. A changeable tap line with a rotary vane pump (type PFEIFFER Company DMO 10 M, final pressure approx. $<1 \cdot 10^{-3}$ mbar) was used. The remaining water in the used nitrogen (purification degree 5.0, AIR LIQUIDE Company) was removed by using a column filled with P_4O_{10} . For handling and storing of hydrolysis and oxidation sensitive compounds, glove boxes (Types MB 150 BG-1, M. BRAUN Company, Lab Master 130, M. BRAUN Company) with nitrogen inert gas atmosphere were used. Reactions requiring temperatures over 200 °C were carried out in a WOOD's metal bath.^[263]

7.1.1 Solvents, Compounds and Starting Materials

All used absolute solvents were dried by using standard literature descriptions and were stored over absorption columns filled with aluminium oxide/molecular sieves 3Å/R3-11G-catalyst (BASF Company).^[264] Compounds marked with corresponding reference " [Lit] ", are literature known as shown in the table of compounds, or were synthesised according to a literature known procedure. Compounds which have not been marked have been synthesised for the first time. The commercially available compounds are marked by € and were purchased. Unless mentioned otherwise, they were used without any further purification.

Starting materials: The following compounds were synthesised according to literature known procedures: $[M(NR)_2Cl_2]$ with $M = Mo, W$ and $R = tBu, Mes$, as described in section 7.15.1,^[265,266] $[M^{RE}(hmds)_3]$,^[267–270] $[Cp^*CrCl_2]$,^[271] $[M(NMe_2)_4]$ with $M = Si, Ti$ €.

7.1.2 Column Chromatography

For purifications using column chromatography, as stationary phase silica gel 60 (pore size 0.040-0.063 nm) obtained from MERCK Company was used. The thin layer chromatography (TLC) was done using aluminium TLC plates 60 F₂₅₄ obtained from MERCK Company. For preparative TLC, glass plates 60 F₂₅₄ obtained from MERCK Company with a silica thickness of

Experimental Section

~210-270 μm were used. The compounds were scratched off the plate and washed off as described in more detail in the respective experimental procedure. For detection a UV-lamp ($\lambda = 254$ (short wave) , 365 nm (long wave)) was used or the compounds were dyed with liquid dips. Therefore, a KMnO_4 -dip (9 g KMnO_4 , 60 g K_2CO_3 , 1 mL glacial acid in 0.9 L water) or a Cer-dip (Cer-(IV)-sulfate, sulfuric acid) was chosen.^[272]

7.1.3 MPLC: Sepacore System BÜCHI

The separation of precursors was carried out by using a medium pressure column chromatography (MPLC), BÜCHI Sepacore System „Preparative Chromatography“. The columns were filled and packed using a dry fill set at a final pressure of 10 bar. A pump module C-601 in combination with a pump module C-610 was used. The substrates were added onto the column in dry form adsorbed on silica or liquid, dissolved in <20 mL of the respective solvent. The products were in general washed with pentane and eluted with the solvent described in the corresponding section. If not mentioned otherwise, <50 times weight amount silica gel/product was used and a pressure <10 bar. The detection was done using a UV-Vis sensor C-640 with four UV-Vis lamps at 254 nm and in the respective absorption area of the compounds/by-products. The fractions were collected with a fraction collector C-660.

7.1.4 Assembly of DSSCs

For assembling of dye sensitized solar cells (DSSCs) glass substrates were used, which have been supplied with semiconducting oxide layers (ITO or FTO). On this layers of mesoporous TiO_2 films have been prepared. The TiO_2 -substrates were prepared by WALLAUER of the ROLING group, Philipps-Universität Marburg, FB Chemie. The ZnO -mesoporous layers were prepared in cooperation with FALGENHAUER and TINZ of the SCHLETTWEIN group at the Justus-Liebig-Universität Gießen, Department of Physics. The ZnO films were prepared following the literature known procedure of YOSHIDA *et al.*^[226]

7.1.5 Autoclave Reactions

All reactions in which high pressure was needed, were carried out in an autoclave. Therefore, a glass (pressure <10 bar) or a steel autoclave (<100 bar) was used. The 100 mL stainless steel autoclaves *V4A-Edelstahlautoklaven* were constructed by the precision engineering department of the Philipps-Universität Marburg (Department of Chemistry). Solids and liquids were weighed out in a 100 mL teflon flask or in the corresponding glass flask, a magnetic stirrer was added and the autoclave was closed and sealed using EPDM-O-rings of CLEFF DICHTUNG company. The actual pressure was regulated using a manometer. The temperature was adjusted using a corresponding aluminium block in which the thermometer of the magnetic stirrer MR 3003 HEIDOLPH could be added (Pt-100-thermal element). If necessary, the heating block might be preheated (for Pc reactions). If necessary, the glass autoclaves were heated in an oil bath. A sketch of the steel autoclave is displayed in Figure 125.

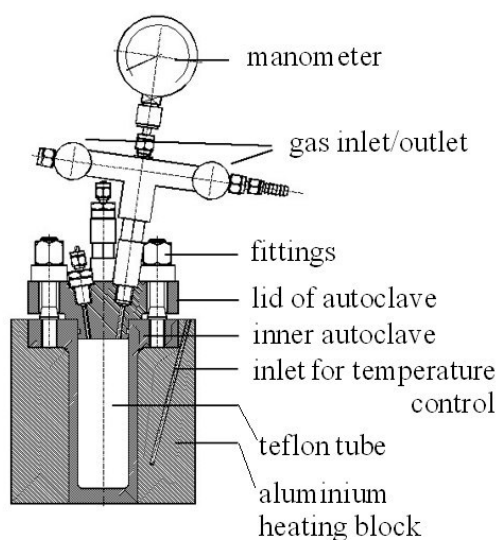


Figure 125: Sketch of the used steel autoclave: *V4A-stainless steel autoclave*.

7.2 Analytical Methods

7.2.1 Elemental Analysis

Elemental analyses were measured at the service department at the Department of Chemistry of the Philipps-Universität Marburg. They were measured with an ELEMENTAR Vario MICRO cube (CHNS-analysis). The values are given in percentage by weight.

7.2.2 NMR Spectroscopy

NMR spectra were measured in the stated deuterated solvents using a device of the type AV II 300 BRUKER Company (^1H : 300.1 MHz, ^{13}C : 75.5 MHz, ^{31}P : 121.5 MHz) or if necessary AV II 600 MHz. Measurements implemented by NMR device of AV III HD 300 MHz, AV III 500 MHz, AV III HD 500 MHz and AV III DRX 400-spectrometer BRUKER Company (^1H : 400.1 MHz, ^{13}C : 100.6 MHz, ^{31}P : 161.9 MHz) were carried out by the service department for NMR spectroscopy at the Department of Chemistry of the Philipps-Universität Marburg. If not mentioned otherwise the measurements were carried out at 300 K.

In the analyses, the chemical shifts δ of the spectra are given in ppm. The assigned protons are written in italic (e.g. CH_2CH_3). The following abbreviations were used:

s = singlet, d = doublet, m = multiplet, b = broadened, H_β = protons in β -position to the pyrrolring, H_α = Protons in α - position to the pyrrole ring. Couplings between the nucleuses X and Y with a spin = $\frac{1}{2}$ over n chemical bonds are given by a coupling constant $^nJ_{X,Y}$ in Hertz.

The calibration of the ^1H NMR and ^{13}C NMR spectra was done by using the residual proton signal and solvent signal of the used solvent (^1H NMR: CDCl_3 : 7.26 ppm, C_6D_6 : 7.15 ppm, $\text{THF-}d_8$: 3.58 ppm, $\text{DMSO-}d_6$: 2.54 ppm, pyridine- d_5 : 8.71 ppm, $\text{C}_6\text{D}_5\text{Br}$: 7.35 ppm, toluene- d_8 : 7.09 ppm. ^{13}C NMR: CDCl_3 : 77.0 ppm, C_6D_6 : 128.1 ppm, $\text{THF-}d_8$: 67.4 ppm, $\text{DMSO-}d_6$: 40.5 ppm, $\text{C}_6\text{D}_5\text{Br}$: 131.8 ppm). The calibration of ^{31}P NMR-spectra was done externally by using 80% phosphorous acid as standard.

Correlation of signals was done by chemical shifts and integrals. Also the splitting, in the form of a typical chemical coupling pattern, was used for correlation of the signals to corresponding protons. The shifts marked with a *, could not be assigned for certain, as in general further described in the additional information below the analysis. Solvent impurities were assigned using literature known values.^[273]

7.2.3 EPR Spectroscopy

EPR samples were prepared according to standard methods. For X-band measurements of the complexes $[\text{Nc}^*\text{M}(\text{NR})\text{Cl}]$ (with $\text{M} = \text{Mo}, \text{W}$ and $\text{R} = t\text{Bu}, \text{Mes}, \text{Ts}$) a 1 mmol solution in toluene was prepared (2.7-2.8 mg in 2 mL toluene) and the EPR quartz tube ($d = 4$ mm) was filled up ~2 cm (max. 3 cm). The samples were prepared under oxygen exclusion, if necessary Ar was bubbled through the prepared solution. The solution was sealed and directly frozen in liquid nitrogen. For Q-Band measurements, in analogy to the X-band, a 2 mmol solution in toluene was prepared in specific glass tubes ($d = 2$ mm) prepared at the Department of Chemistry at the Philipps-Universität Marburg. For X-band measurements a BRUKER company device ESP300 was used, for Q-band measurements a VARIAN company device E15 spectrometer. EPR measurements were carried out by BURGHAUS at the Department of Chemistry at the Philipps-Universität Marburg.

7.2.4 IR Spectroscopy

The IR spectra were measured with a BRUKER Alpha FT-IR spectrometer, which included a diamond measuring cell in ATR mode (*attenuated total reflection*) with neat substances. If necessary, measurements were taken in a glove box under nitrogen atmosphere. For analysis of spectra the following abbreviations were used: vs = very strong, s = strong, m = medium strong, w = weak, vw = very weak, ν = wave number, b = broadened.

7.2.5 UV-Vis Spectroscopy

UV-Vis spectra were done with an UV-1601 PC spectrometer of the SHIMADZU Company or an AVANTES AvaSpec-2048 spectrometer in a quartz cuvette with a coat thickness of 1 cm. The preparation of hydrolysis sensitive compounds was done with absolute solvents in the glove box. For analysis of the spectra the following abbreviations are used: s = strong, m = medium strong, sh = shoulder, b = broadened.

7.2.6 Fluorescence Spectroscopy

Fluorescence spectra were done with a VARIAN Cary Eclipse-spectrometer in fluorescence cuvettes made out of quartz with a coat thickness of 1 cm. The excitation wavelength was between 350-600 nm. Measurements were taken in the range of 400-1000 nm with a scan rate of 600 nm/min. The device shows an error at ~700 nm.

7.2.7 Photophysical Measurements

Photophysical measurements were carried out in cooperation with the group of ZIMČÍK, NOVÁKOVÁ in Hradec Kralove, at the Department of Pharmacy at the Charles University of Prague. The preparation of the samples is described in more detail in the following two sections. For measurements, steady-state fluorescence spectra were measured using an AMINCO-Bowman Series 2 luminescence spectrometer. For singlet oxygen and fluorescence determination, as well as the titration experiments, the dye samples were purified by preparative TLC on Merck aluminium sheets coated with silica gel 60 F254 to ensure high purity. Both, the Φ_{Δ} and Φ_F values, were determined by comparative methods using unsubstituted zinc phthalocyanine (PcZn) as a reference ($\Phi_{\Delta(\text{THF})} = 0.53$, $\Phi_{F(\text{THF})} = 0.32$) for $N_x\text{-[Pc}^*\text{M]}$.^[27,274] The photophysical data for $N_x\text{-[Spc}^*\text{BCl]}$ series were determined with rhodamine G6 ($\Phi_{F(\text{EtOH})} = 0.94$)^[275] and Bengal Rose ($\Phi_{\Delta(\text{MeOH})} = 0.76$)^[276] as reference compounds and long-pass filter FGL455 instead of OG530 for Φ_{Δ} determination.^[193] All of the experiments were performed in triplicate and the data represent the mean values of the measurements (estimated error $\pm 10\%$).

7.2.7.1 Determination of Absolute Fluorescence Quantum Yields

For fluorescence quantum yield, Φ_F , determination, the sample and reference were excited at 598 nm and 490 nm for $N_x\text{-[Pc}^*\text{M]}$ and $N_x\text{-[Spc}^*\text{BCl]}$, respectively, and the absorbance at the Q-band maximum was maintained at less than a relative absorbance of ~0.05 to avoid the inner filter effect. The emission spectra were corrected for the instrument response. The Φ_F values were corrected for the refractive indices of the solvents. The time-resolved fluorescence measurements were performed on FS5 fluorimeter (Edinburgh Instruments) with picosecond pulsed diode lasers excitation at 371 nm (EPL-375, pulse width ~ 68 ps) and 634 nm (EPL-635, pulse width ~ 81 ps). The decay curves were fitted to exponential functions with Fluoracle software (Edinburgh Instruments). The calculation of Φ_F is discussed in section 4.2.5 (p. 82).

7.2.7.2 Measurements of Singlet Oxygen Quantum Yield

As a scavenger for singlet oxygen 1,3-diphenylisobenzofuran (dpbf) was used.^[189,190] For the measurements, first a UV-Vis spectrum of the singlet oxygen scavenger dpbf was measured in a 10 x 10 mm quartz cuvette and the baseline was set, after saturation of the solution with oxygen, for 1 min.^[189,190] Then, the pure sample was added and measured in the dark. After this "second baseline" was set, the sample was illuminated for at least in 5 separate intervals in the shown setup. For illumination, a xenon lamp was used (100 W, ozone free XE DC short arc lamp, Newport). The time of illumination was adjusted in correlation to the decrease of dpbf. The intensity of the singlet oxygen scavenger, dpbf, should not decrease by more than 15% from its initial intensity. The absorption spectrum of the investigated compounds should not change at all. The decreasing intensity of the dpbf was monitored by UV-Vis spectroscopy. The decrease in intensity of the reference compounds was determined, and plotted versus the time of irradiation of the sample

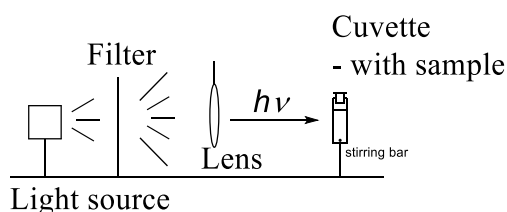


Figure 126: Sketch for determination of singlet oxygen.

Azaphthalocyanines N_x -[Pc^{*}M] with M = 2 H, Zn were measured in THF using [PcZn] as reference. As filter, OG530 was used. Azasubphthalocyanines N_x -[Sp^{*}BCl] were measured in MeOH using Bengal Rose as reference. As filter a FGL455 filter was used. A sketch of the setup is shown in Figure 126. The calculation of Φ_Δ is discussed in section 4.2.5 (p. 82).

7.2.8 Mass Spectrometry

ESI and APCI mass spectra were carried out by the service department for mass spectrometry and elemental analytics of the Philipps-Universität Marburg with a Finnigan LTQ-FT Spectrometer of THERMO FISCHER SCIENTIFIC Company. EI-MS (e. g. for analysis of rare earth metal precursors such as [M_{RE}(hmds)₃]) spectra were measured with a Finnigan MAT95-Spectrometer of THERMO FISCHER SCIENTIFIC Company. For determination of unknown substances on TLC plates a TLC-MS-Interface was used. MALDI-TOF-mass spectra were measured with a Biflex III-Spectrometer of BRUKER Company. Pyrene was used as matrix, or the samples were prepared as described below. MALDI-ToF was partly replaced by an FD

Experimental Section

source. The measurements are in accord with the MALDI-ToF spectra. For LIFDI measurements, AccuTOF-GCv was used, which is a GC TOF mass spectrometer coupled to the respective FD / FI / LIFDI source (DIP, DEP). In all methods, the measured molecular mass is given in mass-to-charge ratio (m/z). Only the signal of the naturally most abundant isotope is given. The abundance isotopic ratio was determined through theoretically calculated values.

Inert MALDI-TOF Samples were prepared in a GB under inert atmosphere. Therefore, the samples (<1 mmol) were dissolved in the corresponding organic solvent (in general MeCN, DCM or toluene). For measurements using a matrix, additional samples were prepared using the corresponding matrix: 2,4,6-trihydroxyacetophenone, pyrene or α -cyano-hydroxycinnamic acid. In the case of the α -cyano-hydroxycinnamic acid, a thin film (thin layer preparation) was prepared to measure the crystals. The others were added on the MALDI metal target in a ratio 1:1 with the sample mixture. After evaporating the solvent, the target was placed in a box, purged with nitrogen before insertion in a MALDI-TOF vacuum chamber. In general, Pcs were measured without matrix.

7.2.9 Cyclic Voltammetry

Cyclovoltammetric Measurements were carried out with a RHD INSTRUMENTS microcell HC cell. The device is coupled to an RHD INSTRUMENTS temperature controller. As interface, IVIUM TECHNOLOGIES IVIUMSTAT Electrochemical Interface & Impedance Analyser was used. The electrodes (Pt, glassy carbon) are constructed within a distance of 30 μm . The Pt working electrode has a surface diameter of 0.25 mm. As solvent, distilled DMSO, DCM ($\text{N}_x\text{-Pc}^*\text{H}_2$) or THF ($\text{N}_x\text{-[Pc}^*\text{Zn]}$) was used, dried over 4 Å molsieve. As conductive salt tetrabutylammoniumhexafluorophosphate (TBAF, *for electrochemical analysis*) was used. The concentration was adjusted between 50-100 mmol/L. The measurements were carried out using a Ag/AgCl pseudo-reference electrode, whereby as reference ferrocene/ferrocenyl as internal standard was used, in correlation to the standard potential E° . Sample preparation and measurements were carried out under inert atmosphere. A <1 mmol solution was used. For controlling and analysis the software product IviumSoft 1.926 of IVIUM TECHNOLOGIES company was used, or later Autolab NOVA of METROHM company. The spectra were plotted in Origin 8 of ORIGINLAB company.

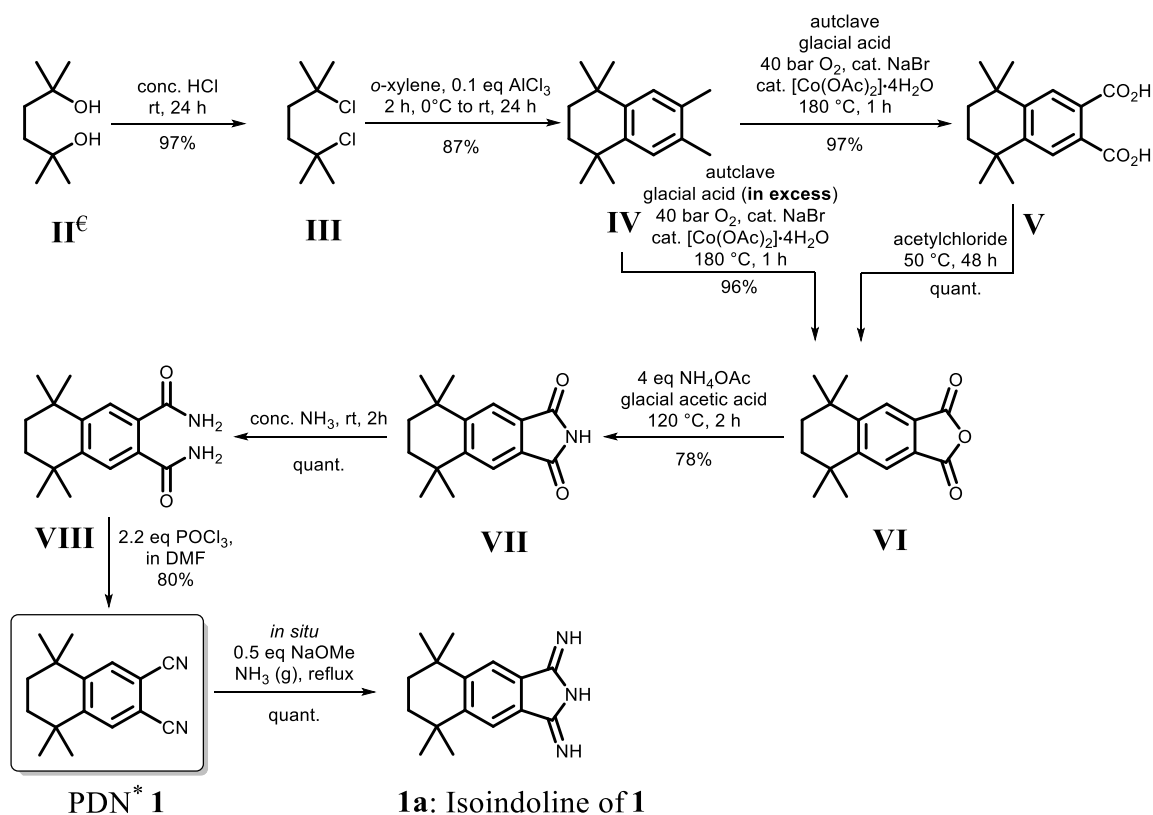
7.3 Syntheses of Phthalonitrile Precursors

The "Experimental Section" is divided in several subsections. According to the "Results and Discussion Section" at first, the ligand synthesis of dinitrile precursors is described, and afterwards, the synthesis of the subphthalocyanines, phthalocyanines, naphthalocyanines, meso-substituted phthalocyanines, metal complexes of subphthalocyanines and finally rare-earth metal sandwich complexes.

The literature known synthesis of all dinitriles are attached to the "Electronic Experimental Section", including NMR spectra and other analysis if present. The synthesis plan of dinitrile precursors are shown before every section.

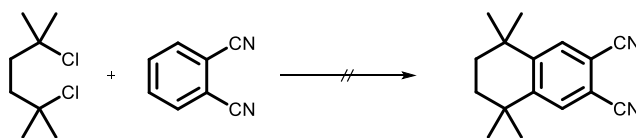
7.3.1 Synthesis of PDN*

The synthesis of the PDN* **1** was carried out according to MIKHALENKO.^[24] The synthesis of 1,1,4,4-tetramethyltetralin-6,7-dicarboxylic acid (VI) was modified by using an overpressure of O₂ in a [Co(OAc)₂]-4H₂O catalytic autoclave reaction.



Experimental Section

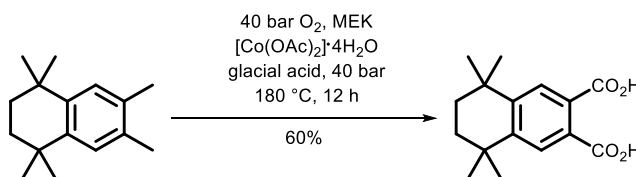
7.3.1.1 Attempt at Direct Synthesis of PDN*



The synthesis was carried out according to a literature reported procedure:^[137] 1.02 g PDN (7.92 mmol, 1 eq) were dissolved with 1.53 g 2,5-dichloro-2,5-dimethylhexane (8.32 mmol, 1.05 eq) in 20 mL DCM. The solution was cooled to $-5\text{ }^{\circ}\text{C}$ and 110 mg AlCl_3 (0.82 mmol, 0.1 eq, excess) were added portionwise. After 1 h, portionwise another 350 mg AlCl_3 (2.62 mmol, >0.3 eq) were added. The solution was stirred overnight and warmed up to rt, before adding 20 mL water. Only educts could be detected by ^1H NMR spectroscopy.

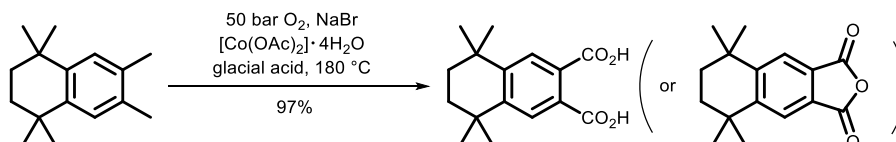
Additional information: Conditions were also varied (by an increase of temperature and time as well as ratios) but no formation of the product was observed in ^1H NMR spectroscopy.

7.3.1.2 Alternative Synthesis of 1,1,4,4-Tetramethyltetralin-6,7-dicarboxylic acid



Method a) The reaction was carried out in an autoclave reaction as described in method b), using 50 bar O_2 and 0.1 eq $[\text{Co}(\text{OAc})_2]\cdot 4\text{H}_2\text{O}$ as catalyst, 5 eq MEK as cocatalyst instead of NaBr, and 5 mL glacial acetic acid/g tetraline as solvent. The mixture was stirred for 12 h while the autoclave was recharged several times with O_2 , until the pressure stayed constant. Workup was carried out according to method b).

Yield: 60% (only carboxylic acid was observed). - ^1H NMR: according to analysis below.



Method b) 15 g tetraline (69.3 mmol, 1 eq) were dissolved in 50 mL glacial acid in a 100 mL teflon tube and added into an autoclave (steel autoclave as visible in “Methods” section 7.1.5). The teflon tube was additionally filled-up with 750 mg $[\text{Co}(\text{OAc})_2]\cdot 4\text{H}_2\text{O}$ (3 mmol, 4 mol%) and 300 mg NaBr (3 mmol, 4 mol%). The mixture was briefly stirred until everything was dissolved. The autoclave was charged with O_2 to a pressure of 20 bar. With stirring, the solution

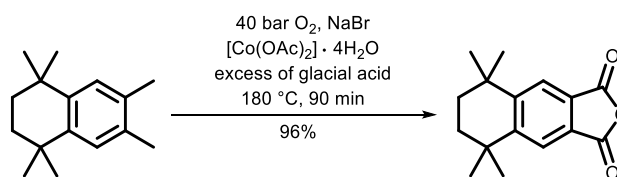
was heated to 180 °C. After a short period of initiation (<30 min) the reaction started and the pressure decreased. The autoclave was recharged with O₂ to 50 bar as often as necessary, until the pressure stayed constant at about 50 bar. After 2 h, the reaction was complete. The reaction may also be stirred overnight. The resulting solution was concentrated under reduced pressure and was washed with water to remove Co-salts and NaBr traces. The product can be additionally precipitated in 20% aq. HCl (500 mL/20 g acid), followed by filtration and washing with water.

Yield: 18.5 g, 67 mmol, 97%. - ¹H NMR (DMSO-*d*₆, 300 MHz): δ = 13.07 (s, 2 H, COOH), 7.57 (s, 2 H, Ar-CH), 1.66 (s, 4 H, -CH₂), 1.25 (s, 12 H, -CH₃) ppm. - MS (ESI(+), MeOH): *m/z* = 277.1436, cal. for C₁₆H₂₀O₄+H₁: 277.1434. - **Elemental analysis** (C₁₆H₂₀O₄, M = 276.33): *find.* (cal.): C 69.83% (69.55%), H 7.18% (7.30%), N 7.53% (0.00%).

Additional information: In some cases, the corresponding anhydride was detected by ¹H NMR spectroscopy. The amount of anhydride is dependent on the amount of glacial acid used in the reaction in ratio to the tetraline amount. No other by-products could be observed. A complete turnover was determined. The high nitrogen value in elemental analysis is caused by the measurement in closed setup in the glovebox, neither in the synthesis nor in precursor steps were nitrogen containing chemicals used.

7.3.1.3 Alternative Synthesis of the Anhydride of

1,1,4,4-Tetramethyltetralin-6,7-dicarboxylic acid



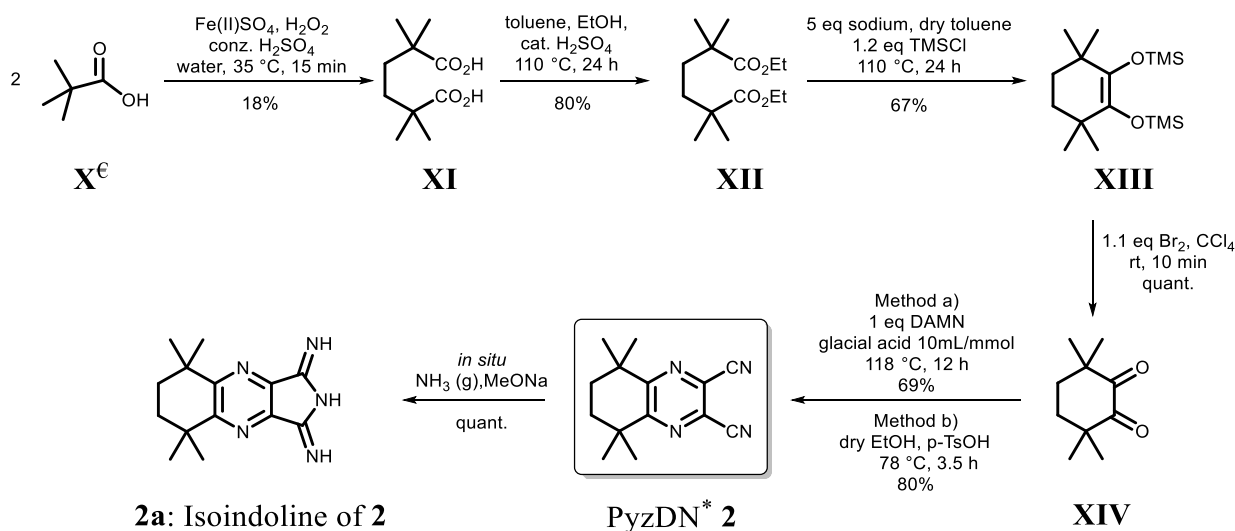
50 mg NaBr (486 μmol, ~3.5 mol%), 125 mg [Co(OAc)₂]₄H₂O (502 μmol, ~3.5 mol%), 3.00 g tetraline (13.9 mmol, 1 eq) were added into an autoclave (steel autoclave as visible in “Methods” section 7.1.5) and dissolved in 10 mL glacial acid. The autoclave was charged with 20 bar O₂ and heated to 180 °C for 90 min. The pressure increased to 30 bar, dropped down to 20 bar and was recharged to 30-40 bar two more times. The autoclave was recharged as often as needed, until the pressure stayed constant. Carboxylic acid anhydride was precipitated out of the solution and washed with water. A second/third portion was yielded overnight, filtered, washed with water and finally dried in vacuum.

Yield: 3.43 g, 13.3 mmol, 96%. - ¹H NMR (CDCl₃, 300 MHz): δ = 7.95 (s, 2 H, Ar-CH), 1.76 (s, 4 H, -CH₂), 1.36 (s, 12 H, -CH₃) ppm.

Experimental Section

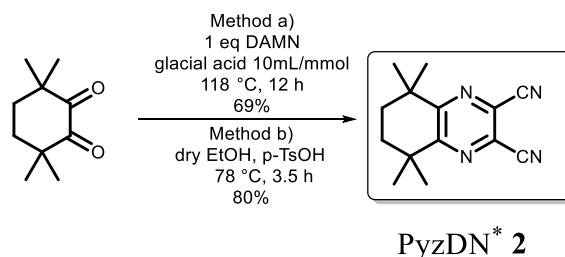
7.3.2 Synthesis of PyzDN*

The synthesis of 3,3,6,6-tetramethylcyclohexane-1,2-dione (**XIV**) was carried out following the procedure of JONES.^[139] The synthesis of PyzDN* **2** was carried out according to the procedure of SEIKEL.^[70]



7.3.2.1 Synthesis of

5,5,8,8-Tetramethyl-5,6,7,8-tetrahydroquinoxaline-2,3-dicarbonitrile^[70]

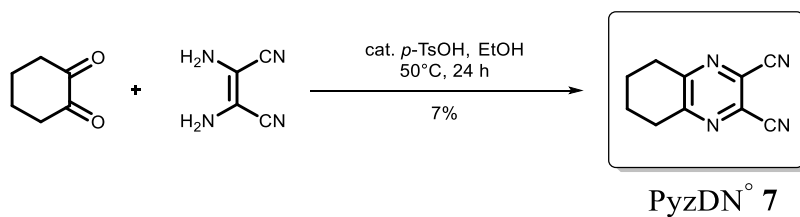


General Procedure 1: Condensation to Pyrazine Dinitriles.

1 eq Diketone was weighed out with 1.2 eq diamine and dissolved in 150 mL EtOH/10 g diketone. Cat. amounts *p*-TsOH (spatula tip) were added, and the solution was stirred for 6 h reflux at 120 °C. After cooling down to rt, the solvent was removed, the crude product was loaded onto silica and was purified by CC. The product was obtained in the form of a white, light yellowish solid.

Yield: 13.1 g, 54.7 mmol, 80%. - *R_f* (PE/DCM 1: 1) = 0.38. - ¹H NMR (CDCl₃, 250 MHz): δ = 1.86 (s, 4 H, -CH₂), 1.36 (s, 12 H, -CH₃) ppm.

Additional Information: For additional purification, the product was sublimed at $5 \cdot 10^{-3}$ mbar, 55 – 95 °C to finally obtain PyzDN* in the form of a white solid.

7.3.3 Synthesis of PyzDN^o [149]

According to General Procedure 1 (p. 204).

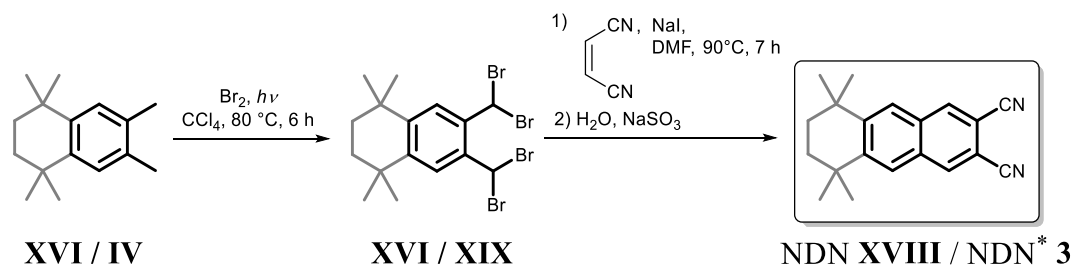
The organic layer was dried over MgSO₄, was filtered and recrystallized from DEE. The product was obtained as a brown powder.

Yield: 7%. - ¹H NMR (DMSO-*d*₆, 300 MHz): δ = 3.02 (q, 2 H, ³J_{H-H} = 6.7 Hz, -CH₂), 1.89 (q, 2 H, ³J_{H-H} = 6.7 Hz, -CH₂) ppm. - ¹³C NMR (DMSO-*d*₆, 75 MHz): δ = 158.2, 129.8, 114.1, 31.7, 20.9 ppm.

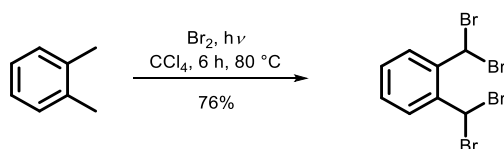
7.4 Synthesis of Aza-/Naphthalonitriles

7.4.1 Synthesis of NDN and NDN*

The synthesis of NDN **XVIII** and NDN* **3** was carried out within the Bachelor-Thesis of VOLLGRAFF,^[140] following the reported procedures of KOVSHEV,^[277] and MIKHALENKO.^[24]



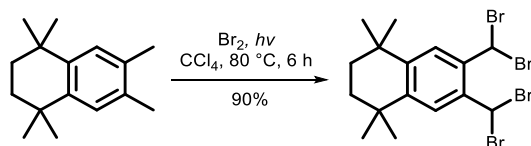
7.4.1.1 Synthesis of 6,7-Bis(dibromomethyl)-xylene^[140]



The synthesis was carried out according to the procedure described in section 7.4.1.2, below. The analysis is accordance with literature values, whereby the product was also converted to the dinitrile without further purification.

Yield: 76%.

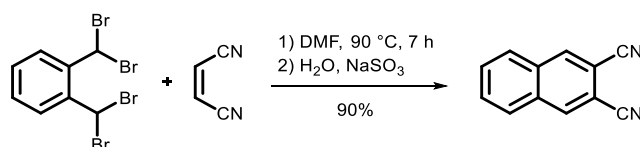
7.4.1.2 Synthesis of 6,7-Bis(dibromomethyl)-1',1',4',4'-tetramethyltetraline^[140]



13.2 g 1,1,4,4,6,7-hexamethyltetraline (61.0 mmol, 1.0 eq) were dissolved in 100 mL CCl₄ and the solution was warmed to 80 °C. The solution was irradiated with UV radiation, and 41.8 g bromine (523 mmol, 8.5 eq) were added dropwise over a period of 6 h. After addition, the solution was refluxed another 2 h. After removing the solvent under reduced pressure, the residue was washed with 10 mL pentane. The powder was dried in vacuum. 6,7-bis(dibromomethyl)-1',1',4',4'-tetramethyltetraline was obtained in the form of yellowish needles.

Yield: 29.2 g, 54.9 mmol, 90%. - $^1\text{H NMR}$ (CDCl_3 , 300 MHz): $\delta = 7.53$ (s, 2 H, Ar-CH), 7.11 (s, 2 H, -CHBr₂), 1.68 (s, 4 H, -CH₂), 1.27 (s, 12 H, -CH₃) ppm. - The $^1\text{H NMR}$ spectrum shows the expected by-products of a bromination. The product was used without further purification, because a purification of the NDN* is easier. - **Elemental analysis:** fnd. (cal.): C 35.59% (36.12%), H 3.59% (3.79%); Br 58.98% (60.08%).

7.4.1.3 Synthesis of 2,3-Naphthalonitrile ^[140]

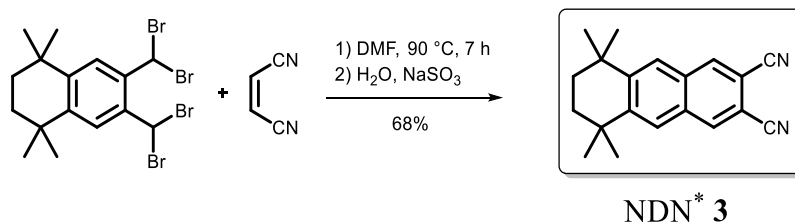


The synthesis was carried out according to the described procedure in section 7.4.1.4, below.

Yield: 90%. - The analysis is accordance with literature values.

7.4.1.4 Synthesis of

1',1',4',4'-Tetramethyl-1',2',3',4'-tetrahydroanthracen-6,7-dicarbonitrile ^[140]

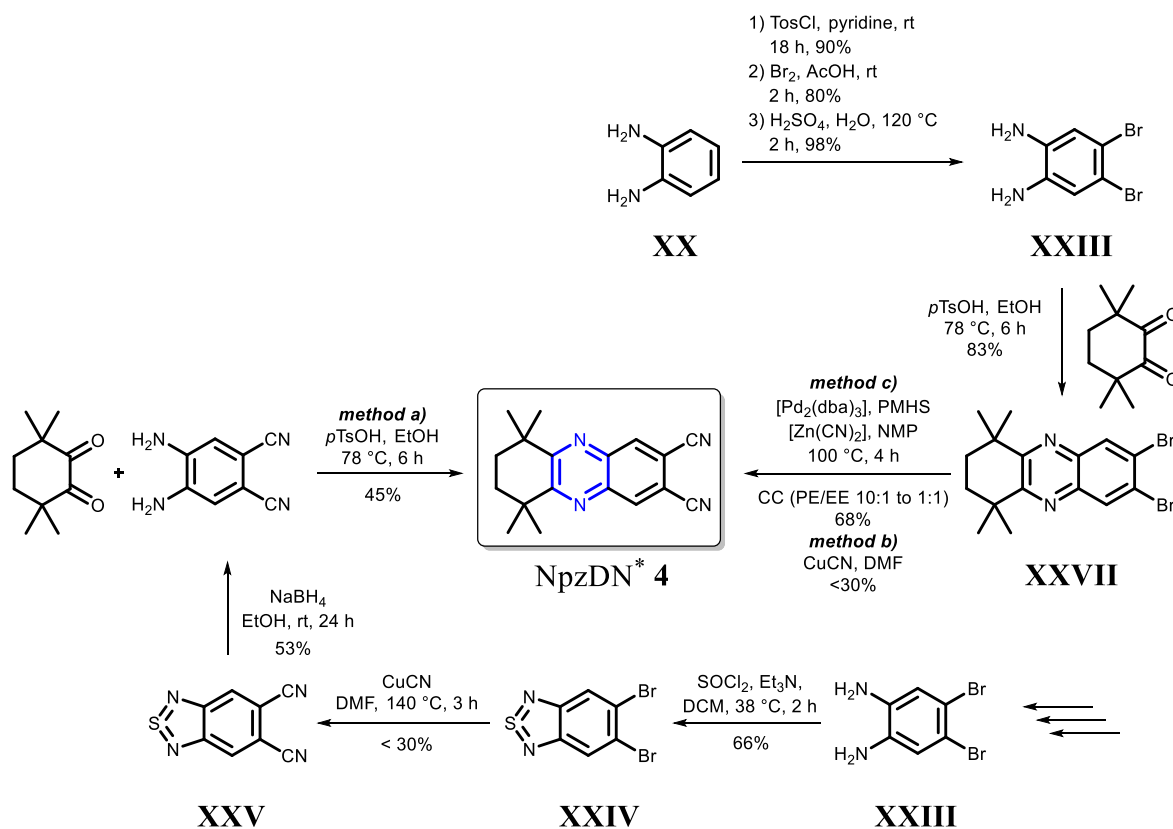


10.0 g 6,7-bis(dibromomethyl)-1,1,4,4-tetramethyltetraline (19.0 mmol, 1.0 eq), 2.63 g fumaronitrile (33.7 mmol, 1.8 eq) and 20.0 g sodium iodide (134 mmol, 7.1 eq) were dissolved in 20 mL DMF and the solution was stirred at 90 °C for 7 h. After 2 h and 4 h, respectively, another portion of fumaronitrile (each 0.3 g, 3.85 mmol, 0.2 eq) was added. The reaction mixture was cooled down to rt, and 20 mL ice water was added. A brownish powder was obtained, which was treated with 200 mL sodium sulfite solution and filtered. The product was purified by CC (toluene). 1,1,4,4-Tetramethyl-1,2,3,4-tetrahydroanthracen-6,7-dicarbonitrile was obtained in the form of a brownish powder. The product was finally sublimed at 120 °C, 10⁻³ mbar, to obtain NDN* in the form of a white solid.

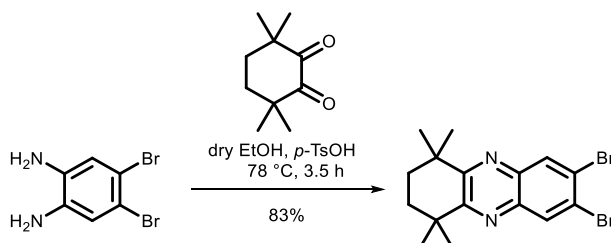
Yield: 3.75 g, 13.0 mmol, 68%. - *R_f* (toluene) = 0.30. - ¹H NMR (CDCl₃, 300 MHz): δ = 8.24 (s, 2 H, Ar-CH-5, H-8), 7.89 (s, 2 H, Ar-CH-1, H-4), 1.80 (s, 4 H, -CH₂), 1.41 (s, 12 H, -CH₃) ppm. - ¹³C NMR (CDCl₃, 75 MHz): δ = 150.7, 135.6, 131.6, 126.3, 116.4, 108.9, 35.3, 34.6, 32.5 ppm. - IR (ATR, 400-4000 cm⁻¹): ν̄ = 2961 (s) 2925 (s), 2857 (m), 2349 (w), 2326 (w), 2230 (m), 1623 (w), 1460 (vs), 1366 (m), 1205 (w), 1110 (m), 920 (vs), 542 (m), 528 (w), 467 (vs) cm⁻¹. - MS (APCI-HRMS(+)): m/z = 311.1523 [M+Na]⁺, cal. for C₂₀H₂₀N₂+Na₁: 311.1519. - **Elemental analysis** (C₂₀H₂₀N₂, M = 288.39 g/mol): *find.* (*cal.*): C 82.50% (83.30%), H 6.97% (6.99%), N 9.53% (9.71%).

7.4.2 Synthesis of NpzDN*

Three different methods were carried out. For all synthetic paths, 4,5-dibromobenzene-1,2-diamine (**XXIII**) was synthesised according to a literature known procedure, starting with *o*-phenylenediamine.^[278] The synthesis of 4,5-dibromobenzene-1,2-diamine (**XXIII**) was carried out by HAMEL in our group. The reaction could be reproduced as described in literature.^[278,279] For method a) this compound was further used for the synthesis of 4,5-diaminophthalonitrile, according to BURMESTER and FAUST.^[279]



7.4.2.1 Synthesis of 7,8-Dibromo-1,1,4,4-tetramethyl-1,2,3,4-tetrahydrophenazine



According to General Procedure 1 (p. 204).

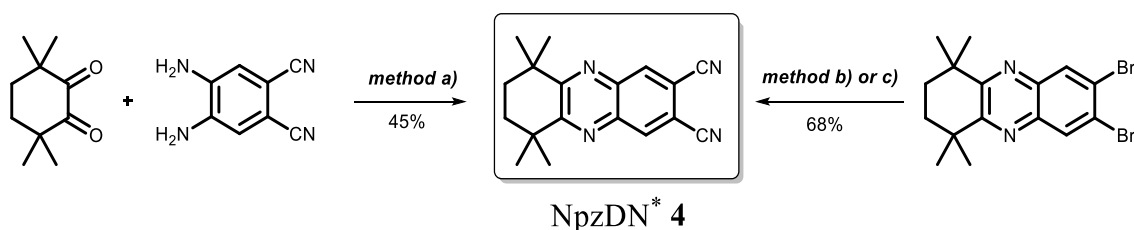
7,8-Dibromo-1,1,4,4-tetramethyl-1,2,3,4-tetrahydrophenazine was purified by CC (DCM).

Experimental Section

Yield: 83%. - **¹H NMR** (CDCl₃, 300 MHz): δ = 8.30 (s, 2 H, Ar-CH), 1.88 (s, 4 H, -CH₂), 1.40 (s, 12 H, -CH₃) ppm. - **¹³C NMR** (CDCl₃, 75 MHz): δ = 161.4, 140.4, 132.7, 124.7, 38.3, 33.8, 30.0 ppm. - **IR** (ATR, 400-4000 cm⁻¹): $\tilde{\nu}$ = 2953 (m), 2863 (w), 1720 (w), 1437 (w), 1379 (w), 1357 (w), 1328 (w), 1250 (w), 1215 (w), 1168 (w), 1115 (s), 1053 (w), 1017 (w), 956 (w), 934 (w), 873 (m), 800 (w), 690 (w), 670 (w) cm⁻¹. - **MS** (APCI-HRMS(+), DCM/MeCN): m/z = 398.9890 [M+H]⁺, cal. for C₁₆H₁₈Br₂N₂+H₁: 398.9890. - **Elemental analysis** (C₁₆H₁₈Br₂N₂, M = 398.14 g/mol): *find.* (*cal.*): C 48.66% (48.27%), H 4.59% (4.56%), N 6.93% (7.04%).

Additional information: The reaction can be carried out, using the 1,2-diamino-4,5-dibromobenzene in excess >2 eq. The 1,2-diamino-4,5-dibromobenzene can be removed from the product/regained by filtration.

7.4.2.2 Synthesis of 6,6,9,9-Tetramethyl-6,7,8,9-tetrahydrophenazine-2,3-dicarbonitrile



For synthesis of 6,6,9,9-tetramethyl-6,7,8,9-tetrahydrophenazine-2,3-dicarbonitrile NpzDN* 4 different methods were carried out. The most efficient one, with the best overall yield, was found to be method c).

Method a): According to General Procedure 1 (p. 204), using 4,5-diaminophthalonitrile. Workup was carried out according to method c).

Yield: 45%.

Method b): ROSENMUND-VON-BRAUN reaction, see Electronic Supplement.

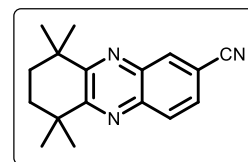
Yield: 30%.

Method c): 300 mg 1,2-diamino-5,6-dibromobenzene (0.75 mmol, 1 eq) were dissolved in 2 mL NMP. Two drops (about 30 mg) PMHS were added. The solution was stirred at 100 °C until the dibromide was completely dissolved. 22 mg [Pd₂(dba)₃] (3 mol%) were added, as well as 15 mg dppf (3.5 mol%). 100 mg [Zn(CN)₂] were added portionwise (4 x 25 mg) every 15 min. When [Zn(CN)₂] is added too fast the yield decreases drastically! The solution was

stirred for 4 h. The conversion was monitored using TLC (PE/EE 5:1). NMP was removed in vacuum, and the resulting solid was purified by CC (PE/EE 10:1 → 1:1).

Yield: 148 mg, 510 μmol, 68%. - R_f (PE/EE 5:1) = 0.31. - $^1\text{H NMR}$ (CDCl_3 , 300 MHz): δ = 8.47 (s, 2 H, Ar-CH), 1.94 (s, 4 H, -CH₂), 1.44 (s, 12 H, -CH₃) ppm. - $^{13}\text{C NMR}$ (CDCl_3 , 75 MHz): δ = 165.5, 141.6, 136.6, 115.2, 113.0, 39.0, 33.5, 30.0 ppm. - **MS** (APCI-HRMS(+), DCM/MeCN): m/z = 291.1605 [M+H]⁺, cal. for C₁₈H₁₈N₄H₁: 291.1604. - **IR** (ATR, 400-4000 cm⁻¹): $\tilde{\nu}$ = 2965 (m), 2927 (m), 2861 (m), 2235 (w), 1554 (s), 1456 (s), 1397 (w), 1361 (w), 1325 (w), 1257 (m), 1223 (w), 1114 (s), 1055 (w), 1018 (w), 957 (m), 904 (s), 806 (w), 725 (w), 643 (w), 534 (s) cm⁻¹. - **Elemental analysis** (C₁₈N₁₈N₄, M = 290.37 g/mol): **found**. (cal.): C 72.35% (74.46%), H 6.20% (6.25%), N 17.38% (19.30%).

Additional information: As by-product, 6,6,9,9-tetramethyl-6,7,8,9-tetrahydrophenazine-2-carbonitrile was obtained, especially when applying ROSENMUND-VON-BRAUN conditions.



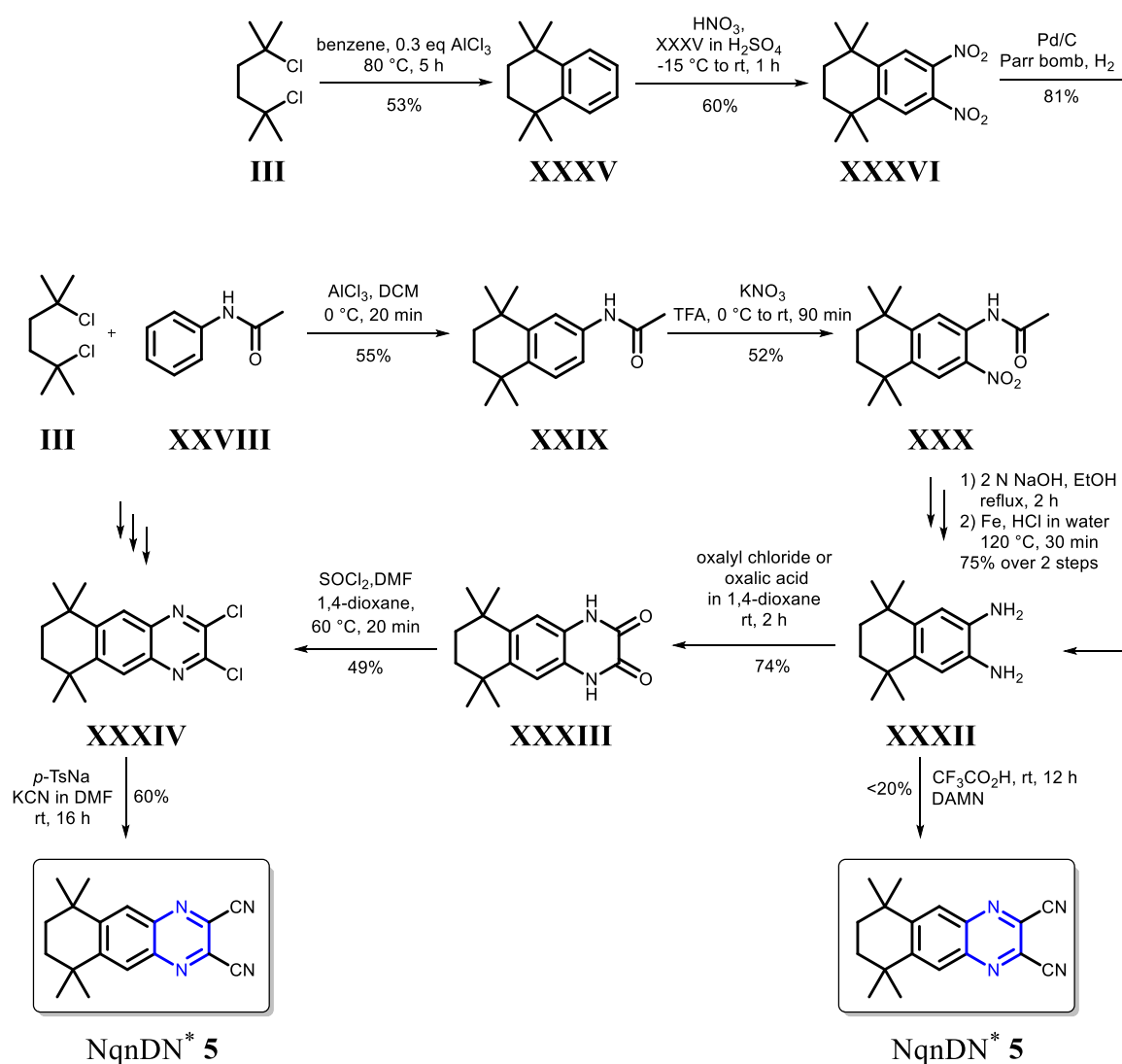
Yield: n.d. - R_f (PE/EE 5:1) = 0.71. - $^1\text{H NMR}$ (CDCl_3 , 300 MHz): δ = 8.37 (d, 1 H, $^3J_{\text{H-H}} = 1.6$ Hz, Ar-CH), 8.06 (d, 1 H, $^3J_{\text{H-H}} = 8.6$ Hz, Ar-CH), 7.77 (dd, 1 H, $^3J_{\text{H-H}} = 1.8, 8.6$ Hz, Ar-CH), 1.93 (s, 4 H, -CH₂), 1.43 (s, 12 H, -CH₃) ppm.

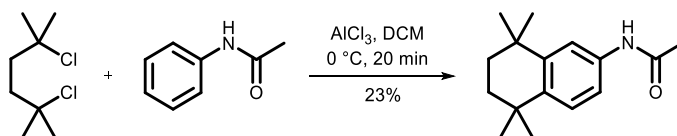
When the reaction of method c) was stirred overnight, a change in colour to green was observed. Here, traces of [Npz^{*}M] are formed, which can be easily removed by CC (PE/EE 10:1 → 1:1).

Experimental Section

7.4.3 Synthesis of NqnDN*

Here, three methods were carried out: Two different synthetic paths were applied to obtain 5,6,7,8-tetrahydro-5,5,8,8-tetramethylnaphthalene-2,3-diamine **XXXII**. It is the precursor for 2,3-dichloro-6,6,9,9-tetramethyl-6,7,8,9-tetrahydrobenzo[*g*]quinoxaline (NqnDN* **5**). Using **XXXII** as starting material, NqnDN* **5** can be obtained in a three step synthesis over compound **XXXIII** and **XXXIV**, as well as in a one step synthesis: a condensation using DISN under acidic conditions. The second synthesis is shorter, but lower yields were obtained.

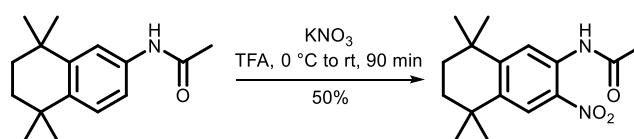


7.4.3.1 Synthesis of 6-Acetamido-1,2,3,4-tetrahydro-1,1,4,4-tetramethylnaphthalene ^[142]

2.03 g Acetanilide (15.0 mmol, 1 eq) were suspended in 20 mL DCM. The solution was cooled to -15 °C (with NaCl/ice), and 5.00 g AlCl₃ (37.4 mmol, >2 eq) were added. A solution of 4.8 g 2,5-dichloro-2,5-dimethylhexane (26.2 mmol, 1.7 eq) in 15 mL DCM was added quickly. The solution was stirred for 90 min, poured onto ice water and the organic phase was separated. The organic phase was washed with K₂CO₃ solution and water, dried over MgSO₄, filtered, concentrated and finally dried in vacuum. The resulting powder was recrystallized from hexane at -25 °C. EtOH/H₂O 1:1 was added, but the brownish slurry could not be removed. EA was added after drying in vacuum. The brownish powder was recrystallized in EA. A white precipitate was formed. The brown solution was removed, and a white solid was collected.

Yield: 837 mg, 3.41 mmol, 23%. - ¹H NMR (DMSO-*d*₆, 300 MHz): δ = 7.50 (d, 1 H, ³J_{H-H} = 7.8 Hz, Ar-CH), 7.34 (dd, 1 H, ⁴J_{H-H} = 2.8 Hz, ³J_{H-H} = 15.3 Hz, Ar-CH), 7.06 (d, 1 H, ³J_{H-H} = 7.4 Hz, Ar-CH), 2.12 (s, 3 H, -CH₃), 1.64 (s, 4 H, -CH₂), 1.26 (s, 6 H, -CH₃), 1.24 (s, 6 H, -CH₃) ppm. *NH was not detected.

7.4.3.2 Synthesis of

6-Acetamido-7-nitro-1,2,3,4-tetrahydro-1,1,4,4-tetramethylnaphthalene ^[142]

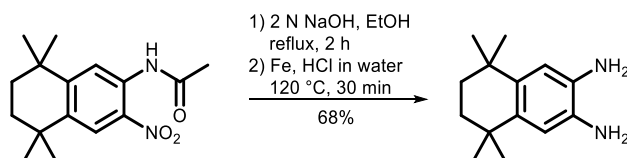
800 mg 1,2,3,4-tetrahydro-1,1,4,4-tetramethyl-6-acetaminonaphthalene (3.26 mmol, 1 eq) were completely dissolved in 2 mL TFA at 0 °C. 362 mg KNO₃ (3.59 mmol, 1.1 eq) were added at once, and the solution was stirred for 90 min while warming up to rt. The solution was poured onto ice and extracted with EA. The organic layer was washed several times with water and NaHSO₄. After drying the organic phase over MgSO₄ and filtration, it was concentrated in vacuum. The product could not be recrystallized as described in literature, so it was purified by CC (PE/EE 1:1) to give a yellowish powder/oil.

Experimental Section

Yield: 473 mg, 1.63 mmol, 50%. - $^1\text{H NMR}$ (CDCl_3 , 300 MHz): $\delta = 10.19$ (s, 1 H, -NH), 8.71 (s, 1 H, Ar-CH), 8.14 (s, 1 H, Ar-CH), 2.27 (s, 3 H, $\text{C}=\text{OCH}_3$), 1.71 (s, 4 H, - CH_2), 1.32 (s, 6 H, - CH_3), 1.29 (s, 6 H, - CH_3) ppm.

7.4.3.3 Synthesis of

5,6,7,8-Tetrahydro-5,5,8,8-tetramethylnaphthalene-2,3-diamine ^[142]



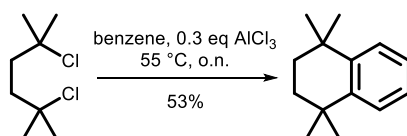
280 mg 6-acetamido-7-nitro-1,2,3,4-tetrahydro-1,1,4,4-tetramethylnaphthalene (0.96 mmol, 1 eq) were refluxed at 120 °C for 2 h in 10 mL 2 N NaOH and 10 mL EtOH. The solution was cooled down to rt, extracted 3 x 20 mL DCM, dried over MgSO_4 and directly converted to the diamine.

$^1\text{H NMR}$ (CDCl_3 , 300 MHz): $\delta = 8.05$ (s, 1 H, Ar-CH), 6.70 (s, 1 H, Ar-CH), 1.67 (s, 4 H, CH_2), 1.27 (s, 6 H, - CH_3), 1.26 (s, 6 H, - CH_3) ppm.

Therefore, 480 mg iron powder were added, as well as 1 mL conc. HCl and 10 mL water. The solution was stirred for 2 h at 120 °C. After cooling down to rt, the solution was neutralized using Na_2CO_3 , extracted 4 x 20 mL with EA, washed with NaCl solution and finally with water before drying over Na_2SO_4 . A yellow solid was obtained, which can be recrystallized from EA/hexane 1:1. White flakes could be obtained after filtration.

Yield: 142 mg, 650 μmol , 68%. - $^1\text{H NMR}$ (CDCl_3 , 300 MHz): $\delta = 6.91$ (s, 2 H, Ar-CH), 3.05 (bs, 4 H, - NH_2), 1.67 (s, 4 H, - CH_2), 1.25 (s, 12 H, - CH_3) ppm.

7.4.3.4 Synthesis of 1,1,4,4-Tetramethyl-1,2,3,4-tetrahydronaphthalene ^[280]



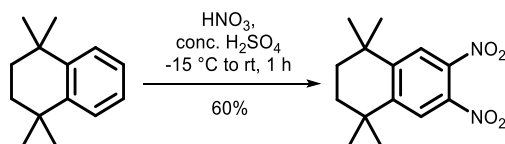
10.09 g 2,5-dichloro-2,5-dimethylhexane (55.1 mmol, 1 eq) were dissolved in 20 mL benzene at rt. Portionwise, 3.5 g AlCl_3 (26.2 mmol, ~0.5 eq, excess) were added to the solution. HCl_{gas} evolved. After stirring for 30 min at 50 °C, the solution was stirred overnight at 55 °C. The

solvent was removed, and DCM was added, as well as 20 mL 5% HCl. The aq. phase was extracted with DCM, washed with NaHCO₃ solution and finally concentrated in vacuum. If necessary, the product was distilled at 80 °C, 10⁻³ mbar. The product was obtained in the form of a yellowish oil.

Yield: 5.51 g, 29.1 mmol, 53%. - **¹H NMR** (CDCl₃, 300 MHz): δ = 7.30 (dd, ³J_{H-H} = 3.5 Hz, ³J_{H-H} = 5.9 Hz, 2 H, Ar-CH), 7.12 (d, ³J_{H-H} = 3.4 Hz, ³J_{H-H} = 5.9 Hz, 2 H, Ar-CH), 1.67 (s, 4 H, -CH₂), 1.27 (s, 12 H, -CH₃) ppm.

7.4.3.5 Synthesis of

1,1,4,4-Tetramethyl-6,7-dinitro-1,2,3,4-tetrahydronaphthalene [148,281]



5.89 g 1,1,4,4-tetramethyl-1,2,3,4-tetrahydronaphthalene (31.3 mmol, 1 eq) were dissolved in 20 mL in H₂SO₄ and slowly dropped into 10 mL HNO₃ at -15 °C. The reaction was stirred for 3 h, while it was warmed up to rt. It was poured onto ice, and extracted with THF or DEE. The organic phase was washed several times with NaHCO₃, with NaCl solution and finally with water. The organic phase was dried over Na₂SO₄, filtered, concentrated and finally dried in vacuum. The product was obtained in the form of a yellow-red powder.

Yield: 5.23 g, 18.8 mmol, 60%. - **¹H NMR** (CDCl₃, 300 MHz): δ = 7.79 (s, 2 H, Ar-CH), 1.73 (s, 4 H, -CH₂), 1.32 (s, 12 H, -CH₃) ppm.

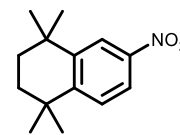
Additional information: The reaction was also carried out in acetic acid anhydride, but only 1,1,4,4-tetramethyl-6-nitro-1,2,3,4-tetrahydronaphthalene was observed.

7.4.3.6 Synthesis of 1,1,4,4-Tetramethyl-6-nitro-1,2,3,4-tetrahydronaphthalene [281]

Following the procedure in section 7.4.3.5. 1,1,4,4-tetramethyl-6,7-dinitro-1,2,3,4-tetrahydronaphthalene was only obtained when lower concentrations of 1,1,4,4-tetramethyl-1,2,3,4-tetrahydronaphthalene were used. Instead, in most cases 1,1,4,4-tetramethyl-6-nitro-1,2,3,4-tetrahydronaphthalene was obtained in the form of a white powder.

Experimental Section

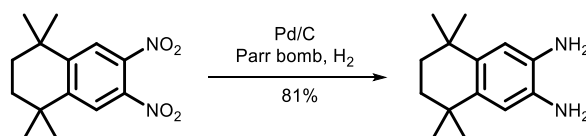
Yield: 5.15 g, 22.1 mmol, 66%. - **¹H NMR** (CDCl₃, 300 MHz): δ = 8.17 (d, ⁴J_{H-H} = 2.5 Hz, 1 H, Ar-CH), 7.94 (dd, ⁴J_{H-H} = 2.5 Hz, ³J_{H-H} = 8.7 Hz, 1 H, Ar-CH), 7.44 (d, ³J_{H-H} = 8.8 Hz, 1 H, Ar-CH), 1.72 (s, 4 H, -CH₂), 1.33 (s, 6 H, -CH₃), 1.31 (s, 6 H, -CH₃) ppm.



To obtain 1,1,4,4-tetramethyl-6,7-dinitro-1,2,3,4-tetrahydronaphthalene, 5.15 g 1,1,4,4-tetramethyl-6-nitro-1,2,3,4-tetrahydronaphthalene (22.1 mmol, 1 eq) were dissolved in 40 mL H₂SO₄ and added dropwise to 20 mL HNO₃ at -10 °C. Then, the mixture was stirred for 3 h while warming up to rt. When the solution was poured onto ice, a reddish solid was obtained. When DEE was added, the powder reacted vigorously, while going into the DEE phase. Nitrogen oxide gases evolved! Workup was carried out as described above. The product was obtained in the form of a yellow-red powder.

7.4.3.7 Synthesis of

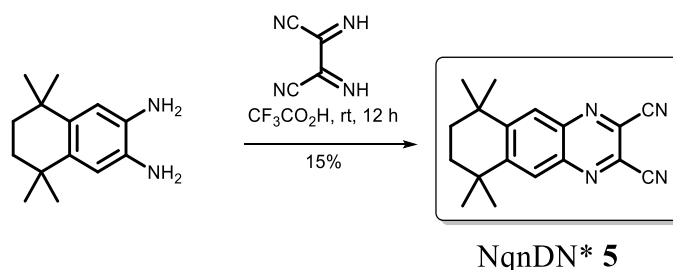
5,5,8,8-Tetramethyl-5,6,7,8-tetrahydronaphthalene-2,3-diamine [142,148]



The reaction was carried out in a glass autoclave. 1.91 g dinitro compound (6.86 mmol, 1 eq) were added to 230 mg Pd/C and suspended in 30 mL 95% aq. EtOH. The autoclave was charged with 15 bar H₂ and was stirred for 30 min. The pressure quickly dropped to 0 bar and the autoclave was recharged several times, while stirring at 10 bar for 3 d. Pd/C was removed by filtration and washed with 10 mL EtOH. The resulting solution was dried over MgSO₄, filtered, and concentrated before drying the resulting powder in vacuum. The product was obtained in the form of a yellow solid.

Yield: 1.21 g, 5.54 mmol, 81%. - Analysis in according with values in section 7.4.3.3.

7.4.3.8 Synthesis of NqnDN* 5 using DISN

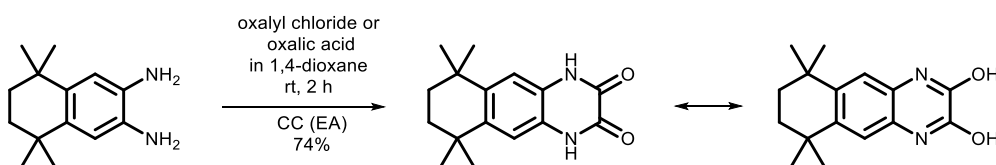


According to a literature known procedure,^[145,147] diiminosuccinonitrile (DISN) was freshly prepared using DAMN and DDQ in MeCN. Therefore, 500 mg DAMN (4.63 mmol, 1 eq) were suspended in 10 mL MeCN. 1.05 g DDQ (4.63 mmol, 1 eq) were added at once, and the solution turned beige-rosé. After 30 min of stirring at rt, the solution was filtered over Celite[®], and the filtrate was concentrated in vacuum.

A mixture of 106 mg DISN (1.00 mmol, 1 eq) and 218 mg phenylenediamine (1.00 mmol, 1 eq) was dissolved in 1 mL TFA at rt. Ammonia slowly bubbled out of the solution. The solution was stirred at rt overnight. The slurry was precipitated into ice-water and extracted with EA, dried over MgSO₄, filtered and the resulting powder was finally dried in vacuum. After purification by CC (PE/DCM 1:1), NqnDN* 5 was obtained in the form of a yellowish solid.

Yield: 42 mg, 0.14 mmol, 15%. - Analysis is in accordance with values in section 7.4.3.11. The synthesis was reproduced by HAMEL in our group yielding up to 20%.

7.4.3.9 Synthesis of

6,6,9,9-Tetramethyl-1,4,6,7,8,9-hexahydrobenzo[g]quinoxaline-2,3-dione

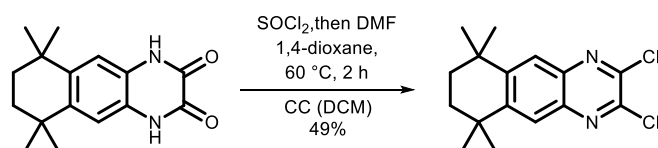
1.20 g 5,6,7,8-tetrahydro-5,5,8,8-tetramethylnaphthalene-2,3-diamine (5.50 mmol, 1 eq) were dissolved in 25 mL 1,4-dioxane. 2.0 mL oxalylchloride (2.96 g, 23.3 mmol, 4.2 eq, excess) in 20 mL 1,4-dioxane were added in two portions dropwise at rt. The solution was stirred for 2 h at rt. After removing the solvent under reduced pressure, the obtained powder was dissolved in EA. The organic phase was extracted with water until the water showed a pH ~5. If necessary, the product was additionally purified by CC (EA).

Experimental Section

Yield: 1.01 g, 3.71 mmol, 74%. - R_f (EA) = 0.90. - $^1\text{H NMR}$ (DMSO- d_6 , 300 MHz): δ = 10.32 (s, 2 H, NH, -OH), 7.37 (s, 2 H, Ar-CH), 1.67 (s, 4 H, -CH₂), 1.25 (s, 12 H, -CH₃) ppm. - $^1\text{H NMR}$ (Acetone- d_6 , 300 MHz): δ = 10.08 (s, 2 H, NH, -OH), 7.76 (s, 2 H, Ar-CH), 1.75 (s, 4 H, -CH₂), 1.32 (s, 12 H, -CH₃) ppm. - **MS** (APCI-HRMS(+)): m/z = 273.1598 [M+H]⁺, cal. for C₁₆H₂₀N₂O₂+H₁: 273.1598.

7.4.3.10 Synthesis of

2,3-Dichloro-6,6,9,9-tetramethyl-6,7,8,9-tetrahydrobenzo[g]quinoxaline

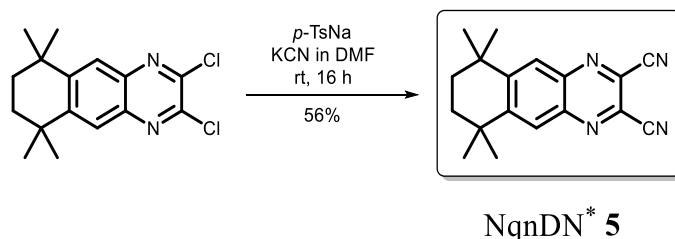


1.01 g dione (3.71 mmol, 1 eq) were dissolved in 20 mL 1,4-dioxane. 2.7 mL thionylchloride (37.2 mmol, 10 eq, excess) were added and stirred for 20 min at 60 °C, before the addition of 2 ml DMF. The solution was stirred at 60 °C for 2 h. After cooling down to rt, the solvent was evaporated under reduced pressure, and the residue was dried in vacuum. The crude product was purified by CC (DCM).

Yield: 555 mg, 1.79 mmol, 49%. - R_f (DCM) = 0.80. - $^1\text{H NMR}$ (CDCl₃, 300 MHz): δ = 7.97 (s, 2 H, Ar-CH), 1.79 (s, 4 H, -CH₂), 1.40 (s, 12 H, -CH₃) ppm. - $^{13}\text{C NMR}$ (CDCl₃, 75 MHz): δ = 151.0, 125.3, 35.2, 34.5, 32.2 ppm. - not all carbons could be detected. - **MS** (APCI-HRMS(+)): m/z = 309.0921 [M+H]⁺, cal. for C₁₆H₁₈Cl₂N₂+H: 309.0920.

7.4.3.11 Synthesis of

6,6,9,9-Tetramethyl-6,7,8,9-tetrahydrobenzo[g]-quinoxaline-2,3-dicarbonitrile



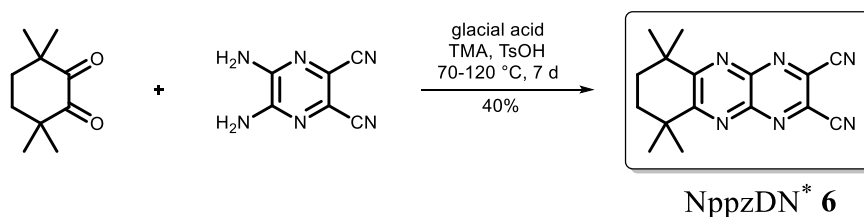
230 mg 2,3-dichloro-6,6,9,9-tetramethyl-6,7,8,9-tetrahydrobenzo[g]quinoxaline (0.74 mmol, 1 eq) were dissolved in 5 mL DMF. 145 mg sodium(I)-*p*-toluenesulfinate (0.74 mmol, 1 eq) were added, and afterwards 111 mg KCN (1.7 mmol, 2.3 eq). The solution was stirred at rt

overnight. The conversion to NqnDN* was monitored by TLC (PE/EE 1:1). After 2 h, no conversion was visible. The solution was stirred overnight. The solvent was removed in vacuum. The resulting brown slurry was purified by CC (PE/DCM 1:1). NpzDN* **5** was obtained in form of a yellow solid.

Yield: 120 mg, 0.41 mmol, 56%. - R_f (PE/DCM 1:1) = 0.5. - $^1\text{H NMR}$ (CDCl_3 , 300 MHz): δ = 8.19 (s, 2 H, Ar-CH), 1.84 (s, 4 H, -CH₂), 1.46 (s, 12 H, -CH₃) ppm. - $^{13}\text{C NMR}$ (CDCl_3 , 75 MHz): δ = 156.3, 140.0, 127.0, 113.7, 35.9, 34.1, 32.3 ppm. - the quaternary carbons could not be detected. - **IR** (ATR, 400-4000 cm^{-1}): $\tilde{\nu}$ = 2965 (m), 2932 (m), 2864 (w), 1469 (s), 1391 (w), 1365 (w), 1259 (s), 1214 (s), 1186 (m), 1164 (m), 1097 (s), 1049 (s), 1021 (s), 888 (m), 870 (m), 797 (s) cm^{-1} . - **MS** (APCI-HRMS(+)): m/z = 291.1602 $[\text{M}+\text{H}]^+$, cal. for $\text{C}_{18}\text{H}_{18}\text{N}_4+\text{H}_1$: 291.1602. - **Elemental analysis** ($\text{C}_{18}\text{N}_{18}\text{N}_4$, $M = 290.37$ g/mol): fnd. (cal.): C 70.74% (74.46%), H 6.54% (6.25%), N 13.80% (19.30%).

Experimental Section

7.4.4 Synthesis of NppzDN*



1.00 g 3,3,6,6-tetramethylcyclohexane-1,2-dione (5.64 mmol, 1 eq) were dissolved in glacial acid with 5,6-diaminopyrazine-2,3-dicarbonitrile (5.64 mmol, 1-1.2 eq). The reaction was monitored by ^1H NMR spectroscopy and TLC. After 7 d, 50% of the dione was converted to the product. The solution was refluxed for another 4 d. The solvent was removed under reduced pressure. The brown slurry was dissolved in DCM and the excess of diamine was filtered off. The solvent was evaporated, and the product was washed with hexane to remove traces of the dione. The product, 6,6,9,9-tetramethyl-6,7,8,9-tetrahydropyrazino[2,3-b]quinoxaline-2,3-dicarbonitrile, was sublimed at 130 °C, 10^{-3} mbar to finally obtain it in the form of a yellow-orange powder.

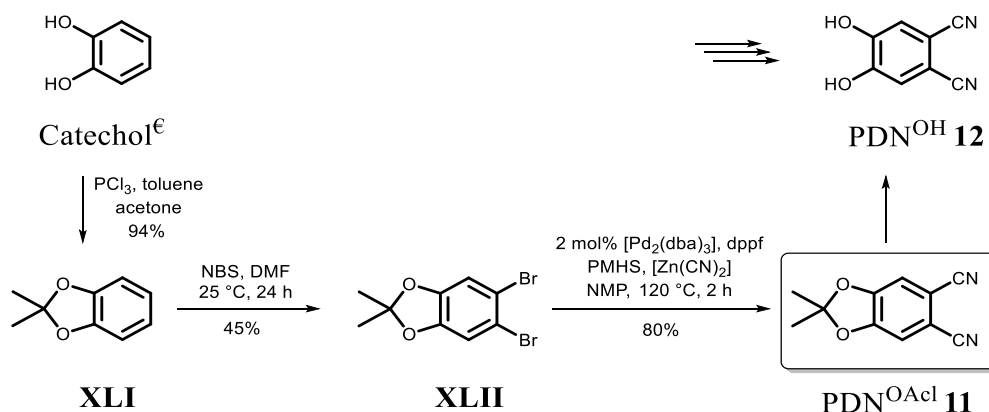
Yield: 400 mg, 1.32 mmol, 40%. - R_f (DCM) = 0.52. - ^1H NMR (CDCl_3 , 300 MHz): δ = 2.02 (s, 4 H, $-\text{CH}_2$), 1.54 (s, 12 H, $-\text{CH}_3$) ppm. - ^{13}C NMR (CDCl_3 , 75 MHz): δ = 172.4, 143.6, 132.9, 112.5, 40.2, 33.1, 30.0 ppm. - **IR** (ATR, 400-4000 cm^{-1}): $\tilde{\nu}$ = 2966 (m), 2931 (m), 2868 (w), 1716 (m), 1458 (m), 1393 (s), 1374 (m), 1256 (w), 1239 (w), 1211 (w), 1166 (w), 1122 (s), 1099 (w), 1059 (w), 1019 (w), 915 (w), 720 (m), 636 (w), 546 (w), 499 (s) cm^{-1} . - **MS** (APCI-HRMS(+), DCM/MeCN): m/z = 293.1510 $[\text{M}+\text{H}]^+$, cal. for $\text{C}_{16}\text{H}_{16}\text{N}_6+\text{H}_1$: 293.1509. - **Elemental analysis:** fnd. (cal.): C 64.15% (65.74%), H 5.57% (5.52%), N 26.56% (28.75%).

Additional information: If necessary, a CC (DCM) was carried out before sublimation. Optimisation of the reaction was attempted. In the first attempt, the reaction was carried out according to General Procedure 1 (p. 204). Here, no formation of NppzDN* 6 was observed. Additionally, different acids (acetic acid anhydride, methyl formate, triethyl orthoformate, or similar acids to act as water scavengers) were added, and the reaction time increased up to 7 d, 78 °C. Full conversion was monitored by TLC after 11 d. Anyway, no higher yields were obtained.

7.5 Synthesis of Functionalised Precursors

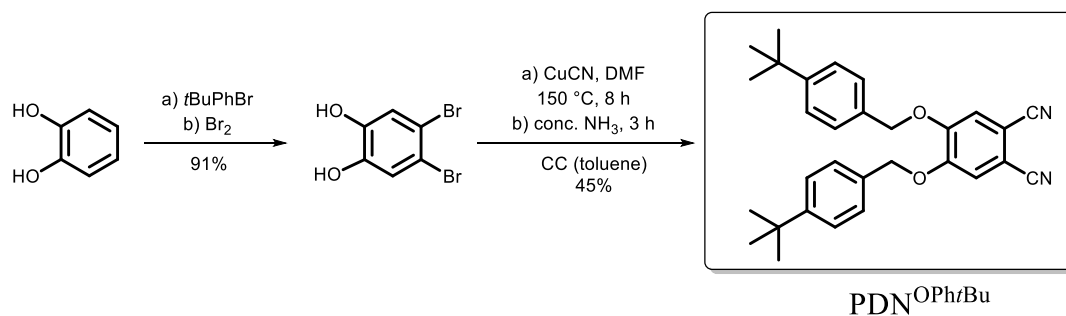
7.5.1 Synthesis of PDN^{OAc}

The synthesis of 5,6-dicyano-2,2-dimethyl-1,3-benzodioxole and precursors (PDN^{OAc} **11**) was carried out according to a literature described procedure.^[136,209] In the final step, compound **11** can be obtained in a ROSENMUND-VON-BRAUN reaction or via a Pd catalysed reaction.



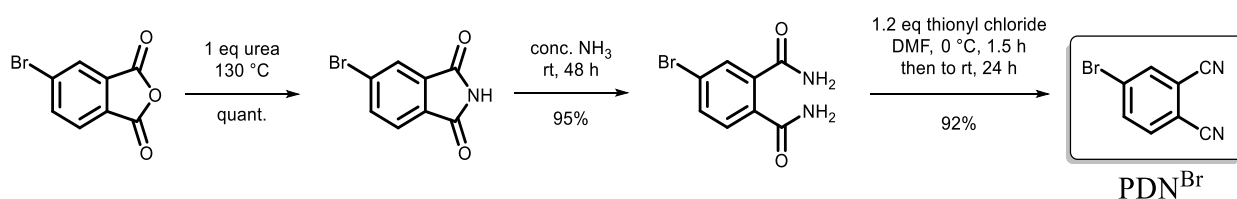
7.5.2 Synthesis of PDN^{O^tBu}

The synthesis of 4,5-bis-(4-*tert*-butylbenzoxy)phthalonitrile was carried out according to a literature known procedure.^[219]



7.5.3 Synthesis of PDN^{Br}

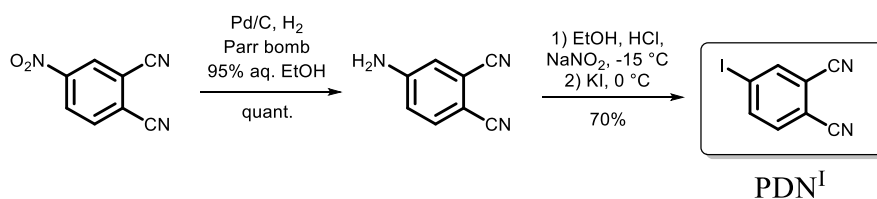
The synthesis was carried out according to the Master-Thesis of LIEBOLD,^[13] according to the literature reported procedure by MÄRKL.^[282]



Experimental Section

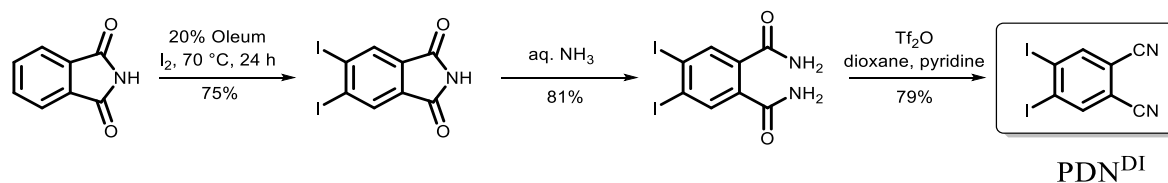
7.5.4 Synthesis of PDN^I

The synthesis was carried out following the reported procedure of ARANYOS.^[283]



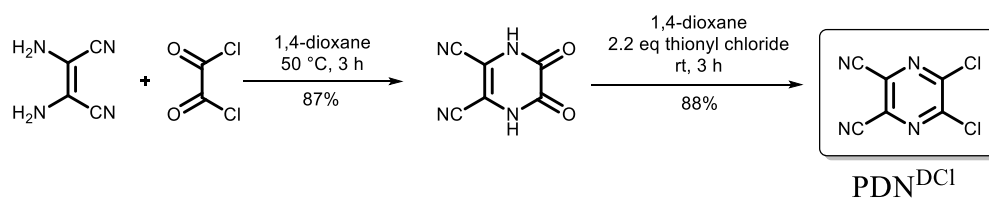
7.5.5 Synthesis of PDN^{DI}

4,5-diiodobenzenedicarbonitrile was synthesised according to a literature known procedure.^[284]



7.5.6 Synthesis of PyzDN^{Cl} and Precursors

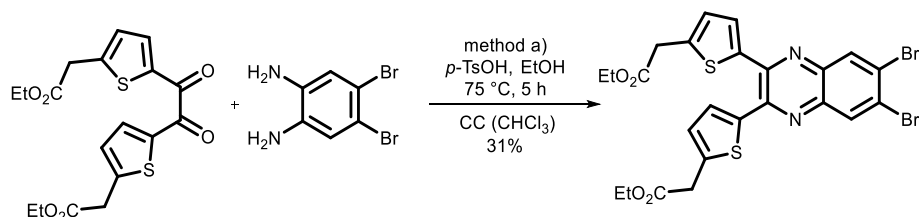
The synthesis was carried out according to the Master-Thesis of LIEBOLD,^[13] according to the literature reported procedure by SUZUKI.^[285]



7.6 Synthesis of QnDN^{TP} and PzDN^{TP}

7.6.1 Synthesis of

Diethyl 2,2'-((6,7-dibromoquinoxaline-2,3-diyl)bis(thiophene-5,2-diyl))diacetate



According to General Procedure 1 (p. 204).

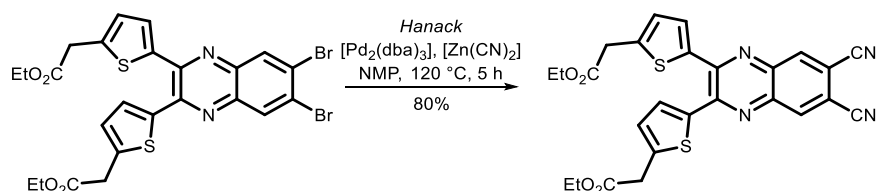
The product was purified by CC (CHCl₃) and obtained in the form of a yellowish powder.

Yield: 31%*. - **R_f** (CHCl₃) = 0.59. - **¹H NMR** (CDCl₃, 300 MHz): δ = 8.33 (s, 2 H, Ar-CH), 7.24 (d, 2 H, ³J_{H-H} = 3.7 Hz, Ar-CH^{Thio}), 6.88 (d, 2 H, ³J_{H-H} = 3.8 Hz, Ar-CH^{Thio}), 4.23 (q, 4 H, ³J_{H-H} = 7.2 Hz, -CH₂), 3.87 (s, 2 H, -CH₂), 1.31 (t, 6 H, ³J_{H-H} = 7.1 Hz, -CH₃) ppm. - **¹H NMR** (CD₂Cl₂, 300 MHz): δ = 8.32 (s, 2 H, Ar-CH), 7.24 (d, 2 H, ³J_{H-H} = 3.7 Hz, Ar^{Thio}-CH), 6.89 (d, 2 H, ³J_{H-H} = 3.8 Hz, Ar^{Thio}-CH), 4.24 (q, 4 H, ³J_{H-H} = 7.2 Hz, -CH₂), 3.88 (s, 2 H, -CH₂), 1.31 (t, 6 H, ³J_{H-H} = 7.1 Hz, -CH₃) ppm. - **¹³C NMR** (CD₂Cl₂, 75 MHz): δ = 170.2, 147.9, 141.0, 140.9, 140.2, 133.1, 130.2, 127.9, 126.6, 61.8, 36.2, 14.4 ppm. - **MS** (APCI-HRMS(+)): m/z = 624.9278 [M+H]⁺, C₂₄H₂₀Br₂N₂O₄S₂+H₁: 624.9284.

*The calculation is based on the dione, whereby the unpurified (unseparated) product was used.

7.6.2 Synthesis of

Diethyl 2,2'-((6,7-dicyanoquinoxaline-2,3-diyl)bis(thiophene-5,2-diyl))diacetate



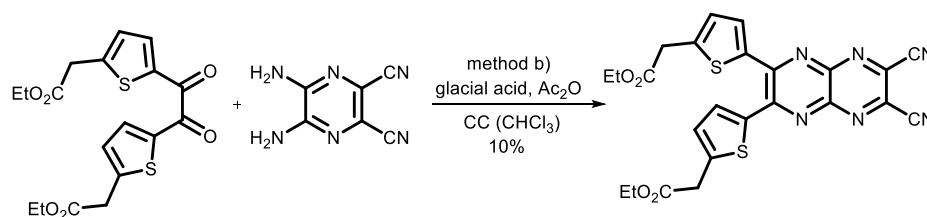
The reaction was carried out according to a literature known procedure.^[136] 100 mg dibromide (160 μ mol, 1 eq) were dissolved in 2 mL DMF, 40 mg PMHS were added as well as 20 mg [Pd₂(dba)₃] (35 μ mol, theo.: 2 mol%) and 10 mg dppf (18 μ mol, theo.: 1.5 mol). Portionwise, 19 mg [ZnCN₂] (160 μ mol, 1 eq) were added, while the solution was stirred for 2 h at 100 °C.

Experimental Section

The resulting brown slurry was purified by CC (DCM). The product was obtained in the form of a yellow solid.

Yield: 67 mg, 128 μmol , 80%. - R_f (DCM) = 0.32. - $^1\text{H NMR}$ (CDCl_3 , 300 MHz): δ = 8.42 (s, 2 H, Ar-CH), 7.46 (d, 2 H, $^3J_{\text{H-H}} = 3.8$ Hz, Ar-CH^{Thio}), 6.92 (d, 2 H, $^3J_{\text{H-H}} = 3.9$ Hz, Ar-CH^{Thio}), 4.28 (q, 4 H, $^3J_{\text{H-H}} = 7.1$ Hz, -CH₂), 3.90 (s, 2 H, -CH₂), 1.34 (t, 6 H, $^3J_{\text{H-H}} = 7.1$ Hz, -CH₃) ppm. - $^{13}\text{C NMR}$ (CDCl_3 , 75 MHz): δ = 193.7, 149.8, 142.4, 140.8, 135.3, 131.3, 127.8, 113.8, 61.5, 35.9, 14.2. - not all quaternary carbon atoms could be detected. - **UV-Vis** (DCM): λ = 416 (s), 322 (s) nm. - **UV-Vis** (Anion, DCM/drop DBU): λ = 627 (s), 407 (s) nm - **MS** (APCI-HRMS(+)): m/z = 517.0998 [M+H]⁺, cal. for C₂₆H₂₀N₄O₄S₂+H₁: 517.0999.

7.6.3 Synthesis of Diethyl 2,2'-((6,7-dicyanopyrazino[2,3-b]pyrazine-2,3-diyl)bis(thiophene-5,2-diyl))diacetate

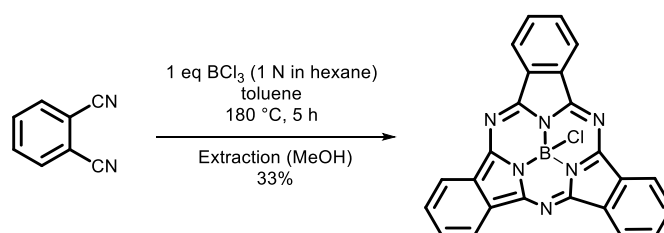


203 mg dione (507 μmol , 1 eq) were dissolved with 88 mg diamine (550 μmol , 1.1 eq) and dissolved in 20 mL glacial acid. The solution was refluxed at 120 °C for 2 h. The reaction was monitored via TLC and was stirred until the dione was completely consumed. The reaction was cooled down to rt, before the solvent was removed by distillation. The crude black product (yellowish shimmer) was purified by CC (DCM).

Yield: 10%. - R_f (DCM) = 0.22. - $^1\text{H NMR}$ (CDCl_3 , 300 MHz): δ = 7.91 (d, 2 H, $^3J_{\text{H-H}} = 3.9$ Hz, Ar-CH^{Thio}), 7.05 (d, 2 H, $^3J_{\text{H-H}} = 3.9$ Hz, Ar-CH^{Thio}), 4.21 (q, 4 H, $^3J_{\text{H-H}} = 7.1$ Hz, -CH₂), 3.88 (s, 4 H, -CH₂), 1.29 (t, 6 H, $^3J_{\text{H-H}} = 7.2$ Hz, -CH₃) ppm. - **UV-Vis** (DCM): λ = 322 (s), 266 (s) nm. - **UV-Vis** (Anion, DCM/drop DBU): λ = 572 (s), 480 (s), 414 (s), 318 (s) nm.

7.7 Synthesis of Symmetrical Subphthalocyanines

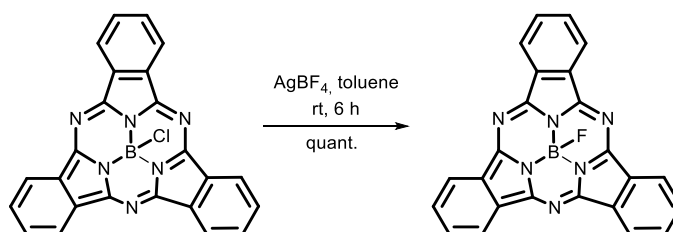
7.7.1 Synthesis of [SpcBCl] ^[164]



4.34 g PDN (33.9 mmol, 1.5 eq) were dissolved in 100 mL 1,2-dichlorobenzene and 23 mL BCl_3 solution (1 M in hexane, 23.0 mmol, 1.0 eq) was added dropwise. The solution was stirred for 5 h at 180 °C during which time the colour turned deep purple. After removing the solvent under reduced pressure, the black solid was washed with MeOH using a SOXHLET extractor. The resulting metallic powder was dried in vacuum.

Yield: 2.15 g, 5.00 mmol, 44%. - **$^1\text{H NMR}$** (CDCl_3 , 300 MHz): $\delta = 8.89\text{-}8.92$ (m, 6H, $-\text{CH}^\alpha$), 7.94-7.97 (m, 6H, $-\text{CH}^\beta$) ppm. - **$^{11}\text{B NMR}$** (CDCl_3 , 67 MHz): $\delta = -13.9$ (s, 1 B, BCl) ppm. - **IR** (ATR, 400-4000 cm^{-1}): $\tilde{\nu} = 1714$ (vw), 1489 (m), 1435 (w), 1435 (w), 1277 (m), 1229 (w), 1193 (m), 1125 (s), 1088 (m), 948 (s), 875 (w), 743 (vs), 692 (s), 626 (s), 526 (m), 563 (m), 506 (w), 439 (m), 410 (vw) cm^{-1} . - **UV-Vis** (toluene): $\lambda = 565$ (s), 547 (sh), 306 (m), nm. - **Fluorescence** (toluene, $\lambda_{\text{ex}} = 350$ nm): $\lambda = 575$ nm. - **MS** (APCI-HRMS(+)): $m/z = 431.0979$ $[\text{M}+\text{H}]^+$, cal. for $\text{C}_{24}\text{H}_{12}\text{B}_1\text{Cl}_1\text{N}_6+\text{H}_1$: 431.0982.

7.7.2 Synthesis of [SpcBF] ^[169,170]



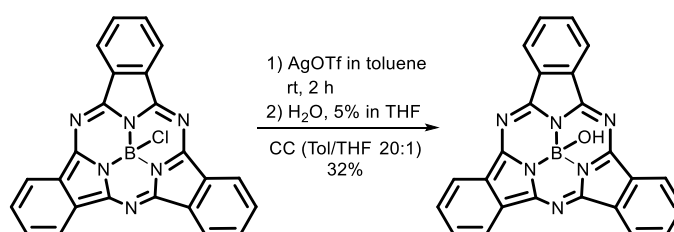
General Procedure 2:^[169,170] Fluorination of [SpcBCl].

1 eq [SpcBCl] was dissolved in toluene with 1.2 eq AgBF_4 . The reaction was monitored by TLC (DCM/EA), while the solution was stirred at rt. The resulting purple powder was purified by CC (DCM/EA 1:1).

Experimental Section

Yield: quant. - $^1\text{H NMR}$ (CDCl_3 , 300 MHz): $\delta = 8.89\text{-}8.86$ (m, 6 H, $-\text{CH}^\beta$), 7.94-7.91 (m, 6 H, $-\text{CH}^\alpha$). - $^{19}\text{F NMR}$ (CDCl_3 , 282 MHz): $\delta = 157$ (m, 1 F, $-\text{BF}$) ppm. - $^{11}\text{B NMR}$ (CDCl_3 , 128 MHz): $\delta = -14.5$ (s, 1 B, $-\text{BF}$) ppm.

7.7.3 Synthesis of [SpCBOH] ^[169,170]



1.05 g [SpCBOH]Cl (2.44 mmol, 1.0 eq) and 0.80 g AgOTf (3.11 mmol, 1.3 eq) were dissolved in 17 ml toluene and stirred for 2 h at rt. After complete formation of [SpCBOH]Cl, monitored by TLC, 1.5 ml H₂O (5% in THF, 4.16 mmol, 1.7 eq) and 0.4 ml triethylamine were added and the mixture was stirred for another 6 h at 40 °C. Again, the formation of [SpCBOH] was monitored by TLC. After removing the solvent in vacuum, the resulting purple solid was purified by CC (DCM/EA 10:1), and separated from [(SpCB)₂O] and partly reformed [SpCBOH]Cl. The product was finally dried in vacuum.

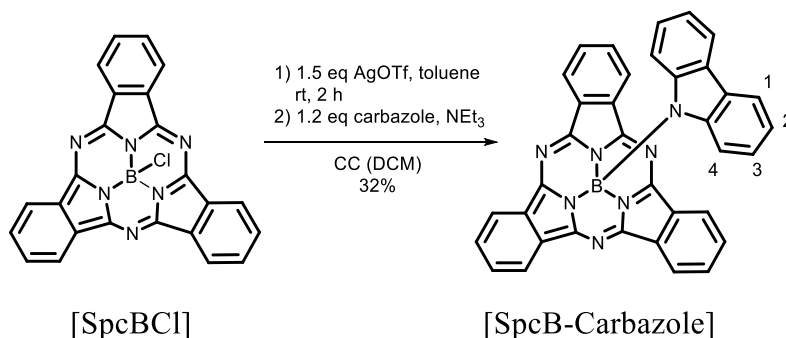
Yield: 279 mg, 0.68 mmol, 32%. - R_f (DCM/EA 10:1) = 0.23. - $^1\text{H NMR}$ (C_6D_6 , 300 MHz): $\delta = 8.72\text{-}8.75$ (m, 6 H, $-\text{CH}^\alpha$), 7.36-7.39 (m, 6 H, $-\text{CH}^\beta$), -1.79-(-1.83) (bs, 1 H, $-\text{OH}$) ppm. - $^{11}\text{B NMR}$ (C_6D_6 , 128 MHz): $\delta = -15.5$ (s, 1 B, $-\text{BOH}$) ppm. - **IR** (ATR, 400-4000 cm^{-1}): $\tilde{\nu} = 3351$ (vw), 1726 (vw), 1609 (vw), 1490 (m), 1450 (w), 1283 (m), 1181 (m), 1089 (s), 1053 (s), 957 (m), 760 (m), 730 (vs), 695 (m), 637 (m), 564 (m), 439 (w) cm^{-1} . - **UV-Vis** (toluene): $\lambda = 561$ (s), 521 (sh), 303 (m) nm. - **Fluorescence** (toluene, $\lambda_{ex} = 505$ nm): $\lambda = 572$ nm. - **MS** (APCI-HRMS(+)): $m/z = 413.1317$ $[\text{M}+\text{H}]^+$, cal. for $\text{C}_{24}\text{H}_{14}\text{B}_1\text{N}_6\text{O}_1+\text{H}_1$: 413.1321. $m/z = 427.1475$ $[\text{M}+\text{Me}]^+$, cal. for $\text{C}_{24}\text{H}_{14}\text{B}_1\text{N}_6\text{O}_1+\text{C}_1\text{H}_3$: 427.1747.

Additional information: Methanolysis occurs during measurement.

By-product (Dimer): **Yield:** 88 mg, 0.11 mmol, 5%. - R_f (DCM/EA 10:1) = 0.52. - $^1\text{H NMR}$ (C_6D_6 , 300 MHz): $\delta = 8.52\text{-}8.55$ (m, 6 H, $-\text{CH}^\alpha$), 7.27-7.30 (m, 6 H, $-\text{CH}^\beta$) ppm. - **IR** (ATR, 400-4000 cm^{-1}): $\tilde{\nu} = 3056$ (vw), 2960 (vw), 1770 (w), 1610 (w), 1491 (m), 1382 (m), 1283 (m), 1228 (w), 1126 (s), 1181 (m), 1077 (m), 952 (w), 799 (w), 736 (vs), 696 (m), 632 (w), 568 (m), 507 (w), 435 (w) cm^{-1} . - **UV-Vis** (DCM): $\lambda = 555$ (sh), 531 (s), 301 (m), 270 (m),

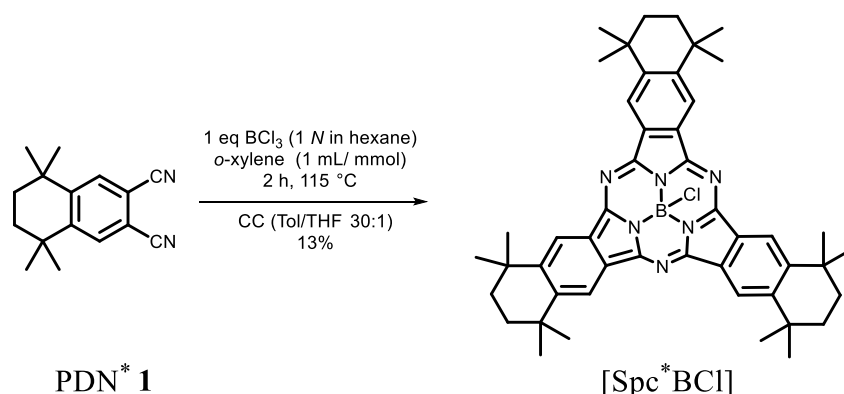
238 (s) nm. - **Fluorescence** (toluene, $\lambda_{ex} = 470$ nm): $\lambda = 620$ (bs), 599 (s) nm. - **MS** (APCI-HRMS(+)): $m/z = 807.2449$ $[M+H]^+$, cal. for $C_{48}H_{24}B_2N_{12}O_1+H_1$: 807.2470.

7.7.4 Synthesis of [SpcB-Carbazole]



7.8 Synthesis of Substituted Subphthalocyanines

7.8.1 Synthesis of [Sp^{c*}BCl] [13,25]



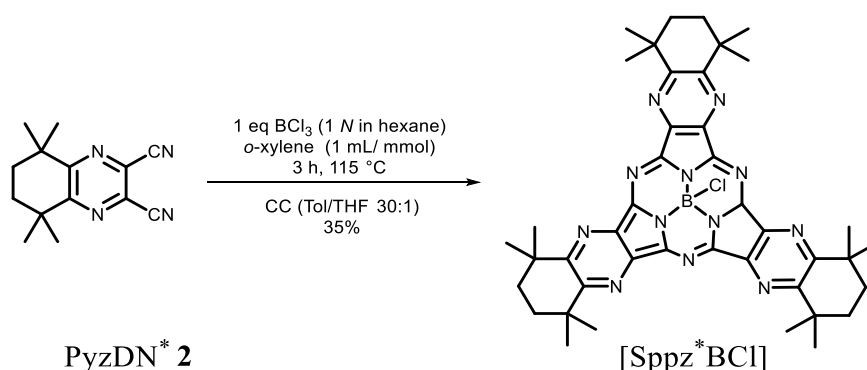
General Procedure 3: Synthesis of [Sp^{c*}BX].

1 eq PDN was dissolved in 2 mL toluene /5 mmol PDN. Fresh BCl₃ solution (1 M in heptane or in *o*-xylene, 3 eq BCl₃ per intended [Sp^{c*}BCl]) was added at once and then heated to 150 °C. The yellowish solution turned deep pink. After heating for about 5 h, the solution was loaded onto a short silica pluck, purified with DCM/EE to remove the boron compounds and then purified by CC (PE/EA 10:1).

Yield: ~5%. - *R_f* (PE/EE 10:1) = 0.4. - ¹H NMR (C₆D₆, 300 MHz): δ = 8.91 (s, 6 H, Ar-CH), 1.65-1.52 (m, 12 H, -CH₂), 1.42 (s, 18 H, -CH₃), 1.10 (s, 18 H, -CH₃) ppm. - ¹H NMR (CD₂Cl₂, 300 MHz): δ = 8.84 (s, 6 H, Ar-CH), 1.94-1.80 (m, 12 H, -CH₂), 1.66 (s, 18 H, -CH₃), 1.44 (s, 18 H, -CH₃) ppm. - ¹³C NMR (CD₂Cl₂, 75 MHz): δ = 149.6, 149.2, 129.4, 120.4, 36.0, 35.3, 32.9, 32.3 ppm. - UV-Vis (DCM): λ = 582 (s), 528 (sh), 318 (s), 267 (s) nm. - Fluorescence (DCM, λ_{ex} = 350 nm): λ = 592 nm. - Φ_F (λ_{ex} = 490 nm) = 0.18. - Φ_Δ = 0.64. - MS (APCI-HRMS(+)): *m/z* = 761.4247 [M+H]⁺, cal. for C₄₈H₅₄B₁Cl₁N₆+H₁: 761.4272. - X-ray: Crystals could be obtained out of CD₂Cl₂ in the NMR tube at rt.

Additional information: In some cases, degradation of [Sp^{c*}BCl] in the form of a fast decolouration was observed in acidic solvents.

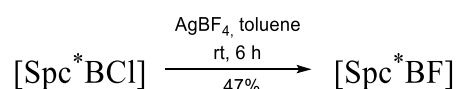
7.8.2 Synthesis of [Sppz*BCl] [13,25]



According to General Procedure 3 (p. 228). The pink solution was purified by CC (Tol/THF 30:1). The pink solid was dried in vacuum.

Yield: 35%. - R_f (Tol/THF 30:1) = 0.35. - R_f (DCM) = 0.6. - $^1\text{H NMR}$ (CDCl_3 , 300 MHz): δ = 1.94–2.07 (m, 12 H, $-\text{CH}_2$), 1.75 (s, 18 H, $-\text{CH}_3$), 1.52 (s, 18 H, $-\text{CH}_3$) ppm. - $^1\text{H NMR}$ (CD_2Cl_2 , 300 MHz): δ = 1.53 (s, 18 H, $-\text{CH}_3$), 1.78 (s, 18 H, $-\text{CH}_3$), 1.96–2.16 (m, 12 H, $-\text{CH}_2$) ppm. - **UV-Vis** (DCM): λ = 534 (s), 489 (sh), 334 (m), 303 (s) nm. - **Fluorescence** (DCM, λ_{ex} = 350 nm): λ = 546 nm. - Φ_F (λ_{ex} = 490 nm) = 0.19. - Φ_A = 0.88. - **MS** (APCI-HRMS(+)): m/z = 767.3964 $[\text{M}+\text{H}]^+$, cal. for $\text{C}_{42}\text{H}_{48}\text{B}_1\text{Cl}_1\text{N}_{12}+\text{H}_1$: 767.3980.

7.8.3 Synthesis of [Spс*BF]



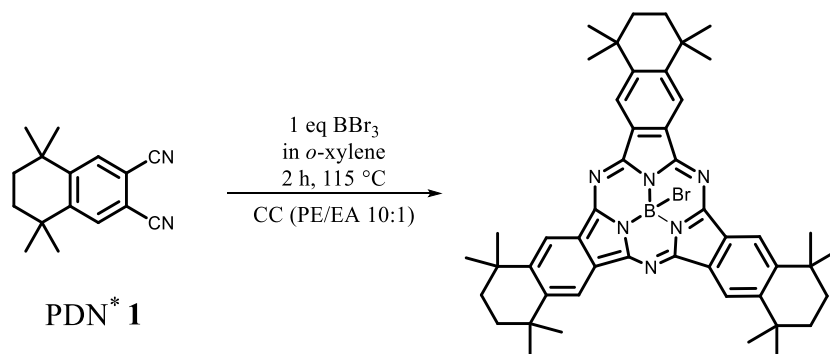
According to General Procedure 2 (p. 225). The reaction was monitored by TLC(PE/EA 1:1). The product was purified by CC (PE/EA 1:1). [Spс*BF] was obtained in the form of a pink solid.

Yield: 47%. - $^1\text{H NMR}$ (CD_2Cl_2 , 300 MHz): δ = 8.82 (s, 6 H, Ar-CH), 1.81-1.93 (m, 12 H, $-\text{CH}_2$), 1.66 (s, 18 H, $-\text{CH}_3$), 1.43 (s, 18 H, $-\text{CH}_3$) ppm. - $^{11}\text{B NMR}$ (CD_2Cl_2 , 128 MHz): δ = -13.8 (d, $^1J_{\text{B-F}}$ = 29.4 Hz, $-\text{BF}$) ppm. - $^{19}\text{F NMR}$ (CD_2Cl_2 , 282 MHz): δ = -158.0 (q, $^1J_{\text{B-F}}$ = 31 Hz) ppm. - **IR** (ATR, 400-4000 cm^{-1}): $\tilde{\nu}$ = 2959 (m), 2929 (m), 2864 (w), 2323 (vw), 1690 (w), 1625 (w), 1558 (w), 1455 (m), 1413 (w), 1375 (m), 1360 (m), 1333 (m), 1262 (m), 1244 (s), 1215 (m), 1184 (m), 1159 (m), 1111 (m), 1083 (s), 1045 (w), 1020 (w), 997 (m), 865 (w), 840 (w), 785 (s), 765 (w), 706 (w), 672 (s), 636 (m), 597 (w), 543 (w), 469 (w), 439 (m) cm^{-1} . - **UV-Vis** (DCM): λ = 577 (s), 320 (m), 265 (s) nm. - **Fluorescence** (DCM, λ_{ex} =

Experimental Section

350 nm): $\lambda = 587$ nm. - **MS** (APCI-HRMS(+)): $m/z = 745.4554$ $[M+H]^+$, cal. for $C_{48}H_{54}B_1F_1N_6+H_1$: 745.4568.

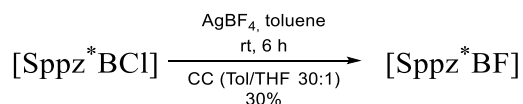
7.8.4 Synthesis of [Sp^c*BBr]



According to General Procedure 3 (p. 228), using BBr_3 . The product was purified by CC (PE/EA 1:1). [Sp^c*BF] was obtained in the form of a pink solid.

Yield: n.d. - **¹H NMR** (CD_2Cl_2 , 300 MHz): $\delta = 8.82$ (s, 6 H, Ar-CH), 1.85-1.89 (m, 12 H, -CH₂), 1.56 (s, 18 H, -CH₃), 1.43 (s, 18 H, -CH₃) ppm. - **¹¹B NMR** (CD_2Cl_2 , 128 MHz): $\delta = -15.5$ (s) ppm. - **IR** (ATR, 400-4000 cm^{-1}): $\tilde{\nu} = 3359$ (w), 3185 (w), 2958 (m), 2922 (s), 2853 (m), 1727 (w), 1658 (m), 1632 (m), 1601 (m), 1548 (w), 1458 (s), 1440 (m), 1379 (m), 1364 (m), 1302 (m), 1259 (s), 1206 (m), 1160 (w), 1083 (s), 1048 (s), 1021 (s), 968 (w), 938 (w), 892 (w), 844 (w), 797 (s), 766 (w), 734 (w), 708 (s), 539 (w) cm^{-1} . - **UV-Vis** (DCM): $\lambda = 578$ (s), 319 (m), 281 (s) nm. - **Fluorescence** (DCM, $\lambda_{ex} = 350$ nm): $\lambda = 591$ nm. - **MS** (APCI-HRMS(+)): $m/z = 725.4475$ $[M+H]^+$, cal. for $C_{48}H_{54}B_1N_6+H_1$: 725.4502. - Loss of bromide occurs within the measurement. $m/z = 757.4748$ $[M-Br,+OMe]^+$, cal. for $C_{49}H_{55}B_1N_6+O_1C_1H_3$: 757.4765. - Methanolysis occurs within the measurement.

7.8.5 Synthesis of [Sp^p*BF]

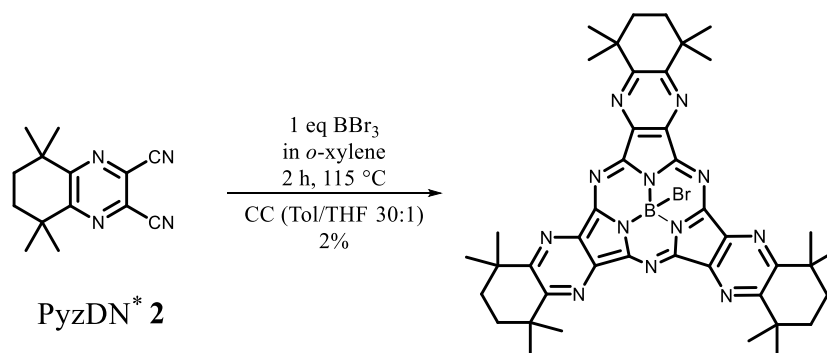


According to General Procedure 2 (p. 225). The pink solution was purified by CC (Tol/THF 30:1). The product was obtained in the form of a reddish solid.

Yield: 30%. - **¹H NMR** (CD_2Cl_2 , 300 MHz): $\delta = 2.00$ -2.08 (m, 12 H, -CH₂), 1.78 (s, 18 H, -CH₃), 1.53 (s, 18 H, -CH₃) ppm. - **¹¹B NMR** (CD_2Cl_2 , 128 MHz): $\delta = -14.24$ (s) ppm. -

^{19}F NMR (CD_2Cl_2 , 282 MHz): $\delta = -156.7$ (q, $^1J_{\text{B-F}} = 31$ Hz) ppm. - **UV-Vis** (DCM): $\lambda = 534$ (s), 333 (m), 302 (s) nm. - **Fluorescence** (DCM, $\lambda_{\text{ex}} = 350$ nm): $\lambda = 547$ nm. - **MS** (APCI-HRMS(+)): $m/z = 751.4260$ [$\text{M}+\text{H}^+$], cal. for $\text{C}_{42}\text{H}_{48}\text{B}_1\text{F}_1\text{N}_{12}+\text{H}_1$: 751.4282.

7.8.6 Synthesis of [Sppz^*BBr]

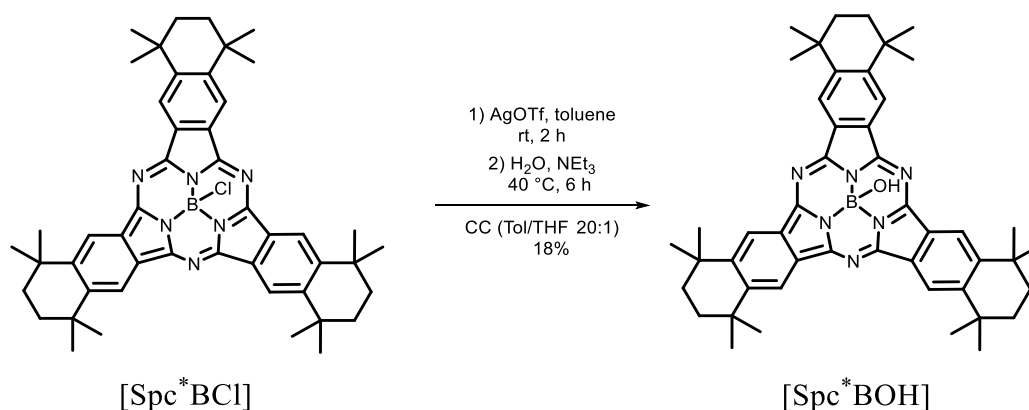


According to General Procedure 3 (p. 228), using BBr_3 . The pink solution was purified by CC (Tol/THF 30:1). The product was obtained in the form of a reddish solid.

Yield: 2%. - **^1H NMR** (CD_2Cl_2 , 300 MHz): $\delta = 2.03$ - 2.08 (m, 12 H, $-\text{CH}_2$), 1.78 (s, 18 H, $-\text{CH}_3$), 1.53 (s, 18 H, $-\text{CH}_3$) ppm. - **^{11}B NMR** (CD_2Cl_2 , 128 MHz): $\delta = -17.0$ (s) ppm. - **IR** (ATR, 400 - 4000 cm^{-1}): $\tilde{\nu} = 2964$ (m), 2931 (m), 2864 (m), 2232 (vw), 1721 (w), 1557 (vw), 1519 (m), 1457 (s), 1362 (s), 1345 (m), 1302 (w), 1260 (m), 1245 (s), 1219 (m), 1189 (w), 1129 (s), 1088 (m), 1020 (s), 941 (w), 865 (m), 801 (m), 781 (m), 706 (m), 670 (m), 582 (m), 527 (w), 469 (w), 442 (w), 408 (w) cm^{-1} . - **UV-Vis** (DCM) $\lambda = 534$ (s), 313 (s), 225 (m) nm. - **Fluorescence** (DCM, $\lambda_{\text{ex}} = 350$ nm): $\lambda = 546$ nm. - **MS** (APCI-HRMS(+)): $m/z = 813.3422$ [$\text{M}+\text{H}^+$], cal. for $\text{C}_{42}\text{H}_{48}\text{B}_1\text{Br}_1\text{N}_{12}+\text{H}_1$: 813.3468.

Experimental Section

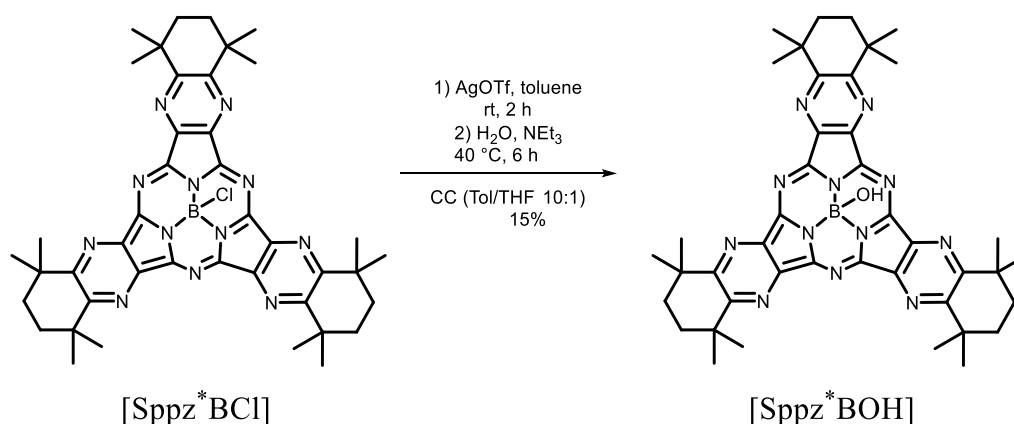
7.8.7 Synthesis of [Sp^c*BOH] [242]



56 mg [Sp^c*BCl] (73.6 μmol, 1.0 eq) and 23 mg AgOTf (89.5 μmol, 1.2 eq) were dissolved in 8 mL toluene and stirred for 2.5 h at rt. 0.4 ml H₂O (0.5% in THF, 111 μmol, 1.5 eq) and 10 μL triethylamine (98.8 μmol, 1.3 eq) were added and stirred for another 6 h at 40 °C. After removing the solvent in vacuum, the solid was purified by CC (Tol/THF 20:1) and finally dried in vacuum.

Yield: 10 mg, 13.5 μmol, 18%. - **R_f** (Tol/THF 20:1) = 0.40. - **¹H NMR** (C₆D₆, 300 MHz): δ = 8.94 (s, 6 H, -CH), 1.53-1.67 (m, 12 H, -CH₂), 1.42 (s, 18 H, -CH₃), 1.11 (s, 18 H, -CH₃) ppm. - **IR** (ATR, 400-4000 cm⁻¹): $\tilde{\nu}$ = 463 (vw), 499 (m), 543 (w), 625 (vw), 704 (m), 733 (m), 797 (vs), 895 (m), 1019 (vs), 1046 (vs), 1089 (vs), 1260 (s), 1364 (m), 1430 (s), 1461 (s), 1545 (w), 1599 (m), 1728 (w), 2358 (vw), 2860 (w), 2925 (m), 2960 (m), 3204 (vw), 3330 (vw) cm⁻¹. - **UV-Vis** (toluene): λ = 382 (m), 557 (sh), 575 (s) nm. - **Fluorescence** (toluene, λ_{ex} = 480 nm): λ = 596 nm. - **MS** (APCI-HRMS(+)): m/z = 743.4592 [M+H]⁺, cal. for C₄₈H₅₆B₁N₆O₁+H₁: 743.4611. m/z = 757.4752 [M+OMe]⁺, cal. for C₄₈H₅₅B₁N₆O₁+C₁H₃: 757.4768. - Methanolysis occurs within the measurement.

7.8.8 Synthesis of [Sppz*BOH] [242]



40 mg [Sppz*BCl] (52.2 μmol , 1.0 eq) and 22 mg AgOTf (85.6 μmol , 1.6 eq) were dissolved in 4 mL toluene and stirred for 3.5 h at rt. After removing the solvent under reduced pressure, the resulting solid was directly* loaded onto silica, was washed with pentane and purified by CC (Tol/THF 10:1). The solvent was removed under reduced pressure, and the red solid was dried in vacuum.

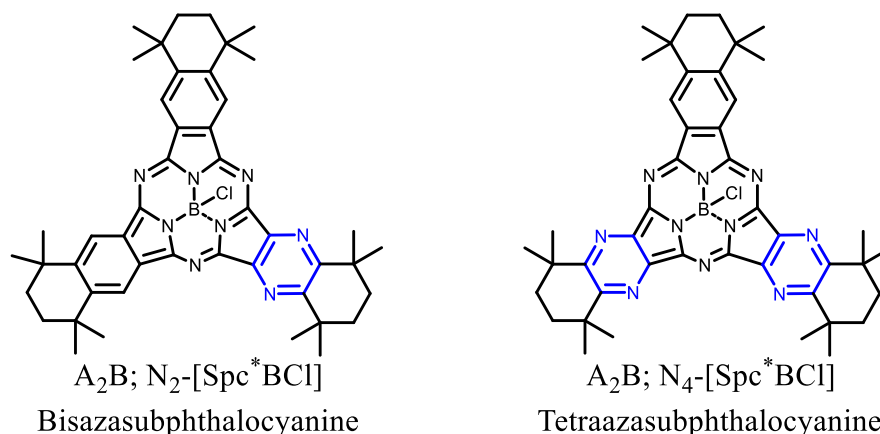
Yield: 6 mg, 8.0 μmol , 15%. - R_f (Tol/THF 10:1) = 0.21. - $^1\text{H NMR}$ (CDCl_3 , 300 MHz): δ = 1.93-2.06 (m, 12 H, $-\text{CH}_2$), 1.74 (s, 18 H, $-\text{CH}_3$), 1.52 (s, 18 H, $-\text{CH}_3$) ppm. - **IR** (ATR, 400-4000 cm^{-1}): $\tilde{\nu}$ = 3261 (w), 2961 (s), 2929 (s), 2866 (m), 1721 (vs), 1560 (vw), 1459 (s), 1386 (m), 1367 (m), 1260 (s), 1153 (m), 1091 (s), 1064 (s), 1024 (vs), 867 (w), 800 (s), 721 (m), 701 (w), 515 (w), 467 (w) cm^{-1} . - **UV-Vis** (DCM): λ = 536 (s), 596 (sh), 305 (m) nm. - **Fluorescence** (toluene, λ_{ex} = 400 nm): λ = 550 nm. - **MS** (APCI-HRMS(+)): m/z = 749.4312 $[\text{M}+\text{H}]^+$, cal. for $\text{C}_{42}\text{H}_{49}\text{B}_1\text{N}_{12}\text{O}_1+\text{H}_1$: 749.4325. m/z = 777.4633 $[\text{M}+\text{OEt}]^+$, cal. for $\text{C}_{42}\text{H}_{49}\text{B}_1\text{N}_{12}\text{O}_1+\text{C}_2\text{H}_5$: 777.4636. - Ethanolysis occurs within the measurement.

Additional information: *By addition of THF/ H_2O , and formation of TfOH, degradation of [Sppz*BOTf] was observed. So, the formation of [Sppz*BOH] occurs on the silica of the CC. The completion of the formation of [Sppz*BOH] was monitored by the absence of ^{19}F in ^{19}F NMR spectroscopy.

7.9 Synthesis of Azasubphthalocyanines

According to General Procedure 3 (p. 228), using PDN*/PyzDN* in a 1:1 ratio. After evaporation of the solvent, the solid residue was loaded onto silica and the crude product was purified via gradient CC (Tol → Tol/THF).

7.9.1 Synthesis of Azasubphthalocyanines N_x-[Spc*BCl]



[Spc*BCl]: Yield: <1%. - The product was identified by using UV-Vis and MS. The analysis is in accordance to the one described in section 7.8.1.

N₂-[Spc*BCl]: Yield: 8 mg, 10.5 μ mol, 1%. - **¹H NMR** (CDCl₃, 300 MHz): δ = 8.87 (s, 2 H, Ar-CH), 8.78 (s, 2 H, Ar-CH), 1.77-1.55 (m, 12 H, -CH₂), 1.38 (s, 9 H, -CH₃), 1.35 (s, 9 H, -CH₃), 1.05 (s, 9 H, -CH₃), 1.03 (s, 9 H, -CH₃) ppm. - **UV-Vis** (DCM): λ = 572 (s), 519 (sh), 327 (m), 303 (s) nm. - **Fluorescence** (DCM, λ_{ex} = 350 nm): λ = 577 nm. - Φ_F (λ_{ex} = 490 nm) = 0.24. - Φ_A = 0.67. - **MS** (APCI-HRMS(+)): m/z = 763.4162 [M+H]⁺, cal. for C₄₆H₅₃B₁Cl₁N₈+H₁: 763.4177.

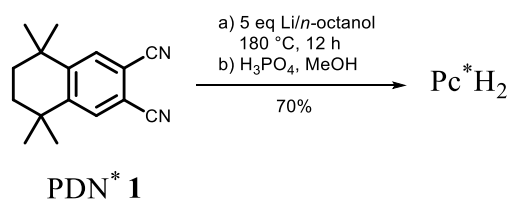
N₄-[Spc*BCl]: Yield: 12 mg, 15.7 μ mol, 2%. - **¹H NMR** (CDCl₃, 300 MHz): δ = 8.78 (s, 2 H, Ar-CH), 1.66-1.51 (m, 12 H, -CH₂), 1.38 (s, 9 H, -CH₃), 1.38 (s, 9 H, -CH₃), 1.35 (s, 9 H, -CH₃), 1.35 (s, 9 H, -CH₃) ppm. - **UV-Vis** (DCM): λ = 557 (s), 506 (sh), 330 (s), 296 (s) nm. - **Fluorescence** (DCM, λ_{ex} = 350 nm): λ = 567 nm. - Φ_F (λ_{ex} = 490 nm) = 0.22. - Φ_A = 0.65. - **MS** (APCI-HRMS(+)): m/z = 765.4069 [M+H]⁺, cal. for C₄₄H₅₁B₁Cl₁N₁₀+H₁: 765.4082.

[Sppz*BCl]: Yield: <1%. - The analysis is in accordance to the one described in section 7.8.2.

Additional information: For the synthesis of N_x-[Spc*BCl], depending on the desired product, the corresponding ratios of dinitriles was varied. In the ¹H NMR spectra, dinitriles traces were observed.

7.10 Synthesis of Symmetrical Phthalocyanines

7.10.1 Synthesis of Pc^*H_2 [24]

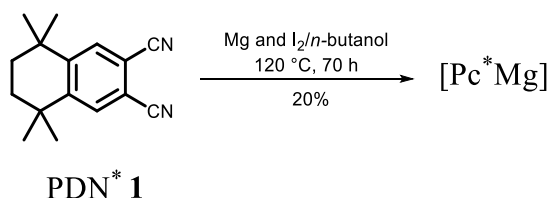


General Procedure 4: Synthesis of Pcs using the Li/*n*-octanol method.

4 eq PDN were dissolved in a Li/*n*-octanol solution (5 eq Li in 10 mL *n*-octanol/g PDN) and were allowed to stir in a preheated oil bath at 160 °C - 180 °C for 8 h. After cooling down to rt, the green solution was diluted with MeOH and the formed $[\text{Pc}^{(*)}\text{Li}_2]$ was protonated with H_3PO_4 (1 mL/g formed Pc). The solution was macerated with MeOH, until the washing solution became clear in colour. The obtained green powder was sublimed in vacuum.

Yield: 70%. - **$^1\text{H NMR}$** (CDCl_3 , 300 MHz): $\delta = 9.91$ (s, 8 H, Ar-CH), 1.79 (s, 16 H, - CH_2), 1.54 (s, 48 H, - CH_3), -0.01 (s, 2 H, -NH) ppm. - **IR** (ATR, 400-4000 cm^{-1}): $\tilde{\nu} = 3346$ (vw), 3243 (vw), 2956 (w), 2914 (w), 2859 (w), 2362 (m), 2350 (m), 2326 (m), 1501 (w), 1384 (w), 1261 (w), 1185 (w), 1049 (s), 1012 (s), 977 (w), 949 (w), 895 (m), 847 (m), 770 (m), 756 (m), 650 (m), 512 (m), 442 (m), 421 (m) cm^{-1} . - **CV** (DCM, $[\text{TBA}]\text{PF}_6$, Fc): $E_{\text{ox}1} = 0.67$, $E_{\text{red}1} = -0.91$, $E_{\text{red}2} = -1.36$ V. - **UV-Vis** (DCM): $\lambda = 710$ (s), 677 (s), 647 (sh), 615 (sh), 343 (s), 295 (sh), 231 (sh) nm. - **MS** (APCI-HRMS(+)): $m/z = 955.6096$ $[\text{M}+\text{H}]^+$, cal. for $\text{C}_{64}\text{H}_{75}\text{N}_8$: 955.6109.

7.10.2 Synthesis of $[\text{Pc}^*\text{Mg}]$



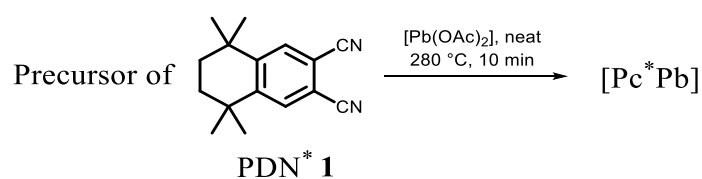
25 mg Mg turnings (1.04 mmol, 2 eq) were dissolved in 10 mL *n*-butanol by adding an iodine crystal at 120 °C. The solution was stirred for 24 h. After cooling down to rt, 430 mg PDN^* (1.80 mmol, 1 eq) were added and the solution was stirred for 70 h, at 120 °C. After 1 h, a change in colour to turquoise was observed. After cooling down to rt, the solvent was

Experimental Section

evaporated under reduced pressure. 10 mL pentane were added and the crude product was purified with a filter column CC (PE/DCM).

Yield: 88.2 mg, 90.2 μmol , 20%. - **$^1\text{H NMR}$** (C_6D_6 , 300 MHz): $\delta = 9.98$ (s, 8 H, Ar-CH), 1.82 (s, 16 H, -CH₂), 1.58 (s, 48 H, -CH₃) ppm. - **UV-Vis** (DCM): $\lambda = 692$ (s), 650 (w, sh), 354 (s), 294 (s) nm. - **MS** (APCI-HRMS(+)): $m/z = 977.5809$ [M+H]⁺, cal. for $\text{C}_{64}\text{H}_{72}\text{N}_8\text{Mg}_1+\text{H}_1$: 977.5803.

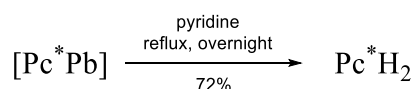
7.10.3 Synthesis of [Pc*Pb] [25]



1.95 g PDN* (8.18 mmol, 2.5 eq) were melted at 280 °C with 1.13 g [Pb(OAc)₂] \cdot 3H₂O (3.15 mmol, 1 eq) and a spatula of ammonium heptamolybdate, for 10 min. The resulting blue/black solid was washed with 3 x 50 mL MeOH and 50 mL hexane and finally dried in vacuum.

Yield: 522 mg, 0.45 mmol, 22%. - **$^1\text{H NMR}$** (CD_2Cl_2 , 300 MHz): $\delta = 9.37$ (s, 8 H, Ar-CH), 2.07 (s, 16 H, -CH₂), 1.83 (s, 24 H, -CH₃), 1.73 (s, 24 H, -CH₃) ppm. - **UV-Vis** (DCM): $\lambda = 733$ (s), 705 (sh), 659 (sh), 357 (s), 272 (s) nm.

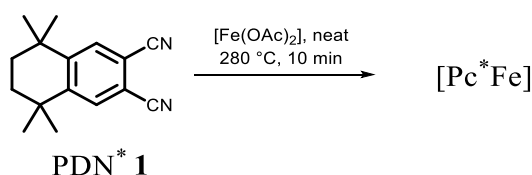
7.10.4 Synthesis of Pc*H₂ using [Pc*Pb] [25]



The reaction was carried out according to a literature described procedure.

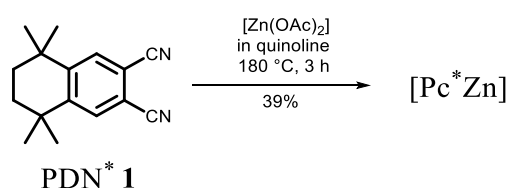
Yield: 72%. - $^1\text{H NMR}$ values are in accordance with the values in section 7.10.1.

Additional information: The synthesis of [Pc*Pb] was carried out using PDN precursors such as the imine, diamide or even carboxylic acid. Therefore, an excess of urea was used in the neat reaction.

7.10.5 Synthesis of [Pc*Fe] ^[133]

500 mg PDN* (2.14 mmol, 4 eq) were melted with 111 mg [Fe(OAc)₂] (0.64 mmol, 1.2 eq) in a preheated metal bath at 280 °C with a spatula tip of urea. After 15 min, the green powder was cooled down to rt. It was washed with 40 mL hexane, 40 mL DEE and finally with 40 mL MeOH. The resulting powder was dried in vacuum. To remove residual salts, the product was purified by CC (Tol/THF gradient).

MS (APCI-HRMS(+)): $m/z = 1009.5302$ [M+H]⁺, cal. for C₆₄H₇₂N₈Fe₁+H₁: 1009.5303.

7.10.6 Synthesis of [Pc*Zn] ^[25]

Method a) 500 mg PDN* (2.10 mmol, 4 eq), 230 mg [Zn(OAc)₂] \cdot 2H₂O (1.05 mmol, 2 eq) and a spatula tip of urea were stirred in 3 mL quinoline at 180 °C, for 3 h. After cooling down to rt, the mixture was washed with 3 x 20 mL MeOH, and once with 20 mL hexane. The resulting blue green powder was dried in vacuum.

Yield: 83 mg, 81.5 μ mol, 39%. - The analysis is in accordance to literature values. - Φ_{F} ($\lambda_{\text{ex}} = 350$ nm) = 0.28; - ($\lambda_{\text{ex}} = 598$ nm) = 0.31. - $\Phi_{\Delta} = 0.59$.

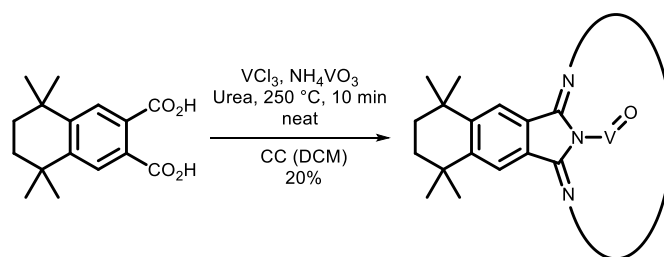
Method b) 500 mg PDN* (2.10 mmol, 4 eq), 78 mg [ZnCl₂] (0.58 mmol, 1.1 eq) and cat. amounts of urea were heated up to 230 °C for 30 min. After melting, a change in colour to green was observed. The resulting product was washed with MeOH and hexane. The resulting blue green powder was dried in vacuum.

Yield: 89 mg, 87.8 μ mol, 42%.

Additional information: In aq. DCM degradation was observed. The UV-Vis spectrum was measured in the glovebox.

Experimental Section

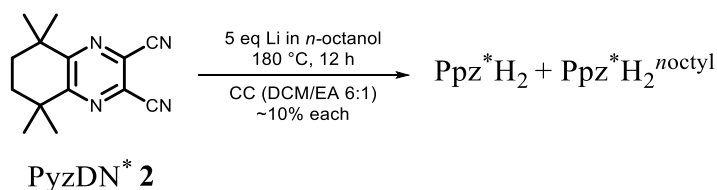
7.10.7 Alternative Synthesis of [Pc*VO] [20,25]



4 eq 1,1,4,4-tetramethyltetralin-6,7-dicarboxylic acid were melted with 1 eq VCl_3 and an excess of NH_4VO_3 . The product was washed with 4 x 50 mL MeOH until the colour of the solution became clear and finally with 40 mL hexane. The product was obtained in the form of a dark green powder.

Yield: 20%. - **IR** (ATR, 400-4000 cm^{-1}): $\tilde{\nu} = 2957$ (m), 2921 (m), 2859 (m), 1615 (w), 1501 (m), 1456 (m), 1432 (m), 1401 (m), 1386 (m), 1360 (m), 1326 (s), 1304 (m), 1260 (m), 1189 (m), 1115 (m), 1078 (s), 1048 (m), 1007 (m), 989 (m), 953 (w), 935 (w), 902 (w), 869 (m), 795 (m), 776 (m), 760 (m), 707 (m), 664 (w), 544 (w), 453 (w) cm^{-1} . - **MS** (APCI-HRMS(+)): $m/z = 1020.339$ $[\text{M}+\text{H}]^+$, cal. for $\text{C}_{64}\text{H}_{72}\text{N}_8\text{O}_1\text{V}_1+\text{H}_1$: 1020.5339. - **Elemental analysis** ($\text{C}_{64}\text{H}_{72}\text{N}_8\text{O}_1\text{V}_1$, 1020.28 g/mol): *find.* (*cal.*): C: 72.13% (75.34%), H: 7.16% (7.11%), N: 10.11% (10.98%).

7.10.8 Synthesis of Ppz*H₂ [70]



According to General Procedure 4 (p. 235). The product mixture was separated by CC (DCM/EA 6:1).

Yield: 10%. - R_f (DCM/EA 6:1) = 0.35. - **¹H NMR** (CDCl_3 , 300 MHz): $\delta = 2.22$ (s, 16 H, $-\text{CH}_2$), 1.93 (s, 48 H, $-\text{CH}_2$), -1.02 (s, 2 H, $-\text{NH}$) ppm. - **IR** (ATR, 400-4000 cm^{-1}): $\tilde{\nu} = 2960$ (vw), 2927 (vw), 2857 (vw), 1458 (vw), 1361 (vw), 1329 (vw), 1256. (vw), 1198 (vw), 1142 (vw), 1012 (s), 878 (vw), 853 (vw), 829 (vw), 768 (vw), 757 (vw), 748 (vw), 688 (vw), 676 (vw), 669.72 (w), 585 (s), 506 (m), 465 (vw), 434 (vw), 405 (vw) cm^{-1} . - **CV** (THF, $[\text{TBA}]\text{PF}_6$, Fc): $E_{\text{ox}1} = 0.87$, $E_{\text{red}1} = -1.05$, $E_{\text{red}2} = -1.37$ V. - **UV-Vis** (DCM): $\lambda = 655$ (s), 621 (s),

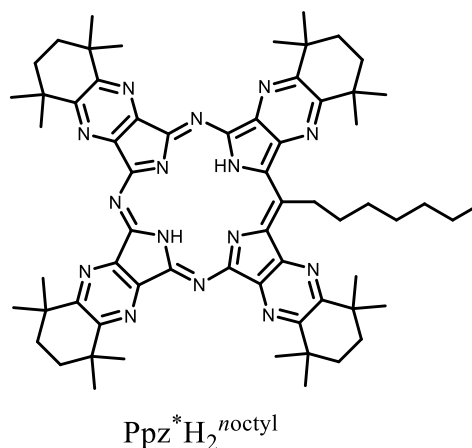
576 (s), 343 (s), 231 (s) nm. - Φ_F ($\lambda_{ex} = 350$ nm) = 0.27; - ($\lambda_{ex} = 598$ nm) = 0.30. - $\Phi_{\Delta} = 0.57$. -
MS (APCI-HRMS(+)): $m/z = 963.5732$ [M+H]⁺, cal. for C₅₆H₆₆N₁₆+H₁: 963.5729.

Additional information: The compound could not be sublimed in vacuum without degradation, >10⁻⁵ bar. As by-product, Ppz*H₂^{noctyl} was observed, see 7.10.9.

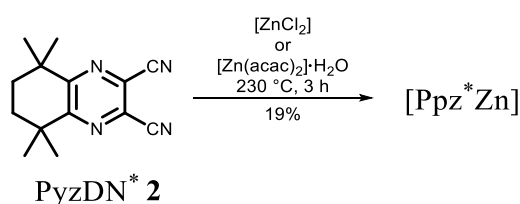
7.10.9 Isolation of Ppz*H₂^{noctyl}

As by-product in the synthesis of Ppz*H₂, in section 7.10.8, Ppz*H₂^{noctyl} was found. Ppz*H₂^{noctyl} was separated by CC (DCM/EA 8:1 → 6:1). The by-product was not separated in literature and is here described for the first time.^[201]

Yield: 7%. - R_f (DCM/EA 6:1) = 0.5. - **¹H NMR** (CD₂Cl₂, 300 MHz): $\delta = 6.46$ (m, 3 H, -CH₃), 2.53 (m, 2 H, -CH₂), 2.26 (s, 16 H, -CH₂), 1.95 (s, 48 H, -CH₃), 1.89 (bs, 2 H, -CH₂), 1.79 (bs, 8 H, -CH₂), -0.82 (s, 2 H, -NH) ppm. - **UV-Vis** (DCM): $\lambda = 653$ (s), 617 (s), 438 (s), 363 (s), 305 (s) nm. - **MS** (APCI-HRMS(+)): $m/z = 1060.6870$ [M+H]⁺, cal. for C₆₄H₈₁N₁₅+H₁: 1060.6872.



7.10.10 Synthesis of [Ppz*Zn]^[70]



Method a) 50 mg Ppz*H₂ (51.9 μ mol, 1 eq) were dissolved in 2 mL pyridine with 20 mg [Zn(acac)₂] \cdot H₂O (77.9 μ mol, 1.5 eq). The solution was stirred at 120 °C for 2 d. The solvent was removed in vacuum and after washing the product with water, the resulting blue powder was purified by TLC (PE/EE 8:1).

Yield: 39 mg, 38.0 μ mol, 73%. - The analysis is in accordance with literature values.

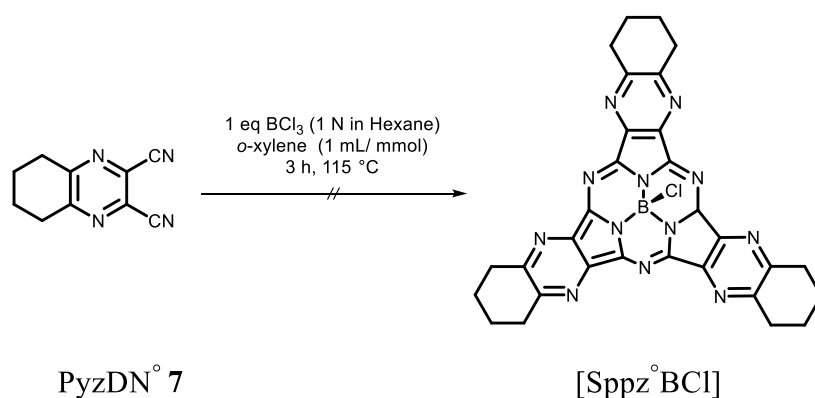
Experimental Section

Method b) 500 mg (2.08 mmol, 4 eq) PyzDN* were melted with 78 mg [ZnCl₂] (57 mmol, 1.1 eq) at 230 °C. The resulting blue powder was washed with 20 mL H₂O, 2 x 20 mL EtOH and finally with 20 mL DEE. The resulting blue powder was dried in vacuum.

Yield: 40 mg, 39.0 μmol, 19%. - The analysis is according to literature.

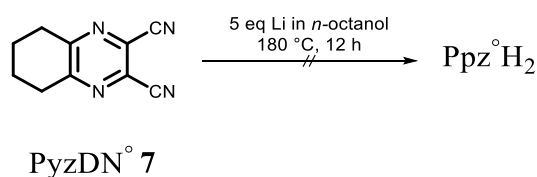
Attempt c) 500 mg (2.08 mmol, 4 eq) PyzDN* were dissolved in quinoline 78 mg [ZnCl₂] (57 mmol, 1.1 eq) and warmed up to 230 °C. A brown slurry was obtained, which was wasted, because no Ppz traces could be detected by using MS or UV-Vis spectroscopy.

7.10.11 Attempt to Synthesise [Sppz^oBCl]

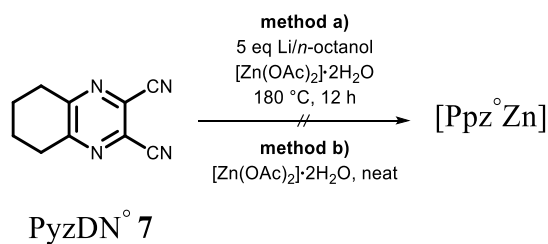


According to General Procedure 3 (p. 228). A black solution was obtained. No Spc traces could be detected by using MS or UV-Vis spectroscopy.

7.10.12 Attempt to Synthesise Ppz^oH₂



According to General Procedure 4 (p. 235). A brown liquid was obtained. No products could be detected by using MS or UV-Vis spectroscopy.

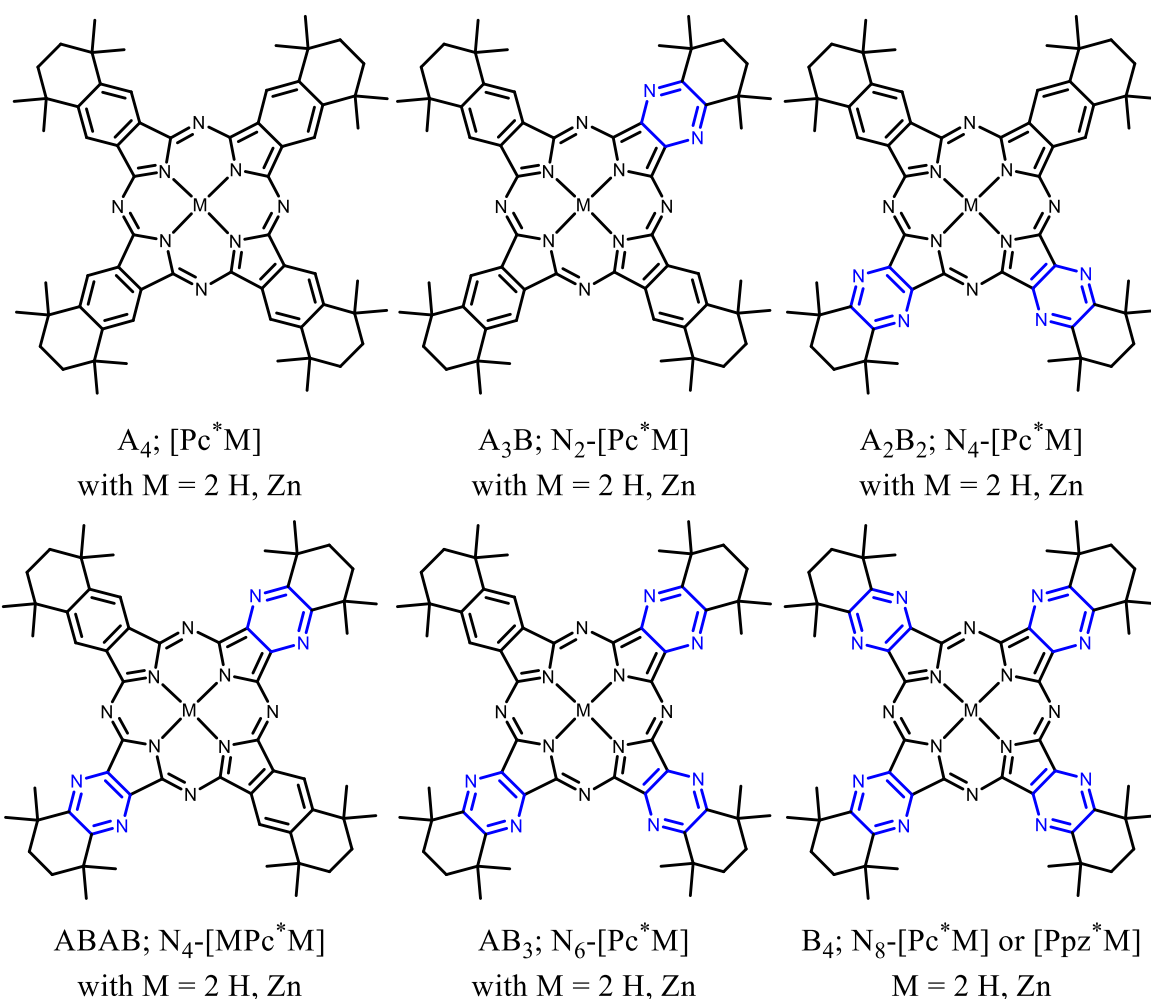
7.10.13 Attempt to Synthesise [Ppz^oZn]

attempt a) 100 mg PyzDN^o (543 μmol , 1 eq) were dissolved in 2 mL *n*-octanol with 22 mg urea and 131 mg $[\text{Zn}(\text{OAc})_2] \cdot 2\text{H}_2\text{O}$ (597 μmol , 1.1 eq). The solution was heated to 130 °C and a drop of DBU was added. After 2 min, the solution changed colour to green, then black-reddish and finally it turned blue. The solution was stirred at 130 °C for 20 h. The black solution was purified by macerating it with H_3PO_4 and MeOH.

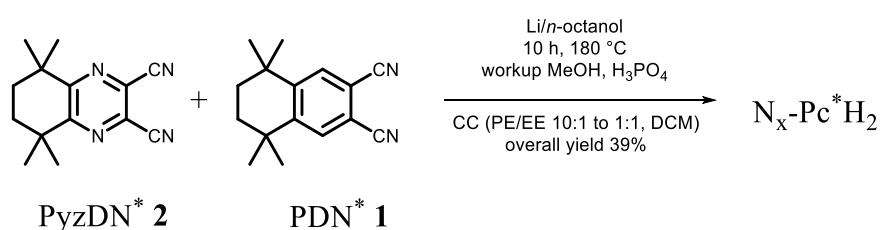
attempt b) 100 mg PyzDN^o (543 μmol , 1 eq) were melted with 22 mg urea and 131 mg $[\text{Zn}(\text{OAc})_2] \cdot 2\text{H}_2\text{O}$ (597 μmol , 1.1 eq). A black powder was obtained.

In both methods, neither in UV-Vis nor in MS could any traces of Ppz be found.

7.11 Synthesis of Asymmetrical Phthalocyanines: $N_x\text{-Pc}^*\text{H}_2$



7.11.1 Synthesis of $N_x\text{-Pc}^*\text{H}_2$ [25]



According to General Procedure 4 (p. 235), using $\text{PyzDN}^* \text{ 2}/\text{PDN}^* \text{ 1}$ in a 1:1 ratio. The solution turned dark green. The isomers were separated by CC (PE(40/60)/EE gradient). At first, Pc^*H_2 and $\text{N}_2\text{-Pc}^*\text{H}_2$ were eluted, then ABAB and the symmetrical $\text{A}_2\text{B}_2 \text{N}_4\text{-Pc}^*\text{H}_2$ were eluted. After changing the solvent to PE/EE 1:1 a mixture of $\text{A}_2\text{B}_2 \text{N}_4\text{-Pc}^*\text{H}_2$ and $\text{AB}_3 \text{N}_6\text{-Pc}^*\text{H}_2$ was eluted. Finally, Ppz^*H_2 was eluted with pure DCM. In a second CC (DCM), $\text{A}_2\text{B}_2 \text{N}_4\text{-Pc}^*\text{H}_2$ and $\text{AB}_3 \text{N}_6\text{-Pc}^*\text{H}_2$ were separated.

Pc*H₂: Yield: 2%. - The analysis is in accordance with values in section 7.10.1. - Φ_F ($\lambda_{ex} = 350$ nm) = 0.44; - ($\lambda_{ex} = 598$ nm) = 0.45. - $\Phi_{\Delta} = 0.16$.

N₂-Pc*H₂: Yield: 4%. - ¹H NMR (CDCl₃, 300 MHz): $\delta = 9.69$ (s, 2 H, Ar-CH), 9.65 (s, 2 H, Ar-CH), 9.42 (s, 2 H, Ar-CH), 2.19 (s, 4 H, -CH₂), 2.07 (s, 8 H, -CH₂), 2.04 (s, 4 H, -CH₂), 1.90 (s, 12 H, -CH₃), 1.83 (s, 12 H, -CH₃), 1.81 (s, 12 H, -CH₃), 1.81 (s, 12 H, -CH₃), -0.07 (s, 2 H, -NH) ppm. - ¹³C NMR (C₆D₆, 75 MHz): $\delta = 160.6, 149.8, 149.2, 148.6, 137.0, 133.0, 132.2, 122.2, 121.6, 39.1, 36.1, 36.1, 35.9, 35.4, 35.3, 34.7, 32.9, 32.8, 32.7, 30.9$ ppm. - not all quartary atoms could be detected. - IR (ATR, 400-4000 cm⁻¹): $\tilde{\nu} = 3475$ (vw), 3297 (vw), 2956 (m), 2921 (m), 2855 (m), 2555 (vw), 2348 (vw), 1711 (m), 1688 (m), 1621 (m), 1539 (m), 1498 (s), 1460 (m), 1382 (m), 1358 (m), 1328 (m), 1301 (s), 1258 (m), 1242 (m), 1188 (m), 1159 (m), 1140 (m), 1119 (m), 1089 (m), 1071 (m), 1022 (s), 999 (m), 980 (m), 891 (m), 848 (m), 804 (m), 755 (s), 722 (m), 681 (s), 622 (m), 541 (m) cm⁻¹. - CV (DCM, [TBA]PF₆, Fc): E_{ox1} = 0.43, E_{red1} = -1.23, E_{red2} = -1.65 V. - UV-Vis (DCM): $\lambda = 687$ (s), 619 (sh), 340 (s), 306 (s), 232 (s) nm. - Φ_F ($\lambda_{ex} = 350$ nm) = 0.31; - ($\lambda_{ex} = 598$ nm) = 0.33. - $\Phi_{\Delta} = 0.14$. - MS (APCI-HRMS(+)): $m/z = 957.5992$ [M+H]⁺, cal. for C₆₂H₇₂N₁₀+H₁: 957.6014. - **Elemental analysis** (C₆₂H₇₂N₁₀, M = 957.30 g/mol): *find.* (*cal.*): C: 75.29% (77.79%), H: 8.92% (7.58%), N: 10.14% (14.63%).

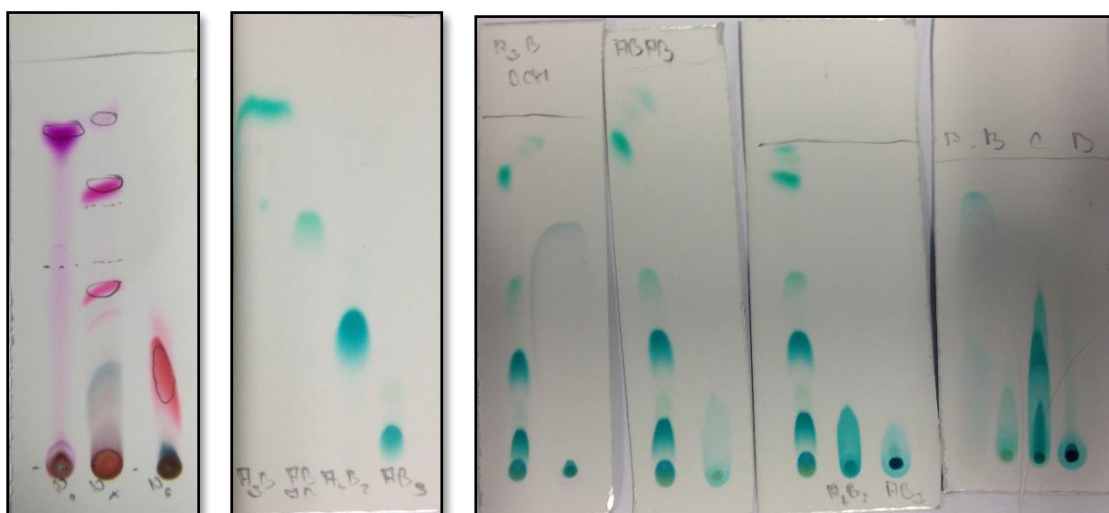
A₂B₂ N₄-Pc*H₂: Yield: 17%. - ¹H NMR (CDCl₃, 300 MHz): $\delta = 9.56$ (s, 2 H, Ar-CH), 9.50 (s, 2 H, Ar-CH), 2.20 (s, 8 H, -CH₂), 2.05 (s, 8 H, -CH₂), 1.91 (s, 24 H, -CH₃), 1.81 (s, 12 H, -CH₃), 1.80 (s, 12 H, -CH₃), -0.04 (s, 2 H, -NH) ppm. - ¹H NMR (Pyridine-*d*₅, 300 MHz): $\delta = 9.87$ (s, 2 H, Ar-CH), 9.68 (s, 2 H, Ar-CH), 1.94 (s, 8 H, -CH₂), 1.76 (s, 8 H, -CH₂), 1.72 (s, 12 H, -CH₃), 1.67 (s, 12 H, -CH₃), 1.46 (s, 12 H, -CH₃), 1.37 (s, 12 H, -CH₃), -0.26 (s, 2 H, -NH) ppm. - ¹H NMR (C₆D₆, 300 MHz): $\delta = 9.83$ (s, 2 H, Ar-CH), 9.82 (s, 2 H, Ar-CH), 1.86 (s, 8 H, -CH₂), 1.79 (s, 8 H, -CH₂), 1.75 (s, 24 H, -CH₃), 1.48 (s, 12 H, -CH₃), 1.38 (s, 12 H, -CH₃), -0.31 (s, 2 H, -NH) ppm. - ¹³C NMR (C₆D₆, 75 MHz): $\delta = 162.4, 150.0, 149.6, 145.1, 144.4, 135.2, 134.8, 122.7, 122.0, 39.4, 39.3, 36.1, 36.0, 35.2, 34.6, 34.5, 32.7, 32.7, 21.1, 30.8$ ppm. - IR (ATR, 400-4000 cm⁻¹): $\tilde{\nu} = 3526$ (w), 3284 (w), 2915 (s), 2857 (s), 1736 (w), 1638 (w), 1553 (w), 1496 (w), 1455 (s), 1381 (w), 1358 (m), 1328 (m), 1300 (s), 1254 (m), 1242 (m), 1190 (m), 1162 (m), 1148 (m), 1128 (m), 1083 (w), 1048 (w), 1019 (s), 1001 (s), 983 (s), 949 (w), 936 (w), 893 (m), 851 (m), 828 (m), 761 (s), 752 (s), 717 (m), 700 (m), 679 (m), 623 (w), 560 (w), 543 (m), 507 (m), 443 (w), 429 (w) cm⁻¹. - CV (DCM, [TBA]PF₆, Fc): E_{ox1} = 0.28, E_{red1} = -1.47, E_{red2} = -1.79 V. - UV-Vis (DCM): $\lambda = 680$ (s), 656 (s), 625 (sh), 348 (s), 232 (s) nm. - Φ_F ($\lambda_{ex} = 350$ nm) = 0.13; - ($\lambda_{ex} = 598$ nm) = 0.14. - $\Phi_{\Delta} = 0.07$. - MS (APCI-

Experimental Section

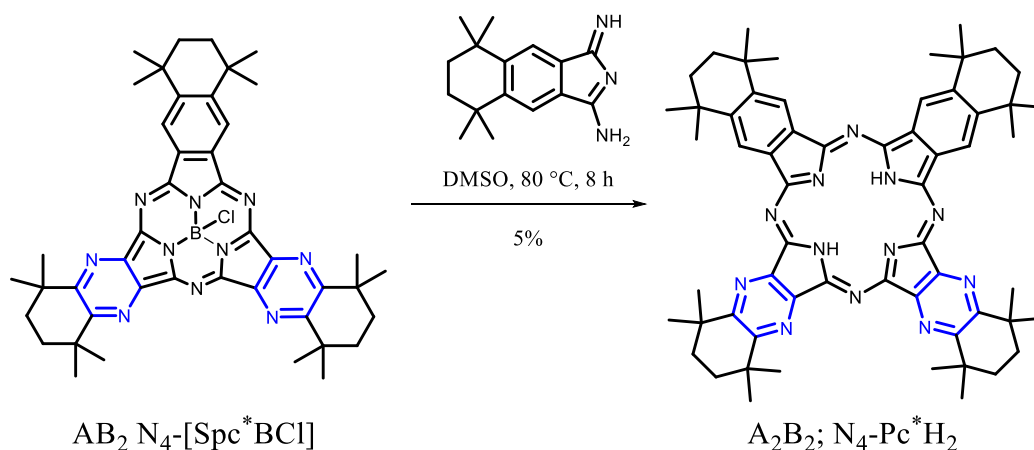
HRMS(+): $m/z = 959.5921$ $[M+H]^+$, cal. for $C_{60}H_{70}N_{12}+H_1$: 959.5919. - **Elemental analysis** ($C_{60}H_{70}N_{12}$, $M = 959.28$ g/mol): *find.* (*cal.*): C: 72.03% (75.12%), H: 7.36% (7.36%), N: 16.36% (17.52%).

N_6 -Pc*H₂: **Yield:** 9%. - **1H NMR** ($CDCl_3$, 300 MHz): $\delta = 9.75$ (s, 2 H, Ar-CH), 2.22 (s, 4 H, -CH₂), 2.19 (s, 12 H, -CH₂), 1.93 (s, 12 H, -CH₃), 1.91 (s, 12 H, -CH₃), 1.90 (s, 12 H, -CH₃), 1.83 (s, 12 H, -CH₃), -0.53 (s, 2 H, -NH) ppm. - **^{13}C NMR** (C_6D_6 , 75 MHz): $\delta = 162.0, 139.1, 131.3, 134.1$ (w), 132.9 (w), 132.9 (w), 131.3 (w), 127.1 (w), 123.1, 46.0, 41.3 (w), 39.7, 39.3, 36.3, 34.5, 32.8, 31.8, 31.7, 31.1, 30.9, 30.8, 29.8, 29.5, 29.3, 29.2, 28.6, 28.1, 27.5, 27.5 ppm. - 6 weak signal, marked with (w); not all quaternary atoms could be detected. - **IR** (ATR, 400-4000 cm^{-1}): $\tilde{\nu} = 3291$ (w), 2957 (s), 2924 (s), 2856 (s), 1727 (s), 1693 (s), 1637 (m), 1540 (m), 1503 (m), 1457 (s), 1411 (m), 1381 (m), 1360 (m), 1330 (m), 1305 (m), 1281 (m), 1257 (s), 1192 (s), 1157 (w), 1139 (m), 1127 (s), 1086 (m), 1072 (m), 1021 (s), 995 (s), 952 (m), 935 (w), 893 (w), 852 (m), 828 (m), 804 (m), 756 (m), 744 (s), 719 (s), 700 (w), 677 (s), 631 (m), 542 (w), 506 (w), 466 (w), 429 (w) cm^{-1} . - **CV** (DCM, [TBA]PF₆, Fc): $E_{ox1} = 0.35$, $E_{red1} = -1.47$, $E_{red2} = -1.82$ V. - **UV-Vis** (DCM): $\lambda = 660$ (s), 597 (sh), 343 (s), 234 (s) nm. - Φ_F ($\lambda_{ex} = 350$ nm) = 0.05; - ($\lambda_{ex} = 598$ nm) = 0.03. - $\Phi_{\Delta} = 0.04$. - **MS** (APCI-HRMS(+)): $m/z = 961.5825$ $[M+H]^+$, cal. for $C_{58}H_{68}N_{14}+H_1$: 961.5824. - **Elemental analysis** ($C_{58}H_{68}N_{14}$, $M = 961.25$ g/mol): *find.* (*cal.*): C: 71.99% (72.47%), H: 9.49% (7.13%), N: 12.38% (20.40%).

Ppz*H₂: **Yield:** 9%. - The analysis is in accordance with values in section 7.10.8. - Φ_F ($\lambda_{ex} = 350$ nm) = 0.03; - ($\lambda_{ex} = 598$ nm) = 0.03. - $\Phi_{\Delta} = 0.05$.



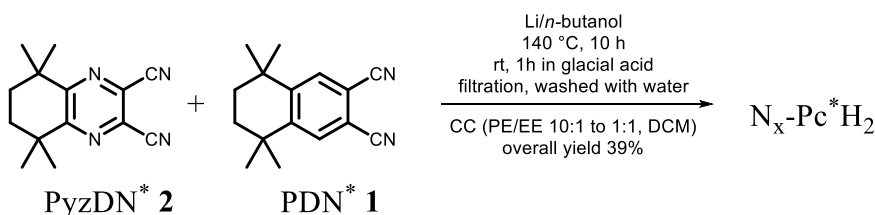
Pictures of TLC plates, before and after separation / Zn-insertion. Left: TLC plate (Tol, drop thf) of N_x -[SpC*BCl], middle: TLC plate (DCM) of N_x -Pc*H₂, right: TLC plate (DCM) of N_x -[Pc*Zn] (right spots) in comparison to unseparated N_x -Pc*H₂ (left spot).

7.11.2 Attempt to Synthesise ABAB N₄-Pc*H₂ in a Ring-Expansion

General Procedure 5: KOBAYASHI Ring-Expansion of Subphthalocyanines.^[45]

AB₃ N₆-Pc*H₂ and A₂B₂ N₄-Pc*H₂ could be obtained by inserting 1.1 eq isoindoline of PDN* into the corresponding subphthalocyanine [Spz*BCl] or N₄-[SpC*BCl]. Therefore, a solution of 1 eq isoindoline **1a** and 1 eq subphthalocyanine was stirred in DMSO at 120 °C for 8 h. After removing the solvent under reduced pressure, the product was purified by CC (PE/EA 1:1). AB₃ N₆-Pc*H₂ and A₂B₂ N₄-Pc*H₂ could be identified by using ¹H NMR, UV-Vis spectroscopy and APCI-HRMS. All data correlated with that described in section 7.11.1.

Yield: 5% (A₂B₂ N₄-Pc*H₂). - The analysis is in accordance with the data in section 7.11.1 (p. 242).

7.11.3 Synthesis of ABAB N₄-Pc*H₂

According to General Procedure 4 (p. 235), excepted that *n*-butanol was used instead of *n*-octanol. After cyclisation, the solvent was removed in vacuum, 50% aq. acetic acid was added and the solution was stirred for another 30 min. The solution was concentrated in vacuum, filtered, and was washed with water until the filtrate became neutral. ABAB N₄-Pc*H₂ was purified by CC (PE/EA 4:1). For photophysical experiments, the separation was additionally carried out by preparative TLC (PE/EE 4:1).

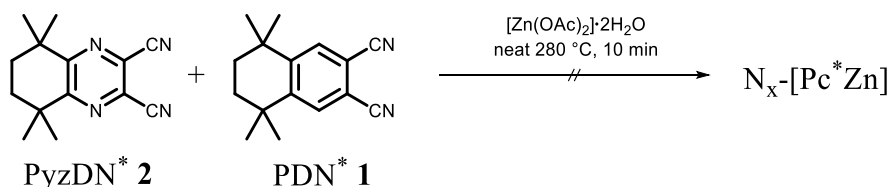
Experimental Section

ABAB N₄-Pc*H₂: Yield: <1%. - *R_f* (PE/EA 4:1) = 0.53. - ¹H NMR (CDCl₃, 300 MHz): δ = 9.79 (s, 4 H, Ar-CH), 2.22 (s, 8 H, -CH₂), 2.11 (s, 8 H, -CH₂), 1.90 (s, 24 H, -CH₃), 1.85 (s, 24 H, -CH₃), -0.68 (s, 2 H, -NH) ppm. - ¹³C NMR (C₆D₆, 75 MHz): δ = 36.5, 33.0, 29.8 ppm.* - CV (DCM, [TBA]PF₆, Fc): E_{ox1} = 0.28, E_{red1} = -1.47, E_{red2} = -1.79 V. - UV-Vis (DCM): λ = 672 (s), 642 (sh), 607 (s), 347 (s), 309 (s) nm. - Fluorescence (DCM, λ_{ex} = 350 nm): λ = 696 nm. - Φ_F (λ_{ex} = 350 nm) = 0.16; - (λ_{ex} = 598 nm) = 0.16. - Φ_Δ = 0.10. - MS (APCI-HRMS(+)): *m/z* = 959.5922 [M+H]⁺, cal. for C₆₀H₇₀N₁₂+H₁: 959.5919.

*only the methyl/methylene carbons could be detected.

7.11.4 Synthesis of N_x-[Pc*Zn]

7.11.4.1 Synthesis of N_x-[Pc*Zn] in a Neat Reaction [25]



488 mg PDN* (2.05 mmol, 4 eq), 521 mg PyzDN* (2.17 mmol, 4.4 eq), cat. amounts of urea (241 mg) and 688 mg [Zn(OAc)₂]·2H₂O (3.14 mmol, excess) were heated to 255 °C in a preheated metal bath for 5 min. The green/blue solid was extracted with DCM, loaded onto silica and purified by gradient CC (DCM/EE 95:1 → 1:1).

N₂-[Pc*Zn]: Yields: <1%. - ¹H NMR (CDCl₃, 300 MHz): δ = 7.07* (s, 6 H, Ar-CH), 1.17 (s, 16 H, -CH₂), 0.71 (s, 48 H, -CH₃) ppm. - MS (APCI-HRMS(+)): *m/z* = 1019.5158 [M+H]⁺, cal. for C₆₂H₇₀N₁₀Zn₁+H₁: 1019.5149.

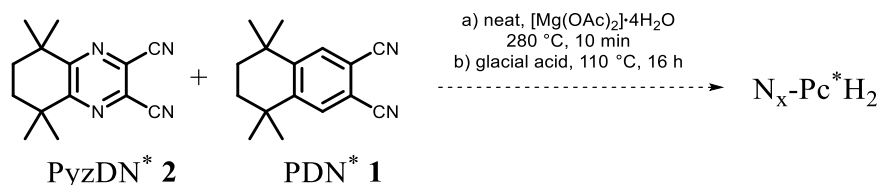
N₄-[Pc*Zn]: Yields: <1%. - ¹H NMR (CDCl₃, 300 MHz): δ = 7.71* (s, 2 H, Ar-CH), 1.44 (s, 8 H, -CH₂), 1.34 (s, 8 H, -CH₂), 1.23 (s, 24 H, -CH₃), 0.96 (s, 24 H, -CH₃) ppm. - ¹³C NMR (C₆D₆, 75 MHz): δ = 168.0, 164.2, 163.7, 151.8, 144.7, 130.8, 122.1, 38.6, 35.2, 34.6, 33.7, 31.4, 29.9 ppm. - UV-Vis (DCM): λ = 667 (s), 398 (s), 359 (sh), 298 (s) nm. - MS (APCI-HRMS(+)): *m/z* = 1021.5062 [M+H]⁺, cal. for C₆₀H₆₈N₁₂Zn₁+H₁: 1021.5054.

N₆-[Pc*Zn]: Yields: <1%. - UV-Vis (DCM): λ = 642 (s), 398 (s), 359 (sh), 298 (s) nm. - MS (APCI-HRMS(+)): *m/z* = 1023.4963 [M+H]⁺, cal. for C₅₈H₆₆N₁₄Zn₁+H₁: 1023.4959.

Additional information: *The different products could not be separated as it was possible in case of N_x-Pc*H₂. In MS, instead of product peaks, ligand peaks at *m/z* = 270-290 were

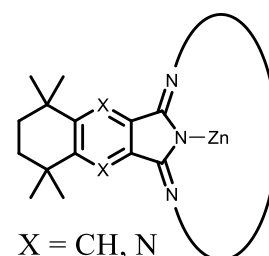
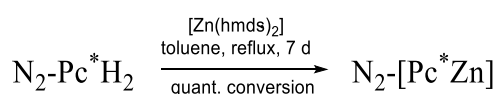
observed as 100% peaks. In the NMR spectra, only high-field shifted protons were observed. The NMR shifts of the aromatic protons suggest a degradation of the N_x -[Pc*Zn].

7.11.4.2 Attempt to Synthesise N_x -Pc*H₂ in a neat reaction using [Mg(OAc)₂]



502 mg PDN* (2.10 mmol, 2 eq) and 511 mg PyzDN* (2.10 mmol, 2 eq) were heated up to 280 °C within a 247 mg [Mg(OAc)₂]·4H₂O (1.20 mmol, 1.1 eq) mixture. After 10 min, the green powder was cooled down to rt, 40 mL glacial acidic acid were added and stirred at 110 °C overnight. After removing AcOH in vacuum, the powder was washed several times with MeOH. The products could not be separated in sufficient amounts and purity.

7.11.4.3 Synthesis of N_2 -[Pc*Zn] on NMR Scale

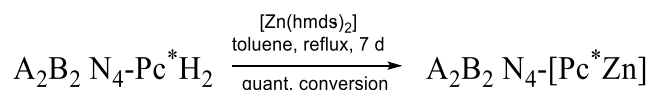


General Procedure 6: Synthesis of [PcZn] using [Zn(hmnds)₂] and PcH₂.

1 eq N_x -Pc*H₂ was dissolved in dry toluene (2 mL/100 mg N_x -Pc*H₂) and 10 eq [Zn(hmnds)₂] were added at rt. The solution was stirred at 110 °C, overnight. The reaction was monitored by TLC. The obtained blue powder was washed with DEE, to dissolve and remove [Zn(hmnds)₂]/HHMDS residues. Finally, the products were purified over a short filter column of silica.

N_2 -[Pc*Zn]: **Yield:** quant. - **R_f** (Tol/THF 20:1) = 0.80. - **¹H NMR** (C₆D₆, 300 MHz): δ = 9.97 (s, 4 H, Ar-CH), 9.94 (s, 2 H, Ar-CH), 1.92 (s, 4 H, -CH₂), 1.86 (s, 12 H, -CH₃), 1.80 (s, 12 H, -CH₂), 1.56 (s, 24 H, -CH₃), 1.46 (s, 12 H, -CH₃) ppm. - **UV-Vis** (DCM): λ = 675 (s), 613 (sh), 360 (s), 228 (s) nm. - **Fluorescence** (DCM, λ_{ex} = 350 nm): λ = 697 nm. - **Φ_F** (λ_{ex} = 350 nm) = 0.24; - (λ_{ex} = 598 nm) = 0.25. - **Φ_Δ** = 0.63. - **MS** (APCI-HRMS(+)): m/z = 1019.5139 [M+H]⁺, cal. for C₆₂H₇₀N₁₀Zn₁+H₁: 1019.5149.

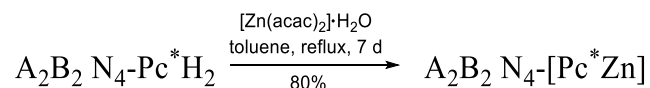
7.11.4.4 Synthesis of A₂B₂ N₄-[Pc*Zn] on NMR Scale



According to General Procedure 6 (p. 247).

A₂B₂ N₄-[Pc*Zn]: Yield: quant. - **¹H NMR** (C₆D₆, 300 MHz): δ = 9.93 (s, 2 H, Ar-CH), 9.91 (s, 2 H, Ar-CH), 1.91 (s, 8 H, -CH₂), 1.83 (s, 8 H, -CH₂), 1.78 (s, 24 H, -CH₃), 1.53 (s, 12 H, -CH₃), 1.43 (s, 12 H, -CH₃) ppm. - **¹H NMR** (CD₂Cl₂, 300 MHz): δ = 9.59 (s, 2 H, Ar-CH), 9.56 (s, 2 H, Ar-CH), 2.24 (s, 8 H, -CH₂), 2.08 (s, 8 H, -CH₂), 1.93 (s, 12 H, -CH₃), 1.92 (s, 12 H, -CH₃), 1.83 (s, 12 H, -CH₃), 1.82 (s, 12 H, -CH₃) ppm. - **IR** (ATR, 400-4000 cm⁻¹): $\tilde{\nu}$ = 2959 (m), 2924 (m), 2857 (m), 2381 (m), 2349 (m), 2326 (m), 1536 (w), 1493 (w), 1468 (w), 1460 (w), 1361 (w), 1336 (w), 1308 (w), 1256 (s), 1192 (w), 1149 (w), 1086 (s), 1014 (s), 901 (m), 866 (w), 796 (s), 746 (w), 698 (w), 662 (m), 508 (w), 449 (w), 429 (w) cm⁻¹. - **UV-Vis** (DCM): λ = 666 (s), 601 (sh), 361 (s) nm. - **Fluorescence** (DCM, λ_{ex} = 350 nm): λ = 680 nm. - Φ_F (λ_{ex} = 350 nm) = 0.26; - (λ_{ex} = 598 nm) = 0.30. - Φ_Δ = 0.64. - **MS** (APCI-HRMS(+)): m/z = 1021.5043 [M+H]⁺, cal. for C₆₀H₆₈N₁₂Zn₁+H₁: 1021.5054.

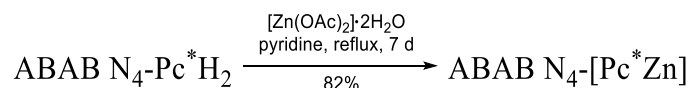
7.11.4.5 Synthesis of A₂B₂ N₄-[Pc*Zn] using [Zn(acac)₂]



20 mg N₄-Pc*H₂ (20 μmol, 1 eq) were dissolved in 1 mL DMF with 9 mg [Zn(acac)₂]₂·H₂O (30 μmol, 1.5 eq) and were stirred for 2 d at 120 °C. The crude product was purified by CC (DCM/EE 1:1).

Yield: 80%. - **R_f** (Tol/THF 20:1) = 0.74. - **UV-Vis** (DCM): λ = 667 (s), 398 (s), 359 (sh), 298 (s) nm. - **MS** (APCI-HRMS(+)): m/z = 1021.5058 [M+H]⁺, cal. for C₆₀H₆₈N₁₂Zn+H₁: 1021.5054.

The disadvantage of this synthesis is that a degradation of the pyrazinoporphyrazine compounds might be observed if too many equivalents of the [Zn(acac)₂]₂·H₂O are added. By using the route with [Zn(hmds)₂] no degradation was observed, even though high temperatures of 100 °C and >10 eq of the [Zn(hmds)₂] were used.

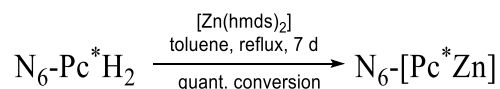
7.11.4.6 Synthesis of N₄-[Pc*Zn] using [Zn(OAc)₂]

General Procedure for the Synthesis of N_x-[Pc*Zn] using [Zn(OAc)₂]:

1 eq ABAB or A₂B₂ N₄-Pc*H₂ was dissolved in pyridine and 1.2 eq [Zn(OAc)₂]^{*}·2H₂O were added. After refluxing for 1 h, the reaction was monitored by TLC (DCM), and was stirred for another 1 h. The resulting blue solutions were concentrated in vacuum, filtered, and washed with an excess of water. After washing the product off the filter paper using CHCl₃/MeOH 3:1, the blue product was dried in vacuum and purified by preparative TLC or CC (Tol/THF 20:1).

ABAB N₄-[Pc*Zn]: Yield: 82%. - *R_f* (Tol/THF 20:1) = 0.63. - **¹H NMR** (C₆D₆, 300 MHz): δ = 9.96 (s, 4 H, Ar-CH), 1.91 (s, 8 H, -CH₂), 1.85 (s, 24 H, -CH₃), 1.78 (s, 8 H, -CH₂), 1.45 (s, 24 H, -CH₃) ppm. - **UV-Vis** (DCM): λ = 687 (s), 657 (s), 631 (sh), 596 (sh), 357 (s) nm. - **Φ_F** (λ_{ex} = 350 nm) = 0.16; - (λ_{ex} = 598 nm) = 0.18. - **Φ_Δ** = 0.73. - **MS** (APCI-HRMS(+)): *m/z* = 1021.5073 [M+H]⁺, cal. for C₆₀H₆₈N₁₂Zn₁+H₁: 1021.5054.

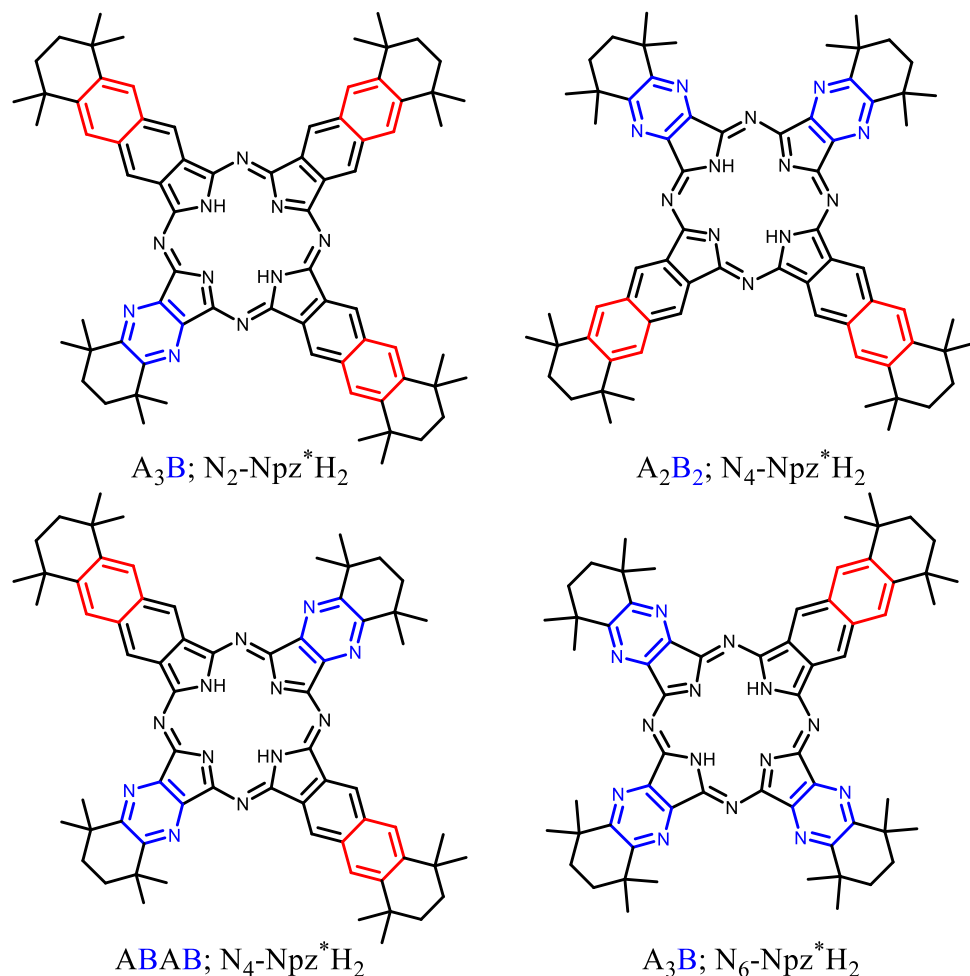
A₂B₂ N₄-[Pc*Zn]: Yield: 76%. - The analysis is in accordance with the data described above.

7.11.4.7 Synthesis of N₆-[Pc*Zn]

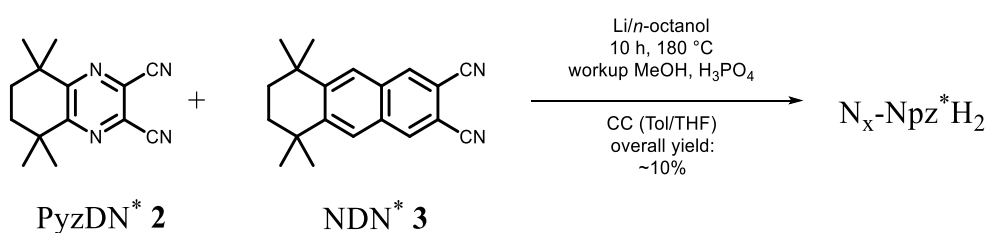
According to General Procedure 6 (p. 247).

Yield: quant. - *R_f* (Tol/THF 20:1) = 0.32. - **¹H NMR** (C₆D₆, 300 MHz): δ = 9.96 (s, 2 H, Ar-CH), 1.89 (s, 12 H, -CH₂), 1.83 (s, 12 H, -CH₃), 1.79 (s, 24 H, -CH₃), 1.76 (s, 4 H, -CH₂), 1.43 (s, 12 H, -CH₃) ppm. - **IR** (ATR, 400-4000 cm⁻¹): ν̃ = 2959 (w), 2926 (w), 2856 (w), 1458 (w), 1308 (m), 1230 (s), 1204 (s), 1149 (s), 1128 (s), 981 (s), 867 (m), 802 (m), 745 (m), 696 (m), 638 (m), 553 (m), 505 (s), 432 (w) cm⁻¹. - **UV-Vis** (DCM): λ = 662 (s), 649 (s), 357 (s), 227 (s) nm. - **Fluorescence** (DCM, λ_{ex} = 350 nm): λ = 673 nm. - **Φ_F** (λ_{ex} = 350 nm) = 0.24; - (λ_{ex} = 598 nm) = 0.27. - **Φ_Δ** = 0.62. - **MS** (APCI-HRMS(+)): *m/z* = 1023.4959 [M+H]⁺, cal. for C₅₈H₆₆N₁₄Zn₁+H₁: 1023.4959.

7.12 Synthesis of Asymmetrical Azanaphthalocyanines: $N_x-Npz^*H_2$



7.12.1 Synthesis of $N_x-Npz^*H_2$ [196]



According to General Procedure 4 (p. 235), using $PyzDN^* 2$ / $NDN^* 3$ in a 1:3 ratio. The products were separated by using CC (Tol/THF 100 \rightarrow 20:1). In accordance with the separation of $N_x-Pc^*H_2$, the products were eluted with an increased number of pyrazine units [-N=] (increasing substitution of [-CH=] by [-N=]).

Nc^*H_2 :^[24] **Yield:** <1%. - Nc^*H_2 was identified by using UV-Vis spectroscopy and MS.

$N_2-Npz^*H_2$: **Yield:** 3%. - R_f (Tol/THF 1:1) = 0.95. - 1H NMR (C_6D_6 , 300 MHz): δ = 9.43 (s, 2 H, Ar-CH^{inner}), 9.27 (s, 2 H, Ar-CH^{inner}), 9.20 (s, 2 H, Ar-CH^{inner}), 8.48 (s, 2 H, Ar-CH), 8.29 (s, 2 H, Ar-CH), 8.00 (s, 2 H, Ar-CH), 2.07 (s, 4 H, -CH₂^{Ppz}), 2.01 (s, 12 H, -CH₃^{Ppz}), 1.91

(s, 8 H, $-CH_2^{Nc}$), 1.86 (s, 4 H, $-CH_2^{Nc}$), 1.64 (s, 24 H, $-CH_3^{Nc}$), 1.58 (s, 24 H, $-CH_3^{Nc}$), 0.45 (s, 2 H, $-NH$) ppm. - **IR** (ATR, 400-4000 cm^{-1}): $\tilde{\nu}$ = 2957 (m), 2923 (m), 2855 (m), 1726 (w), 1258 (m), 1089 (s), 1016 (s), 909 (m), 857 (w), 796 (s), 754 (m), 709 (m), 469 (m) cm^{-1} . - **CV** (DCM, [TBA]PF₆, Fc): E_{ox2} = 0.29, E_{ox1} = -0.32, E_{red1} = -1.69, E_{red2} = -2.02 V. - **UV-Vis** (DCM): λ = 773 (s), 735 (s), 693 (sh), 334 (s) nm. - **MS** (APCI-HRMS(+)): m/z = 1106.6431 [M+H]⁺, cal. for C₇₄H₇₈N₁₀+H₁: 1106.6405.

A₂B₂ N₄-Npz*H₂: Yield: 3%. - R_f (Tol/THF 1:1) = 0.78. - **¹H NMR** (CDCl₃, 300 MHz): δ = 9.56 (s, 2 H, Ar-CH^{inner}), 9.48 (s, 2 H, Ar-CH^{inner}), 8.42 (s, 2 H, Ar-CH), 8.41 (s, 2 H, Ar-CH), 2.15 (s, 8 H, $-CH_2^{Ppz}$), 1.95 (s, 8 H, $-CH_2^{Nc}$), 1.87 (s, 12 H, $-CH_3^{Ppz}$), 1.84 (s, 12 H, $-CH_3^{Ppz}$), 1.62 (s, 12 H, $-CH_3^{Nc}$), 1.60 (s, 12 H, $-CH_3^{Nc}$), 1.08 (s, 2 H, $-NH$) ppm. - **IR** (ATR, 400-4000 cm^{-1}): $\tilde{\nu}$ = 2956 (m), 2923 (m), 2857 (m), 1550 (m), 1456 (m), 1381 (m), 1358 (m), 1331 (m), 1306 (m), 1256 (s), 1204 (w), 1187 (w), 1151 (w), 1129 (w), 1100 (s), 1047 (s), 1017 (s), 935 (m), 911 (w), 856 (m), 798 (s), 752 (s), 730 (m), 703 (m), 678 (m), 663 (m), 469 (m) cm^{-1} . - **CV** (DCM, [TBA]PF₆, Fc): (E_{ox2} = 0.16), E_{ox1} = -0.25, E_{red1} = -1.74, E_{red2} = -2.11 V. - **UV-Vis** (DCM): λ = 723 (s), 687 (s), 651 (sh), 258 (s), 338 (s) nm. - **MS** (APCI-HRMS(+)): m/z = 1081.6046 [M+Na]⁺, cal. for C₆₈H₇₄N₁₂+Na₁: 1081.6052.

N₆-Npz*H₂: Yield: 2%. - R_f (Tol/THF 1:1) = 0.71. - **¹H NMR** (CDCl₃, 300 MHz): δ = 9.85 (s, 2 H, Ar-CH^{inner}), 8.04 (s, 2 H, Ar-CH), 1.91 (s, 4 H, $-CH_2^{Ppz}$), 1.88 (s, 12 H, $-CH_3^{Ppz}$), 1.86 (s, 8 H, $-CH_2^{Ppz}$), 1.81 (s, 12 H, $-CH_3^{Ppz}$), 1.79 (s, 12 H, $-CH_3^{Ppz}$), 1.78 (s, 4 H, $-CH_2^{Nc}$), 1.50 (s, 12 H, $-CH_3^{Nc}$), -0.11 (s, 2 H, $-NH$) ppm. - **IR** (ATR, 400-4000 cm^{-1}): $\tilde{\nu}$ = 2965 (m), 2879 (m), 1473 (m), 1259 (m), 1087 (m), 1016 (m), 930 (w), 879 (w), 832 (s), 797 (s), 738 (m), 669 (m), 556 (s), 437 (m) cm^{-1} . - **CV** (DCM, [TBA]PF₆, Fc): E_{ox1} = 0.02*, E_{red1} = -1.63, E_{red2} = -2.18 V. - **UV-Vis** (DCM): λ = 717 (s), 678 (s), 341 (s) nm. - **MS** (APCI-HRMS(+)): m/z = 1033.5803 [M+Na]⁺, cal. for C₆₂H₇₀N₁₄+Na₁: 1033.5800.

*CV values for N₆-Nc*H₂ could not be assigned for certain. Here, only approximated values are given. New measurements in different solvents have to be carried out.

Additional information: The procedure was carried out for a second time, using Li/*n*-butanol suspension. The solution was refluxed at 160 °C for 3 h. After cooling down to rt, the solvent was removed in vacuum, and 10 mL 50% aq. AcOH were added. The solution was stirred for another 30 min before filtration. The filtrate was washed with water until it became neutral. The powder was dried in vacuum and separated by preparative TLC.

Experimental Section

7.12.2 Synthesis of N₄-Npz*H₂

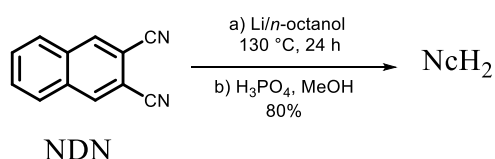
According to General Procedure 4 (p. 235): ABAB N₄-Npz*H₂ was synthesised in a separate procedure using PyzDN*/NDN* in a 1.5:1 ratio.

ABAB N₄-Npz*H₂: Yield: <1%. - **R_f** (Tol/THF 20:1) = 0.85. - **¹H NMR** (C₆D₆/drop CD₂Cl₂, 300 MHz): δ = 9.88 (s, 4 H, Ar-CH), 8.08 (s, 4 H, Ar-CH), 1.93 (s, 24+8 H, -CH₃, -CH₂), 1.80 (s, 8 H, -CH₂), 1.52 (s, 24 H, -CH₃), 0.09 (s, 2 H, -NH) ppm. - **UV-Vis** (DCM): λ = 777 (s), 715 (s), 690 (s), 641 (sh), 342 (s) nm. - **Fluorescence** (DCM, λ_{ex} = 350 nm): λ = 808 nm. - **MS** (APCI-HRMS(+)): m/z = 1059.6240 [M+H]⁺, cal. for C₆₈H₇₄N₁₂+H₁: 1059.6232.

7.13 Synthesis of Naphthalocyanines

For the synthesis of $[\text{Nc}^*\text{M}]$ complexes, several established methods similar to the synthesis of $[\text{Pc}^*\text{M}]$ were carried out. The different syntheses are summarised in the discussion section. Known phthalocyanines have been synthesised by MIKHALENKO, and were reproduced by VOLLGRAFF. New naphthalocyanines were part of the bachelor thesis of VOLLGRAFF and were therefore synthesised for the first time.

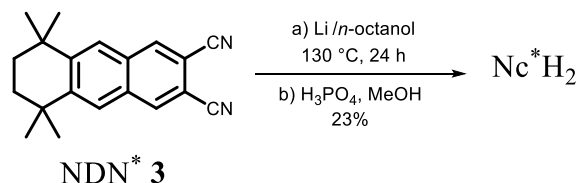
7.13.1 Synthesis of NcH_2 [24]



Modified known literature procedure:^[286] 357 mg lithium (51.5 mmol, 5.0 eq) were suspended for 2 h at 60 °C in 10 mL *n*-octanol. 1.83 g 2,3-naphthalindicarbonitrile (10.3 mmol, 1.0 eq) were added at once and placed in a preheated oil bath at 130 °C. Within 10 min, the solution turned green and was stirred for another 24 h. After cooling down to rt, 60 mL MeOH and 2.5 mL H_3PO_4 were added, and the solution was macerated with 3 x 60 mL MeOH. The brownish powder was finally dried in vacuum.

Yield: 1.45 g, 8.2 mmol, 80%. - **IR** (ATR, 400-4000 cm^{-1}): $\tilde{\nu} = 2924$ (vw), 1019 (s), 885 (m), 753 (w), 586 (m), 506 (w) cm^{-1} . - **UV-Vis** (DCM): $\lambda = 765$ (s), 734 (sh), 687 (sh), 235 (m) nm. - **Fluorescence** (DCM, $\lambda_{\text{ex}} = 750$ nm): $\lambda = 785$ nm. - **MS** (MALDI-ToF(+)): $m/z = 714.193$ $[\text{M}+\text{H}]^+$.

7.13.2 Synthesis of Nc^*H_2 [24]



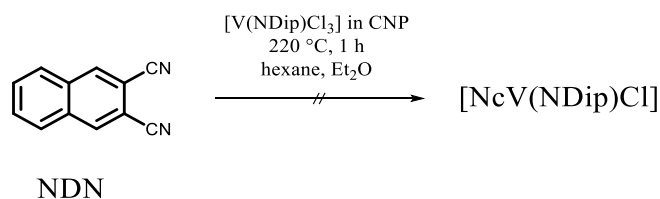
Modified known literature procedure: ^[24,140] 180 mg lithium (25.9 mmol, 5.0 eq) were suspended for 2 h at 60 °C in 10 mL *n*-octanol. 1.51 g NDN^* (5.24 mmol, 1.0 eq) were added at once, placed in a preheated oil bath at 130 °C and were stirred for 24 h. After cooling down

Experimental Section

to rt, 60 mL MeOH and 2.5 mL H₃PO₄ were added and the solution was macerated with 3 x 60 mL MeOH. The brownish powder was finally dried in vacuum.

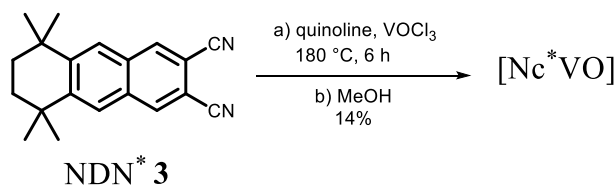
Yield: 351 mg, 1.20 mmol, 23%. - **¹H NMR** (C₆D₆, 300 MHz): δ = 9.43 (s, 8 H, Ar-CH), 8.50 (s, 8 H, Ar-CH), 1.94 (s, 16 H, -CH₂), 1.71 (s, 48 H, -CH₃) ppm. - **IR** (ATR, 400-4000 cm⁻¹): $\tilde{\nu}$ = 3287 (vw), 2956 (s), 2923 (s), 2856 (s), 2325 (w), 1458 (s), 1106 (s), 1015 (vs), 906 (s), 753 (m), 465 (m) cm⁻¹. - **UV-Vis** (DCM): λ = 797 (s), 761 (sh), 710 (sh), 370 (m), 325 (m) nm. - **Fluorescence** (DCM, λ_{ex} = 750 nm): λ = 805 nm. - **MS** (MALDI-ToF(+)): m/z = 1154.985 [M+H]⁺. - **Elemental analysis** (C₈₀H₈₂N₈, 1155.56 g/mol): *find.* (*cal.*): C: 77.22% (83.15%), H: 7.54% (7.15%), N: 7.61% (9.70%).

7.13.3 Attempt to Synthesise [NcV(NDip)Cl]



4 eq of NDN and 1 eq of [V(NDip)Cl₃]*dme* were dissolved in CNP. The solution was stirred at 220 °C for 1 h. The solution turned black. No product could be observed either in UV-Vis, or in MALDI-ToF.

7.13.4 Synthesis of [Nc*VO] [4]

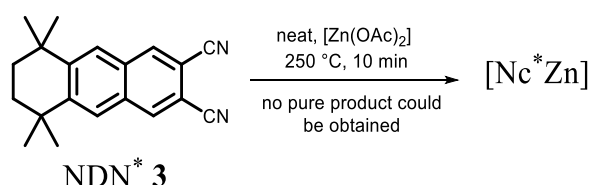


250 mg NDN* (868 μ mol, 4.0 eq) were dissolved in 1 mL quinoline. The solution was stirred with 38 mg vanadyltrichlorid (0.22 mmol, 1.0 eq) in a preheated oil bath for 6 h at 180 °C. After cooling down to rt, the mixture was macerated with 3 x 50 mL MeOH and finally dried in vacuum. A dark green powder was obtained.

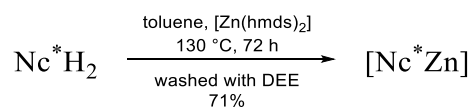
Yield: 37 mg, 30.0 μ mol, 14%. - **IR** (ATR, 400-4000 cm⁻¹): $\tilde{\nu}$ = 3064 (br), 2957 (m), 2922 (m), 2858 (m), 2358 (vw), 2339 (vw), 1637 (w), 1500 (m), 1460 (m), 1409 (s), 1107 (vs), 1087 (vs), 981 (s), 909 (m), 804 (s), 747 (m), 731 (m), 609 (m), 469 (s) cm⁻¹. - **UV-Vis** (DCM):

$\lambda = 830$ (s), 788 (sh), 737 (m), 367 (m), 330 (m) nm. - **MS** (MALDI-ToF(+)): $m/z = 1219.762$ $[M+H]^+$. - **Elemental analysis** ($C_{80}H_{80}N_8V_1O_1$, 1235.52 g/mol): *find.* (*cal.*): C: 74.90% (78.73%), H: 6.25% (6.61%), N: 9.16% (9.18%).

7.13.5 Synthesis of $[Nc^*Zn]$ [24]



Method a) Modified known literature procedure:^[24] 250 mg NDN^* (867 μmol , 4.0 eq) and 48 mg $[\text{Zn}(\text{OAc})_2] \cdot 2\text{H}_2\text{O}$ (217 μmol , 1.0 eq) were weighed out in a flask and were melted at 250 $^\circ\text{C}$ for 1 h. After cooling down to rt, the green solid was washed with 3 x 20 mL MeOH and finally dried in vacuum. A green powder was obtained. No spectroscopically pure product was obtained.

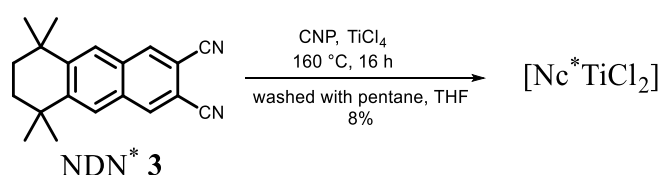


Method b) 100 mg $\text{Nc}^* \text{H}_2$ (86.5 μmol , 1.0 eq) and 134 mg $[\text{Zn}(\text{hmds})_2]$ (348 μmol , 4.0 eq) were dissolved in 2 mL toluene. The solution was warmed up to 130 $^\circ\text{C}$ and 1 mL $[\text{Zn}(\text{hmds})_2]$ was added. After 30 min another aliquot of $[\text{Zn}(\text{hmds})_2]$ solution was added, and was stirred for 72 h at 130 $^\circ\text{C}$. After cooling down to rt, the solvent was evaporated and the residue was washed with DEE. A greenish-brown powder was obtained.

Yield: 188 mg, 154 μmol , 71%. - **$^1\text{H NMR}$** (C_6D_6 , 300 MHz): only low-field shifted protons at 10.83 ppm and 9.07 ppm were detected. - **IR** (ATR, 400-4000 cm^{-1}): $\tilde{\nu} = 2956$ (m), 2909 (m), 2860 (m), 1460 (m), 1398 (m), 1338 (s), 1294 (m), 1109 (vs), 1092 (s), 1035 (s), 1020 (s), 906 (s), 729 (m), 467 (m) cm^{-1} . - **UV-Vis** (DCM): $\lambda = 792$ (s), 704 (w), 327 (m) nm. - **Fluorescence** (DCM, $\lambda_{\text{ex}} = 750$ nm): $\lambda = 794$ nm. - **MS** (MALDI-ToF(+)): $m/z = 1218.572$ $[M+H]^+$. - **Elemental analysis** ($\text{C}_{80}\text{H}_{80}\text{N}_8\text{Zn}_1$, 1218.95 g/mol): *find.* (*cal.*): C: 69.90% (78.83%), H: 6.14% (6.62%), N: 7.03% (9.19%).

Experimental Section

7.13.6 Synthesis of $[\text{Nc}^*\text{TiCl}_2]$ ^[140]

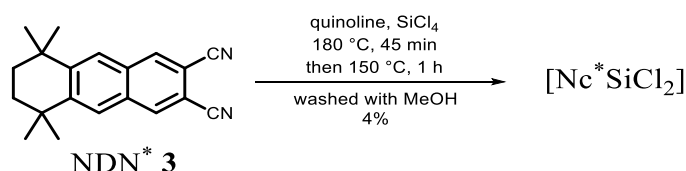


500 mg NDN* (174 μmol , 4.0 eq) and 83.4 mg TiCl_4 (44.6 μmol , 1.0 eq) were dissolved in 2 mL CNP in a preheated oil bath at 160 $^\circ\text{C}$. The solution was stirred for 16 h. After cooling down to rt, the solution was washed with 5 x 20 mL pentane until the solution got clear. The resulting solid was further washed with 5 x 20 mL THF before drying in vacuum. The product was obtained in the form of violet microcrystals.

Yield: 47 mg, 36.9 μmol , 8%. - **$^1\text{H NMR}$** (C_6D_6 , 300 MHz): only low-field shifted protons at 9.96 and 8.64 ppm were detected. - **IR** (ATR, 400-4000 cm^{-1}): $\tilde{\nu}$ = 3049 (vw), 2925 (m), 2860 (m), 1475 (m), 1460 (m), 1336 (m), 1292 (vs), 1107 (s), 1070 (s), 936 (s), 738 (m), 730 (m), 467 (s) cm^{-1} . - **UV-Vis** (DCM): λ = 827 (s), 782 (sh), 737 (m), 446 (m), 311 (m) nm. - **Fluorescence** (DCM, λ_{ex} = 750 nm): λ = 839 nm. - **MS** (MALDI-ToF(+)): m/z = 1271.108 $[\text{M}]^+$; m/z = 1235.923 $[\text{M}-\text{Cl}]^+$; m/z = 1216.904 $[\text{M}=\text{O}]^+$. - **Elemental analysis** ($\text{C}_{80}\text{H}_{80}\text{N}_8\text{Ti}_1\text{Cl}_2$, 1272.31 g/mol): *find.* (*cal.*): C: 74.05% (75.52%), H: 6.52% (6.34%), N: 9.08% (8.81%).

Additional information: Observed fragments, $[\text{MO}]$ and $[\text{M}-\text{Cl}]$, result from the MALDI-ToF measurement, because the target is a short time on air before measurement.

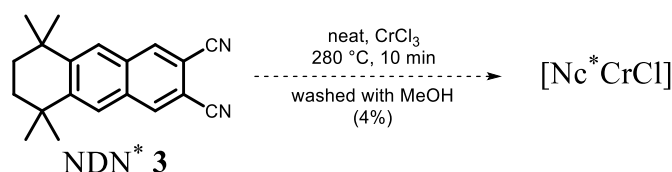
7.13.7 Synthesis of $[\text{Nc}^*\text{SiCl}_2]$ ^[140]



501 mg NDN* (1.74 mmol, 1.0 eq) and cat. amounts of ammonium heptamolybdate were dissolved in 2 mL quinoline. 444 mg SiCl_4 (2.61 mmol, 1.5 eq) were added and stirred in a preheated oil bath for 45 min at 180 $^\circ\text{C}$. After cooling down to 150 $^\circ\text{C}$, the solution was stirred for another 1 h. After cooling down to rt, the mixture was macerated with 3 x 50 mL MeOH and finally dried in vacuum. The product was obtained in the form of a green powder.

Yield: 24 mg, 19.3 μmol , 4%. - **$^1\text{H NMR}$** (CDCl_3 , 300 MHz): $\delta = 10.21$ (s, 8 H, Ar-CH), 8.59 (s, 8 H, Ar-CH), 1.56 (s, 16 H, $-\text{CH}_2$), 1.35 (s, 48 H, $-\text{CH}_3$) ppm. - **IR** (ATR, 400-4000 cm^{-1}): $\tilde{\nu} = 2956$ (m), 2923 (m), 2859 (m), 1461 (m), 1386 (m), 1294 (s), 1207 (w), 1107 (s), 1087 (vs), 911 (s), 769 (m), 565 (w), 471 (s) cm^{-1} . - **UV-Vis** (DCM): $\lambda = 851$ (s), 803 (sh), 756 (m), 378 (m), 355 (m) nm. - **Fluorescence** (DCM, $\lambda_{\text{ex}} = 750$ nm): $\lambda = 818$ nm. - **MS** (MALDI-ToF(+)): $m/z = 1250.930$ $[\text{M}+\text{H}]^+$. - **Elemental analysis** ($\text{C}_{80}\text{H}_{80}\text{N}_8\text{Si}_1\text{Cl}_2$, 1252.53 g/mol): *find.* (*cal.*): C: 63.22% (76.71%), H: 5.77% (6.44%), N: 7.99% (8.95%).

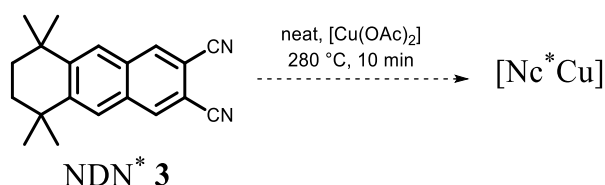
7.13.8 Synthesis of $[\text{Nc}^*\text{CrCl}]$ [140]



250 mg NDN^* (868 μmol , 1.0 eq) and 138 mg CrCl_3 (871 μmol , 1.0 eq) were heated for 15 min at 280 $^\circ\text{C}$ in a preheated metal bath. After cooling down to rt, the mixture was macerated with 3 x 50 mL MeOH and finally dried in vacuum. Violet microcrystals were obtained, but the resulting substance was not obtained in sufficient amounts and was not pure enough for full analysis. Anyway, it could only be detected by UV-Vis spectroscopy and MS spectrometry.

(**Yield:** 11 mg, 8.86 μmol , 4%.) - **UV-Vis** (DCM): $\lambda = 805$ (m), 707 (m), 355 (s), 299 (s) nm. - **Fluorescence** (DCM, $\lambda_{\text{ex}} = 750$ nm): $\lambda = 811$ nm. - **MS** (MALDI-ToF(+)): $m/z = 1239.879$ $[\text{M}+\text{H}]^+$.

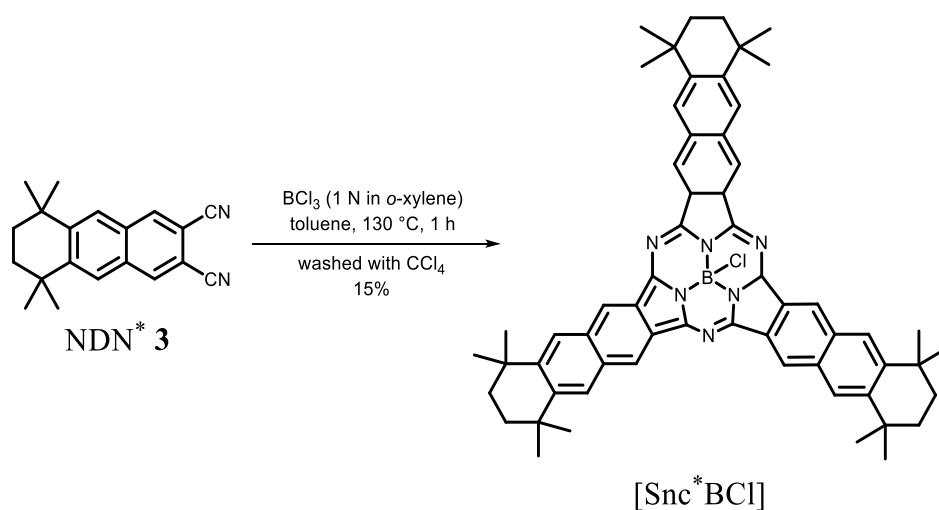
7.13.8.1 Synthesis of $[\text{Nc}^*\text{Cu}]$ [140]



A neat reaction carried out, using 1 eq $[\text{Cu}(\text{OAc})_2]$, 4 eq NDN^* and cat. amounts of urea. The flask was placed in a preheated metal bath at 280 $^\circ\text{C}$, for 10 min. The resulting dark powder was washed with 3 x 30 mL MeOH. No spectroscopically pure product was obtained, but it was observed in MS. - **MS** (MALDI-ToF(+)): $m/z = 1216.513$ $[\text{M}+\text{H}]^+$.

Experimental Section

7.13.9 Synthesis of [Snc*BCl] ^[140]

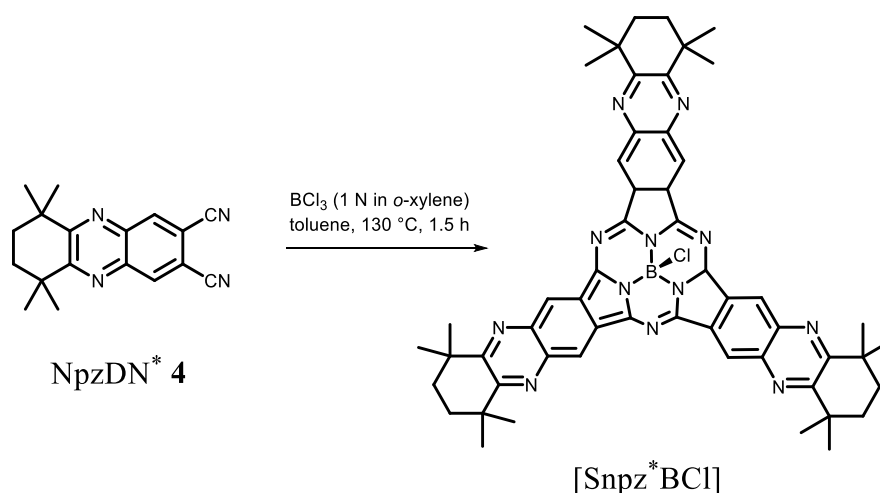


250 mg NDN* (868 μ mol, 1.5 eq) were dissolved in 2 mL toluene. 0.46 mL BCl₃ solution (1 M in *o*-xylene, 460 μ mol, 1.0 eq) were added and the solution was stirred at 130 °C for 1 h. After cooling down to rt, the solvent was removed, and the brownish solid was washed with 3 x 20 mL hexane and tetrachlormethane.* The resulting solid was dried in vacuum.

Yield: 78 mg, 85.3 μ mol, 15%. - **IR** (ATR, 400-4000 cm⁻¹): $\tilde{\nu}$ = 3214 (br), 2959 (m), 2927 (m), 2862 (m), 1595 (m), 1458 (vs), 1363 (s), 1340 (s), 1106 (s), 917 (m), 782 (s), 756 (s), 466 (m) cm⁻¹. - **UV-Vis** (DCM): λ = 676 (m), 379 (m), 284 (s), nm. - **Fluorescence** (DCM, λ_{ex} = 600 nm): λ = 692 nm. - **MS** (MALDI-ToF(+)): m/z = 913.736 [M+H]⁺.

Additional information: *CC and filtration under inert atmosphere was attempted but leads to a degradation of the Snc.

7.13.10 Attempt to Synthesise [Snpz*BCl]

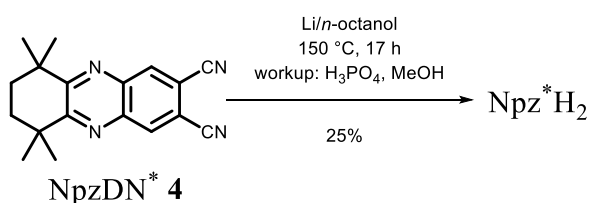


100 mg NpzDN* (0.34 mmol, 1 eq) were dissolved in 1 mL toluene. 0.3 mL BCl₃ solution (1 M in *o*-xylene, 0.3 mL, 0.3 mmol) were added and the solution was heated to 130 °C and was stirred for 1.5 h. The solvent was removed in vacuum and the resulting green powder was loaded onto a short plug of silica. The resulting crude product was again purified by CC (PE/EE 20:1) and a weak blue fraction was collected, which was wasted. The solvent was changed to (Tol/THF) and another deep blue fraction was collected. The final product was analysed by preparative TLC. The product was obtained in the form of a blue powder.

Yield: <5%. - *R_f* (toluene) = 0.2. - ¹H NMR: (C₆D₆, 300 MHz): δ = 9.65 (s, 6 H, Ar-CH), 2.05-1.84 (m, 12 H, -CH₂), 1.58 (s, 18 H, -CH₃), 1.47 (s, 18 H, -CH₃) ppm. - ¹H NMR: (CD₂Cl₂, 300 MHz): δ = 9.49 (s, 6 H, Ar-CH), 1.97-1.89 (m, 12 H, -CH₂), 1.62 (s, 18 H, -CH₃), 1.49 (s, 18 H, -CH₃) ppm. - while measuring the ¹H NMR spectrum, degradation/oxidation of the [Snpz*BCl] was observed. - **UV-Vis** (DCM): λ = 638 (s), 578 (sh), 296 (s) nm. - **Fluorescence** (DCM, λ_{ex} = 350 nm): λ = 653 nm - **MS** (MALDI-ToF(+)): m/z = 915.263 [M+OMe, -Cl]⁺. - Methanolysis is caused by chosen conditions of ionisation.

7.14 Synthesis of Azanaphthalocyanines

7.14.1 Synthesis of Npz^*H_2

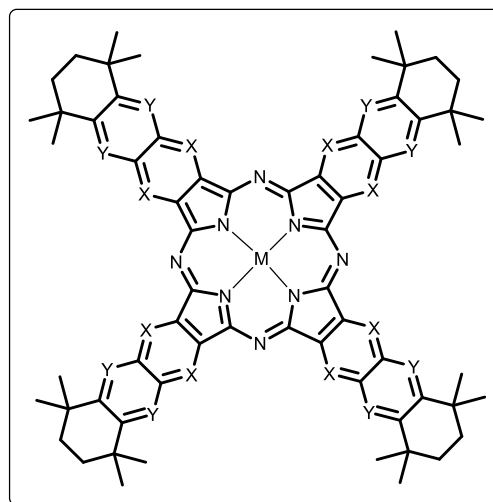


20 mg lithium (2.8 μmol , 8 eq) were dissolved in 3 mL *n*-octanol at 75 $^\circ\text{C}$ and were stirred for 30 min. When the solution became clear, it was cooled down to rt and 100 mg NpzDN^* (0.34 mmol, 1 eq) were added at once. The solution was stirred for 17 h in a preheated oil bath at 150 $^\circ\text{C}$. 40 mL MeOH were added as well as 1.5 mL H_3PO_4 .

The solution was macerated with 3 x 50 mL MeOH and 50 mL hexane, and the resulting green powder was finally dried in vacuum.

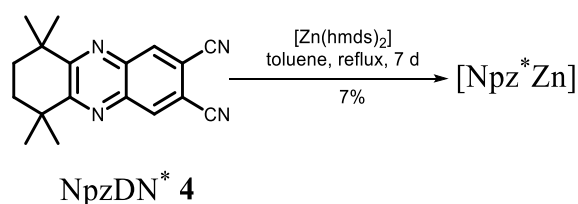
Yield: 25 mg, 21.5 μmol , 25%. - **$^1\text{H NMR}$** (Bromobenzene- d_5 , 300 MHz): δ = 9.45 (s, 8 H, Ar-CH), 2.32 (s, 16 H, $-\text{CH}_2$), 2.06 (s, 48 H, $-\text{CH}_3$), -1.15 (bs, 2 H, $-\text{NH}$) ppm. - **IR** (ATR, 400-4000 cm^{-1}): $\tilde{\nu}$ = 2920 (m), 2860 (m), 1446 (m), 1377 (w), 1357 (w), 1325 (s), 1253 (s), 1111 (s), 1074 (w), 1050 (w), 1009 (s), 953 (w), 888 (m), 813 (w), 752 (m), 712 (w), 669 (w), 616 (w) cm^{-1} . - **UV-Vis** (DCM): λ = 764 (s), 726 (sh), 683 (s), 342 (bs) nm. - **MS** (MALDI-ToF(+)): m/z = 1163.746 $[\text{M}]^+$ - Intensity of measured MALDI-ToF is low ($2 \cdot 10^3$). - **Elemental analysis** ($\text{C}_{72}\text{H}_{74}\text{N}_{16}$, $M = 1163.50$ g/mol): fnd. (cal.): C: 73.49% (74.33%), H: 6.48% (6.41%), N: 18.33% (19.26%).

Additional information: APCI-HRMS was attempted using the same sample as in MALDI-ToF but no product, only degraded products ($m/z \sim 290$) could be observed.



Nc^*H_2 : X = Y = CH with M = 2 H, Zn
 Npz^*H_2 : X = CH; Y = N with M = 2 H, Zn
 Nqn^*H_2 : X = N; Y = CH with M = Zn
 Nppz^*H_2 : X = Y = N with M = Zn

7.14.2 Synthesis of [Npz*Zn]

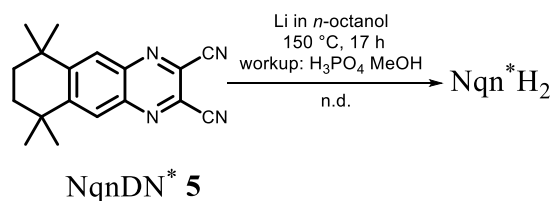


According to General Procedure 6 (p. 247). The purple powder was macerated with hexane and DEE. The product was obtained in the form of a purple solid.

Yield: 7%. - **¹H NMR** (Pyridine-*d*₅, 300 MHz): δ = 10.52 (bs, 8 H, Ar-CH), *2.20 (s, 16 H, -CH₂), *1.98 (s, 48 H, -CH₃) ppm. - **IR** (ATR, 400-4000 cm⁻¹): $\tilde{\nu}$ = 2958 (m), 2929 (m), 1450 (w), 1373 (w), 1330 (w), 1257 (m), 1120 (s), 1032 (s), 894 (m), 842 (m), 801 (m), 725 (w), 593 (s), 465 (w) cm⁻¹. - **UV-Vis** (DCM): λ = 754 (s), 717 (s), 674 (s), 361 (bs) nm. - **MS** (MALDI-ToF(+)): m/z = 1224.615 [M]⁺.

*could not be assigned for certain, caused by very low solubility, but low-field shifted protons are clearly visible.

Additional information: The reaction was carried out using pyridine/[Zn(acac)₂] \cdot 2H₂O in excess.

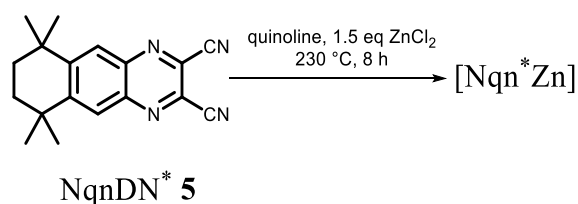
7.14.3 Synthesis of Nqn*H₂

According to General Procedure 4 (p. 235). 110 mg NqnDN* (379 μ mol, 1 eq) were dissolved in 2 mL Li/*n*-octanol solution and were stirred for 17 h in a preheated oil bath at 150 °C. The product was obtained in the form of a dark green powder. Besides the Nqn*H₂, a formation of the meso-substituted pyrazine derivatives was observed. In the obtained mass spectrum, a ~3:2:1 ratio of Nqn*H₂^{2xnoctyl}/Nqn*H₂^{noctyl}/Nqn*H₂ was observed.

Yield: n. d. - **UV-Vis** (DCM): λ = 729 (s), 706 (s), 674 (s), 414 (s), 353 (sh), 253 (s) nm. - **Fluorescence** (DCM, λ_{ex} = 350 nm): λ = 742 nm. - **MS** (MALDI-ToF(+)): Nqn*H₂^{2xnoctyl}: m/z = 1358.833 [M+H]⁺, (100%); Nqn*H₂^{noctyl}: m/z = 1262.735 [M+H]⁺, (50%); Nqn*H₂: m/z = 1165.691 [M+H]⁺, (20%).

Experimental Section

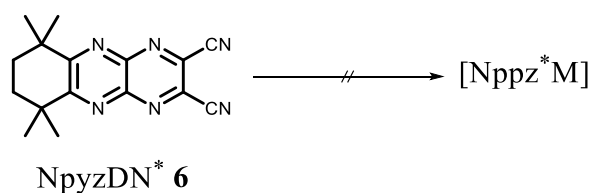
7.14.4 Synthesis of [Nqn*Zn]



71 mg NqnDN* (0.24 mmol, 4 eq) were weighed out together with 13 mg [ZnCl₂] (91.7 μmol, 1.5 eq). A spatula tip of ammonium heptamolybdate was added as well as 2 mL quinoline. The solution was heated in a preheated oil bath at 230 °C, for 8 h. A change in colour to green was observed. The solution was cooled down to rt. The black solution was poured into 50 mL ice/MeOH mixture. The black/greenish precipitate was filtered off and was washed with MeOH and water. The yellowish solution was discarded and the black powder was dried in air and finally in vacuum.

Yield: 21 mg, 17.1 μmol, 29%. - **¹H NMR** (C₆D₆/drop pyridine-*d*₅, 300 MHz): δ = 8.76 (s, 8 H, Ar-CH), 1.85 (s, 16 H, -CH₂), 1.69 (s, 48 H, -CH₃) ppm.* - **UV-Vis** (CB/drop pyridine): λ = 721 (s), 686 (s), 658 (s), 369 (s) nm. - **Fluorescence** (CB/drop pyridine, λ_{ex} = 350 nm): λ = 732 nm. - **MS** (APCI-MS(+)): *m/z* = 1226.670 [M+H]⁺. - **MS** (MALDI-ToF(+)): *m/z* = 1226.518 [M+H]⁺.

*sample includes quinoline residues.

7.14.5 Attempt to Synthesise [Nppz**M*]

Several established methods were attempted to yield [Nppz**M*], but no conversion to the respective Nppz*H₂ could be detected. Different attempts are summarized in the table below. [Nppz*Zn] could be observed in a reaction in quinoline, at 240 °C, after stirring the mixture overnight with [ZnCl₂]. The product was poured onto ice, filtered as described for other N_{x,y}-[Npz*Zn], see section 7.14.1 (p. 260).

Precursor	Solvent	Additive	Metal precursor	ΔT	time
NpyzDN*	Li/n-octanol			24 h	180 °C
NpyzDN*	n-octanol	dbu/ammonium heptamolybdate		12 h	180 °C
NpyzDN*	CNP		[ZnCl ₂]	12 h	240 °C
NpyzDN*		Urea	[Pb(OAc) ₂ ·H ₂ O]	10 min	290 °C
NpyzDN*	CNP	Urea	[Zn(acac) ₂ ·H ₂ O]	12 h	220 °C
NpyzDN*	Neat	ammonium heptamolybdate	[Mg(OAc) ₂]	10 min	280 °C
NpyzDN*	Neat	Urea	[ZnCl ₂] or [Zn(OAc) ₂]	20 min	280 °C

[Nppz*Zn]: Yield: n. d. - **UV-Vis** (DCM, raw product): λ = 712 (s) main absorption/Q-band observed. - **MS** (MALDI-ToF(+)): *m/z* = 1236.542 [M+H]⁺.

7.15 Azaphthalocyanine Complexes of Molybdenum and Tungsten

7.15.1 Synthesis of Precursors

7.15.1.1 Synthesis of [Mo(NMes)₂Cl₂·dme] [266]

Was carried out according to the procedure described in literature.

Yield: 75%. - ¹H NMR (C₆D₆, 300 MHz): δ = 6.56 (s, 4 H, Ar-CH), 3.42 (bs, 6 H, -CH₃), 3.24 (s, 4 H, -CH₂), 2.67 (s, 12 H, Mes-CH₃^{inner}), 2.02 (s, 6 H, Mes-CH₃^{outer}) ppm.

7.15.1.2 Synthesis of [W(NMes)₂Cl₂·dme] [266]

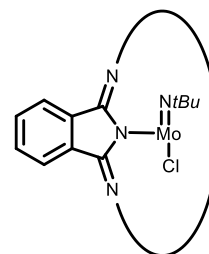
Was carried out according to the procedure described in literature.

Yield: 77%. - ¹H NMR (C₆D₆, 300 MHz): δ = 6.72 (s, 4 H, Ar-CH), 3.45 (bs, 6 H, -CH₃), 3.13 (s, 4 H, -CH₂), 2.74 (s, 12 H, Mes-CH₃^{inner}), 2.16 (s, 6 H, Mes-CH₃^{outer}) ppm.

7.15.2 Synthesis of [PcMo(NtBu)Cl] [69]

General Procedure 7: Synthesis of [PcM(NR)Cl] with M = Mo, W and R = *t*Bu or Mes.

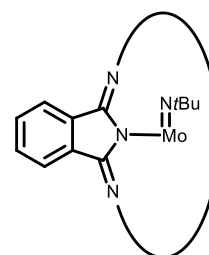
4 eq (aza)naphthalonitrile were dissolved with 1 eq [M(NR)₂Cl₂·solv] in 1 mL CNP/0.5 mmol (aza)naphthalonitrile in a preheated oil-bath at 215 °C, and were stirred for 1-2 h. The solution was cooled down to rt, was washed several times with hexane and then with MeCN (or DEE) until the washings became clear. The resulting brown-green powder was dried in vacuum.



Yield: 67%. - **UV-Vis** (DCM): λ = 715 (s), 646 (s), 360 (s), 293 (s) nm. - **MS** (MALDI-ToF(+)): *m/z* = 681.386 [M-Cl]⁺. - **Elemental analysis:** (C₃₆H₂₅Mo₁Cl₁N₉, 715.07 g/mol): *find.* (cal.): C: 58.24% (60.47%), H: 4.09% (3.52%), N: 15.42% (17.63%).

7.15.3 Attempt to Synthesise [PcMoNtBu] [25]

1 eq [PcMo(NtBu)Cl] was treated with 1 eq C₈K in THF. The reaction was stirred for 1 h while changing the colour to a deep purple. After filtration and washing with toluene, a pink solid was obtained. By oxidation in air, the product changed colour to green.

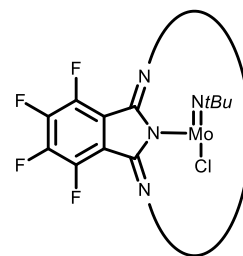


7.15.4 Synthesis of [Pc^FMo(*Nt*Bu)Cl]

According to General Procedure 7 (p. 264).

Yield: n.d. - **UV-Vis** (DCM): $\lambda = 723$ (s), 685 (sh), 352 (s), 298 (s) nm. -

MS (MALDI-ToF(+)): $m/z = 969.090$ [M-Cl]⁺; 913.065 [M-Cl, -*t*Bu]⁺.

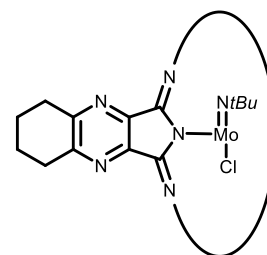


7.15.5 Attempt to Synthesise [Ppz^oMo(*Nt*Bu)Cl]

According to General Procedure 7 (p. 264).

Yield: n.d. - **MS** (MALDI-ToF(+)): $m/z = 906.270$ [M-Cl]⁺; 890.225

[M-Cl, -CH₃]⁺; 871.288 [M-Cl, 2x-CH₃]⁺; 850.290 [M-Cl, -*t*Bu]⁺.



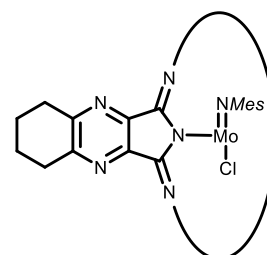
In UV-Vis spectroscopy, only a strong increasing band with decreasing wavelength was observed. The product appears insoluble in common organic solvents.

7.15.6 Attempt to Synthesise [Ppz^oMo(NMes)Cl]

According to General Procedure 7 (p. 264).

Yield: n.d. - **MS** (MALDI-ToF(+)): $m/z = 967.297$ [M+H]⁺.

In UV-Vis spectroscopy, a strong increasing band with decreasing wavelength was observed. The product appears insoluble in common organic solvents.

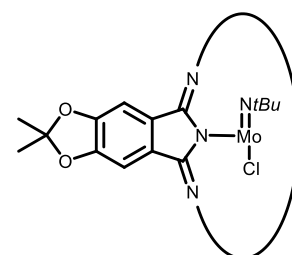


7.15.7 Synthesis of [Pc^{OAc}Mo(*Nt*Bu)Cl]

According to General Procedure 7 (p. 264).

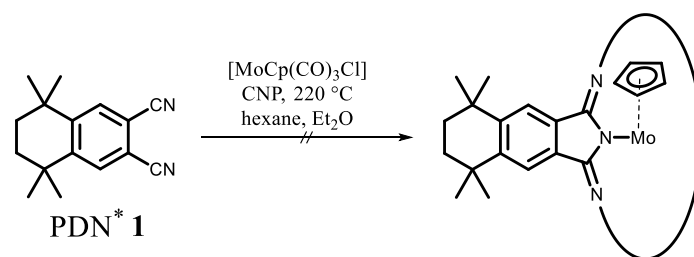
Yield: n.d. - **UV-Vis** (DCM): $\lambda = 714$ (s), 644 (s), 476 (s), 390 (s), 374 (s), 296 (s) nm. - **MS** (MALDI-ToF(+)): $m/z = 969.314$ [M-Cl]⁺;

919.507 [M-Cl, -*t*Bu]⁺.



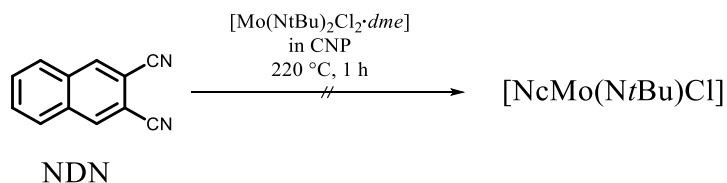
Experimental Section

7.15.8 Attempt to Synthesis [Pc*Mo(Cp)Cl]



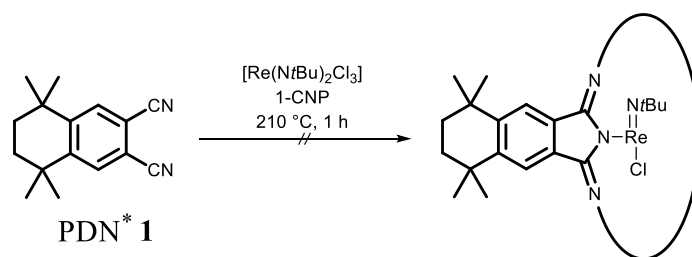
4 eq PDN* were dissolved in CNP and stirred in a preheated oil-bath for 1 h. Gas evolved. Neither in UV-Vis spectroscopy nor in MALDI-ToF spectrometry could traces of Pc be observed.

7.15.9 Attempt to Synthesis [NcMo(NtBu)Cl]



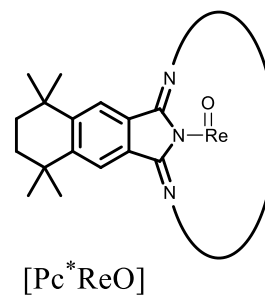
According to General Procedure 7 (p. 264): 4 eq of NDN and 1 eq of [Mo(NtBu)₂Cl₂·dme] were dissolved in 2 mL CNP/100 mg NDN at 220 °C and were stirred for 1 h. A brown powder was obtained. The formation of the product could be observed in MALDI-ToF, but it appears to be very insoluble, so that no clear Q-band could be identified in UV-Vis spectroscopy. The product was not analysed any further.

Yield: 31%. - **MS** (MALDI-ToF(+)): $m/z = 881.154$ [M-Cl]⁺; 824.070 [M-Cl, -tBu]⁺ (100%).

7.15.10 Attempt to Synthesise [$\text{Pc}^*\text{Re}(\text{NtBu})\text{Cl}$]

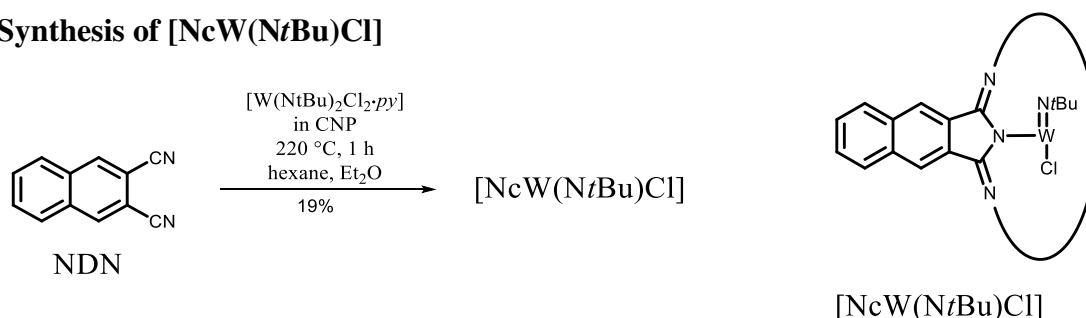
250 mg $\text{Pc}^* \mathbf{1}$ (1.05 mmol, 4 eq) were mixed with 125 mg $[\text{Re}(\text{NtBu})_2\text{Cl}_3]$ (0.29 mmol, 1.1 eq), dissolved in 1-CNP , and were stirred in a preheated oil-bath at $210\text{ }^\circ\text{C}$ for 1 h. After cooling down to rt, to the brown solution 20 mL hexane was added, the solution was macerated first with hexane, and then with DEE until it became clear. The product was obtained in the form of a black powder. As product, $[\text{Pc}^*\text{ReO}]$ was obtained.

MS (MALDI-ToF(+)): $m/z = 1155.559$ $[\text{M}]^+$.



7.16 Azanaphthalocyanine Complexes of Molybdenum and Tungsten $N_{x,y}$ -[Nc**M*(NR)Cl] with R = *t*Bu, Mes, and M = Mo, W

7.16.1 Synthesis of [NcW(N*t*Bu)Cl]



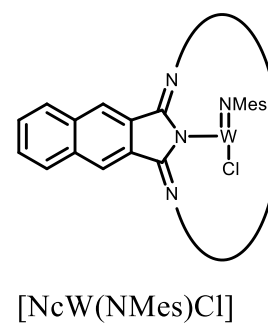
According to General Procedure 7 (p. 264).

Yield: 19%. - **IR** (ATR, 400-4000 cm^{-1}): $\tilde{\nu}$ = 3053 (w), 2946 (w), 2891 (w), 2802 (w), 2708 (w), 2598 (w), 2500 (w), 2382 (w), 2349 (w), 2324 (m), 2297 (w), 2166 (w), 1666 (w), 1636 (w), 1591 (m), 1510 (w), 1472 (w), 1443 (w), 1400 (m), 1356 (m), 1335 (m), 1260 (m), 1194 (w), 1078 (s, br), 1020 (m), 887 (w), 802 (s), 752 (s), 712 (m), 675 (m), 469 (s), 449 (m) cm^{-1} . - **UV-Vis** (DCM): λ = 846 (s), 750 (s), 361 (s) nm. - **MS** (MALDI-ToF(+)): m/z = 967.154 [M-Cl]⁺, 911.087 [M-Cl, -*t*Bu]⁺. - **Elemental analysis** (C₅₂H₃₃W₁Cl₁N₉, 1003.19 g/mol): *find.* (cal.): C: 41.47 (62.26), H: 3.65 (3.32), N: 9.03 (12.57) S: 0.80 (0.00).

7.16.2 Synthesis of [NcW(NMes)Cl]

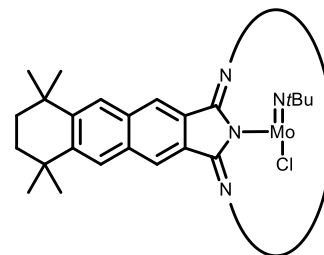
According to General Procedure 7 (p. 264).

Yield: 64%. - **IR** (ATR, 400-4000 cm^{-1}): $\tilde{\nu}$ = 2976 (w), 2914 (w), 2382 (m), 2348 (m), 2324 (m), 1981 (m), 1660 (m), 1606 (m), 1568 (m), 1315 (m), 1256 (w), 1084 (m), 974 (m), 811 (s), 756 (s), 672 (m), 617 (w), 583 (w), 472 (s), 445 (s) cm^{-1} . - **UV-Vis** (DCM): λ = 860 (s), 766 (sh), 354 (s), 341 (s) nm. - **MS** (MALDI-ToF(+)): m/z = 1029.182 [M-Cl]⁺. - **Elemental analysis** (C₅₇H₃₅W₁Cl₁N₉, 1065.26 g/mol): *find.* (cal.): C: 48.99 (64.27), H: 3.86 (3.31), N: 7.69 (11.83), S: 0.11 (0.00).



7.16.3 Synthesis of $N_{0,0}$ -[Nc*Mo(NtBu)Cl]

According to General Procedure 7 (p. 264). The product was obtained in form of a black solid.



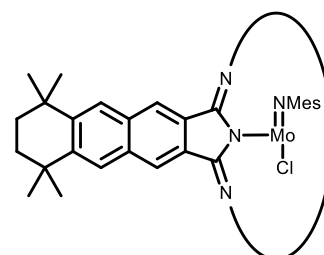
Yield: 17%. - **EPR** (Q-band, 2 M in toluene, 100 K, 34.5225 GHz):

$g = 1.9866, 1.9772, 1.9721$. $A = 3.2, 2.7, 7.0$. Line width: 2.5, 2.0, 2.1 mT. - **EPR** (Q-band, 2 M in toluene, rt, 34.523 GHz): $g_{\text{iso}} = 1.9788$, $a_{\text{iso}} = 4.63$ mT. - **IR** (ATR, 400-4000 cm^{-1}): $\tilde{\nu} = 2954$ (m), 2921 (m), 2859 (m), 1460 (m), 1360 (m), 1330 (s), 1291 (m), 1230 (w), 1212 (w), 1181 (w), 1142 (w), 1104 (m), 1079 (s), 1026 (m), 930 (w), 907 (w), 847 (w), 799 (w), 767 (w), 724 (w), 467 (m) cm^{-1} . - **UV-Vis** (DCB): $\lambda = 869$ (s), 779 (sh), 382 (s), 295 (s) nm. - **MS** (MALDI-ToF(+)): $m/z = 1321.441$ $[\text{M}-\text{Cl}]^+$. - **MS** (FD): $m/z = 1321.6357$ $[\text{M}]^+$, cal. for $\text{C}_{84}\text{H}_{89}\text{Mo}_1\text{N}_9$: 1321.6295. - higher, negligible aberrations in LIFDI measurements are caused by the not optimized internal standard used in measurements. - **Elemental analysis** ($\text{C}_{84}\text{H}_{89}\text{Cl}_1\text{Mo}_1\text{N}_9$, $M = 1356.11$ g/mol): fnd. (cal.): C: 68.38% (74.40%), H: 6.42% (6.62%), N: 8.39% (9.30%). - low value of carbon is caused by incomplete combustion, because MoC or WC compounds are formed.

Additional information: An aberration of collinearity of g and a observed. The EULER angle of 362° is negligible.

7.16.4 Synthesis of $N_{0,0}$ -[Nc*Mo(NMes)Cl]

According to General Procedure 7 (p. 264). The product was washed with hexane and DEE. The product was obtained in the form of a light grey powder.

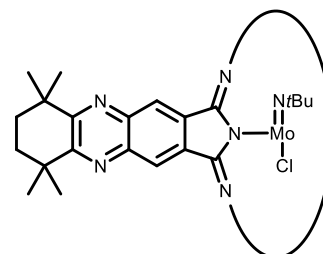


Yield: 52%. - **EPR** (Q-band, 2 M in toluene, 100 K, 34.5252 GHz): $N_{0,0}$ -[Nc*Mo(NMes)Cl]
 $g = 1.9833, 1.9830, 1.9796$. $A = 2.0, 3.5, 7.1$. Line width: 4.8, 1.4, 3.4 mT. - **EPR** (Q-band, 2 M in toluene, rt, 34.5236 GHz): $g_{\text{iso}} = 1.9779$, $a_{\text{iso}} = 4.58$ mT. - **IR** (ATR, 400-4000 cm^{-1}): $\tilde{\nu} = 2956$ (m), 2923 (m), 2860 (m), 1603 (w), 1460 (m), 1408 (w), 1358 (s), 1332 (s), 1317 (m), 1294 (w), 1182 (w), 1105 (s), 1080 (s), 1051 (w), 1027 (w), 908 (m), 849 (w), 766 (w), 725 (w), 467 (m) cm^{-1} . - **UV-Vis** (DCB): $\lambda = 897$ (s), 807 (sh), 382 (s), 295 (s) nm. - **MS** (MALDI-ToF(+)): $m/z = 1383.556$ $[\text{M}-\text{Cl}]^+$. - **MS** (FD): $m/z = 1383.6391$ $[\text{M}]^+$, cal. for $\text{C}_{89}\text{H}_{91}\text{Mo}_1\text{N}_9$: 1383.6452. - higher, negligible aberrations in LIFDI measurements, are caused by the not optimized internal standard used in measurements. - **Elemental analysis** ($\text{C}_{89}\text{H}_{91}\text{Cl}_1\text{Mo}_1\text{N}_9$, $M = 1418.18$ g/mol): fnd. (cal.): C: 70.90% (75.38%), H: 6.45% (6.47%), N: 7.70% (8.89%).

Additional information: New structural information was obtained from EPR spectroscopy. The splitting is not caused by the chlorine atom rather than by the axial nitrogen atom. The crystal structures of [PcMo(*t*Bu)Cl] ^[69], as well as the elemental analysis, verifies the axial chlorine atom. Here, for the first time FD measurements could resolve the structure with a chlorine atom in a high resolution. In addition, Q-band EPR spectroscopy measurements were carried out. The structure of both compounds was verified: a C_{2v} symmetry in case of the N_{x,y}-[Nc*Mo(NMes)Cl] and a lower symmetry for the N_{x,y}-[Nc*Mo(N*t*Bu)Cl] complexes. The axial/rhombic splitting of *g*-tenors is clearly visible. The symmetry axis is the chlorine - central metal center – axial substituent vector.

7.16.5 Synthesis of N_{0,8}-[Nc*Mo(N*t*Bu)Cl]

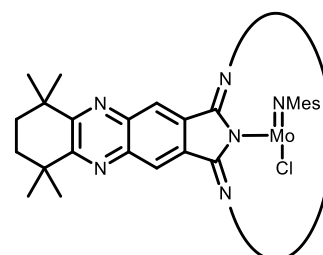
According to General Procedure 7 (p. 264). The product was washed with hexane and MeCN. The product was obtained in the form of a light-grey powder.



Yield: <2%. - **IR** (ATR, 400-4000 cm⁻¹): $\tilde{\nu}$ = 2963 (m), 1258 (m), 1008 (s), 862 (w), 789 (s), 698 (w), 665 (w) cm⁻¹. - **UV-Vis** (DCB): λ = 812 (s), 732 (sh), 374 (s), 335 (s), 292 (s) nm. - **MS** (MALDI-ToF(+)): m/z = 1329.480 [M-Cl]⁺.

7.16.6 Synthesis of N_{0,8}-[Nc*Mo(NMes)Cl]

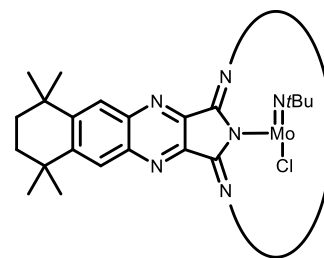
According to General Procedure 7 (p. 264). The product was washed with hexane and Et₂O. The product was obtained in the form of a brown powder.



Yield: ~5%. - **IR** (ATR, 400-4000 cm⁻¹): $\tilde{\nu}$ = 2960 (m), 2925 (m), 2862 (m), 1600 (m), 1553 (w), 1518 (w), 1452 (m), 1408 (w), 1378 (w), 1360 (w), 1329 (w), 1298 (w), 1257 (s), 1116 (s), 1097 (s), 1074 (s), 1053 (s), 1017 (s), 851 (w), 794 (s), 727 (m), 697 (m) cm⁻¹. - **UV-Vis** (DCB): λ = 834 (s) nm.* - **MS** (MALDI-ToF(+)): m/z = 1391.661 [M-Cl]⁺. *strong B-band was found in DCB.

7.16.7 Synthesis of $N_{8,0}$ -[Nc*Mo(NtBu)Cl]

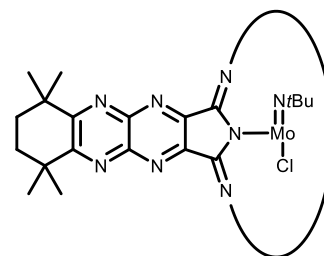
According to General Procedure 7 (p. 264). The product was washed with hexane and Et₂O. The product was obtained in the form of a dark green powder.



Yield: n.d. - **IR** (ATR, 400-4000 cm⁻¹): $\tilde{\nu}$ = 2961 (s), 2894 (s), 2804 (w), 1603 (m), 1560 (m), 1507 (m), 1468 (s), 1402 (m), 1366 (m), 1259 (s), 1211 (m), 1179 (s), 1145 (s), 1092 (m), 1052 (m), 1023 (m), 959 (m), 888 (m), 797 (s), 766 (m), 719 (m), 661 (w), 541 (w), 451 (w) cm⁻¹. - **UV-Vis** (DCM): λ = 761 (s), 691 (sh), 352 (s), 294 (s) nm. - **MS** (MALDI-ToF(+)): m/z = 1329.571 [M-Cl]⁺, 1275.571 [M-Cl, -tBu]⁺. - **Elemental analysis** (C₇₆H₈₁Cl₁Mo₁N₁₇, M = 1364.01 g/mol): *find.* (*cal.*): C: 63.80 (66.92), H: 5.73 (5.99), N: 6.35 (17.46).

7.16.8 Synthesis of $N_{8,8}$ -[Nc*Mo(NtBu)Cl]

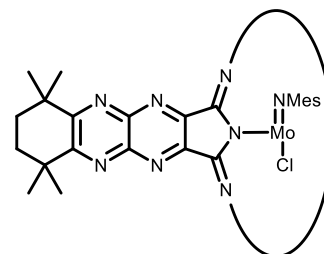
According to General Procedure 7 (p. 264). The product was washed with hexane and MeCN. The product was obtained in the form of a green solid.



Yield: 23%. - **IR** (ATR, 400-4000 cm⁻¹): $\tilde{\nu}$ = 2962 (m), 2930 (m), 2892 (w), 2865 (m), 1612 (w), 1535 (w), 1456 (m), 1426 (m), 1361 (w), 1317 (w), 1242 (s), 1207 (s), 1118 (s), 1091 (s), 1056 (s), 927 (w), 723 (s), 628 (s), 592 (w), 505 (s), 451 (w), 434 (m) cm⁻¹. - **UV-Vis** (DCM): λ = 729 (s), 673 (sh), 374 (s), 294 (s) nm. - **MS** (MALDI-ToF(+)): m/z = 1336.824 [M-Cl]⁺. - **Elemental analysis** (C₆₈H₇₃Cl₁Mo₁N₂₅, M = 1371.92 g/mol): *find.* (*cal.*): C: 57.15% (59.53%), H: 5.29% (5.36%), N: 23.28% (25.52%).

7.16.9 Attempt to Synthesise $N_{8,8}$ -[Nc*Mo(NMes)Cl]

According to General Procedure 7 (p. 264). The product was washed with hexane and Et₂O. The product was obtained in the form of a green powder. Not enough substance for full analysis was obtained.



$N_{8,8}$ -[Nc*Mo(NMes)Cl]

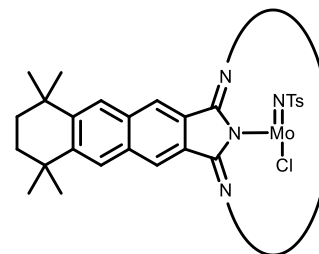
Yield: n.d. - **IR** (ATR, 400-4000 cm⁻¹): $\tilde{\nu}$ = 2958 (m), 2927 (m), 2864 (m), 1599 (w), 1568 (w), 1532 (w), 1505 (w), 1454 (m), 1426 (m), 1383 (w), 1360 (w), 1319 (w), 1243 (m), 1208 (w),

Experimental Section

1163 (m), 1117 (s), 1056 (m), 1018 (m), 725 (w), 627 (w), 505 (w) cm^{-1} . - **MS** (MALDI-ToF(+)): $m/z = 1391.537$ $[\text{M}-\text{Cl}]^+$.

7.16.10 Attempt to Synthesise $\text{N}_{0,0}$ - $[\text{Nc}^*\text{Mo}(\text{NTs})\text{Cl}]$

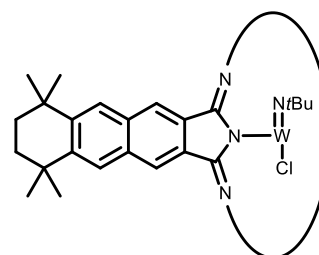
According to General Procedure 7 (p. 264). A black powder was obtained. The product could neither be identified in UV-Vis spectroscopy nor in MALDI-ToF.



$\text{N}_{0,0}$ - $[\text{Nc}^*\text{Mo}(\text{NTs})\text{Cl}]$

7.16.11 Synthesis of $\text{N}_{0,0}$ - $[\text{Nc}^*\text{W}(\text{NtBu})\text{Cl}]$

According to General Procedure 7 (p. 264). The product was washed with hexane and DEE. The product was obtained in form of a brown solid.

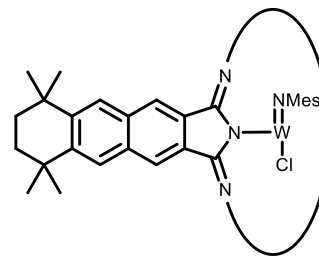


Yield: 37%. - **IR** (ATR, 400-4000 cm^{-1}): $\tilde{\nu} = 2956$ (m), 2892 (m), 2802 (m), 1460 (m), 1366 (w), 1331 (m), 1295 (w), 1261 (m), 1213 (w), 1105 (s), 1080 (s), 1051 (w), 1026 (m), 908 (w), 743 (w), 725 (w), 468 (m), 449 (w) cm^{-1} . - **UV-Vis** (DCM): $\lambda = 871$ (s), 769 (sh), 379 (s), 361 (s), 292 (s) nm. - **MS** (MALDI-ToF(+)): $m/z = 1407.765$ $[\text{M}-\text{Cl}]^+$. - **MS** (FD): $m/z = 1442.6336$ $[\text{M}]^+$, cal. for $\text{C}_{84}\text{H}_{89}\text{Cl}_1\text{W}_1\text{N}_9$: 1442.6339. - **MS** (FD): $m/z = 1407.6805$ $[\text{M}-\text{Cl}]^+$, cal. for $\text{C}_{84}\text{H}_{89}\text{W}_1\text{N}_9$: 1407.6750. - **Elemental analysis** ($\text{C}_{84}\text{H}_{89}\text{Cl}_1\text{W}_1\text{N}_9$, $M = 1443.99$ g/mol): **find.** (cal.): C: 61.55% (69.87%), H: 6.19% (6.21%), N: 8.43% (8.36%). - low value of carbon is caused by incomplete combustion, because WN or WC compounds are formed. High variations of carbon values in different measurements, while hydrogen and nitrogen values are similar.

Additional information: EPR X-band was measured.

7.16.12 Synthesis of $\text{N}_{0,0}$ - $[\text{Nc}^*\text{W}(\text{NMes})\text{Cl}]$

According to General Procedure 7 (p. 264). The product was washed with hexane and DEE. The product was obtained in the form of a light-grey powder.

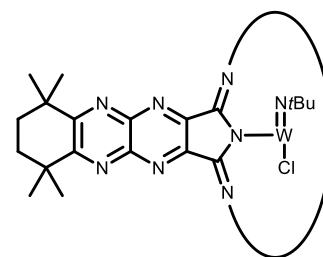


Yield: >82%. - **IR** (ATR, 400-4000 cm^{-1}): $\tilde{\nu} = 2957$ (s), 2924 (s), 2860 (s), 1602 (s), 1563 (s), 1458 (m), 1407 (m), 1382 (m), 1359 (m), 1334 (m), 1317 (m),

1295 (m), 1257 (w), 1211 (w), 1198 (w), 1182 (w), 1145 (w), 1106 (s), 1082 (s), 1048 (m), 1026 (w), 968 (w), 911 (w), 850 (w), 793 (s), 766 (s), 731 (w), 664 (w), 468 (m), 448 (m) cm^{-1} . - **UV-Vis** (DCM): $\lambda = 881$ (s), 784 (s), 360 (s) nm. - **MS** (MALDI-ToF(+)): $m/z = 1469.597$ $[\text{M}-\text{Cl}]^+$. - **MS** (FD): $m/z = 1469.6977$ $[\text{M}-\text{Cl}]^+$, cal. for $\text{C}_{89}\text{H}_{91}\text{W}_1\text{N}_9$: 1469.6907. - **Elemental analysis** ($\text{C}_{89}\text{H}_{91}\text{Cl}_1\text{W}_1\text{N}_{17}$, $M = 1506.06$ g/mol): *find.* (*cal.*): C: 52.29 (79.98), H: 5.53 (6.09), N: 12.47 (8.37), S: 0.14 (0.00).

7.16.13 Synthesis of $\text{N}_{8,8}\text{-}[\text{Nc}^*\text{W}(\text{NtBu})\text{Cl}]$

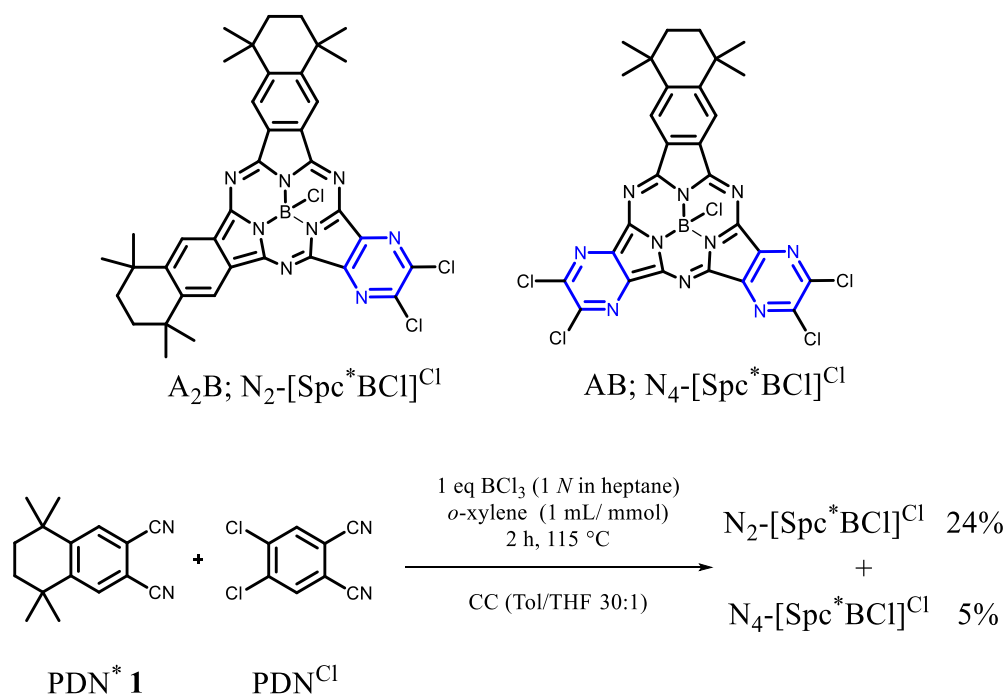
According to General Procedure 7 (p. 264). The product was washed with hexane and DEE. The product was obtained in form of a dark green solid.



Yield: 56%. - **IR** (ATR, 400-4000 cm^{-1}): $\tilde{\nu} = 2963$ (m), 2930 (m), $\text{N}_{8,8}\text{-}[\text{Nc}^*\text{W}(\text{NtBu})\text{Cl}]$ 2866 (m), 1609 (w), 1575 (w), 1536 (w), 1518 (w), 1455 (m), 1432 (m), 1401 (m), 1380 (m), 1361 (w), 1244 (s), 1201 (m), 1165 (m), 1117 (s), 1057 (m), 1019 (m), 795 (w), 768 (s), 724 (m), 663 (w), 507 (s) cm^{-1} . - **UV-Vis** (DCM): $\lambda = 717$ (s), 658 (s), 364 (s), 293 (s) nm. - **MS** (MALDI-ToF(+)): $m/z = 1425.571$ $[\text{M}-\text{Cl}]^+$. - **Elemental analysis** ($\text{C}_{68}\text{H}_{73}\text{Cl}_1\text{W}_1\text{N}_{25}$, $M = 1459.80$ g/mol): *find.* (*cal.*): C: 54.45% (55.95%), H: 4.94% (5.04%), N: 18.16% (23.99%).

7.17 Functionalised Azasubphthalocyanines

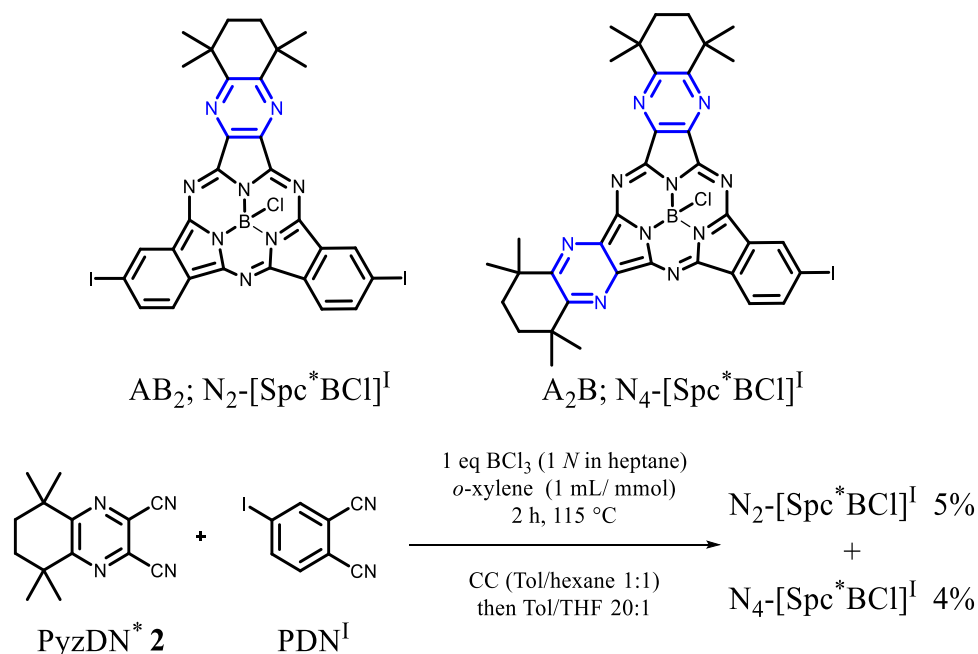
7.17.1 Synthesis of N_x -[Spc*BCl]^{Cl} [13]



According to General Procedure 3 (p. 228), using PDN^*/PDN^{Cl} in a 1:1 ratio.

$A_2B; N_2-[Spc^*BCl]$: Yield: 24%. - ¹H NMR (CD₂Cl₂, 300 MHz): δ = 8.89 (s, 2 H, Ar-CH), 8.76 (s, 2 H, Ar-CH), 2.23-1.80 (m, 12 H, -CH₂), 1.64 (s, 9 H, -CH₃), 1.44 (s, 9 H, -CH₃), 1.40 (s, 9 H, -CH₃) ppm. - according to master thesis. - **X-ray**: Crystals could be obtained out in the NMR tube from CD₂Cl₂. - The analysis is in accordance to literature values.

$AB_2; N_4-[Spc^*BCl]$: Yield: 5%. - The analysis is in accordance to literature values.

7.17.2 Synthesis of N_x -[Spc*BCl]^I

According to General Procedure 3 (p. 228), using PzDN*/PDN^I in a 1:1 ratio.

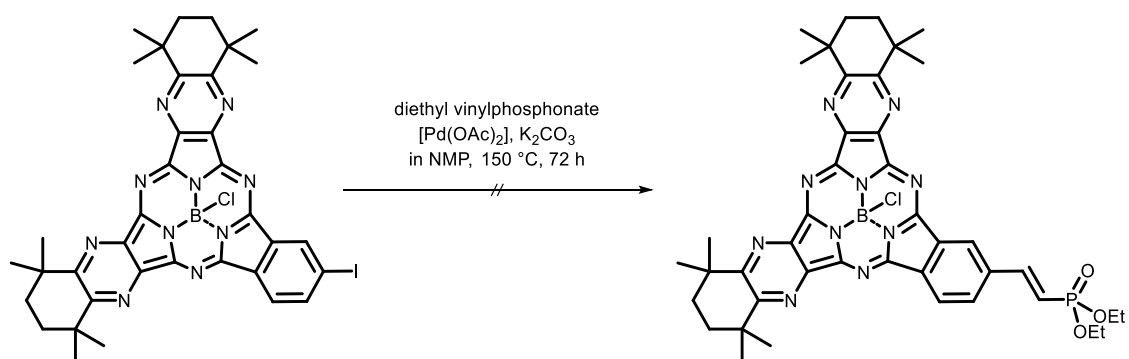
AB₂; N₂-[Spc*BCl]^I: Yield: 5%. - ¹H NMR (CDCl₃, 300 MHz): δ = 9.36 (s, 1 H, Ar-CH), 9.35 (s, 1 H, Ar-CH), 8.73 (d, 1 H, ³J_{H-H} = 8.3 Hz, Ar-CH), 8.59 (d, 1 H, ³J_{H-H} = 8.2 Hz, Ar-CH), 8.27 (dd, 2 H, ³J_{H-H} = 8.3 Hz, ⁴J_{H-H} = 3.1 Hz, Ar-CH), 2.96-1.92 (m, 4 H, -CH₂), 1.75 (s, 6 H, -CH₃), 1.48 (s, 6 H, -CH₃) ppm. - UV-Vis (DCM): λ = 561 (s), 515 (sh), 273 (s), 233 (s) nm. - MS (APCI-HRMS): m/z = 794.9914 [M+H]⁺, cal. for C₃₀H₂₂B₁Cl₁I₂N₈+H₁: 794.9916.

A₂B; N₄-[Spc*BCl]^I: Yield: 4%. - ¹H NMR (CDCl₃, 300 MHz): δ = 9.43 (s, 1 H, Ar-CH), 8.76 (d, ³J_{H-H} = 8.3 Hz, 1 H, Ar-CH), 8.38 (d, ³J_{H-H} = 8.3 Hz, 1 H, Ar-CH), 2.07-2.00 (m, 8 H, -CH₂), 1.77 (s, 6 H, -CH₃), 1.74 (s, 6 H, -CH₃), 1.51 (s, 12 H, -CH₃) ppm. - ¹³C NMR (CD₂Cl₂, 75 MHz): δ = 163.6, 163.3, 151.3*, 150.2*, 147.5*, 147.3*, 145.9*, 140.5, 133.3*, 132.6, 131.0*, 129.4*, 124.5, 97.9, 39.6, 34.4, 34.4, 31.1, 31.0, 30.3 ppm. - not all quaternary carbons could be detected. - UV-Vis (DCM): λ = 548 (s), 505 (s), 294 (s), 242 (s) nm. - MS (APCI-HRMS): m/z = 781.1948 [M+H]⁺, cal. for C₃₆H₃₅B₁Cl₁I₁N₁₀+H₁: 781.1951.

*could not be assigned for certain, because of low intensity of signals.

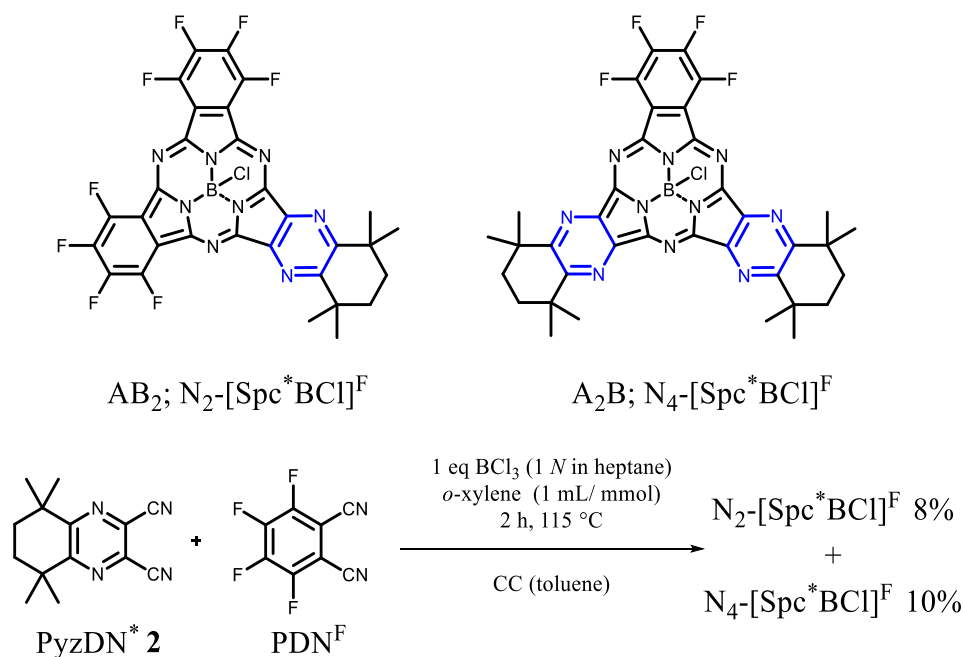
Experimental Section

7.17.3 Attempt of N_4 -[Spc*BCI]^{vPA}



According to literature described HECK coupling conditions. The reaction was monitored by TLC (DCM/THF 4:1). A conversion could be observed, but during purification, a change in colour of the subphthalocyanine from purple to light green could be observed.

7.17.4 Synthesis of N_x -[Spc*BCI]^F



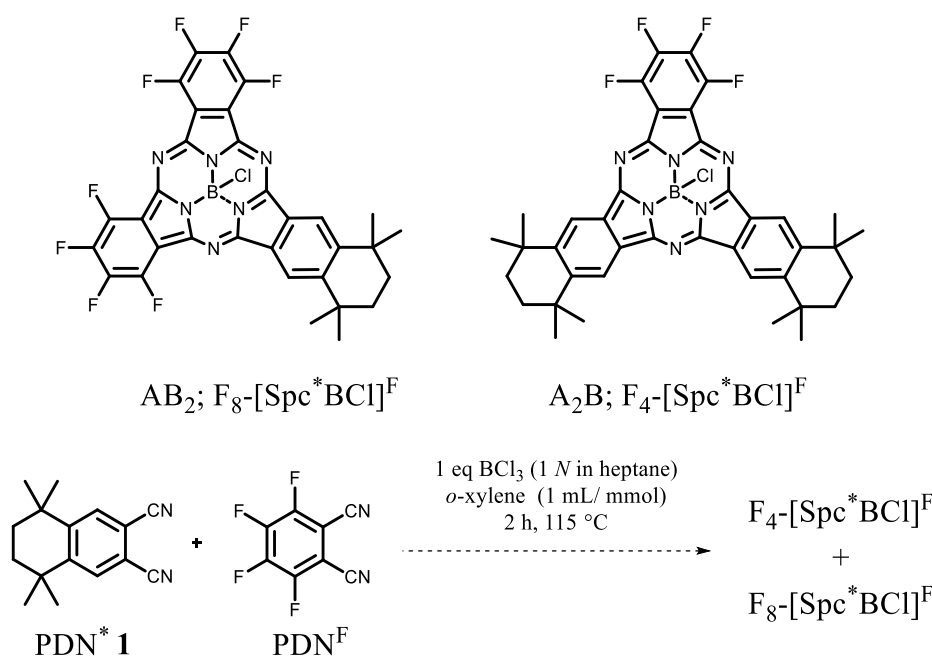
According to General Procedure 3 (p. 228), using PyzDN^{*}/PDN^F in a 1:1 ratio. The products were separated by CC (toluene).

A₂B; F₈/N₂-[Spc*BCI]^F: Yield: 8%. - R_f (toluene) = 0.27. - ¹H NMR (toluene-*d*₈/drop CD₂Cl₂, 300 MHz): δ = 2.10-1.96 (m, 4 H, -CH₂), 1.74 (s, 8 H, -CH₃), 1.50 (s, 8 H, -CH₃) ppm. - ¹³C NMR (toluene-*d*₈/drop CD₂Cl₂, 75 MHz): δ = 39.9, 34.4, 31.1, 30.5 ppm. - not all carbons could be detected. - UV-Vis (DCM): λ = 550 (s), 503 (sh), 296 (s) nm. - Fluorescence (DCM,

$\lambda_{ex} = 350$ nm): $\lambda = 561$ nm. - **MS** (APCI-HRMS(+)): $m/z = 687.1218$ $[M+H]^+$, cal. for $C_{30}H_{16}B_1Cl_1F_8N_8+H_1$: 687.1230.

AB₂; F₄/N₄-[Spc*BCl]^F: **Yield**: 10%. - **R_f** (toluene) = 0.61. - **¹H NMR** (toluene-*d*₈/CD₂Cl₂, 300 MHz): $\delta = 2.16$ -1.97 (m, 8 H, -CH₂), 1.79 (s, 8 H, -CH₃), 1.76 (s, 8 H, -CH₃), 1.54 (s, 8 H, -CH₃), 1.53 (s, 8 H, -CH₃) ppm. - **¹³C NMR** (toluene-*d*₈/drop CD₂Cl₂, 75 MHz): $\delta = 164.2$, 39.8, 34.5, 34.4, 31.2, 30.5 ppm. - not all carbons could be detected. - **UV-Vis** (DCM): $\lambda = 563$ (s), 513 (sh), 296 (s) nm. - **Fluorescence** (DCM, $\lambda_{ex} = 350$ nm): $\lambda = 578$ nm. - **MS** (APCI-HRMS(+)): $m/z = 727.2593$ $[M+H]^+$, cal. for $C_{36}H_{32}B_1Cl_1F_4N_{10}+H_1$: 727.2608.

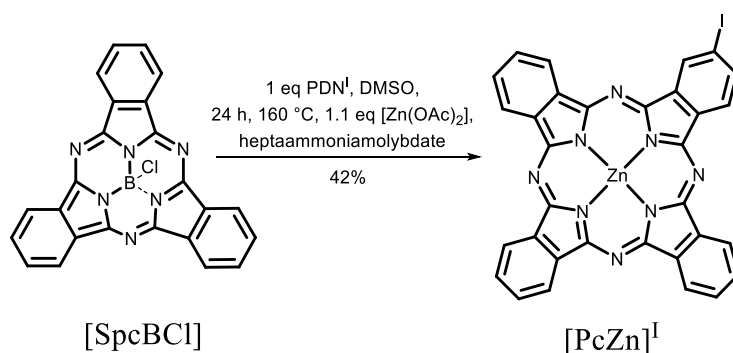
7.17.5 Attempt to Synthesise F_x-[Spc*BCl]^F



According to General Procedure 3 (p. 228), using PDN^{*}/PDN^F in a 1:1 ratio. The products were not obtained in sufficient purity after by CC (EA/PE 3:1). As main product, [Spc*BCl] was obtained, which could be separated. Further attempts might be carried out, varying the ratio of PDN^{*}/PDN^F.

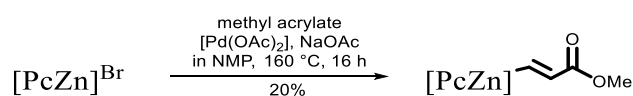
A₂B; F₄-[Spc*BCl]: **MS** (APCI-HRMS(+)): $m/z = 723.2781$ $[M+H]^+$, cal. for $C_{40}H_{36}B_1Cl_1F_4N_6+H_1$: 723.2799.

AB₂; F₈-[Spc*BCl]: **MS** (APCI-HRMS(+)): $m/z = 685.1306$ $[M+H]^+$, cal. for $C_{32}H_{18}B_1Cl_1F_8N_6+H_1$: 685.1325.

7.18.2 Synthesis of [PcZn]^I

According to the procedure described in 7.18.1.

Yield: 42%. - **¹H NMR** (Pyridine-*d*₅, 300 MHz): δ = 8.17–8.21 (m, 6 H, Ar-CH), 8.49 (dd, 1 H, ⁴*J*_{H-H} = 1.2, ³*J*_{H-H} = 7.9 Hz, Ar-CH), 9.12 (d, 1 H, ³*J*_{H-H} = 7.8 Hz, Ar-CH), 9.57–9.60 (m, 6 H, Ar-CH), 9.82 (d, 1 H, ⁴*J*_{H-H} = 1.2 Hz, Ar-CH) ppm. - **IR** (ATR, 400-4000 cm⁻¹): $\tilde{\nu}$ = 1595 (w), 1482 (m), 1408 (w), 1330 (s), 1283 (m), 1162 (m), 1115 (m), 1089 (s), 1061 (m), 1034 (w), 946 (w), 888 (s), 819 (w), 771 (m), 752 (s), 718 (vs), 637 (w), 572 (w), 526 (w), 500 (m), 431 (m) cm⁻¹. - **UV-Vis** (DCM): λ = 671 (s), 607 (s), 343 (s), 285 (s), 236 (s) nm. - **MS** (MALDI-ToF(+), DCM/MeCN): *m/z* = 701.969 [M]⁺. - **MS** (APCI-HRMS(+)): *m/z* = 702.9828 [M+H]⁺, cal. for C₃₂H₁₅I₁N₈Zn₁+H₁: 702.9829 (100% Peak); 577.2 [M-I]⁺. - **MS** (APCI-HRMS(-)): *m/z* = 701.9759 [M-H]⁻, cal. for C₃₂H₁₅I₁N₈Zn₁-H₁: 701.9759. - **Elemental analysis:** (C₃₂H₁₅I₁N₈Zn₁, M = 703.81 g/mol): *find.* (cal.) C: 56.69 (54.61), H: 2.43 (2.15), N: 16.21 (15.92).

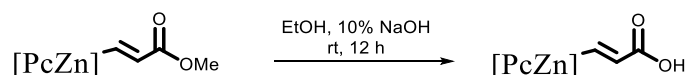
7.18.3 Synthesis of [PcZn]^{vCA}

According to literature described procedure.^[13]

Yield: 20%. - **¹H NMR** (DMSO-*d*₆, 300 MHz): δ = 9.23 (m, 8 H, Ar-CH), 8.19 (m, 7 H, Ar-CH), 3.16 (d, 3 H, -OCH₃)* ppm. - **IR** (ATR, 400-4000 cm⁻¹): $\tilde{\nu}$ = 2826 (w), 1639 (w), 1607 (w), 1484 (w), 1454 (w), 1406 (w), 1327 (m), 1282 (w), 1163 (w), 1112 (m), 1083 (m), 1056 (w), 1023 (m), 976 (m), 885 (w), 803 (m), 770 (s), 751 (w), 720 (w), 633 (w), 570 (w), 502 (w) cm⁻¹. - **UV-Vis** (DCM or DMSO): λ = 673 (s), 608 (s), 346 (s) nm. - **MS** (MALDI-ToF(+), MeCN): *m/z* = 660.658 [M+H]⁺.

*could not be assigned for certain. Only low-field shifted protons were detected.

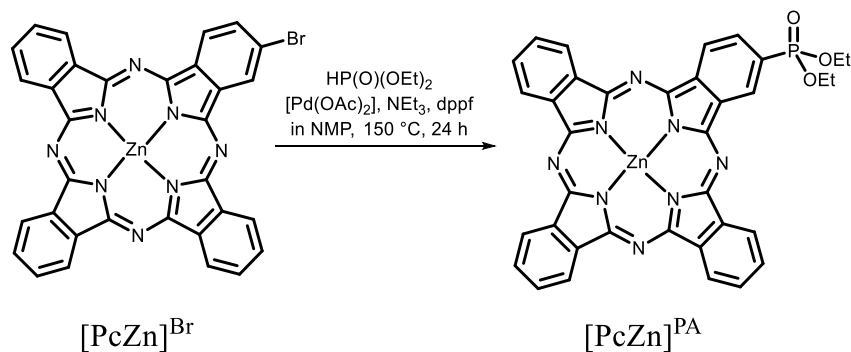
Experimental Section



To obtain $[\text{PcZn}]^{\text{vCA}}$, the methyl ester was deprotected using 10 mL EtOH in 2 mL aq. 10% NaOH solution/100 mg methyl ester. The solution was refluxed overnight and neutralized with HCl. The blue solid was filtered and washed with water.

Yield: n.d. - **IR** (ATR, 400-4000 cm^{-1}): $\tilde{\nu} = 3326$ (m), 3153 (m), 3051 (m), 2917 (m), 2851 (m), 2323 (w), 1706 (w), 1602 (w), 1468 (w), 1405 (w), 1325 (m), 1166 (w), 1064 (s), 953 (w), 882 (w), 720 (s), 568 (w), 458 (w) cm^{-1} . - **UV-Vis** (DCM or DMSO): $\lambda = 673$ (s), 608 (s), 346 (s) nm. - **MS** (MALDI-ToF(+), MeCN): $m/z = 647.676$ $[\text{M}+\text{H}]^+$.

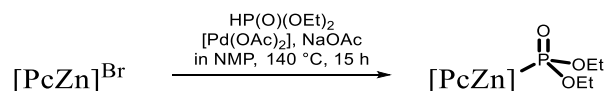
7.18.4 Synthesis of $[\text{PcZn}]^{\text{PA}}$



Method a) 300 mg $[\text{PcZn}]^{\text{Br}}$ (0.45 mmol, 1 eq) were dissolved in 2 mL NMP. 0.1 mL diethyl phosphite, 2 mg $[\text{Pd}(\text{OAc})_2]$ and 5 mg dppf were added. The solution was heated to 150 °C for 15 h. After cooling down to rt, the blue solution was washed several times with MeOH until the MeOH solution became clear. The product was purified by CC (Tol/THF 10:1).

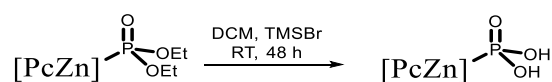
Yield: <2%. - **^1H NMR** (DMSO- d_6 , 300 MHz): $\delta = 9.35$ (m, 7 H, Ar-CH), 8.25 (m, 8 H, Ar-CH), 2.18* (t, 4 H, $^3J_{\text{H-H}} = 8.0$ Hz, -CH₂), 1.91* (q, 6 H, $^3J_{\text{H-H}} = 7.9$ Hz, $^3J_{\text{H-H}} = 14.5$ Hz, -CH₃) ppm. - **^1H NMR** (C₆D₆, 300 MHz): $\delta = 9.74$ (m, 8 H, Ar-CH), 7.93 (m, 7 H, Ar-CH), 3.02 (bs, 6 H, CH₃)*, 1.36 (bs, 4 H, CH₂)* ppm. - **^{31}P NMR** (C₆D₆, 300 MHz): $\delta = -53.17$ ppm. - **UV-Vis** (DCM or DMSO): $\lambda = 673$ (s), 608 (s), 346 (s) nm. - **MS** (MALDI-ToF(+), MeCN): $m/z = 713.248$ $[\text{M}+\text{H}]^+$; 685.397 $[\text{M}-\text{Et}]^+$ (100% Peak); 657.699 $[\text{M}-2\text{Et}]^+$; 573.664 $[\text{M}-\text{P}(\text{O})(\text{OEt})_2]^*$. - **Elemental analysis** (C₃₆H₂₅N₈O₃P₁Zn₁, M = 714.00 g/mol): fnd. (cal.): C: 62.81% (60.56%), H: 3.64% (3.53%), N: 14.45% (15.69%).

*could not be assigned for certain.



Method b) 300 mg $[\text{PcZn}]^{\text{Br}}$ (0.45 mmol, 1 eq) were dissolved in 3 mL NMP, 0.1 mL diethylphosphite (200 mg, 0.6 mmol, 1.3 eq) were added with 0.1 mL NEt_3 (0.6 mmol, 1.3 eq), 2 mg $[\text{Pd(OAc)}_2]$ and 2 mg dppf. The solution was stirred at 160 °C, overnight. DBU was added, and the solution was stirred for 1 h while cooling down to rt. Workup was carried out as described in method a).

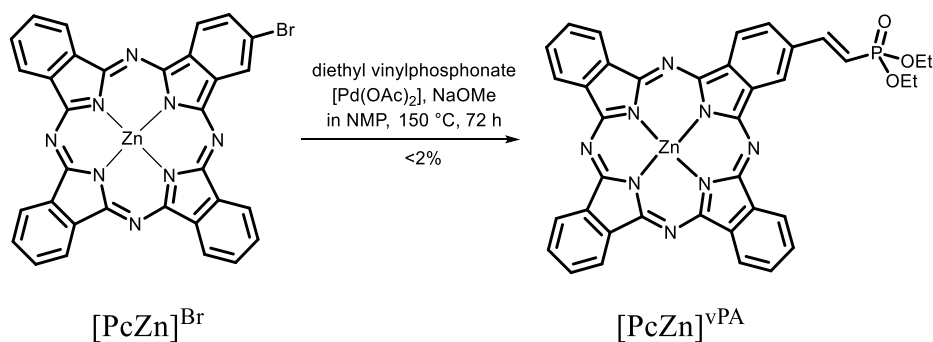
MS (MALDI-ToF(+), without Matrix, MeCN): $m/z = 837.333$ $[\text{M}+\text{H}]^+$, cal. for $\text{C}_{43}\text{H}_{37}\text{N}_{10}\text{O}_3\text{P}_1\text{Zn}_1$: 837.213 ($[\text{PcZn}\cdot\text{dbu}]^{\text{PA}}$), 685.397 $[\text{M}-\text{Et}]^+$.



Deprotection was carried out, using a literature known procedure of MASATO *et al.*^[222] Therefore, 1 eq $[\text{PcZn}]^{\text{PA}}$ was suspended in DCM and 5 eq TMSBr were added. A change in colour could be observed; from dark blue to green. After stirring for 2 h, water was added and the reaction was stirred for another 1 h. The resulting blue solid was purified with 3 x 30 mL MeOH and finally dried in vacuum.

Yield: n.d. - **$^1\text{H NMR}$** ($\text{DMSO}-d_6$, 300 MHz): $\delta = 9.23$ (m, 7 H, Ar-CH), 8.19 (m, 8 H, Ar-CH), -0.06 (bs, 2 H, -OH) ppm. - **UV-Vis** (DCM and DMSO): $\lambda = 673$ (s), 608 (s), 346 (s) nm. - **MS** (APCI-HRMS(+)): $m/z = 1339.1915$ $[2\text{M}]^+$, cal. for $\text{C}_{64}\text{H}_{34}\text{N}_{16}\text{O}_6\text{P}_2\text{Zn}_2+\text{Na}_1$: 1339.0771. - Only a dimeric species could be observed in MS, intensity of measured APCI-HRMS is much too weak (rel. intensity of $2.86 \cdot 10^{-3}$), the aberration is high, but the isotopic pattern matches perfectly. - **Elemental analysis** ($\text{C}_{32}\text{H}_{17}\text{N}_8\text{O}_3\text{P}_1\text{Zn}_1$, $M = 657.89$ g/mol): *find.* (*cal.*): C: 56.96% (58.42%), H: 2.44% (2.60%), N: 16.37% (17.03%).

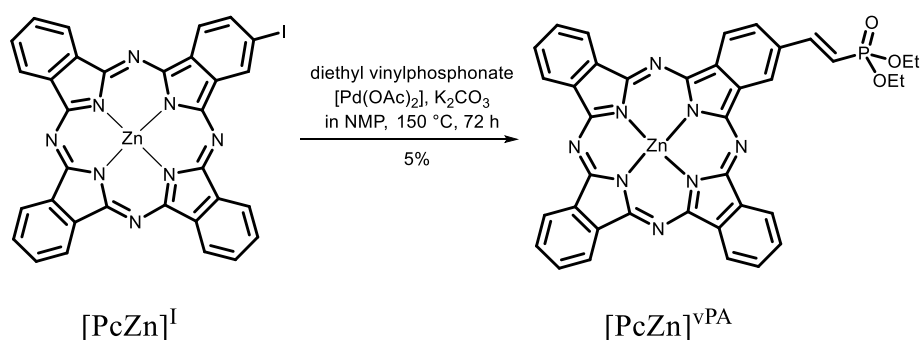
7.18.5 Synthesis of [PcZn]^{vPA}



Method a) 250 mg [PcZn]^{Br} (0.38 mmol, 1 eq), 18 mg [Pd(OAc)₂] and 52 mg K₂CO₃ (theo. 10%) were dissolved in 3 mL NMP under inert atmosphere. 0.1 mL diethyl vinylphosphonate (excess) were added and the solution was stirred for 24 h, at 160 °C. The solvent was distilled off. The crude product was purified by CC (Tol/THF 3:1).

Yield: <math><2\%</math>. - **R_f** (Tol/THF 3:1) = 0.95. - **¹H NMR** (DMSO-*d*₆, 300 MHz): δ = 9.29 (m, 7 H, Ar-CH), 8.21 (m, 8 H, Ar-CH), 2.15* (t, 4 H, -CH₂), 1.19* (q, 6 H, -CH₃) ppm. - **IR** (ATR, 400-4000 cm⁻¹): $\tilde{\nu}$ = 3052 (w), 3044 (w), 2344 (w), 1712 (m), 1658 (m), 1606 (m), 1483 (m), 1284 (m), 1056 (m), 1014 (m), 942 (w), 920 (s), 892 (s), 889 (s), 820 (m), 772 (m), 752 (w), 718 (s), 631 (m), 598 (m), 571 (m), 531 (m), 503 (m), 428 (w) cm⁻¹. - **UV-Vis** (DCM): λ = 672 (s), 640 (sh), 607 (s), 343 (s) nm. - **MS** (MALDI-ToF(+), without Matrix, THF, MeCN): m/z = 739.349 [M+H]⁺; 713.178 [M-OEt]⁺; 685.346 [M-2OEt]⁺. - **Elemental analysis** (C₃₈H₂₇N₈O₃P₁Zn₁, M = 740.05 g/mol): *find.* (*cal.*): C: 61.50% (61.67%), H: 4.18% (3.68%), N: 13.97% (15.14%).

*could not be assigned for certain. Only low-field shifted protons were detected.

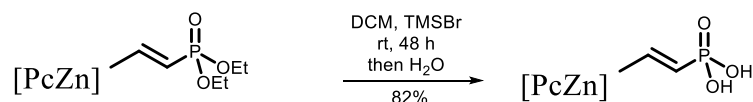


Method b) 150 mg [PcZn]^I (0.21 mmol, 1 eq), 15 mg [Pd(OAc)₂] (66.8 μmol, 0.3 eq), and 41 mg K₂CO₃ (0.29 mmol, 1 eq) were dissolved in 3 mL NMP under inert atmosphere. 0.05 mL diethyl vinylphosphonate was added and the solution was stirred for 72 h at 160 °C. After

cooling down to rt, the solvent was removed by distillation in vacuum, 70 – 90 °C, 5·10⁻³ bar. The product was purified by CC (Tol/THF 1:1).

Yield: 5%. - The analysis is in accordance with the data described above.

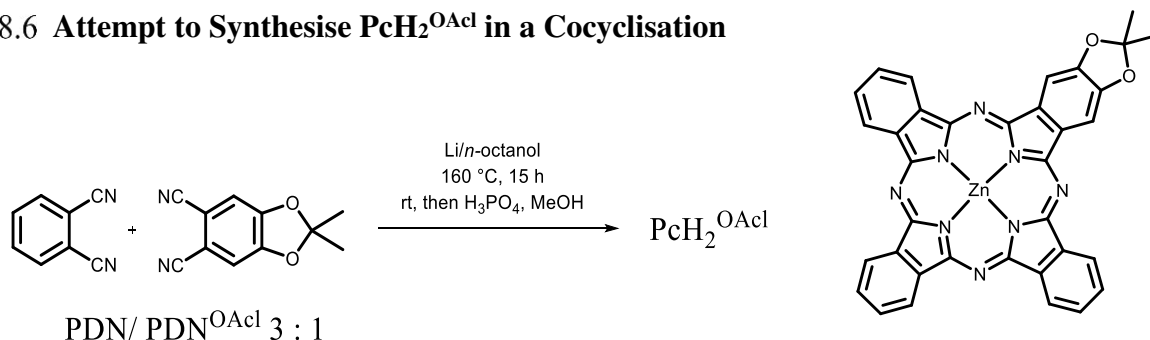
Deprotection was carried out according to the procedure described above in section 7.18.4.



Yield: 82%. - R_f (Tol/THF 3:1) = 0.1. - **¹H NMR** (DMSO-*d*₆, 300 MHz): δ = 9.51 (m, 7 H, Ar-CH), 8.16 (m, 8 H, Ar-CH), 2.87* (bt, 4 H, -CH₂), 2.56* (bq, 6 H, -CH₃) ppm. - **IR** (ATR, 400-4000 cm⁻¹): $\tilde{\nu}$ = 3180 (w), 3047 (w), 2960 (m), 2913 (w), 2740 (w), 2345 (w), 1720 (w), 1463 (w), 1323 (m), 1257 (m), 1014 (s), 868 (w), 791 (s), 718 (m), 476 (w) cm⁻¹. - **UV-Vis** (DCM): λ = 673 (s), 644 (sh), 608 (s), 343 (s) nm. - **MS** (MALDI-ToF(+), without Matrix, dissolved DCM diluted with MeCN): m/z = 683.324 [M]⁺. Also π -stacked phthalocyanine [2M]⁺ observed. - **Elemental analysis** (C₃₄H₁₉N₈O₃P₁Zn₁, M = 683.95 g/mol): *find.* (*cal.*): C: 57.75% (59.71%), H: 2.60% (2.80%), N: 16.21% (16.38%).

*could not be assigned for certain. Only low-field shifted protons were detected.

7.18.6 Attempt to Synthesise PcH₂OAc^l in a Cocyclisation



According to General Procedure 4 (p. 235). A separation by CC (Tol/THF, PE/EE, PE/DCM, or MeCN) was not successful. All compounds could be observed in different fractions.

¹H NMR (Pyridine-*d*₅, 300 MHz): low-field shifted protons were observed, indicating a mixture of compounds after CC. - **MS** (APCI-HRMS(+)): m/z = 587.1941 [M+H]⁺, *cal.* for C₃₅H₂₂N₈O₂+H₁: 587.1938. - **MS** (APCI-HRMS(+)): m/z = 659.2152 [M+H]⁺, *cal.* for C₃₈H₂₆N₈O₄+H₁: 659.2150. - **MS** (APCI-HRMS(+)): m/z = 731.2361 [M+H]⁺, *cal.* for C₄₁H₃₀N₈O₆+H₁: 731.2361.

Experimental Section

7.18.7 Synthesis of [PcZn]^{OAc}

According to General Procedure 5 (p. 245).

Yield: 30%. - **¹H NMR** (Pyridine-*d*₅, 300 MHz): δ = 9.72 (m, 7 H, Ar-CH), 8.23 (m, 2 H, Ar-CH), 2.48 (s, 6 H, CH₃) ppm. - **IR** (ATR, 400-4000 cm⁻¹): $\tilde{\nu}$ = 2360 (w), 2339 (w), 1698 (w), 1468 (m), 1407 (w), 1330 (m), 1284 (m), 120 (m), 1114 (s), 1085 (s), 1054 (s), 720 (s) cm⁻¹. - **UV-Vis** (DCM): λ = 671 (s), 644 (sh), 607 (sh), 344 (s), 227 (s) nm. - **MS** (APCI-HRMS(+)): m/z = 649.1087 [M+H]⁺, cal. for C₃₅H₂₀N₈O₂Zn₁+H₁: 649.1073. - **MS** (MALDI-ToF(+)): m/z = 648.674 [M]⁺.

7.18.8 Synthesis of [PcZn]^{O^{Ph}tBu} [219]

The compound is known from literature,^[219] but was synthesised in a modified procedure: 710 mg [SpcBCl] (1.64 mmol, 1 eq) were dissolved with 741 mg PDN^{O^{Ph}tBu} (1.64 mmol, 1 eq) and 395 mg [Zn(OAc)₂·2H₂O] (1.80 mmol, 1.1 eq) in 2 mL DMSO. A spatula tip of urea was added and the solution was stirred for 72 h at 160 °C. After cooling down to rt, the solvent was removed by vacuum distillation, dried at 140 °C in vacuum, and was finally purified by CC (PE/THF 3:1). The product was obtained in the form of a green powder.

Yield: 421 mg, 0.47 mmol, 28%. - **MS** (MALDI-ToF(+)): m/z = 901.231 [M+H]⁺. ¹H NMR and UV-Vis spectroscopic data are in accordance with literature values.

7.18.9 Synthesis of [PcZn]^{OH} [219]

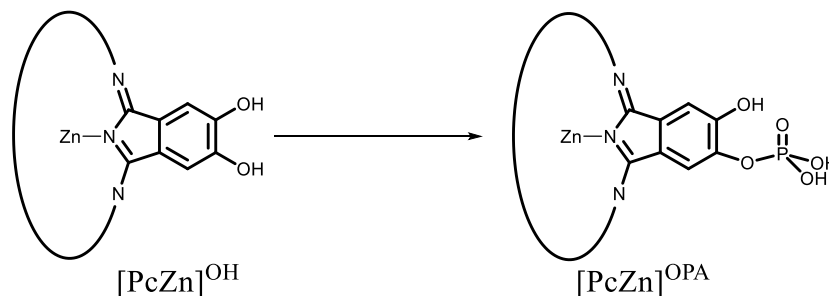
General Procedure 8: Synthesis of [PcZn]^{OH}.^[209]

[PcZn]^{OAc} or [PcZn]^{O^{Ph}tBu} were completely dissolved in conc. H₂SO₄ (2 mL/100 mg Pc). A change in colour was observed, from blue to red. The solution was stirred for about 30 min at rt. Water was added and a blue powder precipitated. The resulting blue solid was filtered off and was washed with water until it became neutral. Finally, it was dried in vacuum and [PcZn]^{OH} was obtained in the form of a deep blue powder.

Yield: quant. - **¹H NMR** (Pyridine-*d*₅, 300 MHz): δ = 9.59 (s, 7 H, Ar-CH), 8.17 (s, 2 H, Ar-CH), *2.00 (s, 6 H, -CH₃) ppm. - **IR** (ATR, 400-4000 cm⁻¹): $\tilde{\nu}$ = 3043 (w, bs, OH), 2961 (w), 2921 (w), 2848 (w), 1480 (m), 1406 (m), 1326 (m), 1284 (m), 1258 (m), 1158 (w), 1084 (s), 1013 (s), 881 (m), 794 (s), 746 (m), 722 (s) cm⁻¹. - **UV-Vis** (DCM): λ = 671 (s), 644 (sh), 607 (sh), 344 (s), 227 (s) nm. - **MS** (MALDI-ToF(+)): m/z = 609.043 [M+H]⁺.

Additional information: *could not be assigned for certain. Compared to UV-Vis spectroscopic data of $[\text{PcZn}]^{\text{OAc}}$, a weak hypsochromic shift was observed.

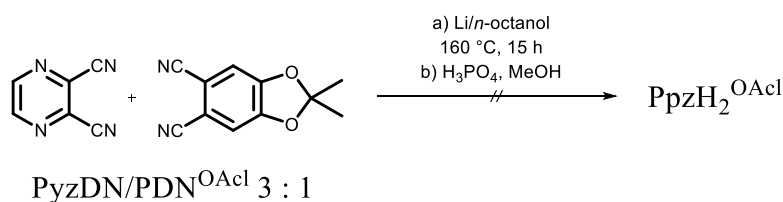
7.18.10 Attempt to Synthesise $[\text{PcZn}]^{\text{OPA}}$



10 mg $[\text{PcZn}]^{\text{OH}}$ (16.4 μmol , 1 eq) were dissolved in 1.5 mL pyridine- d_5 , and a drop phosphorylchloride was added. The solution was stirred overnight. 0.05 mL water were added and the solution was stirred for another 1 h. The solvent was removed in vacuum and finally extracted with chloroform until the aqueous phase became clear. The product was dried in vacuum.

Conversion: quant. - MS (MALDI-ToF): $m/z = 689.239$ $[\text{M}+\text{H}]^+$.

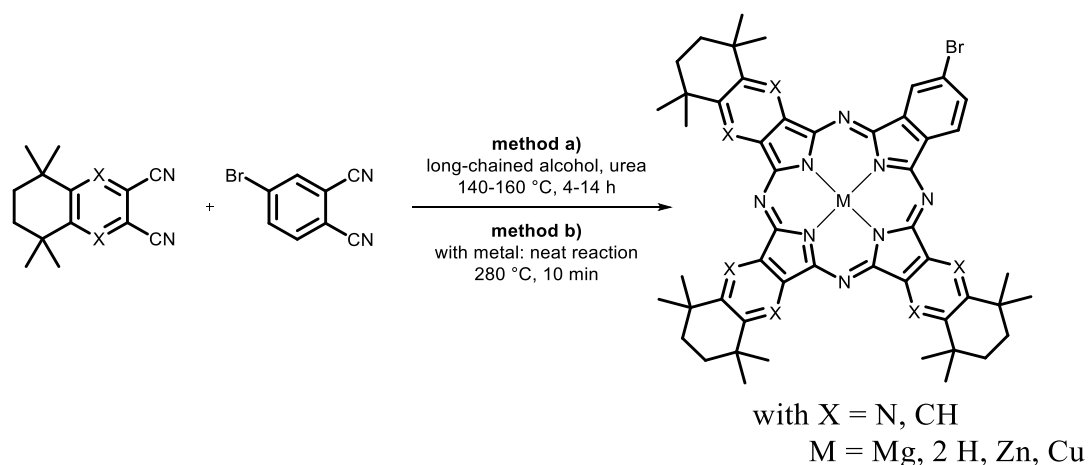
7.18.11 Attempt to Synthesise $\text{PpzH}_2^{\text{OAc}}$



205 mg lithium were dissolved in 6 mL *n*-octanol at 90 °C within 10 min. The solution was cooled down to rt, a mixture of 506 mg PyzDN (3.85 mmol, 3 eq) and 260 mg PDN^{OAc} (1.6 mmol, 1 eq) were added and stirred in a preheated oil bath at 160 °C for 10 h. No pyrazinoporphyrazine traces could be detected by using MS and UV-Vis spectroscopy.

7.19 Synthesis of Alkyl Substituted Functionalised Phthalocyanines

7.19.1 Attempts to Synthesise Soluble, Functionalised Phthalocyanines [PcM]^{FG}



General Procedures:

Method a) All dinitriles PDN^{*} or PzDN^{*}/PDN^{Br} have been used in a ratio of 2:1. For synthesis of metal free phthalocyanine derivatives, the dinitriles were dissolved in a high boiling solvent such as quinoline or CNP (5 mL/g dinitrile mixture). Urea or ammonium heptamolybdate was added in cat. amounts. Then, the solution was stirred for about 12 h at 140-160 °C under argon in a preheated oil-bath, while a colour change to deep blue was observed. Finally, the solvent was removed by distillation. The product was washed with hexane and MeOH, and finally purified by a short CC. The formation of Pc^{*}H₂^{FG} was controlled by using TLC, UV-Vis and MS.

Method b) Metal phthalocyanines [Pc^{*}M]^{FG} have been synthesised in a neat reaction: Therefore, dinitriles PDN^{*} or PzDN^{*}/PDN^{Br} were used in a ratio of 2:1. Metal precursors such as [M(OAc)₂·xH₂O] or [MCl₂] were added as well as urea or ammonium heptamolybdate in cat. amounts. The mixture was placed in a preheated WOOD's metal bath. The corresponding precursors were stirred for 10 min at 280 °C. The resulting mixture was washed with MeOH and hexane. When a change in colour to green or blue was observed, the resulting powder was dried and was purified by CC. For [Pc^{*}Zn]^{FG}, a degradation could be observed when chloride containing solvents were used.

Following HECK coupling reactions was calculated based on the molar amount of used bromine dinitrile.

Analytic Investigations: All bromine precursors could be identified in APCI-HRMS or MALDI-ToF and UV-Vis spectroscopy, but not separated by CC. In some cases, a separation using preparative TLC is possible. Also, the low-field shifted protons could be observed by using ^1H NMR spectroscopy.

$[\text{Pc}^*\text{Zn}]^{\text{Br}}$: MS (APCI-HRMS(+)): $m/z = 987.3208$ $[\text{M}+\text{H}]^+$, cal. for $\text{C}_{56}\text{H}_{57}\text{Br}_1\text{N}_8\text{Zn}_1+\text{H}_1$: 987.3239.

$[\text{Pc}^*\text{Zn}]^{\text{I}}$: MS (APCI-HRMS(+)): $m/z = 1033.3114$ $[\text{M}+\text{H}]^+$, cal. for $\text{C}_{56}\text{H}_{57}\text{I}_1\text{N}_8\text{Zn}_1+\text{H}_1$: 1033.3115.

$[\text{Pc}^*\text{Mg}]^{\text{Br}}$: MS (APCI-HRMS(+)): $m/z = 947.3769$ $[\text{M}+\text{H}]^+$, cal. for $\text{C}_{56}\text{H}_{57}\text{Br}_1\text{Mg}_1\text{N}_8+\text{H}_1$: 947.3807. - MS (APCI-HRMS(+)): $m/z = 946.3729$ $[\text{M}]^+$, cal. for $\text{C}_{56}\text{H}_{57}\text{Br}_1\text{Mg}_1\text{N}_8$: 946.3729.

7.19.1.1 Attempt to Synthesise $[\text{Pc}^*\text{Cu}]^{\text{vCA}}$

The synthesis was carried out following method b), using $\text{PDN}^*/\text{PDN}^{\text{I}}$, 1 mol% $[\text{Pd}(\text{OAc})_2]$, 10% NaOAc and 100 eq acrylic acid methylester. The mixture was dissolved in 5 mL NMP/ g $[\text{Pc}^*\text{M}]^{\text{I}}$ and was stirred at 160 °C for 24 h. The reaction was monitored by using TLC. Under chosen conditions a demetallation of the phthalocyanine was observed. Thereby, $[\text{Cu}(\text{OAc})_2]$ was formed and Pd inserted into the phthalocyanine and a mixture of the desired product, the palladium phthalocyanine, the bromide compounds and the acrylate anchor + isomers was obtained.

$[\text{Pc}^*\text{Cu}]$: MS (APCI-HRMS(+)): $m/z = 1016.5246$ $[\text{M}+\text{H}]^+$, cal. for $\text{C}_{64}\text{H}_{72}\text{Cu}_1\text{N}_8+\text{H}_1$: 1016.5249.

$[\text{Pc}^*\text{Cu}]^{\text{vCA}}$: MS (APCI-HRMS(+)): $m/z = 989.4281$ $[\text{M}+\text{H}]^+$, cal. for $\text{C}_{60}\text{H}_{62}\text{Cu}_1\text{N}_8\text{O}_2+\text{H}_1$: 989.4286.

$[\text{Pc}^*\text{Pd}]^{\text{vCA}}$: MS (MALDI-ToF(+)): $m/z = 1033.664$ $[\text{M}]^+$.

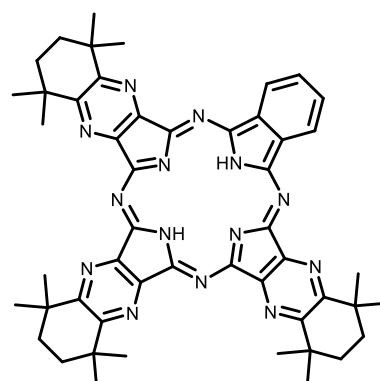
7.19.1.2 Attempt to Synthesise $[\text{Pc}^*\text{Zn}]^{\text{vCA}}$

$[\text{Pc}^*\text{Zn}]^{\text{vCA}}$ was synthesised according to the procedure described above. The product was purified by CC (Tol/THF 20:1). $[\text{Pc}^*\text{Zn}]$ was eluted first, followed by $[\text{Pc}^*\text{Zn}]^{\text{vCA}}$ and the A_2B_2 -type Pc in a mixture in three fractions. Then, AB_3 -type Pc was eluted and finally the B_4 -type compound. Again, the separation of the products was attempted by CC (PE/Tol/THF 20:20:1) but not obtained in sufficient purity. The products might be separated by using preparative TLC.

Experimental Section

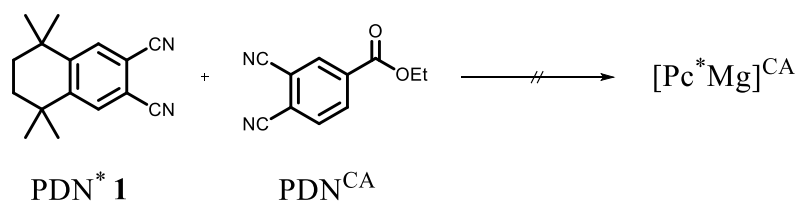
7.19.1.3 Attempt to Synthesis $\text{Pc}^*\text{H}_2\text{Br}$

500 mg PzDN^* (2.08 mmol, 1 eq) were dissolved with 433 mg PDN^{Br} (2.09 mmol, 1 eq) in 10 mL of a freshly prepared Li/n -octanol solution, using 200 mg Li. The solution was warmed up to 160 °C for 24 h in a preheated oil bath. After extraction with 3 mL H_3PO_4 and 50 mL MeOH, the solution was washed with 2 x 50 mL MeOH before purification by CC (PE(40/60)/EE 50:50 \rightarrow 80:1).

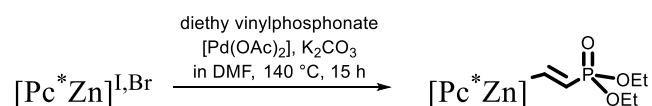


$^1\text{H NMR}$ (C_6D_6 , 300 MHz): aromatic protons at 9.32 ppm, as well as $-\text{NH}$ at -1.96 ppm were observed. - **UV-Vis** (DCM): $\lambda = 660$ (s), 635 (s), 345 (s) nm. - **MS** (APCI-HRMS(+)): $m/z = 851.4700$ [$\text{M}+\text{H}$] $^+$, cal. for $\text{C}_{50}\text{H}_{54}\text{N}_{14}+\text{H}_1$: 851.4729.

7.19.1.4 Attempt to Synthesis $[\text{Pc}^*\text{Mg}]^{\text{CA}}$



230 mg PDN^* (0.97 mmol, 2.6 eq) were dissolved with 75 mg PDN^{CA} (0.37 mmol, 1 eq), 40 mg ammonium heptamolybdate, 240 mg $[\text{MgCl}_2]\cdot 6\text{H}_2\text{O}$ (1.18 mmol, excess) in 1 mL CNP. A drop of DBU was added, and the solution was placed in a preheated oil bath at 200 °C. The solution was stirred for 24 h. The yellowish solution changed colour to a brown liquid. After cooling down to rt, the product was washed with MeOH and hexane. No product could be observed either in UV-Vis spectroscopy or MS.

7.19.1.5 Attempt to Synthesise $[\text{Pc}^*\text{Zn}]^{\text{vPA}}$ 

Method a) The synthesis was carried out using 2 mol% Pd/C (Pd 10% on charcoal), 1.5 eq K_2CO_3 , and 5 eq vinylphosphonate. The mixture was suspended in DMF and was stirred at 140 °C for 15 h. The reaction was monitored by TLC. No traces of a Pc were observed using UV-Vis spectroscopy and MS.

Method b) $[\text{PcZn}]^{\text{Br}}$ was dissolved in 2 mL NMP and was stirred at 180 °C for 48 h with 4 mol% $[\text{Pd}(\text{OAc})_2]$ 1.5 eq K_2CO_3 , and >20 eq vinylphosphonate. No traces of a Pc were observed either in UV-Vis spectroscopy or MS.

Method c) Synthesis of $[\text{Pc}^*\text{Zn}]^{\text{I}}$ in neat reaction with $[\text{Zn}(\text{OAc})_2] \cdot 2\text{H}_2\text{O}$. The product mixture was purified using CC (DCM). The product mixture was obtained in the form of a green solid.

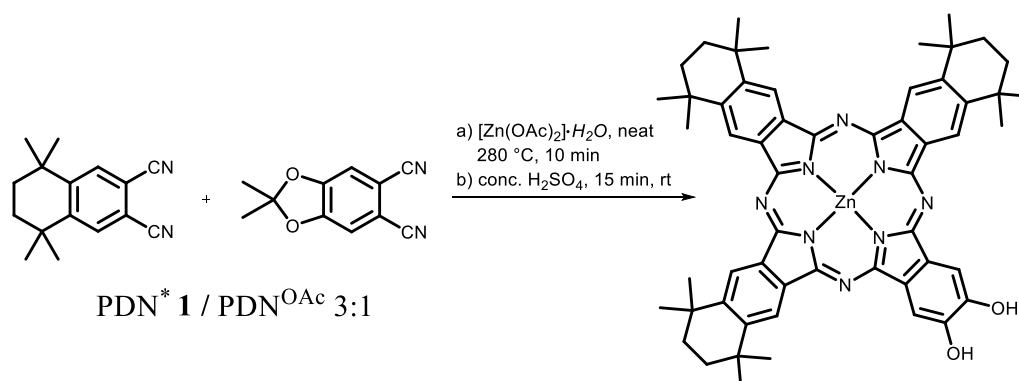
MS (APCI-HRMS(+)): $m/z = 1033.3114$ $[\text{M}+\text{H}]^+$, cal. for $\text{C}_{56}\text{H}_{58}\text{I}_1\text{N}_8\text{Zn}_1+\text{H}_1$: 1033.3115.

The palladium catalysed reaction was carried out using vinylphosphonate and $[\text{Pd}(\text{OAc})_2]$ in DMF. The solution was stirred at 120 °C for 9 h. The reaction was monitored using TLC and ^{31}P NMR spectroscopy. The solvent was removed under reduced pressure. The resulting green powder was purified by CC (PE/EE 6:1 \rightarrow PE/EE 4:1).

Yield: 10%. - ^{31}P NMR (solution, 101 MHz): $\delta = 27.59$ ppm. - **UV-Vis** (DCB): $\lambda = 684$ (s), 619 (sh), 355 (s), 238 (s) nm.

7.20 Synthesis of Alkyl Substituted Hydroxy Pc*/Ppz*

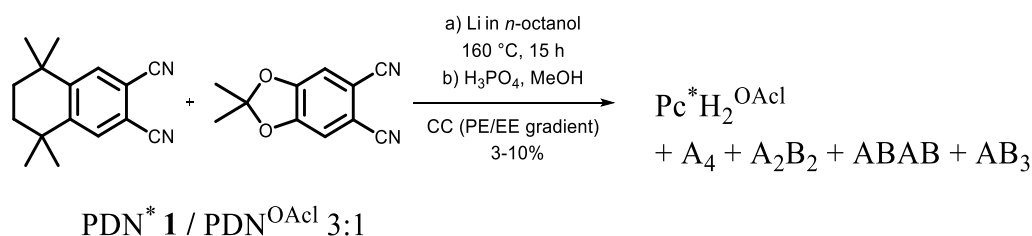
7.20.1 Attempt to Synthesise [Pc*Zn]^{OH} in a Neat Reaction



According to General Procedure 4 (p. 235), followed by General Procedure 8 (p. 284). The products could not be separated by CC.

Yield: 333 mg mixture of isomers. - **MS** (APCI-HRMS(+)): $m/z = 939.4035$ $[\text{M}+\text{H}]^+$, cal. for $\text{C}_{56}\text{H}_{58}\text{N}_8\text{O}_2\text{Zn}_1+\text{H}_1$: 939.4047.

7.20.2 Synthesis of Pc*H₂OAc



According to General Procedure 4 (p. 235), using $\text{Pc}^* / \text{Pc}^* \text{N}^{\text{OAc}}$ in a 3:1 ratio. The mixture was added onto silica and was separated by CC (PE/EE 10:1 \rightarrow 1:1 in gradient). At first, $\text{Pc}^* \text{H}_2$ was eluted, then A_3B $\text{Pc}^* \text{H}_2 \text{OAc}$, before the other isomers A_2B_2 in a mixture with ABAB and AB_3 were eluted.

Pc*H₂: **Yield:** 40 mg, 41.9 μmol , 3%. - R_f (PE/EE 10:1) = 0.89. - The analysis (^1H NMR, UV-Vis spectroscopy and MS) is in accordance with the values in section 7.10.1.

Pc*H₂OAc: **Yield:** 128 mg, 0.14 mmol, 10%. - R_f (PE/EE 10:1) = 0.77. - ^1H NMR (C_6D_6 , 300 MHz): $\delta = 9.93$ (s, 2 H, Ar-CH), 9.85 (s, 2 H, Ar-CH), 9.74 (s, 2 H, Ar-CH), 9.09 (s, 2 H, Ar-CH), 1.83 (s, 6 H, $-\text{CH}_3^{\text{OAc}}$), 1.79 (s, 4 H, $-\text{CH}_2$), 1.62 (s, 8 H, $-\text{CH}_2$), 1.53 (s, 12 H, $-\text{CH}_3$), 0.39 (s, 24 H, $-\text{CH}_3$), -0.29 (s, 2 H, -NH) ppm. - ^1H NMR (Pyridine- d_5 , 300 MHz): $\delta =$

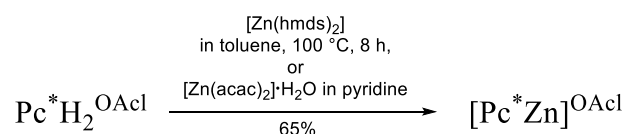
9.94 (s, 2 H, Ar-CH), 9.85 (s, 2 H, Ar-CH), 9.73 (s, 2 H, Ar-CH), 9.01 (s, 2 H, Ar-CH), 2.16 (s, 4 H, -CH₂), 1.91 (s, 12 H, -CH₂), 1.87 (s, 6 H, -CH₃^{OAc}), 1.70 (s, 12 H, -CH₃), 1.56 (s, 24 H, -CH₃), -0.39 (s, 2 H, -NH) ppm. - ¹³C NMR (C₆D₆, 75 MHz): δ = 151.1, 148.6, 147.8, 122.0, 121.6, 121.3, 119.7, 102.6, 99.7, 35.9, 35.9, 32.8, 29.8, 29.7, 29.2, 26.1 ppm. - IR (ATR, 400-4000 cm⁻¹): ν̄ = 3449 (w), 3297 (w), 3071 (m), 2958 (m), 2924 (m), 2857 (m), 2348 (w), 2325 (w), 1727 (w), 1617 (w), 1457 (s), 1375 (m), 1362.86 (m), 1298 (m), 1260 (m), 1207 (m), 1078 (s), 1000 (s), 975 (s), 860 (m), 799 (m), 767 (s), 681 (s), 543 (m), 495 (m), 447 (m), 413 (m) cm⁻¹. - UV-Vis (DCM): λ = 707 (s), 670 (s), 651 (sh), 607 (sh), 343 (s), 296 (s) nm. - MS (APCI-HRMS(+)): m/z = 917.5229 [M+H]⁺, cal. for C₅₉H₆₄N₈O₂H₁: 917.5225. Second π-stacked molecule could be observed: 1834.0357 [M+H]⁺, cal. for C₁₁₈H₁₂₈N₁₆O₄+H₁: 1834.0357. - **Elemental analysis** (C₅₉H₆₄N₈O₂, M = 917.1919 g/mol): cal. (fnd.): C: 73.67% (77.26%), H: 7.31% (7.03%), N: 10.03% (12.22%).

Isomeric mixture:* **A₂B₂, ABAB:** Yield: 79 mg, 83.6 μmol, 6%. - R_f (PE/EE 10:1) = 0.63. - ¹H NMR (C₆D₆, 300 MHz): δ = 9.78 (s, 2 H, Ar-CH), 9.72 (s, 2 H, Ar-CH), 8.77 (s, 2 H, Ar-CH), 8.63 (s, 2 H, Ar-CH), 2.13-2.05 (m, 8 H, -CH₂), 1.69 (s, 12 H, -CH₃), 1.65 (s, 12 H, -CH₃), 1.59 (s, 12 H, -CH₃^{OAc}), 1.54 (s, 24 H, -CH₃^{OAc}), -1.37 (s, 2 H, -NH) ppm. - UV-Vis (DCM): λ = 699 (s), 664 (s), 645 (sh), 609 (sh), 343 (s), 295 (sh) nm. - MS (APCI-HRMS(+)): m/z = 879.4339 [M+H]⁺, cal. for C₅₄H₅₄N₈O₄+H₁: 879.4341.

AB₃: Yield: 5 mg, 5.95 μmol, <1%. - R_f (PE/EE 10:1) = 0.26. - ¹H NMR (C₆D₆, 300 MHz): δ = 9.64 (s, 2 H, Ar-CH^{OAc}), 8.77 (s, 2 H, Ar-CH^{OAc}), 8.67 (s, 2 H, Ar-CH^{OAc}), 8.37 (s, 2 H, Ar-CH), 2.01 (s, 4 H, -CH₂), 1.82 (s, 18 H, -CH₃^{OAc}), 1.75 (s, 12 H, -CH₃), -2.57 (bs, 2 H, -NH) ppm. - UV-Vis (DCM): λ = 694 (s), 687(s), (638 (sh)), 596 (sh), 345 (s), 294 (s) nm. - MS (APCI-HRMS(+)): m/z = 841.3450 [M+H]⁺, cal. for C₆₄H₇₄N₈+H₁: 841.3457.

*The isomeric mixture can be assigned by using ¹H NMR spectroscopy. The observed ratio of A₂B₂/ABAB is almost 1:1.

7.20.3 Synthesis of [Pc*Zn]^{OAc}



60 mg Pc*H₂^{OAc} (65.4 μmol, 1 eq) were dissolved in 2 mL toluene before adding 185 mg [Zn(hmds)₂] (479 μmol, 7.5 eq) at once. The solution was stirred for 8 h at 100 °C. After

Experimental Section

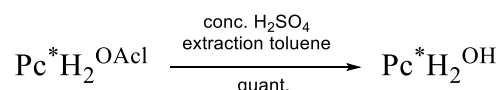
cooling down to rt the solution was concentrated in vacuum and was washed with 2 x 20 mL DEE to remove the hmids residues. The green powder was dried in vacuum.

Yield: 42 mg, 42.8 μmol , 65%. - $^1\text{H NMR}$ (C_6D_6 , 300 MHz): δ = 10.03 (s, 2 H, Ar-CH), 10.01 (s, 2 H, Ar-CH), 9.91 (s, 2 H, Ar-CH), 9.26 (s, 2 H, Ar-CH), 1.85 (s, 8 H, -CH₂), 1.82 (s, 4 H, -CH₂), 1.65 (s, 12 H, -CH₂), 1.60 (s, 12 H, -CH₃), 1.59 (s, 12 H, -CH₃), 1.56 (s, 6 H, -CH₃^{OAc}) ppm. - $^1\text{H NMR}$ (THF-*d*⁸, 300 MHz): δ = 10.49 (s, 2 H, Ar-CH), 9.47 (s, 2 H, Ar-CH), 9.45 (s, 2 H, Ar-CH), 8.75 (s, 2 H, Ar-CH) ppm. - the signals of alkyl moieties are overlapping with the thf signals. - **UV-Vis** (DCM): λ = 685 (s), 616 (sh), 346 (s), 294 (s) nm. - **Fluorescence** (DCM, λ_{ex} = 350 nm): λ = 693 nm. - **MS** (APCI-HRMS(+)): m/z = 979.4330 [M+H]⁺, cal. for C₅₉H₆₂N₈O₂Zn₁+H₁: 979.4360. - **MS** (MALDI-ToF(+)): m/z = 980.870 [M+H]⁺, also the π -stacked molecule might be observed 1962.535 [2M+H]⁺.

Alternative Synthesis: 84 mg Pc*H₂^{OAc} (92 mmol, 1 eq) and 22 mg [Zn(acac)₂] \cdot 2H₂O (101 mmol, 1.1 eq) were dissolved in 2 mL toluene and stirred at 50 °C for 7 d. The reaction was monitored by TLC. After concentration in vacuum, the obtained powder was washed with hexane and MeOH. The green powder was dried in vacuum.

Yield: 59%.

7.20.4 Synthesis of Pc*H₂^{OH}

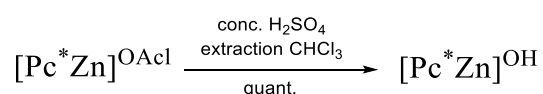


According to General Procedure 8 (p. 284). The green powder was dissolved in 100 mL toluene/100 mg product and was washed with aq. NaHCO₃ until the solution became neutral. The organic phase was dried over MgSO₄, filtered and the solvent was removed under reduced pressure. The product was dried in vacuum to obtain finally the diol in the form of a dark green powder.

Yield: quant. - $^1\text{H NMR}$ (C_6D_6 /drop pyridine-*d*₅ 300 MHz): δ = 9.93 (s, 2 H, Ar-CH), 9.79 (s, 2 H, Ar-CH), 9.62 (s, 2 H, Ar-CH), 9.42 (s, 2 H, Ar-CH), 1.83 (s, 8 H, -CH₂), 1.80 (s, 4 H, -CH₂), 1.59 (s, 12 H, -CH₃), 1.55 (s, 24 H, -CH₃), -0.30 (s, 2 H, -NH) ppm. - $^1\text{H NMR}$ (Pyridine-*d*₅): δ = 12.81 (bs, 2 H, -OH), 10.01 (s, 2 H, Ar-CH), 9.86 (s, 2 H, Ar-CH), 9.72 (s, 2 H, Ar-CH), 9.57 (s, 2 H, Ar-CH), 1.89 (s, 8 H, -CH₂), 1.86 (s, 4 H, -CH₂), 1.67 (s, 12 H, -CH₃), 1.56 (s, 24 H, -CH₃), -0.08 (s, 2 H, -NH) ppm. - $^{13}\text{C NMR}$ (C_6D_6 , 75 MHz): δ = 150.1,

123.5, 122.1, 36.1-35.1, 34.6, 33.7, 33.0, 32.3, 31.4, 30.1 ppm. - not all quaternary carbon atoms could be detected, because of the low solubility of the sample. - **IR** (ATR, 400-4000 cm^{-1}): $\tilde{\nu}$ = 2952 (m), 2919 (m), 2854 (m), 1612 (w), 1502 (w), 1458 (m), 1381 (w), 1359 (m), 1305 (w), 1184 (w), 1119 (m), 1090 (s), 1015 (s), 977 (m), 896 (w), 848 (w), 802 (w), 756 (s), 682 (s), 540 (w), 450 (w) cm^{-1} . - **UV-Vis** (DCM): λ = 707 (s), 673 (s), 652 (sh), 612 (sh), 342 (s), 295 (s) nm. - **CV** (THF, TBAF, Ferrocene/Ferrocenyl): E_{ox1} = 0.00, E_{red1} = -1.68, E_{red2} = -2.11 V. - **MS** (APCI-HRMS(+)): m/z = 877.4909 $[\text{M}+\text{H}]^+$, cal. for $\text{C}_{56}\text{H}_{60}\text{N}_8\text{O}_2+\text{H}_1$: 877.4912.

7.20.5 Synthesis of $[\text{Pc}^*\text{Zn}]^{\text{OH}}$



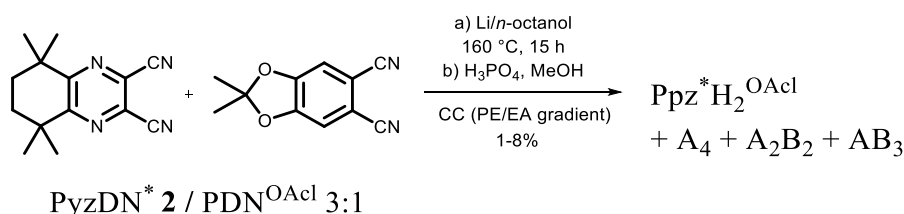
According to General Procedure 8 (p. 284). The resulting green solid of $[\text{Pc}^*\text{Zn}]^{\text{OH}}$ was collected in 100 mL toluene/100 mg product, neutralised with NaHCO_3 , dried over MgSO_4 , filtered and finally concentrated and dried in vacuum.

Yield: quant. - **$^1\text{H NMR}$** (C_6D_6 /drop pyridine- d_5 , 300 MHz): δ = 9.96 (s, 2 H, Ar-CH), 9.93 (s, 2 H, Ar-CH), 9.82 (s, 2 H, Ar-CH), 9.55 (s, 2 H, Ar-CH), 1.84 (s, 8 H, -CH₂), 1.80 (s, 4 H, -CH₂), 1.61 (s, 12 H, -CH₃), 1.54 (s, 24 H, -CH₃) ppm. - **IR** (ATR, 400-4000 cm^{-1}): $\tilde{\nu}$ = 3201 (broadened, m), 2955 (m), 2921 (m), 2855 (m), 1701 (w), 1611 (w), 1466 (m), 1428 (m), 1380 (m), 1361 (m), 1309 (s), 1259 (m), 1188 (w), 1074 (s), 1048 (s), 1023 (s), 984 (s), 897 (m), 864 (m), 800 (s), 747 (m), 696 (m), 619 (m), 540 (w), 448 (w) cm^{-1} . - **UV-Vis** (DCM): λ = 686 (s), 654 (sh), 618 (s), 355 (s), 292 (s) nm. - **CV** (THF, TBAF, Ferrocene/Ferrocenyl): E_{ox1} = -0.65, E_{red1} = -2.61, E_{red2} = -3.04 V.* - **MS** (APCI-HRMS(+)): m/z = 939.4056 $[\text{M}+\text{H}]^+$, cal. for $\text{C}_{56}\text{H}_{58}\text{N}_8\text{O}_2\text{Zn}_1+\text{H}_1$: 939.4047. - **MS** (MALDI-ToF(+)): m/z = 940.356 $[\text{M}]^+$; 1879.751 $[\text{2M}]^+$. - **Elemental analysis:** ($\text{C}_{56}\text{H}_{58}\text{N}_8\text{O}_2\text{Zn}_1$, 940.51 g/mol): *find.* (*cal.*): C: 65.19% (71.52%), H: 6.99% (6.22%), N: 7.82% (11.91%), O: 7.80 (3.40) - traces of sulfuric acid.

Additional information: Less harsh conditions were attempted, but even in aq. TFA reflux, for 7 d no conversion to the diol was observed. The product is almost insoluble in C_6D_6 , so two drops of pyridine were added.

Experimental Section

7.20.6 Synthesis of Ppz*H₂^{OAc}



According to General Procedure 4 (p. 235), using PyzDN*/PDN^{OAc} (1.41 mmol, 1 eq) in a 3:1 ratio. The product was purified by CC (PE/EE in gradient).

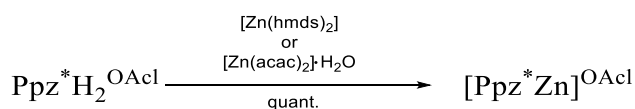
Ppz*H₂^{OAc}: Yield: 100 mg, 0.11 mmol, 8%. - *R_f* (PE/EE 1:1) = 0.95 (eluted with DCM). - **Preparative TLC** (Tol/THF 10:1) = 0.55. - **¹H NMR** (C₆D₆, 300 MHz): δ = 8.95 (s, 2 H, Ar-CH^{OAc}), 1.91 (s, 4 H, -CH₂), 1.90 (s, 8 H, -CH₂), 1.87 (s, 12 H, -CH₃), 1.85 (s, 12 H, -CH₃), 1.85 (s, 12 H, -CH₃), 1.47 (s, 6 H, -CH₃^{OAc}), -1.52 (s, 2 H, -NH) ppm. - **¹³C NMR** (C₆D₆, 75 MHz): δ = 39.3, 34.8, 30.9, 30.9 ppm. - not all quaternary carbon atoms could be detected, because of the low solubility of the sample. - **UV-Vis** (DCM): λ = 657 (s), 630 (sh), 622 (s), 343 (s) nm. - **MS** (APCI-HRMS(+)): *m/z* = 923.4947 [M+H]⁺, cal. for C₅₃H₅₈N₁₄O₂+H₁: 923.4940.

A₂B₂:* Yield: 60 mg, 0.07 mmol, 5%. - *R_f* (PE/EE 1:1) = 0.86. - **¹H NMR** (C₆D₆, 300 MHz): δ = 8.69 (s, 2 H, Ar-CH^{OAc}), 8.52 (s, 2 H, Ar-CH^{OAc}), 1.96 (s, 12 H, -CH₃^{OAc}), 1.90 (s, 8 H, -CH₂), 1.87 (s, 12 H, -CH₂), 1.67 (s, 12 H, -CH₃), -1.52 (s, 2 H, -NH) ppm. - **UV-Vis** (DCM): λ = 662 (s), 642 (s), 335 (s) nm. - **MS** (APCI-HRMS(+)): *m/z* = 883.4158 [M+H]⁺, cal. for C₅₀H₅₀N₁₂O₄+H₁: 883.4151. *here, only the A₂B₂ product was observed.

AB₃: Yield: <1%. - **MS** (APCI-MS(+)): *m/z* = 843.7* [M+H]⁺ (<5%). - **UV-Vis** (DCM): λ = 674 (s), 645 (s), 441 (sh), 347 (s) nm. * intensity to low, no HR possible.

Ppz*H₂: Yield: 78 mg, 0.08 mmol, 6%. - *R_f* (PE/EE 1:1) = 0.04 (eluted with DCM). - Analysis according to section 7.10.8.

7.20.7 Synthesis of [PpzZn*]^{OAc}

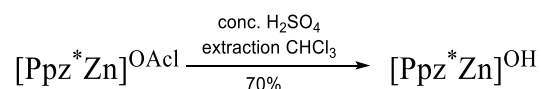


The reaction was carried out on ¹H NMR scale: 5 mg Ppz*H₂^{OAc} (5.42 μ mol, 1 eq) were dissolved in 0.5 mL C₆D₆ and 0.05 mL [Zn(hmnds)₂] were added. The solution was stirred for

1 h at 75 °C. The reaction was monitored by ^1H NMR spectroscopy and finally concentrated in vacuum at 50 °C to removed all volatile compounds. Remaining HMDS traces were removed by washing the product with DEE.

Conversion: quant. - ^1H NMR (C_6D_6 , 300 MHz): $\delta = 9.10$ (s, 2 H, Ar- CH^{OAc}), 1.95 (s, 4 H, - CH_2), 1.92 (s, 8 H, - CH_3), 1.88 (s, 12 H, - CH_3), 1.83 (s, 6 H, - CH_3^{OAc}), 1.80 (s, 12 H, - CH_3), 1.79 (s, 12 H, - CH_3) ppm. - **IR** (ATR, 400-4000 cm^{-1}): $\tilde{\nu} = 2955$ (m), 2918 (m), 2849 (m), 1472 (m), 1407 (m), 1340 (w), 1255 (s), 1213 (m), 1187 (w), 1130 (w), 1083 (m), 1010 (w), 978 (w), 929 (w), 869 (w), 836 (s), 801 (s), 746 (m), 694 (m), 488 (m) cm^{-1} . - **UV-Vis** (DCM): $\lambda = 653$ (s), 362 (s), 227 (s) nm. - **MS** (APCI-HRMS(+)): $m/z = 985.4068$ $[\text{M}+\text{H}]^+$, cal. for $\text{C}_{53}\text{H}_{56}\text{N}_{14}\text{O}_2\text{Zn}_1+\text{H}_1$: 985.4075.

7.20.8 Synthesis of $[\text{Ppz}^*\text{Zn}]^{\text{OH}}$

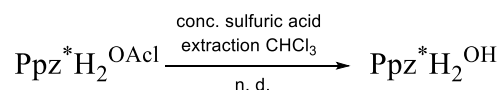


According to General Procedure 8 (p. 284). The resulting green solid of $[\text{Ppz}^*\text{Zn}]^{\text{OH}}$ was collected in 100 mL toluene/100 mg product, neutralised with NaHCO_3 , dried over MgSO_4 , filtered and finally concentrated and dried in vacuum.

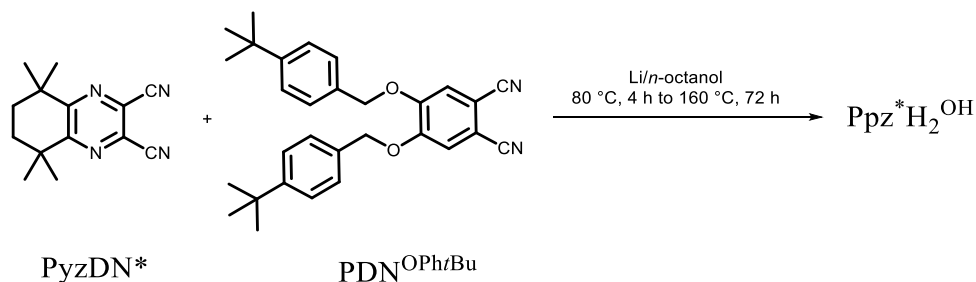
Yield: 70%. - ^1H NMR (C_6D_6 /drop pyridine- d_5 , 300 MHz): $\delta = 9.46$ (s, 2 H, Ar- CH), 1.89 (s, 4 H, - CH_2), 1.83 (s, 8 H, - CH_2), 1.80 (s, 24 H, - CH_3), 1.77 (s, 12 H, - CH_3) ppm. - **IR** (ATR, 400-4000 cm^{-1}): $\tilde{\nu} = 3277$ (w), 2955 (m), 2921 (m), 2856 (m), 1743 (w), 1637 (w), 1457 (m), 1331 (m), 1256 (vs), 1089 (s), 1041 (s), 1017 (s), 868 (m), 801 (m), 747 (m), 694 (m), 552 (w), 432 (w) cm^{-1} . - **UV-Vis** (DCM): $\lambda = 640$ (s), 615 (sh), 582 (s), 353 (s), 297 (s) nm. - **MS** (MALDI-ToF(+)): $m/z = 945.484$ $[\text{M}+\text{H}]^+$.

Experimental Section

7.20.9 Attempt to Synthesise Ppz*H₂^{OH}



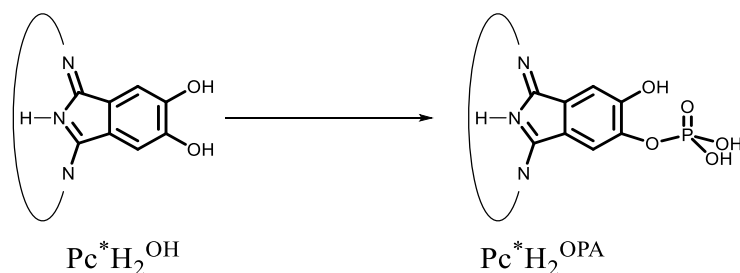
According to General Procedure 8 (p. 284). A decolouration of the solution was observed. Ppz*H₂^{OH} could be identified by using MS and UV-Vis. Other acids such as aq. TFA were used but no conversion to Ppz*H₂^{OH} was observed at 120 °C in toluene, after 4 weeks.



Instead of PDN^{OAcI}, PDN^{OPh/Bu} was used. Under chosen conditions (General Procedure 4 (p. 235)), a direct formation of Ppz*H₂^{OH} was observed. Not enough substance for full characterisation was obtained.

Yield: <2%. - *R_f* (Tol/THF 10:1) = 0.56. - ¹H NMR (C₆D₆, 300 MHz): δ = 9.00 (s, 2H, -CH_{Arom}), 1.86 (s, 12H, -OCCH₃), 1.65 (s, 6H, -CH₂), 1.56 (s, 36H, -CH₃), -0.45 (s, 2H, -NH). - **MS** (MALDI-ToF(+)): *m/z* = 883.430 [M+H]⁺. - **MS** (APCI-MS(+)): *m/z* = 883.620 [M+H]⁺.

7.20.10 Synthesis of Pc*H₂^{OPA}

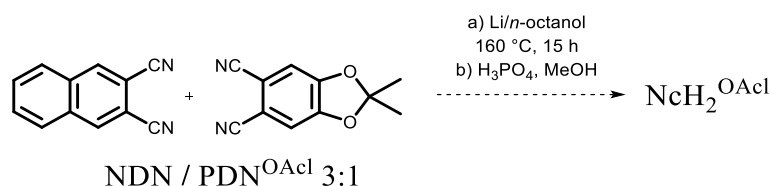


7 mg Pc*H₂^{OH} were dissolved in 5 mL pyridine and a drop of phosphorylchloride was added. After stirring overnight, the raw product was quenched with water, extracted with chloroform until the aqueous phase became clear. The resulting light green powder was finally dried in vacuum.

Yield: n. d. - **MS** (MALDI-ToF(+)): *m/z* = 957.524 [M+H]⁺. - **UV-Vis** (DCM): λ = 708 (s), 676 (sh), 649 (sh), 343 (s) nm.

7.21 Synthesis of Lower Symmetric Naphthalocyanines

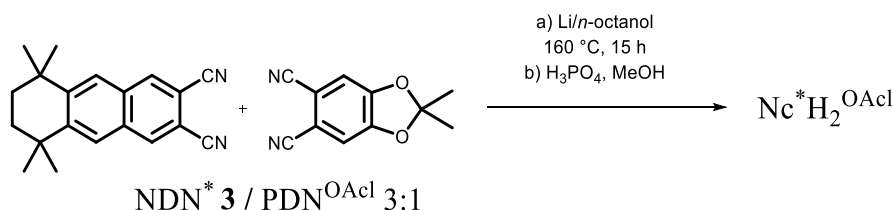
7.21.1 Attempt to Synthesise $\text{NcH}_2^{\text{OAcI}}$



According to General Procedure 4 (p. 235), using NDN/PDN^{OAcI} in a 3:1 ratio. A separation by CC (Tol/THF in gradient) was not successful.

NcH₂^{OAcI}: MS (MALDI-ToF(+)): $m/z = 736.272$ $[\text{M}+\text{H}]^+$. - Not enough product was obtained, for further analysis, but a test reaction could be carried out, see section 7.21.5.

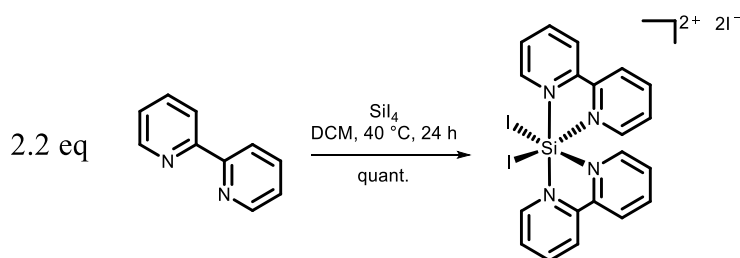
7.21.2 Attempt to Synthesise $\text{Nc}^*\text{H}_2^{\text{OAcI}}$



According to General Procedure 4 (p. 235), using NDN*/PDN^{OAcI} in a 3:1 ratio. The separation was carried out by CC (PE/EE 30:1 in gradient). At first, $\text{Nc}^*\text{H}_2^{\text{OAcI}}$ was obtained, followed by Nc^*H_2 . Not enough product was obtained for complete analysis.

Yield: <2%. - **UV-Vis** (DCM): $\lambda = 743$ (s), 440 (bs), 316 (s), 276 (s), 246 (s) nm. - **MS** (MALDI-ToF(+)): $m/z = 1066.757$ $[\text{M}+\text{H}]^+$.

7.21.3 Synthesis of *cis*-Bis(2,2'-bipyridine)diiodosilicium (IV) iodide ^[287]

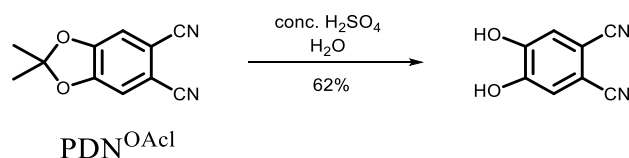


1.00 g SiI_4 (1.87 mmol, 1 eq) were dissolved in 10 mL DCM with 641 mg 2,2'-bipyridine (4.11 mmol, 2.2 eq). The solution was stirred for 16 h at 40 °C. After cooling down to rt, the

Experimental Section

resulting red solid was washed 2 x 20 mL DCM before drying in vacuum. The resulting red solid could be used for the following synthesis 7.21.5 without any further purification.

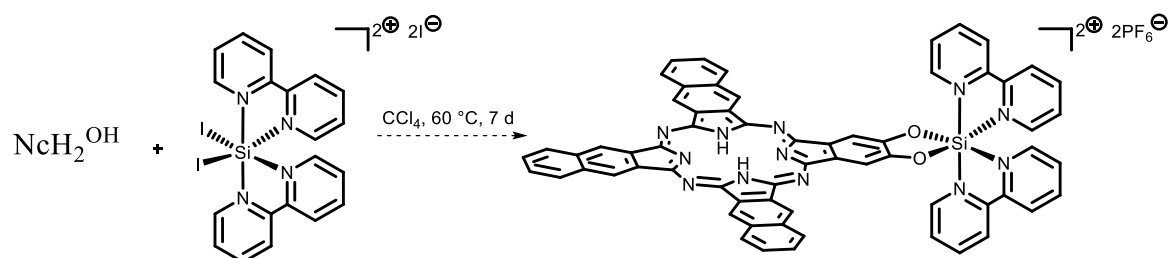
7.21.4 Synthesis of 4,5-Dihydroxyphthalonitrile



501 mg 5,6-dicyano-2,2-dimethyl-1,3-benzodioxole (2.5 mmol, 1 eq) were completely dissolved in 4 mL H₂SO₄ and then poured onto ice water. The white powder was filtered and the precipitate was washed with chloroform. After drying in vacuum, 4,5-dihydroxyphthalonitrile was obtained in the form of a white powder.

Yield: 249 mg, 1.55 mmol, 62%. - ¹H NMR (DMSO-*d*₆, 300 MHz): δ = 10.98 (bs, 2 H, -OH), 7.70 (s, 2 H, Ar-CH) ppm.

7.21.5 Attempt to Synthesise [NcSi(bipy)₂]

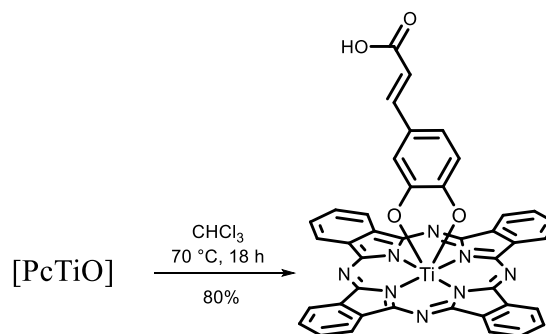


43 mg NcH₂^{OH} (62 μ mol, 1 eq) were suspended with 66 mg [Si(bipy)₂]²I (74 μ mol, 1.2 eq) in 2 mL CCl₄ and stirred at 60 °C over 7 d. 1 mL water was added as well as 250 mg NH₄PF₆ (1.5 mmol, excess). The solution was stirred over 3 d. The resulting powder was macerated several times with water and MeOH and PE. A conversion to the product could be observed by using MS and UV-Vis. The product was quite insoluble and insufficient amounts for full analysis were obtained.

MS (MALDI-ToF(+)): m/z = 1035.602 [M]²⁺.

7.21.6 Synthesis of [PcTi(Cat^{vinyl}CO₂H)] [25]

320 mg [PcTiO] (0.56 mmol, 1 eq) and 201 mg 4-(E)-vinyl-2-carboxylic catechol (1.17 mmol, 2 eq) were dissolved in 10 mL chloroform and stirred at 70 °C for 18 h. After cooling down to rt, the solvent was removed in vacuum and the obtained blue solid was washed with MeOH until it became clear. The solid was dried in vacuum.



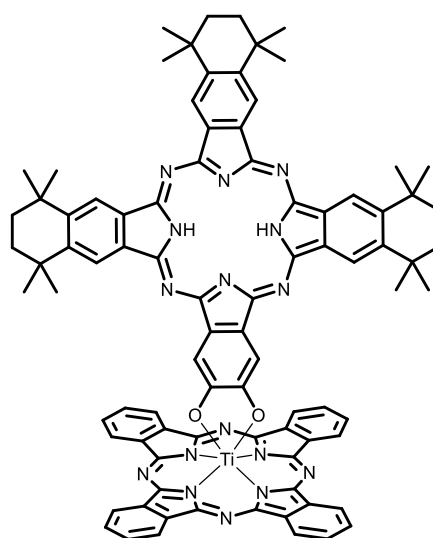
Yield: 331 mg, 0.45 mmol, 80%. - **IR** (ATR, 400-4000 cm⁻¹): $\tilde{\nu}$ = 1702 (m), 1626 (m), 1606 (w), 1504 (w), 1476 (w), 1422 (w), 1378 (w), 1332 (s), 1289 (w), 1267 (w), 1235 (w), 1220 (w), 1205 (w), 1161 (w), 1142 (w), 1117 (w), 1072 (w), 1048 (w), 951 (w), 896 (w), 852 (w), 827 (w), 807 (w), 774 (w), 751 (w), 726 (s), 664 (w), 640 (m), 606 (w), 560 (w), 539 (w), 507 (w), 422 (m) cm⁻¹. - literature described peaks at 2800 cm⁻¹ are visible, but very weak. - **UV-Vis** (DCM): λ = 691 (s), 349 (s), 291 (s), 265 (s) nm. - **Fluorescence** (DCM, λ_{ex} = 350 nm): λ = 700 nm. - **MS** (MALDI-ToF(+)): m/z = 738.323 [M+H]⁺. - **Elemental analysis:** (C₄₁H₂₂N₈O₄Ti₁, 738.53 g/mol): *find.* (*cal.*): C: 65.66% (66.68%), H: 2.98% (3.00%), N: 15.16% (15.17%).

Additional information: In ¹H NMR experiments, low-field shifted protons were observed, but the solubility was not sufficient for detection of the axial ligand.

7.21.7 Synthesis of [PcTiPc*]

10 mg Pc*H₂^{OH} (11.4 μmol, 1 eq) were dissolved in 2 mL chloroform and 10 mg of [PcTiO] (17.4 μmol, 1.5 eq) were added. The solution was stirred for 15 h at 70 °C. After removing the solvent under reduced pressure, the product was macerated with MeOH and hexane. The obtained green powder was purified by CC (Tol/THF 1:1).

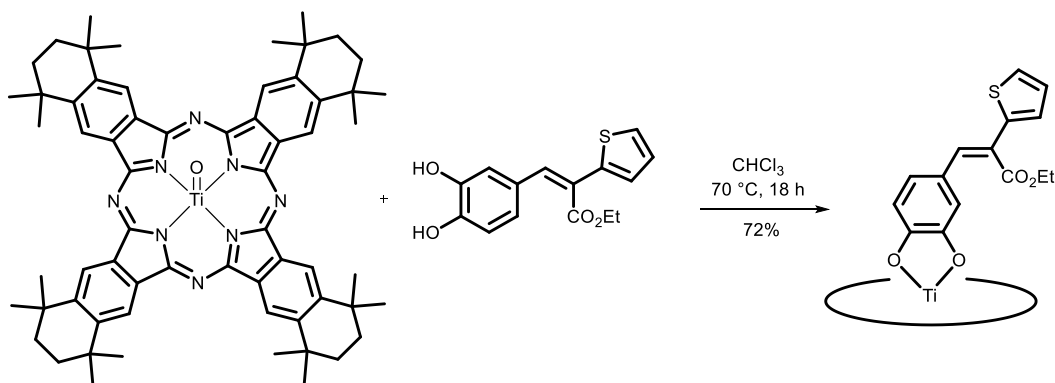
Yield: 13 mg, 9.06 μmol, 79%. - **IR** (ATR, 400-4000 cm⁻¹): $\tilde{\nu}$ = 2957 (m), 2924 (m), 2859 (m), 2359 (w), 1735 (w), 1610 (w), 1505 (w), 1466 (w), 1422 (w), 1383 (w), 1361 (w), 1332 (w), 1305 (m), 1288 (m), 1278 (w), 1205 (w), 1187 (w), 1161 (w), 1117 (w), 1075 (w), 1053 (w), 1013 (w), 977 (s), 948 (s), 894 (s), 868 (s), 849 (w), 828 (w), 800 (w), 777 (w), 769 (w), 751 (w),



Experimental Section

731 (w), 718 (s), 684 (w), 612 (s), 543 (w), 530 (w), 505 (w), 486 (w), 417 (w) cm^{-1} . - **UV-Vis** (CHCl_3): $\lambda = 693$ (s), 364 (s), 393 (s) nm. - **MS** (MALDI-ToF(+)): $m/z = 1435.205$ $[\text{M}+\text{H}]^+$. - **Elemental analysis** ($\text{C}_{88}\text{H}_{74}\text{N}_{16}\text{O}_2\text{Ti}_1$, $M = 1435.50$ g/mol): *find.* (*cal.*): C: 69.36% (73.63%), H: 5.19% (5.20%), N: 14.10% (15.61%).

7.21.8 Synthesis of New Catechol Substituted Titanylphthalocyanines



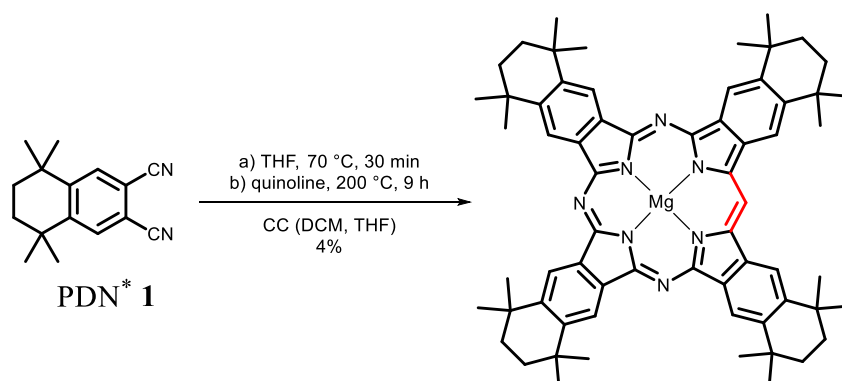
Similar to literature analogues, compare to section 7.21.6.^[25] The reaction was carried out on ^1H NMR scale.

[Pc*TiCat^{vinyl}Tp]: **Yield:** 72%. - ^1H NMR (CD_2Cl_2 , 300 MHz): $\delta = 9.66$ (s, 8 H, $^{Pc}\text{Ar-CH}$), 7.00* (dd, 1 H, $^4J_{\text{H-H}} = 1.0$ Hz, $^3J_{\text{H-H}} = 5.1$ Hz, Ar-CH), 6.67 (s, 1 H, $^{\text{vinyl}}\text{CHCO}_2\text{Et}$), 6.61* (dd, 1 H, $^3J_{\text{H-H}} = 3.5$ Hz, $^3J_{\text{H-H}} = 5.0$ Hz, Ar-CH), 6.32* (dd, 1 H, $^4J_{\text{H-H}} = 0.9$ Hz, $^3J_{\text{H-H}} = 3.4$ Hz, Ar-CH), 5.44 (dd, 1 H, $^4J_{\text{H-H}} = 1.5$ Hz, $^3J_{\text{H-H}} = 8.4$ Hz, Ar-CH), 4.45 (d, 1 H, $^4J_{\text{H-H}} = 1.6$ Hz, Ar-CH), 4.40 (d, 1 H, $^3J_{\text{H-H}} = 8.4$ Hz, Ar-CH), 3.95 (q, 2 H, $^3J_{\text{H-H}} = 7.1$ Hz, $^{-\text{Et}}\text{CH}_2$), 2.07 (s, 16 H, $^{-Pc}\text{CH}_2$), 1.84 (s, 24 H, $^{-Pc}\text{CH}_3$), 1.78 (s, 24 H, $^{-Pc}\text{CH}_3$), 1.05 (t, 3 H, $^3J_{\text{H-H}} = 7.1$ Hz, $^{-\text{Et}}\text{CH}_3$) ppm. - **UV-Vis** (DCM): $\lambda = 717$ (s), 650 (s), 297 (s), 243 (s) nm. - **MS** (MALDI-ToF(+)): $m/z = 1289.589$ $[\text{M}+\text{H}]^+$. - **MS** (APCI-HRMS(+)): $m/z = 1289.5863$ $[\text{M}+\text{H}]^+$, *cal.* for $\text{C}_{79}\text{H}_{84}\text{N}_8\text{O}_4\text{S}_1\text{Ti}_1+\text{H}_1$: 1289.5898.

*could not be assigned for certain.

7.22 Synthesis of Tetrabenzotriazaporphyrins (TBTAP)

7.22.1 Synthesis of [TBTAP**Mg*]



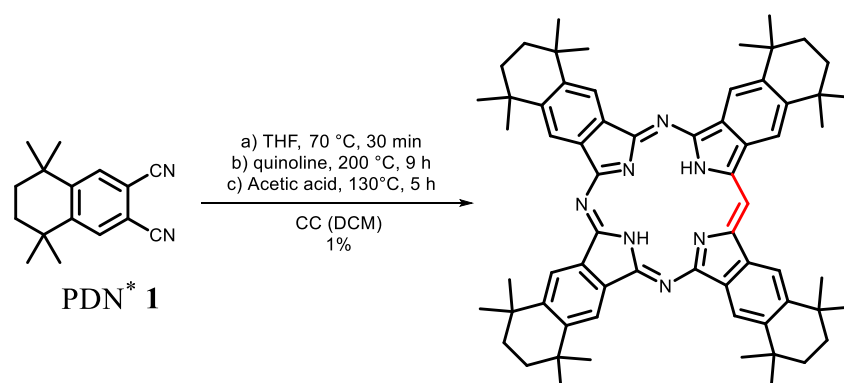
247 mg PDN* (1.04 mmol, 1 eq) were dissolved in 3 mL dry THF. The mixture was warmed to 70 °C and 0.9 mL MeMgBr solution (2.2 M in DEE, 2.1 mmol, 2 eq) were added at once. After 30 min, the solution was cooled to rt, 3 mL quinoline were added and the mixture was stirred in a preheated oilbath at 200 °C, overnight. The product was purified by CC (DCM, then THF).

Yield: 10 mg, 10.5 μmol , 4%. - **$^1\text{H NMR}$** (C_6D_6 , 300 MHz): $\delta = 10.78$ (s, 1 H, $\text{C}^{\text{meso}}\text{CH}$), 9.73 (bs, 4 H, Ar-CH), 9.46 (bs, 2 H, Ar-CH), 1.90 (s, 8 H, - CH_2), 1.87 (s, 8 H, - CH_2), 1.59-1.38 (m, 48 H, - CH_3) ppm. - **UV-Vis** (DCM): $\lambda = 691$ (s), 643 (w, sh), 354 (s), 294 (s) nm. - **Fluorescence** (DCM, $\lambda_{\text{ex}} = 350$ nm): $\lambda = 693$ nm. - **MS** (APCI-HRMS(+)): $m/z = 976.5851$ $[\text{M}+\text{H}]^+$, cal. for $\text{C}_{65}\text{H}_{73}\text{Mg}_1\text{N}_7+\text{H}_1$: 976.5851.

Additional information: [TBTAP**Mg*] was obtained in low yields. Similar to $\text{N}_x\text{-[Pc}^*\text{M]}$, a separation of demetallated TBTAP* H_2 appears much easier.

Experimental Section

7.22.2 Synthesis of TBTAP*H₂

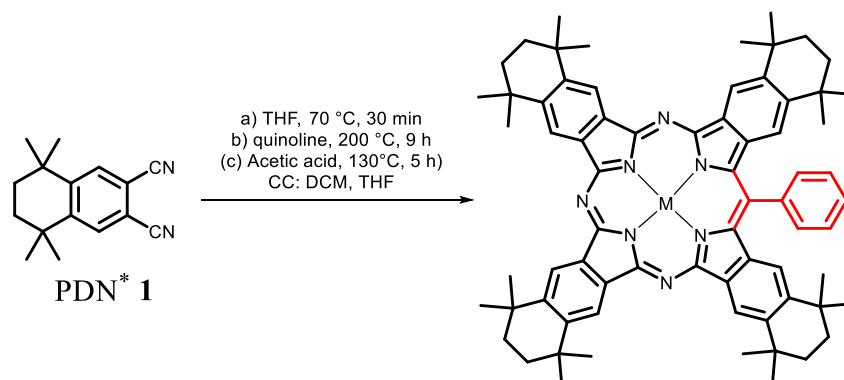


250 mg PDN* (1.05 mmol, 1 eq) were dissolved in 3 mL dry THF. The mixture was heated up to 70 °C and 1.5 mL MeMgBr (2.2 M in DEE, 3.30 mmol, 3.2 eq) were added at once. After 1 h, the solution was cooled to rt, the solvent was removed in vacuum and 3 mL dry quinoline were added. The solution was stirred in a preheated oilbath at 200 °C, overnight. The conversion to TBTAP was monitored by TLC (DCM). After cooling down to rt, 4 mL glacial acid were added and the solution was stirred for another 1 h, at 130 °C. The product was purified by CC (DCM).

TBTAP*H₂: Yield: <1%. - *R_f* (DCM) = 0.67. - ¹H NMR (C₆D₆, 300 MHz): δ = 10.75 (s, 1 H, -CH^{meso}), 10.03 (s, 2 H, Ar-CH), 9.97 (s, 2 H, Ar-CH), 9.96 (s, 2 H, Ar-CH), 9.39 (s, 2 H, Ar-CH), 1.83 (s, 8 H, -CH₂), 1.80 (s, 8 H, -CH₂), 1.60-1.53 (m, 48 H, -CH₃), -0.12 (s, 2 H, -NH) ppm. - UV-Vis (DCM): λ = 701 (s), 661 (s), 631 (sh), 606 (sh), 387 (s), 351 (s), 290 (s) nm. - MS (APCI-HRMS(+)): *m/z* = 954.6153 [M+H]⁺, cal. for C₆₅H₇₅N₇+H₁: 954.6157.

TBDAP*H₂: Yield: <1%. - MS(APCI-HRMS(+)): *m/z* = 953.6196 [M+H]⁺, cal. for C₆₄H₇₆N₆+H₁: 953.6204.

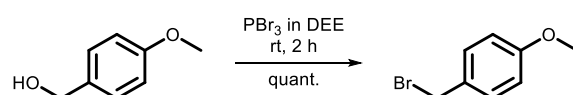
TBMAP*H₂: Yield: <1%. - MS(APCI-HRMS(+)): *m/z* = 952.6252 [M+H]⁺, cal. for C₆₃H₇₇N₅+H₁: 952.6252.

7.22.3 Attempt to Synthesise [TBTAP**M*]^{Ph}

250 mg PDN* (1.05 mmol, 1 eq) were dissolved in 3 mL THF and then 0.5 mL ArMgBr (3.0 M in DEE, 2.10 mmol, 2 eq) were added. The solution was stirred for 1 h at 70 °C. After cooling down to rt, the red solution was concentrated. The obtained red powder was dissolved in 3 mL quinoline and was warmed to 160 °C in a preheated oil bath. The solution was stirred for 5 h. The solvent was evaporated again, 10 mL glacial acid were added and then the mixture was stirred for another 3 h at 120 °C. The glacial acid was removed and the crude product was added onto silica and purified by CC (DCM).*

[TBTAP*Mg]^{Ph}: **Yield:** <1%. - **MS** (APCI-HRMS(+)): $m/z = 1052.6168$ [M+H]⁺, cal. for C₇₁H₇₇Mg₁N₇+H₁: 1052.6164. *obtained as a mixture of isomers.

[TBDAP*Mg]^{Ph}: **MS** (APCI-HRMS(+)): $m/z = 1127.6532$ [M+H]⁺, cal. for C₇₈H₈₂Mg₁N₆+H₁: 1127.6524.

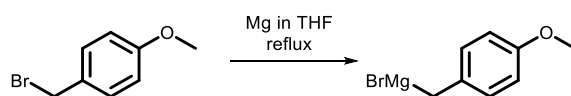
7.22.4 Synthesis of [TBTAP*M]^{PhOMe} and Precursors7.22.4.1 Synthesis of 1-(Bromomethyl)-4-methoxybenzene ^[288]

12.8 g PBr₃ (4.0 mL, 434 mmol, 0.6 eq) were dissolved in 40 mL DEE. To the solution, 9.75 g alcohol (70.0 mmol, 1 eq) were added within 1 h and the solution was allowed to stir over 48 h. The product was purified by extractive workup.

Yield: 14.2 g, 70.5 mmol, quant. - **¹H NMR** (CDCl₃, 300 MHz): $\delta = 7.35$ (d, ³J_{H-H} = 8.7 Hz, 2 H, Ar-CH), 6.89 (d, ³J_{H-H} = 8.7 Hz, 2 H, Ar-CH), 4.51 (s, 2 H, -CH₂), 3.81 (s, 3 H, -OCH₃) ppm.

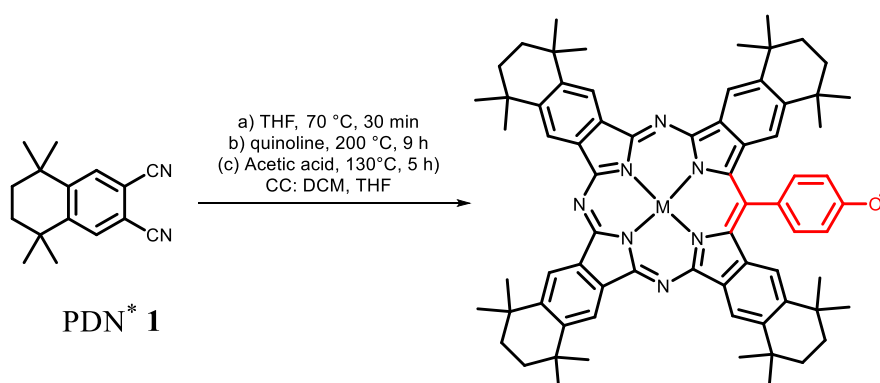
Experimental Section

7.22.4.2 Synthesis of the GRIGNARD reagent of 1-(Bromomethyl)-4-methoxybenzene



Mg was freshly prepared with TMSCl and *i*PrOH in THF. After filtration under inert atmosphere and washing with THF, 1.06 g Mg were weighed out. 50 mL THF were added, and then dropwise 9.65 g 1-(bromomethyl)-4-methoxybenzene (48.0 mmol, 1 eq) in 10 mL THF, while the solution was kept decent boiling. After completed addition, the reaction mixture was titrated to obtain a 1 M solution.

7.22.4.3 Attempt to Synthesise [TBTAP**M*]^{PhOMe}



202 mg PDN* (0.85 mmol, 1 eq) were dissolved in 2 mL of a freshly prepared GRIGNARD solution (1.5 N in THF, 3 mmol, 4 eq). The solution was stirred at 70 °C for 30 min before removing the solvent under reduced pressure. The reddish solid was dissolved in 3 mL quinoline and was stirred for at 180 °C 24 h.

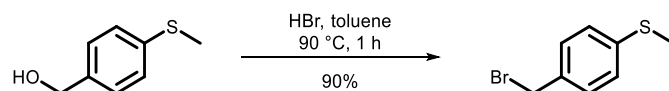
[TBTAP**Mg*]^{PhOMe}: UV-Vis (DCM): $\lambda = 695$ (s), 673 (sh), 624 (ss), 351 (s), 294 (s) nm.

After cooling down to rt, 5 mL glacial acetic acid were added and the solution was stirred for another 5 h at 120 °C. The solvent was evaporated and the crude product was first purified over a filter column to remove the quinoline and then by CC (MeCN /DCM 100:0 \rightarrow 50:50). The product was obtained as a mixture Pc^*H_2 /[TBTAP**H*]^{PhOMe} in a 3:1 ratio.

Yield: <1%. - ¹H NMR (C₆D₆, 300 MHz): $\delta = 10.06$ (s, 4 H, Ar-CH), 9.95 (s, 4 H, Ar-CH), 7.95 (d, 1 H, -CH^{PhOMe}), 7.38 (d, 1 H, -CH^{PhOMe}), 6.79 (d, 1 H, -CH^{PhOMe}), 6.71 (d, 1 H, -CH^{PhOMe}), 3.72 (s, 3 H, -OCH₃), 1.61 (s, 8 H, -CH₂), 1.60 (s, 8 H, -CH₂), 1.37 (s, 24 H, -CH₃), 1.31 (s, 24 H, -CH₃), 0.70 (s, 2 H, -NH) ppm. - UV-Vis (DCM): $\lambda = 709$ (s), 677 (s), 647 (sh),

613 (sh), 343 (s), 294 (s) nm. - **MS** (APCI-HRMS(+)): $m/z = 1060.6572$ $[M+H]^+$, cal. for $C_{72}H_{81}N_7O_1+H_1$: 1060.6575.

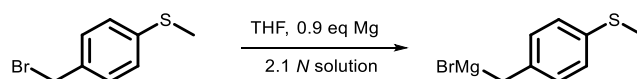
7.22.4.4 Synthesis of 4-(Thiomethyl)benzylbromide



4.03 g 4-thiomethylbenzylalcohol (26.1 mmol, 1 eq) were dissolved in 50 mL toluene. 8 mL HBr (p.a., 47% in water) were added and warmed up to 90 °C for 1 h. The yellowish solution became clear within 20 min. After cooling down to rt, the solution was washed with 2 x 20 mL water, dried over $MgSO_4$ and filtered. The organic phase was concentrated in vacuum.

Yield: 5.10 g, 23.5 mmol, 90%. - 1H NMR ($CDCl_3$, 300 MHz): $\delta = 7.32$ (d, 2 H, Ar-CH), 7.22 (d, 2 H, Ar-CH), 4.48 (s, 2 H, $-CH_2$), 2.48 (s, 3 H, $-SCH_3$) ppm.

7.22.4.5 Synthesis of the GRIGNARD of 4-(Thiomethyl)benzylmagnesiumbromide



The synthesis was carried out according to the procedure described in section 7.22.4.2. A 2.1 M GRIGNARD solution in THF was obtained.

7.22.4.6 Attempt to Synthesis $[TBTAP^*M]^{PhSMe}$

The reaction was carried out according to the procedures described before, in section 7.22.2 (p. 302). Traces of a Pc could neither be detected in UV-Vis nor in MS spectroscopy.

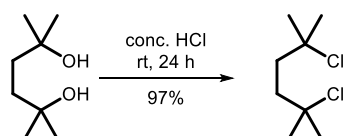
7.22.4.7 Attempt to Synthesis $[TBTAP^*M]^I$

The reaction was carried out according to the procedures described before, in section 7.22.2 (p. 302). A $IArMgCl$ GRIGNARD reagent was used. Traces of a Pc could neither be detected in UV-Vis nor in MS spectroscopy.

7.23 Synthesis of Precursors for a Selective Synthesis of TBTAP*

The synthesis of a precursor for a selective synthesis of a TBTAP* was carried out within the bachelor thesis of PFAFF.^[199]

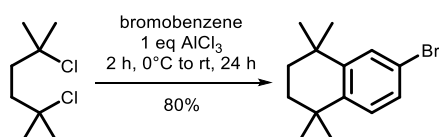
7.23.1 Synthesis of 2,5-Dichloro-2,5-dimethylhexane



The synthesis was carried out according to a literature known procedure.^[24] 22.4 g 2,5-dihydroxy-2,5-dimethylhexane (0.15 mol, 1 eq) were dissolved in 300 mL conc. hydrogen chloride. The solution was stirred overnight at rt. The pinkish solid was filtered, washed with water until the solution became neutral and a white solid was obtained. The solid was dried in vacuum.

Yield: 27.2 g, 0.15 mmol, 97%. - ¹H NMR (CDCl₃, 300 MHz) δ = 1.95 (s, 4 H, -CH₂), 1.60 (s, 12H, -CH₃) ppm.

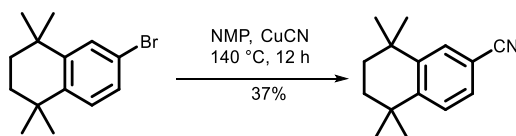
7.23.2 Synthesis of 6-Bromo-1,1,4,4-tetramethyltetralin



The synthesis was carried out in accordance with a literature known procedure.^[199] 2.50 g 2,5-dichloro-2,5-dimethylhexane (13.7 mmol, 1 eq) were dissolved in 20 mL hexane with 1.6 mL bromobenzene (2.40 g, 15 mmol, 1.1 eq), at 0 °C. Slowly 1.8 g AlCl₃ (13.7 mmol, 1.0 eq) were added portionwise while holding the temperature constant. HCl_{gas} evolved. After stirring overnight, slowly 10 mL water were added and the solution was purified with 20 mL 3% aq. HCl, 10 mL water, and 20 mL sat. Na₂CO₃. The organic phase was dried over MgSO₄ and the yellow solution was concentrated and dried in vacuum. A yellow solid was obtained.

Yield: 2.91 g, 10.9 mmol, 80%. - *R_f* (PE/DCM 20:1) = 0.7. - ¹H NMR (CDCl₃, 300 MHz) δ = 7.43 (d, ³J_{H-H} = 2.0, 1 H, Ar-CH), 7.23 (d, ³J_{H-H} = 2.1, 1 H, Ar-CH), 7.43 (s, 1 H, Ar-CH), 1.68 (s, 4 H, CH₂), 1.28 (s, 12 H, CH₃) ppm.

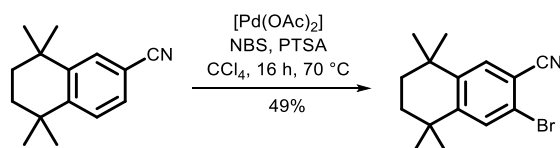
7.23.3 Synthesis of 6-Cyano-1,1,4,4-tetramethyltetralin



The synthesis was carried out according to a literature known procedure.^[199] 9.62 g 1,2,3,4-tetrahydro-1,1,4,4-methyl-6-bromonaphthaline (36.0 mmol, 1 eq) were dissolved in 40 mL NMP. 9.72 g CuCN (109 mmol, 3 eq) were added portionwise. The mixture was stirred at 140 °C, overnight. After cooling down to rt, 400 mL water were added and the residue was filtered and the precipitated powder was collected with EA. The organic phase was separated, washed with water and NaHCO₃ solution and finally dried over MgSO₄. The solvent was removed under reduced pressure and the obtained solid was dried in vacuum. The crude product was purified by CC (DCM/PE 1:1). The product was obtained in the form of a yellow solid.

Yield: 2.81 g, 12.2 mmol, 37%. - *R_f* (DCM/PE 1:1) = 0.9. - ¹H NMR (CDCl₃, 300 MHz): δ = 7.59 (m, 1 H, Ar-CH), 7.38 (d, 2 H, ³J_{H-H} = 1.1 Hz, Ar-CH), 1.69 (s, 4 H, -CH₂), 1.28 (s, 12 H, -CH₃) ppm.

7.23.4 Synthesis of 5-Bromine-6-cyano-1,1,4,4-tetramethyltetralin



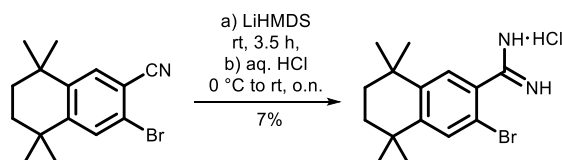
The synthesis was carried out according to a procedure reported by SUN.^[289] 2.14 g 5,5,8,8-tetramethyl-5,6,7,8-tetrahydronaphthalin-2-carbonitrile (10.0 mmol, 1 eq), 1.96 mg NBS (11.0 mmol, 1.1 eq), 951 PTSA (5.0 mmol, 0.5 eq) and 122 mg [Pd(OAc)₂] (0.5 mmol, 0.1 eq) were dissolved in 50 mL CCl₄ and were stirred at 70 °C for 48 h. The solvent was removed under reduced pressure and the resulting brownish powder was dried in vacuum. The product was purified by CC (PE/EE 5:1).

Yield: 1.45 g, 4.96 mmol, 49%. - ¹H NMR (CDCl₃, 300 MHz): δ = 7.57 (s, 1 H, Ar-CH), 7.55 (s, 1 H, Ar-CH), 1.68 (s, 4 H, -CH₂), 1.28 (s, 6 H, -CH₃), 1.26 (s, 6 H, -CH₃) ppm. - ¹H NMR (DMSO-*d*₆, 300 MHz): δ = 7.94 (s, 1 H, Ar-CH), 7.79 (s, 1 H, Ar-CH), 1.63 (s, 4 H, -CH₂), 1.24 (s, 6 H, -CH₃) ppm. - IR (ATR, 400-4000 cm⁻¹): $\tilde{\nu}$ = 2959 (s), 2924 (s), 2856 (m), 1590 (m), 1479 (s), 1460 (s), 1388 (m), 1364 (m), 1260 (s), 1081 (s), 1019 (s), 913 (w), 878 (w), 796 (s), 728 (w), 695 (w), 659 (w), 626 (w), 549 (w), 489 (m). - MS (ESI-HRMS(+)):

Experimental Section

$m/z = 314.0521$ $[M+Na]^+$, cal. for $C_{15}H_{18}Br_1N_1+Na_1$: 314.0515. - **Elemental analysis** ($C_{15}H_{18}N_1Br_1$, $M = 290.00$ g/mol): cal. (fnd.): C: 61.78% (61.65%), H: 6.32% (6.21%), N: 4.73% (4.79%).

7.23.5 Synthesis of 3-Bromo-5,5,8,8-tetramethyl-5,6,7,8-tetrahydronaphthalene-2-carboximidamide ^[199]

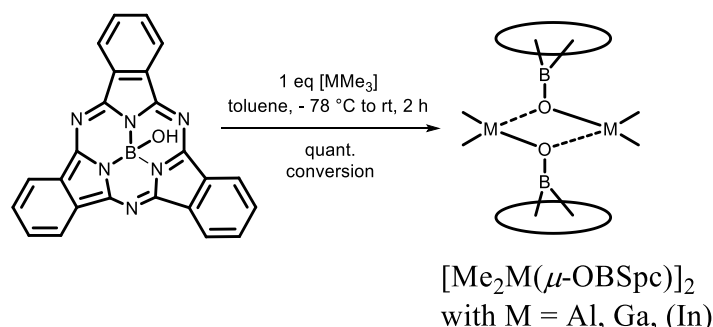


1.09 g 5-bromo-6-cyano-1,1,4,4-tetramethyltetralin (3.73 mmol, 1 eq) were dissolved in 10 mL THF. A ~1 M LiHMDS solution (0.69 g in 6 mL THF, 4.11 mmol, 1.1 eq) was added and the mixture was stirred for 3.5 h at rt. 0.25 mL 6 N HCl were added at 0 °C and the solution was stirred overnight. After recrystallization in the freezer at -20 °C, the product was obtained in the form of white snowflakes. The solvent was removed, and the resulting solid was washed with 5 mL cold DEE. The obtained white powder was dried in vacuum.

Yield: 90 mg, 0.26 mmol, 7%. - **¹H NMR** (DMSO-*d*₆, 300 MHz): $\delta = 9.60$ (bs, 2 H, -NH), 9.47 (bs, 2 H, -NH), 7.72 (s, 1 H, Ar-CH), 7.57 (s, 1 H, Ar-CH), 1.63 (s, 4 H, -CH₂), 1.25 (s, 6 H, -CH₃) ppm. - **IR** (ATR, 400-4000 cm⁻¹): $\tilde{\nu} = 3384$ (m), 3129 (s), 3038 (s), 2820 (m), 1996 (w), 1632 (s), 1400 (s), 1080 (w), 912 (w), 614.68 (m), 460 (s), 420 (s). - **MS** (APCI-HRMS(+)): $m/z = 309.0959$ $[M+H]^+$, cal. for $C_{15}H_{22}Br_1N_2+H_1$: 309.0961.

7.24 Synthesis of $[\text{Me}_2\text{M}(\mu\text{-OBSpc})]_2$ Complexes using $[\text{SpcBOH}]$

7.24.1 Synthesis of $[\text{Me}_2\text{Al}(\mu\text{-OBSpc})]_2$



General Procedure 9: Synthesis of Subphthalocyanine Metal Complexes.^[242]

0.23 mL AlMe_3 (1.1 M in toluene, 253 μmol , 1.0 eq) were added to 5 mL toluene and cooled to $-78\text{ }^\circ\text{C}$. 100 mg $[\text{SpcBOH}]$ (243 μmol , 1.0 eq) in 5 mL toluene were added dropwise. The solution was slowly warmed up to rt and was stirred for 2 h. A change in colour from blue to magenta could be observed. After removing the solvent in vacuum, the resulting solid was washed with DEE and finally dried in vacuum.

Conversion: quant. - **$^1\text{H NMR}$** (C_6D_6 , 300 MHz): $\delta = 8.76\text{-}8.79$ (m, 12 H, $-\text{CH}^a$), $7.34\text{-}7.37$ (m, 12 H, $-\text{CH}^b$), -1.20 (s, 12 H, $-\text{CH}_3$) ppm. - **IR** (ATR, $400\text{-}4000\text{ cm}^{-1}$): $\tilde{\nu} = 3057$ (w), 2922 (w), 1612 (w), 1456 (m), 1432 (m), 1386 (w), 1326 (m), 1287 (w), 1190 (m), 1130 (s), 1084 (m), 1040 (s), 909 (m), 812 (w), 764 (m), 693 (vs), 612 (m), 570 (m), 504 (m), 468 (w), 436 (w) cm^{-1} . - **UV-Vis** (toluene): $\lambda = 561$ (s), 545 (sh), 303 (bs) nm. - **Fluorescence** (toluene, $\lambda_{\text{ex}} = 500\text{ nm}$): $\lambda = 572\text{ nm}$. - **MS** (MALDI-ToF(+)): $m/z = 881.638$ $[\text{M-Me}_4]^+$; $m/z = 864.610$ $[\text{M-Me}]^+$ (100%). - **Elemental analysis:** ($\text{C}_{52}\text{H}_{36}\text{Al}_2\text{B}_2\text{N}_{12}\text{O}_2$, 936.5 g/mol): *find.* (*cal.*): C: 66.98% (66.69%), H: 4.51% (3.87%), N: 14.37% (17.95%).

7.24.2 Synthesis of $[\text{Me}_2\text{Ga}(\mu\text{-OBSpc})]_2$

According to General Procedure 9 (p. 309).

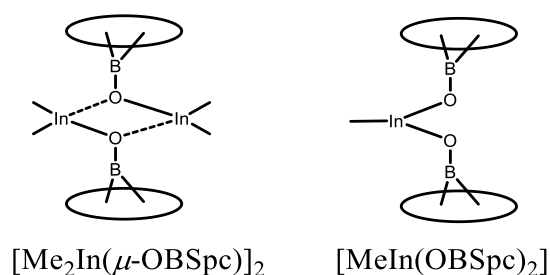
Conversion: quant. - **$^1\text{H NMR}$** (C_6D_6 , 300 MHz): $\delta = 8.78\text{-}8.75$ (m, 6 H, $-\text{CH}^a$), $7.39\text{-}7.36$ (m, 6 H, $-\text{CH}^b$), -0.56 (s, 6 H, Ga- CH_3) ppm. - **UV-Vis** (DCM): $\lambda = 560$ (s), 303 (s), 266 (s) nm. - **Fluorescence** (DCM, $\lambda_{\text{ex}} = 350\text{ nm}$): $\lambda = 576\text{ nm}$. - **MS** (MALDI-ToF(+)): $m/z = 1008.736$ $[\text{M-Me}]^+$ (100%); $[\text{C}_{50}\text{H}_{30}\text{B}_2\text{Ga}_1\text{N}_{12}\text{O}_1]^+$: $m/z = 906.367$ $[\text{M-Me}]^+$.

7.24.3 Attempt to Synthesis $[\text{Me}_2\text{In}(\mu\text{-OBSpc})]_2$

According to General Procedure 9 (p. 309). A mixture of $[\text{Me}_2\text{In}(\mu\text{-OBSpc})]_2$ and $[\text{MeIn}(\text{OBSpc})_2]$ was obtained (proposed structures are shown below).

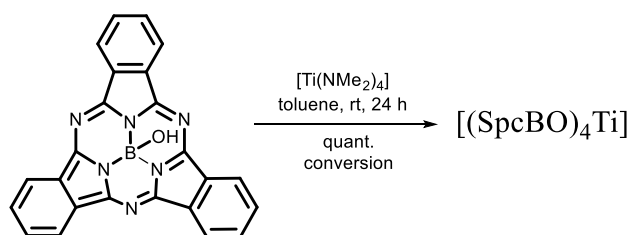
$[\text{Me}_2\text{In}(\mu\text{-OBSpc})]_2$: $^1\text{H NMR}$ (C_6D_6 , 300 MHz): $\delta = 8.81\text{-}8.79$ (m, 6 H, $-\text{CH}^\alpha$), $7.41\text{-}7.37$ (m, 6 H, $-\text{CH}^\beta$), -0.53 (s, 6 H, In-CH_3) ppm. - **MS** (MALDI-ToF(+)): $m/z = 1097.198$ $[\text{M-Me}]^+$, 1070.653 $[\text{M-Me}_3]^+$.

$[\text{MeIn}(\text{OBSpc})_2]$: $^1\text{H NMR}$ (C_6D_6 , 300 MHz): $\delta = 8.60\text{-}8.54$ (m, 6 H, $-\text{CH}^\alpha$), $7.29\text{-}7.27$ (m, 6 H, $-\text{CH}^\beta$), -1.20 (s, 6 H, In-CH_3) ppm. - **MS** (MALDI-ToF(+)): $m/z = 1494.212$ $[\text{M-Me}]^+$.



Additional information: In $^1\text{H NMR}$ spectroscopy, the products can be differentiated by chemical shifts and integrals of $-\text{CH}_3$.

7.24.4 Synthesis of $[(\text{SpcBO})_4\text{Ti}]^{[242]}$

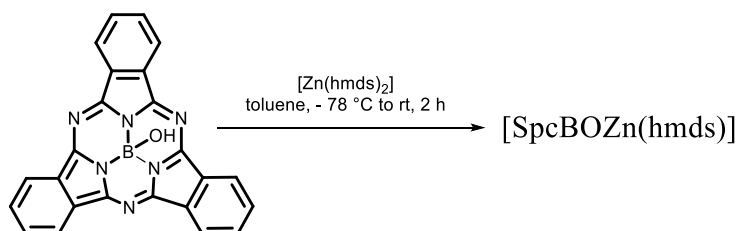


Modification to General Procedure 9 (p. 309): 0.03 mL $[\text{Ti}(\text{NMe}_2)_4]$ (143 μmol , 1.0 eq) were dissolved in 10 mL toluene and added dropwise to a solution of 220 mg $[\text{SpcBOH}]$ (534 μmol , 3.7 eq) in 15 mL toluene, at rt. The mixture was stirred for 5 h. After removing the solvent under reduced pressure, the resulting powder was washed with DEE and finally dried in vacuum.

Conversion: quant. - $^1\text{H NMR}$ (C_6D_6 , 300 MHz): $\delta = 8.79\text{-}8.82$ (m, 6 H, $-\text{CH}^\alpha$), $7.36\text{-}7.40$ (m, 6 H, $-\text{CH}^\beta$) ppm. - $^{13}\text{C NMR}$ (C_6D_6 , 75 MHz): $\delta = 151.1, 132.1, 129.3, 122.1$ ppm. – not all quaternary carbons were detected. - **IR** (ATR, $400\text{-}4000$ cm^{-1}): $\tilde{\nu} = 2962$ (m), 2905 (w), 2850 (w), 2816 (w), 2775 (w), 1635 (m), 1600 (m), 1457 (m), 1432 (m), 1286 (s), 1176 (w),

1156 (w), 1082 (s), 1014 (vs), 867 (vw), 794 (vs), 753 (s), 727 (m), 695 (m), 569 (m), 500 (m) cm^{-1} . - **UV-Vis** (toluene): $\lambda = 561$ (s), 524 (sh), 299 (m). - **Fluorescence** (toluene, $\lambda_{\text{ex}} = 530$ nm): $\lambda = 570$ nm. - **MS** (MALDI-ToF(+)): $m/z = 1693.420$ $[\text{M}+\text{H}]^+$.

7.24.5 Synthesis of [SpcBOZnhmnds]

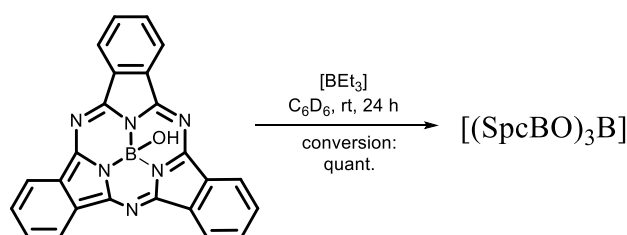


According to General Procedure 9 (p. 309), using [SpcBOH] and $[\text{Zn}(\text{hmnds})_2]$ in a 1:1 ratio.

Conversion: quant. - ^1H NMR (C_6D_6 , 300 MHz): $\delta = 8.84$ - 8.87 (m, 6 H, $-\text{CH}^\alpha$), 7.41 - 7.44 (m, 18 H, $-\text{CH}^\beta$), 0.20 (s, 6 H, $-\text{CH}_3^{\text{hmnds}}$) ppm. - ^{11}B NMR (C_6D_6 , 128 MHz): $\delta = -14.9$ (s), -15.4 (s) ppm. - **UV-Vis** (DCM): $\lambda = 561$ (s), 301 (s), 269 (s) nm. - **MS** (MALDI-ToF(+)): $m/z = 636.886$ $[\text{M}+\text{H}]^+$.

Additional information: In mass spectroscopy and ^{11}B NMR spectroscopy, also $[(\text{SpcBO})_2\text{Zn}]$ was observed: **MS** (MALDI-ToF(+)): $m/z = 886.389$ $[\text{M}]^+$.

7.24.6 Synthesis of $[(\text{SpcBO})_3\text{B}]$



According to General Procedure 9 (p. 309). The synthesis was carried out on NMR scale. 1 eq BEt_3 was dissolved in 5 mL C_6D_6 . Portionwise, a [SpcBOH] solution (3 eq, 1 mL, 2 mL) in C_6D_6 was added. The reaction was monitored by ^1H NMR spectroscopy. The formation of $[\text{SpcBOBEt}_2]$ to $[(\text{SpcBO})_2\text{BEt}]$ and the final desired $[(\text{SpcBO})_3\text{B}]$ could be observed.

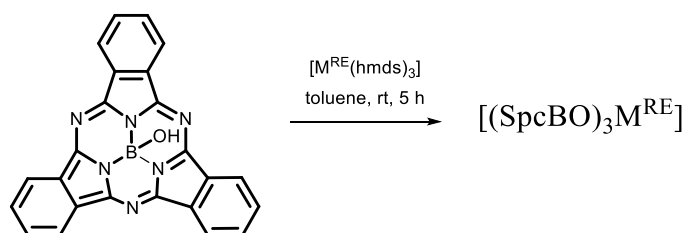
$[(\text{SpcBO})_3\text{B}]$: **Conversion:** quant. - ^1H NMR (C_6D_6 , 300 MHz): $\delta = 8.78$ - 8.72 (m, 12 H, $-\text{CH}^\alpha$), 7.45 - 7.37 (m, 12 H, $-\text{CH}^\beta$) ppm. - **UV-Vis** (DCM): $\lambda = 560$ (s), 524 (sh), 300 (s), 270 (s) nm. - **MS** (MALDI-ToF(+)): $m/z = 1244.528$ $[\text{M}]^+$.

Experimental Section

By-product: (not isolated, observed in NMR experiment)

[(SpcBO)₂BEt]: ¹H NMR (300 MHz, C₆D₆): δ = 8.76-8.73 (m, 12 H, -CH^α), 7.44-7.41 (m, 12 H, -CH^β), -0.29 (t, 3 H, ³J_{H-H} = 7.7 Hz, -CH₃), -1.28 (q, 2 H, ³J_{H-H} = 7.6 Hz, -CH₂) ppm. - **MS** (MALDI-ToF(+)): m/z = 862.378 [M]⁺.

7.24.7 Attempts to Synthesise [(SpcBO)₃M^{RE}]



100 mg [SpcBOH] (243 μmol, 3.0 eq) were dissolved in 5 mL toluene and cooled to 0 °C. 3.1 eq [M^{RE}(hmnds)₃] were dissolved in 5 mL toluene and added very slowly. A change in colour to deep blue was observed. After 5 h, the solution was warmed up to rt, the solvent was evaporated in vacuum and the resulting solid was washed with dry DEE 3 x 10 mL. The solid was dried in vacuum. In all reactions, a weak shift of the aromatic protons of [SpcBOH] was observed, and a weak shift of the Q-band in UV-Vis spectroscopy. Attempts at crystallisation from different solvents were unsuccessful.

7.24.7.1 Attempt to Synthesise [(SpcBO)₃Y]

According to General Procedure 9 (p. 309).

Conversion: quant. - ¹H NMR (C₆D₆, 300 MHz): δ = 8.69-8.72 (m, 6 H, -CH^α), 7.34-7.37 (m, 6 H, -CH^β), ppm. - **IR** (ATR, 400-4000 cm⁻¹): $\tilde{\nu}$ = 3309 (w), 3055 (w), 2949 (w), 2323 (vw), 2114 (vw), 1611 (m), 1454 (s), 1427 (m), 1224 (m), 1188 (s), 1125 (vs), 1066 (s), 949 (w), 838 (w), 734 (vs), 695 (s), 650 (m), 568 (m), 507 (w), 465 (vw), 435 (w) cm⁻¹. - **UV-Vis** (toluene): λ = 561 (s), 545 (sh), 303 (m) nm. - **Fluorescence** (toluene, λ_{ex} = 470 nm): λ = 578 nm. - **Elemental analysis:** (C₇₂H₃₇B₃N₁₈O₃Y₁, 1322.50 g/mol): fnd. (cal.): C 63.67% (65.39%), H 3.66% (2.74%), N 16.21% (19.06%).

7.24.7.2 Attempt to Synthesise [(SpcBO)₃Ce]

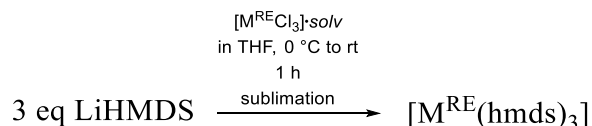
According to General Procedure 9 (p. 309). The synthesis was carried out on NMR scale.

100 mg [SpcBOH] (243 μmol, 3.0 eq) were dissolved in 4 mL toluene and 51 mg [La(hmds)₃] (82 μmol, 3.0 eq) in 5 mL toluene and were added dropwise to the [SpcBOH] solution. The solution was stirred for 4 h at 40 °C. The solvent was removed in vacuum. The resulting green brown solid was washed with DEE and finally dried in vacuum. The complex could neither be identified using MALDI-ToF nor with UV-Vis spectroscopy. No shift of aromatic protons in the ¹H NMR spectrum was observed compared to [SpcBOH].

Yield: n. d. - ¹H NMR (C₆D₆, 300 MHz): δ = 8.59-8.75 (m, 6 H, -CH^α), 7.38-7.53 (m, 18 H, -CH^β), ppm. - ¹¹B NMR (C₆D₆, 128 MHz): δ = -14.7 (s, 1 B, [SpcBOH]), -17.3 (s, 2 B, B-OCe) ppm. - UV-Vis (DCM): λ = 560 (s), 305 (s), 251 (s) nm. - MS (MALDI-ToF(+)): [(SpcBO)₂Ce(hmds)]: m/z = 963.654 [M]⁺.*

*a mixture of [(SpcBO)₂Ce(hmds)] and [SpcBOH] was obtained.

7.25 Synthesis of Rare Earth Metal Phthalocyanines Sandwich-Complexes

7.25.1 General Procedure for Synthesis of [M^{RE}(hmds)₃]^[267-270]

1 eq [GdCl₃]·2*dme* was suspended in 20 mL THF and was cooled in an ice-bath to 0 °C. 3 eq LiHMDS were dissolved in 20 mL THF and added dropwise. The solution was stirred for 1 h at 0 °C before warming up to rt. After another 2 h, the solvent was removed under reduced pressure. The product was dissolved in 50 mL toluene, filtered over Celite[®] and finally washed with 2 x 20 mL toluene. After removing the solvent in vacuum, [Gd(hmds)₃]·*thf* was obtained in the form of a white solid. The product was sublimed in vacuum.

Yield: 34%.

7.26 Synthesis of Known Phthalocyanine Precursors

7.26.1 Synthesis of [PcK₂]

According to procedure described in section 7.26.3.^[25] The product was used without any further purification.

Yield: quant. - **Elemental analysis:** (C₃₂H₁₆K₂N₈, 590.73 g/mol): *find.* (*cal.*): C: 64.80% (65.06%), H: 4.60% (2.73%), N: 13.41% (18.97%).

7.26.2 Synthesis of [Pc*Na₂]

According to literature known procedure.^[25]

51 mg Pc*H₂ (53.4 μmol, 1 eq) were dissolved in 2 mL THF with 49 mg NaHMDS (267 μmol, 5 eq). The solution was stirred at 60 °C for 14 h. The solvent was removed in vacuum to obtain [Pc*Na₂] in the form of a dark blue powder.

Yield: quant. - **¹H NMR** (C₆D₆/drop THF-*d*₈, 300 MHz): δ = 9.42 (bs, 8 H, Ar-CH), 1.93 (s, 16 H, -CH₂), 1.69 (s, 48 H, -CH₃) ppm. - **UV-Vis** (DCM): λ = 686 (s), 345 (s), 288 (s) nm. - **MS** (APCI-HRMS(+)): *m/z* = 999.5752 [M+H]⁺, *cal.* for C₆₄H₇₂N₈Na₂+H₁: 999.5748.

7.26.3 Synthesis of [Pc*K₂]

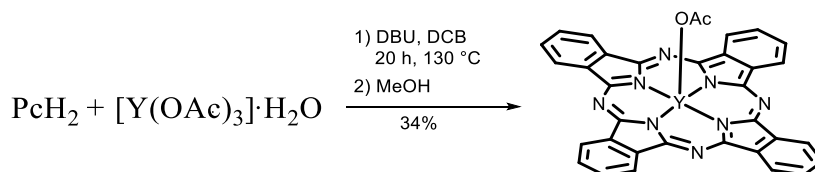
According to literature known procedure.^[25] 1.00 g Pc*H₂ (1.05 mmol, 1 eq) was dissolved in 30 mL THF. 0.27 g KBn (2.10 mmol, 2 eq) were dissolved in 30 mL THF and added dropwise. The solution was stirred overnight at rt. The solvent was removed in vacuum and the product was obtained in the form of a dark green powder.

Yield: 93%. - **¹H NMR** (C₆D₆, 300 MHz): δ = 9.75 (bs, 8 H, Ar-CH), 1.80 (s, 16 H, -CH₂), 1.51 (s, 48 H, -CH₃) ppm. - **UV-Vis** (DCM): λ = 683 (s), 345 (s), 277 (s) nm.

Additional information: Analysis was carried out before dissolving the product in 80 mL THF to get a 13.5 mg/mL solution for conversion to rare earth metal complexes. If necessary, the product was additionally purified by filtration under inert atmosphere.

7.27 Synthesis of Half-Sandwich-Complexes

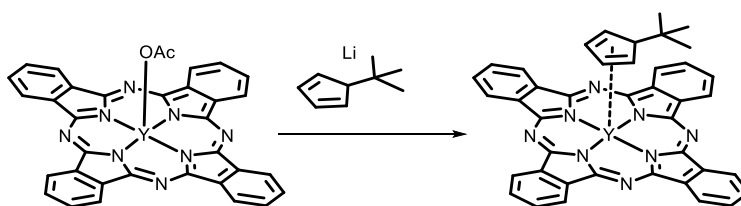
7.27.1 Synthesis von [PcYOAc] ^[256]



1.01 g PcH₂ (2.00 mmol, 1 eq), 0.78 g [Y(OAc)₃]·H₂O (2.92 mmol, 1.5 eq), and 0.7 mL DBU (4.69 mmol, 2.4 eq) were suspended in 10 mL DCB and then stirred for 20 h at 130 °C. After cooling down to rt, the solvent was removed in vacuum and the resulting dark blue powder was washed several times with MeOH. A dark blue powder was obtained, which was dried in vacuum.

Yield: 0.45 g, 0.68 mmol, 34%. - **IR** (ATR, 400-4000 cm⁻¹): $\tilde{\nu}$ = 3270 (w), 3012 (w), 2536 (w), 1967 (w), 1896 (w), 1823 (w), 1723 (w), 1646 (m), 1536 (m), 1498 (m), 1476 (m), 1456 (m), 1436 (m), 1333 (m), 1321 (m), 1301 (m), 1276 (m), 1187 (m), 1155 (m), 1116 (s), 1092 (s), 999 (s), 957 (m), 871 (s), 777 (s), 748 (s), 729 (s), 717 (s), 683 (m), 612 (m), 555 (m), 486 (w), 432 (m) cm⁻¹. - **UV-Vis** (CHCl₃): λ = 693 (m), 656 (m), 340 (s) nm. - **MS** (MALDI-ToF(+)): m/z = 661.652 [M+H]⁺. - **Elemental analysis** (C₃₄H₁₉N₈O₂Y₁, M = 660.47 g/mol): cal. (fnd.) C: 71.79% (61.83%), N: 20.44% (16.97%), H: 3.57% (2.90%).

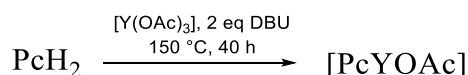
7.27.2 Synthesis of [PcYCp^{tBu}]



To 49 mg [PcYOAc]·dbu (61.6 μmol, 1 eq) were added 69 mg LiCp^{tBu} (538 μmol, 8.5 eq). The solids were suspended in toluene and stirred at 85 °C for 2 d. The product was washed with 3 x 20 mL DEE and finally dried in vacuum.

Yield: n. d. - **UV-Vis** (DCM): λ = 669 (s), 603 (sh), 375 (bs), 331 (bs), 247 (s) nm. - **MS** (MALDI-ToF(+)): m/z = 738.430 [M]⁺.

7.27.3 Synthesis of [PcYOAc] ^[199]



500 mg PcH₂ (0.97 mmol, 1 eq) and 390 mg [Y(OAc)₃]·H₂O (1.37 mmol, 1.5 eq) were dissolved in 1.45 mL DBU and 5 mL DCB. The mixture was stirred at 150 °C, for 40 h. The solution was filtered over a short silica column. The solvent was removed in vacuum, and the blue powder was washed with dry DEE. The product was obtained in the form of a blue solid.

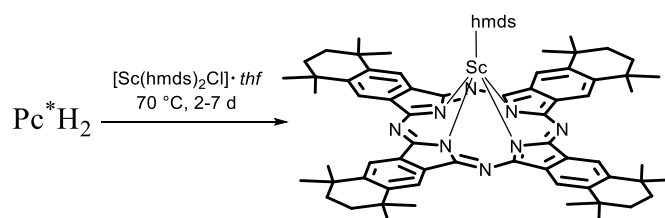
Yield: n. d. - **UV-Vis** (DBU): λ = 697 (s), 661 (s), 643 (sh), 632 (sh), 345 (s) nm. - **MS** (MALDI-ToF(+)): *m/z* = 660.608 [M]⁺.

[PcYOAc]·*dbu*: 52 mg [PcYOAc] were dissolved in 3 mL toluene. 0.3 mL DBU were added. The mixture was stirred at 120 °C, overnight. The solvent was removed in vacuum and the blue solid was washed with 3 x 20 mL DEE.

Yield: n. d. - **¹H NMR** (CD₂Cl₂, 300 MHz): δ = 9.49 (m, 8 H, Ar-CH^α), 8.17 (m, 8 H, Ar-CH^β), 1.26 (s, 3 H, -OAc), 3.21-1.26 (dbu-multiplett) ppm. - **¹H NMR** (Toluene-*d*₈, 300 MHz): δ = 9.56 (m, 8 H, Ar-CH^{non-peri}), 7.86 (m, 8 H, Ar-CH^{peri}), 0.45 (s, 2 H, dbu-CH₂), 0.33 (s, 2 H, dbu-CH₂), 0.27 (s, 2 H, dbu-CH₂), 0.22 (s, 2 H, dbu-CH₂), 0.18 (s, 2 H, dbu-CH₂), 0.17 (s, 2 H, dbu-CH₂), 0.11 (s, 2 H, dbu-CH₂), 0.06 (s, 2 H, dbu-CH₂) ppm. - **¹³C NMR** (CD₂Cl₂, 75 MHz): δ = 155.7, 139.1, 129.4, 123.0, 48.8, 40.4, 34.0, 29.7, 27.8, 25.1, 20.9 ppm. - **UV-Vis** (DBU): λ = 667 (s), 603 (sh), 379 (s) nm. - **UV-Vis** (DCM): λ = 669 (s), 607 (sh), 336 (bs), 252 (s) nm. - **MS** (MALDI-ToF(+)): *m/z* = 660.608 [M-*dbu*]⁺; 745.778 [M(-OAc)]⁺; 753.513 [M(-OAc)·*dbu*]⁺; 825.513 [M+CH]⁺.

7.28 Synthesis of New Soluble [Pc*^{M^{RE}}(R)]

7.28.1 Synthesis of [Pc*^{Sc}(hmds)]



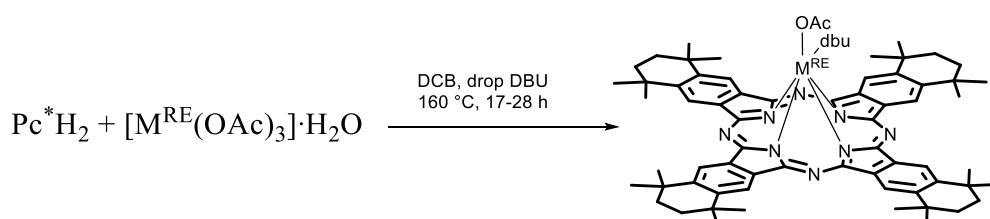
The synthesis was carried out on ¹H NMR scale: 1 eq Pc*H₂ was dissolved in 2 mL C₆D₆. 1.05 eq [Sc(hmds)₂Cl] were added and stirred at 70 °C up to 2 d. The reaction was monitored by ¹H NMR spectroscopy. After the reaction was completed, the solvent was removed in vacuum and the obtained greenish powder was analysed by MALDI-ToF under inert atmosphere.

Conversion: quant. - ¹H NMR (C₆D₆, 300 MHz): δ = 9.97 (s, 8 H, Ar-CH), 1.76 (s, 16 H, CH₂), 1.55 (s, 24 H, CH₃), 1.50 (s, 24 H, CH₃), -1.39 (s, 18 H, SiCH₃) ppm. - MS (MALDI-ToF(+)): m/z = 1152.180 [M+H]⁺.

Additional information: The reaction can be monitored by the splitting of the methyl groups and the low-field shift of the aromatic protons. The reaction was also attempted by using [Pc*^K]₂ and [ScCl₃]. When shorter reaction times are used, [Pc*^{Sc}Cl] can be observed: - MS (MALDI-ToF(+)): m/z = 1031.984 [M-H]⁺.

7.28.2 New Half Sandwich-Complexes of [Pc*^{M^{RE}}(OAc)]·dbu type

The syntheses of half sandwich-complexes were carried out according to the procedures described by PUSHKAREV ET AL.^[257,290] The syntheses were carried out within the Bachelor-Thesis of SWOLANA.^[256]



General Procedure:

1 eq Pc*H₂, ~1.2 eq rare earth metal [M^{RE}(OAc)₃]·H₂O, and 2.2 eq DBU were suspended in 3 mL DCB and were stirred for 17 – 28 h at 160 °C. After cooling down to rt, the mixture was

Experimental Section

dried in vacuum and was washed with MeOH until the solution became clear. After a final filtration, the resulting blue powder was dried in vacuum.

7.28.2.1 Synthesis of [Pc*YOAc]·dbu

Method a) 100 mg Pc*H₂ (104 μmol, 1 eq), 65 mg [Y(OAc)₃]·H₂O (244 μmol, 2.3 eq). The product was obtained in the form of a light green powder.

Yield: 30 mg, 0.03 mmol, 26%. - **IR** (ATR, 400-4000 cm⁻¹): $\tilde{\nu}$ = 2963 (m), 2904 (m), 1560 (w), 1396 (w), 1260 (s), 1016 (s), 862 (m), 796 (s), 699 (m), 661 (m), 586 (m), 504 (m), 482 (m), 468 (m), 459 (m), 438 (m) cm⁻¹. - **UV-Vis** (DCM): λ = 691 (s), 622 (sh), 351 (s), 231 (s) nm. **Fluorescence** (DCM, λ_{ex} = 350 nm): λ = 706 nm. - **MS** (MALDI-ToF(+)): m/z = 1194.747 [M+H]⁺.

Method b) An alternative synthesis was carried out within the Bachelor-Thesis of PFAFF.^[199]

50 mg Pc*H₂ (52.3 μmol, 1 eq) and 20 mg [Y(OAc)₃]·H₂O (68.0 μmol, 1.3) were dissolved in 2 mL toluene and warmed up to 130 °C. After addition of 0.08 mL DBU, the reaction mixture was stirred for 24 h at 130 °C. After cooling down to rt, the solvent was removed in vacuum and the resulting blue solid was washed with DEE. The blue powder was finally dried in vacuum. A turquoise powder was obtained.

Yield: n.d. - **¹H NMR** (CD₂Cl₂, 300 MHz): δ = 9.45 (s, 8 H, Ar-CH), 2.34 (s, 3 H, OAc), 2.05 (bs, 16 H, CH₂), 1.83 (s, 24 H, CH₃), 1.82 (s, 24 H, CH₃) ppm. - **UV-Vis** (DCM): λ = 690 (s), 623 (sh), 350 (m), 246 (w) nm. - **MS** (MALDI-ToF(+)): m/z = 1195.857 [M -OAc +H]⁺, cal. for C₇₃H₈₉N₁₀Y⁺: 1194.633.

7.28.2.2 Synthesis of [Pc*GdOAc]·dbu

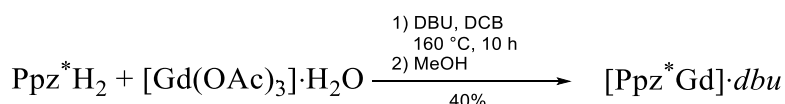
Following the General Procedure, section 7.28.2: 100 mg Pc*H₂ (104 μmol, 1 eq), 47 g [Gd(OAc)₃]·H₂O (156 μmol, 1.5 eq). The product was obtained in the form of a blue solid.

Yield: 2 mg, 1.71 μmol, 2%. - **UV-Vis** (DCM): λ = 696 (m), 628 (sh), 354 (m), 233 (s) nm. - **Fluorescence** (DCM, λ_{ex} = 350 nm): λ = 704 nm. - **MS** (MALDI-ToF(+)): m/z = 1263.738 [M+H]⁺. - Not enough product was obtained for full analysis.

7.28.2.3 Synthesis of [Pc**TbOAc*]*dbu*

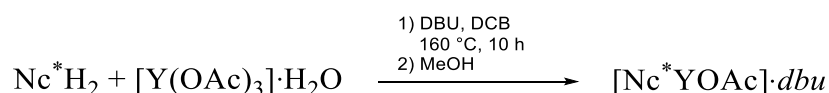
Following the General Procedure, section 7.28.2: 100 mg Pc*H₂ (104 μmol, 1 eq), 54 g [Tb(OAc)₃]*·*H₂O (156 mmol, 1.5 eq). The product was obtained in the form of a turquoise powder.

Yield: 61 mg, 52 μmol, 50%. - **IR** (ATR, 400-4000 cm⁻¹): $\tilde{\nu}$ = 2964 (w), 2361 (m), 2341 (m), 1261 (m), 1032 (s), 800 (s), 668 (w), 600 (m), 508 (m), 496 (m), 472 (m), 451 (m), 436 (m) cm⁻¹. - **UV-Vis** (DCM): λ = 690 (m), 348 (m) nm. - **Fluorescence** (DCM, λ_{ex} = 350 nm): λ = 714 nm. - **MS** (MALDI-ToF(+)): m/z = 1265.788 [M+H]⁺.

7.28.2.4 Synthesis of [Ppz**GdOAc*]*dbu*

100 mg Ppz*H₂ (104 μmol, 1 eq), 47 g [Gd(OAc)₃]*·*H₂O (156 μmol, 1.5 eq), and 0.04 mL DBU (0.30 mmol, 2 eq) were suspended in 4 mL DCB and heated to 160 °C for 10 h. After cooling down to rt, the solvent was removed in vacuum and the resulting light green powder washed with MeOH. The filtered product was dried in vacuum. [Ppz**GdOAc*]*dbu* was obtained in the form of a blue powder.

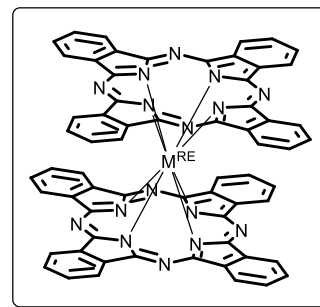
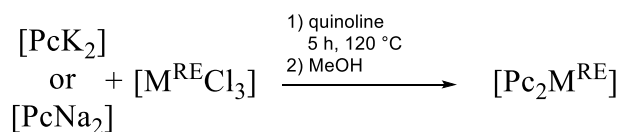
Yield: 49 mg, 41.6 μmol, 40%. - **IR** (ATR, 400-4000 cm⁻¹): $\tilde{\nu}$ = 2962 (w), 1259 (m), 1012 (s), 863 (w), 793 (m), 702 (w), 588 (m) 464 (w), 440 (w) cm⁻¹. - **UV-Vis** (DCM): λ = 646 (m), 628 (m), 297 (m), 238 (s) nm. - **Fluorescence** (DCM, λ_{ex} = 350 nm): λ = 699 nm. - **MS** (MALDI-ToF(+)): m/z = 1263.443 [M-DBU+DCB]⁺.

7.28.2.5 Synthesis of [Nc**YOAc*]*dbu*

Following the General Procedure, section 7.28.2: 100 mg Nc*H₂ (87.0 μmol, 1 eq), 35 mg [Y(OAc)₃]*·*H₂O (132 μmol, 1.7 eq), 0.13 mL DBU. The product was obtained in the form of a grey greenish powder.

Yield: n. d. - **UV-Vis** (DCM): λ = 777 (s), 695 (sh), 335 (m), 248 (m) nm. - **MS** (MALDI-ToF(+)): m/z = 1395.009 [M-OAc]⁺.

7.29 Synthesis of [Pc₂M^{RE}]

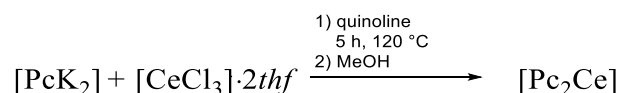


M^{RE} = rare earth metal

General Procedure 10: Synthesis of [Pc₂M^{RE}].

2 eq of [Pc^{*}M₂] with M= Na, K were dissolved with 1 eq [M^{RE}Cl₃] in quinoline and the mixture was stirred at 120 °C for 5 h. The solution was filtered under inert gas over Celite[®]. After oxidation in air, the double-decker sandwich-complexes could be observed. The obtained blue powders were washed with MeOH and finally dried in vacuum. The resulting blue powders were purified by CC.

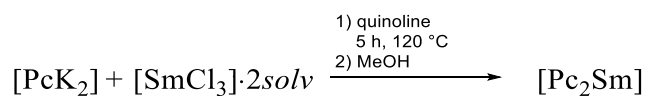
7.29.1 Synthesis of [Pc₂Ce]



According to General Procedure 10 (p. 320): [PcK₂], [CeCl₃]·2*thf* in CNP, 20 h, 180 °C.

Yield: n. d. - **MS** (APCI-HRMS(+)): *m/z* = 1166.46 [M+H]⁺.

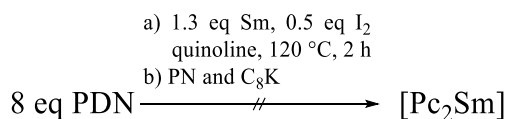
7.29.2 Synthesis of [Pc₂Sm]



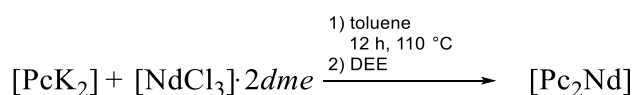
According to General Procedure 10 (p. 320): [PcK₂], [SmCl₃]·2*thf* or [SmCl₃]·2*dme* in CNP, 20 h, 180 °C.

Yield: n. d. - **UV-Vis** (DCM): λ = 642 (s), 338 (s), 292 (sh) nm. - **MS** (APCI-HRMS(+)): *m/z* = 1179.2302 [M+H]⁺, cal. for [C₆₄H₃₂N₁₆Sm₁+H]⁺: 1179.2299. - **MS** (MALDI-ToF(+)): *m/z* = 1178.436 [M]⁺.

Additional information: For verification of the formed sandwich-complex, the MALDI-ToF measurement was carried out using an internal standard.

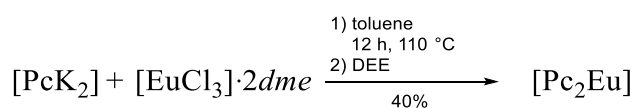
7.29.3 Attempt to Synthesise [Pc₂Sm] in a Neat Reaction

55 mg Sm (366 μmol , 1.3 eq) were added with 38 mg I₂ (150 μmol , 0.5 eq) in 2 mL quinoline. The solution was stirred for 1 h at 120 °C. A change in colour to dark violet was observed. After cooling down to rt, 42 mg C₈K (311 μmol , 1.1 eq) in 2 mL quinoline were added as well as 301 mg PDN (2.35 mmol, 8.3 eq). The solution was stirred for 16 h at 180 °C. After cooling down to rt, 10 mL pentane was added. The solvent was removed and the dark powder was washed several times with MeOH. Neither in UV-Vis nor in MS could [Pc₂Sm] be detected.

7.29.4 Synthesis of [Pc₂Nd]

According to General Procedure 10 (p. 320): [PcK₂], [NdCl₃]·2dme in CNP, 20 h, 180 °C.

Yield: n. d. - **UV-Vis** (DCM): $\lambda = 678$ (s), 654 (sh), 610 (sh), 326 (s), 284 (sh), 228 (m), 216 (s), 208 (s) nm. - **MS** (APCI-HRMS(+)): $m/z = 1169.2214$ [M+H]⁺, cal. for [C₆₄H₃₂N₁₆Nd+H₁]⁺: 1169.2182.

7.29.5 Synthesis of [Pc₂Eu]

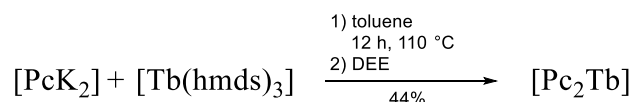
According to General Procedure 10 (p. 320): 300 mg [PcK₂] (0.51 mmol, 1 eq) were suspended in 5 mL toluene with 965 mg [Eu(hmds)₃]/ or 1 eq [EuCl₃]·2dme (1.52 mmol, 3 eq). The solution was refluxed at 110 °C, overnight. After removing the solvent in vacuum, the product was washed several times with DEE. The product was obtained in the form of a blue greyish powder.

Yield: 120 mg, 102 μmol , 40%. - **¹H NMR** (C₆D₆, 300 MHz) $\delta = 11.39$ (m, 16 H, Ar-CH ^{α}), 9.09 (m, 16 H, Ar-CH ^{β}) ppm. - **IR** (ATR, 400-4000 cm⁻¹): $\tilde{\nu} = 3050$ (w), 2951 (w), 2895 (w), 2348 (w), 2326 (w), 1609 (w), 1477 (w), 1405 (w), 1329 (m), 1250 (w), 1160 (w), 1113 (m),

Experimental Section

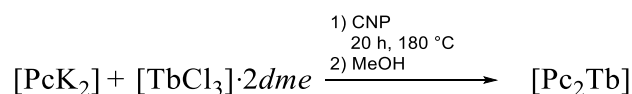
1073 (w), 929 (w), 881 (w), 827 (w), 774 (w), 725 (s), 672 (w), 496 (w), 429 (w) cm^{-1} . - **UV-Vis** (toluene): $\lambda = 668$ (s), 337 (s), 245 (s) nm. - **MS** (MALDI-ToF(+)): $m/z = 1177.283$ $[\text{M}]^+$.

7.29.6 Synthesis of $[\text{Pc}_2\text{Tb}]$



Method a) 100 mg $[\text{PcK}_2]$ (169 μmol , 1 eq) were suspended in 2 mL toluene with 480 mg $[\text{Tb}(\text{hmds})_3]$ (750 μmol , ~5 eq). The solution was stirred at 110 $^\circ\text{C}$, overnight. After removing the solvent in vacuum the product was washed with DEE.

Yield: 42 mg, 35.5 μmol , 44%. - **IR** (ATR, 400-4000 cm^{-1}): $\tilde{\nu} = 2963$ (w), 2349 (w), 2324 (w), 1485 (w), 1408 (w), 1328 (w), 1260 (w), 1021 (s, br), 797 (2), 729 (m), 673 (w), 464 (s) cm^{-1} . - **UV-Vis** (toluene): $\lambda = 666$ (s), 332 (s), 246 (s) nm. - **MS** (MALDI-ToF(+)): $m/z = 1183.540$ $[\text{M}]^+$.



Method b) According to General Procedure 10 (p. 320): $[\text{PcK}_2]$, $[\text{TbCl}_3] \cdot 2\text{dme}$ in CNP, 20 h, 180 $^\circ\text{C}$.

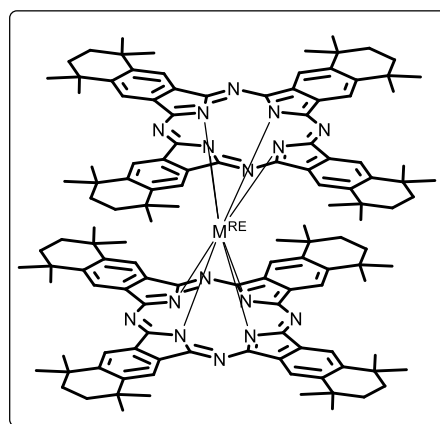
Yield: n. d. - **UV-Vis** (DCM): $\lambda = 638$ (s), 336 (s), 292 (sh), 228 (m), 216 (w), 210 (s), 216 (w) nm. - **MS** (APCI-HRMS(+)): $m/z = 1184.2330$ $[\text{M}+\text{H}]^+$, cal. for $\text{C}_{64}\text{H}_{32}\text{N}_{16}\text{Tb}_1+\text{H}_1$: 1184.2322.

Additional information: In this method, also the triple-decker sandwich-complex was observed when product was handled under inert atmosphere. - **MS** (APCI-HRMS(+)): $m/z = 1856.3090$ $[\text{M}+\text{H}]^+$, cal. for $\text{C}_{96}\text{H}_{48}\text{N}_{24}\text{Tb}_2+\text{H}_1$: 1856.3104.

7.30 Synthesis of $[\text{Pc}^*_2\text{M}^{\text{RE}}]$

General Procedure 11: Synthesis of $[\text{Pc}^*_2\text{M}^{\text{RE}}]$:

To 1 eq Pc^*H_2 , up to 5 eq $[\text{M}^{\text{RE}}(\text{hmds})_3]$ were dissolved in toluene (1 mL/50 mg Pc^*H_2). The solution was stirred for 3-5 d at 120 °C. The reaction was monitored by TLC. The solvent was evaporated, after cooling down to rt. The complexes were washed with hexane and DEE to remove the excess of $[\text{M}^{\text{RE}}(\text{hmds})_3]$. The resulting green-blue powders were dried in vacuum. The crude products were purified by CC (Tol/THF or DCM/PE). For some complexes, insufficient amounts were obtained for full analysis. The complexes are summarised in a table below with the observed MS (MALDI-ToF) data. Some complexes were further analysed, such as Eu and Tb.

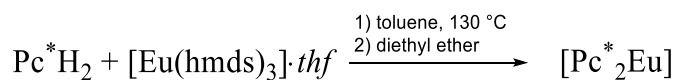


M^{RE} = rare earth metal

Table 19: Additionally, synthesised $[\text{Pc}^*_2\text{M}^{\text{RE}}]$ complexes of insufficient amount for analysis and purity.

$[\text{Pc}^*_2\text{M}^{\text{RE}}]$	$[\text{Pc}^*_2\text{Sc}]$	$[\text{Pc}^*_2\text{Y}]$	$[\text{Pc}^*_2\text{La}]$	$[\text{Pc}^*_2\text{Ce}]$ ^[102]	$[\text{Pc}^*_2\text{Sm}]$	$[\text{Pc}^*_2\text{Nd}]$	$[\text{Pc}^*_2\text{Gd}]$	$[\text{Pc}^*_2\text{Lu}]$
MALDI-ToF / m/z	1951.12 [M+H] ⁺	1995.267 [M+H] ⁺	2044.874 [M+H] ⁺	2048.012 [M+H] ⁺	2059.909 [M+H] ⁺	2051.142 [M+H] ⁺	2063.927 [M+H] ⁺	2079.979 [M+H] ⁺
UV-Vis / nm	692 (s) 625 (sh)	-	-	-	696 (s), 627 (sh)	693 (s), 626 (sh)	692(s), 626 (sh)	696 (s), 638 (sh), 528 (s)
Multiple decker / m/z	3160.24 [M+H] ⁺ [Pc [*] ₃ Sc ₂]	-	-	-	3162.284 [M+H] ⁺ [Pc [*] ₃ Sm ₂]	3145.418 [M+H] ⁺ [Pc [*] ₃ Nd ₂]	3173.900 [M+H] ⁺ [Pc [*] ₃ Gd ₂]	3207.411 [M+H] ⁺ [Pc [*] ₃ Lu ₂]

7.30.1 Synthesis of $[\text{Pc}^*_2\text{Eu}]$ ^[196]



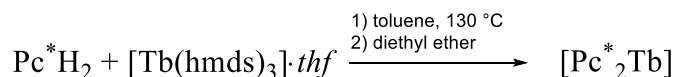
According to General Procedure 11 (p. 323), using 1 eq Pc^*H_2 and 5 eq $[\text{M}^{\text{RE}}(\text{hmds})_3]$. After oxidation in air the double decker sandwich-complex was observed. Triple and multiple decker sandwich-complexes could also be observed in MALDI-ToF spectrum, when the compounds were carefully handled under nitrogen atmosphere.

Yield: n.d. - **IR** (ATR, 400-4000 cm^{-1}): $\tilde{\nu}$ = 2961 (w), 2929 (w), 2860 (w), 2358 (w), 2341 (w), 2306 (w), 1308 (w), 1259 (w), 1021 (s, br), 852 (w), 799 (w), 589 (m), 508 (w), 438 (w) cm^{-1} .

Experimental Section

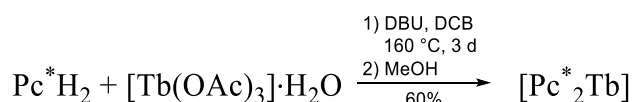
- **UV-Vis** (DCM): $\lambda = 694$ (s), 621 (s), 487 (sh), 353 (s), 329 (sh), 281 (s) nm. - **MS** (MALDI-ToF(+)): $m/z = 2059.012$ [M]⁺.

7.30.2 Synthesis of [Pc*₂Tb]



Method a) According to General Procedure 11 (p. 323). The product was obtained in the form of a light green powder.

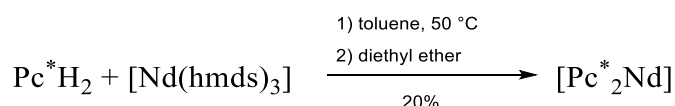
Yield: n. d. - **IR** (ATR, 400-4000 cm⁻¹): $\tilde{\nu} = 2962$ (w), 2861 (w), 2382 (w), 2349 (w), 2325 (m), 2297 (w), 1624 (w), 1309 (w), 1258 (m), 1018 (s, br), 846 (m), 798 (m), 757 (w), 673 (m), 589 (w), 501 (w), 440 (w) cm⁻¹. - **UV-Vis** (DCM): $\lambda = 692$ (s), 625 (sh), 351 (s), 281 (s) nm. - **Fluorescence** (DCM, $\lambda_{ex} = 350$ nm): $\lambda = 712$ nm. - **MS** (MALDI-ToF(+)): $m/z = 2066.008$ [M]⁺. - **MS** (MALDI-ToF(+)): $m/z = 2067.475$ [M+H]⁺.



Method b)^[256] 0.10 g Pc*H₂ (0.10 mmol, 1 eq), 0.03 g [Tb(OAc)₃·H₂O] (0.07 mmol, 0.7 eq), and 0.04 mL DBU (0.27 mmol, 2.7 eq) were suspended in 3 mL DCB and heated to 160 °C for 3 d. The dark green solution was concentrated in vacuum, the residue dissolved in MeOH and separated from the blue-turquoise precipitate. After washing the residue several times, the resulting powder was dried in vacuum. A light green powder was obtained.

Yield: 0.06 g, 0.03 mmol, 60%. -The analysis in accordance to the data above.

7.30.3 Synthesis of [Pc*₂Nd] ^[256]



According to General Procedure 11 (p. 323). The resulting product was washed with DEE. After drying in vacuum a light green powder was obtained.

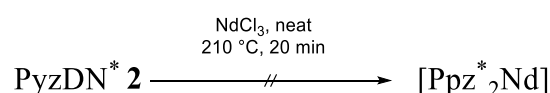
Yield: 20%. - **UV-Vis** (DCM): $\lambda = 693$ (s), 626 (sh), 348 (m), 225 (s) nm. - **MS** (MALDI-ToF(+)): $m/z = 2051.353$ [M]⁺.

7.30.4 Attempt to Synthesise $[\text{Pc}^*{}_{2}\text{Sm}][\text{CoCp}_2]^+$

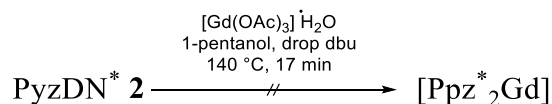
338 mg $[\text{Pc}^*{}_{2}\text{Sm}]$ (24.3 μmol , 1 eq) and 30.8 mg $[\text{Cp}_2\text{Co}]$ (24.3 μmol , 1 eq) were dissolved in 4 mL THF and stirred for 4 d at rt. The solvent was removed in vacuum and the resulting blue powder dissolved in MeCN. Hexane was added.

7.30.5 Attempt to Synthesise $[\text{Pc}^*{}_{2}\text{Lu}][\text{TBA}]^+$

35 mg $[\text{Lu}(\text{hmds})_3]$ (52.3 μmol , 1 eq) and 100 mg Pc^*H_2 (105 μmol , 2 eq) were dissolved in 5 mL toluene and stirred for 3 d at 120 °C. 14 mg tetra-*n*-butylammonium bromide (52.3 μmol , 1 eq) were added and were stirred for 24 h at 120 °C. The solvent was removed in vacuum. Neither could crystals nor product traces be observed in MS or UV-Vis spectroscopy.

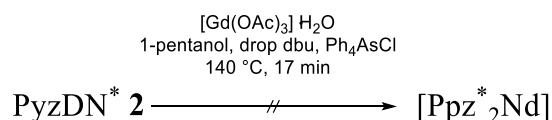
7.30.6 Attempt to Synthesise $[\text{Ppz}^*{}_{2}\text{Nd}]$ 

125 mg $[\text{NdCl}_3] \cdot 2\text{thf}$ (323 μmol , 1.0 eq.) was weighed out with 310 mg PyzDN^* (1.29 mmol, 4 eq) and a spatula tip of $[(\text{NH}_4)_2\text{MoO}_4]$. The flask was placed into a preheated oil bath at 210 °C and stirred for 20 min. After cooling down to rt, the black solid was purified by CC (PE/EE 7:3). No product could be identified either in MALDI or in UV-Vis spectroscopy.

7.30.7 Attempt to Synthesise $[\text{Ppz}^*{}_{2}\text{Gd}]$ 

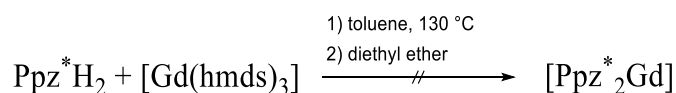
Method a) 54 mg $[\text{Gd}(\text{OAc})_3] \cdot \text{H}_2\text{O}$ (161 μmol , 1 eq) were weighed out with 500 mg PyzDN^* (2.08 mmol, >13 eq) and suspended in 2 mL 1-pentanol. After addition of 2 drops DBU, the solution was placed in a preheated oil bath at 140 °C. The solution was stirred for 14 h. A change in colour to green was observed. After cooling down to rt, the solvent was removed under reduced pressure and the resulting powder was purified by CC (PE/EE 2:1). Neither in MS nor in UV-Vis spectroscopy could pyrazinoporphyrazine traces be detected.

Experimental Section



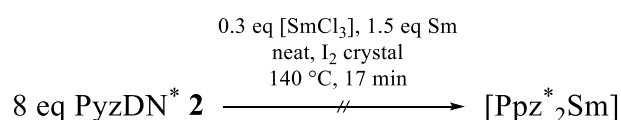
Method b) 55 mg [Gd(OAc)₃·H₂O] (161 μmol, 1 eq), 67 mg Ph₄AsCl (160 μmol, 1 eq) and 538 mg PyzDN* (2.24 mol, 14 eq) were suspended in 2 mL 1-pentanol and were stirred for 18 h at 150 °C in a preheated oil bath. After reaching the temperature, 2 drops of DBU were added. After cooling down to rt, the solvent was removed in vacuum and the dark solid was washed with DEE and hexane. The product was dissolved in DEE. Neither in MS nor in UV-Vis spectroscopy could phthalocyanine traces be detected.

7.30.8 Attempt to Synthesise [Ppz*₂Gd]



298 mg [Gd(hmds)₃] (467 μmol, 3 eq) and 150 mg Ppz*H₂ (156 μmol, 1 eq) were dissolved in 5 mL toluene and heated for 3 d to 120 °C. After cooling down to rt, the solvent was removed in vacuum and the green product was analysed by using MS and UV-Vis spectroscopy. No double-decker sandwich-complex could be observed.

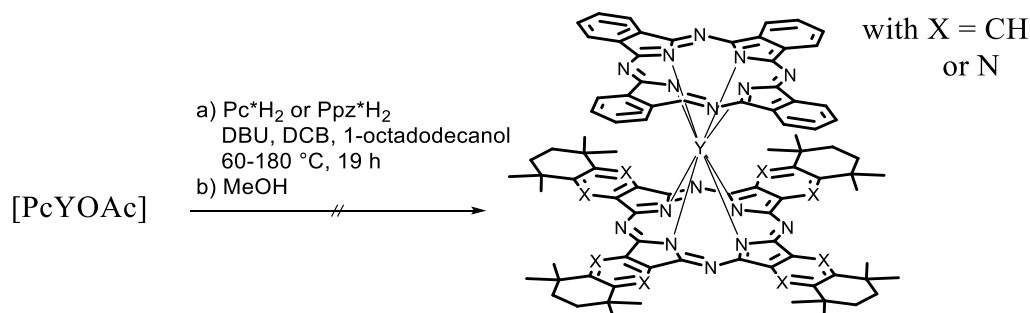
7.30.9 Attempt to Synthesise [Ppz*₂Sm]



510 mg PyzDN* (2.12 mmol, 8.1 eq), 59 mg Sm (392 μmol, 1.5 eq), 29 mg [SmCl₃]·2thf (72.3 μmol, 0.3 eq), and cat. amounts of I₂ were added into a preheated oil bath at 210 °C and stirred for 20 min. After cooling down to rt, the product was dissolved in 6 mL THF, filtered over Celite® and dried in vacuum. The product was washed with MeOH and a blue greenish powder was obtained. Neither in MS nor in UV-Vis spectroscopy could phthalocyanine traces be detected.

7.31 Attempted Synthesis of Heteroleptic Sandwiches [Pc*YPC], [Ppz*YPC]

These attempts were carried out according to the procedures reported by PUSHKAREV *et al.*^[257,290,291] The reactions were carried out within the bachelor thesis of SWOLANA.^[256]



7.31.1 Attempts for Heteroleptic Sandwiches using Pc*, Ppz* and Cp* as ligand

General Procedure for Heteroleptic Sandwiches:

1 eq [PcYOAc], 1 eq Pc*H₂ or Ppz*H₂ and 2 eq DBU were added in 5 mL DCB/100 mg Pc*H₂. 0.1 g 1-octadecanol/100 mg Pc*H₂ were added, and the solution was stirred at 60-180 °C for 1-20 h. After cooling down to rt, the mixture was suspended in 25 mL THF and filtered over Celite®. After removing the solvent in vacuum the obtained powder was dried in vacuum.

7.31.1.1 Attempt to Synthesis [Pc*YPC]

Following the General procedure in section 7.31.1: 30 mg [PcYOAc] (45.4 μmol, 1 eq), 50 mg Pc*H₂ (52.3 μmol, 1 eq), 0.01 mL DBU (0.10 mmol, 2 eq). The desired product could not be isolated. In MS (MALDI-ToF) a weak signal was observed at m/z = 1544.218. By TLC (PE/EE 10:1), a weak green spot was observed.

$R_f = 0.81$. - MS (MALDI-ToF): m/z = 1544.218 [M]⁺.

7.31.1.2 Attempt to Synthesis [Ppz*YPC]

Following the General procedure in section 7.31.1: 30 mg [PcYOAc] (45.4 μmol, 1 eq), 50 mg Ppz*H₂ (52 μmol, 1 eq), 0.01 mL DBU (0.1 mmol, 2 eq). In MS no product could be observed. In UV-Vis spectroscopy Q-band signals at 697 nm and 645 nm could be observed.

7.31.1.3 Attempt to Synthesis [Pc*MoCp(Cl)]

200 mg PDN* (0.84 mmol, 4 eq) were dissolved in 2 mL CNP with 65 mg [MoCp(CO)₃Cl] (231 μmol, 1 eq). The mixture was heated in a preheated oil-bath at 215 °C for 2.5 h. The solution turned green. After cooling down to rt, a black solid was precipitated with hexane. The product was further washed with hexane. Neither in UV-Vis spectroscopy nor in MS could phthalocyanine traces be observed.

7.31.1.4 Attempt to Synthesis [PcEuCp*]

[PcK₂] was freshly prepared by using 2.1 eq KBn and 1 eq PcH₂, in 10 mL THF. After filtration, to the formed [PcK₂], 1 eq [EuCl₃] was added in 10 mL THF at -78 °C. After addition, slowly 1 eq [KCp*] in 5 mL THF was added. The solution was stirred overnight, while warming up to rt. After removing the solvent in vacuum, and filtration over Celite[®] with toluene, the product was analysed by UV-Vis spectroscopy and MS. No traces of the product were detected.

Additional information: It was also attempted to preform the [Cp*EuCl₂] at -78 °C and add it to a solution was [PcK₂]. No sandwich-complex could be observed, neither in MALDI-ToF nor in FD measurements.

7.31.1.5 Attempt to Synthesis [PcTbCp*]

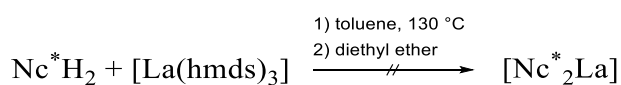
[PcK₂] was freshly prepared by using 2.1 eq KBn and 1 eq PcH₂, in 10 mL THF. After filtration, to the formed [PcK₂], 1 eq [TbCl₃] was added in 10 mL THF at -78 °C. After addition, slowly 1 eq [NaCp*] in 5 mL THF was added. The solution was stirred overnight, while warming up to rt. After removing the solvent in vacuum, and filtration over Celite[®] with toluene, the product was analysed by UV-Vis spectroscopy and MS.

7.31.1.6 Attempt to Synthesis [Pc*CrCp*]

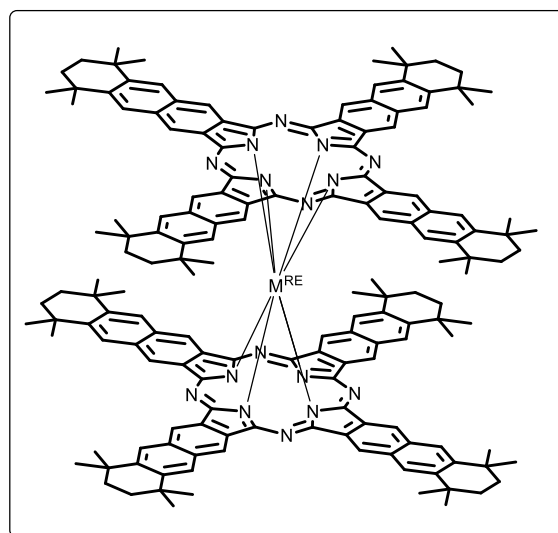
To a solution of 1 eq [Cp*CrCl₂], a freshly prepared solution of 1 eq [Pc*K₂] was added at rt. The solution was stirred at rt, overnight. After removing the solvent in vacuum, the obtained green powder was dissolved in 20 mL toluene and filtered over Celite[®]. The product was concentrated in vacuum and dried. Neither in UV-Vis spectroscopy, nor in MS any product traces were found.

7.32 Synthesis of $[\text{Nc}^*_2\text{M}^{\text{RE}}]$

7.32.1 Attempt to Synthesise $[\text{Nc}^*_2\text{La}]$ [196]

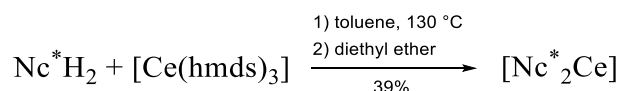


According to General Procedure 11 (p. 323). Several attempts using lower temperatures and fewer equivalents of $[\text{La}(\text{hmds})_3]$ were carried out. No product was observed either in MALDI-ToF or in UV-Vis spectrum. Only free ligand was observed and degraded product.



$\text{M}^{\text{RE}} = \text{rare earth metal}$

7.32.2 Synthesis of $[\text{Nc}^*_2\text{Ce}]$ [140]



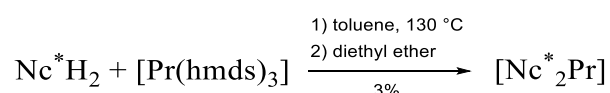
Modification of General Procedure 11 (p. 323): 100 mg Nc^*_2H_2 (86.5 μmol , 1.0 eq) and 216 mg $[\text{Ce}(\text{hmds})_3]$ (34.7 μmol , 4.0 eq) were separately dissolved in 2 mL toluene. The Nc^*_2H_2 solution was warmed up to 130 $^\circ\text{C}$ and 1 mL $[\text{Ce}(\text{hmds})_3]$ solution was added dropwise. The synthesis was monitored by TLC. After 30 min, another 1 mL $[\text{Ce}(\text{hmds})_3]$ solution was added, and the mixture was stirred for 72 h at 130 $^\circ\text{C}$. After cooling down to rt, the solvent was removed in vacuum, the residue was washed several times with DEE. The resulting green powder was dried in vacuum. After a short CC (Tol/THF or DCM/PE) the double-decker sandwich-complex was observed.

Yield: 42 mg, 17.2 μmol , 39%. - **IR** (ATR, 400-4000 cm^{-1}): $\tilde{\nu} = 2954$ (s), 2910 (s), 2858 (s), 1472 (m), 1281 (m), 1261 (m), 1293 (s), 1168 (m), 1106 (s), 1083 (s), 1049 (s), 1030 (s), 864 (s), 693 (m), 661 (m), 465 (m) cm^{-1} . - **UV-Vis** (DCM): $\lambda = 800$ (s), 701 (w), 656 (m), 333 (m) nm. - **Fluorescence** (DCM, $\lambda_{\text{ex}} = 750$ nm): $\lambda = 802$ nm. - **MS** (MALDI-ToF(+)): $m/z = 2445.311$ $[\text{M}]^+$. - **Elemental analysis** ($\text{C}_{160}\text{H}_{160}\text{Ce}_1\text{N}_{16}$, $M = 2447.27$ g/mol): cal. (fnd.): C: 78.53 (66.41), H: 6.59 (6.25), N: 9.16 (7.57).

Additional information: A reduction of the $[\text{Nc}^*_2\text{Ce}]$ sandwich-complex was attempted, as it has been described in literature. Instead of any reaction, still the broadened Q-band at ~ 650 nm was observed, using NaBH_4 , KBH_4 , CaH_2 .

Experimental Section

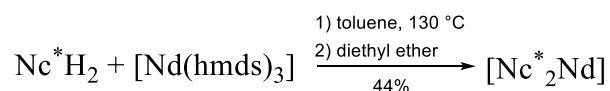
7.32.3 Synthesis of [Nc*₂Pr]



According to General Procedure 11 (p. 323), using [Pr(hmds)₃]. The product was obtained in the form of a light-green solid.

Yield: 3%. - **UV-Vis** (DCM): $\lambda = 797$ (s), 705 (sh), 329 (m) nm. - **MS** (MALDI-ToF(+)): $m/z = 2447.678$ [M]⁺.

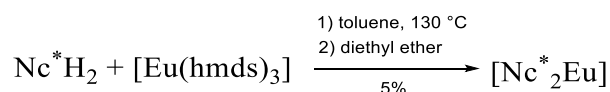
7.32.4 Synthesis of [Nc*₂Nd]



According to General Procedure 11 (p. 323), using [Nd(hmds)₃]. The product was obtained in the form of a greyish-green solid.

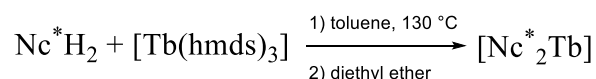
Yield: 44%. - **IR** (ATR, 400-4000 cm⁻¹): $\tilde{\nu} = 2957$ (m), 2923 (m), 2857 (m), 1472 (m), 1384 (m), 1362 (m), 1351 (m), 1316 (m), 1293 (m), 1260 (m), 1182 (m), 1168 (m), 1104 (m), 1048 (s), 1029 (s), 907 (m), 847 (m), 800 (m), 743 (m), 722 (m), 591 (m), 465 (m) cm⁻¹. - **UV-Vis** (DCM): $\lambda = 795$ (s), 700 (m), 644 (m), 339 (m), 251 (m) nm. - **Fluorescence** (DCM, $\lambda_{ex} = 750$ nm): $\lambda = 806$ nm. - **MS** (MALDI-ToF(+)): $m/z = 2450.273$ [M]⁺.

7.32.5 Synthesis of [Nc*₂Eu]



According to General Procedure 11 (p. 323), using [Eu(hmds)₃]. The product was obtained in the form of a green solid. The first attempt to synthesise [EuNc*₂] was carried out by Lange.^[196]

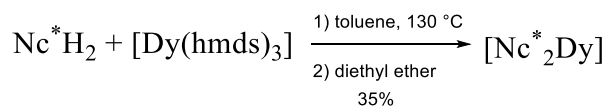
Yield: 5%. - **¹H NMR** (THF-*d*₈, 300 MHz): $\delta = 10.79$ (s, 16 H, Ar-CH), 9.48 (s, 16 H, Ar-CH), 2.57 (s, 48 H, *endo*-CH₃), 2.35 (s, 32 H, -CH₂), 1.96 (s, 48 H, *exo*-CH₃) ppm. - **IR** (ATR, 400-4000 cm⁻¹): $\tilde{\nu} = 2958$ (m), 2926 (m), 2859 (w), 1631 (s, br), 1476 (m), 1386 (w), 1362 (w), 1320 (m), 1296 (m), 1259 (m), 1186 (w), 1105 (m), 1031 (s, br), 908 (w), 847 (w), 802 (m), 747 (m), 725 (m), 601 (w), 591 (m), 465 (w) cm⁻¹. - **UV-Vis** (toluene): $\lambda = 778$ (s), 691 (sh), 517 (sh), 338 (s), 286 (s) nm. - **MS** (MALDI-ToF(+)): $m/z = 2459.217$ [M]⁺.

7.32.6 Synthesis of [Nc*₂Tb]

According to General Procedure 11 (p. 323), using [Tb(hmds)₃]·*thf*. The solution was stirred for 7 d at 130 °C. A dark green solid was obtained. This residue was washed with 2 x 20 mL DEE before drying the resulting powder in vacuum. A light green-greyish powder was obtained.

Yield: n.d. - **UV-Vis** (DCM): λ = 776 (s), *745 (s), 684 (sh), 342 nm. - **MS** (MALDI-ToF(+)): m/z = 2465.008 [M]⁺.

Additional information: The Q-band shift in the UV-Vis spectrum appears quite strong shifted in comparison to the other observed [Nc*₂M^{RE}]. Anyway, a broadened band at ~600 nm was observed which is typical for these sandwich-complexes.

7.32.7 Synthesis of [Nc*₂Dy]

According to General Procedure 11 (p. 323), using [Dy(hmds)₃]. The product was obtained in the form of a green solid.

Yield: 35%. - **UV-Vis** (DCM): λ = 787 (s), 699 (sh), 332 (m) nm. - **MS** (MALDI-ToF(+)): m/z = 2469.590 [M]⁺.

8 References

- [1] A. von Baeyer, A. Emmerling, *Ber. Dtsch. Chem. Ges.* **1870**, 3, 514.
- [2] B. Fugmann, G. Adam, H. Anke, W. Boland, W. Francke, *RÖMPP Lexikon Naturstoffe, 1. Auflage, 1997*, Thieme, **2014**.
- [3] R. Jelly, S. W. Lewis, C. Lennard, K. F. Lim, J. Almog, *Chem. Commun.* **2008**, 3513–3515.
- [4] a) A. C. Dweck, *International Journal of Cosmetic Science* **2002**, 24, 287–302; b) J. P. Forestier, *International Journal of Cosmetic Science* **1982**, 4, 153–174.
- [5] a) A. von Baeyer, H. Caro, *Ber. Dtsch. Chem. Ges.* **1874**, 7, 968; b) A. von Baeyer, *Ber. Dtsch. Chem. Ges.* **1871**, 4, 555; c) A. von Baeyer, *Ber. Dtsch. Chem. Ges.* **1879**, 12, 642.
- [6] R. L. Feller, A. Roy, E. W. FitzHugh, B. H. Berrie, *Artists' pigments. A handbook of their history and characteristics*, National Gallery of Art, Washington, **1986**.
- [7] A. H. Church, *The Chemistry of Paints and Painting*, London : Seeley, Service, **1915**.
- [8] M. Douma, "Pigments through the Ages", can be found under <http://www.webexhibits.org/pigments/indiv/recipe/indianyellow.html>, **2008**.
- [9] a) R. L. Feller, *Artists' Pigments. A handbook of their history and characteristics*, National Gallery of Art; Oxford Univ. Press, Washington, DC, New York, NY, **1986**; b) A. Kuhn, *Reports and Studies in the History of Art* **1968**, 154–202; c) J. Vermeer, "Woman holding a balance", can be found under <http://www.nga.gov/content/ngaweb/Collection/art-object-page.1236.html>, **1664**.
- [10] a) D. G. Stork, J. Coddington (Eds.) *SPIE Proceedings*, SPIE, **2008**; b) Y. Zhao, R. S. Berns, L. A. Taplin, J. Coddington in *SPIE Proceedings* (Eds.: D. G. Stork, J. Coddington), SPIE, **2008**.
- [11] H. von Sonnenburg, W. A. Liedtke, Metropolitan Museum of Art, *Rembrandt/not Rembrandt: in the Metropolitan Museum of Art. Aspects of connoisseurship. Paintings: problems and issues. Paintings, drawings, and prints : art-historical perspectives / Walter Liedtke, Carolyn Logan, Nadine M. Orenstein, Stephanie S. Dickey*, Metropolitan Museum of Art, **1995**.
- [12] D. Wöhrle, G. Schnurpfeil, S. Makarov, O. Suvora, *Chemie in unserer Zeit* **2012**, 46, 12–24.
- [13] M. Liebold, *Masterarbeit*, Philipps-Universität Marburg, Marburg, **2012**.
- [14] N. B. McKeown, *Phthalocyanine Materials: Synthesis, Structure, and Function*, Cambridge University Press, Cambridge, U.K., New York, **1998**.
- [15] A. Braun, J. Tcherniac, *Ber. Dtsch. Chem. Ges.* **1907**, 40, 2709–2714.

References

- [16] J. M. Gottfried, *Surface Science Reports* **2015**, *70*, 259–379.
- [17] J. W. Buchler, *Porphyrins and Metalloporphyrins. in: K.M. Smith (Ed)*, Amsterdam, **1975**.
- [18] R. M. Christie, D. D. Deans, *J. Chem. Soc., Perkin Trans. 2* **1989**, 193.
- [19] S. N. Brumfield, V. W. Foltz, C. M. McGhee, A. L. Thomas, *J. Org. Chem.* **1962**, *27*, 2266–2267.
- [20] M. Hanack, H. Heckmann, R. Polley (Eds.) *Houben Weyl, Methods of Organic Chemistry, F. Aromatic and Heteroaromatic Large Rings*, Thieme-Verlag, Stuttgart, **1997**.
- [21] N. B. McKeown (Ed.) *Science of Synthesis*, Thieme-Verlag, Stuttgart, **2003**.
- [22] a) K. M. Smith, K. M. Kadish, R. Guilard, *Handbook of Porphyrin Science: with Applications to Chemistry, Physics, Materials Science, Engineering, Biology and Medicine (Volume 3)*, World Scientific, **2012**; b) E. A. Luk'yanetz, V. N. Nemykin, *Arkivoc* **2009**, *2010*, 136–208.
- [23] M. J. Cook, A. J. Dunn, S. D. Howe, A. J. Thomson, K. J. Harrison, *J. Chem. Soc., Perkin Trans. 1* **1988**, 2453–2458.
- [24] S. A. Mikhalenko, L. I. Solov'eva, E. A. Luk'yanetz, *The Journal of General Chemistry of the USSR* **1991**, *61*, 996–1003.
- [25] E. Seikel, *Dissertation*, Philipps-Universität Marburg, Marburg, **2012**.
- [26] E. A. Ough, M. J. Stillman, K. A. Creber, *Can. J. Chem.* **1993**, *71*, 1898–1909.
- [27] P. Zimcik, V. Novakova, K. Kopecky, M. Miletin, R. Z. Uslu Kobak, E. Svandrlíkova, L. Váchová, K. Lang, *Inorg. Chem.* **2012**, *51*, 4215–4223.
- [28] N. Kobayashi, N. Sasaki, Y. Higashi, T. Osa, *Inorg. Chem.* **1995**, *34*, 1636–1637.
- [29] C. Adachi, M. A. Baldo, M. E. Thompson, S. R. Forrest, *J. Appl. Phys.* **2001**, *90*, 5048–5051.
- [30] J. Mack, N. Kobayashi, *Chem. Rev.* **2011**, *111*, 281–321.
- [31] D. Wöhrle, M. W. Tausch, W.-D. Stohrer, *Photochemie. Konzepte, Methoden, Experimente*, Wiley-VCH, Weinheim, **1998**.
- [32] M. Quaranta, S. M. Borisov, I. Klimant, *Bioanalytical reviews* **2012**, *4*, 115–157.
- [33] F. Dumoulin, Y. Zorlu, M. Menaf Ayhan, C. Hirel, Ü. Isci, V. Ahsen, *J. Porphyrins Phthalocyanines* **2009**, *13*, 161–165.
- [34] J. A. Elvidge, R. P. Linstead, *J. Chem. Soc.* **1955**, 3536–3544.
- [35] Z. Musil, P. Zimcik, M. Miletin, K. Kopecky, J. Lenco, *Eur. J. Org. Chem.* **2007**, 4535–4542.

- [36] a) N. B. Subbotin, V. N. Nemykin, Y. Z. Voloshin, *Mendeleev Communications* **1993**, 3, 121–122; b) N. Kobayashi, T. Ashida, T. Osa, H. Konami, *Inorg. Chem.* **1994**, 33, 1735–1740; c) T. G. Linßen, M. Hanack, *Chem. Ber.* **1994**, 127, 2051–2057.
- [37] V. N. Nemykin, N. B. Subbotin, N. A. Kostromina, S. V. Volkov, *Mendeleev Communications* **1995**, 5, 71–72.
- [38] C. C. Leznoff, T. W. Hall, *Tetrahedron Letters* **1982**, 23, 3023–3026.
- [39] T. W. Hall, S. Greenberg, C. R. McArthur, Kh, *Nouv. J. Chim.* **1982**, 6, 653–658.
- [40] A. Hirth, A. K. Sobbi, D. Wöhrle, *J. Porphyrins Phthalocyanines* **1997**, 01, 275–279.
- [41] C. C. Leznoff, S. Greenberg, *Chem. Abstr.* **1978**, 88, 171797–171801.
- [42] J. G. Young, W. Onyebuagu, *J. Org. Chem.* **1990**, 55, 2155–2159.
- [43] S. Vigh, H. Lam, P. Janda, A. B. P. Lever, C. C. Leznoff, R. L. Cerny, *Can. J. Chem.* **1991**, 69, 1457–1461.
- [44] T. Fukuda, N. Kobayashi, *Chem. Lett.* **2002**, 31, 866–867.
- [45] N. Kobayashi, R. Kondo, S. Nakajima, T. Osa, *J. Am. Chem. Soc.* **1990**, 112, 9640–9641.
- [46] S. Kudrevich, N. Brasseur, C. La Madeleine, S. Gilbert, J. E. van Lier, *J. Med. Chem.* **1997**, 40, 3897–3904.
- [47] A. Weitemeyer, H. Kliesch, D. Woehrle, *J. Org. Chem.* **1995**, 60, 4900–4904.
- [48] a) N. E. Galanin, E. V. Kudrik, G. P. Shaposhnikov, V. V. Aleksandriiskii, *Russian Journal of Organic Chemistry* **2004**, 40, 723–728; b) S. I. Vagin, M. Hanack, *Eur. J. Org. Chem.* **2002**, 2859; c) S. M. Baum, A. A. Trabanco, A. G. Montalban, A. S. Micallef, C. Zhong, H. G. Meunier, K. Suhling, D. Phillips, A. J. P. White, D. J. Williams et al., *J. Org. Chem.* **2003**, 68, 1665–1670; d) A. G. Montalban, W. Jarrell, E. Riguet, Q. J. McCubbin, M. E. Anderson, A. J. P. White, D. J. Williams, A. G. M. Barrett, B. M. Hoffman, *J. Org. Chem.* **2000**, 65, 2472–2478; e) M. P. Donzello, C. Ercolani, A. A. Gaberkorn, E. V. Kudrik, M. Meneghetti, G. Marcolongo, C. Rizzoli, P. A. Stuzhin, *Chem. Eur. J.* **2003**, 9, 4009–4024.
- [49] T. Fukuda, S. Homma, N. Kobayashi, *Chem. Eur. J.* **2005**, 11, 5205–5216.
- [50] R. H. Platel, T. Teixeira Tasso, W. Zhou, T. Furuyama, N. Kobayashi, D. B. Leznoff, *Chem. Commun.* **2015**, 51, 5986–5989.
- [51] T. Lis, *Acta Crystallogr B Struct Crystallogr Cryst Chem* **1980**, 36, 2042–2046.
- [52] R. Sessoli, H. L. Tsai, A. R. Schake, S. Wang, J. B. Vincent, K. Folting, D. Gatteschi, G. Christou, D. N. Hendrickson, *J. Am. Chem. Soc.* **1993**, 115, 1804–1816.
- [53] R. Sessoli, D. Gatteschi, A. Caneschi, M. A. Novak, *Nature* **1993**, 365, 141–143.

References

- [54] R. A. Layfield, *Organometallics* **2014**, *33*, 1084–1099.
- [55] D. N. Woodruff, R. E. P. Winpenny, R. A. Layfield, *Chemical Reviews* **2013**, *113*, 5110–5148.
- [56] N. Ishikawa, *Polyhedron* **2007**, *26*, 2147–2153.
- [57] N. Ishikawa in *Structure and Bonding*, Vol. 135 (Eds.: J. Jiang, Ö. Bekaroglu), Springer-Verlag Berlin Heidelberg, Berlin, Heidelberg, **2010**.
- [58] T. S. Srivastava, E. B. Fleischer, *J. Am. Chem. Soc.* **1970**, *92*, 5518–5519.
- [59] T. Diebold, B. Chevrier, R. Weiss, *Inorg. Chem.* **1979**, *18*, 1193–1200.
- [60] J. C. Kim, W. S. Rees, V. L. Goedken, *Inorg. Chem.* **1994**, *33*, 3191–3194.
- [61] M. Savy, F. Coowar, J. Riga, J. J. Verbist, G. Bronoel, S. Besse, *J. Appl. Electrochem.* **1990**, *20*, 260–268.
- [62] M. Dieng, O. Contamin, M. Savy, *Electrochimica Acta* **1988**, *33*, 121–126.
- [63] R. A. Sheldon, *Recl. Trav. Chim. Pays-Bas* **1973**, *92*, 253–266.
- [64] M. Gorsch, H. Homborg, *Z. anorg. allg. Chem.* **1998**, *624*, 634–641.
- [65] a) S. J. Edmondson, P. C. Mitchell, *Polyhedron* **1986**, *5*, 315–317; b) T. Nyokong, *Inorganica Chimica Acta* **1989**, *160*, 235–239.
- [66] K. Frick, S. Verma, J. Sundermeyer, M. Hanack, *Eur. J. Inorg. Chem.* **2000**, 1025–1030.
- [67] S. Verma, M. Hanack, *Z. anorg. allg. Chem.* **2003**, *629*, 880–892.
- [68] M. Gorsch, A. Kienast, H. Hueckstaedt, H. Homborg, *Z. anorg. allg. Chem.* **1997**, *623*, 1433–1440.
- [69] W. Darwish, E. Seikel, K. Harms, O. Burghaus, J. Sundermeyer, *Dalton Trans.* **2011**, *40*, 1183–1188.
- [70] E. Seikel, B. Oelkers, O. Burghaus, J. Sundermeyer, *Inorg. Chem.* **2013**, *52*, 4451–4457.
- [71] D. G. Whitten, I. G. Lopp, P. D. Wildes, *J. Am. Chem. Soc.* **1968**, *90*, 7196–7200.
- [72] Peter Erk, Heidi Engelsberg (Ed.) *Phthalocyanines Dyes and Pigments*, Elsevier Science, San Diego, **2003**.
- [73] A. B. Sorokin, *Chemical Reviews* **2013**, *113*, 8152–8191.
- [74] J. Zaumseil, H. Siringhaus, *Chemical Reviews* **2007**, *107*, 1296–1323.
- [75] I. López-Duarte, M. Wang, R. Humphry-Baker, M. Ince, M. V. Martínez-Díaz, M. K. Nazeeruddin, T. Torres, M. Grätzel, *Angew. Chem. Int. Ed.* **2012**, *51*, 1895–1898.
- [76] H. Imahori, T. Umeyama, S. Ito, *Acc. Chem. Res.* **2009**, *42*, 1809–1818.

- [77] E. Palomares, M. V. Martinez-Diaz, S. A. Haque, T. Torres, J. R. Durrant, *Chem. Commun.* **2004**, 2112–2113.
- [78] a) P. Y. Reddy, L. Giribabu, C. Lyness, H. J. Snaith, C. Vijaykumar, M. Chandrasekharam, M. Lakshmikantam, J.-H. Yum, K. Kalyanasundaram, M. Grätzel et al., *Angew. Chem. Int. Ed.* **2007**, *119*, 377–380; b) M. G. Walter, A. B. Rudine, C. C. Wamser, *J. Porphyrins Phthalocyanines* **2010**, *14*, 759–792; c) I. Bruder, J. Schöneboom, R. Dinnebier, A. Ojala, S. Schäfer, R. Sens, P. Erk, J. Weis, *Organic Electronics* **2010**, *11*, 377–387; d) I. Bruder, A. Ojala, C. Lennartz, S. Sundarraaj, J. Schöneboom, R. Sens, J. Hwang, P. Erk, J. Weis, *Solar Energy Materials and Solar Cells* **2010**, *94*, 310–316.
- [79] I. López-Duarte, M. Wang, R. Humphry-Baker, M. Ince, M. V. Martínez-Díaz, M. K. Nazeeruddin, T. Torres, M. Grätzel, *Angew. Chem.* **2012**, *124*, 1931–1934.
- [80] a) Y. Wang, D. Liang, *Advanced materials (Deerfield Beach, Fla.)* **2010**, *22*, 1521–1525; b) K.-Y. Law, *Chem. Rev.* **1993**, *93*, 449–486; c) D. Lee, H. B. Kim, *Korean Journal of Chemical Engineering* **2009**, *26*, 673–678.
- [81] V. Novakova, M. Miletin, K. Kopecky, P. Zimcik, *Chem. Eur. J.* **2011**, *17*, 14273–14282.
- [82] a) V. Novakova, P. Hladík, T. Filandrova, I. Zajícová, V. Krepsová, M. Miletin, J. Lenčo, P. Zimcik, *Physical chemistry chemical physics : PCCP* **2014**, *16*, 5440–5446; b) Y. Bian, J. Jiang, Y. Tao, Choi, Michael T M, R. Li, Ng, Anthony C H, P. Zhu, N. Pan, X. Sun, D. P. Arnold et al., *J. Am. Chem. Soc.* **2003**, *125*, 12257–12267; c) X.-J. Jiang, S.-L. Yeung, P.-C. Lo, W.-P. Fong, D. K. P. Ng, *J. Med. Chem.* **2011**, *54*, 320–330; d) M. Machacek, A. Cidlina, V. Novakova, J. Svec, E. Rudolf, M. Miletin, R. Kučera, T. Simunek, P. Zimcik, *J. Med. Chem.* **2015**, *58*, 1736–1749.
- [83] a) R. W. Boyle, D. Dolphin, *Photochemistry and Photobiology* **1996**, *64* (3), 469–485; b) E. A. Luk'yanets, *J. Porphyrins Phthalocyanines* **1999**, *3*, 424–432; c) A. P. Castano, T. N. Demidova, M. R. Hamblin, *Photodiagnosis and Photodynamic Therapy* **2004**, *1*, 279–293; d) L. B. Josefsen, R. W. Boyle, *British journal of pharmacology* **2008**, *154*, 1–3; e) Leung, S C H, P.-C. Lo, Ng, D K P, W.-K. Liu, K.-P. Fung, W.-P. Fong, *British journal of pharmacology* **2008**, *154*, 4–12.
- [84] D. Wöhrle, *Phthalocyanine – Von Farbmitteln zu photoaktiven Pharmazeutika und optoelektronischen Materialien*, Marburg, **2012**.
- [85] A. Hirth, U. Michelsen, D. Wöhrle, *Chem. Unserer Zeit* **1999**, *33*, 84–94.
- [86] H. I. Pass, *JNCI Journal of the National Cancer Institute* **1993**, *85*, 443–456.

References

- [87] V. Novakova, P. Reimerova, J. Svec, D. Suchan, M. Miletin, H. M. Rhoda, V. N. Nemykin, P. Zimcik, *Dalton Trans.* **2015**, 44, 13220–13233.
- [88] E. A. Luk'yanetz, *J. Porphyrins Phthalocyanines* **1999**, 03, 424–432.
- [89] Agentur für erneuerbare Energien, "Strommix in Deutschland 2014", can be found under <http://www.unendlich-viel-energie.de/strommix-deutschland-2014>, **2015**.
- [90] A. Hagfeldt, G. Boschloo, L. Sun, L. Kloo, H. Pettersson, *Chem. Rev.* **2010**, 110, 6595–6663.
- [91] K. Rudzio, *Die Zeit* **2016**, 71, 18.
- [92] R. Soldt, F. Röth (Fotos), "Ein Raum für Weltverbesserer", can be found under <http://www.faz.net/aktuell/der-deutsche-pavillon-auf-der-expo-2015-in-mailand-13553695.html>, **2015**.
- [93] S. Chhajed, M. F. Schubert, J. K. Kim, E. F. Schubert, *Appl. Phys. Lett.* **2008**, 93, 251108.
- [94] D. M. Chapin, C. S. Fuller, G. L. Pearson, *J. Appl. Phys.* **1954**, 25, 676.
- [95] M. Grätzel, *Nature* **2001**, 414, 338–344.
- [96] C. W. Tang, *Appl. Phys. Lett.* **1986**, 48, 183.
- [97] G. Smestad, M. Grätzel, *Journal of Chemical Education* **1998**, 5, 752–756.
- [98] J. Bisquert, D. Cahen, G. Hodes, S. Rühle, A. Zaban, *J. Phys. Chem. B* **2004**, 108, 8106–8118.
- [99] K. Kalyanasundaram, *Dye-Sensitized Solar Cells*, EFPL Press, **2010**.
- [100] M. K. Nazeeruddin, P. Péchy, T. Renouard, S. M. Zakeeruddin, R. Humphry-Baker, P. Comte, P. Liska, Le Cevey, E. Costa, V. Shklover et al., *J. Am. Chem. Soc.* **2001**, 123, 1613–1624.
- [101] T. Daeneke, T.-H. Kwon, A. B. Holmes, N. W. Duffy, U. Bach, L. Spiccia, *Nat. Chem.* **2011**, 3, 211–215.
- [102] A.-C. Dupuis, "Science Kick. Fritz Haber Institute of the Max Planck Society in Berlin", can be found under <http://www.science-kick.com/special-topics/co-adsorbents>, **2013**.
- [103] A. Yella, H.-W. Lee, H. N. Tsao, C. Yi, A. K. Chandiran, M. K. Nazeeruddin, E. W.-G. Diau, C.-Y. Yeh, S. M. Zakeeruddin, M. Grätzel, *Science* **2011**, 334, 629–634.
- [104] M.-E. Ragoussi, J.-J. Cid, J.-H. Yum, G. de La Torre, D. Di Censo, M. Grätzel, M. K. Nazeeruddin, T. Torres, *Angew. Chem. Int. Ed. Engl.* **2012**, 51, 4375–4378.
- [105] M.-E. Ragoussi, M. Ince, T. Torres, *Eur. J. Org. Chem.* **2013**, 29, 6475–6489.

- [106] M.-E. Ragoussi, J. Malig, G. Katsukis, B. Butz, E. Spiecker, G. de la Torre, T. Torres, D. M. Guldi, *Angew. Chem.* **2012**, *124*, 6527–6531.
- [107] A. N. Cammidge, I. Chambrier, M. J. Cook, D. L. Hughes, M. Rahman, L. Sosa-Vargas, *Chem. Eur. J.* **2011**, *17*, 3136–3146.
- [108] N. B. Chaure, A. N. Cammidge, I. Chambrier, M. J. Cook, A. K. Ray, *ECS Journal of Solid State Science and Technology* **2015**, *4*, P3086-P3090.
- [109] J. Burschka, N. Pellet, S.-J. Moon, R. Humphry-Baker, P. Gao, M. K. Nazeeruddin, M. Grätzel, *Nature* **2013**, *499*, 316–319.
- [110] D. P. McMeekin, G. Sadoughi, W. Rehman, G. E. Eperon, M. Saliba, M. T. Hörantner, A. Haghighirad, N. Sakai, L. Korte, B. Rech et al., *Science (New York, N.Y.)* **2016**, *351*, 151–155.
- [111] T. Glaser, *Chem. Commun.* **2011**, *47*, 116–130.
- [112] O. Kahn, *Acc. Chem. Res.* **2000**, *33*, 647–657.
- [113] R. A. Layfield, J. J. W. McDouall, S. A. Sulway, F. Tuna, D. Collison, R. E. P. Winpenney, *Chemistry* **2010**, *16*, 4442–4446.
- [114] N. Ishikawa, M. Sugita, T. Ishikawa, S.-y. Koshihara, Y. Kaizu, *J. Am. Chem. Soc.* **2003**, *125*, 8694–8695.
- [115] J. D. Rinehart, J. R. Long, *Chem. Sci.* **2011**, *2*, 2078.
- [116] J. A. de Saja, M. L. Rodriguez-Mendez, *Advances in colloid and interface science* **2005**, *116*, 1–11.
- [117] a) A. Parr, A. Krier, R. A. Collins, *Thin Solid Films* **1993**, *230*, 225–228; b) A. Altindal, Z. Öztürk, S. Dabak, Ö. Bekaroğlu, *Sensors and Actuators B: Chemical* **2001**, *77*, 389–394; c) T. Miyata, S. Kawaguchi, M. Ishii, T. Minami, *Thin Solid Films* **2003**, *425*, 255–259.
- [118] A. Wilson, J. D. Wright, *Molecular Crystals and Liquid Crystals Science and Technology. Section A. Molecular Crystals and Liquid Crystals* **1992**, *211*, 321–326.
- [119] A. Schütze, N. Pieper, J. Zacheja, *Sensors and Actuators B: Chemical* **1995**, *23*, 215–217.
- [120] a) M. Trometer, R. Even, J. Simon, A. Dubon, J.-Y. Laval, J. P. Germain, C. Maleysson, A. Pauly, H. Robert, *Sensors and Actuators B: Chemical* **1992**, *8*, 129–135; b) R. Aroca, H. Bolourchi, D. Battisti, K. Najafi, *Langmuir* **1993**, *9*, 3138–3141; c) M. L. Rodriguez-Mendez, R. Aroca, J. A. DeSaja, *Chem. Mater.* **1993**, *5*, 933–937; d) J. Souto, L. Tomilova, R. Aroca, J. A. DeSaja, *Langmuir* **1992**, *8*, 942–946.
- [121] K. R. Rickwood, D. R. Lovett, B. Lukas, J. Silver, *J. Mater. Chem.* **1995**, *5*, 725–729.

References

- [122] B. Liang, Y. Zhang, C. Yuan, Y. Wei, W. Chen, *Sensors and Actuators B: Chemical* **1998**, *46*, 24–29.
- [123] a) D. Campbell, R. A. Collins, *Thin Solid Films* **1997**, *295*, 277–282; b) M. L. Rodriguez-Mendez, R. Aroca, J. A. DeSaja, *Spectrochimica Acta Part A: Molecular Spectroscopy* **1993**, *49*, 965–973.
- [124] J. Jiang, W. Liu, K.-W. Poon, D. Du, D. P. Arnold, D. K. P. Ng, *Eur. J. Inorg. Chem.* **2000**, *2000*, 205–209.
- [125] F. Winquist, P. Wide, I. Lundström, *Analytica Chimica Acta* **1997**, *357*, 21–31.
- [126] Zeit Online, "Ein neuer Weltklimavertrag", can be found under <http://www.zeit.de/thema/klimagipfel-2015>, **2015**.
- [127] Greenpeace, "Ursachen des Klimawandels. Das massenhafte Verbrennen fossiler Energieträger wie Kohle und Öl hat das Klimasystem der Erde aus der Balance gebracht.", can be found under <https://www.greenpeace.de/themen/klimawandel/ursachen-des-klimawandels>, **2015**.
- [128] C. G. Claessens, D. González-Rodríguez, M. S. Rodríguez-Morgade, A. Medina, T. Torres, *Chemical Reviews* **2014**, *114*, 2192–2277.
- [129] M. P. Donzello, C. Ercolani, V. Novakova, P. Zimcik, P. A. Stuzhin, *Coordination Chemistry Reviews* **2016**, *309*, 107–179.
- [130] W. Darwish, *Dissertation*, Philipps-Universität Marburg, Marburg, **2006**.
- [131] S. P. Pujari, L. Scheres, A. T. M. Marcelis, H. Zuilhof, *Angew. Chem.* **2014**, *126*, 6438–6474.
- [132] S. P. Pujari, L. Scheres, A. T. M. Marcelis, H. Zuilhof, *Angew. Chem. Int. Ed.* **2014**, *53*, 6322–6356.
- [133] A. Bayoumi, *Dissertation*, Philipps-Universität Marburg, Marburg, **2015**.
- [134] a) R. C. Palmer, *Industrial and Engineering Chemistry* **1942**, *34*, 1028–1034; b) W. F. Brill, *Industrial and Engineering Chemistry* **1960**, *52*, 837–840; c) A. Onopchenko, J. G. D. Schulz, R. Seekircher, *J. Chem. Soc. D* **1971**, 939.
- [135] a) Sheldon, Roger, A., Kochi, Jay, K., *Metal Catalyzed Oxidations of Organic Compounds*, Academic Press, New York, **1981**; b) B. Cornils, W. A. Herrmann, *Applied Homogeneous Catalysis with Organometallic Compounds*, Wiley-VCH, Weinheim, **1996**.
- [136] Z. Iqbal, A. Lyubimtsev, M. Hanack, *Synlett* **2008**, *15*, 2287–2290.
- [137] N. Alharbi, A. Díaz-Moscoso, G. J. Tizzard, S. J. Coles, M. J. Cook, A. N. Cammidge, *Tetrahedron* **2014**, *70*, 7370–7379.

- [138] D. D. Coffmann, E. L. Jenner, R. D. Lipscomb, *J. Am. Chem. Soc.* **1958**, *80*, 2864–2872.
- [139] P. Jones, G. B. Villeneuve, C. Fei, J. DeMarte, A. J. Haggarty, K. T. Nwe, D. A. Martin, A. M. Lebuis, J. M. Finkelstein, B. J. Gour-Salin et al., *J. Med. Chem.* **1998**, *41*, 3062–3077.
- [140] T. Vollgraf, *Bachelorarbeit*, Philipps-Universität Marburg, Marburg, **2014**.
- [141] a) W. Freyer, L. Q. Minh, *J. Prakt. Chemie* **1987**, *329*, 365–373; b) B. L. Wheeler, G. Nagasubramanian, A. J. Bard, L. A. Schechtman, *J. Am. Chem. Soc.* **1984**, *106*, 7404–7410; c) E. F. Bradbrook, R. P. Linstead, *J. Chem. Soc.* **1936**, 1739–1744.
- [142] L. Eyrolles, H. Kagechika, E. Kawachi, H. Fukasawa, T. Iijima, Y. Matsushima, Y. Hashimoto, K. Shudo, *J. Med. Chem.* **1994**, *37*, 1508–1517.
- [143] K. Hermann, G. Simchen, *Liebigs Annalen der Chemie* **1981**, *2*, 333–341.
- [144] R. W. Begland, D. R. Hartter, *J. Org. Chem.* **1972**, *37*, 4136–4145.
- [145] O. W. Webster, D. R. Hartter, R. W. Begland, W. A. Sheppard, A. Cairncross, *J. Org. Chem.* **1972**, *37*, 4133–4136.
- [146] H. W. Rothkopf, D. Wöhrle, R. Müller, G. Koßmehl, *Chem. Ber.* **1975**, *108*, 875–886.
- [147] O. Hordiyenko, I. Rudenko, I. Zamkova, O. Denisenko, A. Biitseva, A. Arrault, A. Tolmachev, *Synthesis* **2013**, *45*, 3375–3382.
- [148] A. W. Burgstahler, P.-L. Chien, M. O. Abdel-Rahman, *J. Am. Chem. Soc.* **1964**, *86*, 5281–5290.
- [149] H. Onay, B. Esat, R. Öztürk, *Polyhedron* **2010**, *29*, 1314–1316.
- [150] F. D. Popp, *Journal of Heterocyclic Chemistry* **1974**, *11*, 79–82.
- [151] Y.-H. Chen, J.-H. Chang, G.-R. Lee, I.-W. Wu, J.-H. Fang, C.-I. Wu, T.-W. Pi, *Appl. Phys. Lett.* **2009**, *95*, 133302.
- [152] D. D. Díaz, H. J. Bolink, L. Cappelli, C. G. Claessens, E. Coronado, T. Torres, *Tetrahedron Letters* **2007**, *48*, 4657–4660.
- [153] Y.-H. Chen, Y.-J. Chang, G.-R. Lee, J.-H. Chang, I.-W. Wu, J.-H. Fang, S.-H. Hsu, S.-W. Liu, C.-I. Wu, T.-W. Pi, *Organic Electronics* **2010**, *11*, 445–449.
- [154] G. E. Morse, M. G. Helander, J. F. Maka, Z.-H. Lu, T. P. Bender, *ACS Appl. Mater. Interfaces* **2010**, *2*, 1934–1944.
- [155] G. E. Morse, J. S. Castrucci, M. G. Helander, Z.-H. Lu, T. P. Bender, *ACS applied materials & interfaces* **2011**, *3*, 3538–3544.

References

- [156] a) S. Xu, K. Chen, H. Tian, *J. Mater. Chem.* **2005**, *15*, 2676; b) E. Palomares, M. V. Martínez-Díaz, T. Torres, E. Coronado, *Adv. Funct. Mater.* **2006**, *16*, 1166–1170; c) J. V. Ros-Lis, R. Martínez-Mañez, J. Soto, *Chem. Commun.* **2005**, *42*, 5260–5262.
- [157] T. Yasuda, T. Tsutsui, *Molecular Crystals and Liquid Crystals* **2006**, *462*, 3–9.
- [158] a) Z. H. Kafafi, P. A. Lane (Eds.) *SPIE Proceedings*, SPIE, **2009**; b) H. Schmidt, T. Winkler, M. Tilgner, H. Flügge, S. Schmale, T. Bülow, J. Meyer, H.-H. Johannes, T. Riedl, W. Kowalsky in *SPIE Proceedings* (Eds.: Z. H. Kafafi, P. A. Lane), SPIE, **2009**; c) H. H. P. Gommans, D. Cheyns, T. Aernouts, C. Giroto, J. Poortmans, P. Heremans, *Adv. Funct. Mater.* **2007**, *17*, 2653–2658; d) D. Cheyns, B. P. Rand, P. Heremans, *Appl. Phys. Lett.* **2010**, *97*, 33301; e) J. Dai, X. Jiang, H. Wang, D. Yan, *Thin Solid Films* **2008**, *516*, 3320–3323; f) H. Gommans, S. Schols, A. Kadashchuk, P. Heremans, S. C. J. Meskers, *J. Phys. Chem. C* **2009**, *113*, 2974–2979; g) H. H. P. Gommans, D. Cheyns, T. Aernouts, C. Giroto, J. Poortmans, P. Heremans, *Adv. Funct. Mater.* **2007**, *17*, 2653–2658; h) H. Gommans, T. Aernouts, B. Verreet, P. Heremans, A. Medina, C. G. Claessens, T. Torres, *Adv. Funct. Mater.* **2009**, *19*, 3435–3439; i) H. Gommans, B. Verreet, B. P. Rand, R. Muller, J. Poortmans, P. Heremans, J. Genoe, *Adv. Funct. Mater.* **2008**, *18*, 3686–3691; j) I. Hancox, P. Sullivan, K. V. Chauhan, N. Beaumont, L. A. Rochford, R. A. Hatton, T. S. Jones, *Organic Electronics* **2010**, *11*, 2019–2025; k) P. Heremans, D. Cheyns, B. P. Rand, *Accounts of chemical research* **2009**, *42*, 1740–1747; l) X. Jiang, J. Dai, H. Wang, Y. Geng, D. Yan, *Chemical Physics Letters* **2007**, *446*, 329–332; m) C. E. Mauldin, C. Piliago, D. Poulsen, D. A. Unruh, C. Woo, B. Ma, J. L. Mynar, J. M. J. Fréchet, *ACS Appl. Mater. Interfaces* **2010**, *2*, 2833–2838; n) L.-J. Pegg, S. Schumann, R. A. Hatton, *ACS nano* **2010**, *4*, 5671–5678; o) X. Tong, B. E. Lassiter, S. R. Forrest, *Organic Electronics* **2010**, *11*, 705–709; p) J. L. Yang, S. Schumann, R. A. Hatton, T. S. Jones, *Organic Electronics* **2010**, *11*, 1399–1402.
- [159] B. Verreet, B. P. Rand, D. Cheyns, A. Hadipour, T. Aernouts, P. Heremans, A. Medina, C. G. Claessens, T. Torres, *Adv. Energy Mater.* **2011**, *1*, 565–568.
- [160] B. Verreet, S. Schols, D. Cheyns, B. P. Rand, H. Gommans, T. Aernouts, P. Heremans, J. Genoe, *J. Mater. Chem.* **2009**, *19*, 5295–5297.
- [161] K. Cnops, B. P. Rand, D. Cheyns, B. Verreet, M. A. Empl, P. Heremans, *Nature Communications* **2014**, *5*, 3406.
- [162] A. Meller, A. Ossko, *Monatshefte fuer Chemie* **1972**, *103*, 150–155.
- [163] C. G. Claessens, D. González-Rodríguez, C. M. McCallum, R. S. Nohr, H.-P. Schuchmann, T. Torres, *J. Porphyrins Phthalocyanines* **2007**, *11*, 181–188.

- [164] C. G. Claessens, D. González-Rodríguez, B. del Rey, T. Torres, G. Mark, H.-P. Schuchmann, C. von Sonntag, J. G. MacDonald, R. S. Nohr, *Eur. J. Org. Chem.* **2003**, *14*, 2547–2551.
- [165] F. A. Cotton, G. Wilkinson, *Anorganische Chemie*, Verlag Chemie, **1967**.
- [166] H. Hess, *Z. Krist.* **1963**, *118*, 361.
- [167] H. Kietaihl, *Monatsh. Chem.* **1974**, *105*, 405–418.
- [168] a) J. L. Hoard, S. Geller, T. B. Owen, *Acta cryst. (Kopenhagen)* **1951**, *4*, 405; b) *International tables for x-ray crystallography*, Birmingham: The Kynoch Press, **1962**.
- [169] J. Guilleme, D. González-Rodríguez, T. Torres, *Angew. Chem. Int. Ed. Engl.* **2011**, *50*, 3506–3509.
- [170] J. Guilleme, D. González-Rodríguez, T. Torres, *Angew. Chem.* **2011**, *123*, 3568–3571.
- [171] K. Kasuga, T. Idehara, M. Handa, Y. Ueda, T. Fujiwara, K. Isa, *Bull. Chem. Soc. Jpn.* **1996**, *69*, 2559–2563.
- [172] M. S. Rodríguez-Morgade, C. G. Claessens, A. Medina, D. González-Rodríguez, E. Gutiérrez-Puebla, A. Monge, I. Alkorta, J. Elguero, T. Torres, *Chem. Eur. J.* **2008**, *14*, 1342–1350.
- [173] G. E. Morse, J. F. Maka, A. J. Lough, T. P. Bender, *Acta Crystallogr.* **2010**, 3057.
- [174] G. E. Morse, I. Gong, Y. Kowar, A. J. Lough, T. P. Bender, *Crystal Growth & Design* **2014**, *14*, 2138–2147.
- [175] C. H. Macgillavry, G. D. Rieck, K. Lonsdale (Eds.) *International Tables for X-ray crystallography, / The International Union of Crystallography ; Vol. 3*, Kynoch Press, Lincoln, United Kingdom, **1962**.
- [176] a) N. Kobayashi, T. Ishizaki, K. Ishii, H. Konami, *J. Am. Chem. Soc.* **1999**, *121*, 9096–9110; b) M. Geyer, F. Plenzig, M. Hanack, B. del Rey, Á. Sastre, T. Torres, *Synthesis* **1996**, *9*, 1139–1151.
- [177] Michael Kothe, *Masterarbeit*, Philipps-Universität Marburg, Marburg, **2015**.
- [178] K. M. Kadish, K. M. Smith, R. Guilard, *The Porphyrin Handbook: Phthalocyanines - Synthesis*, Academic Press, Amsterdam, **2003**.
- [179] J. Svec, P. Zimcik, L. Novakova, O. A. Rakitin, S. A. Amelichev, P. A. Stuzhin, V. Novakova, *Eur. J. Org. Chem.* **2015**, *3*, 596–604.
- [180] V. N. Nemykin, S. V. Dudkin, F. Dumoulin, C. Hirel, A. G. Gürek, V. Ahsen, *Arkivoc* **2013**, *2014*, 142–204.
- [181] C. C. Leznoff, P. I. Svirskaya, B. Khouw, R. L. Cerny, P. Seymour, A. B. P. Lever, *J. Org. Chem.* **1991**, *56*, 82–90.

References

- [182] E. M. Idelson, *U.S. Patent 4 061 654*, 1977; *Chem. Abstr.* **1977**, 88, 171797.
- [183] a) R. B. Hammond, K. J. Roberts, R. Docherty, M. Edmondson, R. Gairns, *J. Chem. Soc., Perkin Trans. 2* **1996**, 1527–1528; b) J. M. Robertson, *J. Chem. Soc.* **1935**, 615–621.
- [184] M. K. Engel, *Kawamura Rikagaku Kenkyusho Hokoku* **1997**, 1996, 11–54.
- [185] a) T. Furuyama, K. Satoh, T. Kushiya, N. Kobayashi, *J. Am. Chem. Soc.* **2014**, 136, 765–776; b) M. Gsanger, D. Bialas, L. Huang, M. Stolte, F. Wurthner, *Advanced materials (Deerfield Beach, Fla.)* **2016**, 28, 3615–3645.
- [186] C. Würth, M. Grabolle, J. Pauli, M. Spieles, U. Resch-Genger, *Nature Protocols* **2013**, 8, 1535–1550.
- [187] S. Makhseed, B. Ghazal, A. M. Abdelmoniem, V. Novakova, P. Zimcik, *RSC Adv* **2015**, 5, 58854–58864.
- [188] V. Novakova, M. Lásková, H. Vavříčková, P. Zimcik, *Chem. Eur. J.* **2015**, 21, 14382–14392.
- [189] I. B. C. Matheson, J. Lee, B. S. Yamanashi, M. L. Wolbarsht, *J. Am. Chem. Soc.* **1974**, 96, 3343–3348.
- [190] P. B. Merkel, D. R. Kearns, *J. Am. Chem. Soc.* **1975**, 97, 462–463.
- [191] M. Nečedová, P. Magdolen, V. Novakova, M. Cigáň, S. Vlčková, P. Zahradník, A. Fülöpová, *Eur. J. Org. Chem.* **2015**, 2015, 7053–7068.
- [192] a) N. Kobayashi, J. Mack, K. Ishii, M. J. Stillman, *Inorg. Chem.* **2002**, 41, 5350–5363; b) H. Miwa, K. Ishii, N. Kobayashi, *Chem. Eur. J.* **2004**, 10, 4422–4435.
- [193] B. del Rey, U. Keller, T. Torres, G. Rojo, F. Agulló-López, S. Nonell, C. Martí, S. Brasselet, I. Ledoux, J. Zyss, *J. Am. Chem. Soc.* **1998**, 120, 12808–12817.
- [194] Z. Zhao, C.-T. Poon, W.-K. Wong, W.-Y. Wong, H.-L. Tam, K.-W. Cheah, T. Xie, D. Wang, *Eur. J. Inorg. Chem.* **2008**, 2008, 119–128.
- [195] P. Zimcik, E. H. Mørkved, T. Andreassen, J. Lenco, V. Novakova, *Polyhedron* **2008**, 27, 1368–1374.
- [196] Alexander Lange, *Bachelorarbeit*, Philipps-Universität Marburg, Marburg, **2015**.
- [197] A. Díaz-Moscoso, G. J. Tizzard, S. J. Coles, A. N. Cammidge, *Angew. Chem. Int. Ed. Engl.* **2013**, 52, 10784–10787.
- [198] A. Díaz-Moscoso, G. J. Tizzard, S. J. Coles, A. N. Cammidge, *Angew. Chem.* **2013**, 125, 10984–10987.
- [199] K. Pfaff, *Bachelor Arbeit*, Philipps-Universität Marburg, Marburg, **2014**.

- [200] A. N. Cammidge, M. J. Cook, D. L. Hughes, F. Nekelson, M. Rahman, *Chemical communications (Cambridge, England)* **2005**, 930–932.
- [201] P. Zimcik, *Synthesis of Meso Substituted Pyrazinoporphyrazines*. Oral Communication, **2016**, Hradec, Czech Republic.
- [202] a) P. Mehring, A. Beimborn, T. Lühr, C. Westphal, *J. Phys. Chem. C* **2012**, *116*, 12819–12823; b) R. Wu, L. Yan, Y. Zhang, J. Ren, D. Bao, H. Zhang, Y. Wang, S. Du, Q. Huan, H.-J. Gao, *J. Phys. Chem. C* **2015**, *119*, 8208–8212; c) B. Wiggins, K. W. Hipps, *J. Phys. Chem. C* **2014**, *118*, 4222–4230; d) T. A. Pham, F. Song, M. Stöhr, *Physical chemistry chemical physics : PCCP* **2014**, *16*, 8881–8885.
- [203] F. Mitzel, S. FitzGerald, A. Beeby, R. Faust, *Chem. Commun.* **2001**, *24*, 2596–2597.
- [204] a) Y. Zhu, B. Zhang, X. Liu, D.-W. Wang, D. S. Su, *Angew. Chem. Int. Ed. Engl.* **2014**, *53*, 10673–10677; b) Y. Zhu, B. Zhang, X. Liu, D.-W. Wang, D. S. Su, *Angew. Chem.* **2014**, *126*, 10849–10853.
- [205] W. Darwish, E. Seikel, R. Käsmarker, K. Harms, J. Sundermeyer, *Dalton Trans.* **2011**, *40*, 1787–1794.
- [206] A. Morandeira, I. López-Duarte, B. O'Regan, M. V. Martínez-Díaz, A. Forneli, E. Palomares, T. Torres, J. R. Durrant, *J. Mater. Chem.* **2009**, *19*, 5016.
- [207] M. BARTHEL, M. Hanack, *J. Porphyrins Phthalocyanines* **2000**, *4*, 635–638.
- [208] C. Linares-Flores, F. Mendizabal, R. Arratia-Pérez, N. Inostroza, C. Orellana, *Chemical Physics Letters* **2015**, *639*, 172–177.
- [209] A. V. Ivanov, P. A. Svinareva, L. G. Tomilova, N. S. Zefirov, *Russian Chemical Bulletin* **2001**, *50*, 919–920.
- [210] M. Kohn, L. Steiner, *J. Org. Chem.* **1947**, *12*, 30–33.
- [211] A. V. Ivanov, P. A. Svinareva, I. V. Zhukov, L. G. Tomilova, N. S. Zefirov, *Russian Chemical Bulletin* **2003**, *52*, 1562–1566.
- [212] a) G. Märkl, K. Gschwender, I. Rötzer, P. Kreitmeier, *Helvetica Chimica Acta* **2004**, *87*, 825–844; b) A. Sasa, K. Okada, K. Nakamura, S. Okada, *J. Mol. Struct.* **1998**, *446*, 163–178.
- [213] Sebastian M. Marcuccio, Polina I. Svirskaya, Shafrira Greenberg, A. B. P. Lever, Clifford C. Leznoff, Kenneth B. Tomer, *Can. J. Chem.* **1985**, *63*, 3057–3069.
- [214] a) S. Cogal, K. Ocakoglu, A. U. Oksuz, *Inorganica Chimica Acta* **2014**, *423*, 139–144; b) R. Ashokkumar, A. Kathiravan, P. Ramamurthy, *Physical chemistry chemical physics : PCCP* **2014**, *16*, 14139–14149.
- [215] H. Ali, J. E. van Lier, *Tetrahedron Letters* **1997**, *38*, 1157–1160.

References

- [216] H. Ali, S. Ait-Mohand, S. Gosselin, J. E. van Lier, B. Guérin, *J. Org. Chem.* **2011**, *76*, 1887–1890.
- [217] A. Gouloumis, S.-G. Liu, Á. Sastre, P. Vázquez, L. Echegoyen, T. Torres, *Chem. Eur. J.* **2000**, *6*, 3600–3607.
- [218] H. Tian, H. Ali, J. E. van Lier, *Tetrahedron Letters* **2000**, *41*, 8435–8438.
- [219] M. Hu, N. Brasseur, S. Z. Yildiz, J. E. van Lier, C. C. Leznoff, *J. Med. Chem.* **1998**, *41*, 1789–1802.
- [220] a) W. Al-Maksoud, J. Mesnager, F. Jaber, C. Pinel, L. Djakovitch, *J. Organomet. Chem.* **2009**, *694*, 3222–3231; b) J. Tarabay, W. Al-Maksoud, F. Jaber, C. Pinel, S. Prakash, L. Djakovitch, *Applied Catalysis A: General* **2010**, *388*, 124–133; c) Y. Belabassi, S. Alzghari, J.-L. Montchamp, *J. Organomet. Chem.* **2008**, *693*, 3171–3178.
- [221] Y. Kobayashi, A. D. William, *Adv. Synth. Catal.* **2004**, *346*, 1749–1757.
- [222] M. Abe, K. Nishikawa, H. Fukuda, K. Nakanishi, Y. Tazawa, T. Taniguchi, S.-Y. Park, S. Hiradate, Y. Fujii, K. Okuda et al., *Phytochemistry* **2012**, *84*, 56–67.
- [223] C. Richter, M. Beu, D. Schlettwein, *Phys Chem Chem Phys* **2015**, *17*, 1883–1890.
- [224] S. T. Tan, B. J. Chen, X. W. Sun, W. J. Fan, H. S. Kwok, X. H. Zhang, S. J. Chua, *J. Appl. Phys.* **2005**, *98*, 13505.
- [225] N. Sakai, T. Miyasaka, T. N. Murakami, *J. Phys. Chem. C* **2013**, *117*, 10949–10956.
- [226] T. Yoshida, J. Zhang, D. Komatsu, S. Sawatani, H. Minoura, T. Pauporté, D. Lincot, T. Oekermann, D. Schlettwein, H. Tada et al., *Adv. Funct. Mater.* **2009**, *19*, 17–43.
- [227] A. Brennfürer, H. Neumann, M. Beller, *Synlett* **2007**, *2007*, 2537–2540.
- [228] K. S. Petrakis, T. L. Nagabhushan, *J. Am. Chem. Soc.* **1987**, *109*, 2831–2833.
- [229] E. Palomares, M. V. Martínez-Díaz, T. Torres, E. Coronado, *Adv. Funct. Mater.* **2006**, *16*, 1166–1170.
- [230] P. Sullivan, A. Duraud, I. Hancox, N. Beaumont, G. Mirri, J. H. Tucker, R. A. Hatton, M. Shipman, T. S. Jones, *Adv. Energy Mater.* **2011**, *1*, 352–355.
- [231] M. Hanack, M. Geyer, *J. Chem. Soc., Chem. Commun.* **1994**, 2253–2254.
- [232] a) C. G. Claessens, T. Torres, *Eur. J. Org. Chem.* **2000**, 1603–1607; b) C. G. Claessens, T. Torres, *Tetrahedron Letters* **2000**, *41*, 6361–6365.
- [233] Van der Sluis, P., Spek, A. L., *Acta Crystallogr., Sect. A: Found. Crystallogr.* **1990**, *A46*, 194–201.
- [234] A. L. Spek, *Acta crystallographica. Section D, Biological crystallography* **2009**, *65*, 148–155.
- [235] Y. Yamasaki, T. Mori, *Bull. Chem. Soc. Jpn.* **2011**, *84*, 1208–1214.

- [236] R. Potz, M. GöIdner, H. Hückstädt, U. Cornelissen, A. Tutaß, H. Homburg, *Z. anorg. allg. Chem.* **2000**, 626, 588–596.
- [237] R. S. Iglesias, C. G. Claessens, T. Torres, M. A. Herranz, V. R. Ferro, de la Vega, Jose M García, *J. Org. Chem.* **2007**, 72, 2967–2977.
- [238] a) S. Çetindere, B. Çoşut, S. Yeşilot, M. Durmuş, A. Kılıç, *Dyes and Pigments* **2014**, 101, 234–239; b) N. Kobayashi, T. Ishizaki, K. Ishii, H. Konami, *J. Am. Chem. Soc.* **1999**, 121, 9096–9110.
- [239] Y. Yang, *Polyhedron* **2012**, 33, 310–318.
- [240] a) E. Caballero, J. Fernández-Ariza, V. M. Lynch, C. Romero-Nieto, M. S. Rodríguez-Morgade, J. L. Sessler, D. M. Guldi, T. Torres, *Angew. Chem. Int. Ed.* **2012**, 51, 11337–11342; b) E. Caballero, J. Fernández-Ariza, V. M. Lynch, C. Romero-Nieto, M. S. Rodríguez-Morgade, J. L. Sessler, D. M. Guldi, T. Torres, *Angew. Chem.* **2012**, 124, 11499–11504.
- [241] L.-C. Song, F.-X. Luo, H. Tan, X.-J. Sun, Z.-J. Xie, H.-B. Song, *Eur. J. Inorg. Chem.* **2013**, 2013, 2549–2557.
- [242] E. Sharikow, *Bachelorarbeit*, Philipps-Universität Marburg, Marburg, **2013**.
- [243] W. E. Bennett, D. E. Broberg, N. C. Baenziger, *Inorg. Chem.* **1973**, 12, 930–936.
- [244] A. Gieren, W. W. Hoppe, *J. Chem. Soc. D, Chem. Comm.* **1971**, 413–415.
- [245] J. Schwöbel, Y. Fu, J. Brede, A. Dilullo, G. Hoffmann, S. Klyatskaya, M. Ruben, R. Wiesendanger, *Nature Communications* **2012**, 3, 953–957.
- [246] A. de Cian, M. Moussavi, J. Fischer, R. Weiss, *Inorg. Chem.* **1985**, 24, 3162–3167.
- [247] I. S. Kirin, P. N. Moskalev, Y. A. Makashev, *Russ. J. Inorg. Chem. (Engl. Trans.)* **1965**, 10, 1065.
- [248] a) P. N. Maskalev, I. S. Kirin, *Russ. J. Phys. Chem. (Engl. Trans.)* **1972**, 46, 1019; b) P. N. Moskalev, I. S. Kirin, *Russ. J. Inorg. Chem.* **1970**, 15, 7.
- [249] A. G. MacKay, J. F. Boas, G. J. Troup, *Aust. J. Chem.* **1974**, 27, 955–964.
- [250] G. A. Corker, *J. Electrochem. Soc.* **1979**, 126, 1339–1343.
- [251] A. T. Chang, J.-C. Marchon, *Inorganica Chimica Acta* **1981**, 53, L241-L243.
- [252] N. Ishikawa, O. Ohno, Y. Kaizu, *Chemical Physics Letters* **1991**, 180, 51–56.
- [253] a) N. Ishikawa, O. Ohno, Y. Kaizu, *J. Phys. Chem.* **1993**, 97, 1004–1010; b) N. Ishikawa, O. Ohno, Y. Kaizu, H. Kobayashi, *J. Phys. Chem.* **1992**, 96, 8832–8839.
- [254] N. Ishikawa, M. Sugita, N. Tanaka, T. Ishikawa, S.-y. Koshihara, Y. Kaizu, *Inorg. Chem.* **2004**, 43, 5498–5500.

References

- [255] a) N. Ishikawa, M. Sugita, W. Wernsdorfer, *Angew. Chem. Int. Ed. Engl.* **2005**, *44*, 2931–2935; b) N. Ishikawa, M. Sugita, W. Wernsdorfer, *Angew. Chem.* **2005**, *117*, 2991–2995.
- [256] P. Swolana, *Bachelor Arbeit*, Philipps-Universität Marburg, Marburg, **2014**.
- [257] V. E. Pushkarev, M. O. Breusova, E. V. Shulishov, Y. V. Tomilov, *Russ. Chem. Bull.* **2005**, *54*, 2087–2093.
- [258] J. Janczak, R. Kubiak, J. Lisowski, *Polyhedron* **2011**, *30*, 253–258.
- [259] U. Keppeler, W. Kobel, H.-U. Siehl, M. Hanack, *Chem. Ber.* **1985**, *118*, 2095–2104.
- [260] E. Seikel, B. Oelkers, J. Sundermeyer, *Inorg. Chem.* **2012**, *51*, 2709–2717.
- [261] G. Clarisse, M. T. Riou, *Inorganica Chimica Acta* **1987**, *130*, 139–144.
- [262] a) J. W. Buchler, P. Hammerschmitt, I. Kaufeld, J. Löffler, *Chem. Ber.* **1991**, *124*, 2151–2159; b) J. W. Buchler, J. Hüttermann, J. Löffler, *Bull. Chem. Soc. Jpn.* **1988**, *61*, 71–77.
- [263] A. F. Hollemann, E. Wiberg (Eds.) *Lehrbuch der Anorganischen Chemie*, de Gruyter, Berlin, New York, **1995**.
- [264] a) W. Armarego, D. D. Perrin (Eds.) *Purification of Laboratory Chemicals. 4th edition*, Elsevier, Burlington, **1996**; b) W. L. F. Armarego, C. L. L. Chai (Eds.) *Purification of Laboratory Chemicals*, Elsevier/Butterworth-Heinemann, Amsterdam, Boston, **2009**.
- [265] a) Harold H. Fox, Kimo B. Yap, Jennifer Robbins, Shiang Cai, and Richard R. Schrock, *Inorg. Chem.* **1992**, *31*, 2287–2289; b) L. M. Atagi, J. M. Mayer, *Angew. Chem. Int. Ed. Engl.* **1993**, *32*, 439–441.
- [266] U. Radius, J. Sundermeyer, H. Pritzkowb, *Chem. Ber.* **1994**, *127*, 1827–1835.
- [267] Nina Hillesheim, *Dissertation*, Philipps-Universität Marburg, Marburg, **2011**.
- [268] W. A. Herrmann, A. Salzer, *Synthetic Methods of Organometallic and Inorganic Chemistry. Thieme-Verlag, Stuttgart, 1996.*, Thieme-Verlag, Stuttgart, **1996**.
- [269] H. C. Aspinall, D. C. Bradley, M. B. Hursthouse, K. D. Sales, N. P. C. Walker, B. Hussain, *Dalton Trans.* **1989**, *4*, 623–626.
- [270] A. A. Trifonob, D. M. Lyubov, E. A. Fedorova, G. G. Skvortsov, G. K. Fukin, Y. A. Kurskii, M. N. Bochkarev, *Russ. Chem. Bull.* **2006**, *55*, 435–441.
- [271] a) H. Benn, G. Wilke, D. Henneberg, *Angew. Chem.* **1973**, *85*, 1052–1053; b) G. Wilke, H. Benn, R. Goddard, C. Krüger, B. Pfeil, *Inorganica Chimica Acta* **1992**, *198-200*, 741–748; c) H. Benn, G. Wilke, D. Henneberg, *Angew. Chem. Int. Ed. Engl.* **1973**, *12*, 1001–1002.

- [272] H. G. O. Becker, R. Beckert, *Organikum. Organisch-chemisches Grundpraktikum*, Wiley-VCH, Weinheim, **2015**.
- [273] a) G. R. Fulmer, A. J. M. Miller, N. H. Sherden, H. E. Gottlieb, A. Nudelman, B. M. Stoltz, J. E. Bercaw, K. I. Goldberg, *Organometallics* **2010**, *29*, 2176–2179; b) H. E. Gottlieb, V. Kotlyar, A. Nudelman, *J. Org. Chem.* **1997**, *62*, 7512–7515.
- [274] a) L. Kaestner, M. Cesson, K. Kassab, T. Christensen, P. D. Edminson, M. J. Cook, I. Chambrier, G. Jori, *Photochem. Photobiol. Sci.* **2003**, *2*, 660–667; b) P. G. Seybold, M. Gouterman, *Journal of Molecular Spectroscopy* **1969**, *31*, 1–13; c) V. Novakova, M. Miletin, T. Filandrova, J. Lenco, A. Ruzicka, P. Zimcik, *The Journal of organic chemistry* **2014**, *79*, 2082–2093.
- [275] M. Fischer, J. Georges, *Chemical Physics Letters* **1996**, *260*, 115–118.
- [276] P. Gottschalk, J. Paczkowski, D. C. Neckers, *Journal of Photochemistry* **1986**, *35*, 277–281.
- [277] E. V. Kovshev, V. A. Puchnova, E. A. Luk'yanetz, *J. Org. Chem. USSR (Engl. Trans.)* **1971**, *71*, 364.
- [278] F. Mitzel, S. FitzGerald, A. Beeby, R. Faust, *Chem. Eur. J.* **2003**, *9*, 1233–1241.
- [279] C. Burmester, R. Faust, *Synthesis* **2008**, *2008*, 1179–1181.
- [280] H. A. Bruson, J. W. Kroeger, *J. Am. Chem. Soc.* **1940**, *62*, 36–44.
- [281] H. Kagechika, E. Kawachi, Y. Hashimoto, K. Shudo, T. Himi, *J. Med. Chem.* **1988**, *31*, 2182–2192.
- [282] G. Märkl, K. Gschwendner, I. Rötzer, P. Kreitmeier, *HCA* **2004**, *87*, 825–844.
- [283] V. Aranyos, A. M. Castaño, H. Grennberg, M. F. Hawthorne, S. Sjöberg, A. Talec, T. Shono, H. Toftlund, *Acta Chem. Scand.* **1999**, *53*, 714–720.
- [284] D. S. Terekhov, K. J. M. Nolan, C. R. McArthur, C. C. Leznoff, *J. Org. Chem.* **1996**, *61*, 3034–3040.
- [285] T. Suzuki, Y. Nagae, K. Mitsuhashi, *Journal of Heterocyclic Chemistry* **1986**, *23*, 1419–1421.
- [286] S. Nakamura, P. Y. Reddy, H. Tanaka, T. Toru, H. Uchida, H. Yoshiyama, *Synlett* **2002**, *10*, 1649–1652.
- [287] Y. Xiang, *Dissertation*, Philipps-Universität Marburg, Marburg, **2013**.
- [288] A. K. Ghosh, D. D. Anderson, *Org. Lett.* **2012**, *14*, 4730–4733.
- [289] B. Du, X. Jiang, P. Sun, *J. Org. Chem.* **2013**, *78*, 2786–2791.
- [290] V. E. Pushkarev, E. V. Shulishov, Y. V. Tomilov, L. G. Tomilova, *Tetrahedron Letters* **2007**, *48*, 5269–5273.

References

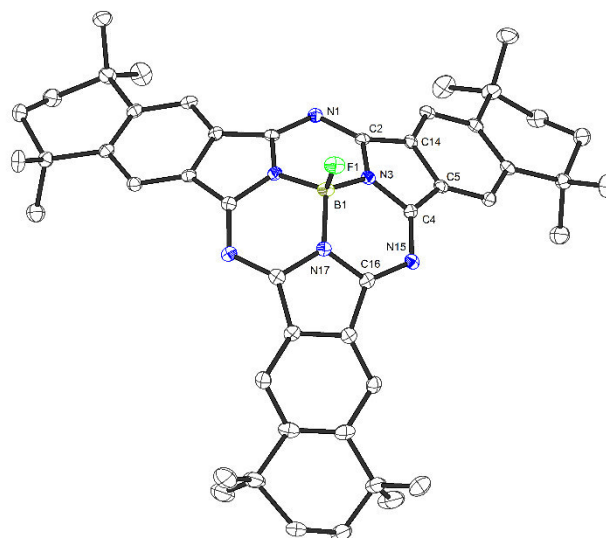
- [291] V. E. Pushkarev, V. V. Kalashnikov, S. A. Trashin, N. E. Borisova, L. G. Tomilova, N. S. Zefirov, *Dalton Trans.* **2013**, *42*, 12083–12086.
- [292] *APEX2*, Bruker AXS Inc., Madison, Wisconsin, USA, **2014**.
- [293] *SAINT*, Bruker AXS Inc., Madison, Wisconsin, USA, **2013**.
- [294] G. M. Sheldrick, *Acta Crystallographica. Section A, Foundations of Crystallography* **2008**, *64*, 112–122.
- [295] G. M. Sheldrick, *SHELXT*, Universität Göttingen, Göttingen, Germany, **2014**.
- [296] G. M. Sheldrick, *SHELXL*, Universität Göttingen, Göttingen, Germany, **2014**.
- [297] K. Brandenburg, *Diamond - Crystal and Molecular Structure Visualization*, Crystal Impact - Dr. H. Putz & Dr. K. Brandenburg GbR, Bonn, Germany, **2014**.
- [298] *SADABS*, Bruker AXS Inc., Madison, Wisconsin, USA, **2014**.
- [299] G. M. Sheldrick, *Acta Crystallogr A Found Adv* **2015**, *71*, 3–8.
- [300] G. M. Sheldrick, *Acta crystallographica. Section C, Structural Chemistry* **2015**, *71*, 3–8.
- [301] C. B. Hübschle, G. M. Sheldrick, B. Dittrich, *Journal of Applied Crystallography* **2011**, *44*, 1281–1284.

9 Crystal Structures

Crystal were measured with a Bruker D8 QUEST area detector. Crystal structures were resolved and refined by Dr. K. Harms of the service Department of Chemistry of the Philipps-Universität Marburg.

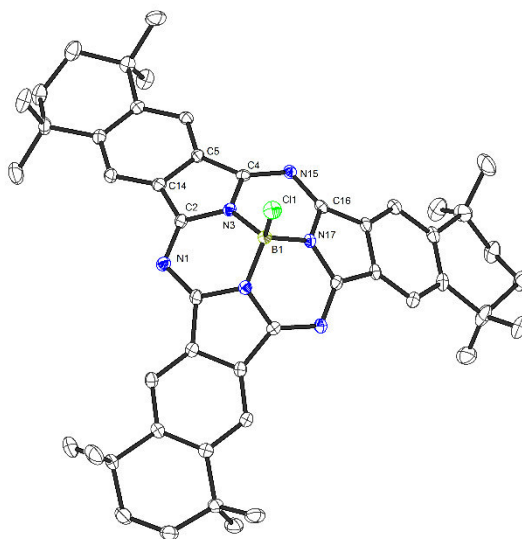
Diffractometer type	Bruker D8 QUEST area detector
Wavelength	0.71073 Å
Temperature	100(2) K
Index ranges	-14<=h<=14, -28<=k<=28, -15<=l<=15
Data collection software	BRUKER APEX2 2014.9-0 ^[292]
Cell refinement software	BRUKER SAINT ^[293]
Data reduction software	SAINT V8.34A (Bruker AXS Inc., 2013) ^[293]
Programs used	XT V2014/1 (Bruker AXS Inc., 2014) ^[294,295] SHELXL-2014/7 (Sheldrick, 2014) ^[294,296] DIAMOND (Crystal Impact) ^[297]

9.1.1 Crystal Structure of [Spc*BF]

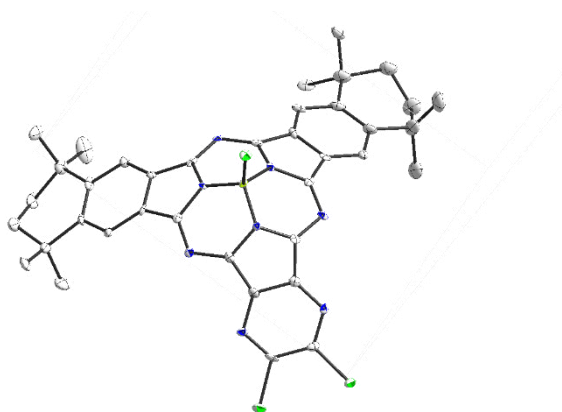


Habitus, colour	plate, red	
Crystal size	0.16 x 0.14 x 0.12 mm ³	
Crystal system	Orthorhombic	
Space group	Cmc2 ₁	Z = 4
Unit cell dimensions	a = 24.5288(15) Å	α = 90°.
	b = 15.7219(8) Å	β = 90°.
	c = 11.4144(6) Å	γ = 90°.
Volume	4401.8(4) Å ³	
Cell determination	5553 peaks with Theta 2.4 to 24.6°.	
Empirical formula	C ₄₉ H ₅₆ B Cl ₂ F N ₆	
Moiety formula	C ₄₈ H ₅₄ B F N ₆ , CH ₂ Cl ₂	
Formula weight	829.70	
Density (calculated)	1.252 Mg/m ³	
Absorption coefficient	0.194 mm ⁻¹	
F(000)	1760	
Solution and refinement:		
Reflections collected	22775	
Independent reflections	3922 [R(int) = 0.0792]	
Completeness to theta = 25.242°	99.9 %	
Observed reflections	3376[I > 2σ(I)]	
Reflections used for refinement	3922	
Absorption correction	Semi-empirical from equivalents ^[298]	
Max. and min. transmission	0.98 and 0.89	
Flack parameter (absolute struct.)	-0.04(4)	
Largest diff. peak and hole	0.256 and -0.227 e.Å ⁻³	
Solution	Direct methods ^[294]	
Refinement	Full-matrix least-squares on F ² ^[294]	
Treatment of hydrogen atoms	Calculated positions, constr. ref.	
Data / restraints / parameters	3922 / 34 / 305	
Goodness-of-fit on F ²	1.076	
R index (all data)	wR2 = 0.0845	
R index conventional [I > 2σ(I)]	R1 = 0.0386	

9.1.2 Crystal Structure of [Spc*BCl]



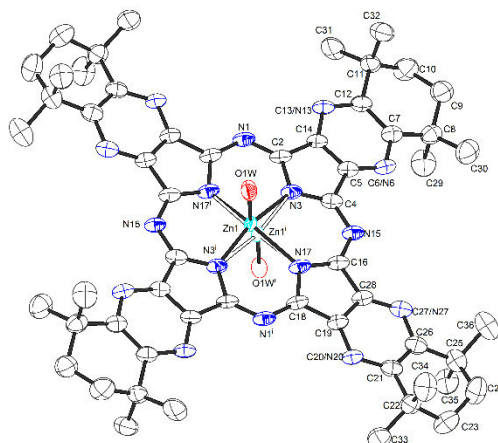
Habitus, colour	prism, colourless	
Crystal size	0.22 x 0.22 x 0.09 mm ³	
Crystal system	Orthorhombic	
Space group	Cmc2 ₁	Z = 4
Unit cell dimensions	a = 24.8236(10) Å	α = 90°.
	b = 16.3090(6) Å	β = 90°.
	c = 10.9728(4) Å	γ = 90°.
Volume	4442.3(3) Å ³	
Cell determination	9874 peaks with Theta 2.4 to 25.4°.	
Empirical formula	C ₄₉ H ₅₆ B Cl ₃ N ₆	
Moiety formula	C ₄₈ H ₅₄ B Cl N ₆ , CH ₂ Cl ₂	
Formula weight	846.15	
Density (calculated)	1.265 Mg/m ³	
Absorption coefficient	0.248 mm ⁻¹	
F(000)	1792	
Solution and refinement:		
Reflections collected	28577	
Independent reflections	4177 [R(int) = 0.0342]	
Completeness to theta = 25.242°	99.9 %	
Observed reflections	4031 [I > 2σ(I)]	
Reflections used for refinement	4177	
Absorption correction	Semi-empirical from equivalents ^[298]	
Max. and min. transmission	0.98 and 0.86	
Flack parameter (absolute struct.)	0.001(14)	
Largest diff. peak and hole	0.283 and -0.192 e.Å ⁻³	
Solution	Direct methods ^[294]	
Refinement	Full-matrix least-squares on F ² ^[294]	
Treatment of hydrogen atoms	Calculated positions, constr. ref.	
Data / restraints / parameters	4177 / 44 / 311	
Goodness-of-fit on F ²	1.049	
R index (all data)	wR2 = 0.0754	
R index conventional [I > 2σ(I)]	R1 = 0.0293	

9.1.4 Crystal Structure of [Spc*BCl]^{Cl}

Habitus, colour	prism, dark	
Crystal size	0.17 x 0.13 x 0.07 mm ³	
Crystal system	Orthorhombic	
Space group	Pna2 ₁	Z = 4
Unit cell dimensions	a = 11.1293(4) Å	α = 90°.
	b = 30.5073(13) Å	β = 90°.
	c = 12.6973(6) Å	γ = 90°.
Volume	4311.1(3) Å ³	
Cell determination	6666 peaks with Theta 2.3 to 25.0°.	
Empirical formula	C ₄₀ H ₄₀ B Cl ₇ N ₈	
Moiety formula	C ₃₈ H ₃₆ B Cl ₃ N ₈ , 2(C H ₂ Cl ₂)	
Formula weight	891.76	
Density (calculated)	1.374 Mg/m ³	
Absorption coefficient	0.501 mm ⁻¹	
F(000)	1840	
Solution and refinement:		
Reflections collected	12571	
Independent reflections	6374 [R(int) = 0.0456]	
Completeness to theta = 25.242°	99.8 %	
Observed reflections	5442[I > 2σ(I)]	
Reflections used for refinement	6374	
Absorption correction	Semi-empirical from equivalents ^[298]	
Max. and min. transmission	0.97 and 0.87	
Flack parameter (absolute struct.)	0.02(4)	
Largest diff. peak and hole	0.552 and -0.569 e.Å ⁻³	
Solution	Direct methods ^[294]	
Refinement	Full-matrix least-squares on F ² ^[294]	
Treatment of hydrogen atoms	Calculated positions, constr. ref.	
Programs used	XT V2014/1 (Bruker AXS Inc., 2014) ^[294,295] SHELXL-2014/7 (Sheldrick, 2014) ^[294,296] DIAMOND (Crystal Impact) ^[297]	
Data / restraints / parameters	6374 / 384 / 591	
Goodness-of-fit on F ²	1.069	
R index (all data)	wR2 = 0.1397	
R index conventional [I > 2σ(I)]	R1 = 0.0569	

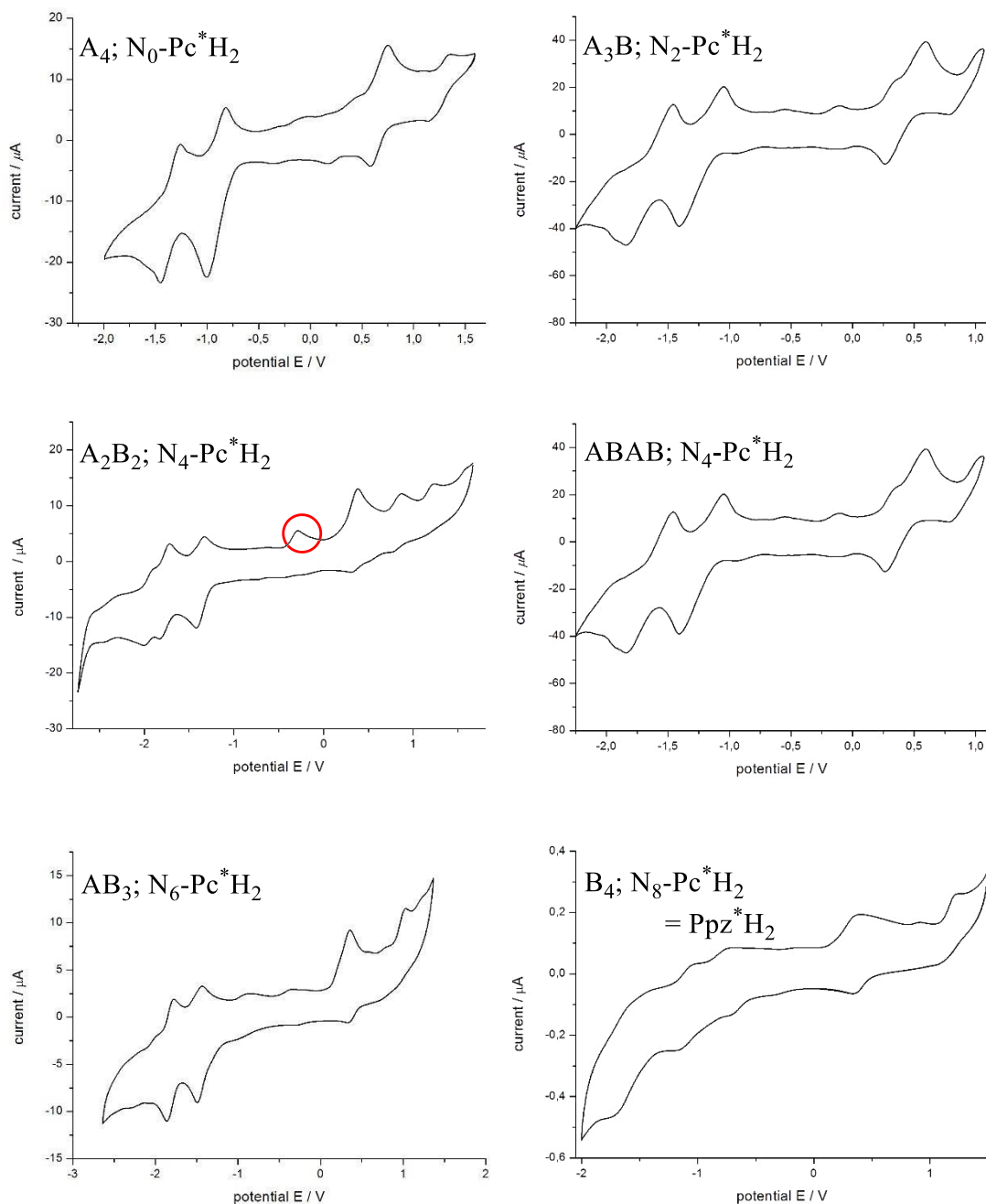
*Die gefüllten Formen in der Kristallstruktur beschreiben Hohlräume in der Zelle, die wahrscheinlich eine kleine Menge an fehlgeordnetem LM enthalten („gesqueezed“).^[233,234,234]

9.1.5 Crystal Structure of $A_2B_2 N_4-[Pc^*Zn \cdot H_2O]$

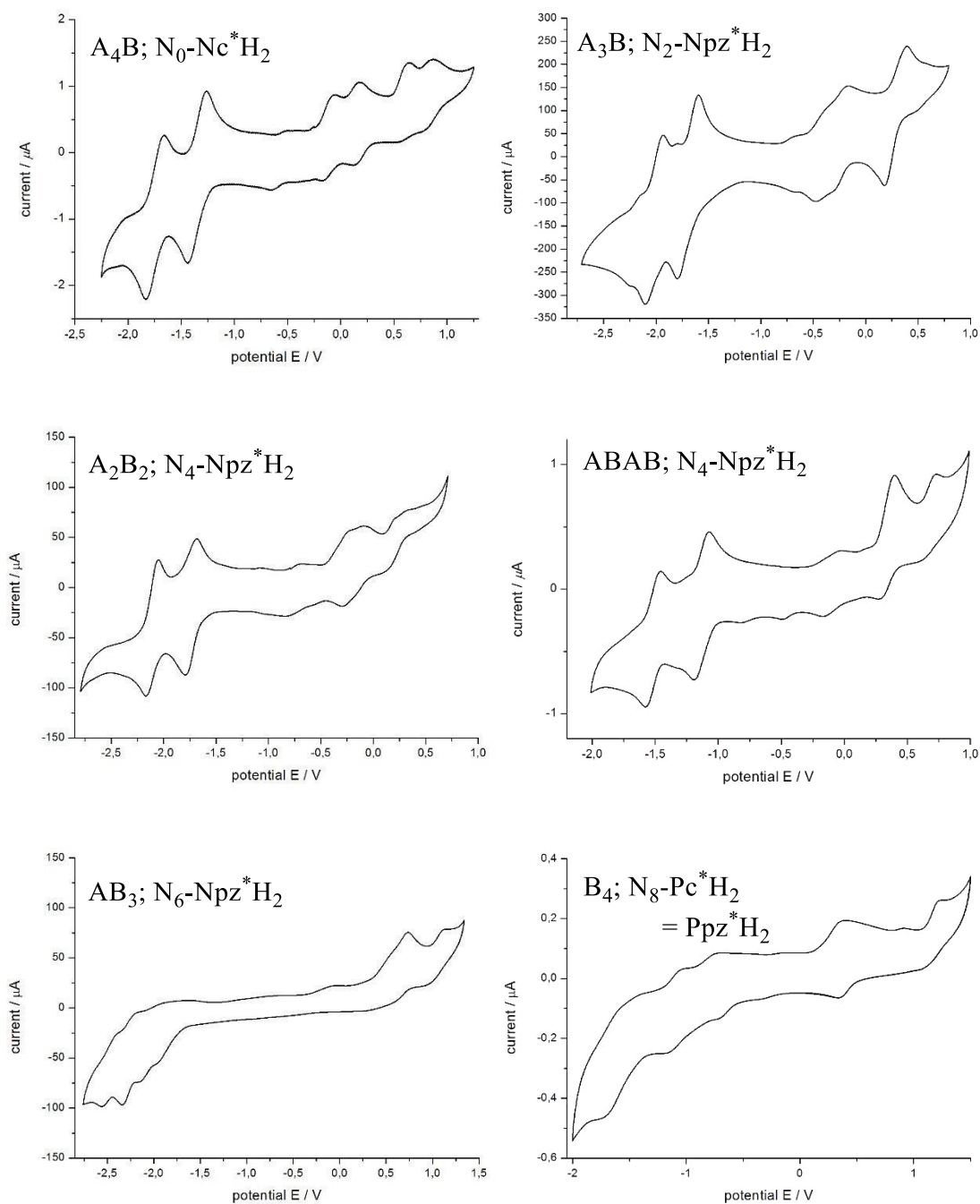


Habitus, colour	prism, dark	
Crystal size	0.27 x 0.06 x 0.03 mm ³	
Crystal system	Monoclinic	
Space group	P2 ₁ /c	Z = 2
Unit cell dimensions	a = 6.0419(5) Å	α = 90°.
	b = 16.2175(13) Å	β = 95.305(3)°.
	c = 31.008(2) Å	γ = 90°.
Volume	3025.3(4) Å ³	
Cell determination	9556 peaks with Theta 2.3 to 25.2°.	
Empirical formula	C ₆₀ H ₇₀ N ₁₂ O Zn	
Moiety formula	C ₆₀ H ₇₀ N ₁₂ O Zn	
Formula weight	1040.65	
Density (calculated)	1.142 Mg/m ³	
Absorption coefficient	0.454 mm ⁻¹	
F(000)	1104	
Solution and refinement:		
Reflections collected	32818	
Independent reflections	5598 [R(int) = 0.0711]	
Completeness to theta = 25.242°	99.9 %	
Observed reflections	4276[I > 2(I)]	
Reflections used for refinement	5598	
Absorption correction	Numerical Mu Calculated ^[298]	
Max. and min. transmission	0.99 and 0.89	
Largest diff. peak and hole	0.288 and -0.347 e.Å ⁻³	
Solution	Direct methods	
Refinement	Full-matrix least-squares on F ²	
Treatment of hydrogen atoms	Calculated positions, constr. ref.	
Programs used	XT V2014/1 (Bruker AXS Inc., 2014) ^[299] SHELXL-2014/7 (Sheldrick, 2014) ^[300] DIAMOND (Crystal Impact) ^[297] ShelXle (Hübschle, Sheldrick, Dittrich, 2011) ^[301]	
Data / restraints / parameters	5598 / 0 / 353	
Goodness-of-fit on F ²	1.021	
R index (all data)	wR2 = 0.1467	
R index conventional [I > 2σ(I)]	R1 = 0.0580	

10 Supplement

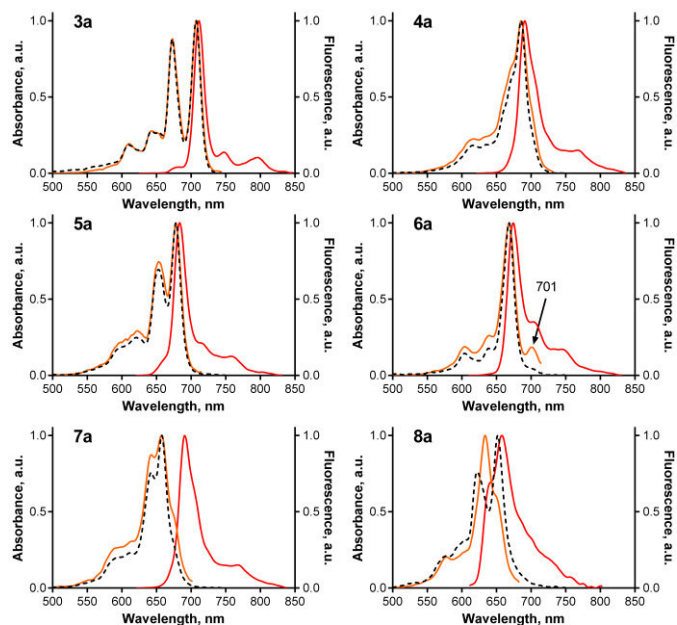
10.1 Cyclovoltammetric Measurements of $N_x\text{-Pc}^*\text{H}_2$ 

Cyclovoltammetric measurements of $N_x\text{-Pc}^*\text{H}_2$. All measurements were carried out in DCM, except of Ppz^*H_2 , which was measured in THF because of solubility. The red circles mark impurities caused by used DCM. In all cases, different scan rates were tested, here, 20 mV/s measurements are shown. The spectra are calibrated using Fc in the final scan, measured in $[\text{TBA}]\text{PF}_6$.

10.2 Cyclovoltammetric Measurements of $N_x-Nc^*H_2$ 

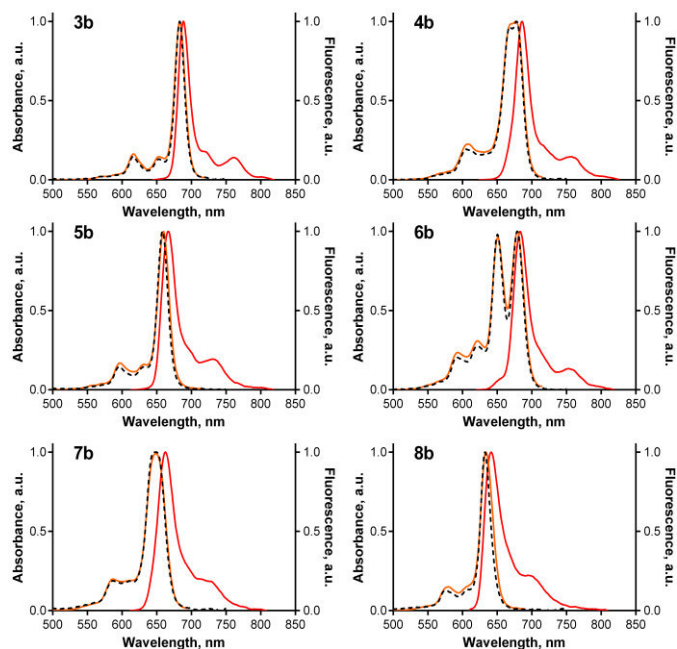
Cyclovoltammetric measurements of $N_x-Np_z^*H_2$. All measurements were carried out in DCM. In all cases, different scan rates were tested, here, 20 mV/s measurements are shown. The spectra are calibrated using Fc in the final scan, measured in $[TBA]PF_6$.

10.3 UV-Vis, FS and Emission spectra of N_x -[Pc**M*] and N_x -[Spc**BCI*]



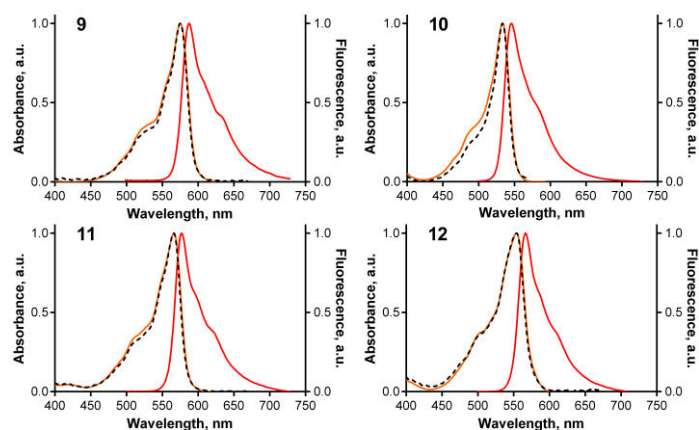
Measurements of N_x -Pc* H_2 in THF.

In orange: excitation, in black (dashed): absorption spectrum, in red: fluorescence.



Measurements of N_x -[Pc**Zn*] in THF.

In orange: excitation, in black (dashed): absorption spectrum, in red: fluorescence.

Measurements of N_x -[Spc^*BCl] in MeOH.

In orange: excitation, in black (dashed): absorption spectrum, in red: fluorescence.

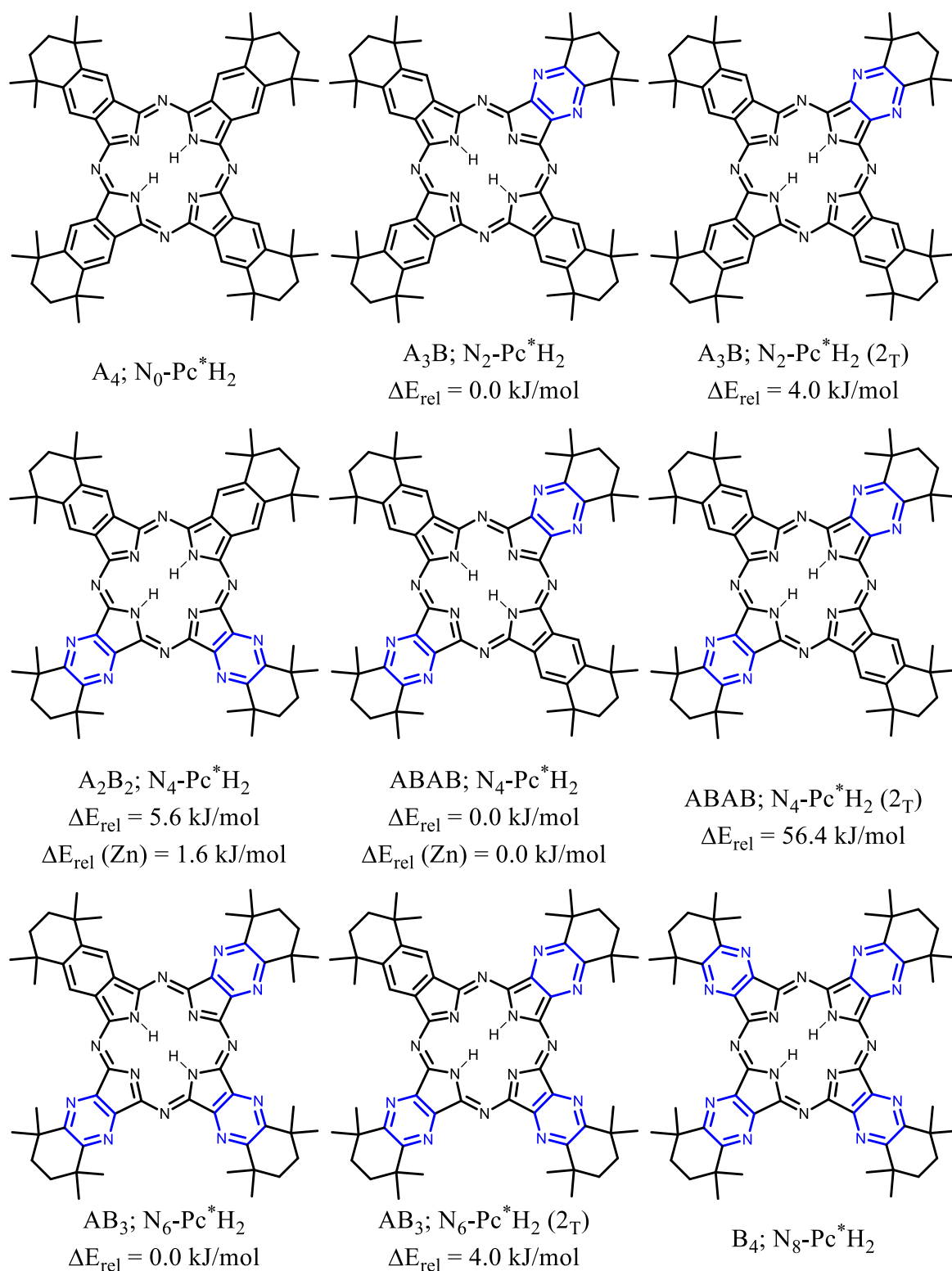
10.4 Photophysical Measurements

Table SI-1: Electronic and photophysical data of N_x -[Pc^*M] in THF and N_x -[Spc^*BCl] in MeOH.^a

	λ_{max} (B-band) / nm	λ_{max} (Q-band) / nm	λ_{F} / nm	τ_{F} / ns ^b	$\Phi_{\text{F}}^{\text{c}}$	Φ_{Δ}^{d}	$\Phi_{\text{F}} + \Phi_{\Delta}$
N_0 - Pc^*H_2	343	707, 673	711	5.52	0.42	0.16	0.58
N_2 - Pc^*H_2	343	686	692	3.45	0.33	0.14	0.47
N_4 - Pc^*H_2 ABAB	358	678, 653	684	1.62	0.14	0.07	0.21
N_4 - Pc^*H_2 A ₂ B ₂	353	668, (701)	674	1.79	0.16	0.10	0.26
N_6 - Pc^*H_2	349	658, 643	664	3.92 (26%), 0.63 (74%)	0.06	0.04	0.10
N_8 - Pc^*H_2	345	652, 623	658	2.15 (29%), 0.36 (71%)	0.03	0.05	0.08
N_0 -[Pc^*Zn]	350	683	689	3.31	0.31	0.59	0.90
N_2 -[Pc^*Zn]	353	679, 668	686	2.69	0.25	0.63	0.88
N_4 -[Pc^*Zn]	356	658	667	3.08	0.35	0.56	0.91
N_4 -[Pc^*Zn]	355	679, 651	687	1.98	0.18	0.73	0.91
N_6 -[Pc^*Zn]	353	648	663	2.69	0.27	0.62	0.89
N_8 -[Pc^*Zn]	347	633	642	2.98	0.30	0.57	0.87
N_0 -[Spc^*BCl]	575	587	12	2.04	0.18	0.65	0.82
N_2 -[Spc^*BCl]	566	577	11	2.19	0.21	0.62	0.82
N_4 -[Spc^*BCl]	555	567	12	2.85	0.23	0.64	0.87
N_6 -[Spc^*BCl]	533	546	13	2.98	0.19	0.69	0.87

^aabsorption maximum (λ_{max}), fluorescence emission maximum (λ_{F}), fluorescence lifetime (τ_{F}), fluorescence quantum yield (Φ_{F}), singlet oxygen quantum yield (Φ_{Δ}). ^b $\lambda_{\text{exc}} = 371$ nm or 634 nm. ^cwith [PcZn] ($\Phi_{\text{F(THF)}} = 0.32$, $\lambda_{\text{exc}} = 598$ nm) and rhodamin G6 ($\Phi_{\text{F(EtOH)}} = 0.94$, $\lambda_{\text{exc}} = 490$ nm) as reference for N_x -[Pc^*M] and N_x -[Spc^*BCl], respectively. ^dwith [PcZn] ($\Phi_{\Delta(\text{THF})} = 0.53$) and bengal rose ($\Phi_{\Delta(\text{MeOH})} = 0.76$) as reference for N_x -[Pc^*M] and N_x -[Spc^*BCl], respectively.

10.5 Theoretical Calculations [a]



[a] The phthalocyanines $N_x\text{-Pc}^*\text{H}_2$ (A_4H_2 , A_3B_1 , A_2B_2 , A_1B_3 and B_4H_2) were computationally investigated by TROMBACH of the TONNER group, at the Department of Chemistry at the Philipps-Universität Marburg. Regioisomers are numbered and tautomers marked (subscript T). Energies are given relative to the most stable isomer (ΔE_{rel}). Zn-substituted phthalocyanines [Pc^*Zn] are derived by substituting the two central H atoms by Zn. Relative isomer energies are given as $\Delta E_{\text{rel}}(\text{Zn})$, no tautomers are found for [Pc^*Zn].

Table SI-2: Computed excitation energies (λ in nm), oscillator strengths (f), frontier orbital gaps ($\Delta_{H-L/L+1}$ in nm) and molecular orbital character of the transitions for the Q-bands. Dipole moment (μ) and isotropic polarizability (α) in a.u.^a

Molecule	λ / nm	$\Delta\lambda$ / nm	f	Character	$\Delta_{H-L/L+1}$ [c]	μ [d]	$\Delta\alpha$ [e]
N ₈ -Pc*H ₂	541	0	0.42	H → L+1	781	0.00	0.0
	536	0	0.53	H → L	818		
N ₆ -Pc*H ₂	550	9	0.56	H → L	861	0.87	23.6
	549	13	0.49	H → L+1	797		
N ₆ -Pc*H ₂ (2T)	559	18	0.47	H → L+1	839	0.92	26.6
	552	16	0.60	H → L	848		
N ₄ -Pc*H ₂ (A ₂ B ₂)	563	22	0.55	H → L+1 (39%) H → L (27%) H → L (41%)	845	1.25	28.3
	559	23	0.63	H → L+1 (18%) H-2 → L+1 (15%)			
N ₄ -Pc*H ₂ (ABAB)	561	20	0.62	H → L	910	0.00	47.8
	560	24	0.55	H → L+1	815		
N ₄ -Pc*H ₂ (ABAB, 2T)	583	42	0.56	H → L+1	892	0.06	61.8
	580	44	0.54	H → L	911		
N ₂ -Pc*H ₂	569	28	0.62	H → L+1	855	0.90	71.1
	564	28	0.72	H → L	915		
N ₂ -Pc*H ₂ (2T)	577	36	0.61	H → L+1	897	0.87	73.3
	571	35	0.69	H → L	900		
N ₀ -Pc*H ₂	580	39	0.69	H → L+1	903	0.00	94.9
	568	32	0.81	H → L	923		
N ₈ -[Pc*Zn]	532	0	0.51	H → L	788	0.00	0.0
	532	0	0.51	H → L+1	788		
N ₆ -[Pc*Zn]	549	17	0.55	H → L	840	0.89	24.6
	544	12	0.59	H → L+1	810		
N ₄ -[Pc*Zn] (A ₂ B ₂)	556	26	0.62	H → L	852	1.25	47.6
	554	22	0.63	H → L+1	848		
N ₄ -[Pc*Zn] (ABAB)	565	33	0.60	H → L	898	0.00	49.5
	557	26	0.63	H → L+1	831		
N ₂ -[Pc*Zn]	566	34	0.69	H → L	897	0.88	71.1
	564	32	0.69	H → L+1	863		
N ₀ -[Pc*Zn]	570	38	0.77	H → L	902	0.00	93.7
	570	38	0.77	H → L+1	901		

[a] Shift relative to Q1/Q2 band of B₄M. [b] dominant MO transitions for the Q-bands (H: HOMO, H-2: HOMO-2, L: LUMO, L+1: LUMO+1).

For A₂B₂H₂₋₁, relative contributions are given in percent. [c] Frontier MO gap of the orbitals given in the “character” column HOMO/LUMO and HOMO/LUMO+1) in nm. [d] All compounds exhibit an in-plane dipole moment only pointing toward the nitrogen-rich parts of the molecule. [e] Polarizabilities are given relative to B₄H₂ ($\alpha = 1091.3$ a.u.) and B₄Zn ($\alpha = 1097.1$ a.u.), respectively.

Danksagung

In erster Linie gilt mein Dank meinem Doktorvater Jörg Sundermeyer für die Möglichkeit, die Arbeit in seiner Gruppe anzufertigen und für die gewissenhafte Betreuung. Dem Zweitgutachter Herrn Prof. Dr. Eric Meggers und dem Prüfungskomitee sei an dieser Stelle gedankt. Dem Sonderforschungsbereich SFB 1083 sowie dem Landesprogramm LOEWE sei für die Finanzierung des Projektes gedankt.

Veronika und Petr sowie dem gesamten Arbeitskreis in Hradec danke ich für die Einführung in die PDT und die Photophysik von Phthalocyaninen, die vielen netten Stunden in Tschechien sowie die Aufklärung des mysteriösen „green spot“. Die gemeinsame Arbeit hat mir sehr viel Freude bereitet!

Nicht zuletzt möchte ich besonders meinen langjährigen Laborpartnern Katrin Schlechter und Marius Hoffmann für die nette Zusammenarbeit und auch die gemeinsamen Pausen danken. Malcolm Bartlett möchte ich besonders für den wissenschaftlichen Austausch sowie das akribische Korrigieren meiner Arbeit danken. Ebenso sei Alexander Venker, Marius Hoffmann und Eugen Sharikow für das Ausmerzen der größten Fehler gedankt. Irene Barth und Lisa Hamel möchte ich für die fleißige Unterstützung im Labor, vor allem gen Ende der Arbeit, danken. Des Weiteren danke ich dem gesamten AK Su mit den derzeitigen und damaligen Mitgliedern für viele nette gemeinsame Stunden und die Zusammenarbeit. Zudem möchte ich mich bei allen Serviceabteilungen, insbesondere bei Tina Krieg, für das Messen der unzähligen MALDIs, bedanken. Herrn Dr. Harms danke ich für das Messen und Lösen viele armorpher Kristallstrukturen. Dr. Olaf Burghaus danke ich für die Einführung in die EPR, die Simulationen und das Messen der Proben, Lukas für das Rechnen der UV-Vis Spektren. Ingo und Luise möchte ich für das Messen der PLs und den wissenschaftlichen Austausch danken, Jane und Jan für Ihre Zeit, mir den Aufbau von Solarzellen näher zubringen und die zahlreichen Messungen. Malte sei bereits jetzt für seine Zeit für die folgenden Untersuchungen der Azanaphthalonitrile gedankt, sowie dem AK Berger für seine Bemühungen die EPR Messungen mit Rechnungen näher zu verstehen.

Im Rahmen dieser Arbeit sind folgende Bachelorarbeiten hervorgegangen: Eugen Sharikow (B.Sc.), Tobias Vollgraff (B.Sc.), Patrick Swolana (B.Sc.), Alexander Lange (B.Sc.). Des Weiteren möchte ich den Vertiefungsstudenten Benjamin Ringler, Leon Maser, Manuel Hartweg, Johannes Jammer, Markus Balmer, Alexander Lange, Anna Reuter, Johanna Plag, und Christian Ritter für ihre Unterstützung und die kreativen Ideen sowie den wissenschaftlichen Austausch danken. Eugen Sharikow sei neben den Vertiefungsprojekten zusätzlich für seine

Unterstützung als Hiwi gedankt. Ohne Eure Mitarbeit wäre diese Arbeit in dem Umfang so nicht möglich gewesen. Des Weiteren sei den AC-MPR Studenten für ihre Beiträge gedankt. Außerhalb der Universität möchte ich meinen langjährigen Kommilitonen und Freunden danken: Lena, Ottfried, Thomas, Arved, Jens – auf dass noch viele Tennis Matches folgen!

Meiner Familie danke ich für die Unterstützung während des Studiums und die vielen schönen gemeinsamen Urlaube. Ann-Kathrin danke ich für die schönen Momente außerhalb der Uni.